

**Secondary Metabolites from Fungi: Isolation,
Structure Elucidation, Bioactivity and Expansion of
the Chemical Diversity**

Inaugural dissertation

for the attainment of the title of doctor
in the Faculty of Mathematics and Natural Sciences
at the Heinrich Heine University Duesseldorf

presented by

Xiaoqin Yu
from Hubei, P. R. China

Duesseldorf, Oct. 2020

from the Institute for Pharmaceutical Biology and Biotechnology
at the Heinrich Heine University Duesseldorf

Published by permission of the
Faculty of Mathematics and Natural Sciences at
Heinrich Heine University Duesseldorf

Supervisor: Prof. Dr. Dr. h.c. Peter Proksch
Co-supervisor: Prof. Dr. Rainer Kalscheuer

Date of the oral examination: 02.12.2020

Declaration of academic honesty/Erklärung

Hiermit erkläre ich ehrenwörtlich, dass ich die vorliegende Dissertation mit dem Titel “Sekundärmetaboliten aus endophytischen Pilzen: Isolierung, Strukturaufklärung, Bioaktivität und Erweiterung des Metabolitenmusters” selbst angefertigt habe. Außer den angegebenen Quellen und Hilfsmitteln wurden keine weiteren verwendet. Diese Dissertation wurde weder in gleicher noch in abgewandelter Form in einem anderen Prüfungsverfahren vorgelegt. Weiterhin erkläre ich, dass ich früher weder akademische Grade erworben habe, noch dies versucht habe.

Düsseldorf, den Oct. 2020

Xiaoqin Yu

Contents

Abstract.....	1
Zusammenfassung	3
1. Introduction	5
1.1. Fungi, important participants in food technology and beverages.....	5
1.2. Rich source and diversity of fungi	6
1.2.1. Coprophilous fungi.....	6
1.2.2. Endophytic fungi	7
1.2.3. Endolichenic fungi	9
1.2.4. Marine-sourced fungi	10
1.3. Pharmaceutical agents originated from fungi	10
1.4. Strategies to expand the diversity of secondary metabolites of fungi	12
1.4.1. OSMAC approach	13
1.4.2. Co-cultivation	14
1.4.3. Genetic modification	14
1.5. Aims of the study	15
2 Publication 1: Indole alkaloids from the coprophilous fungus <i>Aphanoascus fulvescens</i>	16
3 Publication 2: Polyketide derivatives from mangrove derived endophytic fungus <i>Pseudopestalotiopsis theae</i>	41
4 Publication 3: Induction of ambuic acid derivatives by the endophytic fungus <i>Pestalotiopsis lespedezae</i> through an OSMAC approach	157
5 Discussion	226
5.1. Prenylated indole alkaloids from <i>Aphanoascus fulvescens</i>	226
5.2. Acetylenic natural products from <i>Pseudopestalotiopsis theae</i>	228
5.3. Inducing iodinated secondary metabolites through halogen incorporation experiment	230
References	234
List of abbreviations	242
Acknowledgements	244
Curriculum vitae	246

Abstract

Fungi are valuable in the pharmaceutical industry, as well as in other areas, by providing a wide variety of bioactive and structurally novel secondary metabolites. This dissertation describes the investigation of secondary metabolites from the coprophilous fungus *Aphanoascus fulvescens*, the mangrove derived endophytic fungus *Pseudopestalotiopsis theae* and the endophytic fungus *Pestalotiopsis lespedezae*. Halogen incorporation experiments were successfully applied to expand the diversity of secondary metabolites from *Pestalotiopsis lespedezae*, yielding ten new natural products including a remarkably rare iodo organic natural product in the case of pestallic acid Q. The structures of the isolated compounds were established by interpretation of 1D and 2D NMR spectroscopic data together with MS data. In-depth comparison of the NMR and optical rotation data with related literature, modified Mosher's method and TDDFT-ECD calculations were applied to determine the absolute configuration of the new compounds. Okaramines A, C, G, H and cytosporin W showed significant cytotoxicity against the mouse lymphoma cell line L5178Y. Cytosporins V and W showed moderate antibacterial activity against drug-resistant *Acinetobacter baumannii* (ATCC BAA-1605) in combination with sublethal colistin concentrations. This dissertation consists of the following three publications or submitted manuscripts.

Indole alkaloids from the coprophilous fungus Aphanoascus fulvescens

Xiaoqin Yu, Werner E.G. Müller, Zhiyong Guo, Wenhan Lin, Kun Zou, Zhen Liu and Peter Proksch. *Fitoterapia*, 2019, 136, 104168.

The ascomycete fungus *Aphanoascus fulvescens* isolated from goose dung was investigated for its secondary metabolites, yielding five new indole alkaloids okaramines V–Z (**1–5**) and eleven known derivatives (**6–16**). Their structures were determined by 1D, 2D NMR spectra and MS data. Okaramines A, C, G and H showed significant to moderate cytotoxicity against the mouse lymphoma cell line L5178Y with IC₅₀ values ranging from 4.0 to 14.7 µM. Preliminary structure-activity relationships were discussed.

Polyketide derivatives from mangrove derived endophytic fungus Pseudopestalotiopsis theae

Xiaoqin Yu, Werner E. G. Müller, Dieter Meier, Rainer Kalscheuer, Zhiyong Guo, Kun

Zou, Blessing O. Umeokoli, Zhen Liu and Peter Proksch. *Marine drugs*, 2020, **18**, 129.

Chemical investigation of secondary metabolites from the endophytic fungus *Pseudopestalotiopsis theae* led to the isolation of eighteen new polyketide derivatives, pestalotheols I–Q (**1–9**) and cytosporins O–W (**15–23**), together with eight known analogues (**10–14** and **24–26**). The structures of the new compounds were elucidated by HRMS and 1D and 2D NMR data, as well as by comparison with literature data. Modified Mosher's method was applied to determine the absolute configuration of some compounds. Cytosporins W (**23**) showed significant cytotoxicity against the mouse lymphoma cell line L5178Y with an IC₅₀ value of 3.0 µM. Furthermore, cytosporins V (**22**) and W (**23**) showed moderate antibacterial activity against drug-resistant *Acinetobacter baumannii* (ATCC BAA-1605) in combination with sublethal colistin concentrations.

Induction of ambuic acid derivatives by the endophytic fungus Pestalotiopsis lespedezae through an OSMAC approach (submitted)

Xiaoqin Yu, Ying Gao, Marian Frank, Attila Mándi, Tibor Kurtán, Werner E. G. Müller, Rainer Kalscheuer, Zhiyong Guo, Kun Zou, Zhen Liu, Peter Proksch

Ten new ambuic acid derivatives, pestallic acids H–Q (**1–10**) including one new iodinated natural product (**10**) along with two known compounds (**11** and **12**) were obtained through fermentation of the endophytic fungus *Pestalotiopsis lespedezae* on solid rice medium with 3.5% NaI. Compounds **1–10** were undetectable in cultures of this fungus growing on solid rice medium where NaI was either absent or had been replaced by NaCl or NaBr. The structures of the new metabolites were established on basis of 1D/2D NMR and HRESIMS data. Their absolute configurations were determined by modified Mosher's method and TDDFT-ECD calculations. The compounds failed to show antibacterial activity against *S. aureus* (ATCC29213), drug-resistant *Acinetobacter baumannii* (BAA1605) or *Mycobacterium tuberculosis*, as well as cytotoxicity against the mouse lymphoma cell line L5178Y.

Zusammenfassung

Pilze sind für die pharmazeutische Industrie und andere Bereiche wertvoll. Sie liefern eine große Auswahl an bioaktiven und strukturell neuartigen Sekundärmetaboliten. Diese Dissertation beschreibt die Untersuchungen des koprophilen Pilzes *Aphanoascus fulvescens*, des Mangrovenpflanzen-assoziierten endophytischen Pilzes *Pseudopestalotiopsis theae* und des endophytischen Pilzes *Pestalotiopsis lespedezae*. Es wurden erfolgreiche Halogeninkorporationsexperimente an *Pestalotiopsis lespedezae* durchgeführt, die zu einer Erweiterung der Sekundärmetabolitdiversität führten. Hierbei wurden zehn neue Naturstoffe isoliert, einschließlich pestalsäure Q, welche eine bemerkenswert seltene iodorganische Verbindung darstellt. Die Strukturen der neuen Verbindungen wurden durch die Interpretation von 1D und 2D NMR spektroskopischen und massenspektrometrischen Daten aufgeklärt. Zur Aufklärung der absoluten Konfiguration der neuen Verbindungen wurden detaillierte Vergleiche der NMR Spektren und optischen Aktivitäten, die modifizierte Mosher Methode und TDDFT ECD Berechnungen herangezogen. Okaramine A, C, G, H und Cytosporin W zeigten signifikante Zytotoxizität gegen die Mauslymphomzelllinie L5178Y. Cytosporine V und W zeigten moderate antibakterielle Aktivität gegen *Acinetobacter baumannii* (ATCC BAA-1605), wenn sie mit einer subletalen Dosis Colistin kombiniert wurden. Diese Dissertation gliedert sich in drei bereits veröffentlichte oder eingereichte Manuskripte.

Indolalkaloide aus dem koprophilen Pilz Aphanoascus fulvecens

Xiaoqin Yu, Werner E.G. Müller, Zhiyong Guo, Wenhan Lin, Kun Zou, Zhen Liu und Peter Proksch. *Fitoterapia*, 2019, 136, 104168.

Der ascomyzetische Pilz *Aphanoascus fulvescens* wurde aus Gänsekot isoliert. Untersuchungen der Sekundärmetaboliten förderten die fünf neuen Indolalkaloide OkaramineV–Z (1–5) und elf bekannte Derivate (6–16) zu Tage. Ihre Struktur wurde anhand von NMR Spektren und MS Messungen aufgeklärt. Okaramine A, C, G und H zeigten signifikante bis moderate Zytotoxizität gegen Mauslymphomzelllinie L5178Y mit IC₅₀ Werten zwischen 4.0 und 14.7 µM. Eine vorläufige Struktur-Wirkungsbeziehung wurde erarbeitet.

Polyketidderivate aus dem Mangrovenpflanzen-assoziierten endophytischen Pilz

Pseudopestalotiopsis theae.

Xiaoqin Yu, Werner E. G. Müller, Dieter Meier, Rainer Kalscheuer, Zhiyong Guo, Kun Zou, Blessing O. Umeokoli, Zhen Liu und Peter Proksch. *Marine drugs*, 2020, **18**, 129.

Chemische Untersuchungen der Sekundärmetaboliten des endophytischen Pilzes *Pseudopestalotiopsis theae* führten zur Isolation der achtzehn neuen Polyketidderivate Pestalotheole I–Q (**1–9**) und Cytosporine O–W (**15–23**), neben acht bekannten Analoga (**10–14** und **24–26**). Die neuen Strukturen wurden durch HRMS, sowie 1D und 2D NMR Messungen aufgeklärt. Zur Bestimmung der absoluten Konfiguration wurde bei einigen Verbindungen die modifizierte Mosher Methode angewandt. Cytosporin W (**23**) zeigte signifikante Zytotoxizität gegen Mauslymphomzelllinie L5178Y mit einem IC₅₀ Wert von 3.0 µM. Außerdem zeigten Cytosporine V (**22**) und W (**23**) moderate antibakterielle Aktivität gegen einen resistenten Stamm *Acinetobacter baumannii* (ATCC BAA-1605) in Kombination mit einer subletalen Dosis Colistin.

Induktion von Ambuicsäurederivativen im endophytischen Pilz Pestalotiopsis lespedezae durch einen OSMAC Ansatz (eingereicht)

Xiaoqin Yu, Ying Gao, Marian Frank, Attila Mándi, Tibor Kurtán, Werner E. G. Müller, Rainer Kalscheuer, Zhiyong Guo, Kun Zou, Zhen Liu und Peter Proksch

Die zehn neuen Ambuicsäurederivate Pestalsäuren H–Q (**1–10**), unter ihnen ein neuer iodierter Naturstoff (**10**), wurden zusammen mit zwei bekannten Verbindungen (**11** und **12**) aus einer Fermentation des endophytischen Pilzes *Pestalotiopsis lespedezae* auf festem Reismedium nach Zusatz von 3.5% NaI isoliert. Die Verbindungen **1–10** waren weder in Kulturen des Pilzes auf Reismedium ohne NaI, noch in denen mit NaCl oder NaBr nachweisbar. Die Struktur der neuen Metaboliten wurde anhand der 1D/2D NMR Spektren und der HRESIMS Messungen bestimmt. Ihre absolute Konfiguration wurde durch den Einsatz der modifizierten Mosher Methode und TDDFT ECD Berechnungen bestimmt. Die Verbindungen zeigten weder antibakterielle Aktivität gegen *Staphylococcus aureus* (ATCC29213), resistenten *Acinetobacter baumannii* (BAA1605) oder *Mycobacterium tuberculosis*, noch zytotoxische Aktivität gegen Mauslymphomzelllinie L5178Y.

1. Introduction

Fungi are one of the key organisms among microbes. Although they share many common characteristics with animals, plants and other eukaryotic organisms, fungi set themselves apart by their unique chitinous cell wall. Today our understanding of the evaluation and application of fungi is still improving driven by advancing technology. The recent discovery of a 1-0.9-billion-year-old fossil fungus from the shale of the Grassy Bay Formation (Shaler Supergroup, Arctic Canada) showed that early fungi may have appeared half a billion years earlier than previously thought (Loron *et al.*, 2019). Fungi, as our “old friends”, are using their way to participate in human life.

1.1. Fungi, important participants in food technology and beverages

When people talk about “fungi” and “food”, mushrooms may be the first ones to come to mind. Mushrooms, which refer to the sexual structures of basidiomycetes and ascomycetes, are considered as one of the earliest natural foods for humans. The first record for their use dates back to 900 BC (Chang, 1977). Mushrooms can either grow on the ground or underground. Edible mushrooms are popular all over the world since they are rich in protein and low in fat. The existence of edible fungi has historically improved the health and quality of human life (Valverde *et al.*, 2015). In China, around 80 species of mushrooms are used as direct food sources. The examples include *Phallus indusiatus*, *Tricholoma matsutake* and *Termitomyces albuminosus*. Cultivation of edible mushrooms has great potential for expansion of trade all over the world.

In addition to the value as direct food, fungi have participated in production of fermented food and beverages very early. The fact that milk residues were found in pottery vessels in north-western Anatolia, provided the earliest evidence for cheese making around sixth millennium BC in Europe (Salque *et al.*, 2013). Under the right conditions, food molds such as *Penicillium roqueforti* on blue cheese contribute to the aroma and blue spots by producing beneficial secondary metabolites. However, they may also cause contamination with mycotoxins such as roquefortine and PR-toxin if not handled with care (Garcia-Estrada and Martin, 2016). Besides *Penicillii*, *Scopulariopsis* species such as *S. candida* and *S. fusca* also

play important roles in the production of hard cheese. With the increasing demands for fermented dairy products like yogurt, sour cream and cheese which are rich in multiple vitamins and minerals, functional fungi display more advantages as necessary factors for industrial scale production.

Fungi have also influenced the evolution of human drinks. In regard to the beverage industry, especially the production of many fermented alcoholic beverages, such as beer, cider, rum, vodka and whisky, *Saccharomyces cerevisiae* plays an essential role (Parapouli *et al.*, 2020; Patel, 2000). In vinegar production and winery, glucoamylases from *Rhizopus oryzae* are applied to initiate the hydrolysis of starch (Chu *et al.*, 2014). Existing in lots of vegetables and fruits, the weak organic acid, citric acid, is used as a flavoring and preservative in production of candies and soft drinks (Verhoff and Bauweleers, 2000). In industrial scale production for citric acid, species of *Penicilliums* and *Aspergillus* are commonly involved (Show *et al.* 2015).

1.2. Rich sources and diversity of fungi

Natural products, which refer to secondary metabolites in the field of medicinal chemistry, are important sources for drug leads. In addition to prokaryotic bacteria and archaea, eukaryotic fungi, plants and animals are well known producers of bioactive natural products (Zaffiri *et al.*, 2012; Cochrane and Vederas, 2016). Fungal research is a hotspot because the data for approved therapeutic agents show that fungal products and their derivatives account for a considerable proportion of the clinically used drugs (Newman and Cragg, 2020).

Fungi are abundant worldwide and grow in a wide range of habitats. Wild fungal strains can be bio prospected from diverse sources such as the marine environment, associated with animals or plants and even in extreme environments including deep seas, deserts and areas with high salinity. These environments demand a high degree of adaptability and thus contribute to the diversity of fungi and their secondary metabolites. Based on culture-dependent and -independent surveys of the same samples, there are around 12 (11.7–13.2) million estimated fungal species on earth (Wu *et al.*, 2019).

1.2.1. Coprophilous fungi

As saprobic fungi, coprophilous fungi are distributed close to the tracks of herbivores,

such as ducks, rabbits and deer. Decomposing and recycling nutrients from animal dung, dung-inhabiting fungi are of great value for the environment, as well as a source of bioactive agents. Fungal species from genus *Podospora* are well studied and are known as producers of metabolites with antifungal activities. Examples include the new antifungal natural products appenolides A–C, from the coprophilous fungus *Podospora appendiculata* and the polyketide decipinin A produced by coprophilous fungus *Podospora decipiens* when it was cultured in liquid medium (Wang *et al.*, 1993; Che *et al.*, 2002). Furthermore, three undescribed sesquiterpenoids named hypocoprins A–C were obtained during the investigation of coprophilous fungus *Hypocopra rostrata* (TTI-0009, NRRL66178), which was isolated from a sample of horse dung collected in Texas. Hypocoprin A displayed antibacterial activity against the Gram-positive bacteria *Staphylococcus aureus* (ATCC 29213) and *Bacillus subtilis* (ATCC 6051) in disk diffusion assays with 13–14 mm inhibitory zones at 200 µg/disk (Jayanetti *et al.*, 2015).

1.2.2. Endophytic fungi

Endophytic fungi are microorganisms that live harmoniously in certain parts of plants, such as flowers, leaves, roots and fruits without causing any evident disease (Tan and Zou, 2001). In this case a symbiotic relationship between the host and endophytic fungi may be assumed. Host plants provide necessary nutrition for endophytic fungi, while the latter can enhance the growth and resistance of their host (Jia *et al.*, 2016). For instance, *Piriformospora indica* was suggested to help rice plants with higher tolerance towards root herbivory through changes in gibberellin and jasmonate signaling (Cosme *et al.*, 2016).

Fungal endophytes produce different categories of natural products including steroids, terpenoids, xanthenes, alkaloids and flavonoids (Tan and Zou, 2001; El-hawary *et al.*, 2020; Newman and Cragg, 2015). Notably, a number of endophytic fungi are able to produce the same metabolites as their hosts with even higher yields. For example, the highly functionated tetracyclic diterpenoid paclitaxel (Taxol) was discovered in 1971 within the bark of *Taxus brevifolia*, a conifer native to the Pacific Northwest of America (Wani *et al.*, 1971). It is used to treat different types of cancers, such as prostatic, breast, lung and ovarian cancers. However, the limited extractable amount of paclitaxel from wild *Taxus* plants was not able to meet the

increasing demands of the market. Different measures, like complicated chemical synthesis and field cultivation had to be taken, until the appearance of paclitaxel producing fungal endophyte *Taxomyces andreanae* which was derived from the inner bark of pacific yew (*Taxus brevifolia*) in 1993. This discovery could make a higher yield and less time-consuming fermentation possible (Stierle, Strobel and Stierle, 1993).

Fungal endophytes are a prospective reservoir of natural products with unrevealed structures and biological activities. In recent years, numerous research groups have been actively involved in the search for biologically active secondary metabolites (Newman and Cragg, 2020; Jakubczyk and Dussart, 2020). The following natural products are examples of the current endophyte research projects. The nonadride derivative rubratoxin acid A was obtained from the endophytic fungus *Talaromyces purpurogenus*, which was isolated from the leaves of the toxic medicinal plant *Tylophora ovata*. Rubratoxin acid A was able to inhibit nitric oxide (NO) production in lipopolysaccharide (LPS)-induced RAW264.7 cells with an IC₅₀ value of 1.9 µM (Zhao *et al.*, 2019). Chemical investigation of the secondary metabolites from the endophytic fungus *Chaetomium nigricolor* F5, which was derived from the medicinal plant *Mahonia fortunei*, led to the isolation of a novel cytochalasin chamiside A, which possesses a new 6/6/5-fused tricyclic core skeleton and showed moderate antibacterial activity against *Staphylococcus aureus* (Wang *et al.*, 2019). An unusual pyridone alkaloid, asperpyridone A with a pyrano[3,2-*c*] pyridine scaffold and a 1,3-dimethyl-cyclohexane motif, was produced by endophytic fungus *Aspergillus* sp. TJ23 when it was cultured on solid rice medium. Asperpyridone A improved the uptake of glucose by insulin-resistant in HepG2 liver cells, acting as a potential hypoglycemic agent (Qiao *et al.*, 2019).

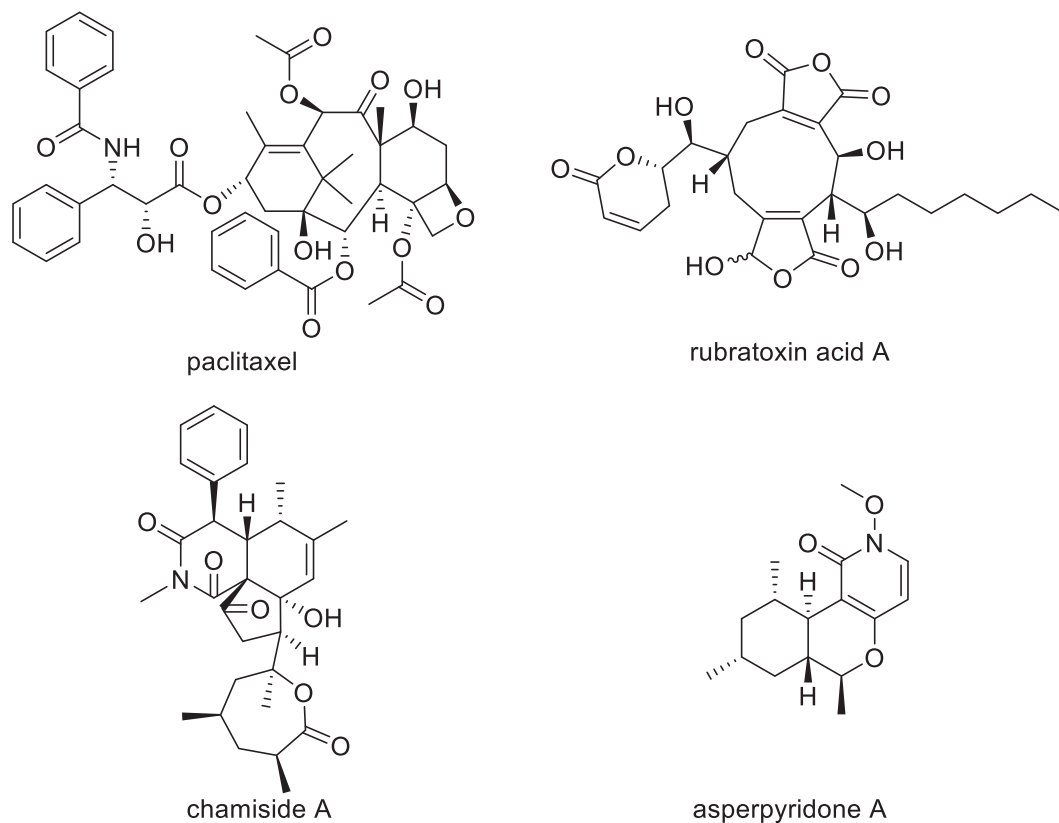


Figure 1.2.2. Structures of compounds from endophytic fungi.

1.2.3. Endolichenic fungi

Compared to endophytic fungi, lichen-associated fungi are even less researched. Until now, only approximately 2% of endolichenic fungi have been investigated for their chemical diversity. However, several reported metabolites produced by endolichenic fungi displayed interesting pharmacological properties (Agrawal *et al.*, 2020). Violaceol-I and violaceol-II produced by the endolichenic fungal strain *Aspergillus* sp. exhibited significant inhibitory activity against A β 42 aggregation with IC₅₀ values of 5.1 and 2.3 μ M, respectively (Zhao *et al.*, 2014). One of the first naturally occurring thiopyranchromenones, preussochromone A and its derivative preussochromone C were obtained from the solid cultures of the endolichenic fungus *Preussia africana*. Both of them displayed potent cytotoxicity against human lung cancer cell line A549, with IC₅₀ values of 8.34 and 5.75 μ M, respectively (Zhang *et al.*, 2012).

The α -pyrones dothideopyrones E and F were produced by the endolichenic fungus *Dothideomycetes* sp. EL003334. Dothideopyrone F was able to inhibit nitric oxide (NO) production in lipopolysaccharide (LPS)-induced BV2 cells with IC₅₀ values of 15.0 ± 2.0 μ M and decreased the mRNA expression levels of pro-inflammatory cytokines, such as tumor

necrosis factor α (TNF- α), interleukin (IL)-1 β as well as IL-6. (Kim *et al.*, 2018). As shown by these examples of secondary metabolites from endolichenic fungi, this potential treasure trove for the discovery of natural compounds with novel structures and bioactivities deserves more attention in the future.

1.2.4. Marine-derived fungi

What are marine-derived fungi? Most of the time, marine-derived fungi refer to fungi which are isolated from marine animals, seawater, sediments, algae or other related habitats (Pang *et al.*, 2016). The ocean ecosystems cover more than 70% of the earth's surface, harboring a wide variety of marine-derived fungi. They contribute to the fast-growing cosmeceuticals and nutricosmetics industry by providing valuable bulk compounds, such as the color agent mutatoxanthin and the whitening agent chrysophanol. Moreover, some of them, for example, marine *Trichoderma* species are able to make use of plant pathogenic fungi through antibiosis competition for nutrients, space and halo tolerance (Chalearmsrimuang *et al.*, 2019). Marine-derived fungi play an important role as a rich source of drug leads (Carroll *et al.*, 2020). From 2000 to 2018, 133 fungal metabolites from marine sources were reported for anti-inflammatory activity (Xu *et al.*, 2019). Moreover, around 131 peptides were known from 17 marine-sourced genera, among them, more than 50% exhibited cytotoxic, antimicrobial and/or antiviral activity. Meanwhile a few of them were reported for antidiabetic, lipid lowering and anti-inflammatory activity (Willems *et al.*, 2020).

Currently, at least thirteen marine-sourced molecules are undergoing advanced clinical trials, while nine drugs of marine origin have already been approved by the Food and Drug Administration (FDA) (Martins *et al.*, 2014). With the development of metabolomic tools used in search of new bioactive marine natural products (Stuart *et al.*, 2020), more drugs derived from marine natural products can be expected in the near future.

1.3. Pharmaceutical agents originating from fungi

Since the discovery of penicillin G from *Penicillium notatum* (Fleming, 1979), fungal metabolites have successfully attracted public attention to searching for new drugs. The wide distribution and rich diversity of fungi make it possible for them to provide different types of

secondary metabolites, including polyketides, terpenes, alkaloids, steroids and peptides. Their various biological activities make them well-suited candidates for antimicrobial, anticancer, antiviral and anti-inflammatory agents (Zhou *et al.*, 2018; Ariantari *et al.*, 2019; Tran-Cong *et al.*, 2019; Yu *et al.*, 2019; El-hawary *et al.*, 2020).

Every year, millions of patients suffer from microbial diseases. Meanwhile, they are being treated with medicines derived from fungi or other microorganisms. Cephalosporin C is one of the famous β -lactam antibiotics firstly isolated from the fungus *Cephalosporium* in the year 1948. So far, five improved generations of cephalosporin analogues have been applied for clinical use with developed activities over those of the natural one (Bryskier, 2000; Hwu, Ethiraj and Hakimelahi, 2003; Singh, 2004; Butler and Paterson, 2020). Similar to the function of penicillins, cephalosporins can inhibit the cell wall synthesis of bacteria by blocking the activity of enzymes which are responsible for crosslinking peptidoglycan, a vital component in the formation of bacterial cell wall.

The first discovered statin was a polyketide derivative named mevastatin (=compactin), which was isolated from *Penicillium citrinum* (Endo, Kuroda and Tsujita, 1976). It was considered as a cholesterol lowering agent (Endo, 2004). However, instead of mevastatin, lovastatin, obtained from culture broths of *Aspergillus terreus*, became the first statin drug approved by the FDA and available to the general public for strong inhibition of 3-hydroxy-3-methyl-glutaryl (HMG)-CoA reductase (Vagelos, 1991). Since lovastatin have been commercialized, more statin derivatives including the hydrophilic statin rosuvastatin, as well as the lipophilic statin, simvastatin, have been introduced to the market successfully (Endo, 2017).

Fingolimod is known as a manufactured analogue related to sphingosine which originated from the fungal secondary metabolite myriocin produced by *Isaria sinclairii* (Fujita *et al.*, 1994). In the year 2010, fingolimod was approved by the U.S. FDA for treatment of multiple sclerosis (Strader, Pearce and Oberlies, 2011). As an immunomodulatory drug for multiple sclerosis, fingolimod acts as functional antagonist of sphingosine-1-phosphate receptors (Chun and Hartung, 2010; Fyrst and Saba, 2010). New progress in surgical techniques makes it possible for organ transplantation with incorporation of organs such as liver and heart.

However, the possible rejection following an organ transplantation poses a great challenge. Fungal drug mycophenolic acid (MPA) was approved by FDA in 2000 as immunosuppressive agent which is now marketed as CellCept® (Eugui *et al.*, 1991; Guzera *et al.*, 2016). Immunosuppressive drugs refer to drugs which can inhibit or prevent the activity of the immune system. Mycophenolic acid, originated from the fungus *Penicillium glaucum* and related fungi (Lafont *et al.*, 1979; Chen *et al.*, 2015), is usually applied in the form of mycophenolate sodium and mycophenolate mofetil to specifically prevent the rejection following kidney, heart and liver transplantations (Knoll *et al.*, 2003; Kobashigawa and Meiser, 2005).

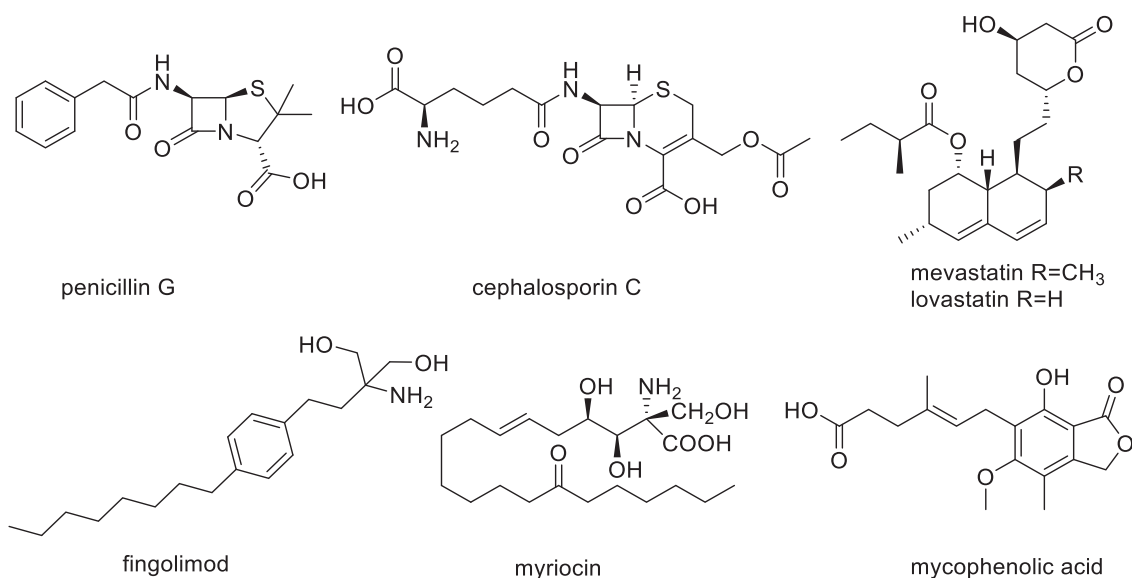


Figure 1.3. Structures of pharmaceutical agents originated from fungi.

1.4. Strategies to expand the diversity of secondary metabolites of fungi

Biosynthetic gene clusters (BGCs) refer to groups of genes which are able to encode a biosynthetic pathway for the production of a specialized metabolite (Pan *et al.*, 2019). It was discovered that fungal species usually harbor 30–100 BGCs. However, the majority of these gene clusters are kept silent under standard laboratory conditions. In order to unlock the trove of metabolic treasures, several successful methods have been developed. Strategies such as the genetic engineering (Choi *et al.*, 2018), One Strain MANY Compounds (OSMAC) approach (Meng *et al.*, 2017), co-cultivation (Liu *et al.*, 2016) and mutagenesis (Zhang and Moore, 2020) have all been successfully applied to activate silent BGCs in bacteria and fungi

(Tomm ,Ucciferri and Ross, 2019).

1.4.1. OSMAC approach

One Strain MAny Compounds (OSMAC) approach is regarded as the most common and effective way to achieve the diversity of secondary metabolites from fungi by cultivating fungi under different conditions, such as media composition, salinity, temperature, pH, oxygen concentration and cultivation status (Pan *et al.*, 2019).

There are several examples which highlight the power of OSMAC approach. Penicanone was reported as the first naturally occurring polyketide that featured a unique highly oxygenated 6/6/8 tricyclic carbon scaffold with a rare bicyclo [5.3.1] hendecane moiety. This compound and its derivative penicanesone A were isolated from the solid rice culture broths of *Penicillium canescens*. Two novel aromatic polyketide dimers which exhibit a special core structure of 6/6/5/6 tetracyclic ring were produced by the same fungus when it was cultured in a liquid medium (zp-2) (Zang *et al.*, 2020). Nine new polyketides were obtained from the fungus *Dothideomycete* sp. CRI7 cultured in Czapek medium prepared from seawater and media containing halide salts, such as potassium bromide (KBr) and potassium iodide (KI). Moreover, different production levels of fungal metabolites indicated that the halide salts can significantly enhance the yields of a crude extract and fungal secondary metabolites (Wijesekera *et al.*, 2017). Through OSMAC approach, fruit and vegetable juice were added to the solid rice media for the cultivation of fungal endophyte *Fusarium tricinctum*, resulting in the isolation of two known compounds fusarielins A and B, and induction of new metabolites fusarielins K and L, along with the upregulation of new natural product fusarielin J as much as 80-fold compared to that from solid rice culture broths. (Hemphill *et al.*, 2017).

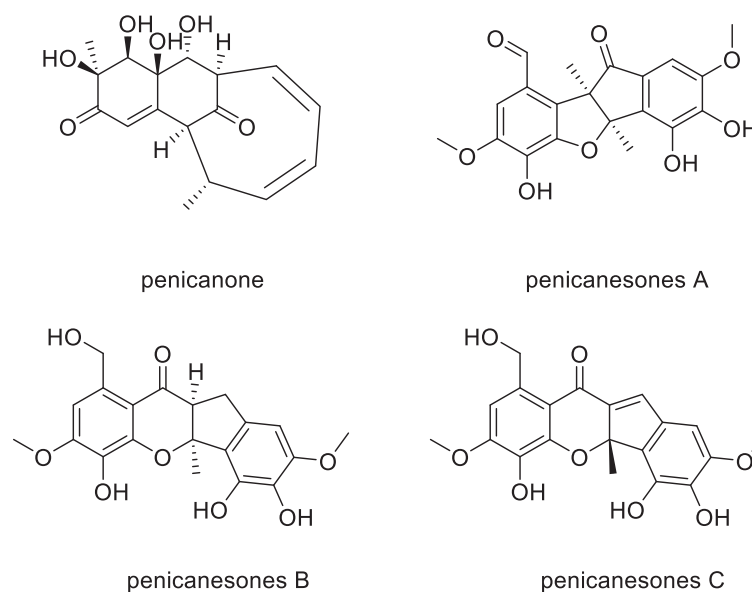


Figure 1.4.1. Structures of compounds produced by *Penicillium canescens*.

1.4.2. Co-cultivation

Most of the time, co-cultivation means mixed fermentation in the same vessel, which includes systems of fungi and bacteria, fungi and fungi, as well as bacteria and bacteria. The competitive environment may force the interactions between them to trigger natural product biosynthesis which usually contribute to the accumulation of constitutively present natural products or new secondary metabolites.

Recent successful cases of this method include the mixed fermentation of the fungal strain *Fusarium tricinctum* together with the bacterium *Bacillus subtilis* 168 trpC2. Co-cultivation on solid rice medium led to a 78-fold upregulation of constitutively expressed secondary metabolites such as lateropyrone and the lipopeptide fusaristatin A. The new secondary metabolites named macrocarpon C, 2-(carboxymethylamino) benzoic acid, and (-)-citreoisocoumarinol were produced only during the co-cultivation (Ola *et al.*, 2013). A series of structurally related C₁₂ polyketides which were different in the geometry and substitution pattern were produced by fungi-fungi co-cultivation of *Phoma* sp. YUD17001 and *Armillaria* sp. Interestingly, none of these metabolites was detected when either fungus grew as axenic cultures thus highlighting the power of co-cultivation (Li *et al.*, 2020).

1.4.3. Genetic modification

Technologies related to the genetic modification for engineering BGCs of microbial

natural products are relatively new compared to the strategies above (Li *et al.*, 2017). It is a powerful tool that can be used to delete unnecessary BGCs to improve the expression of target BGC (Baltz, 2016), or to directly clone (Wang *et al.*, 2016) and edit BGCs to optimize a natural product biosynthetic pattern (Shao *et al.*, 2011). More and more successful cases indicate a bright future for the genetic manipulation of BGCs for natural products as lead compounds.

1.5. Aims of the study

Every moment, millions of people are suffering from different diseases, while at the same time, new kinds of diseases emerge. This generates a great demand for new drugs. As described above, fungi, as rich producers of bioactive natural products bearing novel structures, have attracted a lot of attention for studies on their secondary metabolites. The aim of this study is to search for new bioactive natural products from promising fungal strains including the coprophilous fungus *Aphanoascus fulvescens*, the mangrove derived endophytic fungus *Pseudopestalotiopsis theae* and the endophytic fungus *Pestalotiopsis lespedezae*. These fungi were selected for their putative metabolite novelty based on their research status in scientific databases such as SciFinder and HPLC-DAD analysis of crude extracts combined with an in-house UV spectra library. An OSMAC approach was applied to expand the chemical diversity of fungus *Pestalotiopsis lespedezae*.

The goose-dung-derived coprophilous fungus *Aphanoascus fulvescens* produced five new okaramines indole alkaloids and eleven known analogues. The study on secondary metabolites from mangrove derived endophytic fungus *Pseudopestalotiopsis theae* led to the isolation of twenty-six isoprenylated cyclohexanols, eighteen of them are new natural products. Fermentation of the endophytic fungus *Pestalotiopsis lespedezae* on solid rice containing 3.5 % sodium iodine yielded ten new polyketide derivatives including one new iodinated compound. The absolute configurations of new compounds were determined by comparison of the NMR and specific optical rotation data to the related literature, modified Mosher's method and TDDFT-ECD calculations.

All of the isolated natural products were evaluated for cytotoxicity against the mouse lymphoma cell line L5178Y and for antibacterial activities against *Streptomyces lividans*, *Bacillus subtilis*, *Bacillus cereus* and *Mycobacterium tuberculosis*.

2 Publication 1

Indole alkaloids from the coprophilous fungus *Aphanoascus fulvescens*

Published in “*Fitoterapia*”

Research contribution: the first author contributed 60% to this publication. The first author’s work involved all laboratory work including compound isolation, structure elucidation, and manuscript preparation.

Reprinted by permission from “**Xiaoqin Yu**, Werner E.G. Müller, Zhiyong Guo, Wenhan Lin, Kun Zou, Zhen Liu and Peter Proksch. (2019) Indole alkaloids from the coprophilous fungus *Aphanoascus fulvescens*” *Fitoterapia*, 136, 104168.

Copyright: 2020 Elsevier B.V.



Indole alkaloids from the coprophilous fungus *Aphanoascus fulvescens*

Xiaoqin Yu^{a,b}, Werner E.G. Müller^c, Zhiyong Guo^b, Wenhan Lin^d, Kun Zou^b, Zhen Liu^{a,*}, Peter Proksch^{a,*}

^a Institute of Pharmaceutical Biology and Biotechnology, Heinrich-Heine-University Düsseldorf, Universitätsstrasse 1, 40225 Düsseldorf, Germany

^b Hubei Key Laboratory of Natural Products Research and Development, College of Biological and Pharmaceutical Sciences, China Three Gorges University, Yichang 443002, People's Republic of China

^c Institut für Physiologische Chemie, Universitätsmedizin der Johannes Gutenberg-University Mainz, Duesbergweg 6, 55128 Mainz, Germany

^d State Key Laboratory of Natural and Biomimetic Drugs, Peking University, Beijing 100191, China

ARTICLE INFO

Keywords:

Aphanoascus fulvescens
Indole alkaloids
Okaramine
Cytotoxicity

ABSTRACT

The Ascomycete fungus *Aphanoascus fulvescens* isolated from goose dung was investigated for its secondary metabolites, yielding five new indole alkaloids okaramines V–Z (1–5) and eleven known derivatives (6–16). Their structures were determined by 1D, 2D NMR spectra and HRMS data. Compounds 6, 8, 11 and 12 showed significant to moderate cytotoxicity against the mouse lymphoma cell line L5178Y with IC₅₀ values ranging from 4.0 to 14.7 μM. Preliminary structure-activity relationships are discussed.

1. Introduction

Okaramines, mostly reported from *Penicillium simplicissimum* and *Aspergillus aculeatus*, constitute a family of prenylated indole alkaloids [1]. They are insecticidal compounds due to their toxicity against silkworm larvae and selective activity on glutamate-gated chloride channels (GluCl) [2,3]. These compounds have also inspired many efforts on both biosynthetic research and total synthesis [4–6]. In our ongoing search for new bioactive compounds from Ascomycetes, we isolated the fungus *Aphanoascus fulvescens* from goose dung collected close to the North Sea shore in Northern Germany. *A. fulvescens* belongs to the Ascomycota, and is commonly found in keratin-rich tissues, such as hair, nails and dung that have been cast away from the host [7]. The fungus was reported to have the ability to degrade native feather keratin at pH 7.58 and at a temperature of 28.7 °C [8]. However, its secondary metabolites were rarely investigated except for two amines, WF14865A and B, that were reported as new cathepsins B and L inhibitors with IC₅₀ values in the range of 8.4–72 nM in vitro [9].

Our chemical investigation of *A. fulvescens* led to the isolation of five new okaramine-type indole alkaloids (1–5) together with eleven known derivatives (6–16) (Fig. 1). In this paper, the isolation, structure elucidation and bioactivity of these compounds are reported.

2. Results and discussion

Compound 1 had the molecular formula C₃₂H₃₆N₄O₄ as determined

by HRESIMS, containing an additional oxygen atom when compared to the co-isolated known compound, okaramine C (6) [10]. The ¹H NMR data of 1 (Table 2) displayed the signals for two sets of α,α-dimethylallyl groups, eight olefinic protons assigned to two *ortho*-disubstituted benzene rings, two methylenes and two methines, suggesting a prenylated indole diketopiperazine skeleton similar to okaramine C (6). However, the presence of signals due to an isolated methylene group at C-3 (δ_H 3.26 (d) and 2.26 (d)) and the disappearance of the signal of H-2 in 1 indicated that C-2 of 1 was a quaternary carbon. The attachment of an additional hydroxy group at C-2 in 1 was confirmed by the HMBC correlations from H_{ab}-3, H-8a (δ_H 5.48) and 3'-NH (δ_H 5.83) to C-2 (δ_C 88.9), and from the hydroxy group (δ_H 5.99) and H_{ab}-3 to C-9 (δ_C 166.4). The remaining substructure was determined to be identical to that of okaramine C (6) after detailed analysis of the 2D NMR spectra of 1. Moreover, the relative configuration of 1 was suggested to be identical to that of okaramine C (6) based on the similar NOE correlations. Thus, the structure of 1 was as elucidated as shown in Fig. 1, and the compound was given the trivial name okaramine V. The absolute configuration of okaramine C (6) has been determined by Marfey's method [11] and total synthesis [5]. Okaramine V (1) is assumed to share the same absolute configuration as okaramine C (6) based on the biogenetic relationship between both compounds.

The molecular formula of okaramine W (2) was determined as C₃₂H₃₆N₄O₄ from the HRESIMS data. The ¹H NMR data of 2 (Table 2) were similar to those of okaramine C (6) except for the replacement of a singlet methine proton at C-8a (δ_H 5.52) in 6 [10] by a water-

* Corresponding authors.

E-mail addresses: zhenfeizi0@sina.com (Z. Liu), proksch@uni-duesseldorf.de (P. Proksch).

<https://doi.org/10.1016/j.fitote.2019.05.007>

Reçu le 21 mars 2019; Reçu en forme révisée le 5 mai 2019; accepté le 6 mai 2019

Available online 07 May 2019

0367-326X/ © 2019 Elsevier B.V. All rights reserved.

Publication 1

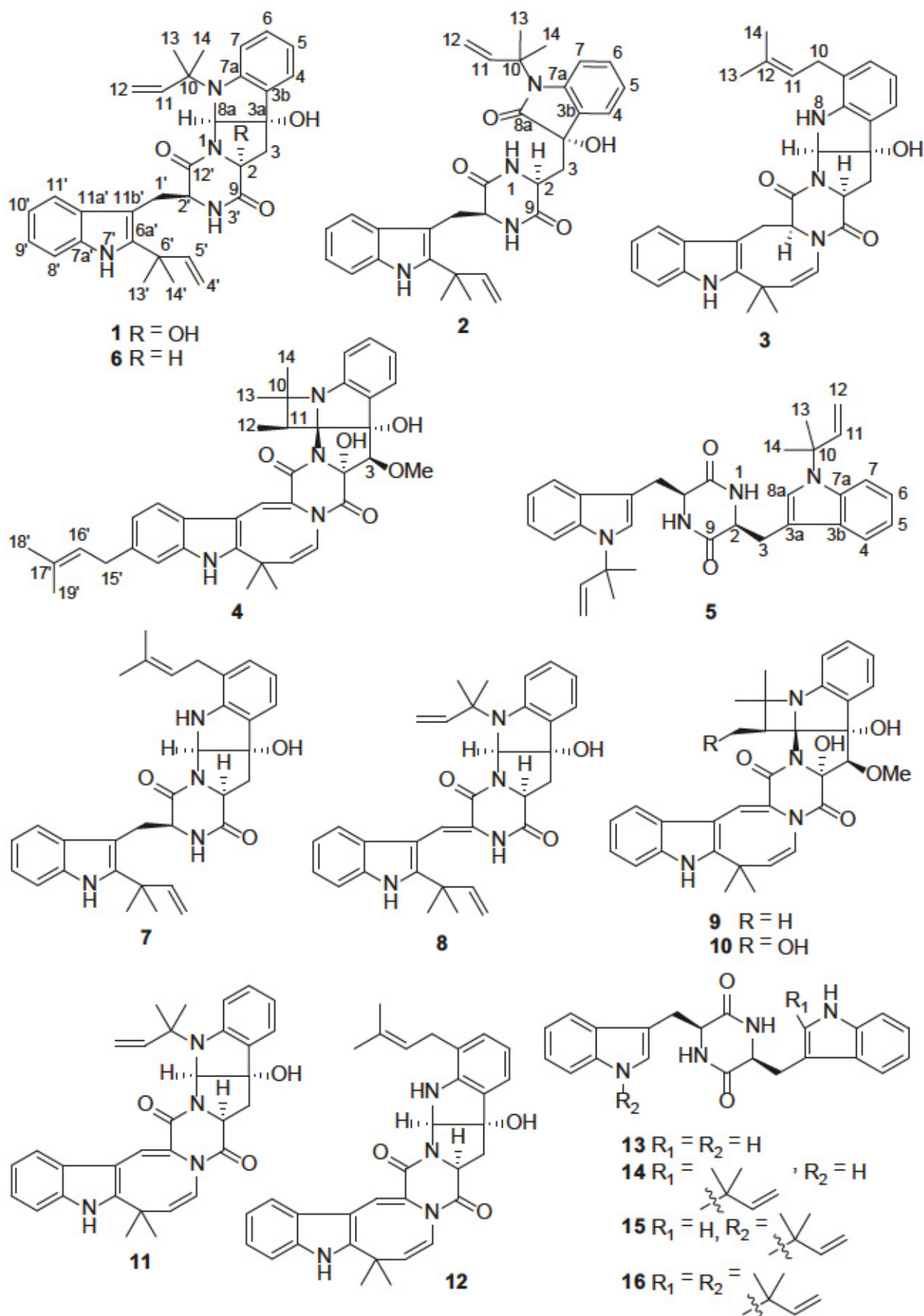


Fig. 1. Structures of compounds 1–16.

Publication 1

Table 1
¹³C NMR Data of Compounds 1–5.

No.	1 ^{a,d}	2 ^{b,d}	3 ^{b,d}	4 ^{c,d}	5 ^{c,d}
2	88.9, C	51.4, CH	58.7, CH	86.7, C	55.2, CH
3	48.2, CH ₂	42.8, CH ₂	42.9, CH ₂	82.3, CH	30.7, CH ₂
3a	85.1, C	74.6, C	86.5, C	84.5, C	106.7, C
3b	131.3, C	133.1, C	130.6, C	139.7, C	128.7, C
4	123.3, CH	124.1, CH	120.8, CH	124.8, CH	119.1, CH
5	118.7, CH	122.8, CH	119.1, CH	122.5, CH	119.3, CH
6	129.8, CH	129.1, CH	129.0, CH	129.0, CH	121.2, CH
7	112.3, CH	114.7, CH	123.0, C	117.3, CH	113.9, CH
7a	147.2, C	143.3, C	146.9, C	149.8, CH	135.9, C
8a	103.4, CH	180.2, C	84.6, CH	93.1, C	125.2, CH
9	166.4, C	168.6, C	169.1, C	163.8, C	167.2, C
10	57.2, C	60.7, C	29.3, CH ₂	62.6, C	59.1, C
11	145.6, CH	145.2, CH	122.1, CH	40.5, CH	143.9, CH
12	112.8, CH ₂	113.1, CH ₂	133.4, C	10.7, CH ₃	113.6, CH ₂
13	26.8, CH ₃	27.9, CH ₃	25.6, CH ₃	25.9, CH ₃	28.0, CH ₃
14	24.8, CH ₃	25.6, CH ₃	17.7, CH ₃	24.8, CH ₃	27.9, CH ₃
1'	27.6, CH ₂	30.6, CH ₂	24.6, CH ₂	113.6, CH	
2'	54.2, CH	56.0, CH	61.4, CH	147.3, C	
4'	112.7, CH ₂	111.6, CH ₂	125.8, CH	121.7, CH	
5'	145.4, CH	147.2, CH	138.9, CH	139.0, CH	
6'	39.0, C	39.8, C	37.2, C	35.9, C	
6a'	141.6, C	142.4, C	140.7, C	147.2, C	
7a'	134.1, C	135.8, C	135.8, C	133.9, C	
8'	110.8, CH	111.5, CH	110.6, CH	110.7, CH	
9'	122.1, CH	121.6, CH	121.3, CH	134.6, C	
10'	120.2, CH	119.5, CH	118.9, CH	121.3, CH	
11'	117.7, CH	118.8, CH	119.9, CH	116.1, CH	
11a'	128.9, C	130.0, C	129.7, C	127.8, C	
11b'	103.5, C	105.4, C	104.6, C	104.2, C	
12'	168.8, C	167.8, C	166.8, C	162.0, C	
13'	27.7, CH ₃	28.4, CH ₃	32.1, CH ₃	27.7, CH ₃	
14'	27.7, CH ₃	28.2, CH ₃	30.0, CH ₃	27.0, CH ₃	
15'				33.5, CH ₂	
16'				123.7, CH	
17'				131.0, C	
18'				25.3, CH ₃	
19'				17.4, CH ₃	
3-OMe				59.5, CH ₃	

^a Recorded in CDCl₃ at 150 MHz.

^b Recorded in acetone-*d*₆ at 150 MHz.

^c Recorded in DMSO-*d*₆ at 150 MHz.

^d Data were extracted from HSQC and HMBC.

exchangeable signal (δ_{H} 5.52, br s, 1-NH) in 2. The COSY correlations between 1-NH/H-2/H_{ab}-3 together with the HMBC correlations from H_{ab}-3 to C-2, C-3a, C-3b, C-8a (δ_{C} 180.2) and C-9 indicated cleavage between 1-N and C-8a and the presence of a carbonyl group at C-8a in 2. Detailed analysis of the 2D NMR spectra of 2 revealed that the remaining substructure and the relative configuration of 2 was identical to those of okaramine C (6).

Based on the HRESIMS data, the molecular formula of 3 was established as C₃₂H₃₄N₄O₃, containing two additional H atoms compared to the co-isolated known compound, okaramine J (7) [11]. Comparison of the ¹H and ¹³C NMR data (Tables 1 and 2) of 3 with 7 revealed the disappearance of a water-exchangeable proton (δ_{H} 5.73, 3'-NH in 7) and the replacement of an olefinic methylene group (δ_{H} 5.13 and 5.07) by an olefinic methine (δ_{H} 5.97, H-4') in 3. This latter proton showed a COSY correlation with H-5' (δ_{H} 5.76) and HMBC correlations with C-9 (δ_{C} 169.1) and C-6' (δ_{C} 37.2), confirming the linkage between 3'-N and C-4' to form an additional ring. The remaining substructure and the relative configuration of 3 was identical to that of okaramine J (7) as indicated by the 2D NMR spectra of 3. The absolute configuration of 3 is suggested to be likewise identical to that of okaramine J (7) based on their biogenetic relationship. Marfey's method [11] and total synthesis [6] had previously been performed to confirm the absolute configuration of okaramine J (7).

Okaramine Y (4) had the molecular formula C₃₈H₄₂N₄O₅ as evident from the HRESIMS data. When compared to okaramine B (9) [12],

okaramine Y (4) exhibited signals of an additional isoprenyl unit (C-15' to C-19', Tables 1 and 2) in addition to the replacement of signals of an *ortho*-disubstituted benzene ring by signals of an 1,2,4-trisubstituted benzene ring at δ_{H} 6.96 (dd, *J* = 8.2, 1.3 Hz, H-10'), 7.19 (d, *J* = 1.3 Hz, H-8') and 7.49 (d, *J* = 8.2 Hz, H-11'). Furthermore, the HMBC correlations from 7'-NH, H-1', H-8', and H-10' to C-11a', from H-8' and H-10' to C-15' and from H₂-15' to C-8', C-9' and C-10' indicated the location of the additional isoprenyl side chain at the C-9' position. Based on the similar NOE relationships, okaramine Y (4) shared the same relative configuration as okaramine B (9).

The molecular formula of compound 5 was determined by HRESIMS as C₃₂H₃₆N₄O₂. The UV and ¹H NMR data of 5 (Table 2) were similar to those of co-isolated cyclo-L-Trp-L-Trp (13) [11]. The only difference between both compounds is the presence of signals attributed to two additional, chemically equivalent α,α -dimethylallyl units at δ_{H} 6.07 (dd, *J* = 17.5, 10.7 Hz, H-11), 5.19 (d, *J* = 10.7 Hz, H₂-12), 5.16 (d, *J* = 17.5 Hz, H₂-12), 1.71 (s, Me-13) and 1.68 (s, Me-14) in 5, which was further supported by the COSY correlations between H-11/H_{ab}-12 and the HMBC correlations from Me-13 and Me-14 to C-10 and C-11. The attachment of the α,α -dimethylallyl unit to N-8 was confirmed by the chemical shift of C-10 (δ_{C} 59.1) and the HMBC correlation from H-8a (δ_{H} 6.64) to C-10. Based on the biogenetic relationship, the absolute configuration of 5 is suggested to be the same as cyclo-L-Trp-L-Trp (13), whose absolute configuration had previously been determined by Marfey's method [11].

The remaining known compounds were identified as okaramines C (6) [10], J (7) [11], G (8) [13], B (9) [12], D (10) [14], A (11) [12], H (12) [15], cyclo-L-Trp-L-Trp (13), cyclo-(6a'- α,α -dimethylallyl-L-Trp)-L-Trp (14), cyclo-(N⁸- α,α -dimethylallyl-L-Trp)-L-Trp (15), cyclo-(N⁸- α,α -dimethylallyl-L-Trp)-(6a'- α,α -dimethylallyl-L-Trp) (16) [11] based on comparison of their spectral data with the literature.

All isolated compounds were tested for their cytotoxicity against the mouse lymphoma cell line L5178Y using the MTT assay. Among them, okaramines H (12), G (8), A (11), and C (6) showed cytotoxicity with IC₅₀ values of 4.0, 12.8, 13.8 and 14.7 μ M, respectively. Some preliminary structure-activity relationships can be concluded based on the bioassay results. Hydroxylation at C-2 (1 vs 6) or cleavage between 1-N and C-8a (2 vs 6) led to total loss of cytotoxicity. When an α,α -dimethylallyl group is attached at 8-N, cleavage between 3'-N and C-4' (8 vs 11) or reduction at $\Delta^{1',2'}$ (6 vs 11) had little effect on cytotoxicity. However, when an isoprenyl group is attached at C-7 instead of 8-N, reduction at $\Delta^{1',2'}$ (3 or 7 vs 12) resulted in total loss of cytotoxicity.

3. Experimental section

3.1. General experimental procedures

Optical rotations were obtained with a Perkin-Elmer-241 MC polarimeter. 1D and 2D NMR spectra were recorded on a Bruker AVANCE DMX 600 NMR spectrometer. Mass spectra (ESI) were recorded with a Finnigan LCQ Deca mass spectrometer and HRMS (ESI) spectra were obtained from a FTHRMS-Orbitrap (Thermo-Finnigan) mass spectrometer. Solvents were distilled prior to use and spectral grade solvents were used for spectroscopic measurements. HPLC analysis was performed with a Dionex UltiMate3400 SD equipped with an LPG-3400SD Pump coupled to a photodiode array detector (DAD3000RS) and the following gradient was used (MeOH, 0.1% HCOOH in H₂O): 0 min (10% MeOH); 5 min (10% MeOH); 45 min (100% MeOH); 60 min (100% MeOH). Column chromatography included Sephadex LH-20 and Merck MN Silica gel 60 M (0.04–0.063 mm). Semi-preparative HPLC was performed using a Merck Hitachi HPLC System (UV detector L-7400; Pump L-7100; Eurosphere-100 C18, 300 \times 8 mm).

Table 2
¹H NMR Data of Compounds 1–5.

No.	1 ^a	2 ^b	3 ^b	4 ^c	5 ^c
2		4.75, m	4.59, dd (11.0, 6.2)		4.18, m
3	3.26, d (14.1)	2.40, dd (14.8, 4.8)	2.51, dd (13.0, 6.2)	4.19, s	3.19, dd (14.4, 3.4)
	2.26, d (14.1)	1.86, dd (14.8, 7.5)	1.75, dd (13.0, 11.0)		2.38, dd (14.4, 8.3)
4	7.31, dd (7.3, 1.0)	7.39, dd (7.4, 1.4)	6.99, d (7.6)	7.39, dd (7.5, 1.2)	7.55, dd (7.5, 1.2)
5	6.80, td (7.3, 0.8)	7.06, td (7.4, 1.1)	6.57, t (7.6)	7.01, td (7.5, 0.8)	7.09, td (7.5, 1.0)
6	7.15, ddd (8.2, 7.3, 1.0)	7.22, ddd (8.0, 7.4, 1.4)	6.80, d (7.6)	7.21, ddd (7.9, 7.5, 1.2)	7.13, ddd (8.0, 7.5, 1.2)
7	6.82, dd (8.2, 0.8)	7.18, dd (8.0, 1.1)		6.73, dd (7.9, 0.8)	7.49, dd (8.0, 1.0)
8a	5.48, s		5.26, br s		6.64, s
10			2.86, m		
			2.79, m		
11	6.01, dd (17.5, 10.7)	6.19, dd (17.6, 10.8)	5.16, t (7.3)		6.07, dd (17.5, 10.7)
12	5.17, d (17.5)	5.24, d (17.6)		1.23, s	5.19, d (10.7)
	5.13, d (10.7)	5.18, d (10.8)			5.16, d (17.5)
13	1.43, s	1.82, s	1.73, s	0.86, s	1.71, s
14	1.40, s	1.73, s	1.66, s	1.66, s	1.68, s
1'	3.72, dd (15.1, 4.0)	3.59, dd (14.8, 3.7)	3.69, br d (14.7)	7.35, s	
	3.16, dd (15.1, 11.6)	3.21, dd (14.8, 10.1)	3.47, br d (14.7)		
2'	4.50, dd (11.6, 4.0)	4.33, m	4.43, br s		
4'	5.19, d (17.5)	5.14, d (17.5)	5.97, d (8.8)	5.66, d (8.2)	
	5.18, d (10.4)	5.07, d (10.6)			
5'	6.14, dd (17.5, 10.4)	6.25, dd (17.5, 10.6)	5.76, d (8.8)	5.91, d (8.2)	
8'	7.35, dd (8.0, 0.9)	7.28, dd (7.9, 1.0)	7.16, d (8.0)	7.19, d (1.3)	
9'	7.20, ddd (8.0, 7.6, 1.1)	7.03, ddd (7.9, 7.4, 1.1)	6.96, m		
10'	7.14, ddd (8.0, 7.6, 0.9)	6.98, ddd (7.8, 7.4, 1.0)	6.97, m	6.96, dd (8.2, 1.3)	
11'	7.50, dd (8.0, 1.1)	7.52, dd (7.8, 1.1)	7.73, d (8.0)	7.49, d (8.2)	
13'	1.56, s	1.59, s	1.44, s	1.56, s	
14'	1.56, s	1.58, s	1.49, s	1.65, s	
15'				3.39, d (7.5)	
16'				5.33, t (7.5)	
18'				1.72, s	
19'				1.71, s	
1-NH		7.35, br s			5.72, br s
2-OH	5.99, s				
3-OMe				3.73, s	
3a-OH		6.08, s	4.92, s		
8-NH			4.81, br s		
3'-NH	5.83, br s	6.74, br s			
7'-NH	8.09, s	9.89, s	9.79, s	11.31, s	

^a Recorded in CDCl₃ at 600 MHz.

^b Recorded in acetone-*d*₆ at 600 MHz.

^c Recorded in DMSO-*d*₆ at 600 MHz.

3.2. Fungal material

The endophytic fungus was isolated from goose dung collected in St. Peter- Oding (North Germany) in March 2017. It was identified as *Aphanoascus fulvescens* by DNA amplification and sequencing of ITS region as previously described [16]. *A. fulvescens* was cultivated on solid rice medium in 30 Erlenmeyer flasks. The rice medium was prepared with demineralized water (110 mL) and rice (100 g) in an Erlenmeyer flask, followed by autoclaving (121 °C, 20 min). The fungus, after it covered the whole surface of a petri dish, was inoculated onto this sterile rice medium under the clean bench and then allowed to grow at 20 °C for 28 days under static conditions.

3.3. Extraction and isolation

The crude EtOAc extract (5.85 g) was subjected to a vacuum liquid chromatography on silica gel with a step gradient elution of *n*-hexane-EtOAc and CH₂Cl₂-MeOH to give six fractions (Fr.A to Fr.F). Fr. B (eluted by 60% *n*-hexane and 40% EtOAc) was subjected to a Sephadex LH-20 column eluted with CH₂Cl₂-MeOH (1:1), followed by purification using semi-preparative HPLC (MeOH-H₂O: 0–2 min, 55%; 2–25 min, from 55% to 80%; 25–30 min, 100%) to yield 1 (2.8 mg), 4 (1.5 mg), 8 (1.2 mg) and 12 (3.3 mg). Fr. C (eluted by 40% *n*-hexane and 60% EtOAc) was fractionated on a Sephadex LH-20 column with MeOH and then separated by semi-preparative HPLC (MeOH-H₂O: 0–2 min, 35%; 2–28 min, from 35% to 58%; 28–30 min, 100%) to yield 9 (1.1 mg), 10

(1.3 mg) and 11 (4.8 mg). Fr. D (eluted by 25% *n*-hexane and 75% EtOAc) was subjected to a silica gel column using CH₂Cl₂-MeOH (15:1) and further separated by semi-preparative HPLC (MeOH-H₂O: 0–2 min, 40%; 2–15 min, from 40% to 55%; 15–30 min, from 55% to 80%; 30–32 min, 100%) to give 2 (2.1 mg), 6 (9.3 mg), 7 (5.8 mg) and 16 (6.4 mg). Fr. E (eluted by 70% CH₂Cl₂ and 30% MeOH) was fractionated on a C-18 reverse phase column using a step gradient of MeCN/H₂O, resulting in 4 subfractions (Fr.E1 to Fr.E4). Fr.E3 were further purified by semi-preparative HPLC (MeOH-H₂O: 0–2 min, 25%; 2–15 min, from 25% to 40%; 15–30 min, from 40% to 65%; 30–32 min, 100%) to yield 3 (2.4 mg), 5 (1.4 mg), 13 (2.1 mg), 14 (1.8 mg) and 15 (2.0 mg).

Okaramine V (1): colorless oil; [α]_D 20 + 30.4 (c 0.1, MeOH); ¹H and ¹³C NMR data, Tables 1 and 2; HRESIMS *m/z* 541.2810 [M + H]⁺ (C₃₂H₃₇N₄O₄, calcd. 541.2809).

Okaramine W (2): light yellow oil; [α]_D 20 – 19.6 (c 0.15, MeOH); ¹H and ¹³C NMR data, Tables 1 and 2; HRESIMS *m/z* 541.2799 [M + H]⁺ (C₃₂H₃₇N₄O₄, calcd. 541.2809).

Okaramine X (3): colorless oil; [α]_D 20 + 52.4 (c 0.15, MeOH); ¹H and ¹³C NMR data, Tables 1 and 2; HRESIMS *m/z* 523.2706 [M + H]⁺ (C₃₂H₃₅N₄O₃, calcd. 523.2704).

Okaramine Y (4): yellow powder; [α]_D 20 + 351 (c 0.1, MeOH); ¹H and ¹³C NMR data, Tables 1 and 2; HRESIMS *m/z* 635.3227 [M + H]⁺ (C₃₈H₄₃N₄O₅, calcd. 635.3228).

Okaramine Z (5): colorless oil; [α]_D 20 – 32.7 (c 0.2, MeOH); ¹H and ¹³C NMR data, Tables 1 and 2; HRESIMS *m/z* 509.2903 [M + H]⁺

Publication 1

(C₃₂H₃₇N₄O₂, calcd. 509.2911).

3.4. Cytotoxicity assay

Cytotoxicity was tested against the L5178Y mouse lymphoma cells using a MTT assay [17]. Experiments were repeated three times and carried out in triplicate. Kahalalide F and 0.1% EGMME/DMSO were used as positive and negative controls, respectively.

Acknowledgment

X.Y. wishes to thank the China Scholarship Council, the Ministry of Education of China, for a doctoral scholarship. P.P. wants to thank the Manchot Foundation for support. We are indebted to Dr. Margareta Proksch for help during sample collection.

Appendix A. Supplementary data

Supplementary data to this article can be found online at <https://doi.org/10.1016/j.fitote.2019.05.007>.

References

- [1] D.K. O'Toole, Characteristics and use of okara, the soybean residue from soy milk production — a review, *J. Agric. Food Chem.* 47 (1999) 363–371.
- [2] S. Furutani, M. Ihara, K. Kai, K. Tanaka, D.B. Sattelle, H. Hayashi, K. Matsuda, Okaramine insecticidal alkaloids show similar activity on both exon 3c and exon 3b variants of glutamate-gated chloride channels of the larval silkworm, *Bombyx mori*, *NeuroToxicology* 60 (2017) 240–244.
- [3] S. Furutani, Y. Nakatani, Y. Miura, M. Ihara, K. Kai, H. Hayashi, K. Matsuda, GluCl a target of indole alkaloid okaramines: a 25 year enigma solved, *Sci. Rep.* 4 (2014) 6190.
- [4] C.Y. Lai, I.W. Lo, R.T. Hewage, Y.C. Chen, C.T. Chen, C.F. Lee, S. Lin, M.C. Tang, H.C. Lin, Biosynthesis of complex indole alkaloids: elucidation of the concise pathway of okaramines, *Angew. Chem. Int. Ed.* 56 (2017) 9478–9482.
- [5] P.R. Hewitt, E. Cleator, S.V. Ley, A concise total synthesis of (+)-okaramine C, *Org. Biomol. Chem.* 2 (2004) 2415–2417.
- [6] J.M. Roe, R.A.B. Webster, A. Ganesan, Total synthesis of (+)-okaramine J featuring an exceptionally facile *N*-reverse-prenyl to *C*-prenyl aza-Claisen rearrangement, *Org. Lett.* 5 (2003) 2825–2827.
- [7] J. Cano, M. Sagués, E. Barrio, P. Vidal, R.F. Castaneda, J. Gené, J. Guarro, Molecular taxonomy of *Aphanoascus* and description of two new species from soil, *Stud. Mycol.* 47 (2002) 153–164.
- [8] J. Bohacz, Biodegradation of feather waste keratin by a keratinolytic soil fungus of the genus *Chrysosporium* and statistical optimization of feather mass loss, *World J. Microbiol. Biotechnol.* 33 (2017) 13.
- [9] T. Otsuka, Y. Muramatsu, T. Nakanishi, H. Hatanaka, M. Okamoto, M. Hino, S. Hashimoto, WF14865A and B, new cathepsins B and L inhibitors produced by *Aphanoascus fulvescens*, *J. Antibiot.* 53 (2000) 449–458.
- [10] H. Hayashi, T. Fujiwara, S. Murao, M. Arai, Okaramine C, a new insecticidal indole alkaloid from *Penicillium simplicissimum*, *Agric. Biol. Chem.* 55 (1991) 3143–3145.
- [11] Y. Shiono, K. Akiyama, H. Hayashi, New okaramine congeners, okaramines J, K, L, M and related compounds, from *Penicillium simplicissimum* ATCC 90288, *Biosci. Biotechnol. Biochem.* 63 (1999) 1910–1920.
- [12] H. Hayashi, K. Takiuchi, S. Murao, M. Arai, Structure and insecticidal activity of new indole alkaloids, okaramines a and b, from *Penicillium simplicissimum* AK-40, *Agric. Biol. Chem.* 53 (1989) 461–469.
- [13] H. Hayashi, A. Sakaguchi, Okaramines G, a new okaramine congener from *Penicillium simplicissimum* ATCC 90288, *Biosci. Biotechnol. Biochem.* 62 (1998) 804–806.
- [14] H. Hayashi, Y. Asabu, S. Murao, M. Arai, New okaramine congeners, okaramines D, E, and F, from *Penicillium simplicissimum* ATCC 90288, *Biosci. Biotechnol. Biochem.* 59 (1995) 246–250.
- [15] H. Hayashi, K. Furutsuka, Y. Shiono, Okaramines H and I, new okaramine congeners, from *Aspergillus aculeatus*, *J. Nat. Prod.* 62 (1999) 315–317.
- [16] J. Kjer, A. Debbab, A.H. Aly, P. Proksch, Methods for isolation of marine-derived endophytic fungi and their bioactive secondary products, *Nat. Protoc.* 5 (2010) 479–490.
- [17] M. Ashour, R. Edrada, R. Ebel, V. Wray, W. Wätjen, K. Padmakumar, W.E.G. Müller, W.H. Lin, P. Proksch, Kahalalide derivatives from the Indian sacoglossan mollusk *Elysia grandifolia*, *J. Nat. Prod.* 69 (2006) 1547–1553.

Support Information

Indole Alkaloids from the Coprophilous Fungus *Aphanoascus fulvescens*

Xiaoqin Yu ^{a,b}, Werner E.G. Müller ^c, Zhiyong Guo ^b, Wenhan Lin ^d, Kun Zou ^b, Zhen Liu ^{a,*}, Peter Proksch ^{a,*}

^a Institute of Pharmaceutical Biology and Biotechnology, Heinrich-Heine-University Düsseldorf, Universitätsstrasse 1, 40225 Düsseldorf, Germany

^b Hubei Key Laboratory of Natural Products Research and Development, College of Biological and Pharmaceutical Sciences, China Three Gorges University, Yichang 443002, People's Republic of China

^c Institut für Physiologische Chemie, Universitätsmedizin der Johannes Gutenberg-University Mainz, Duesbergweg 6, 55128 Mainz, Germany

^d State Key Laboratory of Natural and Biomimetic Drugs, Peking University, Beijing 100191, China

*Corresponding authors.

e-mail: zhenfeizi0@sina.com (Z. Liu),

proksch@uni-duesseldorf.de (P. Proksch)

Table of contents

Figure S1. HR-ESI-MS of 1 .	24
Figure S2. UV spectrum of 1 .	24
Figure S3. ^1H NMR (600 MHz, CDCl_3) spectrum of 1 .	25
Figure S4. ^1H - ^1H COSY (600 MHz, CDCl_3) spectrum of 1 .	25
Figure S5. HSQC (600 MHz, CDCl_3) spectrum of 1 .	26
Figure S6. HMBC (600 MHz, CDCl_3) spectrum of 1 .	26
Figure S7. ROESY (600 MHz, CDCl_3) spectrum of 1 .	27
Figure S8. HR-ESI-MS of 2 .	27
Figure S9. UV spectrum of 2 .	28
Figure S10. ^1H NMR (600 MHz, Acetone- d_6) spectrum of 2 .	28
Figure S11. ^1H - ^1H COSY (600 MHz, Acetone- d_6) spectrum of 2 .	29
Figure S12. HSQC (600 MHz, Acetone- d_6) spectrum of 2 .	29
Figure S13. HMBC (600 MHz, Acetone- d_6) spectrum of 2 .	30
Figure S14. ROESY (600 MHz, Acetone- d_6) spectrum of 2 .	30
Figure S15. HR-ESI-MS of 3 .	31
Figure S16. UV spectrum of 3 .	31
Figure S17. ^1H NMR (600 MHz, Acetone- d_6) spectrum of 3 .	32
Figure S18. ^1H - ^1H COSY (600 MHz, Acetone- d_6) spectrum of 3 .	32
Figure S19. HSQC (600 MHz, Acetone- d_6) spectrum of 3 .	33
Figure S20. HMBC (600 MHz, Acetone- d_6) spectrum of 3 .	33
Figure S21. ROESY (600 MHz, Acetone- d_6) spectrum of 3 .	34
Figure S22. HR-ESI-MS of 4 .	34
Figure S23. UV spectrum of 4 .	35
Figure S24. ^1H NMR (600 MHz, DMSO- d_6) spectrum of 4 .	35
Figure S25. ^1H - ^1H COSY (600 MHz, DMSO- d_6) spectrum of 4 .	36
Figure S26. HSQC (600 MHz, DMSO- d_6) spectrum of 4 .	36
Figure S27. HMBC (600 MHz, DMSO- d_6) spectrum of 4 .	37
Figure S28. ROESY (600 MHz, DMSO- d_6) spectrum of 4 .	37
Figure S29. HR-ESI-MS of 5 .	38
Figure S30. UV spectrum of 5 .	38
Figure S31. ^1H NMR (600 MHz, CDCl_3) spectrum of 5 .	39
Figure S32. ^1H - ^1H COSY (600 MHz, CDCl_3) spectrum of 5 .	39
Figure S33. HSQC (600 MHz, CDCl_3) spectrum of 5 .	40
Figure S34. HMBC (600 MHz, CDCl_3) spectrum of 5 .	40

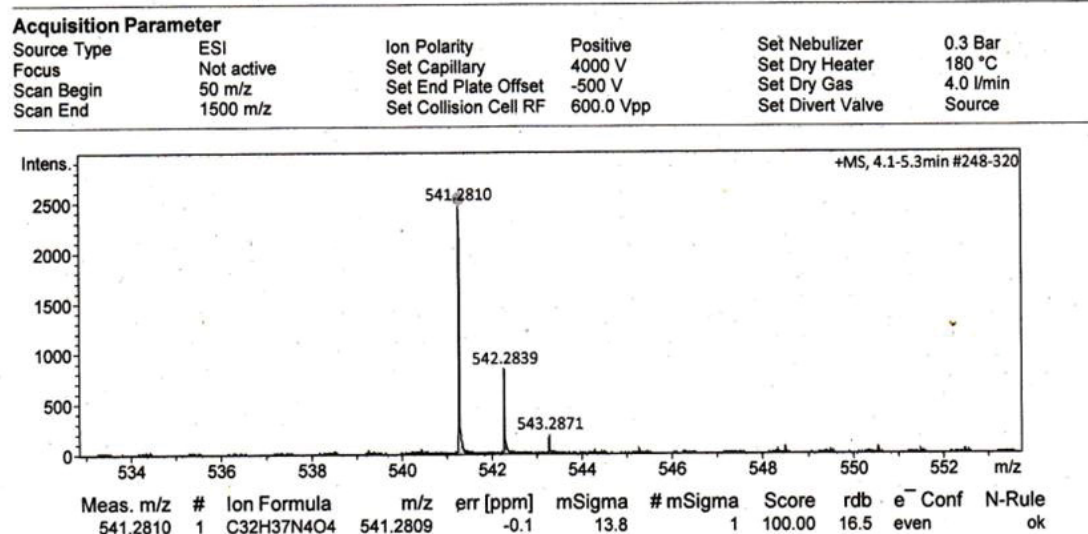


Figure S1. HR-ESI-MS of 1.

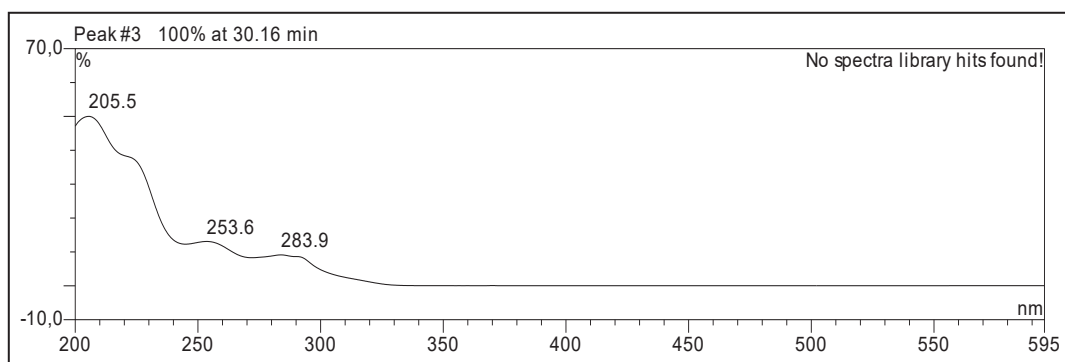


Figure S2. UV spectrum of 1.

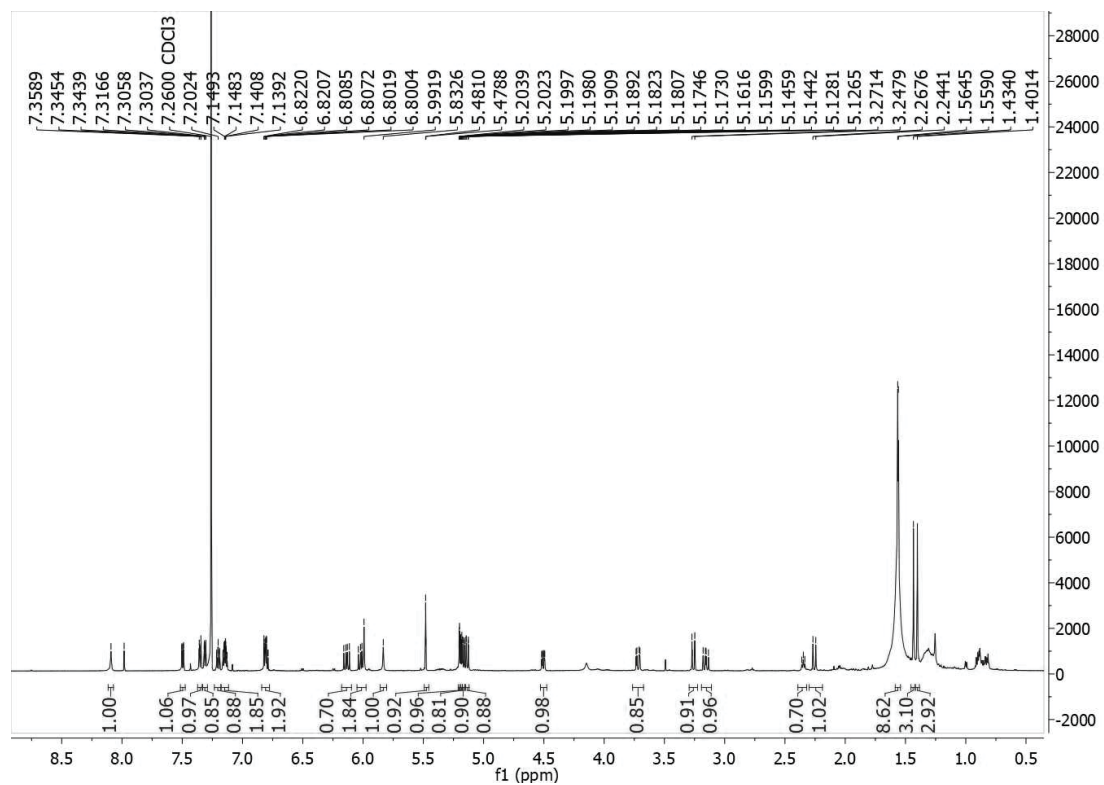


Figure S3. ¹H NMR (600 MHz, CDCl₃) spectrum of **1**.

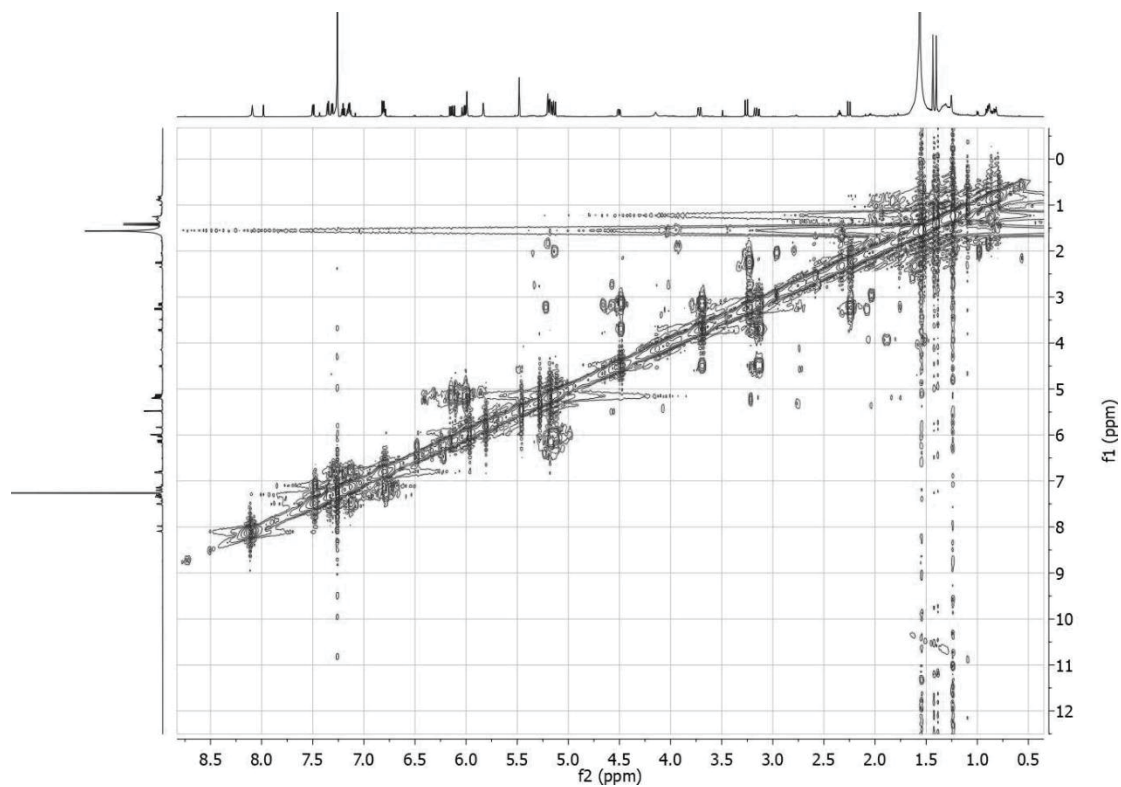


Figure S4. ¹H-¹H COSY (600 MHz, CDCl₃) spectrum of **1**.

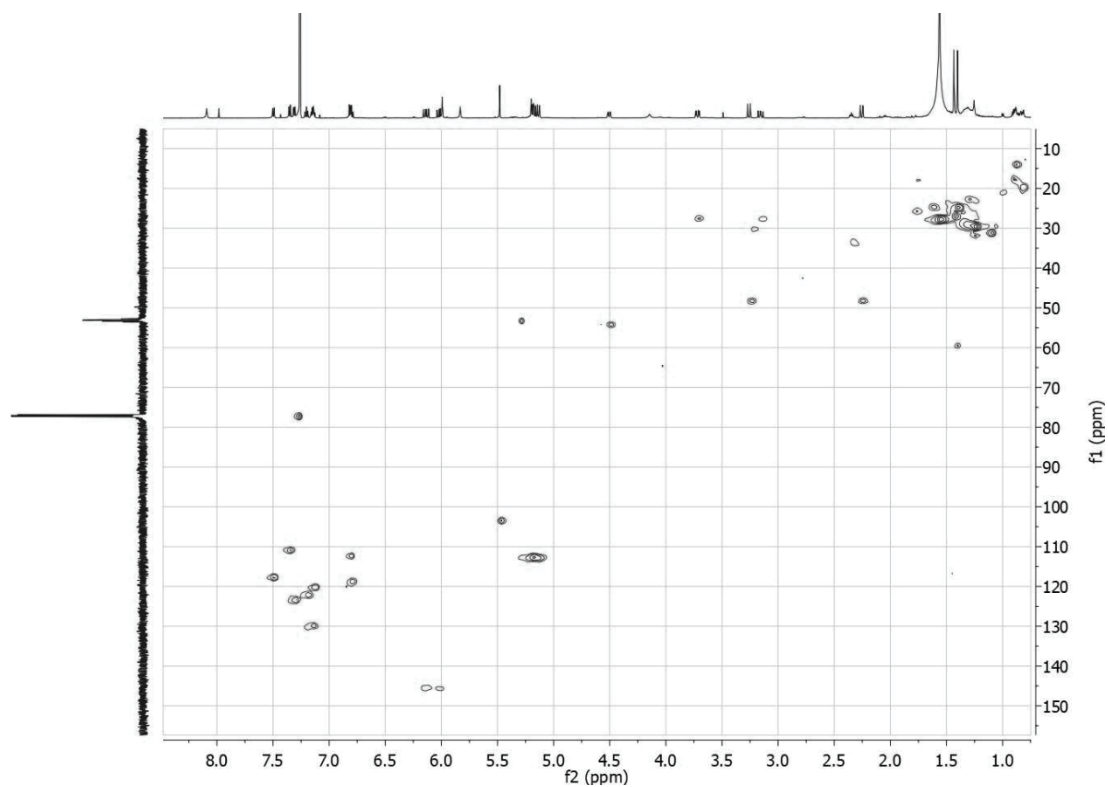


Figure S5. HSQC (600 MHz, CDCl₃) spectrum of **1**.

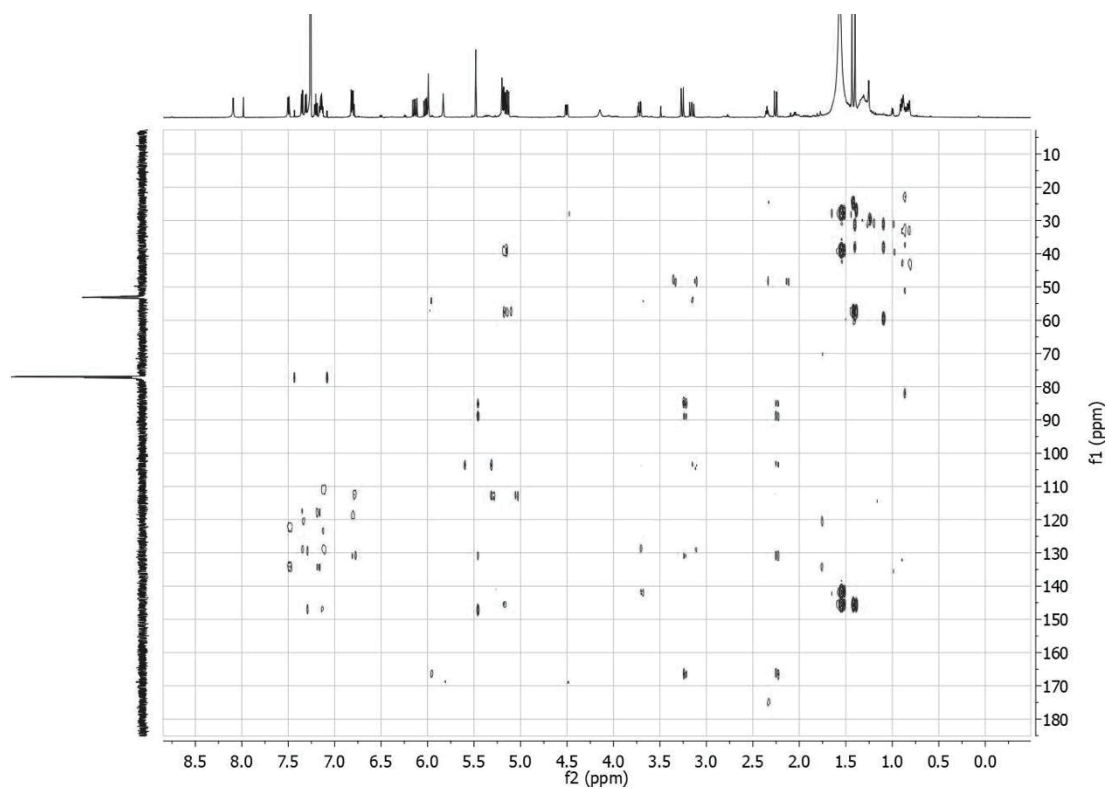


Figure S6. HMBC (600 MHz, CDCl₃) spectrum of **1**.

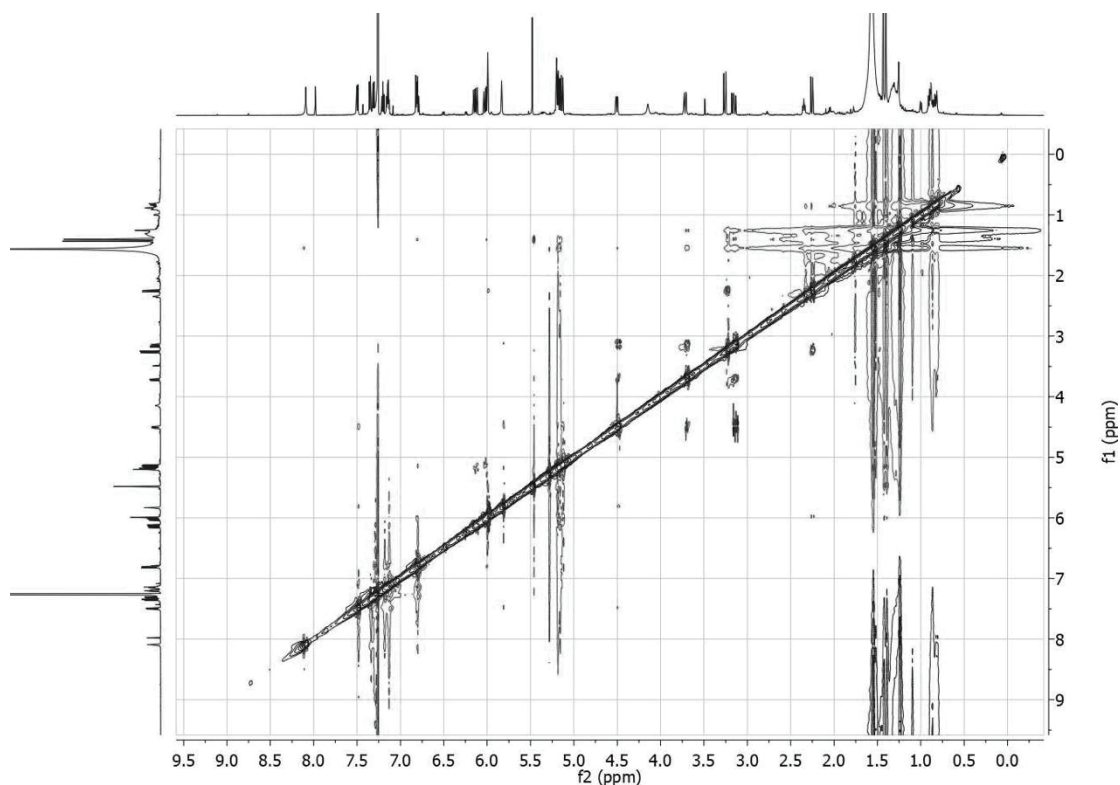


Figure S7. ROESY (600 MHz, CDCl_3) spectrum of **1**.

Acquisition Parameter

Source Type	ESI	Ion Polarity	Positive	Set Nebulizer	0.3 Bar
Focus	Not active	Set Capillary	4000 V	Set Dry Heater	180 °C
Scan Begin	50 m/z	Set End Plate Offset	-500 V	Set Dry Gas	4.0 l/min
Scan End	1500 m/z	Set Collision Cell RF	600.0 Vpp	Set Divert Valve	Source

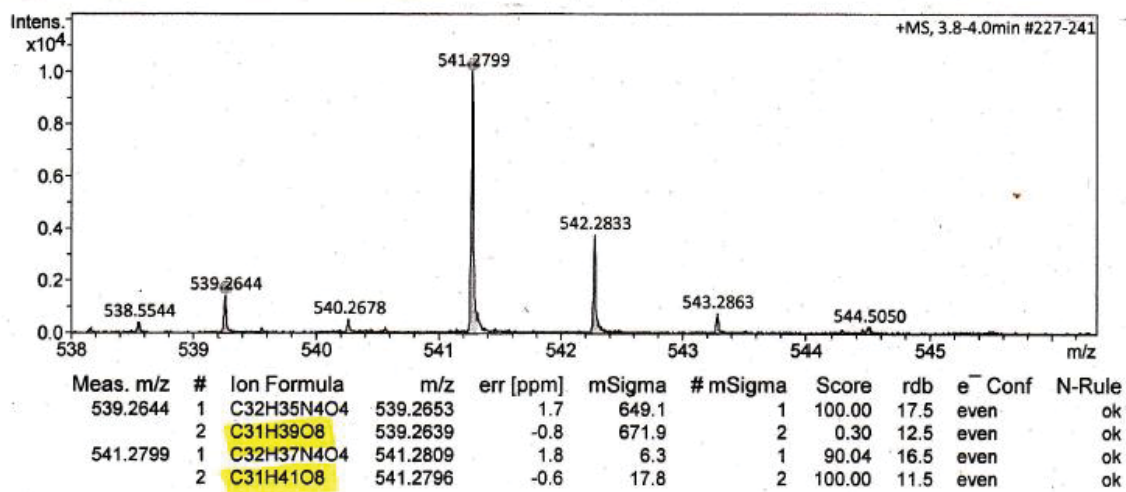


Figure S8. HR-ESI-MS of **2**.

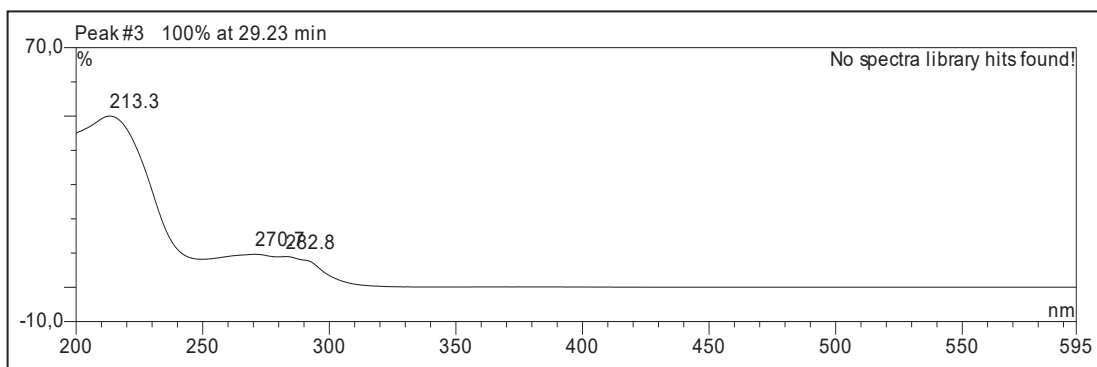


Figure S9. UV spectrum of 2.

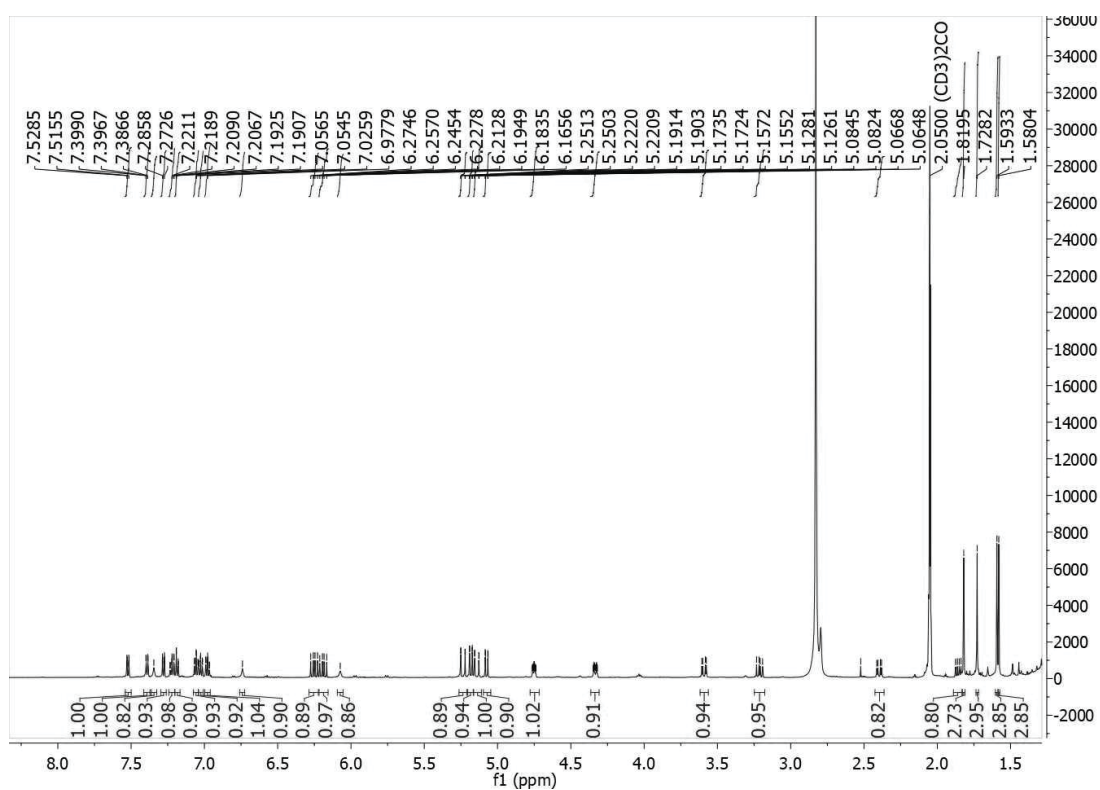


Figure S10. ^1H NMR (600 MHz, Acetone- d_6) spectrum of 2.

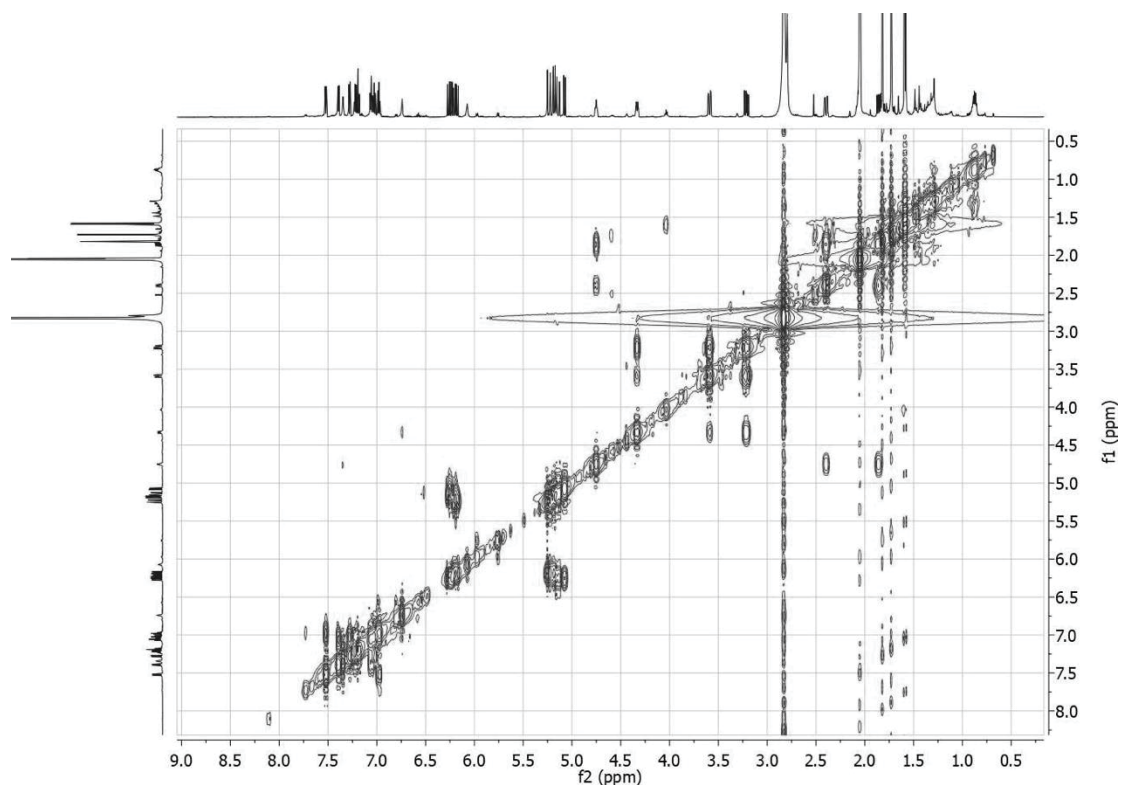


Figure S11. ^1H - ^1H COSY (600 MHz, Acetone- d_6) spectrum of **2**.

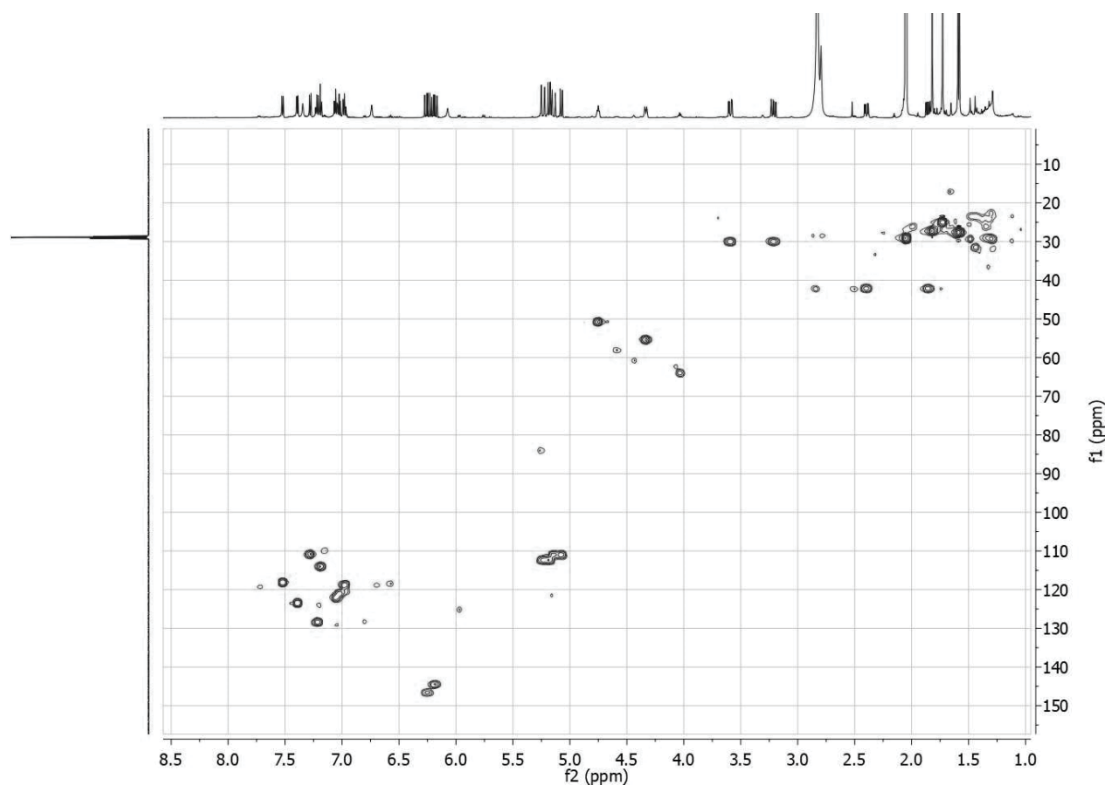


Figure S12. HSQC (600 MHz, Acetone- d_6) spectrum of **2**.

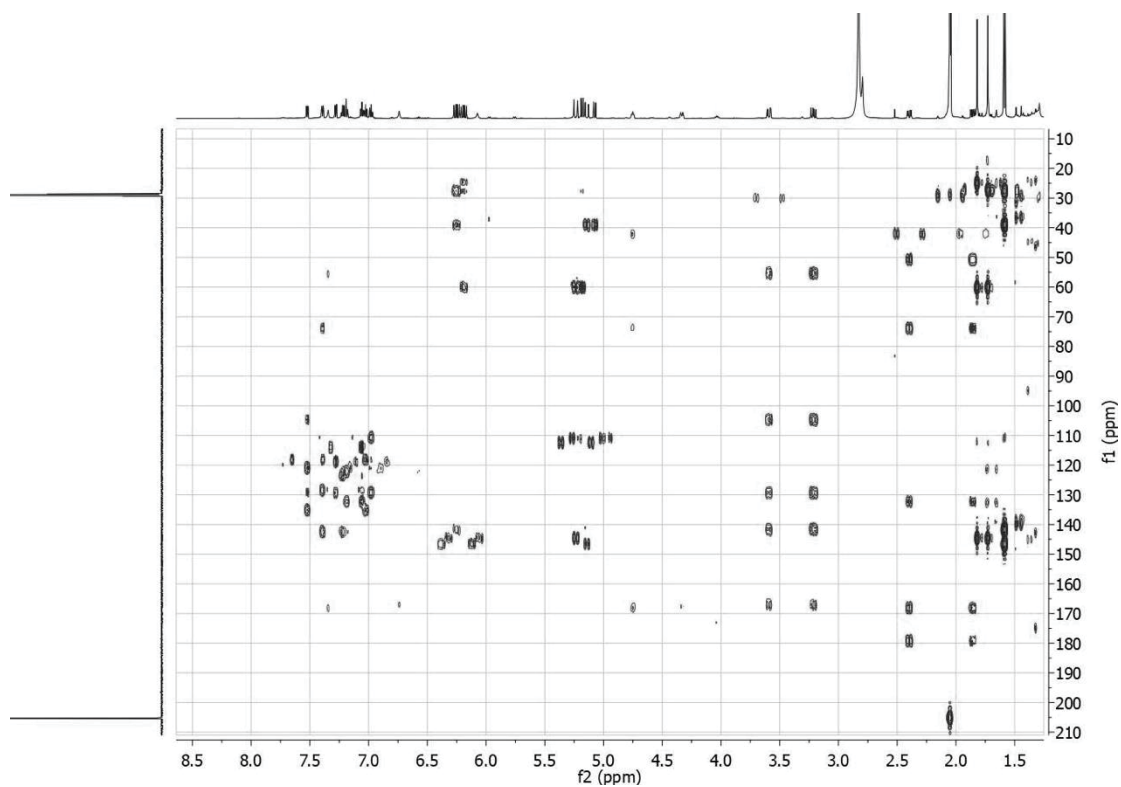


Figure S13. HMBC (600 MHz, Acetone-*d*₆) spectrum of **2**.

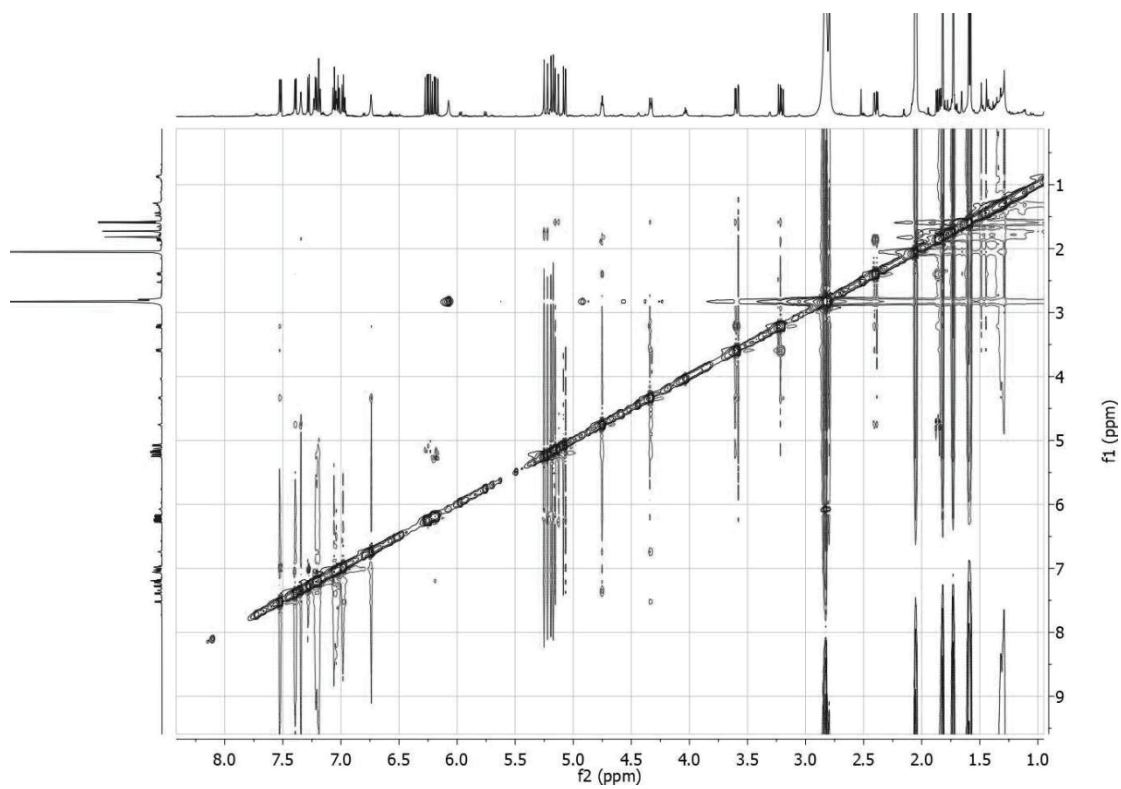
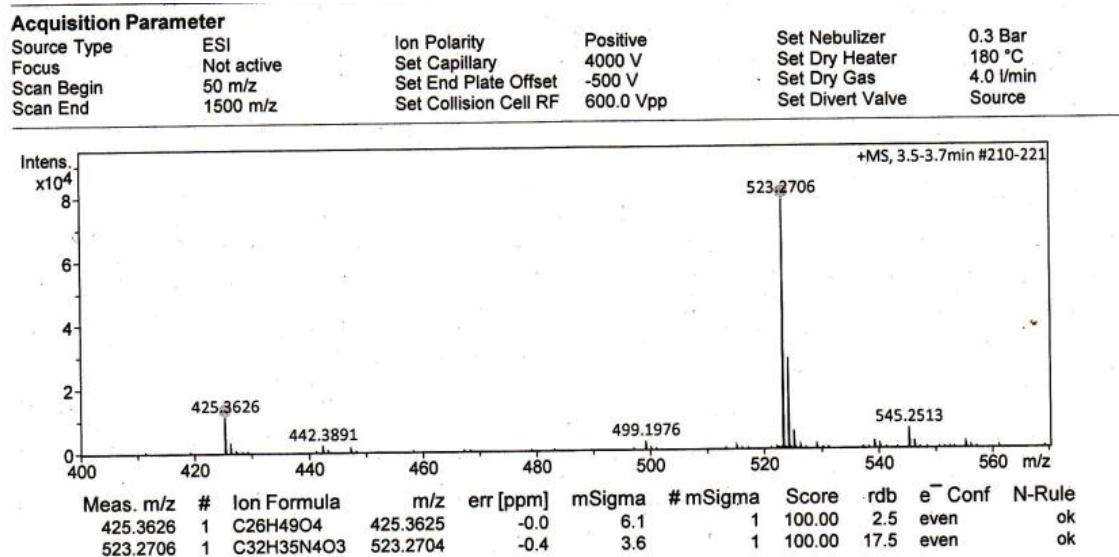
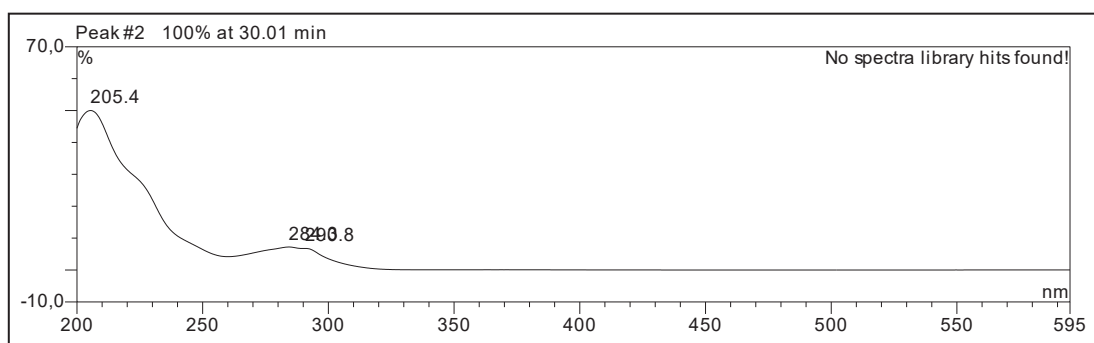


Figure S14. ROESY (600 MHz, Acetone-*d*₆) spectrum of **2**.

Figure S15. HR-ESI-MS of **3**.Figure S16. UV spectrum of **3**.

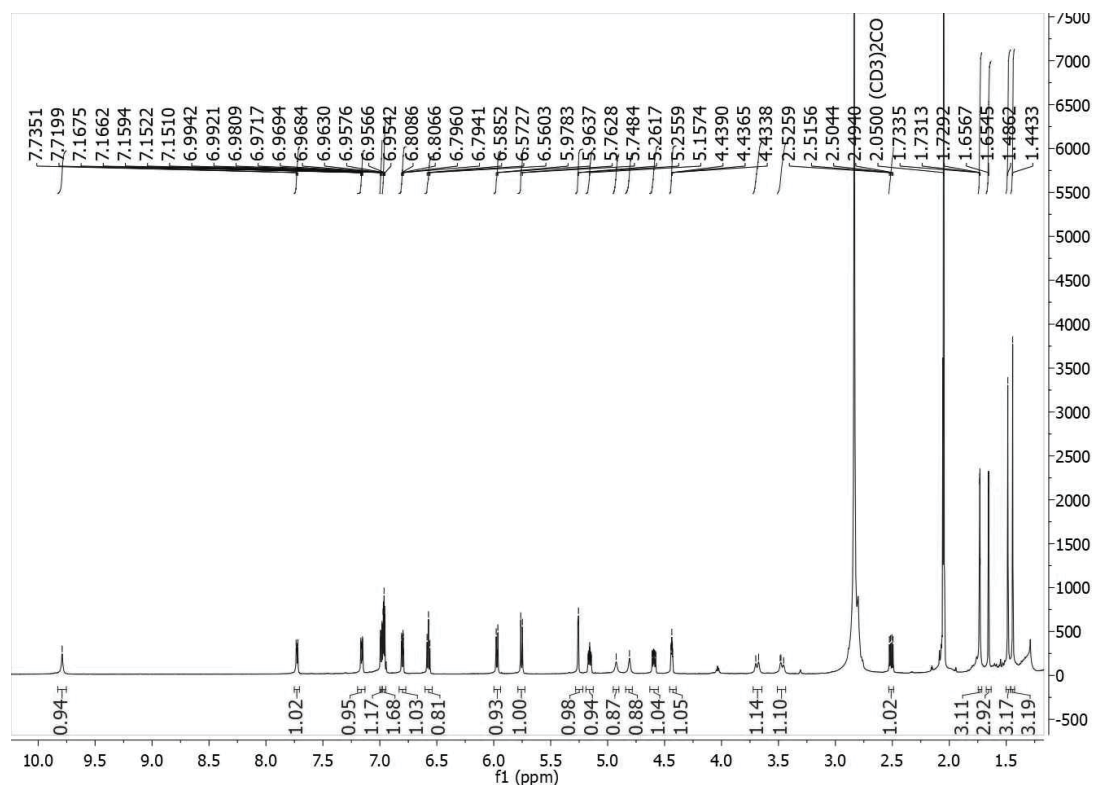


Figure S17. ^1H NMR (600 MHz, Acetone- d_6) spectrum of **3**.

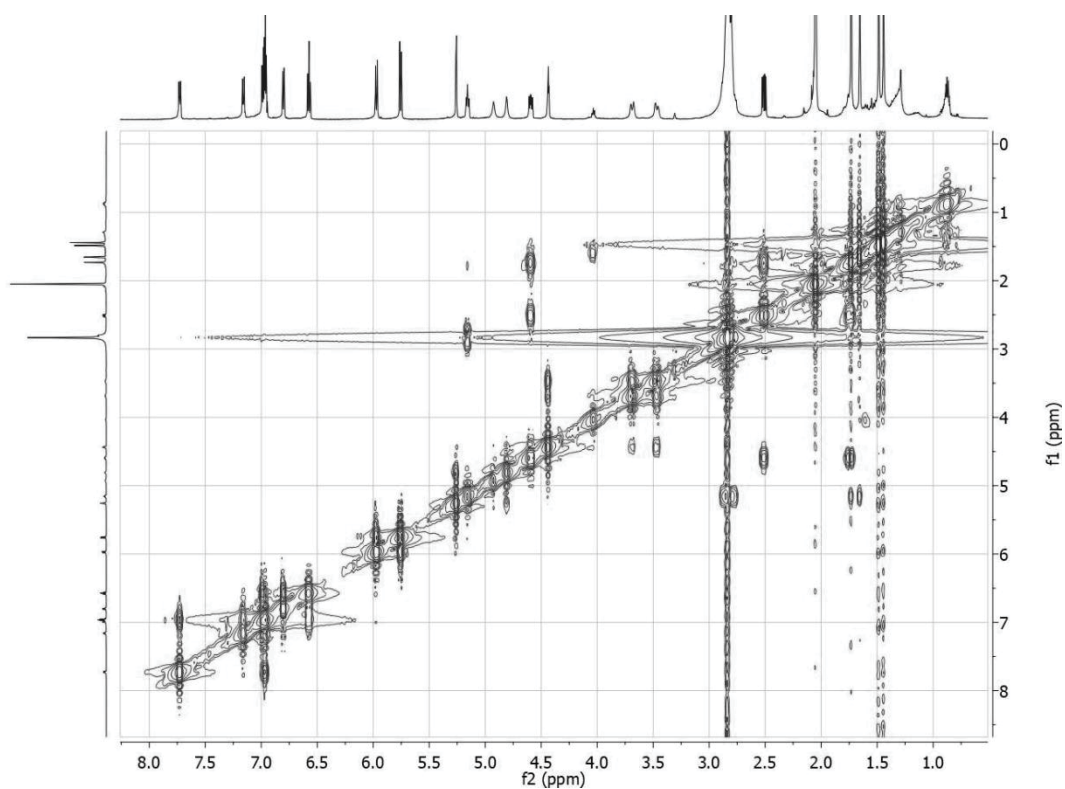


Figure S18. ^1H - ^1H COSY (600 MHz, Acetone- d_6) spectrum of **3**.

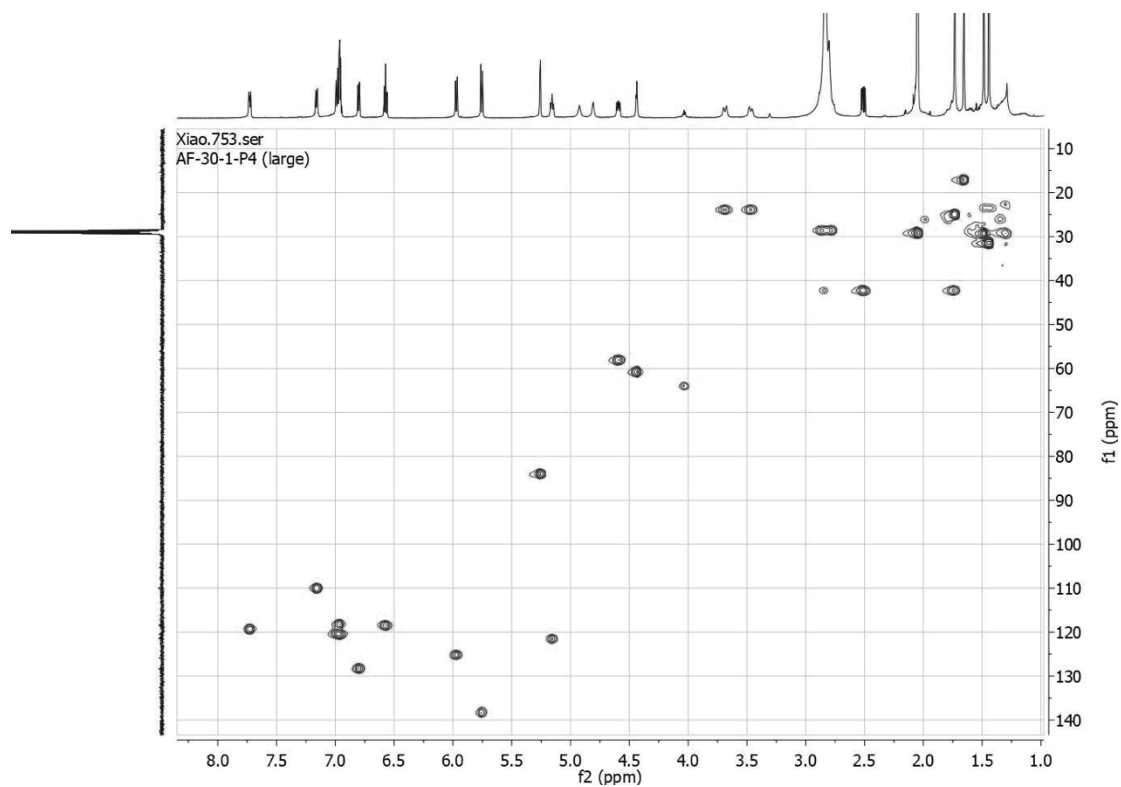


Figure S19. HSQC (600 MHz, Acetone- d_6) spectrum of **3**.

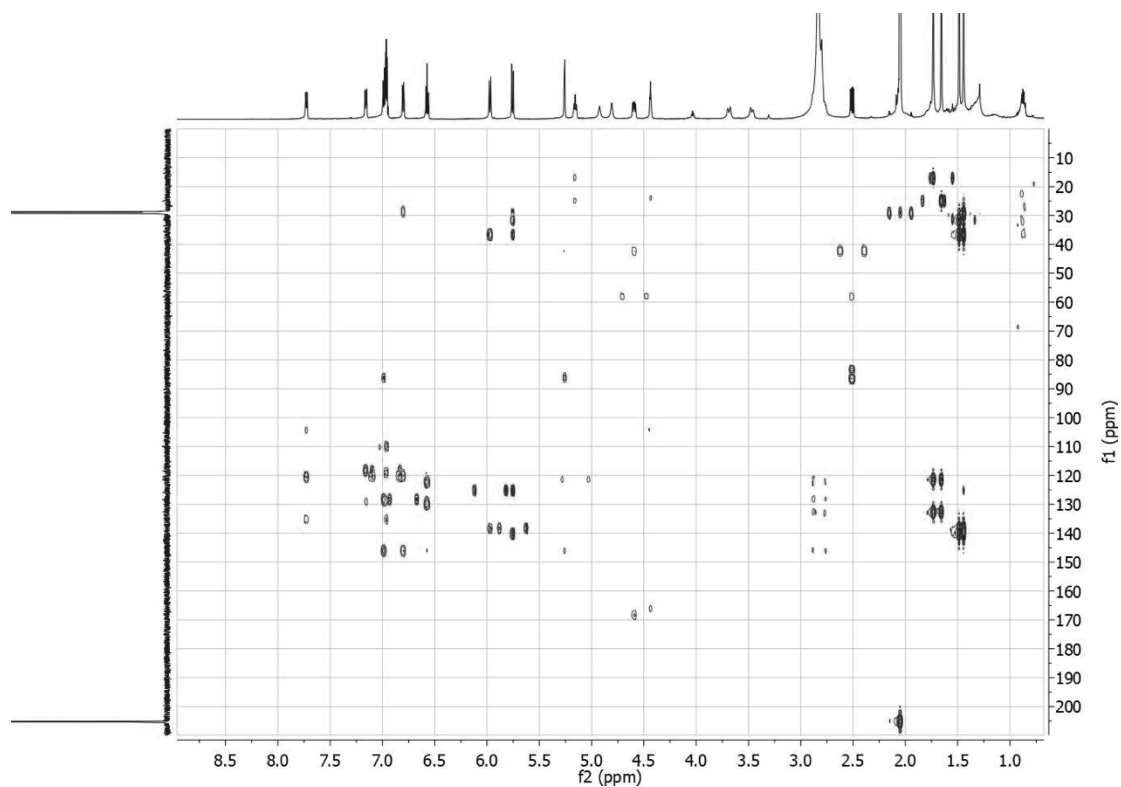


Figure S20. HMBC (600 MHz, Acetone- d_6) spectrum of **3**.

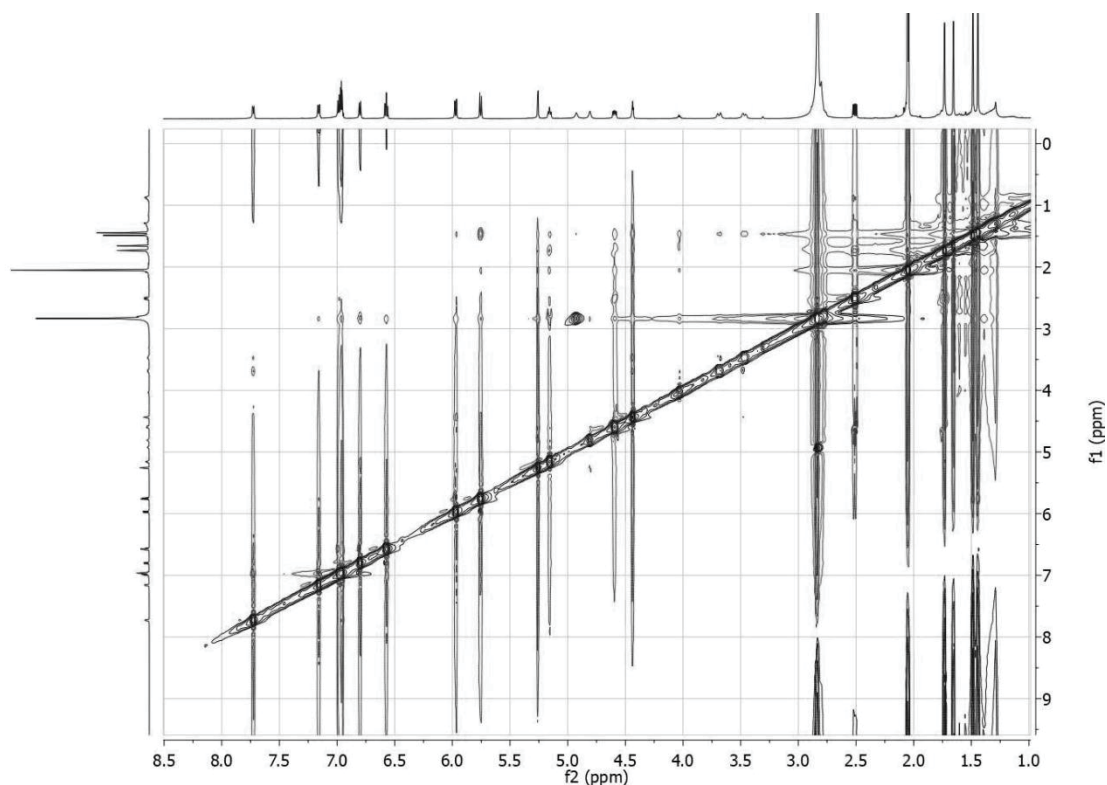


Figure S21. ROESY (600 MHz, Acetone- d_6) spectrum of **3**.

Acquisition Parameter

Source Type	ESI	Ion Polarity	Positive	Set Nebulizer	0.3 Bar
Focus	Not active	Set Capillary	4000 V	Set Dry Heater	180 °C
Scan Begin	50 m/z	Set End Plate Offset	-500 V	Set Dry Gas	4.0 l/min
Scan End	1500 m/z	Set Collision Cell RF	600.0 Vpp	Set Divert Valve	Source

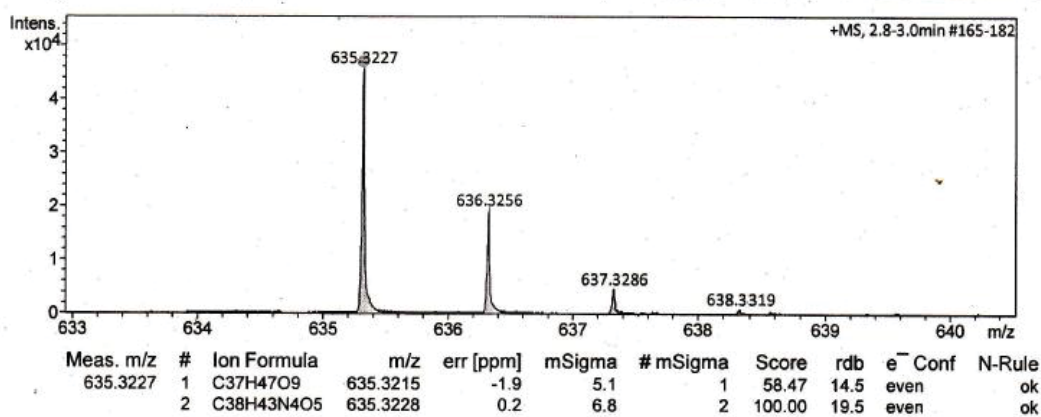


Figure S22. HR-ESI-MS of **4**.

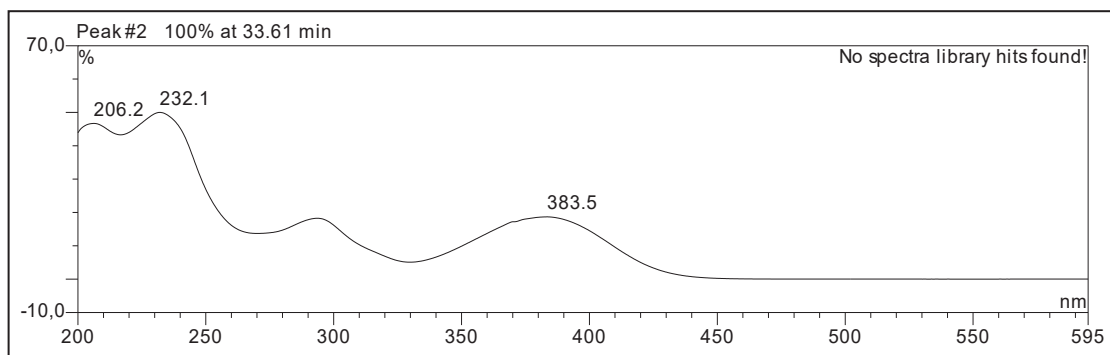


Figure S23. UV spectrum of **4**.

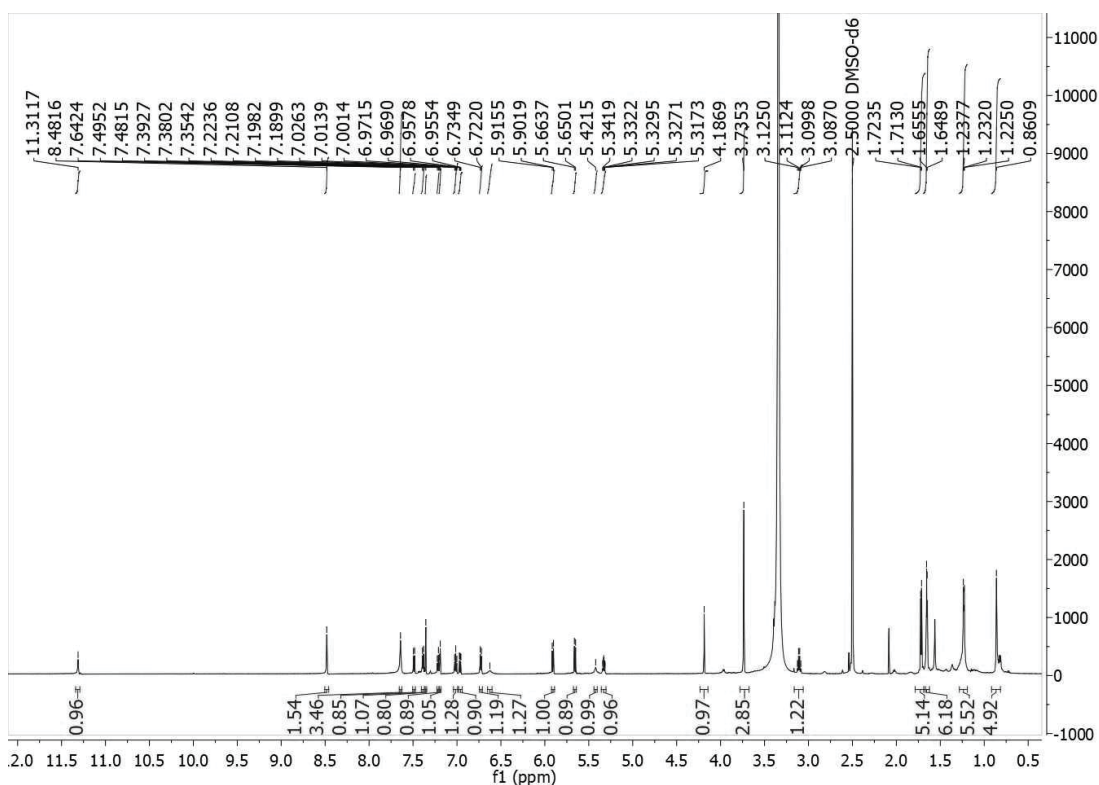


Figure S24. ^1H NMR (600 MHz, $\text{DMSO}-d_6$) spectrum of **4**.

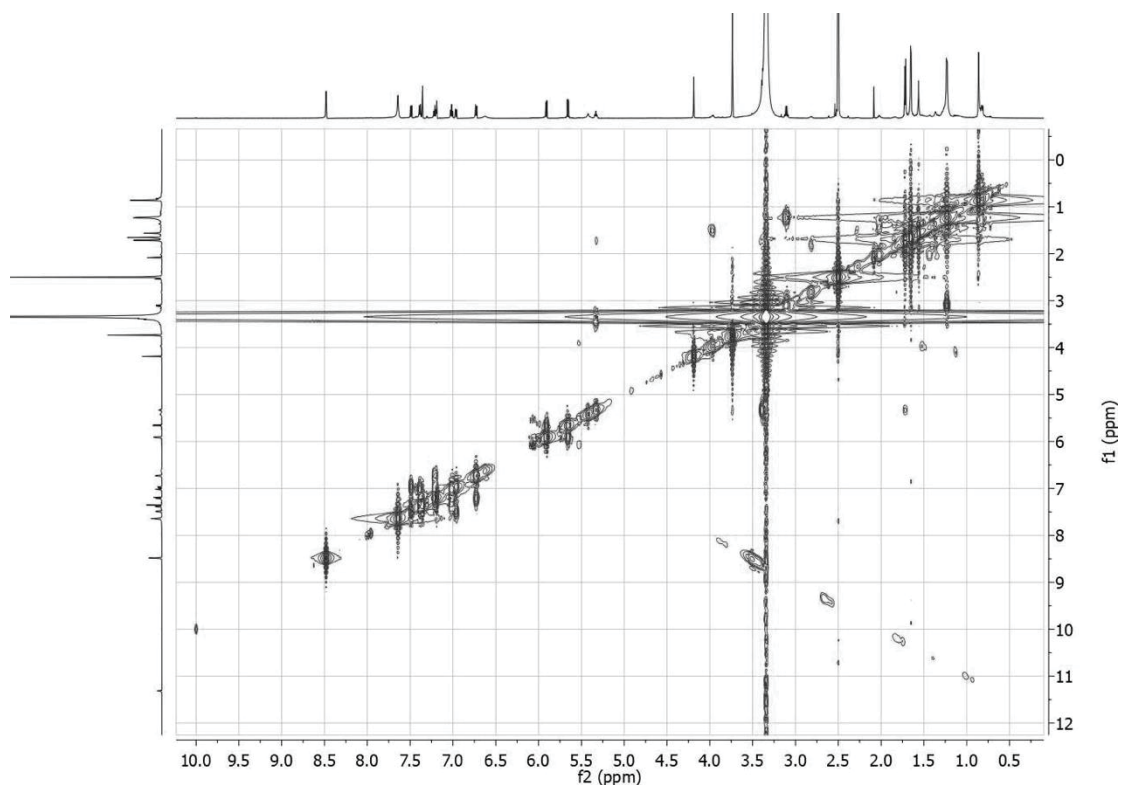


Figure S25. ^1H - ^1H COSY (600 MHz, $\text{DMSO-}d_6$) spectrum of **4**.

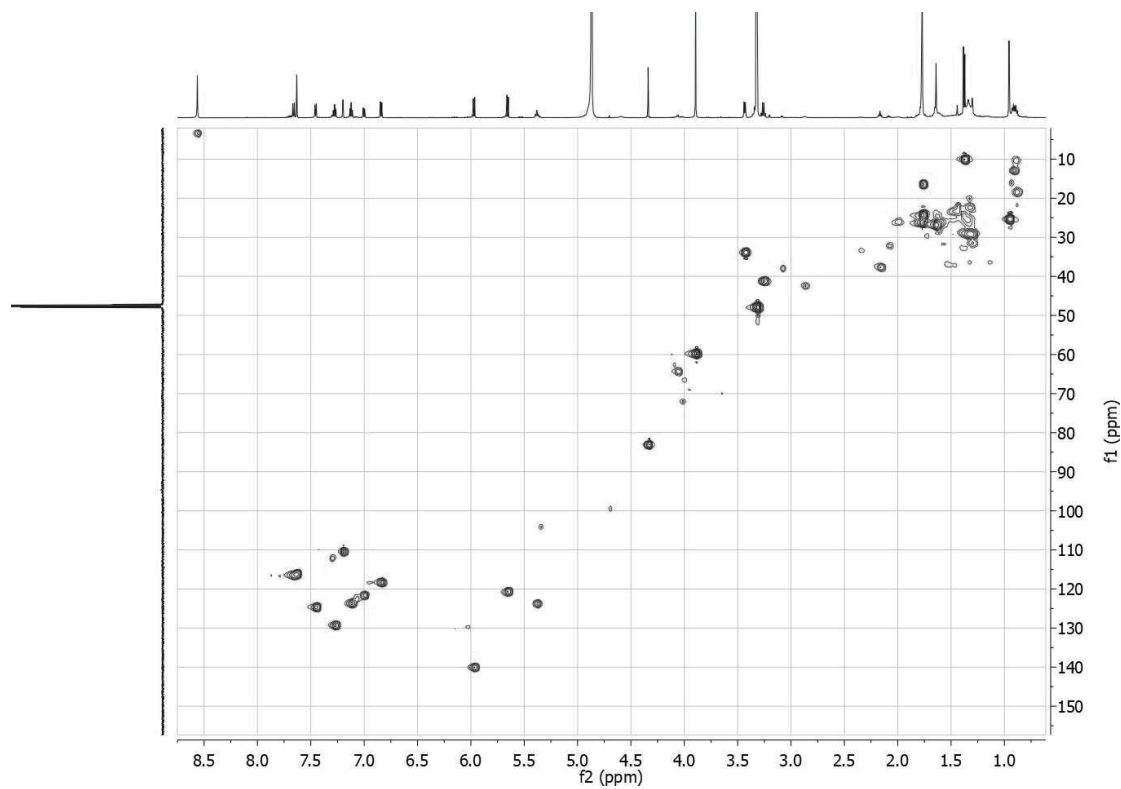


Figure S26. HSQC (600 MHz, $\text{DMSO-}d_6$) spectrum of **4**.

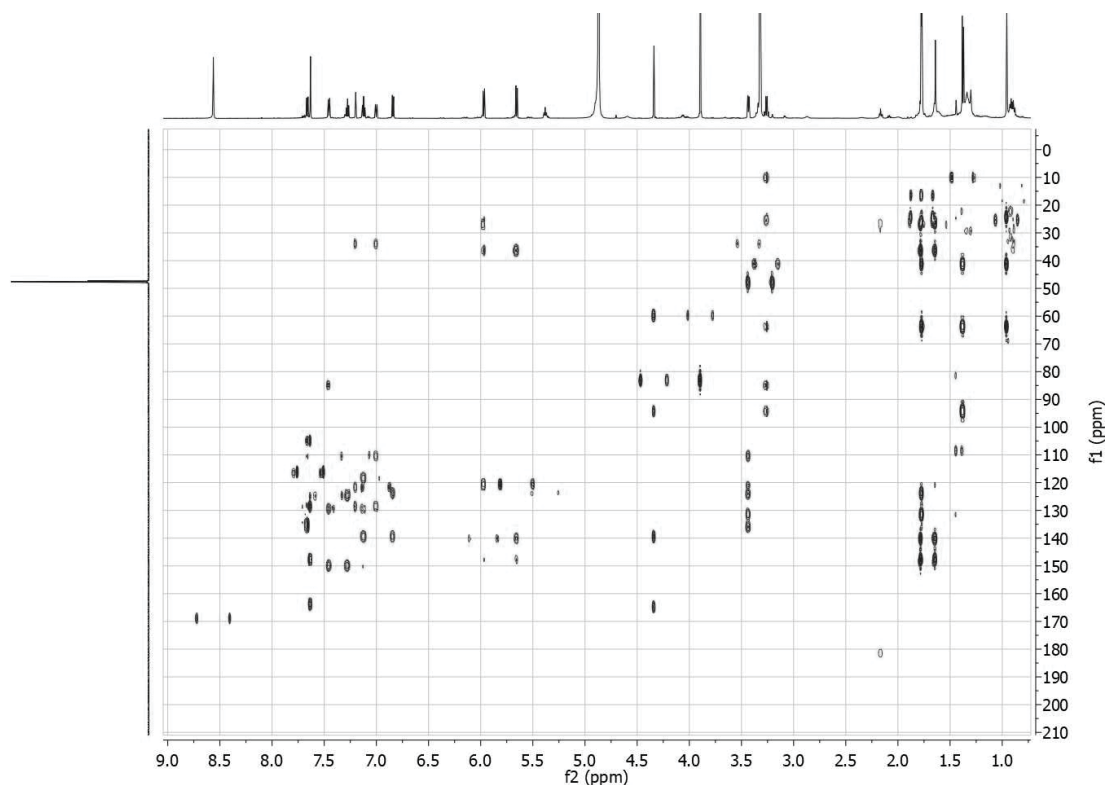


Figure S27. HMBC (600 MHz, DMSO- d_6) spectrum of **4**.

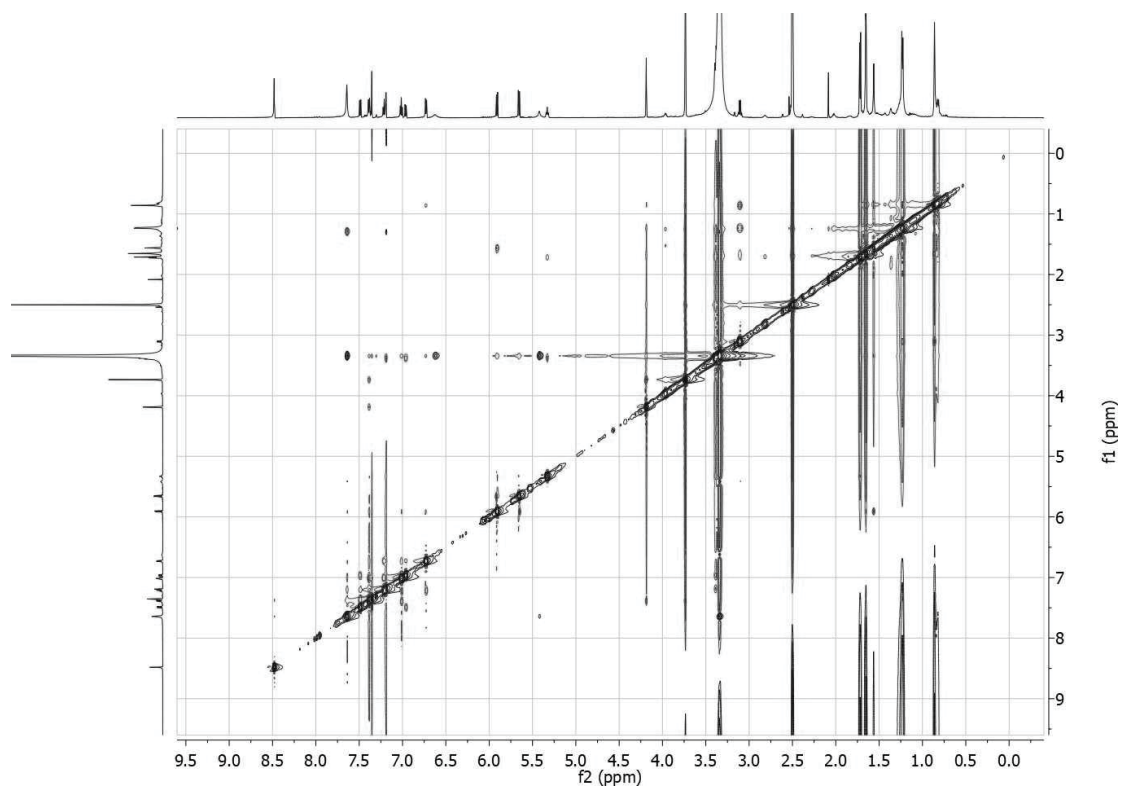
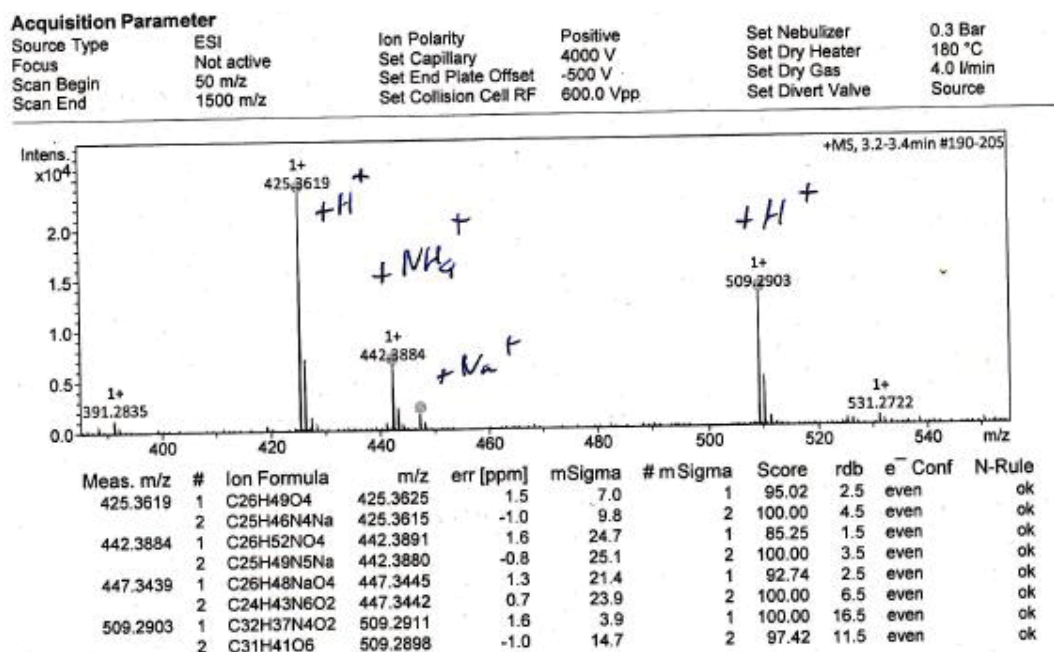
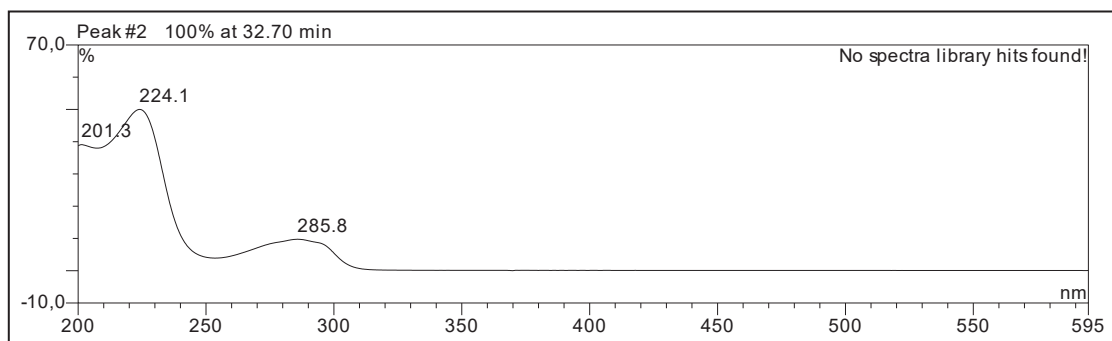


Figure S28. ROESY (600 MHz, DMSO- d_6) spectrum of **4**.

Figure S29. HR-ESI-MS of **5**.Figure S30. UV spectrum of **5**.

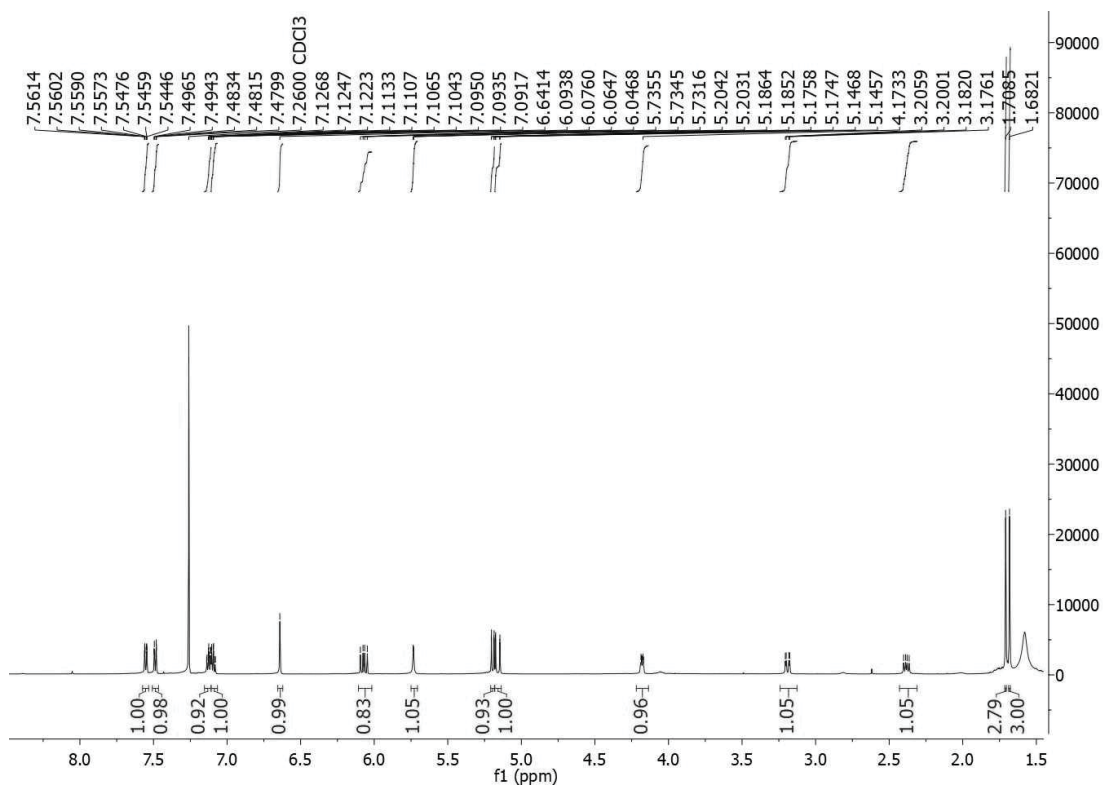


Figure S31. ¹H NMR (600 MHz, CDCl₃) spectrum of **5**.

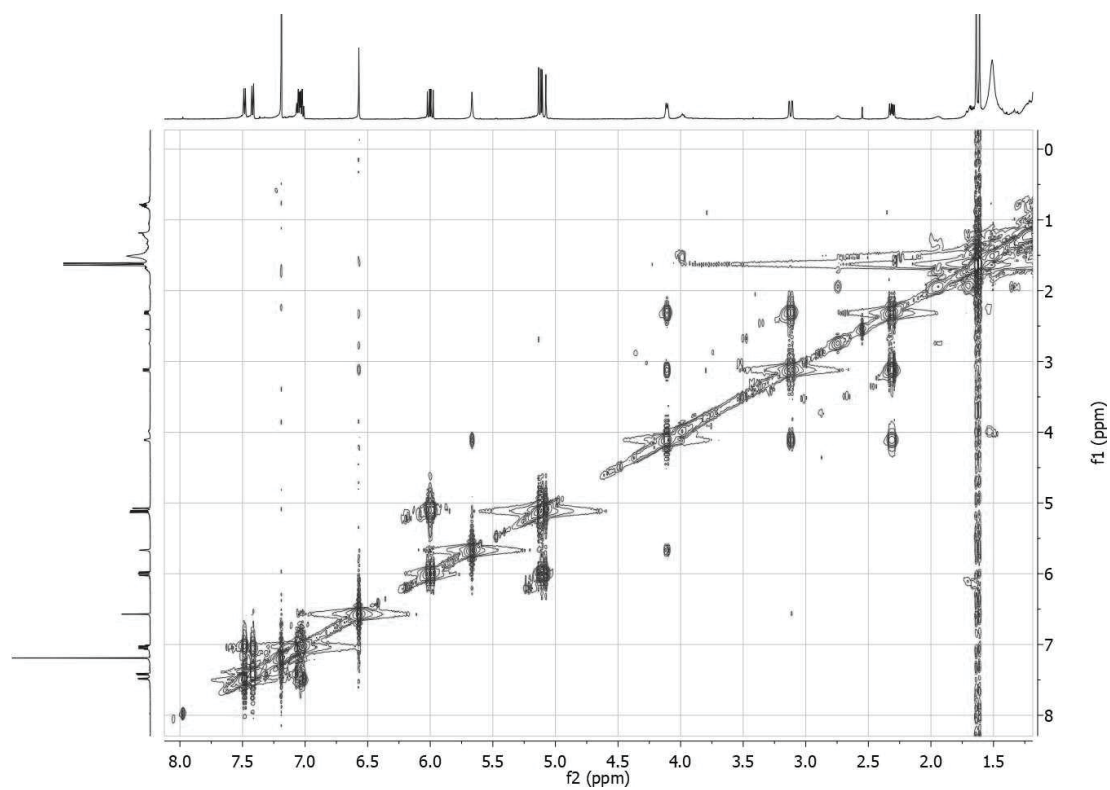


Figure S32. ¹H-¹H COSY (600 MHz, CDCl₃) spectrum of **5**.

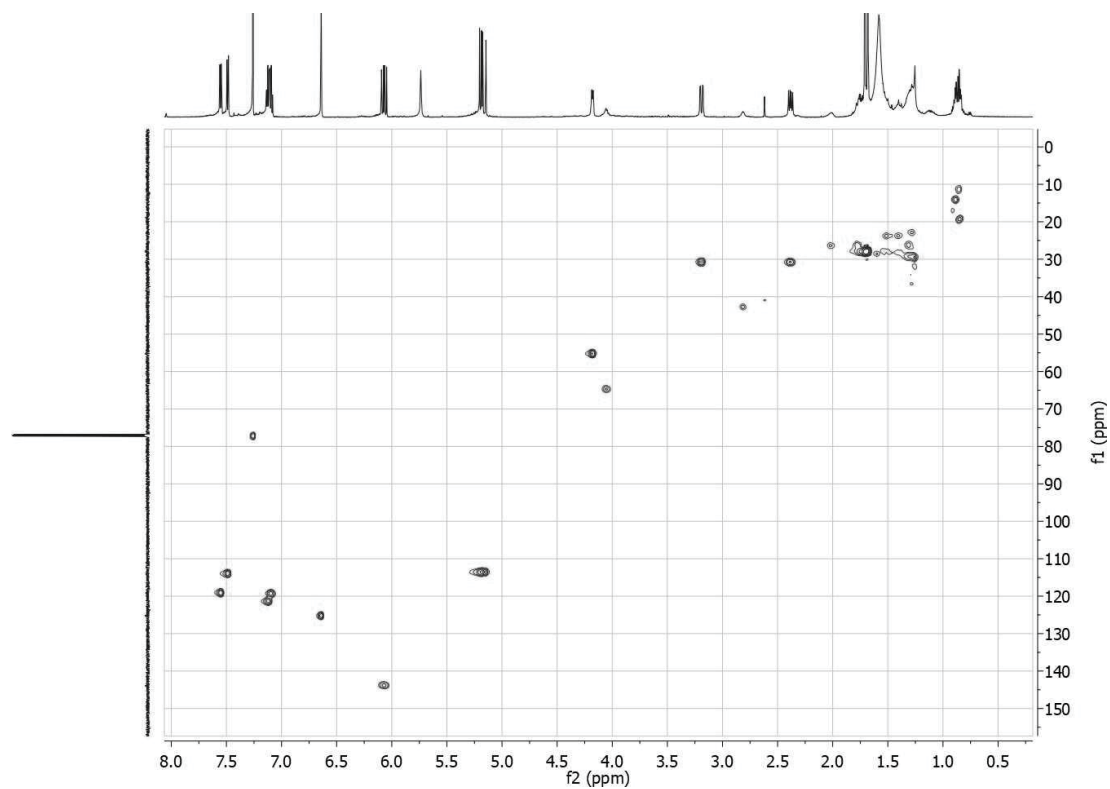


Figure S33. HSQC (600 MHz, CDCl_3) spectrum of **5**.

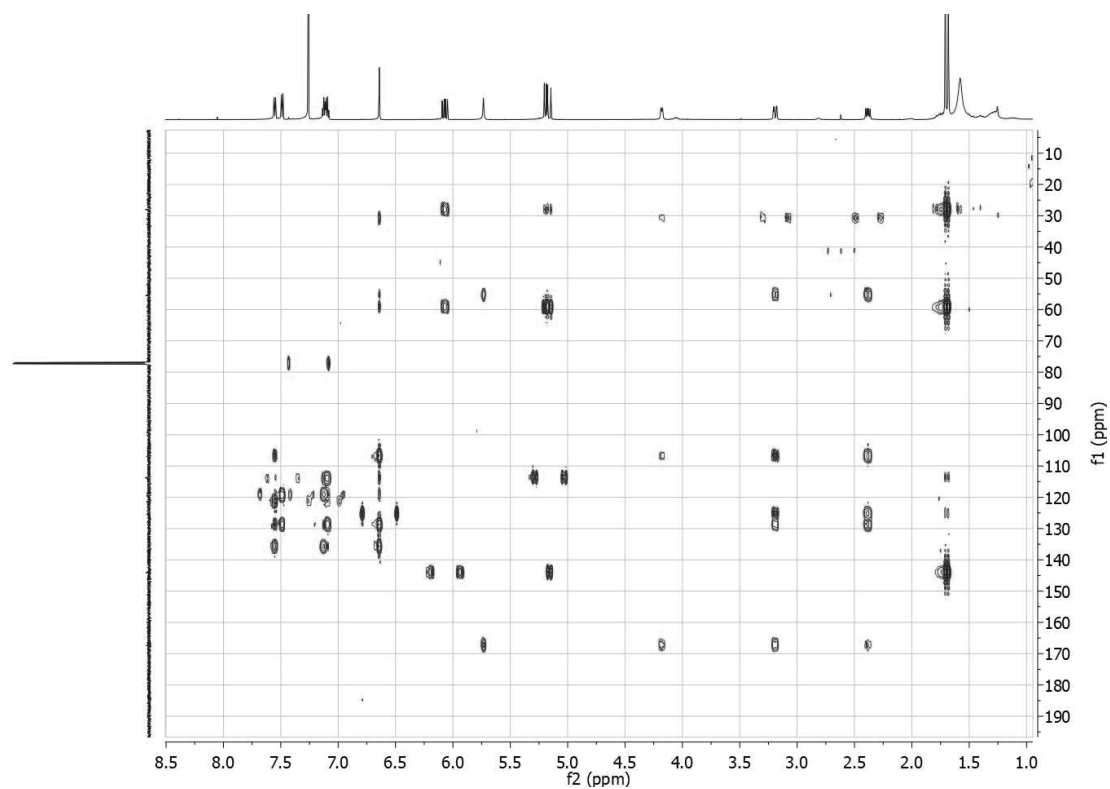


Figure S34. HMBC (600 MHz, CDCl_3) spectrum of **5**.

3 Publication 2

Polyketide derivatives from mangrove derived endophytic fungus *Pseudopestalotiopsis theae*

Published in “*Marine drugs*”

Research contribution: the first author contributed 60% to this publication. The first author’s work involved all laboratory work including the isolation, structure elucidation, and manuscript preparation for all compounds.

Reprinted by permission from “**Xiaoqin Yu**, Werner E. G. Müller, Dieter Meier, Rainer Kalscheuer, Zhiyong Guo, Kun Zou, Blessing O. Umeokoli, Zhen Liu and Peter Proksch. (2020) Polyketide derivatives from mangrove derived endophytic fungus *Pseudopestalotiopsis theae*”. *Marine drugs*, **18**, 129.

Article

Polyketide Derivatives from Mangrove Derived Endophytic Fungus *Pseudopestalotiopsis theae*

Xiaoqin Yu ^{1,2}, Werner E. G. Müller ³ , Dieter Meier ¹, Rainer Kalscheuer ¹ , Zhiyong Guo ², Kun Zou ², Blessing O. Umeokoli ⁴, Zhen Liu ^{1,*}  and Peter Proksch ^{1,2,*}

¹ Institute of Pharmaceutical Biology and Biotechnology, Heinrich Heine University Duesseldorf, 40225 Duesseldorf, Germany; xiyu101@hhu.de (X.Y.); dieter.meier@hhu.de (D.M.); Rainer.Kalscheuer@hhu.de (R.K.)

² Hubei Key Laboratory of Natural Products Research and Development, College of Biological and Pharmaceutical Sciences, China Three Gorges University, Yichang 443002, China; zhyguo@foxmail.com (Z.G.); kzou@ctgu.edu.cn (K.Z.)

³ Institute of Physiological Chemistry, Universitätsmedizin der Johannes Gutenberg-Universität Mainz, 55128 Mainz, Germany; wmueller@uni-mainz.de

⁴ Department of Pharmaceutical and Medicinal Chemistry, Nnamdi Azikiwe University, 420281 Awka, Nigeria; blessingumeokoli@gmail.com

* Correspondence: zhenfeizi0@sina.com (Z.L.); proksch@uni-duesseldorf.de (P.P.); Tel.: +49-211-81-14163 (Z.L. & P.P.)

Received: 5 February 2020; Accepted: 20 February 2020; Published: 23 February 2020



Abstract: Chemical investigation of secondary metabolites from the endophytic fungus *Pseudopestalotiopsis theae* led to the isolation of eighteen new polyketide derivatives, pestalotheols I–Q (1–9) and cytosporins O–W (15–23), together with eight known analogs (10–14 and 24–26). The structures of the new compounds were elucidated by HRMS and 1D and 2D NMR data, as well as by comparison with literature data. Modified Mosher’s method was applied to determine the absolute configuration of some compounds. Compound 23 showed significant cytotoxicity against the mouse lymphoma cell line L5178Y with an IC₅₀ value of 3.0 µM. Furthermore, compounds 22 and 23 showed moderate antibacterial activity against drug-resistant *Acinetobacter baumannii* (ATCC BAA-1605) in combination with sublethal colistin concentrations.

Keywords: *Pseudopestalotiopsis theae*; endophytic fungus; polyketide; cytotoxicity

1. Introduction

Since the discovery of antibacterial penicillin from *Penicillium notatum*, there have been tremendous achievements with regard to the development of fungal drugs [1]. The antifungal medicine griseofulvin, which was initially isolated from *Penicillium griseofulvum*, has been applied for the treatment of ringworm in skin and nails in animals and humans [2]. Lovastatin, the first commercial statin isolated from a fermentation broth of *Aspergillus terreus*, has been used to treat high blood cholesterol and reduce the risk of cardiovascular disease [3]. The immunosuppressant agent cyclosporine was isolated from the fungus *Tolypocladium inflatum* [4]. Endophytic fungi occur in all plants investigated up to now and are important for the fitness and survival of their hosts [5]. The chemically remarkably creative fungal genus *Pestalotiopsis* contains around 234 described fungal species listed in Index Fungorum, including 44 taxol producers [6,7]. *Pestalotiopsis* has attracted considerable attention due to the abundance and diversity of secondary products found in members of this genus [8,9]. Pestalachloride A, a new chlorinated benzophenone alkaloid produced by *Pestalotiopsis adusta*, showed potent antifungal activity against *Fusarium culmorum* with an IC₅₀ value of 0.89 µM [10]. The first chlorinated pupukeanane derivative, chloropupukeananin, which was isolated from fermentation broth of *Pestalotiopsis fici*,

isolated from fermentation broth of *Pestalotiopsis fici*, inhibited HIV-1 replication in C8166 cells with an IC_{50} of 0.01 μ M [11]. *Pestalotiopsis fici* A-163, a blue trichothecium, produced a polyketide and a triterpene obtained from the culture of *Pestalotiopsis fici* both exhibited cytotoxicity against Hepa-2 cells with IC_{50} values of 8.9 μ M [12]. *Pestalotiopsis fici* A-163, a blue trichothecium, produced a polyketide and a triterpene obtained from the culture of *Pestalotiopsis fici* both exhibited cytotoxicity against Hepa-2 cells with IC_{50} values of 8.9 μ M [12]. *Pestalotiopsis fici* A-163, a blue trichothecium, produced a polyketide and a triterpene obtained from the culture of *Pestalotiopsis fici* both exhibited cytotoxicity against Hepa-2 cells with IC_{50} values of 8.9 μ M [12].

In previous studies from our group, cytotoxic 14-membered macrolides were obtained from the mangrove-derived fungus *Pestalotiopsis mucronata* with IC_{50} values ranging from 0.77 to 5.66 μ M [14]. In the present study, the endophytic fungus *Pseudopestalotiopsis thaeae*, which was previously reported as *Pestalotiopsis thaeae* and taxonomically revised in 2014 [7], was isolated from roots of the mangrove plant *Rhizophora racemosa* collected at Lagos, Nigeria. Fermentation of this fungus on solid rice yielded eight highly ketone polyketide macrolides (1–9), (11–13), and (15–17) and a tetracyclic compound (14) (15–23) in addition to congeners (Figure 1). In this paper, the isolation, elucidation, and bioactivity of all isolated compounds are reported.

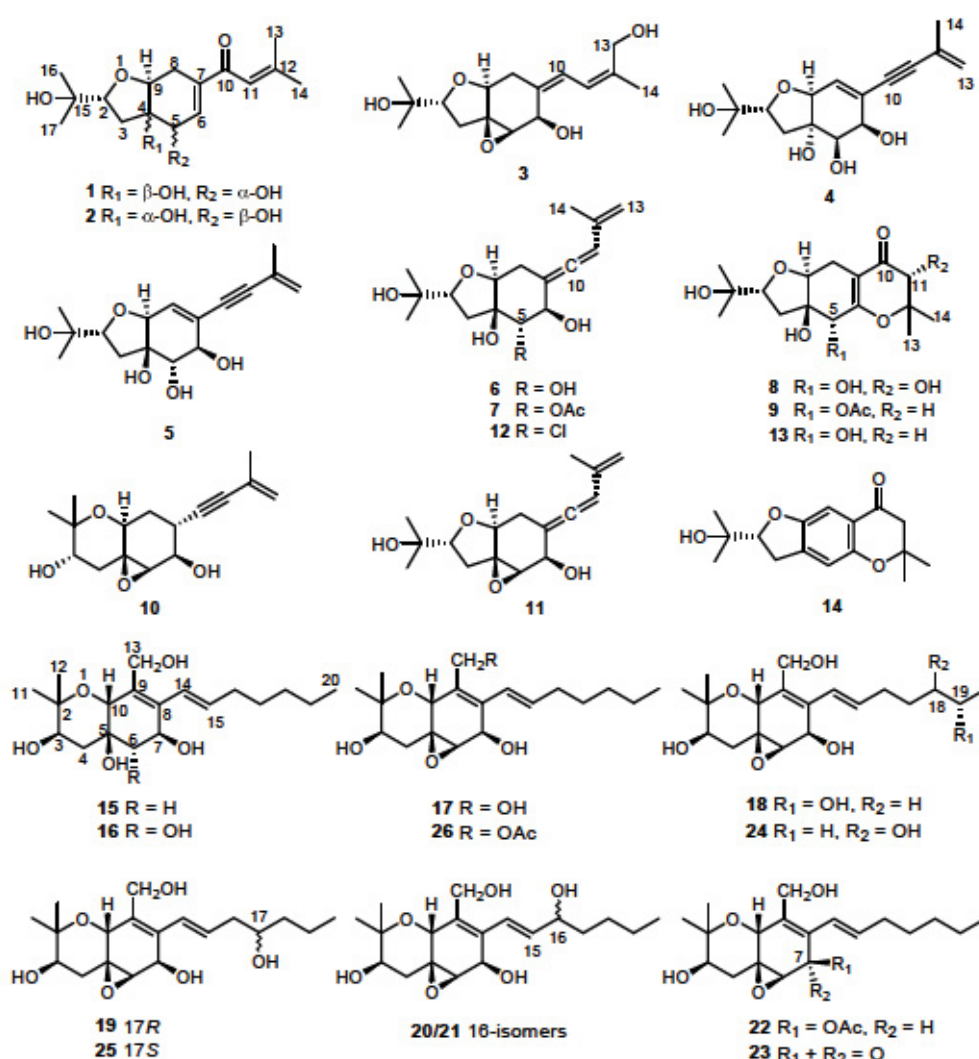


Figure 1. Structures of compounds 1–26 isolated from *Pseudopestalotiopsis thaeae*.

2. Results and Discussion

Compound 1 was obtained as yellowish gel. The molecular formula of 1 was determined as $C_{14}H_{20}O_5$ by HRESIMS data, indicating five degrees of unsaturation. The ^{13}C NMR data (Table 1) for 1 revealed the presence of a carbonyl at δ_c 191.9 (C-10), four olefinic carbons at δ_c 153.7 (C-12), 138.7 (C-7), 138.0 (C-6), and 120.7 (C-11), five oxygenated carbons at δ_c 84.2 (C-2), 77.8 (C-4), 76.5 (C-9), 76.8

(C-9), 70.8 (C-15), and 68.9 (C-5), two methylene groups at δ_C 34.0 (C-3) and 25.7 (C-8), together with four methyls at δ_C 27.2 (C-14), 25.9 (C-17), 25.8 (C-16), and 20.5 (C-13), accounting for three degrees of unsaturation. Thus, compound **1** was suggested to be bicyclic in nature. The COSY correlations between H-2/H-3ab, OH-5/H-5/H-6, H-8/H-9, together with the HMBC correlations from H-2 to H-9, from OH-4 to C-3, C-4, C-5, and C-9, from H-5 to C-4 and C-9, from H-6 to C-4 and C-8, and from H-8ab to C-4, C-6, C-7, and C-9, established the presence of a tetrahydrofuranocyclohexene moiety with two hydroxy groups at C-4 and C-5. Additional HMBC correlations from Me-14 to C-11, C-12, and C-13, and from H-11, H-6 and H-8a to C-10 indicated the attachment of a 3-methyl-1-oxobut-2-en-1-yl side chain at C-7. Moreover, the location of a 2-hydroxyisopropyl subunit at C-2 was confirmed by the HMBC correlations from Me-16(17) to C-2, C-15 and C-17(16), and from OH-15 to C-2, C-15, C-16, and C-17. Thus, the planar structure of **1** was established as shown. The relative configuration of **1** was elucidated by coupling constants and NOE correlations (Figure 2). The large values of $J_{H-2/H-3a}$ (9.9 Hz) and $J_{H-9/H-8b}$ (10.7 Hz) suggested trans-diaxial orientation of these protons. The NOE correlations from H-9 to Me-16, H-3a, OH-5, and H-8a, and between H-3a and OH-5 indicated these protons to be on the same side, whereas the NOE correlations from OH-4 to H-2, H-3b, H-5, and H-8b confirmed they were in opposite orientation. Based on the summarized results (Figure 3) of the modified Mosher's method, the absolute configuration of C-5 was determined to be *S*, thereby assigning 2*R*, 4*R*, 5*S*, 9*S* absolute configuration for pestalothol I (**1**).

Table 1. NMR Data of compounds 1–3.

No.	1 ^a		2 ^{a,c}		3 ^b	
	δ_C , Type	δ_H (J in Hz)	δ_C , Type	δ_H (J in Hz)	δ_C , Type	δ_H (J in Hz)
2	84.2, CH	3.95, dd (9.9, 6.4)	84.1, CH	3.57, dd (8.3, 5.7)	86.0, CH	4.07, dd (9.4, 6.7)
3	34.0, CH ₂	2.20, dd (12.4, 9.9)	36.1, CH ₂	2.08, dd (13.5, 8.3)	31.0, CH ₂	2.55, dd, (13.3, 9.4)
4	77.8, C	1.60, dd (12.4, 6.4)	82.5, C	1.81, dd (13.5, 5.7)	69.5, C	1.72, dd, (13.3, 6.7)
5	68.9, CH	4.05, dd (5.3, 4.6)	72.3, CH	4.24, dd (5.0, 2.5)	60.1, CH	3.75, d (2.8)
6	138.0, CH	6.71, dd (4.6, 2.3)	141.0, CH	6.69, t (2.5)	64.6, CH	4.65, dd (8.8, 2.8)
7	138.7, C		137.8, C		135.5, C	
8	25.7, CH ₂	2.53, dd (16.0, 5.3)	26.8, CH ₂	2.54, dd (16.9, 3.9)	35.4, CH ₂	2.50, dd (12.1, 11.5)
9	76.3, CH	2.09, ddd (16.0, 10.7, 2.3)	82.7, CH	2.14, ddd (16.9, 5.4, 2.5)	127.6, CH	2.21, dd, (12.1, 4.8)
10	191.9, C	3.63, dd (10.7, 5.3)	190.1, C	4.05, dd (5.4, 3.9)	77.7, CH	3.86, dd (11.5, 4.8)
11	120.7, CH	6.57, s	120.0, CH	6.59, s	122.8, CH	6.25, d (11.7)
12	153.7, C		153.6, C		139.9, C	6.29, d (11.7)
13	20.5, CH ₃	2.00, s	20.5, CH ₃	2.00, s	60.9, CH ₂	4.21, dd (12.5, 5.3)
14	27.2, CH ₃	1.90, s	27.1, CH ₃	1.90, s	4.16, dd (12.5, 5.3)	1.85, s
15	70.8, C		70.9, C		22.0, CH ₃	
16	25.8, CH ₃	1.07, s	26.0, CH ₃	1.09, s	71.9, C	
17	25.9, CH ₃	1.01, s	26.7, CH ₃	0.99, s	26.6, CH ₃	1.23, s
4-OH		4.54, s		5.37, s	25.8, CH ₃	1.09, s
5-OH		5.38, d (5.3)		5.52, d (5.0)		
6-OH						3.97, d (8.8)
13-OH						3.70, t (5.3)
15-OH		4.16, s		4.75, s		3.34, s

^a Recorded at 600 MHz (¹H) and 150 MHz (¹³C) in DMSO-*d*₆. ^b Recorded at 600 MHz (¹H) and 150 MHz (¹³C) in Acetone-*d*₆. ^c Data extracted from the HSQC and HMBC spectra.

C₁₆H₂₂O₅ by HRESIMS, suggesting the replacement of the chlorine atom at C-4 by a hydroxy group in **4**, which was supported by the observation of four hydroxy groups at δ_H 5.08, 5.05, 4.77, and 4.31 in the ¹H NMR spectrum of **4** rather than three signals of hydroxy groups in truncateol K. On the basis of the 2D NMR spectroscopic data of **4**, the remaining substructure and relative configuration of **4** were determined to be identical to truncateol K.

Table 2. NMR Data of compounds 4–6.

No.	4 ^a		5 ^{a,b}		6 ^a	
	δ_C , Type	δ_H (J in Hz)	δ_C , Type	δ_H (J in Hz)	δ_C , Type	δ_H (J in Hz)
2	85.2, CH	3.73, dd (8.1, 7.7)	84.6, CH	4.01, dd (9.6, 6.4)	83.7, CH	3.86, dd (9.9, 6.3)
3	37.5, CH ₂	2.43, dd (13.0, 7.7) 1.79, dd (13.0, 8.1)	33.5, CH ₂	2.12, dd (12.0, 9.6) 1.59, dd (12.0, 6.4)	34.1, CH ₂	2.12, dd (12.0, 9.9) 1.53, dd (12.0, 6.3)
4	79.1, C		76.4, C		79.8, C	
5	71.8, CH	3.60, t (4.0)	72.5, CH	3.81, d (3.7)	71.1, CH	3.83, d (3.8)
6	67.6, CH	4.11, dd (9.0, 4.0)	74.1, CH	3.73, d (9.1)	74.9, CH	4.01, s
7	124.1, C		122.2, C		102.2, C	
8	134.0, CH	5.87, d (3.2)	132.9, CH	6.10, d (1.7)	27.8, CH ₂	2.52, ddd (12.4, 11.9, 3.9)
9	81.2, CH	4.10, d (3.2)	77.1, CH	4.35, d (1.7)	77.4, CH	2.23, dd (11.9, 4.4)
10	88.6, C		88.8, C		204.6, C	3.81, dd (12.4, 4.4)
11	90.2, C		88.7, C		95.7, CH	5.92, d (3.9)
12	126.4, C		126.0, C		139.0, C	
13	122.1, CH ₂	5.32, s 5.27, s	121.6, CH ₂	5.30, s 5.26, s	113.5, CH ₂	4.93, s 4.82, s
14	23.2, CH ₃	1.87, s	23.0, CH ₃	1.87, s	19.5, CH ₃	1.69, s
15	70.2, C		70.5, C		70.5, C	
16	25.9, CH ₃	1.07, s	25.8, CH ₃	1.10, s	26.1, CH ₃	1.07, s
17	26.4, CH ₃	1.00, s	25.5, CH ₃	0.99, s	25.9, CH ₃	0.98, s
4-OH		5.05, s		4.68, s		5.22, s
5-OH		4.77, d (4.0)		5.47, d (3.7)		5.28, d (3.8)
6-OH		5.08, d (9.0)		4.72, d (9.1)		5.74, br s
15-OH		4.31, s		4.23, s		4.17, s

^a Recorded at 600 MHz (¹H) and 150 MHz (¹³C) in DMSO-*d*₆. ^b Data extracted from the HSQC and HMBC spectra.

Compound **5** has the same planar structure as **4** based on the 1D and 2D NMR spectroscopic data as well as on the HRESIMS data of **5**. However, the NOE interactions of **5** differed from those of **4** as also observed between **1** and **2**. In the ROESY spectrum of **5**, correlations from H-9 to Me-16, H-3a and OH-5, and from OH-5 to H-3a and H-6 were found, indicating they were on the same side. On the other hand, the NOE correlations between H-3b/H-2, H-2/OH-4, OH-4/H-5, H-5/OH-6 placed those protons on the other side of the ring. Hence the relative configuration of **5** was elucidated as 2*R**, 4*R**, 5*S**, 6*R**, 9*S** whereas that of **4** was 2*R**, 4*S**, 5*R**, 6*R**, 9*S**.

The molecular formula of pestalothol N (**6**) was deduced as C₁₆H₂₄O₅ from the HRESIMS data. The NMR data (Table 2) of **6** were compatible with those of the co-isolated known compound truncateol H (**12**) except for the lack of the chloride atom at C-5 [16]. Instead, the COSY correlation between the D₂O changeable proton at δ_H 5.28 and H-5 (δ_H 3.83) suggested C-5 to be hydroxylated. Similar NOE interactions were observed for **6** and **12**, indicating the relative configuration of **6** to be identical to that of **12**, for which the absolute configuration had previously been determined by Mosher's reaction and by the X-ray data of its 6-epimer [16].

Pestalothol O (**7**) was obtained as colorless oil. The molecular formula of **7** was determined as C₁₈H₂₆O₆ by HRESIMS, containing an additional acetyl group when compared to **6**, which was further supported by the presence of a carbonyl carbon at δ_C 169.2 and a methyl group at δ_C 20.5 and δ_H 2.09 in the NMR data of **7** (Table 3). The location of this additional acetyl group at C-5 was evident from the HMBC correlation from H-5 (δ_H 5.01) to the carbonyl carbon of the acetyl group. Analysis of 1D and 2D NMR data of **7** concluded its remaining substructure to be the same as **6**. The absolute configuration of

C-6 in **7** was determined as *R* by comparison of chemical shifts between its methoxyphenylacetic acid (MPA) esters (Figure 3).

Table 3. NMR Data of compounds **7**–**9**.

No.	7 ^a		8 ^b		9 ^{a,c}	
	δ_C , Type	δ_H (J in Hz)	δ_C , Type	δ_H (J in Hz)	δ_C , Type	δ_H (J in Hz)
2	83.5, CH	3.88, dd (9.6, 6.4)	86.1, CH	4.13, dd (10.1, 6.4)	84.4, CH	3.95, dd (9.5, 6.5)
3	34.0, CH	1.83, dd (12.3, 9.6)	35.0, CH ₂	2.49, dd (12.5, 10.1)	33.9, CH ₂	1.80, dd (12.5, 9.5)
4	77.8, C	1.62, dd (12.3, 6.4)	80.1, C	1.77, dd (12.5, 6.4)	76.4, C	1.66, dd (12.5, 6.5)
5	72.0, CH	5.01, d (2.5)	72.2, CH	4.08, d (5.1)	71.3, CH	5.28, s
6	71.7, CH	4.04, d (2.5)	168.3, C		162.3, C	
7	101.5, C		107.0, C		110.0, C	
8	27.4, CH ₂	2.56, ddd (12.4, 12.0, 3.9)	22.4, CH ₂	2.70, dd (14.9, 5.7)	21.3, CH ₂	2.55, dd (14.9, 5.5)
9	78.0, CH	2.31, dd (12.0, 4.4)	76.9, CH	2.11 (dd, 14.9, 10.6)	76.5, CH	2.01, dd (14.9, 10.7)
10	204.4, CH	3.76, dd (12.4, 4.4)	194.6, C	3.91, dd (10.6, 5.7)	191.9, C	3.63, dd (10.7, 5.5)
11	96.5, CH	6.02, d (3.9)	76.1, CH	4.13, d (2.8)	46.4, CH ₂	2.65, d (16.7)
12	138.2, C		84.4, C		80.4, C	2.42, d (16.7)
13	114.5, CH ₂	4.99, s	26.9, CH ₃	1.49, s	27.3, CH ₃	1.36, s
14	19.5, CH ₃	4.88, s	16.5, CH ₃	1.14, s	23.4, CH ₃	1.24, s
15	70.5, C	1.71, s	72.0, C		70.5, C	
16	25.9, CH ₃	1.09, s	26.7, CH ₃	1.18, s	26.1, CH ₃	0.99, s
17	26.0, CH ₃	0.98, s	25.6, CH ₃	1.09, s	25.6, CH ₃	1.08, s
4-OH		5.45, s		3.97, s		5.31, s
5-OH				5.09, d (5.1)		
6-OH		5.91, br s				
11-OH				4.30, d (2.8)		
13-OH		4.24, s				
15-OH				3.22, s		4.25, s
5-OAc	20.6, CH ₃	2.00, s			20.5, CH ₃	2.09, s
	169.2, C				169.5, C	

^a Recorded at 600 MHz (¹H) and 150 MHz (¹³C) in DMSO-*d*₆. ^b Recorded at 600 MHz (¹H) and 150 MHz (¹³C) in Acetone-*d*₆. ^c Data extracted from the HSQC and HMBC spectra.

Based on the HRESIMS data, the molecular formula of compound **8** was deduced as C₁₆H₂₅O₇, containing one additional oxygen atom when compared to the isolated known derivative, pestalothol A (**13**) [17]. The COSY correlation between the D₂O changeable proton at δ_H 4.30 and H-11 (δ_H 4.13) and the HMBC correlations from H-11 to C-10, C-12, C-13, and C-14 confirmed the replacement of the methylene group by a hydroxy group at C-11 in **8**. Compounds **8** and **13** share the same relative configuration at C-2, C-4, C-5, and C-9 as evident from their similar coupling constants and NOE relationships. Moreover, Mosher's method was applied to determine the absolute configuration at C-5 and C-11 of **8**. Due to the influence of multiple MPA moieties, anomalous $\Delta\delta$ values were observed for Me-13 (−0.27) and Me-14 (+0.06). The absolute configuration at C-5 and C-11 of **8** was tentatively assigned as *R* (Figure 3). Therefore, the 2*R*, 4*R*, 5*R*, 9*S*, and 11*R* absolute configuration was assigned for pestalothol P (**8**).

The HRESIMS of pestalothol Q (**9**) showed the pseudomolecular ion peak at 355.1754 [M + H]⁺, indicating the molecular formula of C₁₈H₂₇O₇. The UV spectrum and the NMR data of **9** suggested it to be an analog of pestalothol A [17], with addition of an acetyl group as evident from signals in the ¹H and ¹³C NMR spectroscopic data at δ_H 2.09, δ_C 169.5 and 20.5. The HMBC correlations from H-5 (δ_H 5.28) to the carbonyl carbon of the acetyl group indicated the attachment of the acetyl group at C-5. Based on the similar coupling constants and NOE relationships, the relative configuration of **9** was suggested to be identical to that of **13**. Thus, pestalothol Q (**9**) was elucidated to be 5-acetoxy derivative of pestalothol A (**13**).

Cytosporin O (**15**) was obtained as yellowish gel. The molecular formula of **15** was established as $C_{19}H_{32}O_5$ from the HRESIMS data, indicating four degrees of unsaturation. The ^{13}C NMR data (Table 4) displayed signals of four olefinic carbons at δ_C 133.8 (C-8), 132.1 (C-15), 132.0 (C-9), and 126.0 (C-14), accounting for two degrees of unsaturation. Therefore, **15** was suggested to contain a bicyclic skeleton. In addition, six oxygenated carbons at δ_C 74.9 (C-2), 70.6 (C-3), 70.0 (C-10), 69.3 (C-5), 63.9 (C-7), and 57.7 (C-13), and three methyls at δ_C 27.9 (C-11), 16.1 (C-12), and 13.9 (C-20) were observed. Upon analysis of the 1D and 2D NMR data, **15** was suggested to be a derivative of cytosporin D [18] except for the replacement of signals of the epoxy ring at C5/C6 by an additional D_2O exchangeable proton at δ_H 5.07 (s, OH-5) and an additional methylene group at δ_C 35.7, and δ_H 2.00, 1.54 (CH₂-6). The HMBC correlations from OH-5 to C-4, C-5, C-6, and C-10, together with the COSY correlations between H-6ab and H-7, indicated a hydroxy group at C-5 and a methylene group at C-6. Thus, the planar structure of **15** was established as shown. The large coupling constant (15.7 Hz) revealed *E*-geometry of the double bond at C-15/C-16. The NOE interactions between H-10/OH-5, OH-5/H-4b, H-4b/H-10, H-10/Me-12, Me-12/H-4b indicated those protons to be orientated on the same side, whereas the NOE correlations between Me-11/H-3, H-3/H-4a, H-3/H-6a, H-6a/H-7 supported them to be on the opposite side (Figure 4).

Table 4. NMR Data of compounds 15–17.

No.	15 ^a		16 ^a		17 ^b	
	δ_C , Type	δ_H (J in Hz)	δ_C , Type	δ_H (J in Hz)	δ_C , Type	δ_H (J in Hz)
2	74.9, C		75.0, C		75.4, C	
3	70.6, CH	3.20, dt (12.0, 4.9)	69.8, CH	3.78, dt (11.4, 5.5)	72.1, CH	3.38, dt (11.7, 5.0)
4	42.7, CH ₂	1.75, dd (12.8, 4.9) 1.65, dd (12.8, 12.0)	42.3, CH ₂	2.00, dd (13.2, 5.5) 1.68, dd (13.2, 11.4)	35.8, CH ₂	2.04, dd (12.7, 11.7) 1.50, dd (12.7, 5.0)
5	69.3, C		69.2, C		58.1, C	
6	35.7, CH ₂	2.00, dd (13.9, 4.3) 1.54, d (13.9)	75.3, CH	3.55, d (8.0)	61.8, CH	3.24, d (2.7)
7	63.9, CH	4.30, dd (7.6, 4.3)	69.5, CH	4.11, d (7.6)	64.8, CH	4.47, dd (7.3, 2.7)
8	133.8, C		131.8, C		132.9, C	
9	132.0, C		131.7, C		130.0, C	
10	70.0, CH	3.87, s	70.1, CH	4.01, s	65.4, CH	4.34, s
11	27.9, CH ₃	1.07, s	27.7, CH ₃	1.06, s	27.7, CH ₃	1.12, s
12	16.1, CH ₃	1.10, s	16.4, CH ₃	1.13, s	16.1, CH ₃	1.16, s
13	57.7, CH ₂	4.21, dd (11.9, 4.0) 3.81, dd (11.9, 6.2)	57.5, CH ₂	4.24, dd (11.9, 4.2) 3.92, dd (11.9, 6.2)	58.0, CH ₂	4.09, br d (11.6) 3.79, br d (11.6)
14	126.0, CH	6.36, d (15.7)	126.4, CH	6.44, d (15.8)	124.9, CH	6.06, d (15.8)
15	132.1, CH	5.90, dt (15.7, 7.0)	132.1, CH	5.91, dt (15.8, 7.0)	134.5, CH	5.85, dt (15.8, 6.8)
16	32.8, CH ₂	2.10, m	32.8, CH ₂	2.12, m	33.0, CH ₂	2.06, m
17	28.6, CH ₂	1.37, m	28.6, CH ₂	1.38, m	28.5, CH ₂	1.36, m
18	30.8, CH ₂	1.27, m	30.8, CH ₂	1.27, m	30.8, CH ₂	1.27, m
19	22.0, CH ₂	1.29, m	22.0, CH ₂	1.29, m	22.0, CH ₂	1.28, m
20	13.9, CH ₃	0.86, t (6.9)	13.9, CH ₃	0.87, t (6.9)	13.9, CH ₃	0.86, t (7.0)
3-OH		4.76, d (4.9)		4.70, d (5.5)		5.05, d (5.0)
5-OH		5.07, s		5.16, s		
6-OH				3.98, d (8.0)		
7-OH		4.75, d (7.6)		4.88, d (7.6)		4.92, d (7.3)
13-OH		4.53, dd (6.2, 4.0)		4.54, dd (6.2, 4.2)		4.55, br s

^a Recorded at 600 MHz (1H) and 150 MHz (^{13}C) in DMSO- d_6 . ^b Recorded at 300 MHz (1H) and 75 MHz (^{13}C) in DMSO- d_6 .

3-OH	4.76, d (4.9)	4.70, d (5.5)	5.05, d (5.0)
5-OH	5.07, s	5.16, s	
6-OH		3.98, d (8.0)	
7-OH	4.75, d (7.6)	4.88, d (7.6)	4.92, d (7.3)
13-OH	4.53, dd (6.2, 4.0)	4.54, dd (6.2, 4.2)	4.55, br s

Mar. Drugs 2024, 18, 1890
 Rec-2024-18-1890 (1H) and 150 MHz (13C) in DMSO-d6. b Recorded at 300 MHz (1H) and 75 MHz (13C) in DMSO-d6.

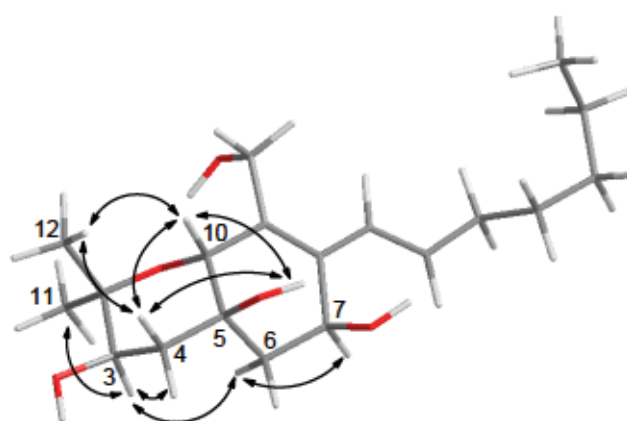


Figure 4. Key NOE correlations for compound **15**.

Compound **16** has the molecular formula $C_{19}H_{32}O_6$ as deduced from the sodium adduct ion at m/z 379.2094 $[M + Na]^+$ in HRESIMS, containing an additional oxygen atom when compared to **15**. The NMR data (Table 4) of **16** resembled those of **15** except for the replacement of a methylene group by an oxygenated methine at δ_H 7.53 and δ_C 3.55 (CH-5.5) (Table 4). The presence of an additional D₂O-exchangeable proton at δ_H 3.98 and its COSY correlation with H-6 hydroxy group at δ_H 6.70. Therefore, it was identified as 6-hydroxy-14-dehydroxy-15-cytoporin (**16**). The relative configuration at C-3, C-5, C-6, C-7, and C-10 in **16** was determined to be identical to that of **15** by comparison of their coupling constants and NOE relationships. In addition, the NOE correlations from OH-6 to H-3 and H-7, and from H-6 to 5-OH and 7-OH confirmed α -orientation of OH-6 in **16**.

The HRESIMS as well as 1D and 2D NMR data of cytoporin Q (**17**) suggested that it possessed the same planar structure as the known cytoporin D bearing an epoxy ring at C-5/C-6 [18]. The NOE correlations observed in **17** between H-10/Me-12, Me-12/H-4a, H-4a/H-10, and between Me-11/H-3, H-3/H-4b, H-4b/H-6, indicated that **17** shared the same relative configuration at C-3, C-5, C-6, and C-10 as cytoporin D. However, the relative configuration at C-7 could not be determined by NOE relationships or J values. Therefore, the modified Mosher's method was applied to determine the absolute configuration at C-3 and C-7 of **17**. In order to exclude the influence of the primary alcohol at C-13, 4,4'-dimethoxytrytyl chloride (DMT-Cl) was used for protection before Mosher's reaction, yielding compound **17a**. Meanwhile, Mosher's reaction was also conducted with the coisolated known compound cytoporin F (**26**) [19], bearing an acetyl group attached to C-13. The differences in chemical shifts of (R)- and (S)-MPA esters assigned 3R and 7R absolute configuration for both **17a** and cytoporin F (**26**) (Figure 3). Thus, **17** was identified as 7-epimer of cytoporin D and has the absolute configuration of 3R, 5S, 6R, 7R, and 10R. Cytoporin D had been firstly reported from the fungus *Eutypella scoparia* derived from a marine pulmonate mollusk [18], while cytoporins F–K were produced by *Pestalotiopsis theae*, an endophyte from leaves of *Turraeanthus longipes* [19]. From biogenetic considerations and the results of Mosher's reaction, it is reasonable to revise the absolute configurations of cytoporins F–K [19] as 3R, 5S, 6R, 7R, and 10R, the same as **17** rather than that of cytoporin D.

The molecular formula of cytoporin R (**18**) was determined as $C_{19}H_{30}O_6$ by HRESIMS, with an additional oxygen atom compared to cytoporin Q (**17**). A methyl doublet at δ_H 1.03 (Me-20) was found in the 1H NMR data of **18** instead of a methyl triplet in **17** (Table 5). Detailed examination of the 2D NMR spectroscopic data revealed **18** to be the 19-OH substituted analog of cytoporin Q (**17**). Similar NOE interactions were observed in **18** as for **17**, indicating that both compounds shared the same relative configuration regarding the ring system. Due to the low amount, cytoporin R (**18**) was subjected for Mosher's method directly without protecting the primary alcohol at C-13. The absolute configuration at C-19 of side chain was determined as S (Figure 3). From biogenetic considerations, the remaining stereocenters of **18** are assumed to share the same absolute configuration as cytoporin Q (**17**).

Table 5. NMR Data of compounds 18–20.

No.	18 ^a		19 ^{b,c}		20 ^{b,c}	
	δ_C , Type	δ_H (J in Hz)	δ_C , Type	δ_H (J in Hz)	δ_C , Type	δ_H (J in Hz)
2	75.4, C		75.2, C		75.2, C	
3	72.1, CH	3.39, m	71.8, CH	3.38, dt (11.8, 5.0)	71.8, CH	3.38, dt (11.8, 4.9)
4	35.8, CH ₂	2.04, m 1.50, dd (12.7, 5.0)	35.5, CH ₂	2.05, dd (12.6, 11.8) 1.50, dd (12.6, 5.0)	35.5, CH ₂	2.05, dd (12.7, 11.8) 1.50, dd (12.7, 4.9)
5	58.1, C		57.7, C		57.7, C	
6	61.8, CH	3.24, d (2.5)	61.5, CH	3.25, d (2.6)	61.5, CH	3.25, d (2.5)
7	64.8, CH	4.48, dd (7.6, 2.5)	64.5, CH	4.48, dd (7.4, 2.6)	64.4, CH	4.49, d (7.5, 2.5)
8	132.9, C		132.5, C		132.3, C	
9	130.0, C		129.8, C		130.4, C	
10	65.4, CH	4.34, s	65.1, CH	4.34, s	65.0, CH	4.35, s
11	27.7, CH ₃	1.12, s	27.5, CH ₃	1.12, s	27.4, CH ₃	1.12, s
12	16.1, CH ₃	1.16, s	15.8, CH ₃	1.16, s	15.8, CH ₃	1.16, s
13	58.0, CH ₂	4.09, dd (12.0, 2.0) 3.79, dd (12.0, 3.5)	57.7, CH ₂	4.11, dd (11.9, 2.3) 3.79, dd (11.9, 4.2)	57.6, CH ₂	4.12, dd (11.9, 2.0) 3.79, dd (11.9, 4.0)
14	124.9, CH	6.06, d (15.9)	126.2, CH	6.08, d (16.0)	122.8, CH	6.20, d (16.0)
15	134.6, CH	5.85, dt (15.9, 7.0)	131.4, CH	5.88, dt (16.0, 7.2)	137.8, CH	5.86, dd (16.0, 6.2)
16	33.1, CH ₂	2.05, m	41.5, CH ₂	2.15, m	71.0, CH ₂	3.95, m
17	25.2, CH ₂	1.40, m 1.34, m	69.2, CH	3.46, m	36.9, CH ₂	1.40, m
18	38.5, CH ₂	1.33, m 1.30, m	38.4, CH ₂	1.36, m 1.27, m	27.0, CH ₂	1.28, m
19	65.6, CH	3.57, m	18.1, CH ₂	1.38, m 1.27, m	21.9, CH ₂	1.27, m
20	23.7, CH ₃	1.03, d (6.1)	13.8, CH ₃	0.85, t (6.9)	13.7, CH ₃	0.86, t (6.9)
3-OH		5.06, d (4.5)		5.07, d (5.0)		5.07, d (4.9)
7-OH		4.94, d (7.6)		4.92, d (7.4)		4.94, d (7.5)
13-OH		4.56, dd (3.5, 2.0)		4.56, dd (4.2, 2.3)		4.58, dd (4.0, 2.0)
16-OH						4.62, d (4.0)
17-OH				4.34, br s		
19-OH		4.31, d (4.3)				

^a Recorded at 300 MHz (¹H) and 75 MHz (¹³C) in DMSO-*d*₆. ^b Recorded at 600 MHz (¹H) and 150 MHz (¹³C) in DMSO-*d*₆. ^c Data extracted from the HSQC and HMBC spectra.

Compound **19** has the same molecular formula of C₁₉H₃₀O₆ as cytosporin R (**18**) as determined by the HRESIMS data. After detailed analysis of the 1D and 2D NMR spectroscopic data of **19**, both compounds were found to differ in the position of the hydroxy group in the side chain. The COSY correlations between the D₂O exchangeable proton at δ_H 4.34 and H-17 (δ_H 3.46), and between H-14/H-15/H-16ab/H-17 confirmed that C-17 was hydroxylated in **19**. Therefore, compound **19** was suggested to be the C-17 epimer of cytosporin K (**25**) [19]. Similar NOE correlations were observed in **19** and **25**, suggesting that both compounds share the same relative configuration regarding the bicyclic ring core. Due to the low amount of cytosporin S (**19**), Mosher's reaction was carried out for its 17-epimer cytosporin K (**25**) [19], whose absolute configuration in the side chain was uncertain before. Comparison of the chemical shifts of (*R*)- and (*S*)-MPA esters of **25** (Figure 3) suggested 17*S* absolute configuration for cytosporin K (**25**). Thus, 17*R* absolute configuration was proposed for cytosporin S (**19**).

Cytosporins T and U (**20** and **21**) have the same molecular formula of C₁₉H₃₀O₆ as deduced by the HRESIMS data. Their NMR data (Table 5 and Table 6) were comparable to those of **19**. However, the olefinic proton at H-15 appeared as dd in **20** and **21** rather than as dt in **19**, suggesting the hydroxy group in the side chain to be located at C-16 in **20** and **21** rather than at C-17 in **19**. This was further supported by the COSY correlations observed between H-14/H-15/H-16/H-17ab, as well as between H-17 and a D₂O exchangeable proton in **20** and **21**. Detailed analysis of the 2D NMR spectroscopic data of **20** and **21** revealed that the remaining substructure was identical to that of **19**. Cytosporins T and U (**20** and **21**) only differ in the absolute configuration in the side chain, as found for **19** and **25**. The absolute configuration at C-16 of both compounds was not determined due to the low amounts.

Table 6. NMR Data of compounds 21–23.

No.	21 ^a		22 ^b		23 ^{b,c}	
	δ_C , Type	δ_H (J in Hz)	δ_C , Type	δ_H (J in Hz)	δ_C , Type	δ_H (J in Hz)
2	75.4, C		75.7, C		76.7, C	
3	72.0, CH	3.39, dt (11.8, 4.9)	71.8, CH	3.42, dt (11.8, 4.9)	71.9, CH	3.45, dt (11.6, 5.0)
4	35.8, CH ₂	2.05, dd (12.6, 11.8) 1.50, dd (12.6, 4.9)	35.2, CH ₂	2.06, dd (12.7, 11.8) 1.53, dd (12.7, 4.9)	34.0, CH ₂	2.21, dd (12.8, 11.6) 1.63, dd (12.8, 5.0)
5	57.9, C		58.0, C		61.1, C	
6	61.7, CH	3.25, d (2.3)	58.1, CH	3.39, d (2.8)	59.3, CH	3.54, d (1.2)
7	64.8, CH	4.48, dd (7.3, 2.3)	67.6, CH	5.85, d (2.8)	195.8, C	
8	132.5, C		128.0, C		130.3, C	
9	130.7, C		133.4, C		148.2, C	
10	65.3, CH	4.35, s	64.7, CH	4.40, s	64.5, CH	4.74, d (1.2)
11	27.7, CH ₃	1.12, s	27.6, CH ₃	1.13, s	27.5, CH ₃	1.16, s
12	16.1, CH ₃	1.16, s	16.1, CH ₃	1.17, s	16.1, CH ₃	1.24, s
13	58.0, CH ₂	4.12, dd (11.8, 4.1) 3.79, dd (11.8, 5.0)	57.6, CH ₂	4.11, dd (12.0, 4.4) 3.78, dd (12.0, 5.8)	58.1, CH ₂	4.26, dd (13.5, 2.1) 4.02, dd (13.5, 4.5)
14	123.3, CH	6.18, d (16.0)	123.8, CH	6.04, d (16.1)	120.6, CH	6.04, m
15	138.2, CH	5.86, dd (16.0, 6.1)	133.9, CH	5.49, dt (16.1, 7.0)	138.4, CH	6.03, m
16	71.3, CH	3.94, m	32.6, CH ₂	2.04, m	33.0, CH ₂	2.10, m
17	37.1, CH ₂	1.40, m 1.34, m	28.4, CH ₂	1.32, m	28.2, CH ₂	1.37, m
18	27.2, CH ₂	1.27, m	30.6, CH ₂	1.23, m	30.7, CH ₂	1.26, m
19	22.2, CH ₂	1.25, m	21.9, CH ₂	1.27, m	21.9, CH ₂	1.28, m
20	14.0, CH ₃	0.86, t (6.9)	13.9, CH ₃	0.86, t (6.8)	13.9, CH ₃	0.86, t (7.0)
3-OH		5.07, d (4.9)		5.12, d (4.9)		5.26, d (5.0)
7-OH		4.91, d (7.3)				
13-OH		4.57, dd (5.0, 4.1)		4.73, dd (5.8, 4.4)		5.17, dd (4.5, 2.1)
16-OH		4.64, d (4.5)				
7-OAc			20.6, CH ₃ 170.0, C	2.02, s		

^a Recorded at 300 MHz (¹H) and 75 MHz (¹³C) in DMSO-*d*₆. ^b Recorded at 600 MHz (¹H) and 150 MHz (¹³C) in DMSO-*d*₆. ^c Data extracted from the HSQC and HMBC spectra.

The NMR data of compound **22** were similar to those of cytosporin F(**26**) [19], and both compounds have the same molecular formula as evident from the HRESIMS data. However, the shielded methylene group at C-13 (δ_C 57.6, δ_H 4.11 and 3.78 in **22** vs. δ_C 63.2, δ_H 4.74 and 4.67 in **26**), and the deshielded oxygenated methine at C-7 (δ_H 5.85 in **22** vs. δ_H 4.63 in **26**) in **22** suggested that the acetoxy moiety was attached at C-7 in **22** rather than at C-13 in **26**, which was further confirmed by the HMBC correlation from H-7 to the carbonyl carbon (δ_C 170.0) of the acetoxy moiety. The remaining substructure of **22** was elucidated to be identical to that of **26**. Based on the similar NOE correlations and the biogenetic relationship between **22** and **26**, compound **22** was suggested to share the same 3*R*, 5*S*, 6*R*, 7*R*, and 10*R* absolute configuration as **26**.

The molecular formula C₁₉H₂₈O₅ was suggested for cytosporin W (**23**) by the HRESIMS data, indicating an additional degree of unsaturation when compared to **17**. The absence of one D₂O changeable proton in the ¹H NMR data (Table 6), along with the HMBC correlations from H-6 (δ_H 3.54) and H-14 (δ_H 6.04) to a carbonyl carbon at δ_C 195.8 indicated a ketone carbonyl to be located at C-7, which accounted for the additional degree of unsaturation. The remaining structure including the relative configuration was determined to be identical to that of **17** after detailed analysis of the 2D NMR spectroscopic data of **23**.

The remaining known compounds were identified as truncateols B (**10**), D (**11**), and H (**12**) [16], pestalothols A (**13**) and D (**14**) [17], cytosporins J (**24**), K (**25**), and F (**26**) [19]. Both new compounds pestalothol O (**7**) and Q (**9**) contain acetoxy group at C-5. In order to exclude the possibility that they might be artifacts formed during the extraction with EtOAc, relative compounds pestalothol N (**6**) and pestalothol A (**13**) were incubated in EtOAc for 48 h at room temperature. Unchanged retention time and molecular weight from HPLC together with MS results indicated that they were natural products rather than artifacts.

In previous report, cytosporins A–C were known as angiotensin II binding inhibitors [20], while cytosporin L was active against the bacteria *Micrococcus lysodeikticus* and *Enterobacter aerogenes* with MIC values of 3.12 μ M [21,22]. In the present study, all isolated compounds were tested for their cytotoxicity and antibacterial activity. Only compound 23, with a carbonyl group at C-7 instead of a hydroxy group, showed significant cytotoxicity against the mouse lymphoma cell line L5178Y with an IC_{50} value of 3.0 μ M, even stronger than that of the positive control kahalalide F (IC_{50} 4.3 μ M), whereas the other compounds were not active ($IC_{50} > 20 \mu$ M), suggesting the importance of α,β -unsaturated ketone moiety in 23 for cytotoxicity. In the antibacterial activity assay, none of the isolated compounds were active against the Gram-positive bacteria *Staphylococcus aureus* (ATCC 29213) and *Mycobacterium tuberculosis* (H37Rv) and the Gram-negative bacterium *Pseudomonas aeruginosa* (ATCC 27853) and drug-resistant *Acinetobacter baumannii* (ATCC BAA-1605) (MIC $> 100 \mu$ M). However, in combination with a sublethal colistin concentration of 0.1 μ M, compounds 22 and 23 displayed antibacterial activity against drug-resistant *Acinetobacter baumannii* (ATCC BAA-1605) with MIC values of 50 and 100 μ M, respectively.

3. Materials and Methods

3.1. General Experimental Procedures

Optical rotations were measured with a Jasco P-2000 polarimeter (JASCO, Tokyo, Japan). Analytical HPLC was performed with a Dionex UltiMate-3400SD system coupled to an LPG-3400SD pump and a DAD300RS photodiode array detector (Dionex Softron, Germering, Germany). The analytical column (125 \times 4 mm) was prefilled with Eurosphere-10 C18 (Knauer, Berlin, Germany), following the program: 0 min (10% MeOH); 5 min (10% MeOH); 35 min (100% MeOH); 45 min (100% MeOH). NMR spectra were recorded with Bruker ARX 300 or 600 NMR spectrometers (Bruker, Karlsruhe, Germany). Chemical shifts were referenced to the solvent residual peaks. HRESIMS were recorded on a UHR-QTOF maXis 4G mass spectrometer (Bruker Daltonics, Bremen, Germany). Column chromatography was conducted with Merck MN silica gel 60M (0.04–0.063 mm). TLC plates precoated with silica gel F₂₅₄ (Merck) were used with detection under 254 and 366 nm. Distilled and spectral grade solvents were used for column chromatography and spectroscopic measurements, respectively. Semipreparative HPLC was performed using a Merck Hitachi HPLC System (UV detector L-5410; pump L-5100; Eurosphere-100 C18, 300 \times 8 mm), with a mixture of MeOH-H₂O or MeCN-H₂O as mobile phase.

3.2. Fungal Material

The fungus was isolated from roots of the mangrove plant *Rhizophora racemosa* collected around Lagos in October 2017. It was identified as *Pseudopestalotiopsis theae* (GenBank accession number MN814071) by DNA amplification and sequencing of its ITS region as described before [23].

3.3. Fermentation, Extraction, and Isolation

The fungus was cultivated on solid rice medium in 10 Erlenmeyer flasks (1 L with 100 g rice and 110 mL demineralized water per flask, autoclaved at 121 °C for 20 min before inoculation). EtOAc (700 mL) was added to each flask after fermentation of 14 days at 20 °C. The fungal cultures were subjected to shaking at 140 rpm for 8 h following addition of EtOAc. After removal of the solvent under reduced pressure, the obtained residue (12.4 g) was subjected to liquid–liquid partition between *n*-hexane and MeOH. After HPLC analysis of both phases, only the methanolic phase was further chromatographically investigated.

The MeOH fraction (8.1 g) was subjected to a vacuum liquid silica gel column chromatography using a gradient solvent system of *n*-hexane and EtOAc (100:1 to 0:100; *v/v*) to obtain seven fractions (Fr. 1–7). Following Sephadex LH-20 column (60 \times 3 cm) chromatography with MeOH as mobile phase, Fr. 3 (1.8 g) was separated into four subfractions (Fr. 3.1–3.4). Fr. 3.4 (0.6 g) was then subjected to vacuum liquid RP-18 column (60 \times 200 mm) chromatography using a solvent gradient (from 100%

H₂O to 100% MeOH) to give five subfractions (Fr.3.4.1–3.4.5). Compounds **6** (4.0 mg), **7** (2.5 mg), **9** (2.2 mg), **10** (5.0 mg), **11** (15 mg), **12** (1.9 mg), **14** (1.7 mg), **22** (3.1 mg), and **23** (2.9 mg) were obtained by semipreparative HPLC (MeOH-H₂O: 0–2 min, 40%; 2–27 min, from 40% to 60%; 27–32 min, 100%) from Fr.3.4.1 (110 mg). Fr. 4 (2.7 g) was subjected to vacuum liquid RP-18 column chromatography (60 × 200 mm) using a solvent gradient (from 100% H₂O to 100% MeCN) to give seven subfractions (Fr. 4.1–4.7). Compounds **1** (2.5 mg), **2** (1.6 mg), **4** (3.0 mg), **5** (1.4 mg), **18** (3.7 mg), and **24** (5.8 mg) were obtained by semipreparative HPLC (MeCN-H₂O: 0–2 min, 8%; 2–22 min, from 8% to 20%; 22–30 min, 100%) from Fr.4.3 (210.0 mg), while compounds **15** (3.3 mg), **16** (3.0 mg), **17** (37.2 mg), and **26** (13.0 mg) were obtained by semipreparative HPLC (MeOH-H₂O: 0–2 min, 30%; 2–22 min, from 30% to 60%; 22–30 min, 100%) from Fr.4.6 (200.0 mg). Following similar procedures, Fr. 5 (1.8 g) was also separated by vacuum liquid RP-18 column (60 × 200 mm) chromatography to give four subfractions (Fr.5.1–Fr.5.4). Compounds **13** (3.5 mg), **19** (1.5 mg), **20** (1.3 mg), **21** (3.8 mg), and **25** (6.2 mg) were obtained from Fr. 5.3 (130 mg) by semipreparative HPLC (MeOH-H₂O: 0–2 min, 38%; 2–22 min, from 38% to 58%; 22–30 min, 100%), while compounds **3** (2.5 mg) and **8** (4.1 mg) were obtained by semipreparative HPLC (MeCN-H₂O: 0–2 min, 5%; 2–22 min, from 5% to 15%; 22–30 min, 100%) from Fr. 5.4 (68.0 mg).

Pestalothol I (**1**): colorless oil; $[\alpha]_D^{20} +115$ (c 0.25, MeOH); UV (MeOH) λ_{\max} 219 nm; ¹H and ¹³C NMR data, Table 1; HRESIMS m/z 297.1694 [M + H]⁺ (C₁₆H₂₅O₅, calcd. 297.1697), 319.1513 [M + Na]⁺ (C₁₆H₂₄O₅Na, calcd. 319.1516).

Pestalothol J (**2**): colorless oil; $[\alpha]_D^{20} -12$ (c 0.20, MeOH); UV (MeOH) λ_{\max} 268 nm; ¹H and ¹³C NMR data, Table 1; HRESIMS m/z 297.1700 [M + H]⁺ (C₁₆H₂₅O₅, calcd. 297.1702).

Pestalothol K (**3**): colorless oil; $[\alpha]_D^{20} +111$ (c 0.25, MeOH); UV (MeOH) λ_{\max} 246 nm; ¹H and ¹³C NMR data, Table 1; HRESIMS m/z 297.1700 [M + H]⁺ (C₁₆H₂₅O₅, calcd. 297.1702).

Pestalothol L (**4**): colorless oil; $[\alpha]_D^{20} -60$ (c 0.30, MeOH); UV (MeOH) λ_{\max} 260 nm; ¹H and ¹³C NMR data, Table 2; HRESIMS m/z 317.1362 [M + Na]⁺ (C₁₆H₂₂O₅Na, calcd. 317.1359).

Pestalothol M (**5**): colorless oil; $[\alpha]_D^{20} +17$ (c 0.25, MeOH); UV (MeOH) λ_{\max} 262 nm; ¹H and ¹³C NMR data, Table 2; HRESIMS m/z 317.1360 [M + Na]⁺ (C₁₆H₂₂O₅Na, calcd. 317.1359).

Pestalothol N (**6**): colorless oil; $[\alpha]_D^{20} +47$ (c 0.15, MeOH); UV (MeOH) λ_{\max} 219 nm; ¹H and ¹³C NMR data, Table 2; HRESIMS m/z 319.1518 [M + Na]⁺ (C₁₆H₂₄O₅Na, calcd. 319.1516).

Pestalothol O (**7**): colorless oil; $[\alpha]_D^{20} +35$ (c 0.22, MeOH); UV (MeOH) λ_{\max} 218 nm; ¹H and ¹³C NMR data, Table 3; HRESIMS m/z 361.1619 [M + Na]⁺ (C₁₈H₂₆O₆Na, calcd. 361.1622).

Pestalothol P (**8**): colorless oil; $[\alpha]_D^{20} +89$ (c 0.22, MeOH); UV (MeOH) λ_{\max} 282 nm; ¹H and ¹³C NMR data, Table 3; HRESIMS m/z 329.1595 [M + H]⁺ (C₁₆H₂₅O₇, calcd. 329.1595).

Pestalothol Q (**9**): colorless oil; $[\alpha]_D^{20} +121$ (c 0.15, MeOH); UV (MeOH) λ_{\max} 279 nm; ¹H and ¹³C NMR data, Table 3; HRESIMS m/z 355.1754 [M + H]⁺ (C₁₈H₂₇O₇, calcd. 355.1757).

Cytosporin O (**15**): colorless oil; $[\alpha]_D^{20} -8$ (c 0.30, MeOH); UV (MeOH) λ_{\max} 243 nm; ¹H and ¹³C NMR data, Table 4; HRESIMS m/z 363.2144 [M + Na]⁺ (C₁₉H₃₂O₅Na, calcd. 363.2142).

Cytosporin P (**16**): colorless oil; $[\alpha]_D^{20} -4$ (c 0.35, MeOH); UV (MeOH) λ_{\max} 240 nm; ¹H and ¹³C NMR data, Table 4; HRESIMS m/z 379.2094 [M + Na]⁺ (C₁₉H₃₂O₆Na, calcd. 379.2091).

Cytosporin Q (**17**): colorless oil; $[\alpha]_D^{20} +16$ (c 0.22, MeOH); UV (MeOH) λ_{\max} 237 nm; ¹H and ¹³C NMR data, Table 4; HRESIMS m/z 356.2432 [M + NH₄]⁺ (C₁₉H₃₄O₅N, calcd. 356.2431).

Cytosporin R (**18**): colorless oil; $[\alpha]_D^{20} +6$ (c 0.20, MeOH); UV (MeOH) λ_{\max} 239 nm; ¹H and ¹³C NMR data, Table 5; HRESIMS m/z 355.2117 [M + H]⁺ (C₁₉H₃₁O₆, calcd. 355.2121).

Cytosporin S (**19**): colorless oil; $[\alpha]_D^{20} +14$ (c 0.10, MeOH); UV (MeOH) λ_{\max} 239 nm; ¹H and ¹³C NMR data, Table 5; HRESIMS m/z 377.1934 [M + Na]⁺ (C₁₉H₃₀NaO₆, calcd. 377.1935).

Cytosporin T (20): colorless oil; $[\alpha]_D^{20} -1$ (c 0.20, MeOH); UV (MeOH) λ_{\max} 238 nm; ^1H and ^{13}C NMR data, Table 5; HRESIMS m/z 377.1931 $[\text{M} + \text{Na}]^+$ ($\text{C}_{19}\text{H}_{30}\text{O}_6\text{Na}$, calcd. 377.1935).

Cytosporin U (21): colorless oil; $[\alpha]_D^{20} +4$ (c 0.20, MeOH); UV (MeOH) λ_{\max} 237 nm; ^1H and ^{13}C NMR data, Table 6; HRESIMS m/z 372.2381 $[\text{M} + \text{NH}_4]^+$ ($\text{C}_{19}\text{H}_{34}\text{NO}_6$, calcd. 372.2381), 377.1935 $[\text{M} + \text{Na}]^+$ ($\text{C}_{19}\text{H}_{30}\text{O}_6\text{Na}$, calcd. 377.1935).

Cytosporin V (22): colorless oil; $[\alpha]_D^{20} -21$ (c 0.30, MeOH); UV (MeOH) λ_{\max} 237 nm; ^1H and ^{13}C NMR data, Table 6; HRESIMS m/z 398.2537 $[\text{M} + \text{NH}_4]^+$ ($\text{C}_{21}\text{H}_{36}\text{NO}_6$, calcd. 398.2537), 403.2089 $[\text{M} + \text{Na}]^+$ ($\text{C}_{21}\text{H}_{32}\text{O}_6\text{Na}$, calcd. 403.2091).

Cytosporin W (23): colorless oil; $[\alpha]_D^{20} -4$ (c 0.10, MeOH); UV (MeOH) λ_{\max} 215, 281 nm; ^1H and ^{13}C NMR data, Table 6; HRESIMS m/z 359.1829 $[\text{M} + \text{Na}]^+$ ($\text{C}_{19}\text{H}_{28}\text{O}_5\text{Na}$, calcd. 359.1829).

3.4. Preparation of (R)- and (S)-MTPA Esters

Compound **1** (0.8 mg) was dissolved in pyridine- d_6 (500 μL) and then transferred to an NMR tube. (S)-MTPACl (10.0 μL , 0.050 mmol) was added quickly. By shaking the NMR tube, the reagent and the dissolved compound were mixed. After 10 h at room temperature, ^1H NMR data were obtained for the (R)-MTPA ester (**1a**). Following the same protocol, the (S)-MTPA ester (**1b**) was produced. A similar procedure was applied for compound **8**.

3.5. Preparation of Compound 17a

Compound **17** (10 mg, 0.030 mmol) was dissolved in anhydrous CH_2Cl_2 (3 mL) together with catalytic amount of DMAP and 10.0 mg of 4,4'-dimethoxytrytil chloride (0.030 mmol, DMTCl) at room temperature for 2 h. After removal of the solvent, preparative thin-layer chromatography was used for purification, using CH_2Cl_2 -MeOH (95:5), to give compound **17a**.

3.6. Preparation of (R)- and (S)-MPA Esters

Compound **7** (0.8 mg, 0.002 mmol), along with DMAP (0.5 mg, 0.004 mmol), N,N' -dicyclohexylcarbodiimide (0.8 mg, 0.004 mmol, DCC) and (R)-MPA (0.7 mg, 0.004 mmol), was mixed in anhydrous CH_2Cl_2 (0.3 mL). The solvent was removed after 2 h at room temperature. The (R)-MPA ester (**7a**) was obtained from the crude product by semipreparative HPLC (MeOH- H_2O : 0–2 min, 40%; 2–15 min; 15–25 min, 100%). Following a similar procedure, the (S)-MPA ester (**7b**) was obtained by using (S)-MPA. The above steps were also applied to compounds **17a**, **18**, **25**, and **26**.

3.7. Cytotoxicity and Antibacterial Assay

The MTT method was applied for the cytotoxicity assay against the mouse lymphoma cell line L5178Y as described before [24]. Antibacterial activity against Gram-positive bacteria *Staphylococcus aureus* (ATCC 29213) and *Mycobacterium tuberculosis* (H37Rv), and the Gram-negative bacteria *Pseudomonas aeruginosa* (ATCC 27853) and drug-resistant *Acinetobacter baumannii* (ATCC BAA-1605), was evaluated using the microdilution method in alignment with the CLSI guidelines using Muller Hinton broth for bacteria and 7H9 broth for *Mycobacteria* [25]. Additionally, the antibacterial activity was performed in combination with sublethal concentrations of the antibiotic colistin (0.1 μM) for drug-resistant *A. baumannii* (ATCC BAA-1605) to elucidate synergistic effects of the combinatory therapy.

Supplementary Materials: The following are available online at <http://www.mdpi.com/1660-3397/18/2/129/s1>, UV, HRMS, 1D and 2D NMR spectra of all the new compounds **1–9** and **15–23** as well as spectra for Mosher's esters of **1**, **7**, **8**, **17**, **18**, **25** and **26**.

Author Contributions: Investigation, X.Y., W.E.G.M., D.M., R.K., Z.G., and K.Z.; resources, B.O.U.; writing—original draft preparation, X.Y.; writing—review and editing and supervision, Z.L. and P.P. All authors have read and agreed to the published version of the manuscript.

Funding: This project was supported by grants of the DFG (GRK 2158, project number 270650915) to P.P. and R.K. and by the Manchot Foundation to P.P.

Acknowledgments: Xiaoqin Yu is grateful to China Scholarship Council, the Ministry of Education of China for a doctoral scholarship.

Conflicts of Interest: The authors declare no conflict of interest.

References

1. Surup, F.; Stadler, M. Natural products in the chemical industry. Von Bernd Schaefer. *Angew. Chem.* **2015**, *127*, 8999–9000. [\[CrossRef\]](#)
2. Petersen, A.B.; Rønne, M.H.; Larsen, T.O.; Clausen, M.H. The Chemistry of Griseofulvin. *Chem. Rev.* **2014**, *114*, 12088–12107. [\[CrossRef\]](#) [\[PubMed\]](#)
3. Tobert, J.A. Lovastatin and beyond: The history of the HMG-CoA reductase inhibitors. *Nat. Rev. Drug Discov.* **2003**, *2*, 517–526. [\[CrossRef\]](#)
4. Watts, R.; Clunie, G.; Hall, F.; Marshall, T. *Rheumatology*; Oxford University Press: New York, NY, USA, 2009; p. 558.
5. Kusari, S.; Pandey, S.P.; Spiteller, M. Untapped mutualistic paradigms linking host plant and endophytic fungal production of similar bioactive secondary metabolites. *Phytochem.* **2013**, *91*, 81–87. [\[CrossRef\]](#) [\[PubMed\]](#)
6. Deshmukh, S.; Prakash, V.; Ranjan, N. Recent advances in the discovery of bioactive metabolites from *Pestalotiopsis*. *Phytochem. Rev.* **2017**, *71*, 882. [\[CrossRef\]](#)
7. Maharachchikumbura, S.; Hyde, K.; Groenewald, J.; Xu, J.; Crous, P. *Pestalotiopsis* revisited. *Stud. Mycol.* **2014**, *79*, 121–186. [\[CrossRef\]](#)
8. Xu, J.; Ebada, S.S.; Proksch, P. *Pestalotiopsis* a highly creative genus: Chemistry and bioactivity of secondary metabolites. *Fungal Divers.* **2010**, *44*, 15–31. [\[CrossRef\]](#)
9. Yang, X.-L.; Zhang, J.-Z.; Luo, D.-Q. The taxonomy, biology and chemistry of the fungal *Pestalotiopsis* genus. *Nat. Prod. Rep.* **2012**, *29*, 622. [\[CrossRef\]](#)
10. Li, E.; Jiang, L.; Guo, L.; Zhang, H.; Che, Y. Pestalachlorides A–C, antifungal metabolites from the plant endophytic fungus *Pestalotiopsis adusta*. *Bioorganic Med. Chem.* **2008**, *16*, 7894–7899. [\[CrossRef\]](#)
11. Liu, L.; Liu, S.; Jiang, L.; Chen, X.; Guo, L.; Che, Y. ChemInform Abstract: Chloropupukeanin, the First Chlorinated Pupukeanane Derivative, and Its Precursors from *Pestalotiopsis fici*. *ChemInform* **2008**, *39*, 1397–1400. [\[CrossRef\]](#)
12. Ding, G.; Zhang, F.; Chen, H.; Guo, L.; Zou, Z.; Che, Y. Pestaloquinols A and B, Isoprenylated Epoxyquinols from *Pestalotiopsis* sp. *J. Nat. Prod.* **2011**, *74*, 286–291. [\[CrossRef\]](#) [\[PubMed\]](#)
13. Zhang, Y.L.; Ge, H.M.; Li, F.; Song, Y.C.; Tan, R.X. New Phytotoxic Metabolites from *Pestalotiopsis* sp. HC02, a Fungus Residing in *Chondracris rosea* Gut. *Chem. Biodivers.* **2008**, *5*, 2402–2407. [\[CrossRef\]](#) [\[PubMed\]](#)
14. Liu, S.; Dai, H.; Makhoulfi, G.; Heering, C.; Janiak, C.; Hartmann, R.; Mandi, A.; Kurtán, T.; Müller, W.E.G.; Kassack, M.U.; et al. Cytotoxic 14-Membered Macrolides from a Mangrove-Derived Endophytic Fungus, *Pestalotiopsis microspora*. *J. Nat. Prod.* **2016**, *79*, 2332–2340. [\[CrossRef\]](#)
15. Zhao, Y.; Liu, N.; Proksch, P.; Zhou, D.; Lin, W. Truncateols O–V, further isoprenylated cyclohexanols from the sponge-associated fungus *Truncatella angustata* with antiviral activities. *Phytochemistry* **2018**, *155*, 61–68. [\[CrossRef\]](#)
16. Zhao, Y.; Si, L.; Liu, N.; Proksch, P.; Zhou, D.; Lin, W. Truncateols A–N, new isoprenylated cyclohexanols from the sponge-associated fungus *Truncatella angustata* with anti-H1N1 virus activities. *Tetrahedron* **2015**, *71*, 2708–2718. [\[CrossRef\]](#)
17. Li, E.; Tian, R.; Liu, S.; Chen, X.; Guo, L.; Che, Y. Pestalotheols A–D, Bioactive Metabolites from the Plant Endophytic Fungus *Pestalotiopsis theae*. *J. Nat. Prod.* **2008**, *71*, 664–668. [\[CrossRef\]](#) [\[PubMed\]](#)
18. Ciavatta, M.L.; López-Gresa, M.P.; Gavagnin, M.; Nicoletti, R.; Manzo, E.; Mollo, E.; Guo, Y.-W.; Cimino, G. Cytosporin-related compounds from the marine-derived fungus *Eutypella scoparia*. *Tetrahedron* **2008**, *64*, 5365–5369. [\[CrossRef\]](#)
19. Akone, S.H.; El Amrani, M.; Lin, W.; Lai, D.; Proksch, P. Cytosporins F–K, new epoxyquinols from the endophytic fungus *Pestalotiopsis theae*. *Tetrahedron Lett.* **2013**, *54*, 6751–6754. [\[CrossRef\]](#)

20. Stevens-Miles, S.; Goetz, M.A.; Bills, G.; Giacobbe, R.A.; Tkacz, J.S.; Chang, R.S.L.; Mojena, M.; Martín, I.; Díez, M.T.; Pelae, F.; et al. Discovery of an Angiotensin II Binding Inhibitor from a *Cytospora* sp. Using Semi-automated Screening Procedures. *J. Antibiot.* **1996**, *49*, 119–123. [[CrossRef](#)]
21. Liao, H.-X.; Sun, D.-W.; Zheng, C.-J.; Wang, C. A new hexahydrobenzopyran derivative from the gorgonian-derived Fungus *Eutypella* sp. *Nat. Prod. Res.* **2017**, *31*, 1640–1646. [[CrossRef](#)]
22. Rivera-Chávez, J.; Zacatenco-Abarca, J.; Morales-Jiménez, J.; Martínez-Aviña, B.; Hernández-Ortega, S.; Aguilar-Ramírez, E. Cuautepestalorin, a 7,8-Dihydrochromene–Oxoisochromane Adduct Bearing a Hexacyclic Scaffold from *Pestalotiopsis* sp. IQ-011. *Org. Lett.* **2019**, *21*, 3558–3562. [[CrossRef](#)] [[PubMed](#)]
23. Kjer, J.; Debbab, A.; Aly, A.H.; Proksch, P. Methods for isolation of marine-derived endophytic fungi and their bioactive secondary products. *Nat. Protoc.* **2010**, *5*, 479–490. [[CrossRef](#)] [[PubMed](#)]
24. Ashour, M.; Edrada, R.; Ebel, R.; Wray, V.; Wätjen, W.; Padmakumar, K.; Müller, W.E.G.; Lin, W.H.; Proksch, P. Kahalalide Derivatives from the Indian Sacoglossan Mollusk *Elysia grandifolia*. *J. Nat. Prod.* **2006**, *69*, 1547–1553. [[CrossRef](#)] [[PubMed](#)]
25. Hecht, D.W.; Citron, D.M.; Cox, M.; Jacobus, N.; Jenkins, S.G.; Onderdonk, A.; Wexler, H.M. *Methods for Antimicrobial Susceptibility Testing of Anaerobic Bacteria: Approved Standard*; Clinical and Laboratory Standards Institute: Wayne, PA, USA, 2007; pp. 1–47.



© 2020 by the authors. Licensee MDPI, Basel, Switzerland. This article is an open access article distributed under the terms and conditions of the Creative Commons Attribution (CC BY) license (<http://creativecommons.org/licenses/by/4.0/>).

Support Information

Polyketide derivatives from mangrove derived endophytic fungus *Pseudopestalotiopsis theae*

Xiaoqin Yu ^{1,2}, Werner E. G. Müller ³, Dieter Meier ¹, Rainer Kalscheuer ¹, Zhiyong Guo ², Kun Zou ², Blessing O. Umeokoli ⁴, Zhen Liu ^{1,*} and Peter Proksch ^{1,2,*}

¹ Institute of Pharmaceutical Biology and Biotechnology, Heinrich-Heine-University Duesseldorf, 40225 Duesseldorf, Germany; xiyu101@hhu.de (X.Y.); dieter.meier@hhu.de (D.M.); Rainer.Kalscheuer@hhu.de (R.K.)

² Hubei Key Laboratory of Natural Products Research and Development, College of Biological and Pharmaceutical Sciences, China Three Gorges University, Yichang 443002, People's Republic of China; zhyguoctgu@foxmail.com (Z.G.); kzou@ctgu.edu.cn (K.Z.)

³ Institute of Physiological Chemistry, Universitätsmedizin der Johannes Gutenberg-Universität Mainz, 55128 Mainz, Germany; wmueller@uni-mainz.de (W.E.G.M.)

⁴ Department of Pharmaceutical and Medicinal Chemistry, Nnamdi Azikiwe University, Awka, Nigeria; blessingumeokoli@gmail.com (B.O.U.)

* Correspondence: zhenfeizi0@sina.com (Z.L.); proksch@uni-duesseldorf (P.P.); Tel.: +49-211-81-14163

Table of contents

Figure S1. HRESIMS of 1.....	63
Figure S2. UV spectrum of 1.....	63
Figure S3. ¹ H-NMR (600 MHz, DMSO- <i>d</i> ₆) spectrum of 1.....	64
Figure S4. ¹³ C-NMR (150 MHz, DMSO- <i>d</i> ₆) spectrum of 1.....	64
Figure S5. ¹ H- ¹ H COSY (600 MHz, DMSO- <i>d</i> ₆) spectrum of 1.....	65
Figure S6. HSQC (600 MHz, DMSO- <i>d</i> ₆) spectrum of 1.....	65
Figure S7. HMBC (600 MHz, DMSO- <i>d</i> ₆) spectrum of 1.....	66
Figure S8. ROESY (600 MHz, DMSO- <i>d</i> ₆) spectrum of 1.....	66
Figure S9. HRESIMS of 2.....	67
Figure S10. UV spectrum of 2.....	67
Figure S11. ¹ H-NMR (600 MHz, DMSO- <i>d</i> ₆) spectrum of 2.....	68
Figure S12. ¹ H- ¹ H COSY (600 MHz, DMSO- <i>d</i> ₆) spectrum of 2.....	68
Figure S13. HSQC (600 MHz, DMSO- <i>d</i> ₆) spectrum of 2.....	69
Figure S14. HMBC (600 MHz, DMSO- <i>d</i> ₆) spectrum of 2.....	69
Figure S15. ROESY (600 MHz, DMSO- <i>d</i> ₆) spectrum of 2.....	70
Figure S16. HRESIMS of 3.....	70
Figure S17. UV spectrum of 3.....	71
Figure S18. ¹ H-NMR (600 MHz, Acetone- <i>d</i> ₆) spectrum of 3.....	71
Figure S19. ¹³ C-NMR (150 MHz, Acetone- <i>d</i> ₆) spectrum of 3.....	72
Figure S20. ¹ H- ¹ H COSY (600 MHz, Acetone- <i>d</i> ₆) spectrum of 3.....	72
Figure S21. HSQC (600 MHz, Acetone- <i>d</i> ₆) spectrum of 3.....	73
Figure S22. HMBC (600 MHz, Acetone- <i>d</i> ₆) spectrum of 3.....	73
Figure S23. ROESY (600 MHz, Acetone- <i>d</i> ₆) spectrum of 3.....	74
Figure S24. HRESIMS of 4.....	74
Figure S25. UV spectrum of 4.....	75
Figure S26. ¹ H-NMR (600 MHz, DMSO- <i>d</i> ₆) spectrum of 4.....	75
Figure S27. ¹³ C-NMR (150 MHz, DMSO- <i>d</i> ₆) spectrum of 4.....	76
Figure S28. ¹ H- ¹ H COSY (600 MHz, DMSO- <i>d</i> ₆) spectrum of 4.....	76
Figure S29. HSQC (600 MHz, DMSO- <i>d</i> ₆) spectrum of 4.....	77
Figure S30. HMBC (600MHz, DMSO- <i>d</i> ₆) spectrum of 4.....	77
Figure S31. ROESY (600 MHz, DMSO- <i>d</i> ₆) spectrum of 4.....	78
Figure S32. HRESIMS of 5.....	78
Figure S33. UV spectrum of 5.....	78
Figure S34. ¹ H-NMR (600 MHz, DMSO- <i>d</i> ₆) spectrum of 5.....	79
Figure S35. ¹ H- ¹ H COSY (600 MHz, DMSO- <i>d</i> ₆) spectrum of 5.....	79
Figure S36. HSQC (600 MHz, DMSO- <i>d</i> ₆) spectrum of 5.....	80
Figure S37. HMBC (600MHz, DMSO- <i>d</i> ₆) spectrum of 5.....	80
Figure S38. ROESY (600 MHz, DMSO- <i>d</i> ₆) spectrum of 5.....	81
Figure S39. HRESIMS of 6.....	81
Figure S40. UV spectrum of 6.....	82
Figure S41. ¹ H-NMR (600 MHz, DMSO- <i>d</i> ₆) spectrum of 6.....	82
Figure S42. ¹³ C-NMR (150 MHz, DMSO- <i>d</i> ₆) spectrum of 6.....	83
Figure S43. ¹ H- ¹ H COSY (600 MHz, DMSO- <i>d</i> ₆) spectrum of 6.....	83

Figure S44. HSQC (600 MHz, DMSO- <i>d</i> ₆) spectrum of 6	84
Figure S45. HMBC (600 MHz, DMSO- <i>d</i> ₆) spectrum of 6	84
Figure S46. ROESY (600 MHz, DMSO- <i>d</i> ₆) spectrum of 6	85
Figure S47. HRESIMS of 7	85
Figure S48. UV spectrum of 7	85
Figure S49. ¹ H-NMR (600 MHz, DMSO- <i>d</i> ₆) spectrum of 7	86
Figure S50. ¹³ C-NMR (150 MHz, DMSO- <i>d</i> ₆) spectrum of 7	86
Figure S51. ¹ H- ¹ H COSY (600 MHz, DMSO- <i>d</i> ₆) spectrum of 7	87
Figure S52. HSQC (600 MHz, DMSO- <i>d</i> ₆) spectrum of 7	87
Figure S53. HMBC (600 MHz, DMSO- <i>d</i> ₆) spectrum of 7	88
Figure S54. ROESY (600 MHz, DMSO- <i>d</i> ₆) spectrum of 7	88
Figure S55. HREISMS of 8	89
Figure S56. UV spectrum of 8	89
Figure S57. ¹ H-NMR (600 MHz, Acetone- <i>d</i> ₆) spectrum of 8	90
Figure S58. ¹³ C-NMR (150 MHz, Acetone- <i>d</i> ₆) spectrum of 8	90
Figure S59. ¹ H- ¹ H COSY (600 MHz, Acetone- <i>d</i> ₆) spectrum of 8	91
Figure S60. HSQC (600 MHz, Acetone- <i>d</i> ₆) spectrum of 8	91
Figure S61. HMBC (600 MHz, Acetone- <i>d</i> ₆) spectrum of 8	92
Figure S62. ROESY (600 MHz, Acetone- <i>d</i> ₆) spectrum of 8	92
Figure S63. HREISMS of 9	93
Figure S64. UV spectrum of 9	93
Figure S65. ¹ H-NMR (600 MHz, DMSO- <i>d</i> ₆) spectrum of 9	94
Figure S66. ¹ H- ¹ H COSY (600 MHz, DMSO- <i>d</i> ₆) spectrum of 9	94
Figure S67. HSQC (600 MHz, DMSO- <i>d</i> ₆) spectrum of 9	95
Figure S68. HMBC (600 MHz, DMSO- <i>d</i> ₆) spectrum of 9	95
Figure S69. ROESY (600 MHz, DMSO- <i>d</i> ₆) spectrum of 9	96
Figure S70. HREISMS of 15	96
Figure S71. UV spectrum of 15	97
Figure S72. ¹ H-NMR (600 MHz, DMSO- <i>d</i> ₆) spectrum of 15	97
Figure S73. ¹³ C-NMR (150 MHz, DMSO- <i>d</i> ₆) spectrum of 15	98
Figure S74. ¹ H- ¹ H COSY (600 MHz, DMSO- <i>d</i> ₆) spectrum of 15	98
Figure S75. HSQC (600 MHz, DMSO- <i>d</i> ₆) spectrum of 15	99
Figure S76. HMBC (600 MHz, DMSO- <i>d</i> ₆) spectrum of 15	99
Figure S77. ROESY (600 MHz, DMSO- <i>d</i> ₆) spectrum of 15	100
Figure S78. HREISMS of 16	100
Figure S79. UV spectrum of 16	101
Figure S80. ¹ H-NMR (600 MHz, DMSO- <i>d</i> ₆) spectrum of 16	101
Figure S81. ¹³ C-NMR (150 MHz, DMSO- <i>d</i> ₆) spectrum of 16	102
Figure S82. ¹ H- ¹ H COSY (600 MHz, DMSO- <i>d</i> ₆) spectrum of 16	102
Figure S83. HSQC (600 MHz, DMSO- <i>d</i> ₆) spectrum of 16	103
Figure S84. HMBC (600 MHz, DMSO- <i>d</i> ₆) spectrum of 16	103
Figure S85. ROESY (600 MHz, DMSO- <i>d</i> ₆) spectrum of 16	104
Figure S86. HREISMS of 17	104
Figure S87. UV spectrum of 17	105

Figure S88. ^1H -NMR (300 MHz, $\text{DMSO-}d_6$) spectrum of 17	105
Figure S89. ^{13}C -NMR (75 MHz, $\text{DMSO-}d_6$) spectrum of 17	106
Figure S90. ^1H - ^1H COSY (300 MHz, $\text{DMSO-}d_6$) spectrum of 17	106
Figure S91. HSQC (300 MHz, $\text{DMSO-}d_6$) spectrum of 17	107
Figure S92. HMBC (300 MHz, $\text{DMSO-}d_6$) spectrum of 17	107
Figure S93. ROESY (300 MHz, $\text{DMSO-}d_6$) spectrum of 17	108
Figure S94. HREISMS of 18	108
Figure S95. UV spectrum of 18	109
Figure S96. ^1H -NMR (300 MHz, $\text{DMSO-}d_6$) spectrum of 18	109
Figure S97. ^{13}C -NMR (75 MHz, $\text{DMSO-}d_6$) spectrum of 18	110
Figure S98. ^1H - ^1H COSY (300 MHz, $\text{DMSO-}d_6$) spectrum of 18	110
Figure S99. HSQC (300 MHz, $\text{DMSO-}d_6$) spectrum of 18	111
Figure S100. HMBC (300 MHz, $\text{DMSO-}d_6$) spectrum of 18	111
Figure S101. ROESY (300 MHz, $\text{DMSO-}d_6$) spectrum of 18	112
Figure S102. HREISMS of 19	112
Figure S103. UV spectrum of 19	113
Figure S104. ^1H -NMR (600 MHz, $\text{DMSO-}d_6$) spectrum of 19	113
Figure S105. ^1H - ^1H COSY (600 MHz, $\text{DMSO-}d_6$) spectrum of 19	114
Figure S106. HSQC (600MHz, $\text{DMSO-}d_6$) spectrum of 19	114
Figure S107. HMBC (600MHz, $\text{DMSO-}d_6$) spectrum of 19	115
Figure S108. ROESY (600 MHz, $\text{DMSO-}d_6$) spectrum of 19	115
Figure S109. HREISMS of 20	116
Figure S110. The UV spectrum of 20	116
Figure S111. The ^1H -NMR (600 MHz, $\text{DMSO-}d_6$) spectrum of 20	117
Figure S112. ^1H - ^1H COSY (600 MHz, $\text{DMSO-}d_6$) spectrum of 20	117
Figure S113. HSQC (600 MHz, $\text{DMSO-}d_6$) spectrum of 20	118
Figure S114. HMBC (600 MHz, $\text{DMSO-}d_6$) spectrum of 20	118
Figure S115. ROESY ((600 MHz, $\text{DMSO-}d_6$) spectrum of 20	119
Figure S116. HREISMS of 21	119
Figure S117. UV spectrum of 21	120
Figure S118. ^1H -NMR (300 MHz, $\text{DMSO-}d_6$) spectrum of 21	120
Figure S119. ^{13}C -NMR (75 MHz, $\text{DMSO-}d_6$) spectrum of 21	121
Figure S120. ^1H - ^1H COSY (300 MHz, $\text{DMSO-}d_6$) spectrum of 21	121
Figure S121. HSQC (300 MHz, $\text{DMSO-}d_6$) spectrum of 21	122
Figure S122. HMBC (300 MHz, $\text{DMSO-}d_6$) spectrum of 21	122
Figure S123. ROESY (300 MHz, $\text{DMSO-}d_6$) spectrum of 21	123
Figure S124. HREISMS of 22	123
Figure S125. UV spectrum of 22	124
Figure S126. ^1H -NMR (600 MHz, $\text{DMSO-}d_6$) spectrum of 22	124
Figure S127. ^{13}C -NMR (150 MHz, $\text{DMSO-}d_6$) spectrum of 22	125
Figure S128. ^1H - ^1H COSY (600 MHz, $\text{DMSO-}d_6$) spectrum of 22	125
Figure S129. HSQC (600 MHz, $\text{DMSO-}d_6$) spectrum of 22	126
Figure S130. HMBC (600 MHz, $\text{DMSO-}d_6$) spectrum of 22	126
Figure S131. ROESY (600 MHz, $\text{DMSO-}d_6$) spectrum of 22	127

Figure S132. HREISMS of 23 .	127
Figure S133. UV spectrum of 23 .	128
Figure S134. ^1H -NMR (600 MHz, $\text{DMSO-}d_6$) spectrum of 23 .	128
Figure S135. ^1H - ^1H COSY (600 MHz, $\text{DMSO-}d_6$) spectrum of 23 .	129
Figure S136. HSQC (600 MHz, $\text{DMSO-}d_6$) spectrum of 23 .	129
Figure S137. HMBC (600 MHz, $\text{DMSO-}d_6$) spectrum of 23 .	130
Figure S138. ROESY (600 MHz, $\text{DMSO-}d_6$) spectrum of 23 .	130
Figure S139. ^1H -NMR (600 MHz, $\text{Prydine-}d_5$) spectrum of 1a .	131
Figure S140. ^1H - ^1H COSY (600 MHz, $\text{Prydine-}d_5$) spectrum of 1a .	131
Figure S141. ESIMS of 1a .	132
Figure S142. ^1H -NMR (600 MHz, $\text{Prydine-}d_5$) spectrum of 1b .	132
Figure S143. ^1H - ^1H COSY (600 MHz, $\text{Prydine-}d_5$) spectrum of 1b .	133
Figure S144. ESIMS of 1b .	133
Figure S145. ^1H -NMR (600 MHz, CD_3OD) spectrum of 7a .	134
Figure S146. ^1H - ^1H COSY (600 MHz, CD_3OD) spectrum of 7a .	134
Figure S147. ESIMS of 7a .	135
Figure S148. ^1H -NMR (600 MHz, CD_3OD) spectrum of 7b .	135
Figure S149. ^1H - ^1H COSY (600 MHz, CD_3OD) spectrum of 7b .	136
Figure S150. ESIMS of 7b .	136
Figure S151. ^1H -NMR (600 MHz, CD_3OD) spectrum of 8a .	137
Figure S152. ^1H - ^1H COSY (600 MHz, CD_3OD) spectrum of 8a .	137
Figure S153. ROESY (600 MHz, CD_3OD) spectrum of 8a .	138
Figure S154. ESIMS of 8a .	138
Figure S155. ^1H -NMR (600 MHz, CD_3OD) spectrum of 8b .	139
Figure S156. ^1H - ^1H COSY (600 MHz, CD_3OD) spectrum of 8b .	139
Figure S157. ROESY (600 MHz, CD_3OD) spectrum of 8b .	140
Figure S158. ESIMS of 8b .	140
Figure S159. ^1H -NMR (600 MHz, CD_3OD) spectrum of 17a .	141
Figure S160. ESIMS of 17a .	141
Figure S161. ^1H -NMR (600 MHz, CD_3OD) spectrum of 17b .	142
Figure S162. ^1H - ^1H COSY (600 MHz, CD_3OD) spectrum of 17b .	142
Figure S163. ESIMS of 17b .	143
Figure S164. ^1H -NMR (600 MHz, CD_3OD) spectrum of 17c .	143
Figure S165. ^1H - ^1H COSY (600 MHz, CD_3OD) spectrum of 17c .	144
Figure S166. ESIMS of 17c .	144
Figure S167. ^1H -NMR (600 MHz, CD_3OD) spectrum of 18a .	145
Figure S168. ^1H - ^1H COSY (600 MHz, CD_3OD) spectrum of 18a .	145
Figure S169. ESIMS of 18a .	146
Figure S170. ^1H -NMR (600 MHz, CD_3OD) spectrum of 18b .	146
Figure S171. ^1H - ^1H COSY (600 MHz, CD_3OD) spectrum of 18b .	147
Figure S172. ESIMS of 18b .	147
Figure S173. ^1H -NMR (600 MHz, CD_3OD) spectrum of 25a .	148
Figure S174. ^1H - ^1H COSY (600 MHz, CD_3OD) spectrum of 25a .	148
Figure S175. ESIMS of 25a .	149

Figure S176. ^1H -NMR (600 MHz, CD_3OD) spectrum of 25b	149
Figure S177. ^1H - ^1H COSY (600 MHz, CD_3OD) spectrum of 25b	150
Figure S178. ESIMS of 25b	150
Figure S179. ^1H -NMR (600 MHz, CD_3OD) spectrum of 26a	151
Figure S180. ^1H - ^1H COSY (600 MHz, CD_3OD) spectrum of 26a	151
Figure S181. ESIMS of 26a	152
Figure S182. ^1H -NMR (600 MHz, CD_3OD) spectrum of 26b	152
Figure S183. ^1H - ^1H COSY (600 MHz, CD_3OD) spectrum of 26b	153
Figure S184. ESIMS of 26b	153
Table S1. SMILES table of 1–26	154
Table S2. Results of cytotoxicity and antibacterial activity assay of 1–26	155

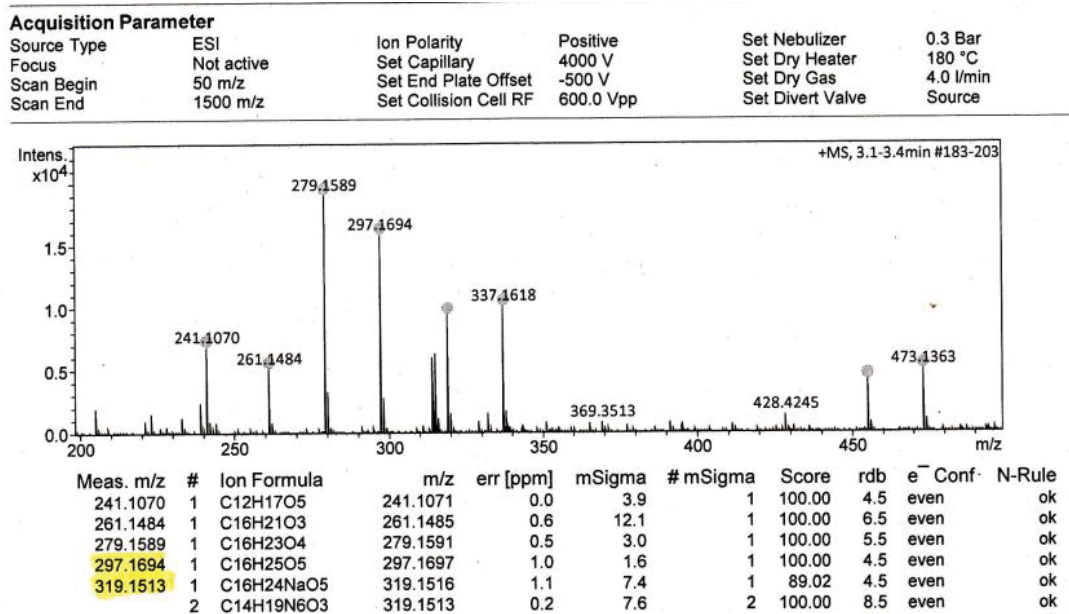


Figure S1. HRESIMS of 1.

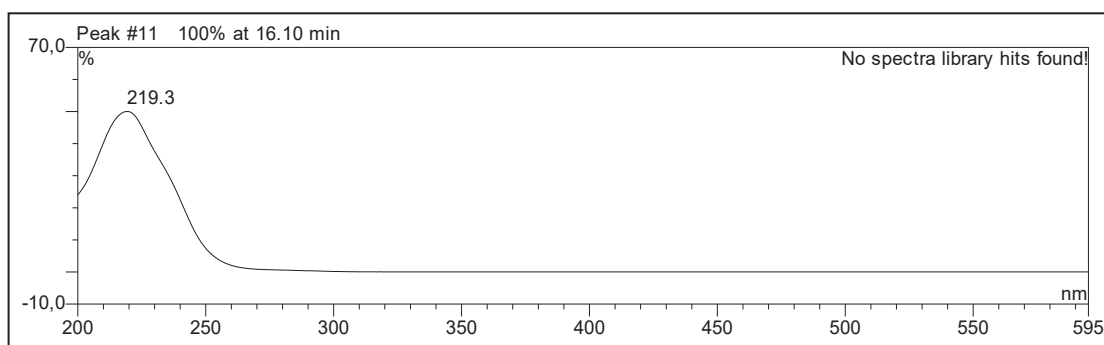


Figure S2. UV spectrum of 1.

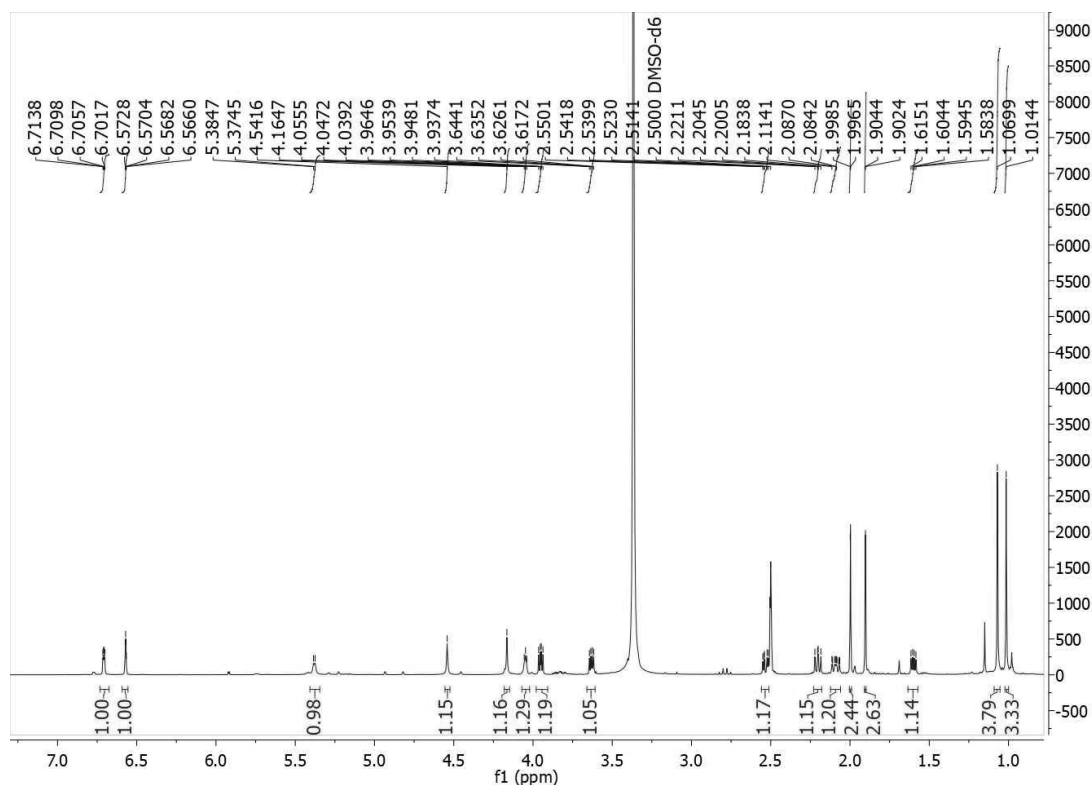


Figure S3. ¹H-NMR (600 MHz, DMSO-*d*₆) spectrum of 1.

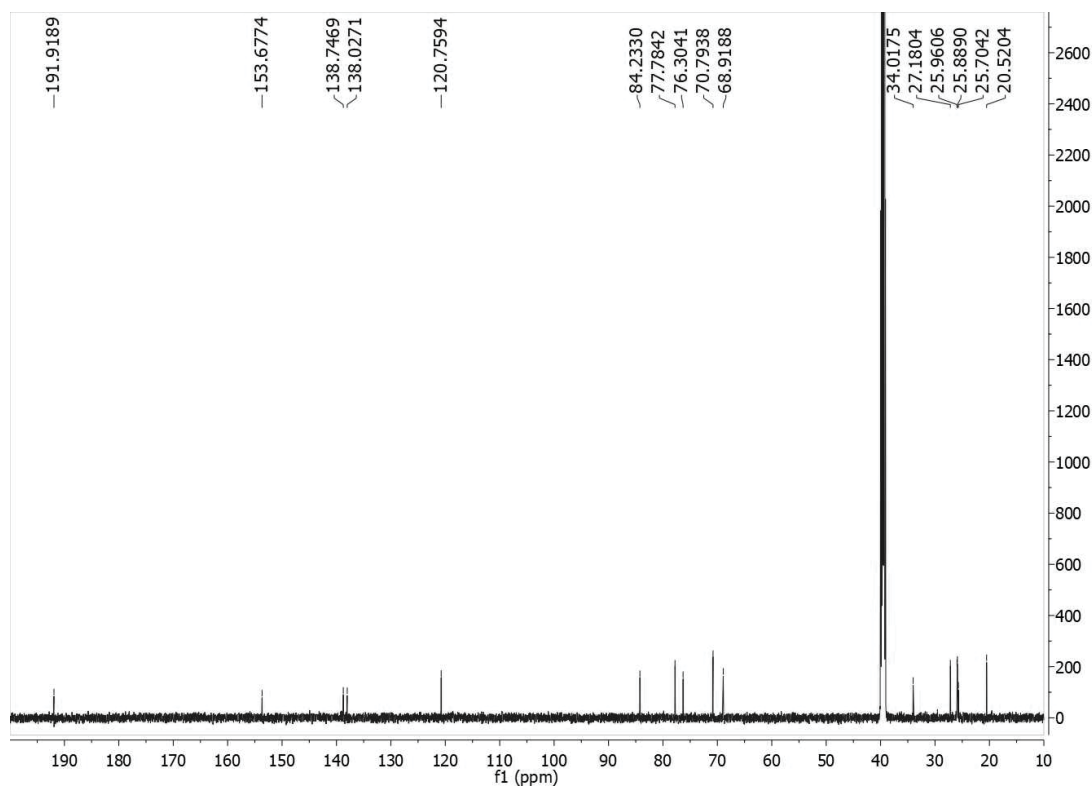


Figure S4. ¹³C-NMR (150 MHz, DMSO-*d*₆) spectrum of 1.

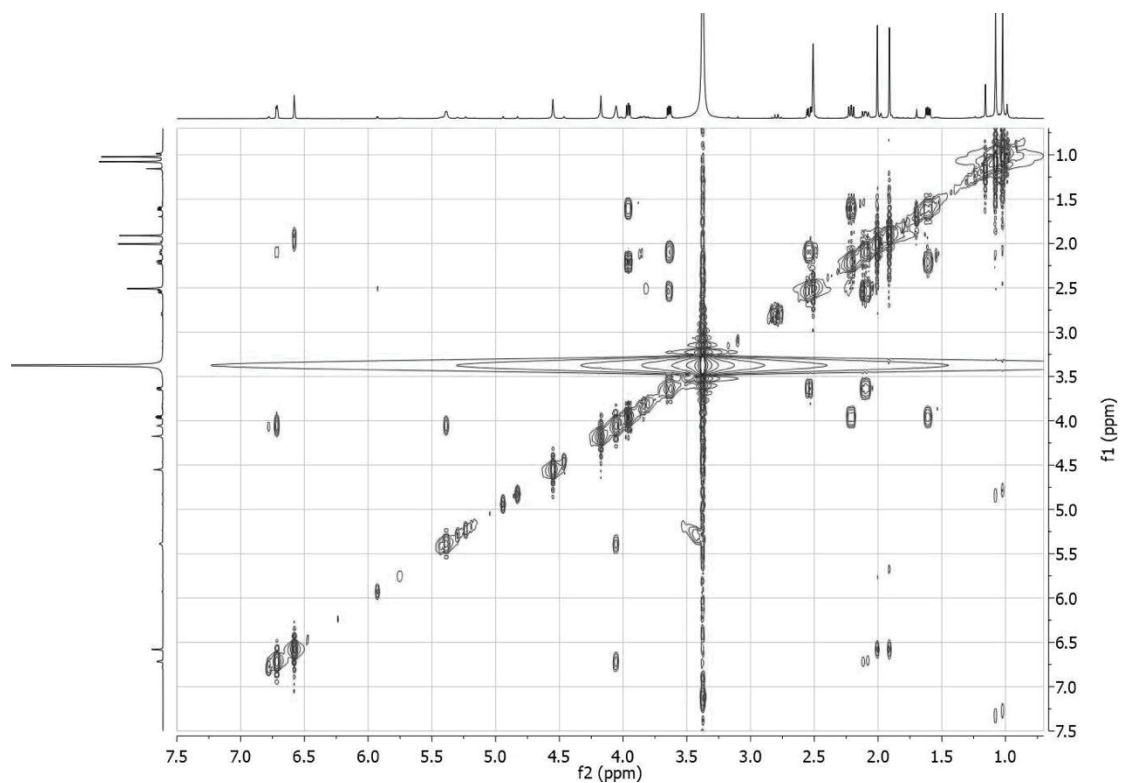


Figure S5. ^1H - ^1H COSY (600 MHz, $\text{DMSO}-d_6$) spectrum of **1**.

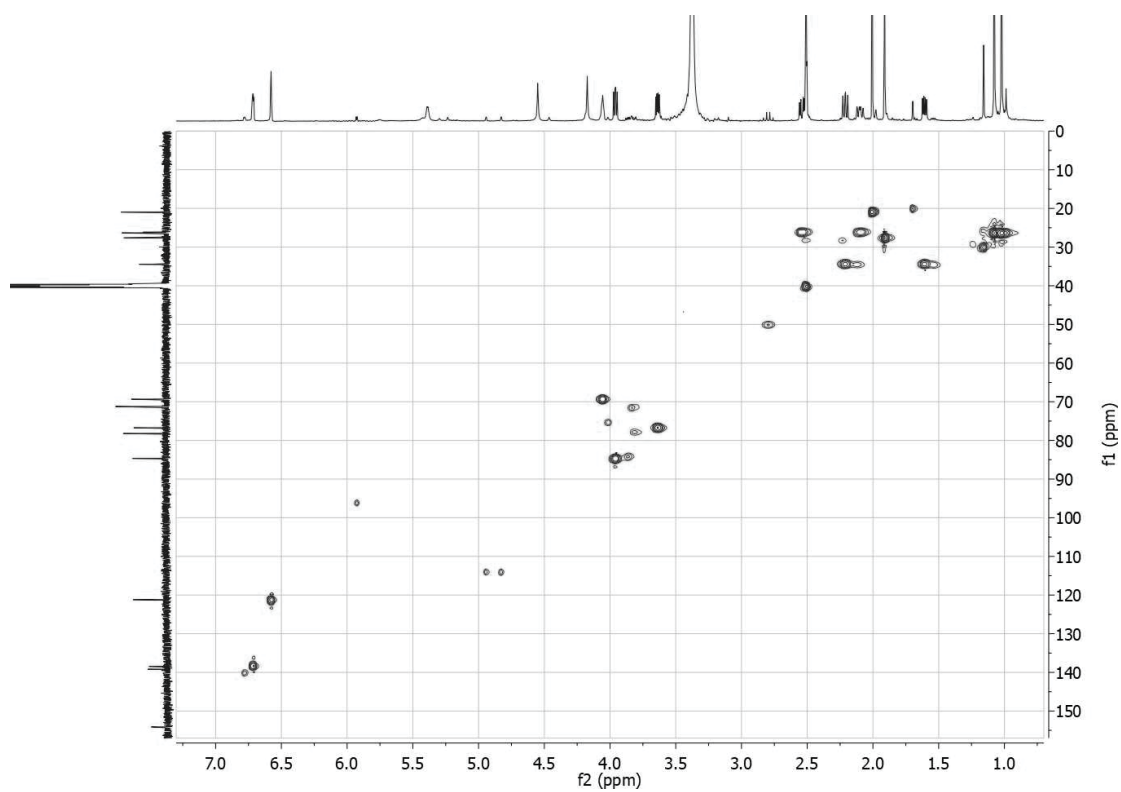


Figure S6. HSQC (600 MHz, $\text{DMSO}-d_6$) spectrum of **1**.

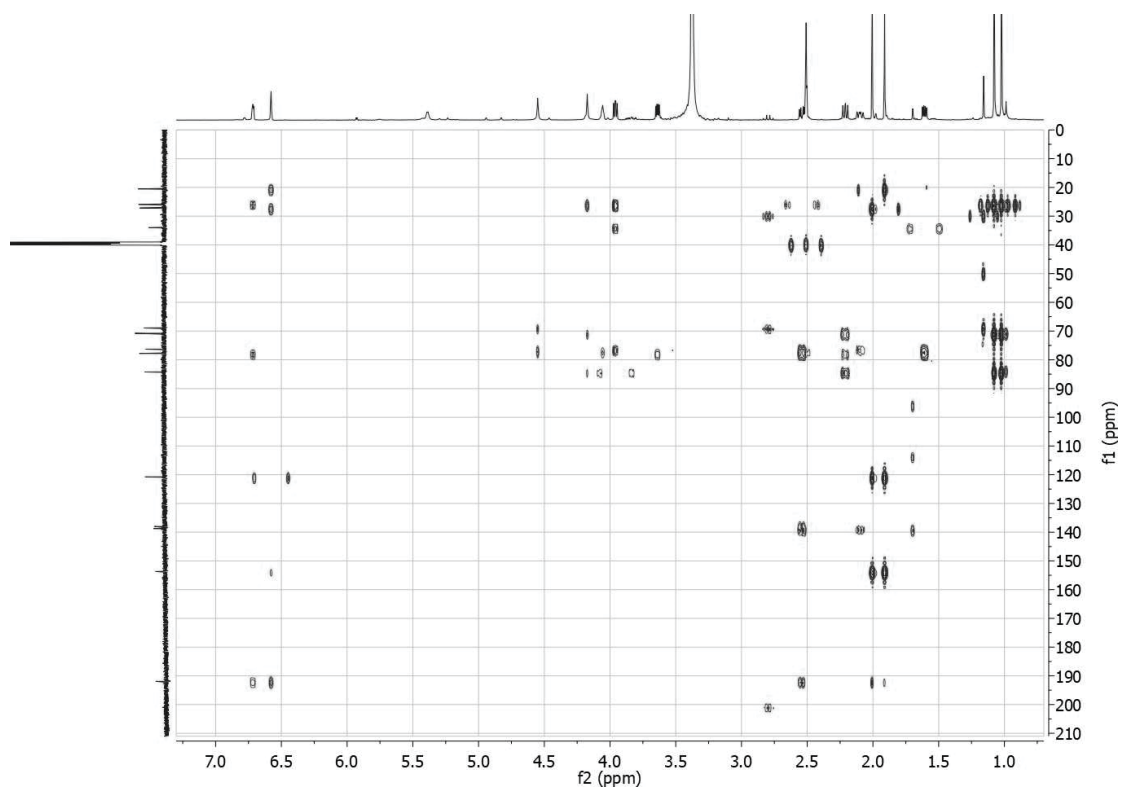


Figure S7. HMBC (600 MHz, DMSO-*d*₆) spectrum of **1**.

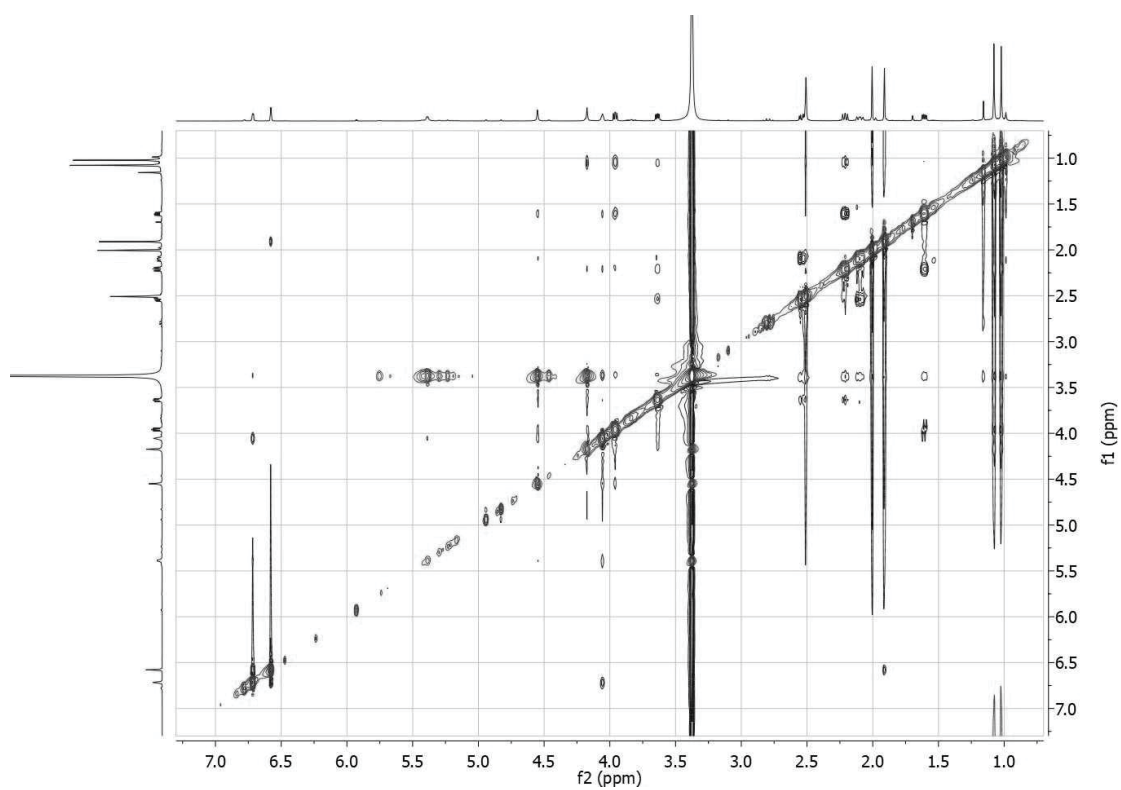


Figure S8. ROESY (600 MHz, DMSO-*d*₆) spectrum of **1**.

10 #364-494 RT: 7.32-8.62 AV: 65 NL: 8.07E6

T: FTMS {1,1} + p ESI Full ms [120.00-2000.00]

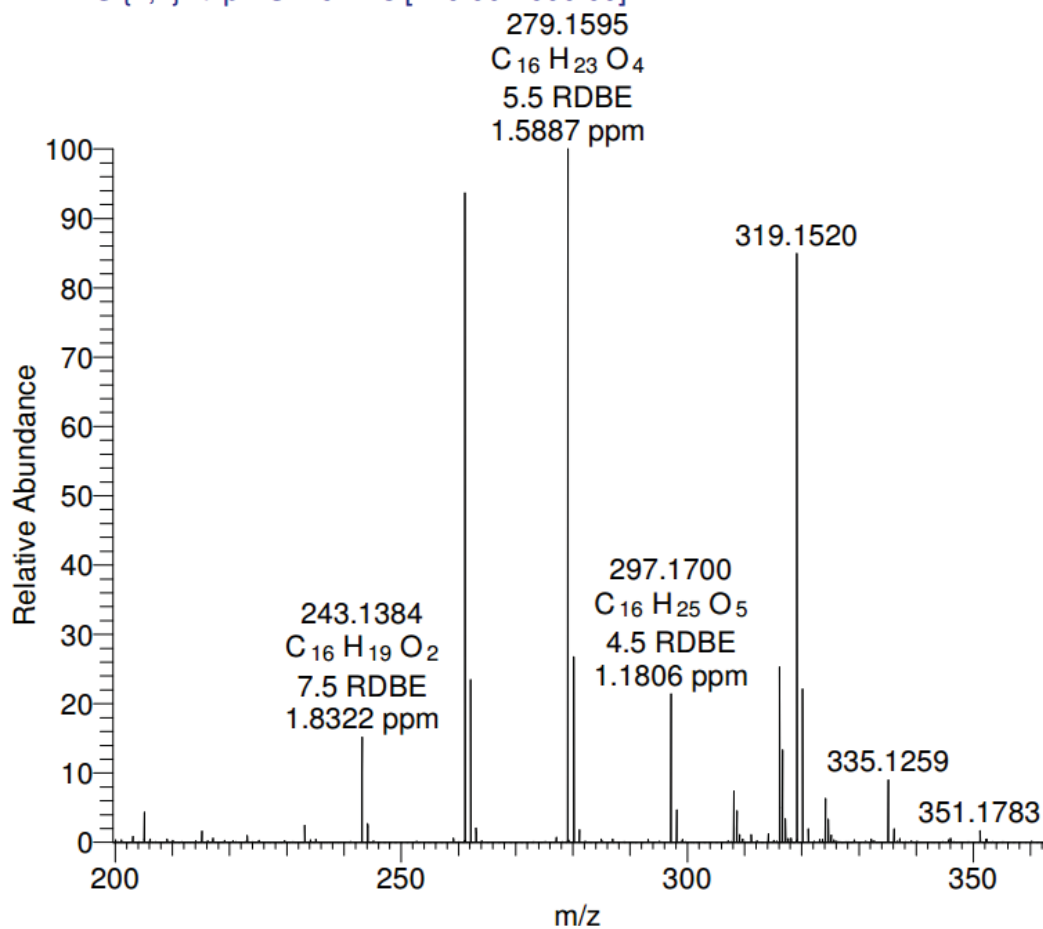


Figure S9. HRESIMS of 2.

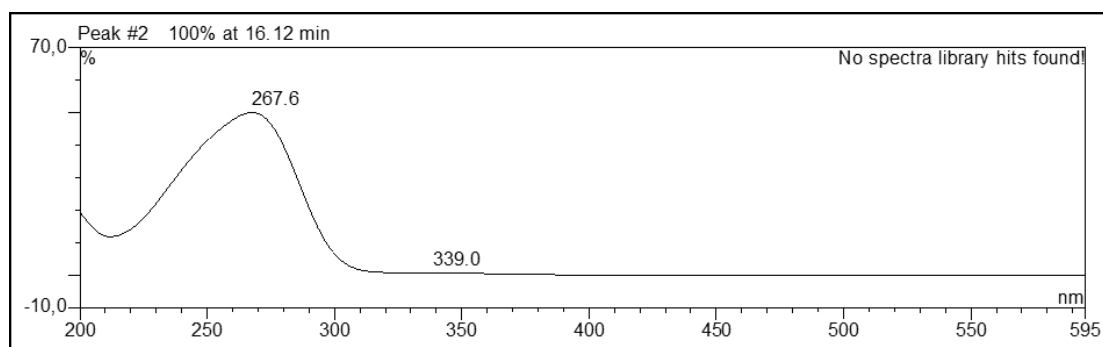


Figure S10. UV spectrum of 2.

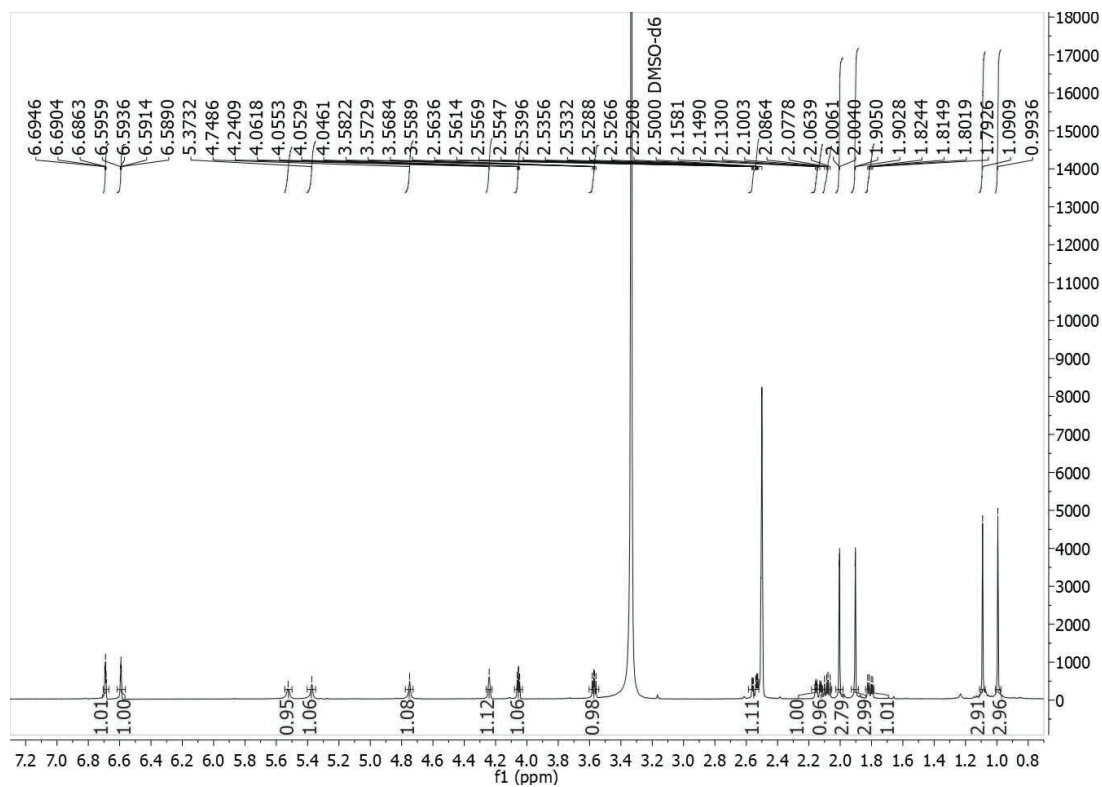


Figure S11. ¹H-NMR (600 MHz, DMSO-*d*₆) spectrum of **2**.

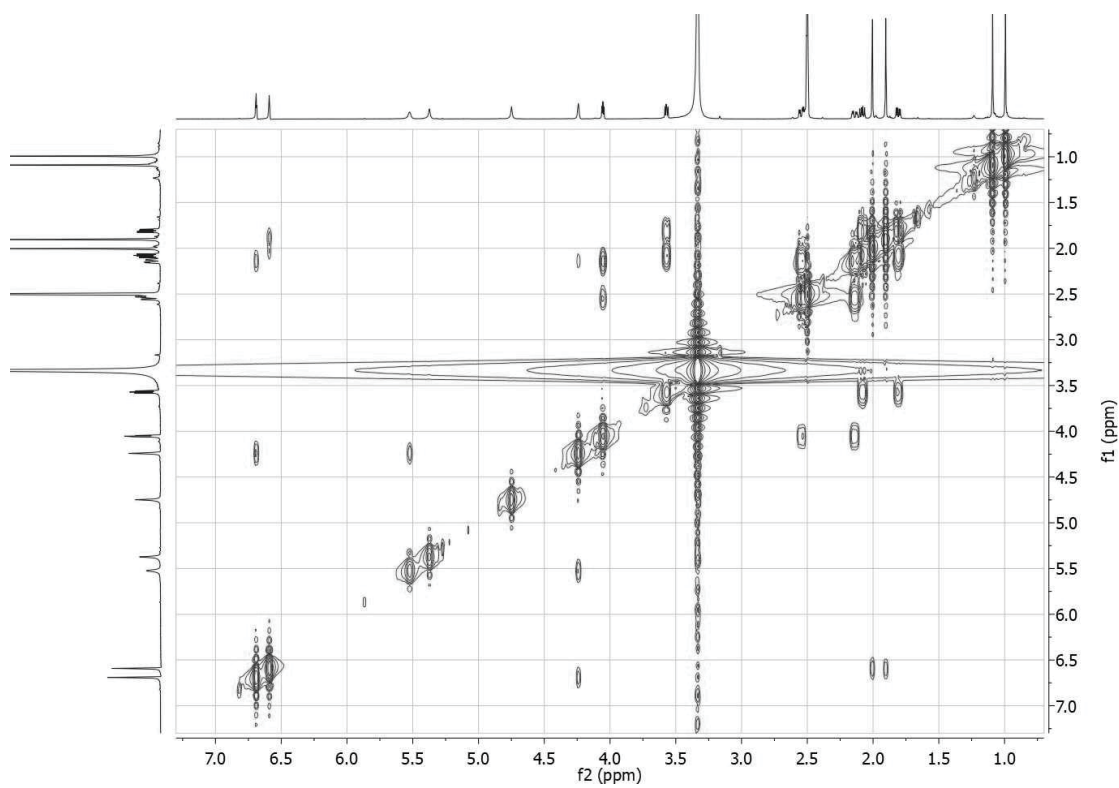


Figure S12. ¹H-¹H COSY (600 MHz, DMSO-*d*₆) spectrum of **2**.

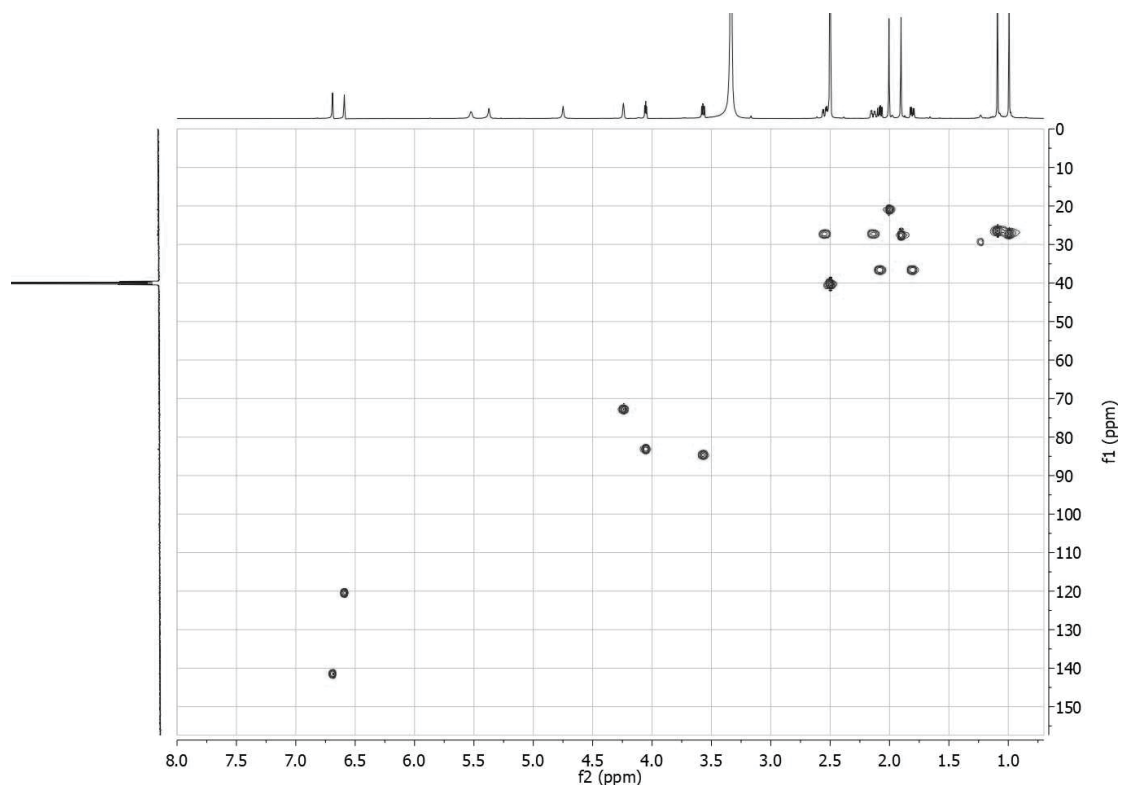


Figure S13. HSQC (600 MHz, DMSO-*d*₆) spectrum of **2**.

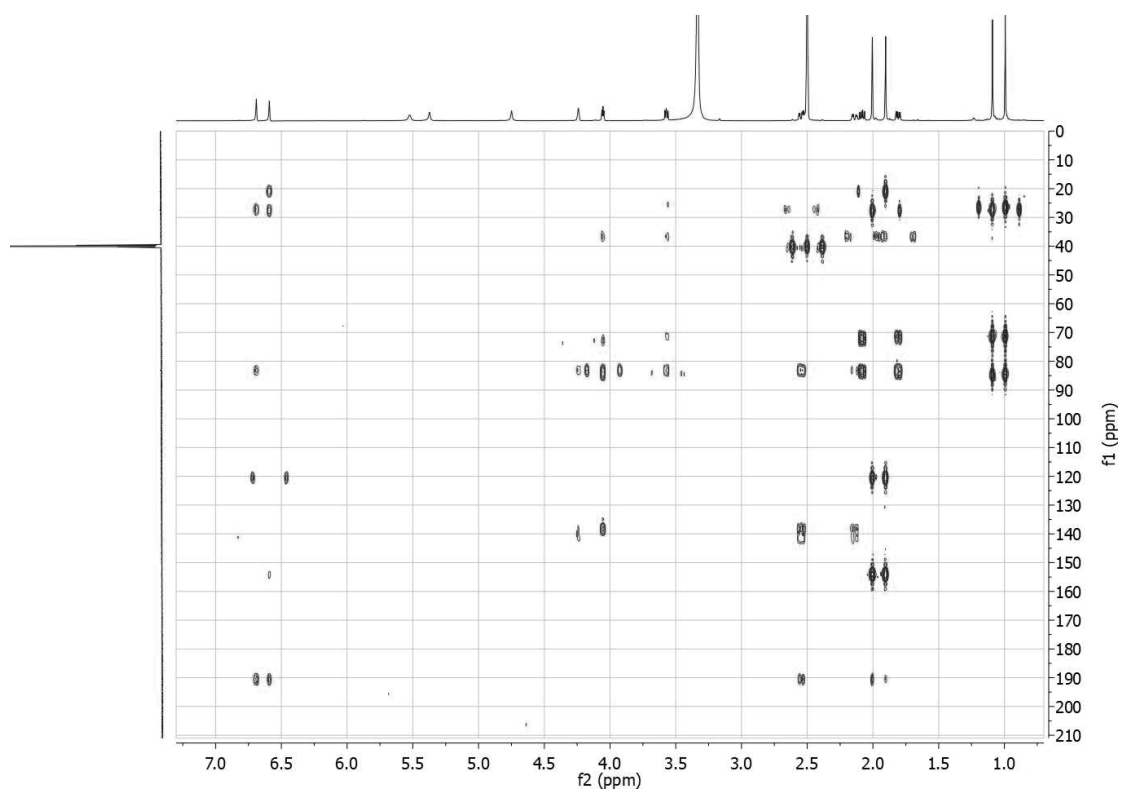


Figure S14. HMBC (600 MHz, DMSO-*d*₆) spectrum of **2**.

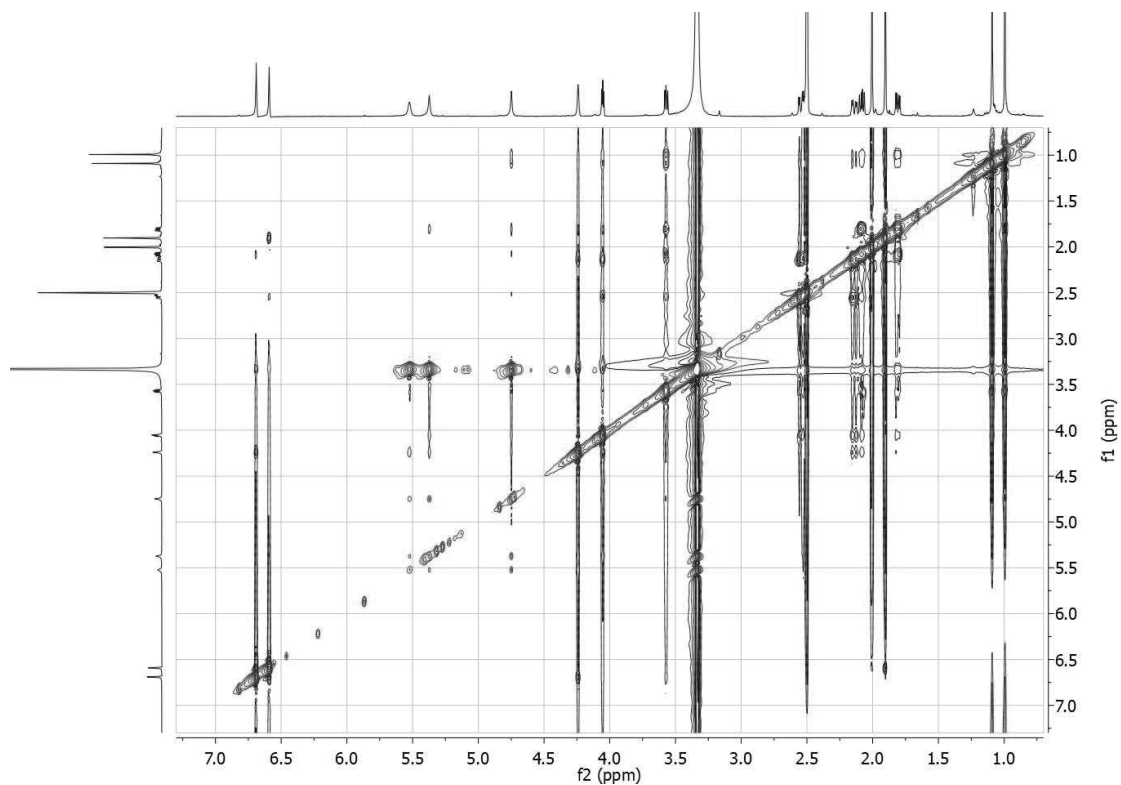


Figure S15. ROESY (600 MHz, DMSO-*d*₆) spectrum of **2**.

9 #182-268 RT: 3.72-5.19 AV: 43 SB: 365 5.66-16.82 , 0.59-4.37 NL: 6.32E5
T: FTMS {1,1} + p ESI Full ms [120.00-2000.00]

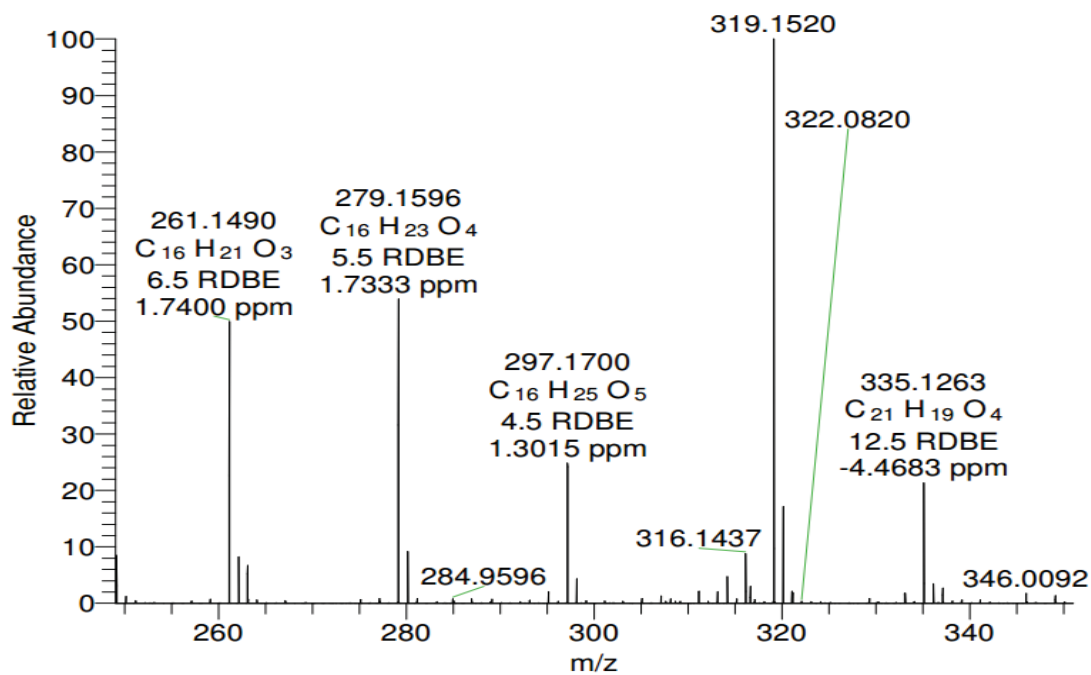


Figure S16. HRESIMS of **3**.

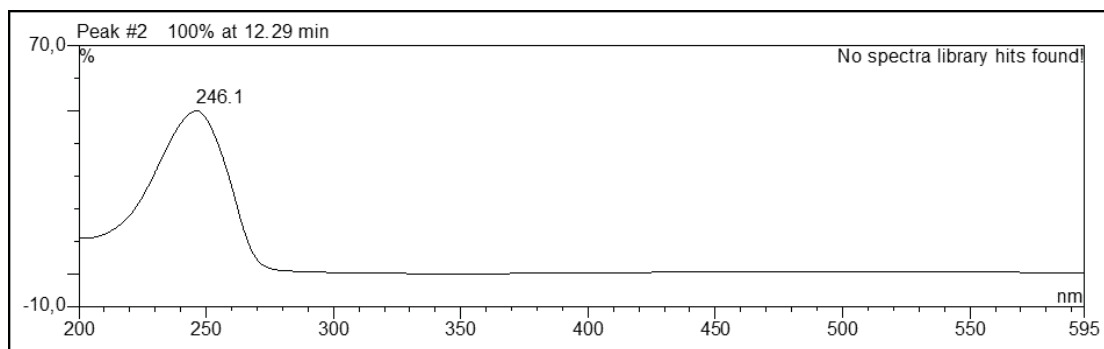


Figure S17. UV spectrum of **3**.

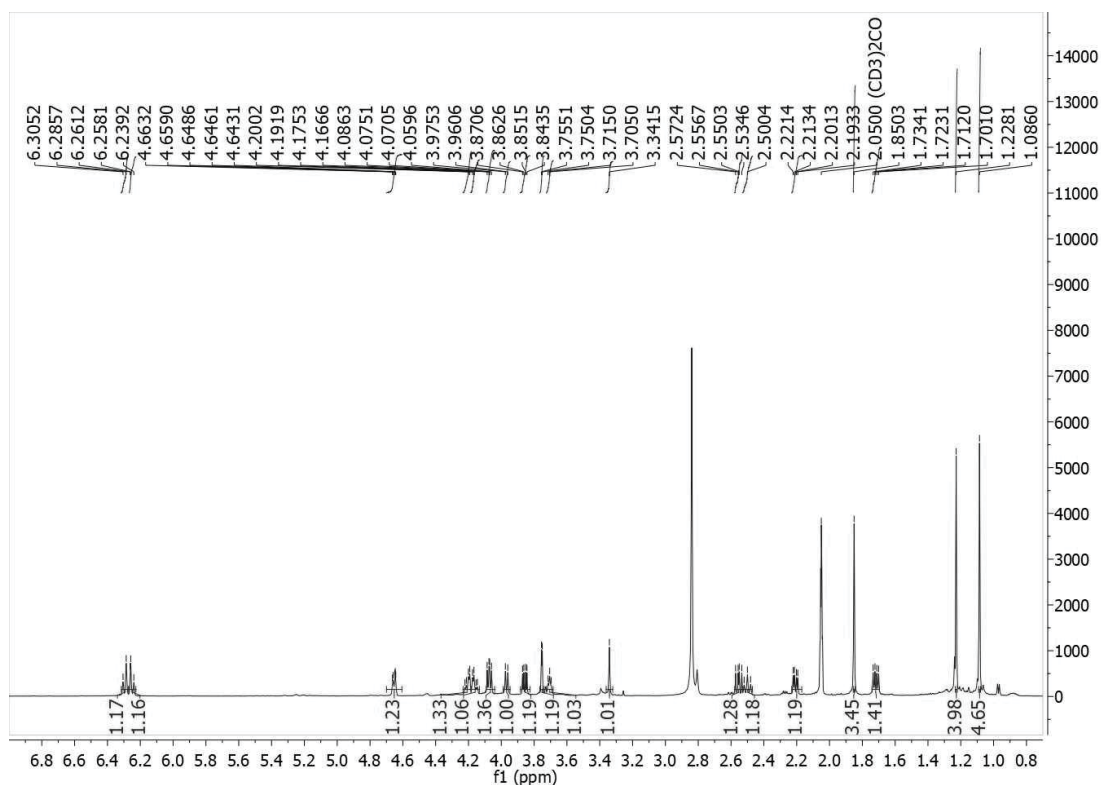


Figure S18. ^1H -NMR (600 MHz, Acetone- d_6) spectrum of **3**.

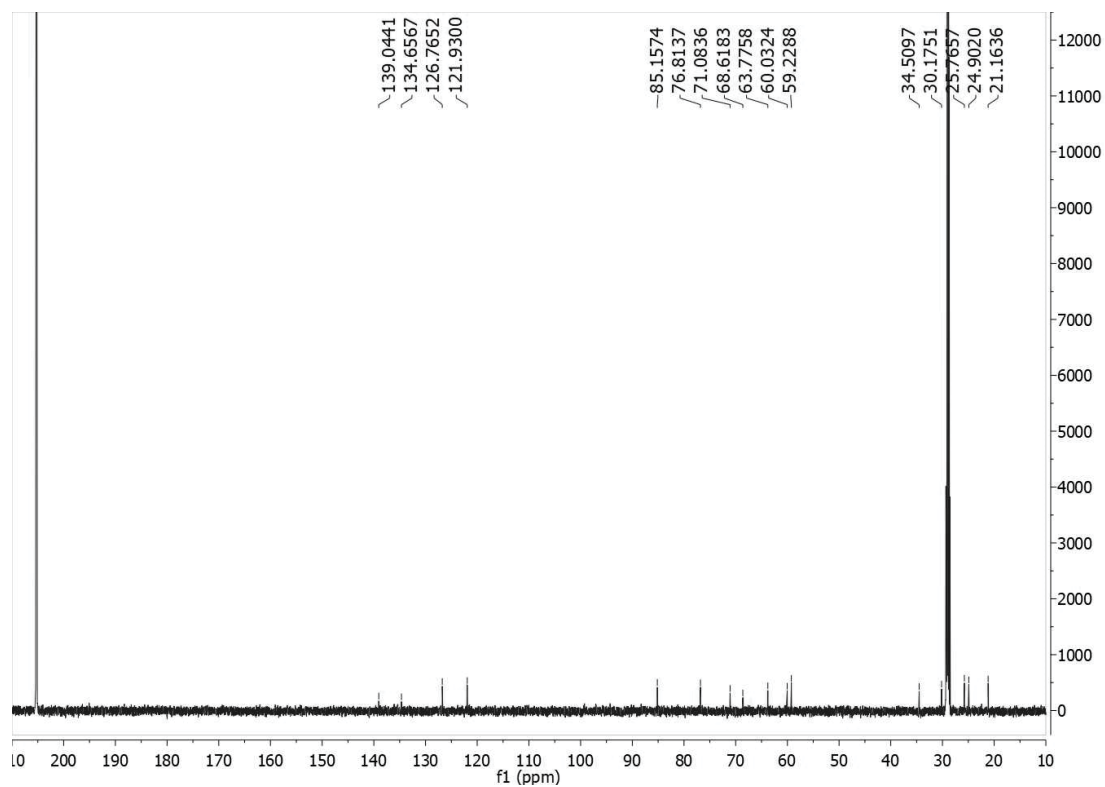


Figure S19. ^{13}C -NMR (150 MHz, Acetone- d_6) spectrum of **3**.

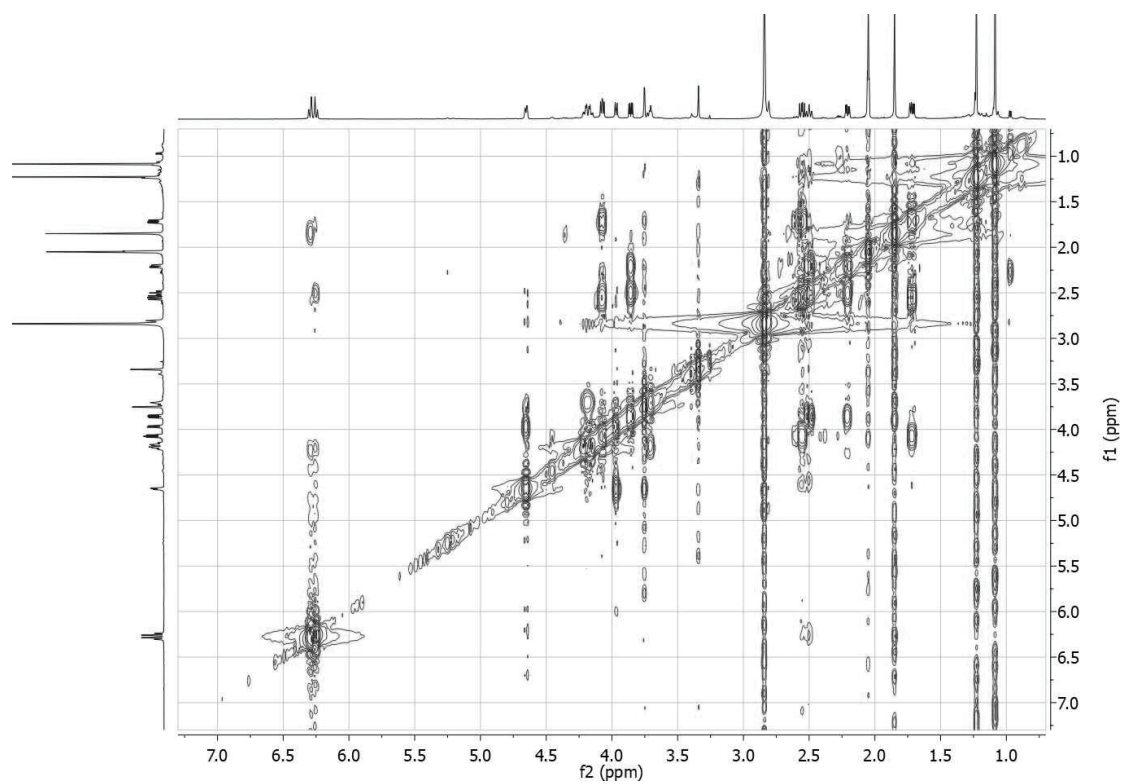


Figure S20. ^1H - ^1H COSY (600 MHz, Acetone- d_6) spectrum of **3**.

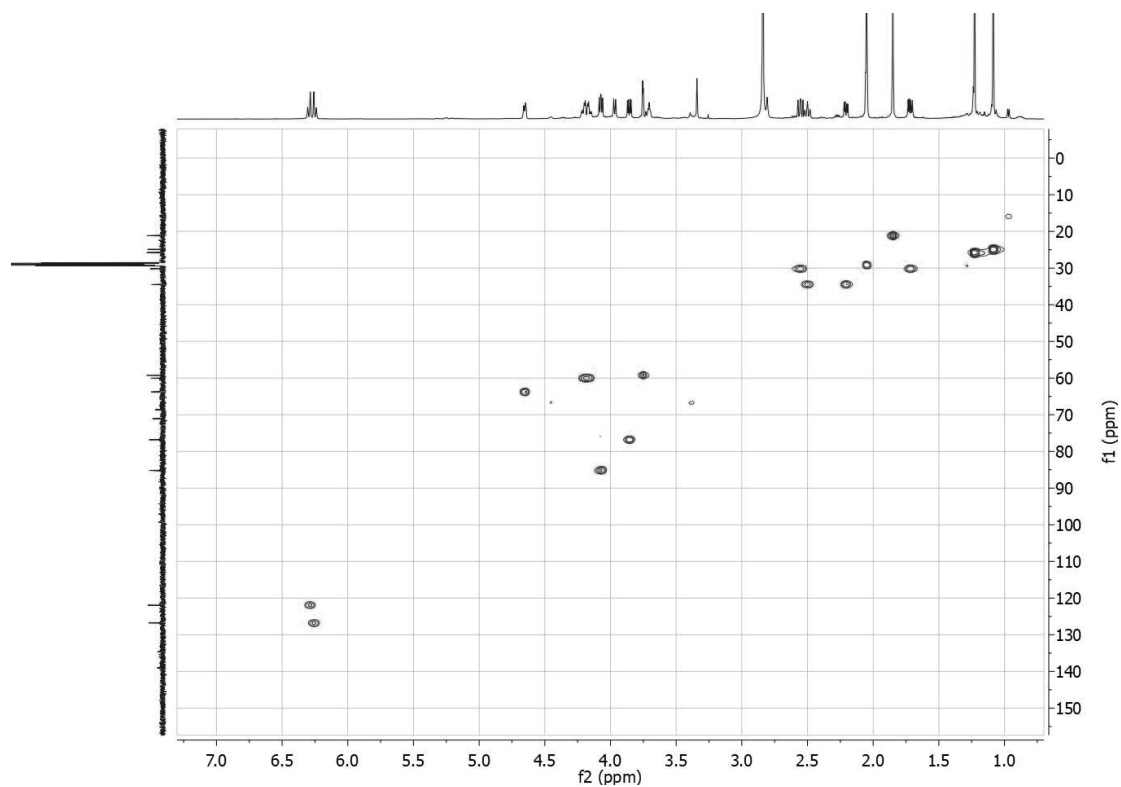


Figure S21. HSQC (600 MHz, Acetone-*d*₆) spectrum of **3**.

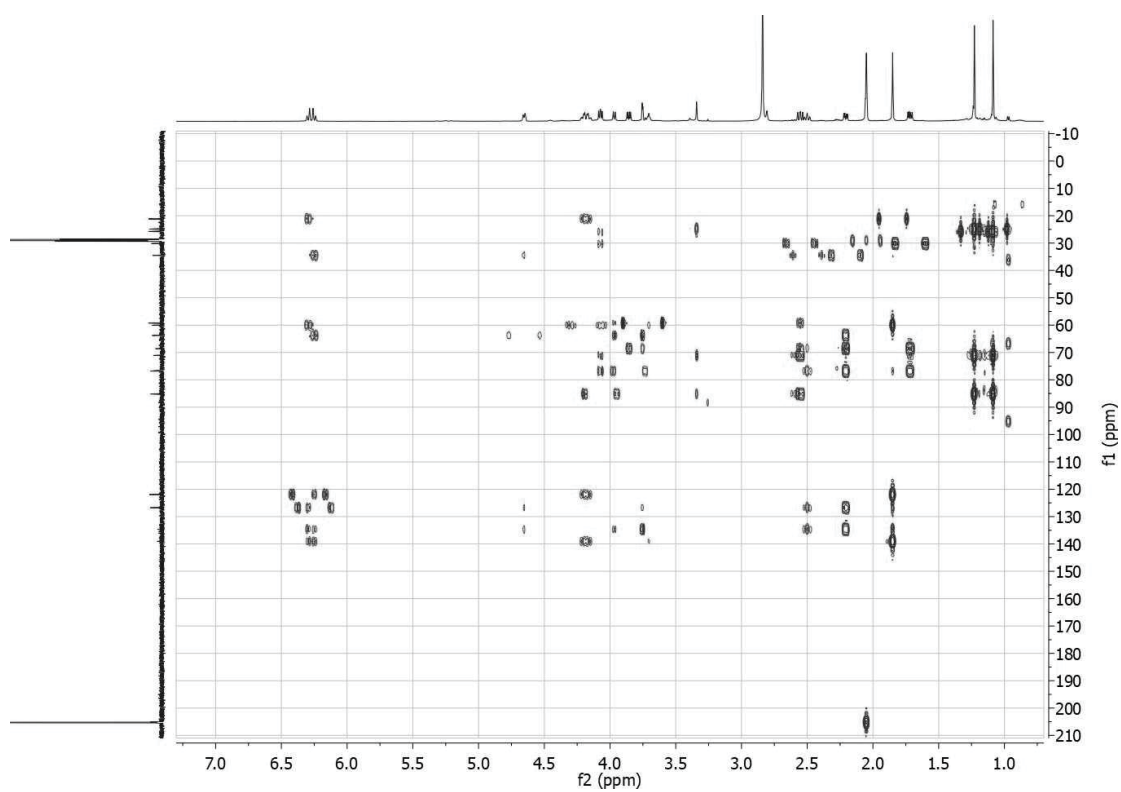


Figure S22. HMBC (600 MHz, Acetone-*d*₆) spectrum of **3**.

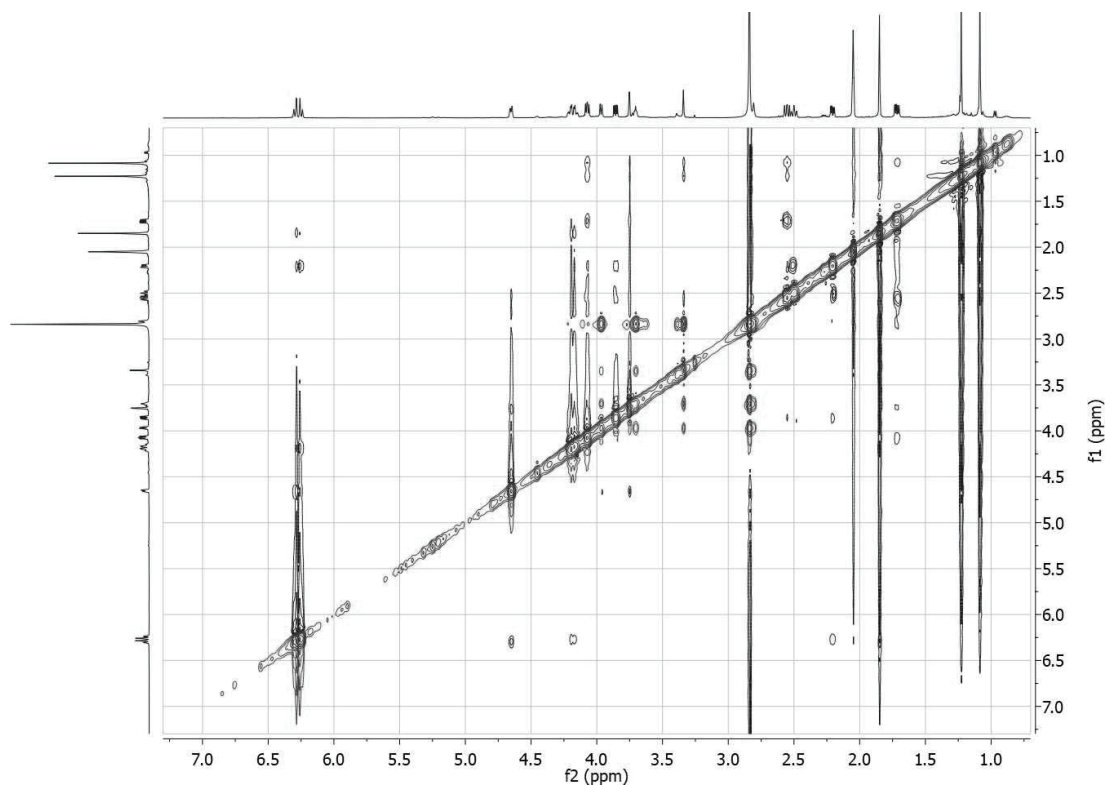


Figure S23. ROESY (600 MHz, Acetone- d_6) spectrum of **3**.

Acquisition Parameter

Source Type	ESI	Ion Polarity	Positive	Set Nebulizer	0.3 Bar
Focus	Not active	Set Capillary	4000 V	Set Dry Heater	180 °C
Scan Begin	50 m/z	Set End Plate Offset	-500 V	Set Dry Gas	4.0 l/min
Scan End	1500 m/z	Set Collision Cell RF	600.0 Vpp	Set Divert Valve	Source

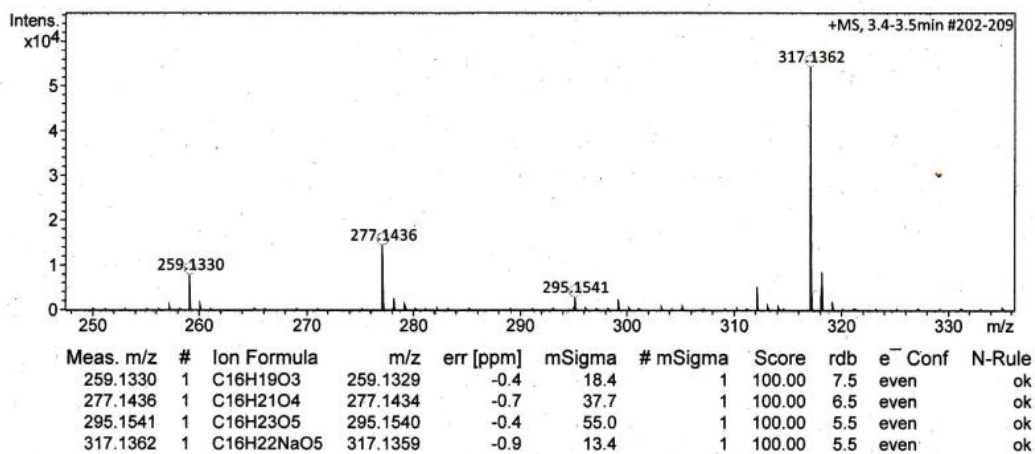


Figure S24. HRESIMS of **4**.

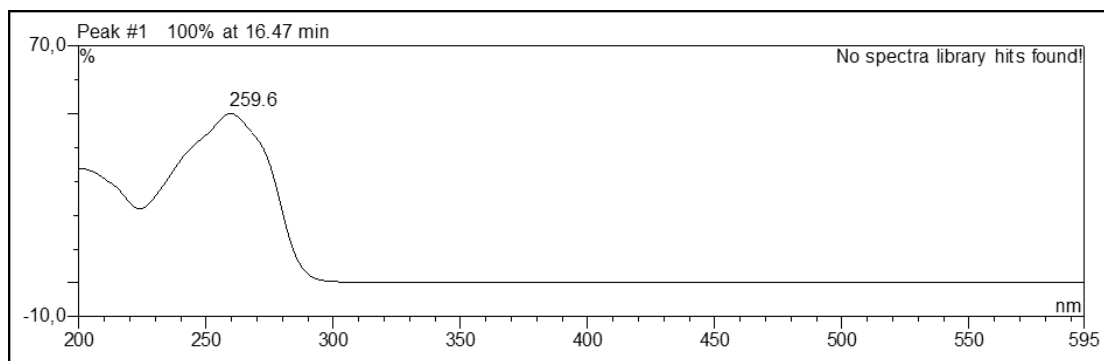


Figure S25. UV spectrum of **4**.

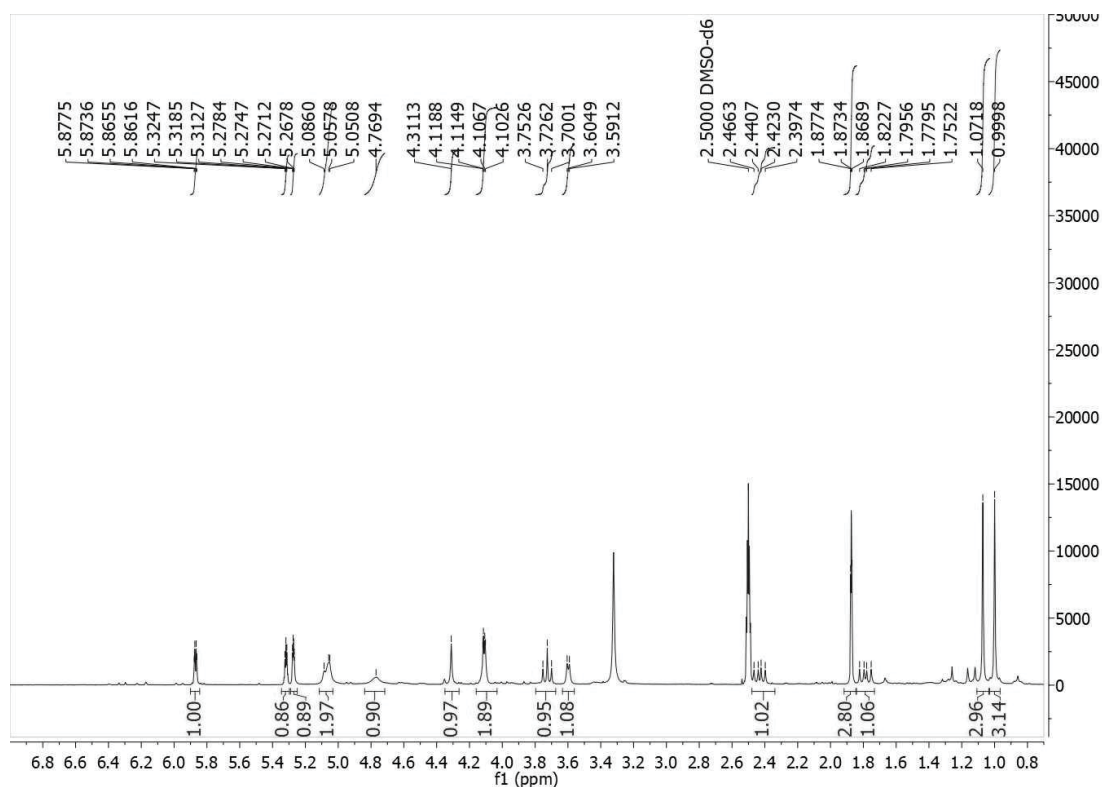


Figure S26. ^1H -NMR (600 MHz, $\text{DMSO}-d_6$) spectrum of **4**.

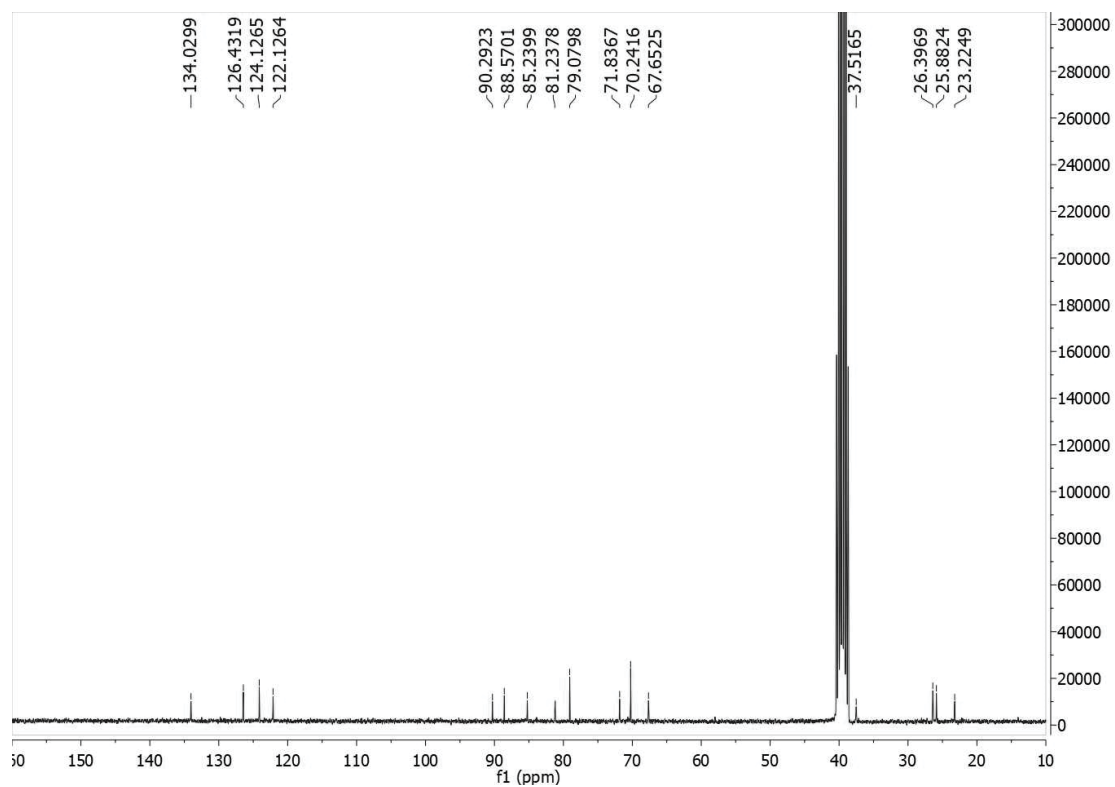


Figure S27. ^{13}C -NMR (150 MHz, $\text{DMSO}-d_6$) spectrum of **4**.

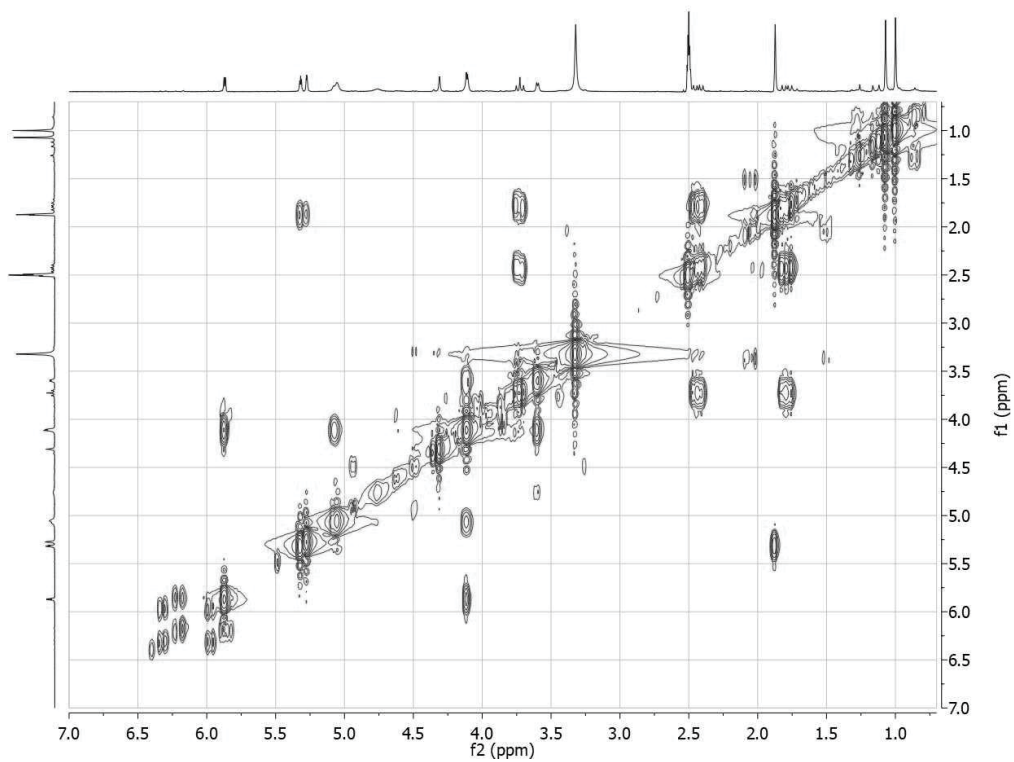


Figure S28. ^1H - ^1H COSY (600 MHz, $\text{DMSO}-d_6$) spectrum of **4**.

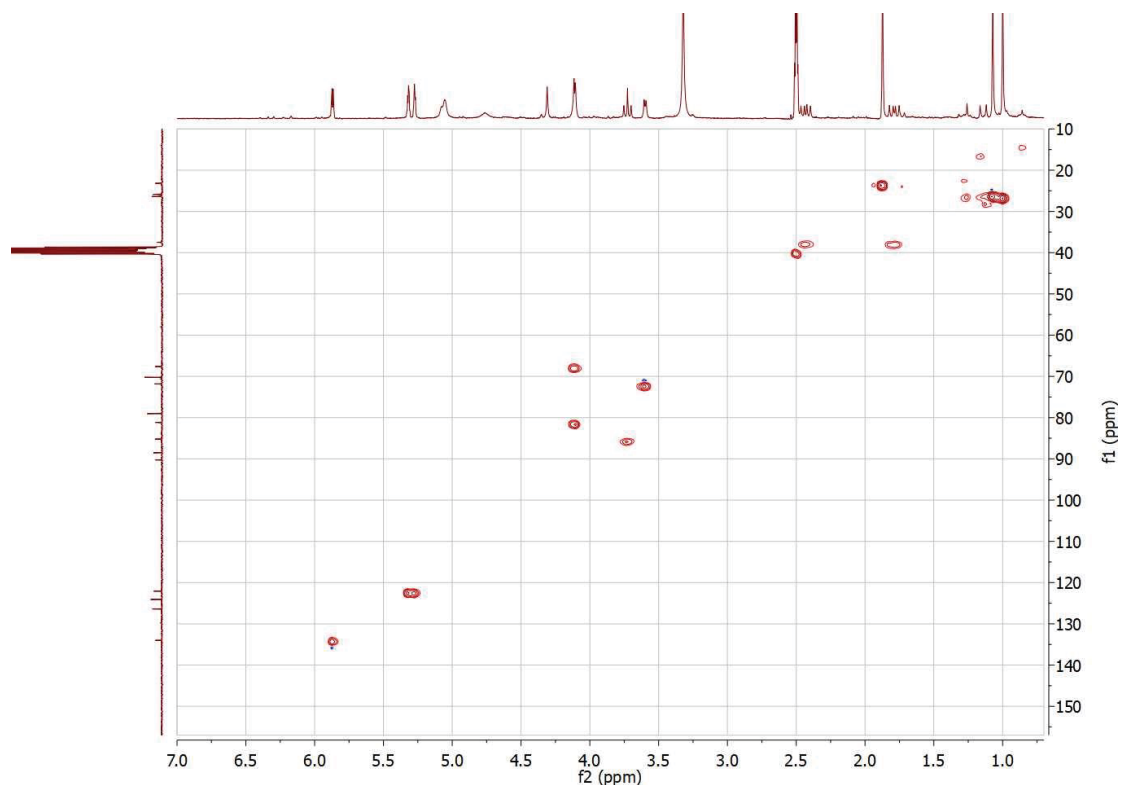


Figure S29. HSQC (600 MHz, DMSO- d_6) spectrum of **4**.

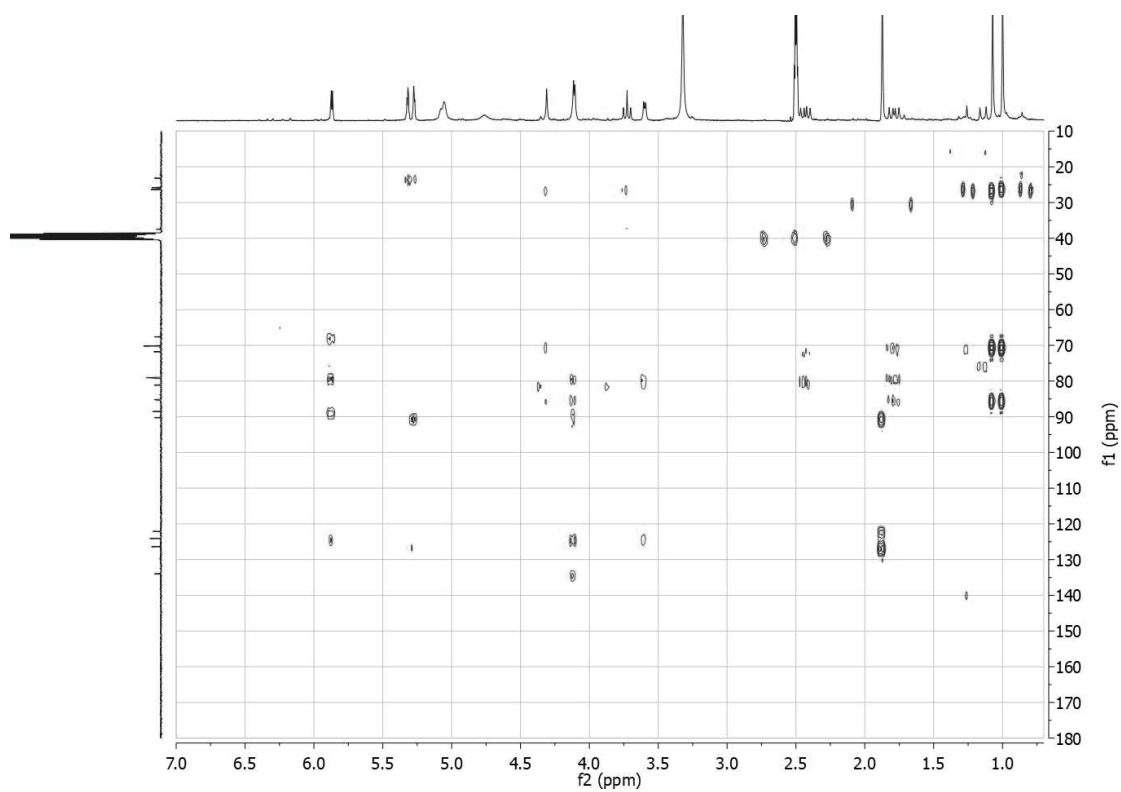
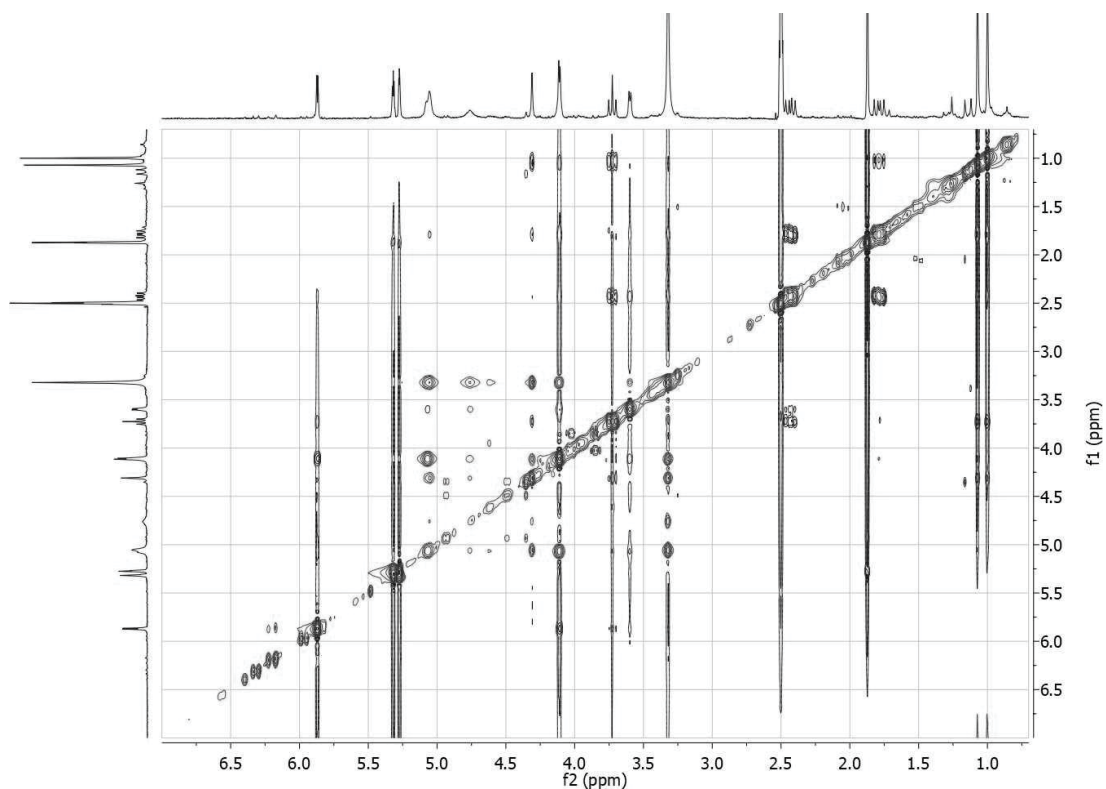
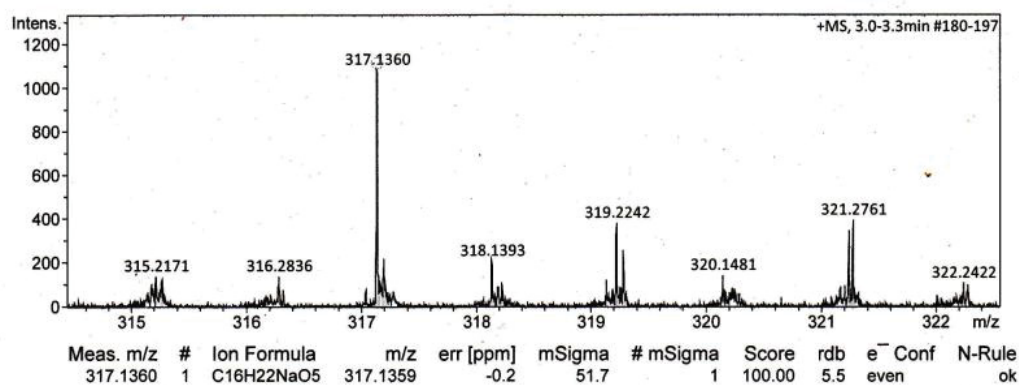
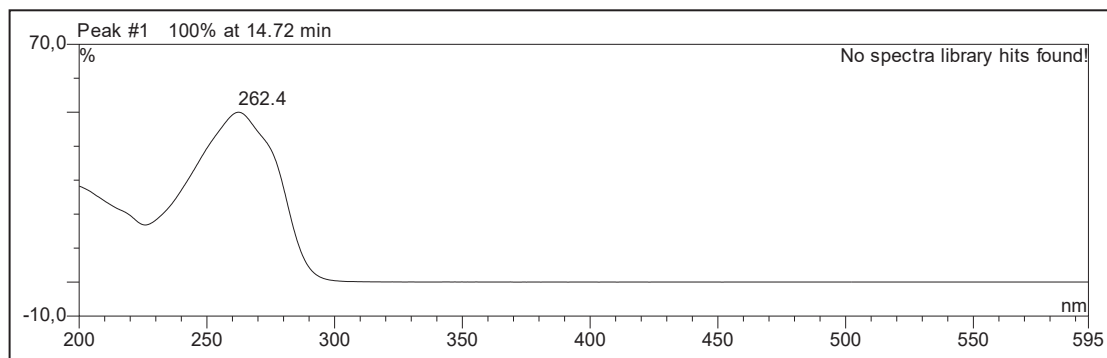


Figure S30. HMBC (600 MHz, DMSO- d_6) spectrum of **4**.

Figure S31. ROESY (600 MHz, DMSO- d_6) spectrum of **4**.**Acquisition Parameter**

Source Type	ESI	Ion Polarity	Positive	Set Nebulizer	0.3 Bar
Focus	Not active	Set Capillary	4000 V	Set Dry Heater	180 °C
Scan Begin	50 m/z	Set End Plate Offset	-500 V	Set Dry Gas	4.0 l/min
Scan End	1500 m/z	Set Collision Cell RF	600.0 Vpp	Set Divert Valve	Source

Figure S32. HRESIMS of **5**.Figure S33. UV spectrum of **5**.

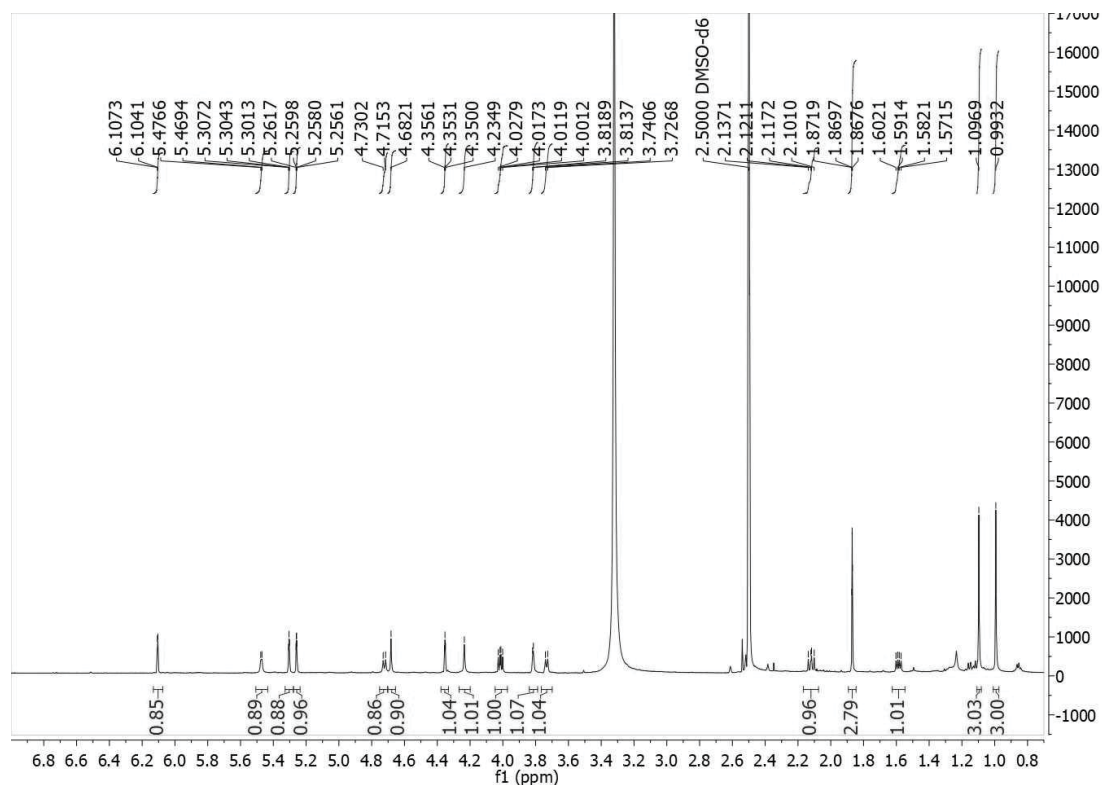


Figure S34. ¹H-NMR (600 MHz, DMSO-*d*₆) spectrum of **5**.

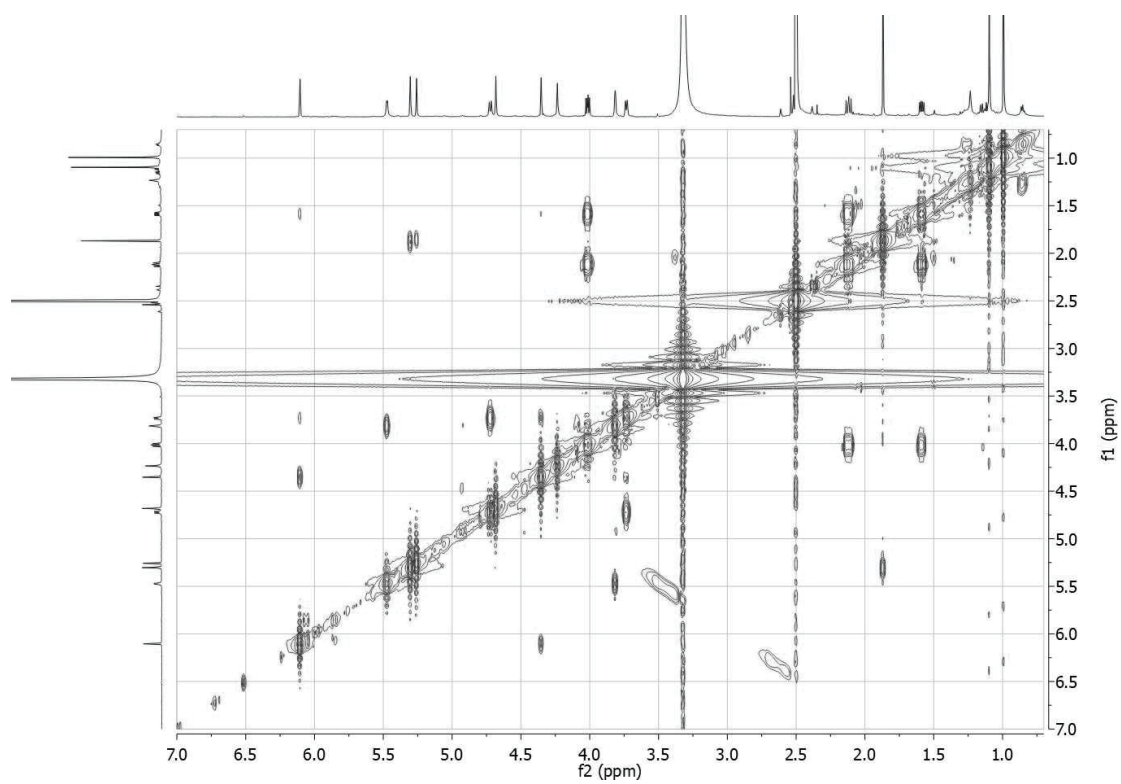


Figure S35. ¹H-¹H COSY (600 MHz, DMSO-*d*₆) spectrum of **5**.

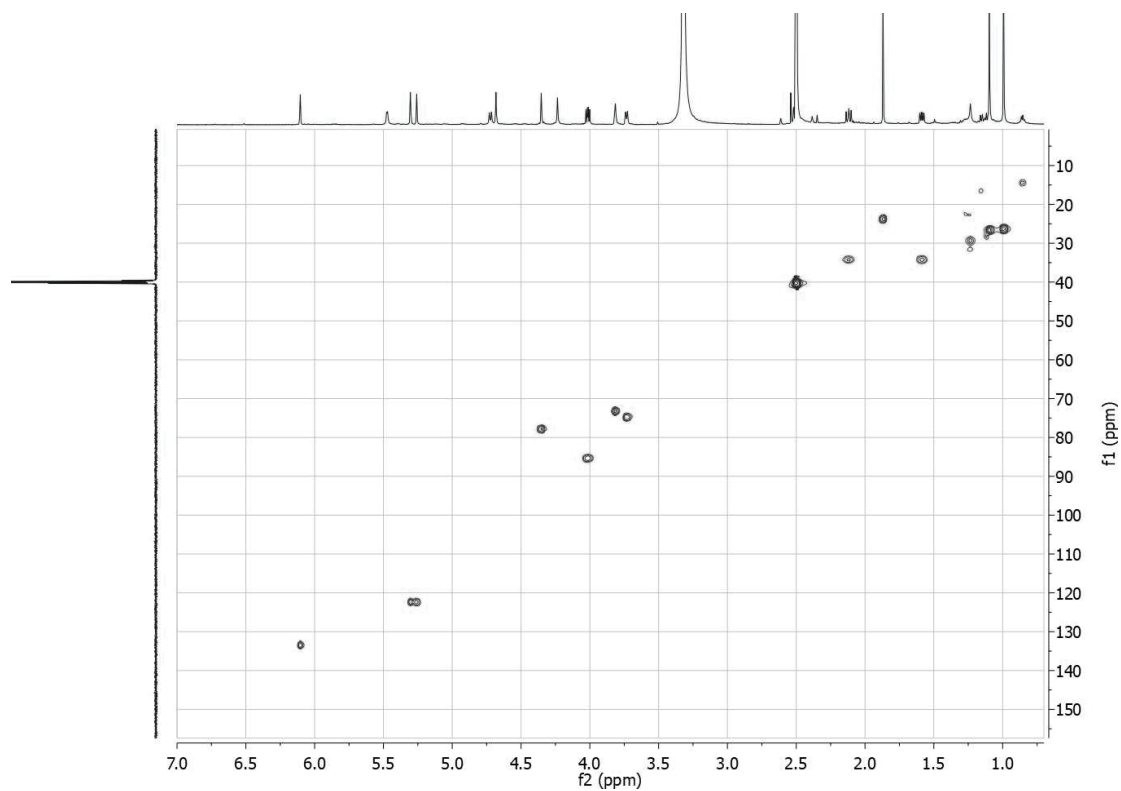


Figure S36. HSQC (600 MHz, DMSO- d_6) spectrum of **5**.

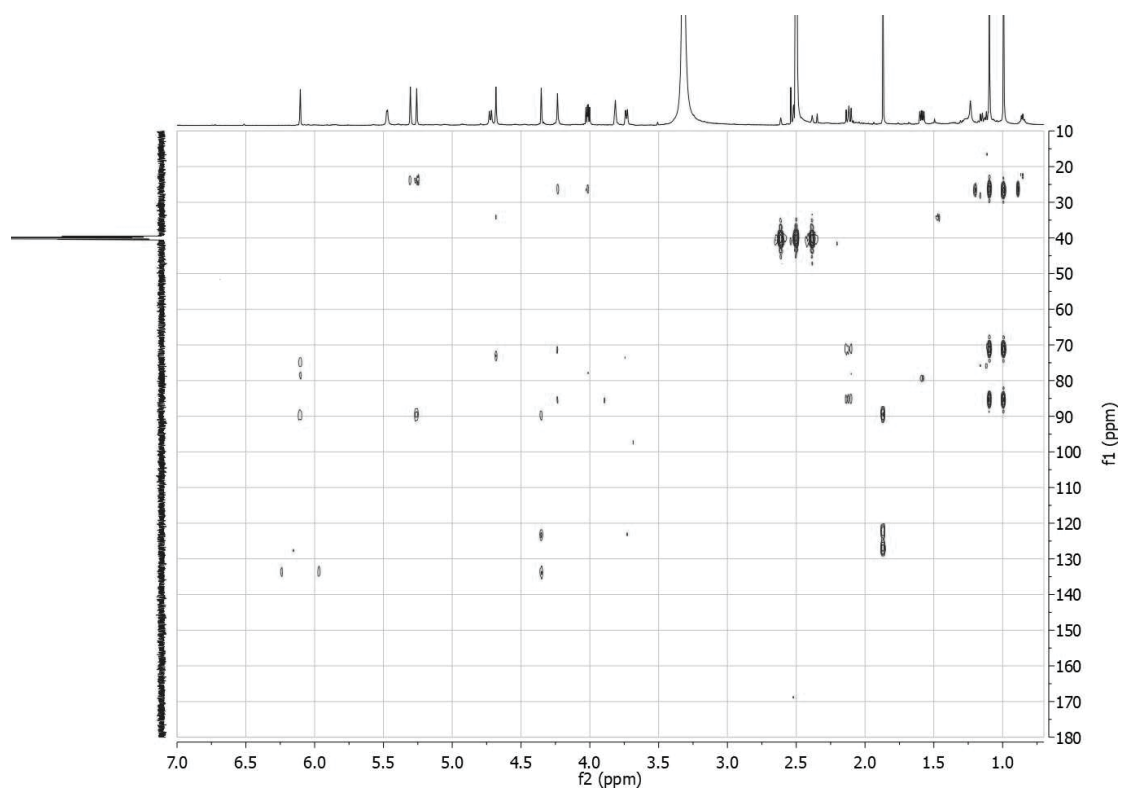
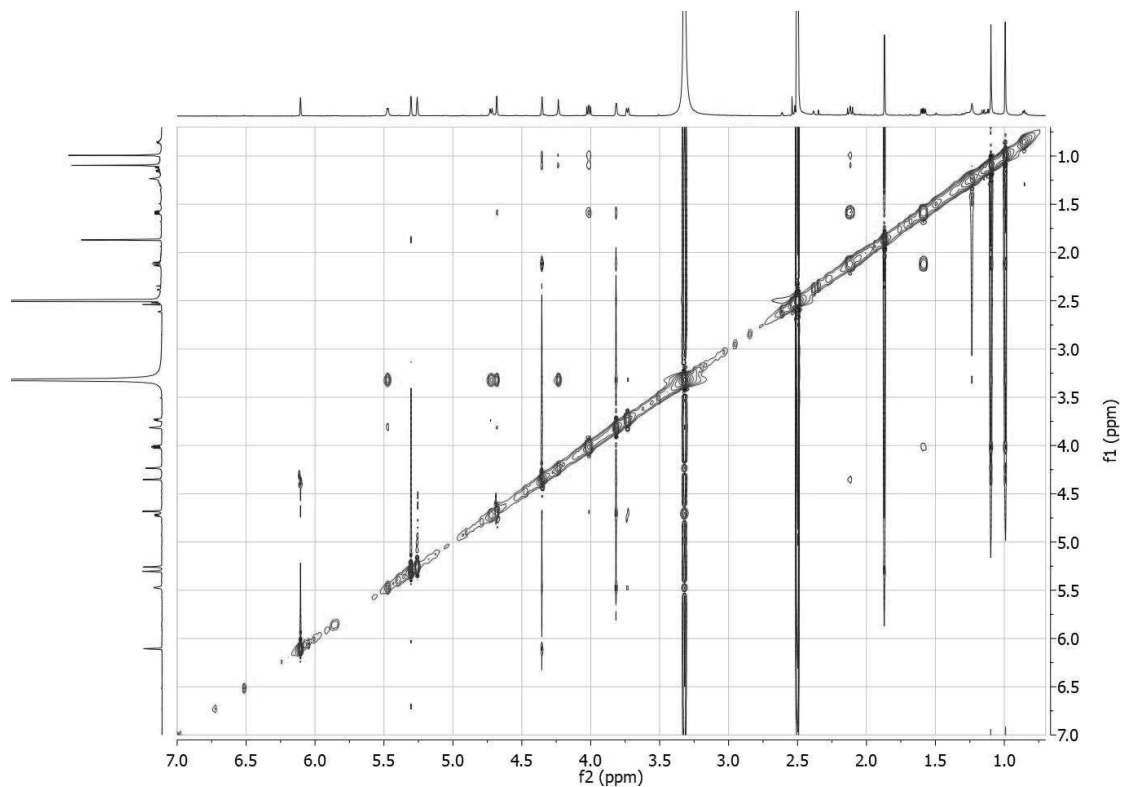
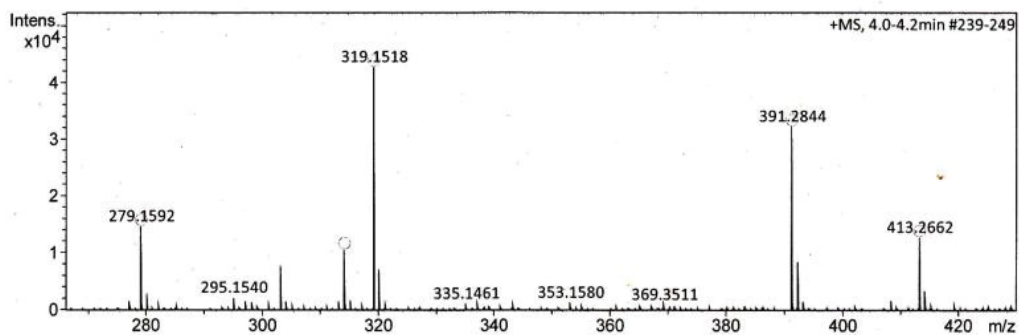


Figure S37. HMBC (600MHz, DMSO- d_6) spectrum of **5**.

Figure S38. ROESY (600 MHz, DMSO-*d*₆) spectrum of **5**.**Acquisition Parameter**

Source Type	ESI	Ion Polarity	Positive	Set Nebulizer	0.3 Bar
Focus	Not active	Set Capillary	4000 V	Set Dry Heater	180 °C
Scan Begin	50 m/z	Set End Plate Offset	-500 V	Set Dry Gas	4.0 l/min
Scan End	1500 m/z	Set Collision Cell RF	600.0 Vpp	Set Divert Valve	Source



Meas. m/z	#	Ion Formula	m/z	err [ppm]	mSigma	# mSigma	Score	rdb	e ⁻ Conf	N-Rule
279.1592	1	C17H19N4	279.1604	4.4	9.7	1	57.04	10.5	even	ok
	2	C16H23O4	279.1591	-0.4	10.4	2	100.00	5.5	even	ok
	3	C15H20N4Na	279.1580	-4.2	12.9	3	55.47	7.5	even	ok
314.1963	1	C16H28NO5	314.1962	-0.5	8.9	1	100.00	3.5	even	ok
	2	C15H25N5NaO	314.1951	-3.9	10.9	2	55.67	5.5	even	ok
	3	C17H24N5O	314.1975	3.8	22.6	3	44.40	8.5	even	ok
319.1518	1	C14H19N6O3	319.1513	-1.4	6.7	1	90.01	8.5	even	ok
	2	C13H23N2O7	319.1500	-5.6	7.5	2	40.26	3.5	even	ok
	3	C16H24NaO5	319.1516	-0.5	7.8	3	100.00	4.5	even	ok
	4	C17H20N4NaO	319.1529	3.7	20.8	4	45.83	9.5	even	ok

Figure S39. HRESIMS of **6**.

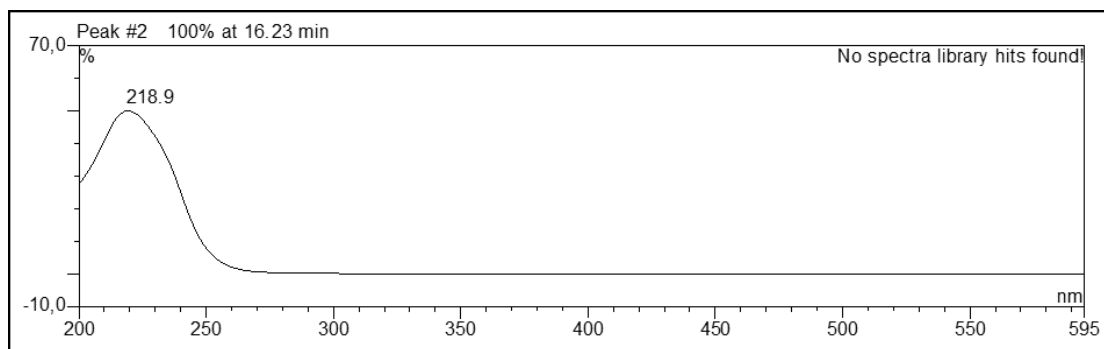


Figure S40. UV spectrum of **6**.

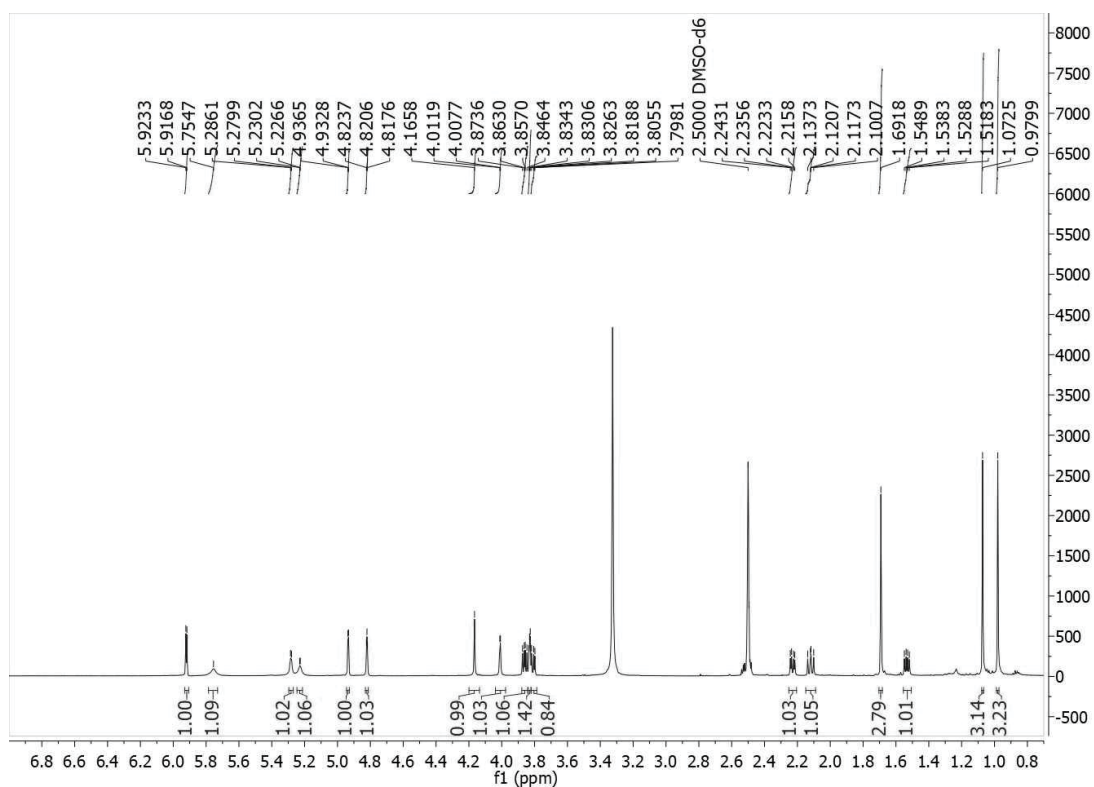


Figure S41. ^1H -NMR (600 MHz, $\text{DMSO}-d_6$) spectrum of **6**.

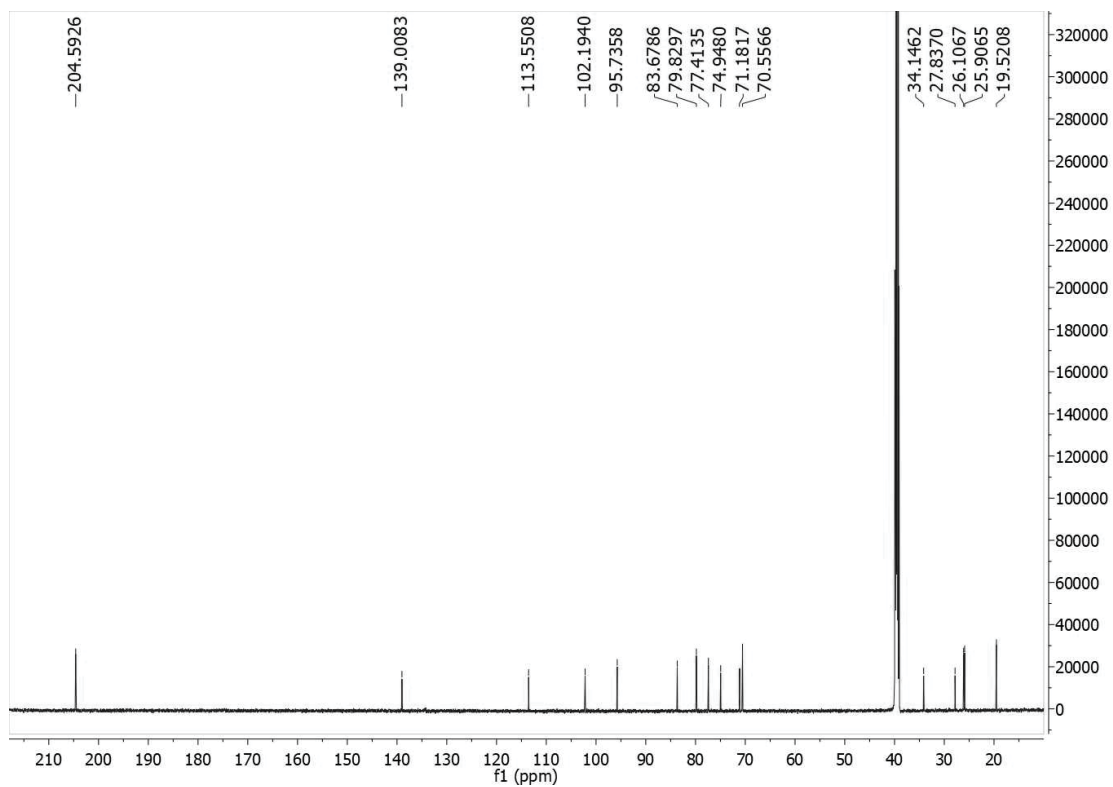


Figure S42. ^{13}C -NMR (150 MHz, $\text{DMSO}-d_6$) spectrum of 6.

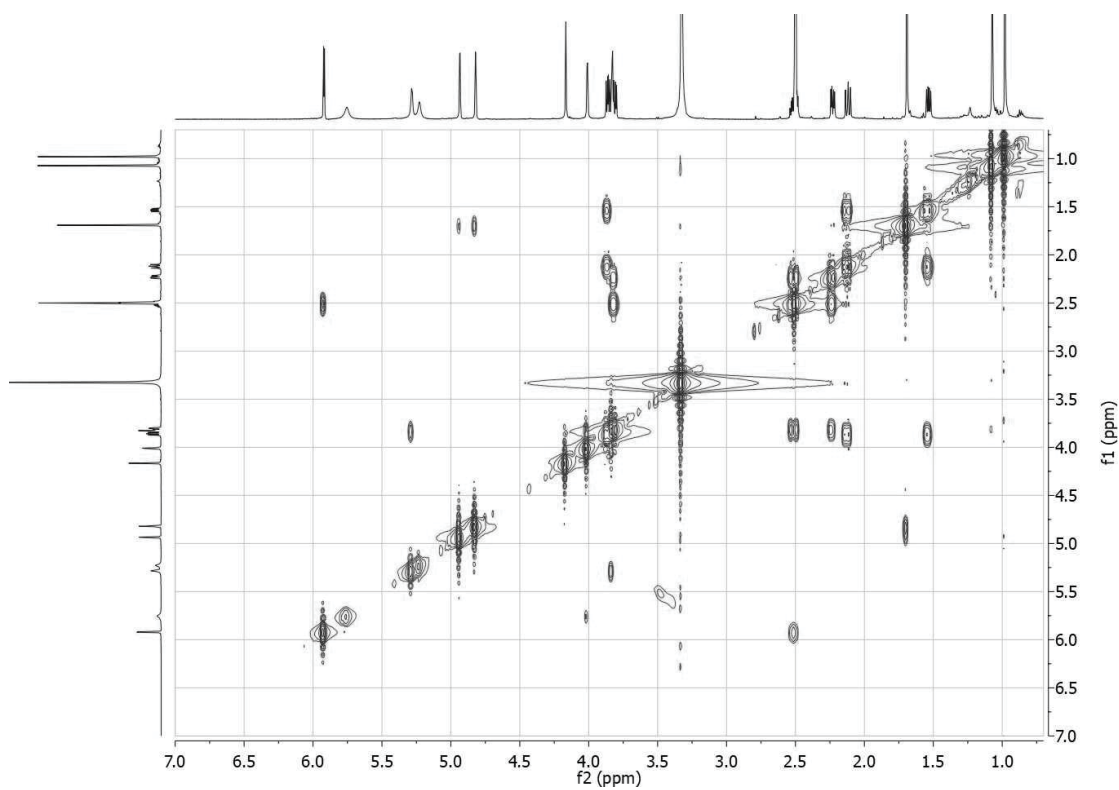


Figure S43. ^1H - ^1H COSY (600 MHz, $\text{DMSO}-d_6$) spectrum of 6.

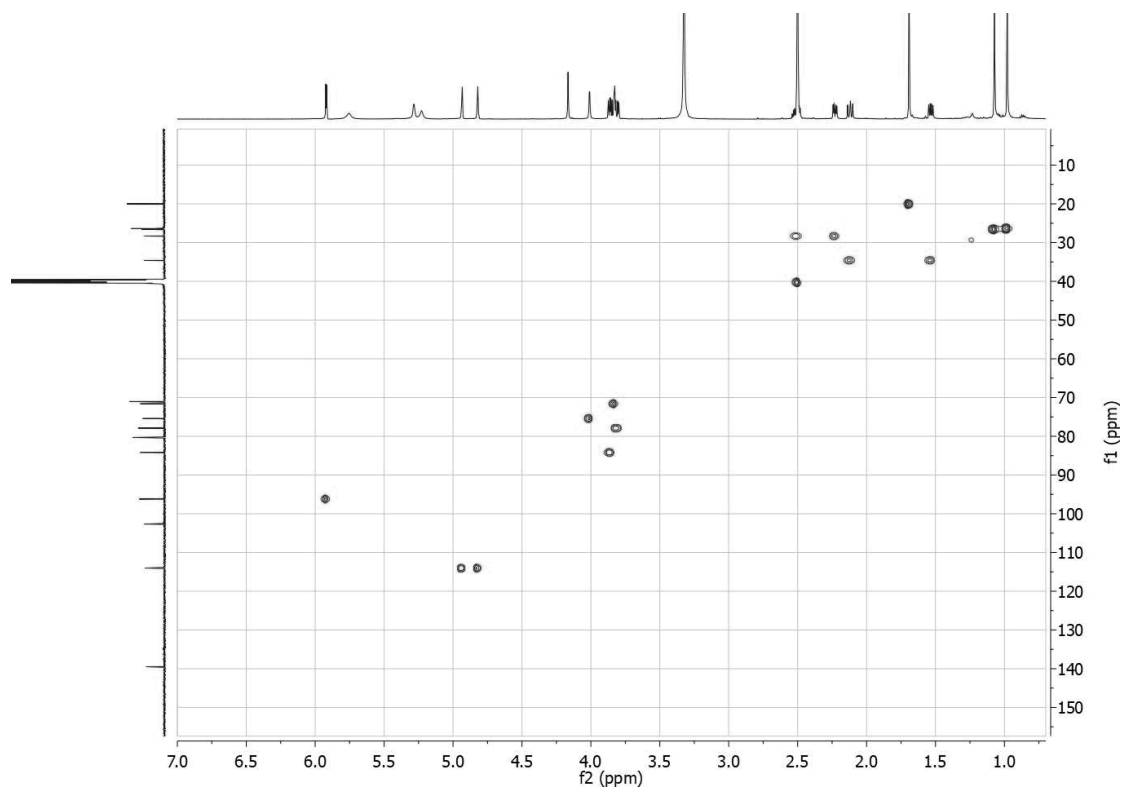


Figure S44. HSQC (600 MHz, DMSO-*d*₆) spectrum of **6**.

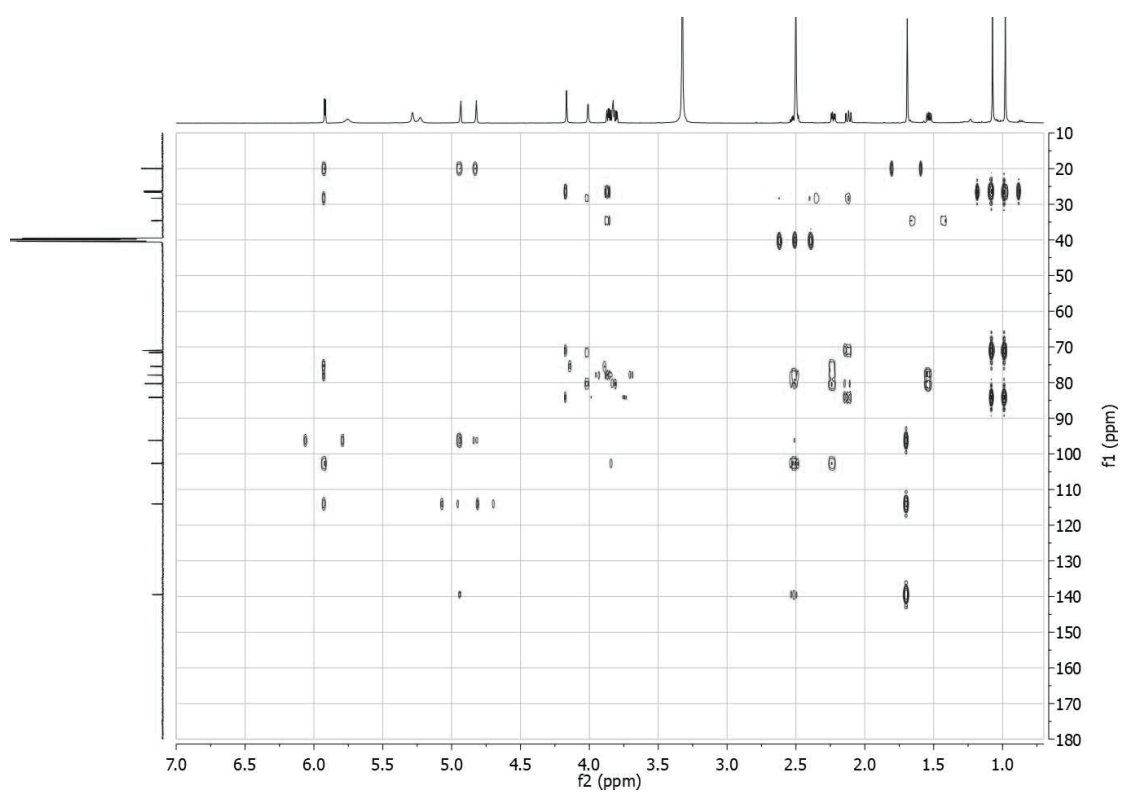
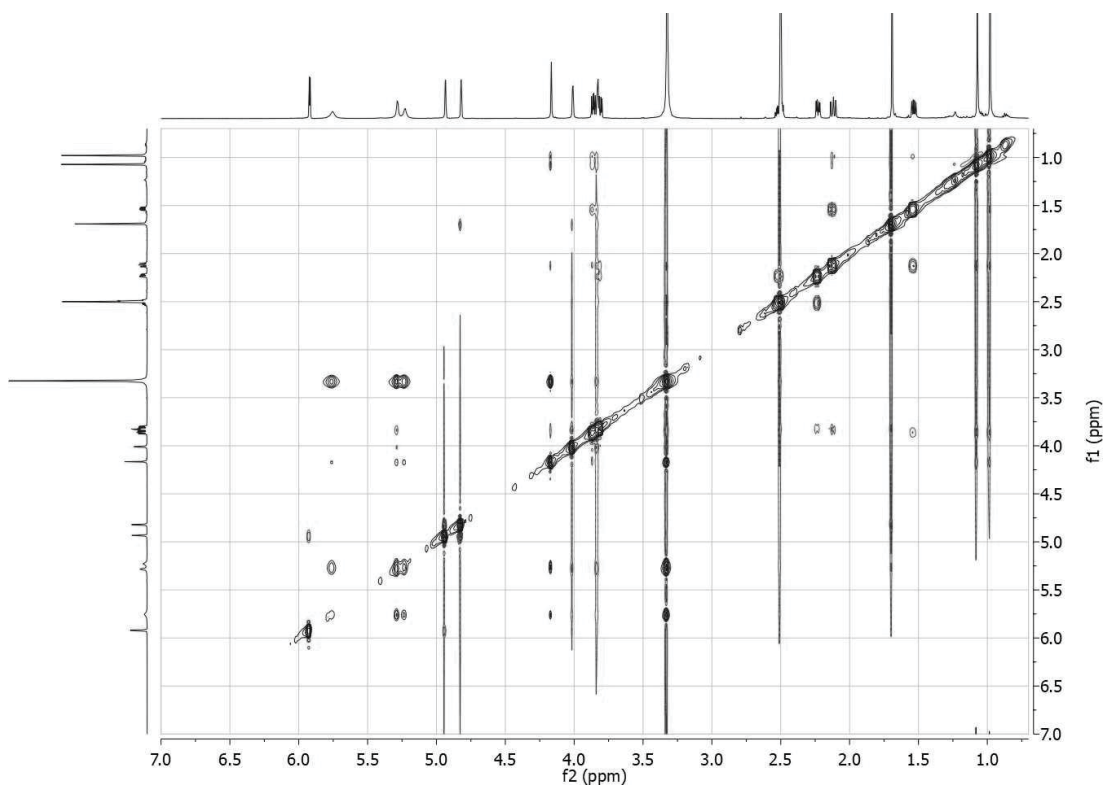
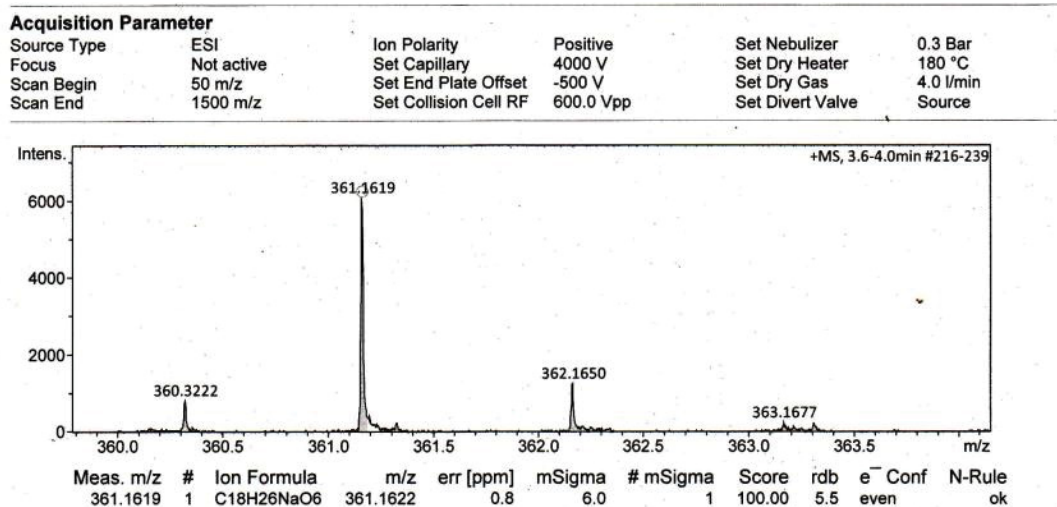
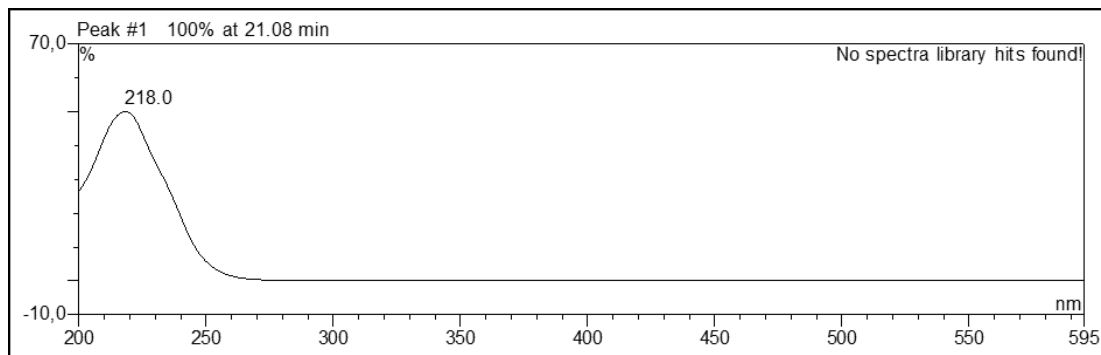


Figure S45. HMBC (600 MHz, DMSO-*d*₆) spectrum of **6**.

Figure S46. ROESY (600 MHz, DMSO-*d*₆) spectrum of **6**.Figure S47. HRESIMS of **7**.Figure S48. UV spectrum of **7**.

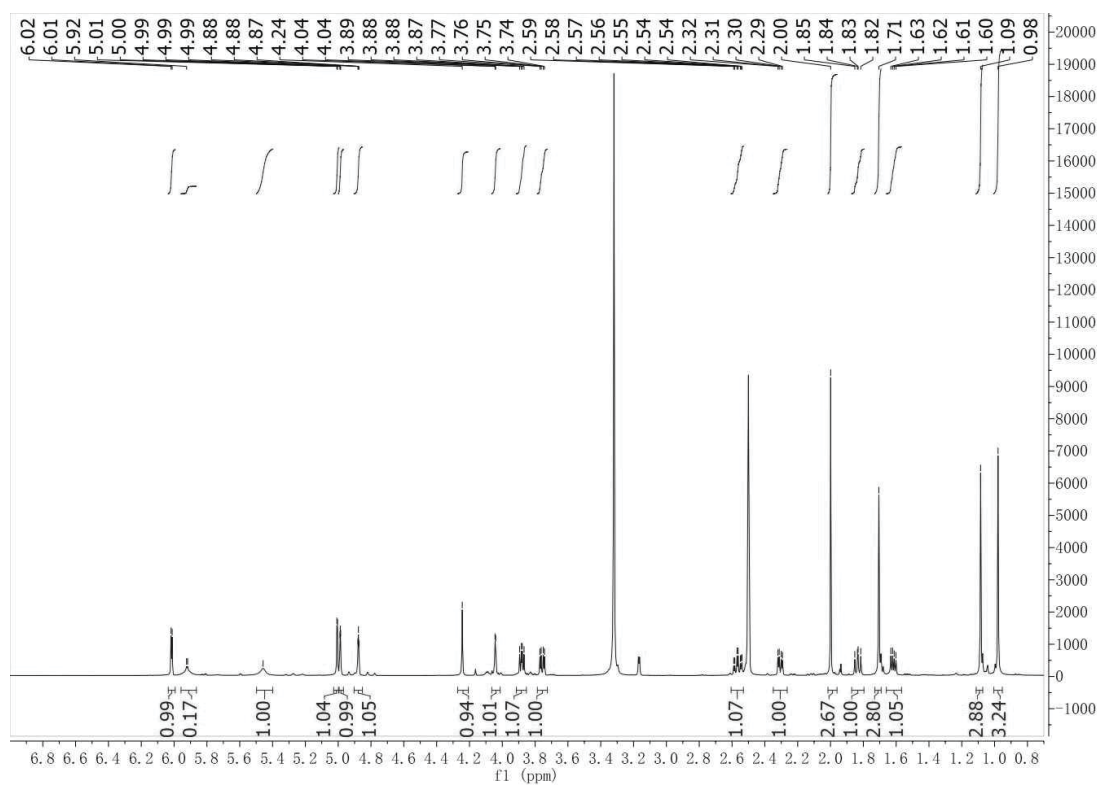


Figure S49. ¹H-NMR (600 MHz, DMSO-*d*₆) spectrum of 7.

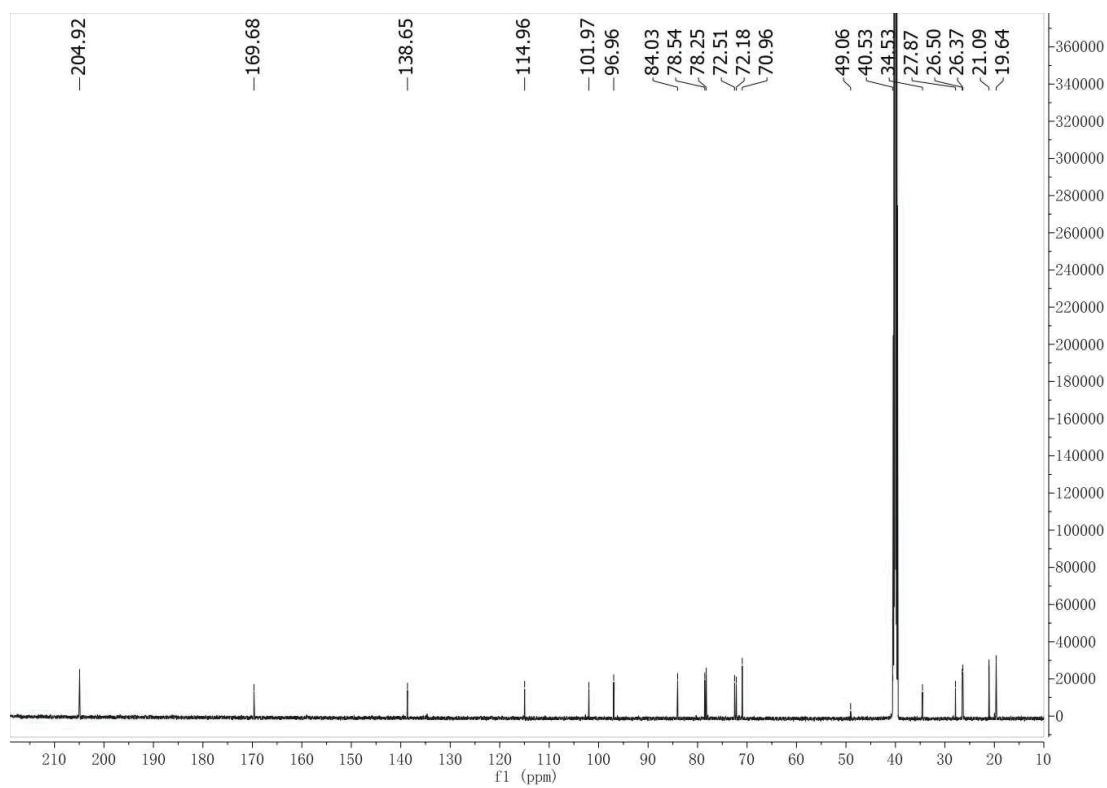


Figure S50. ¹³C-NMR (150 MHz, DMSO-*d*₆) spectrum of 7.

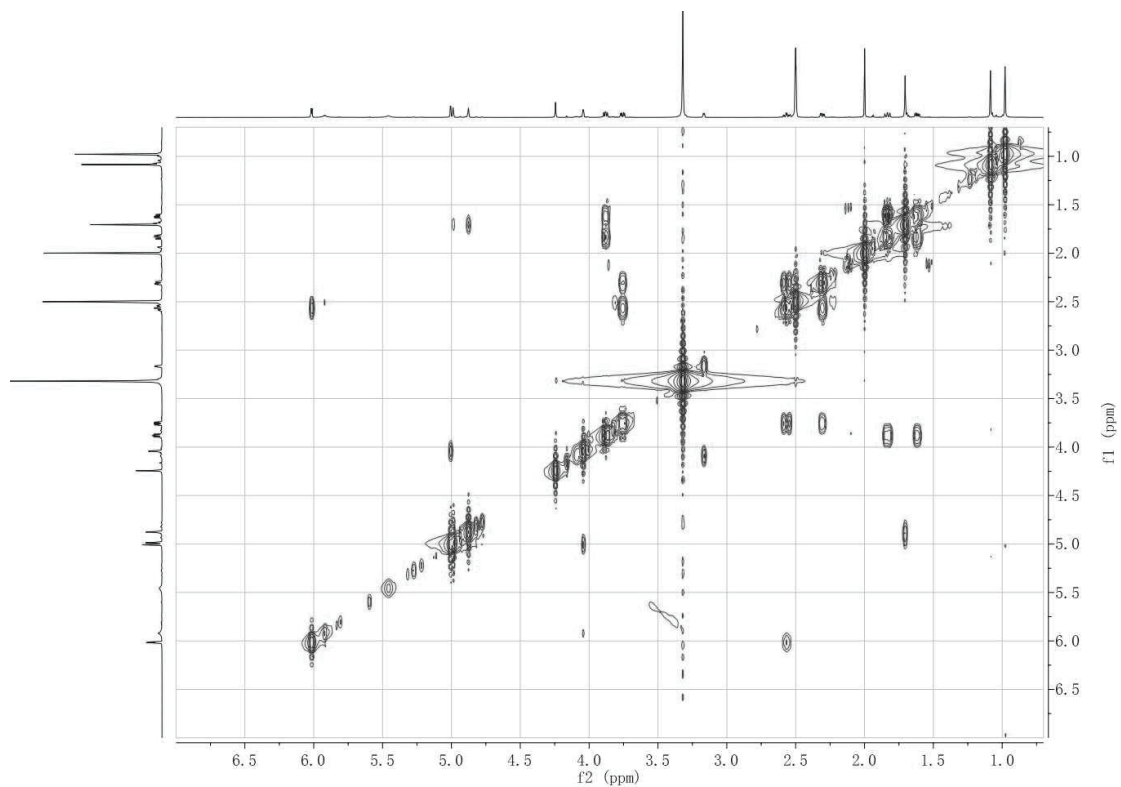


Figure S51. ^1H - ^1H COSY (600 MHz, $\text{DMSO}-d_6$) spectrum of **7**.

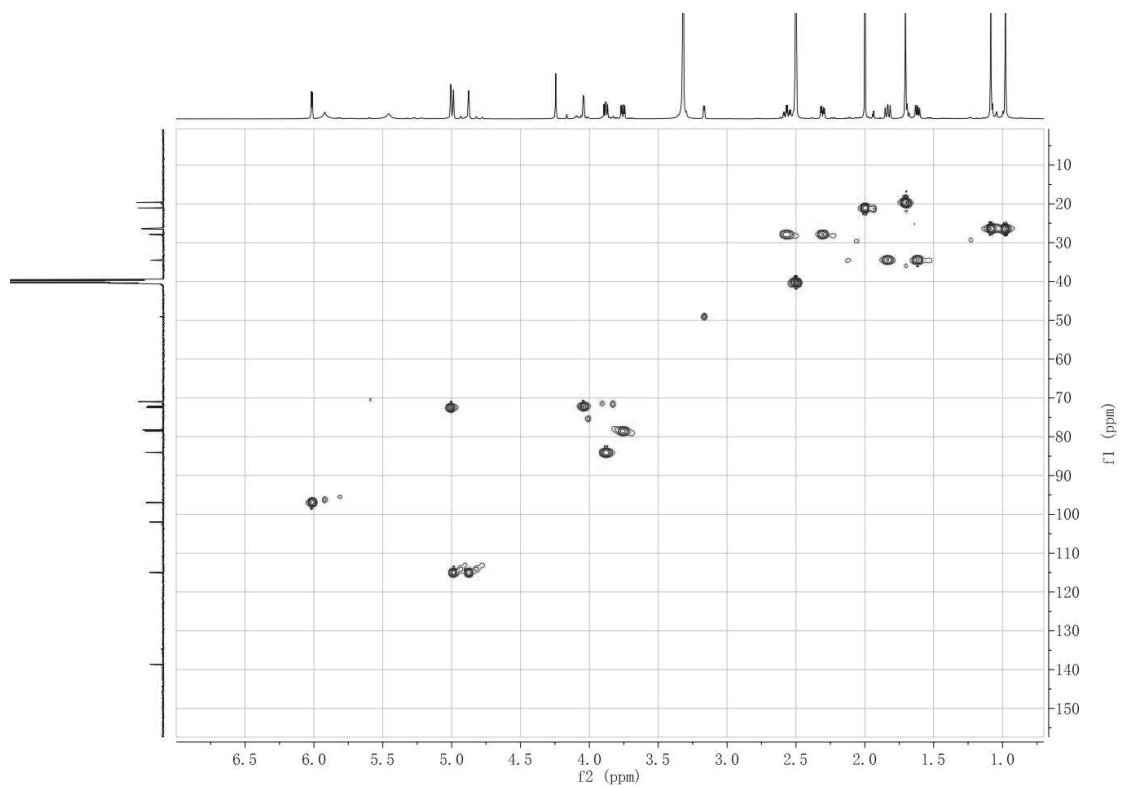


Figure S52. HSQC (600 MHz, $\text{DMSO}-d_6$) spectrum of **7**.

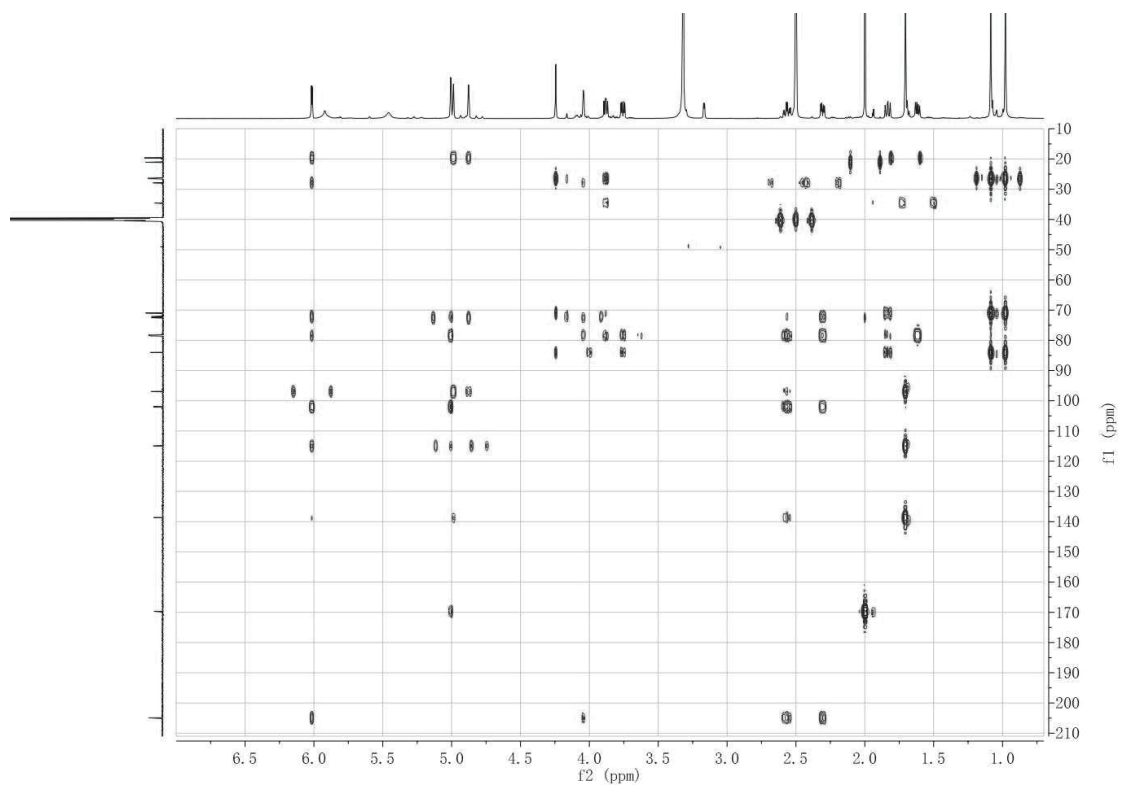


Figure S53. HMBC (600 MHz, DMSO-*d*₆) spectrum of **7**.

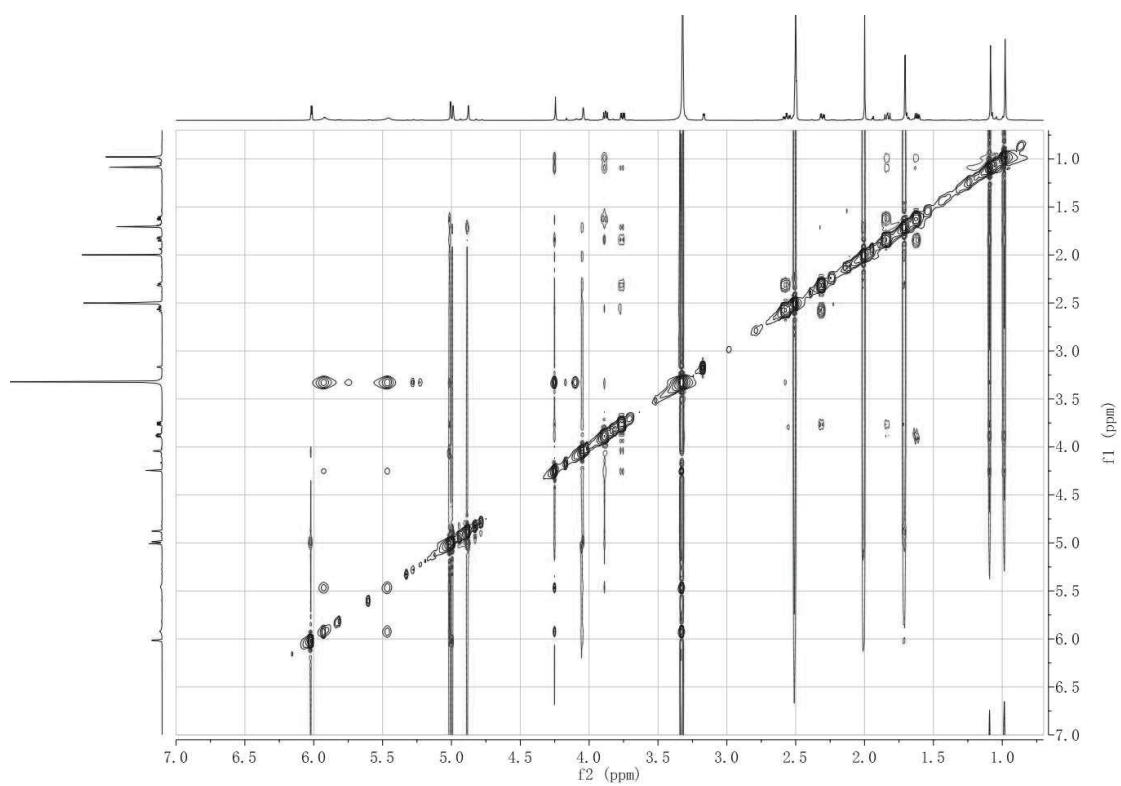


Figure S54. ROESY (600 MHz, DMSO-*d*₆) spectrum of **7**.

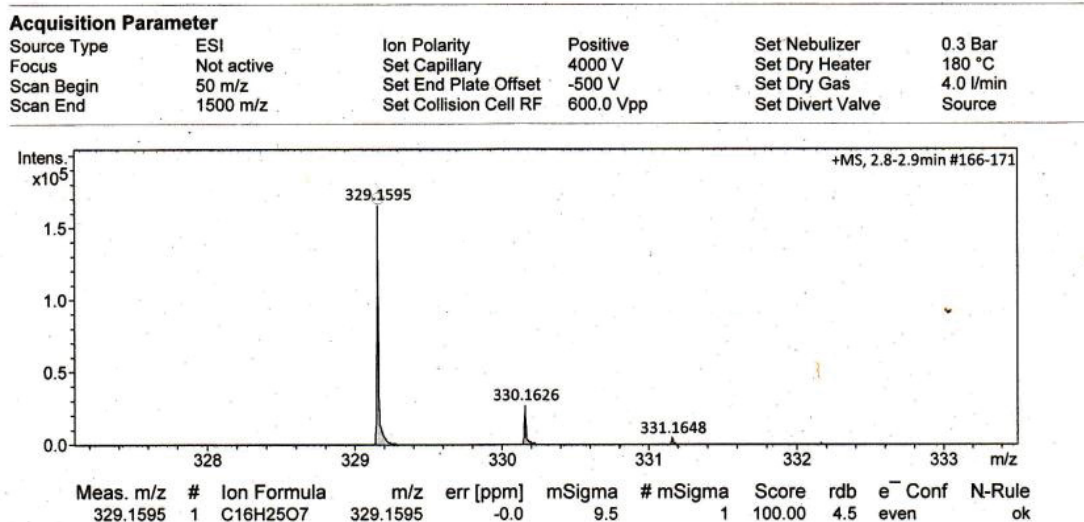


Figure S55. HREISMS of 8.

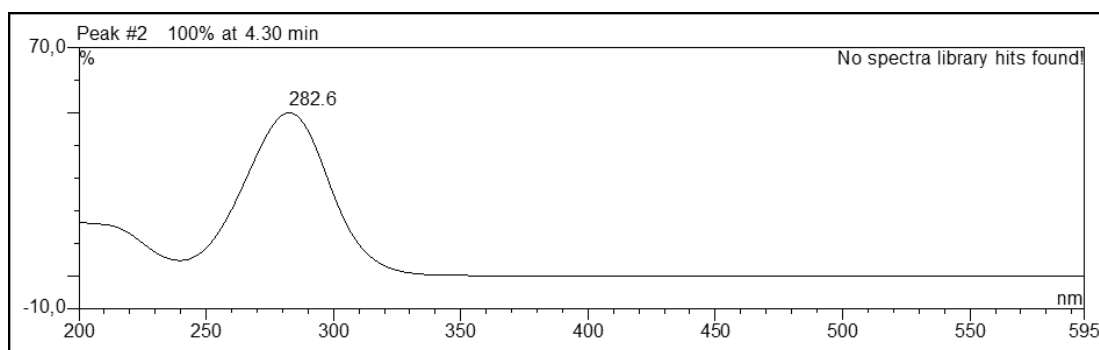


Figure S56. UV spectrum of 8.

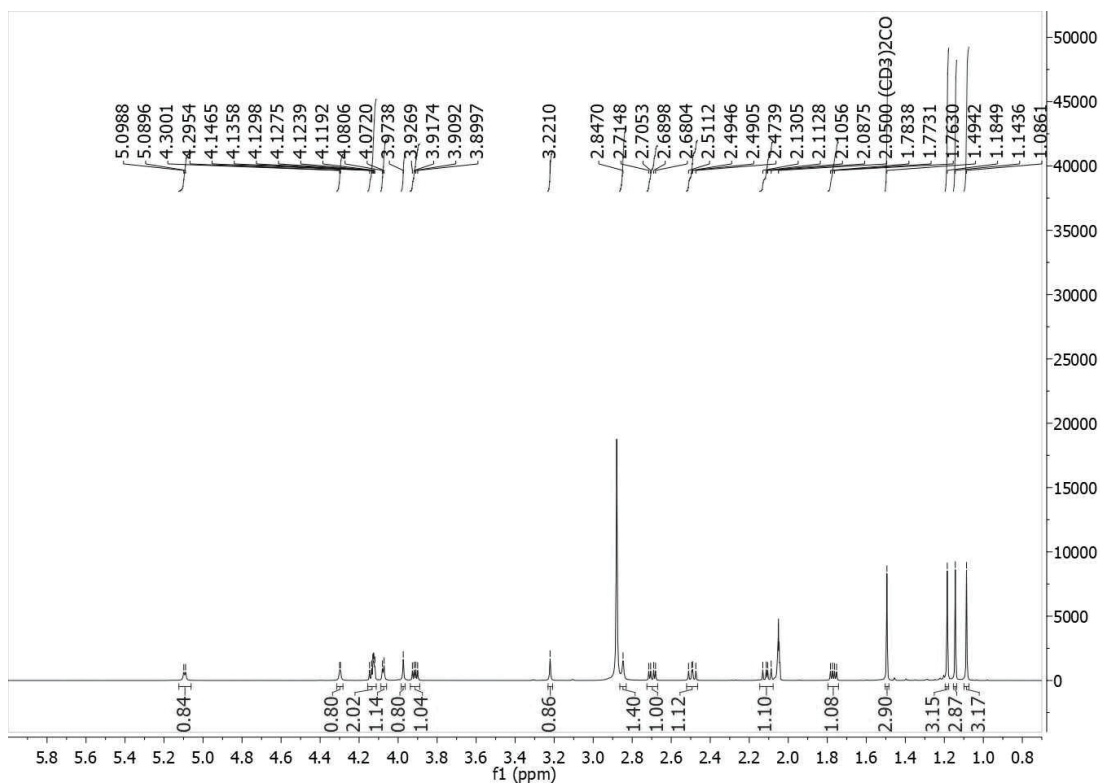


Figure S57. ¹H-NMR (600 MHz, Acetone-*d*₆) spectrum of **8**.

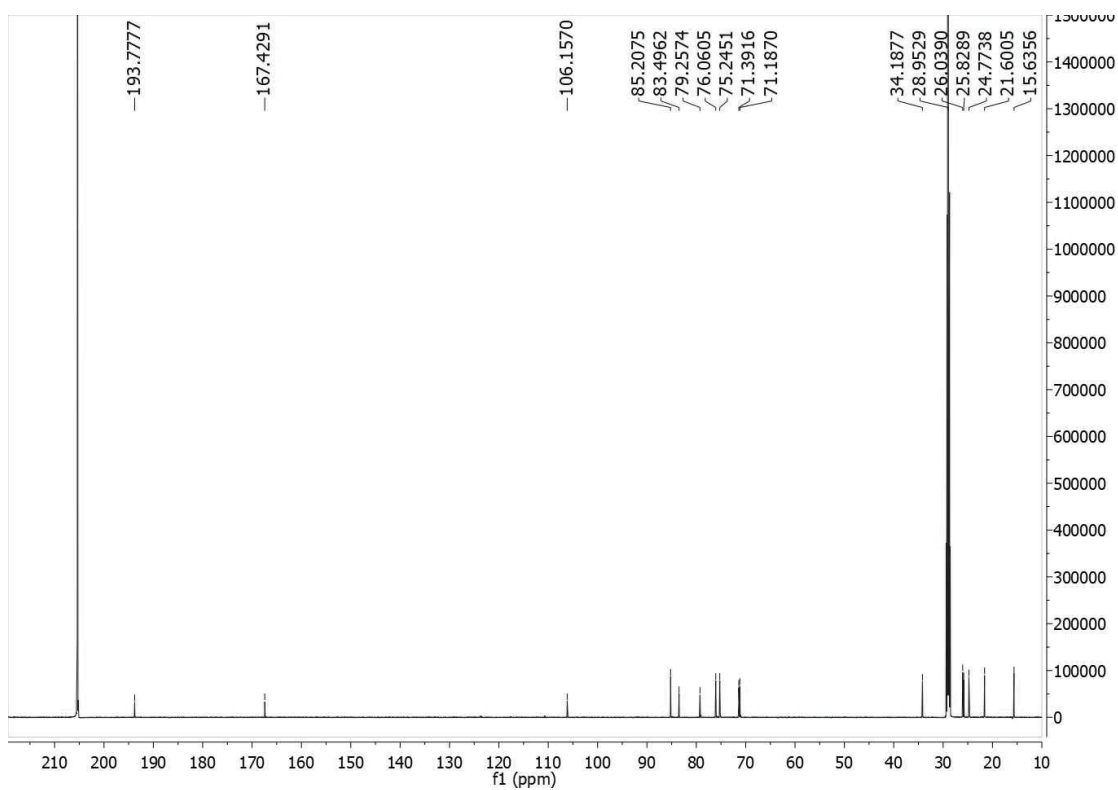


Figure S58. ¹³C-NMR (150 MHz, Acetone-*d*₆) spectrum of **8**.

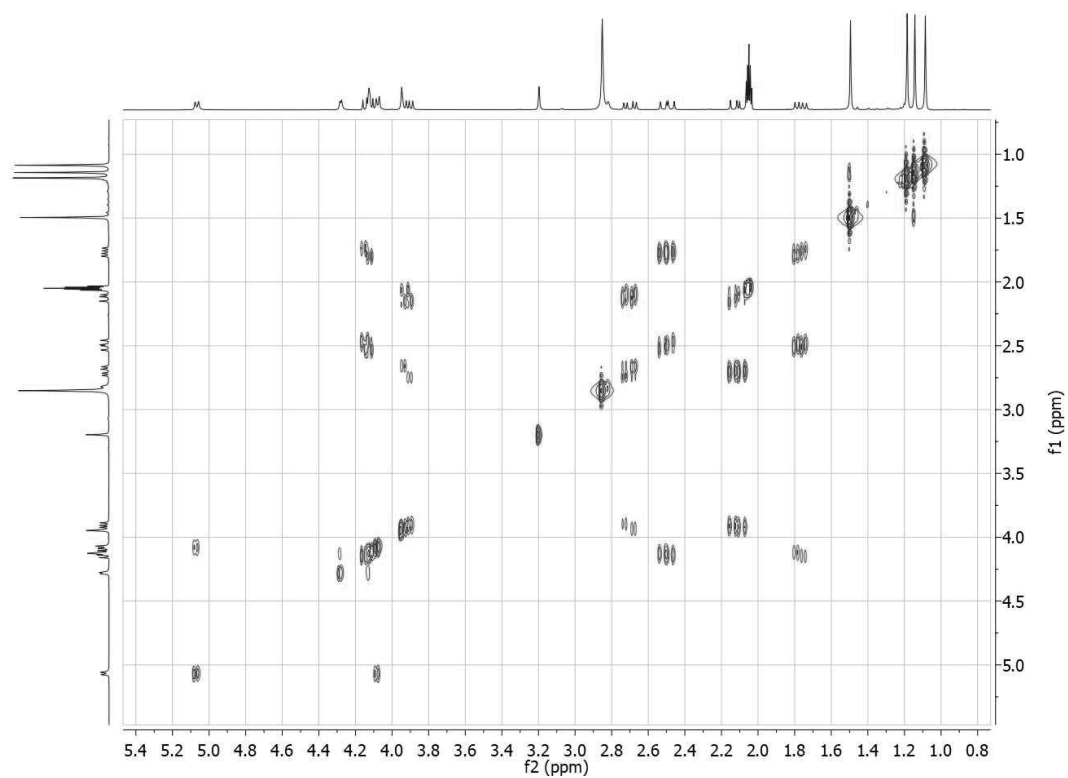


Figure S59. ^1H -H COSY (600 MHz, Acetone- d_6) spectrum of **8**.

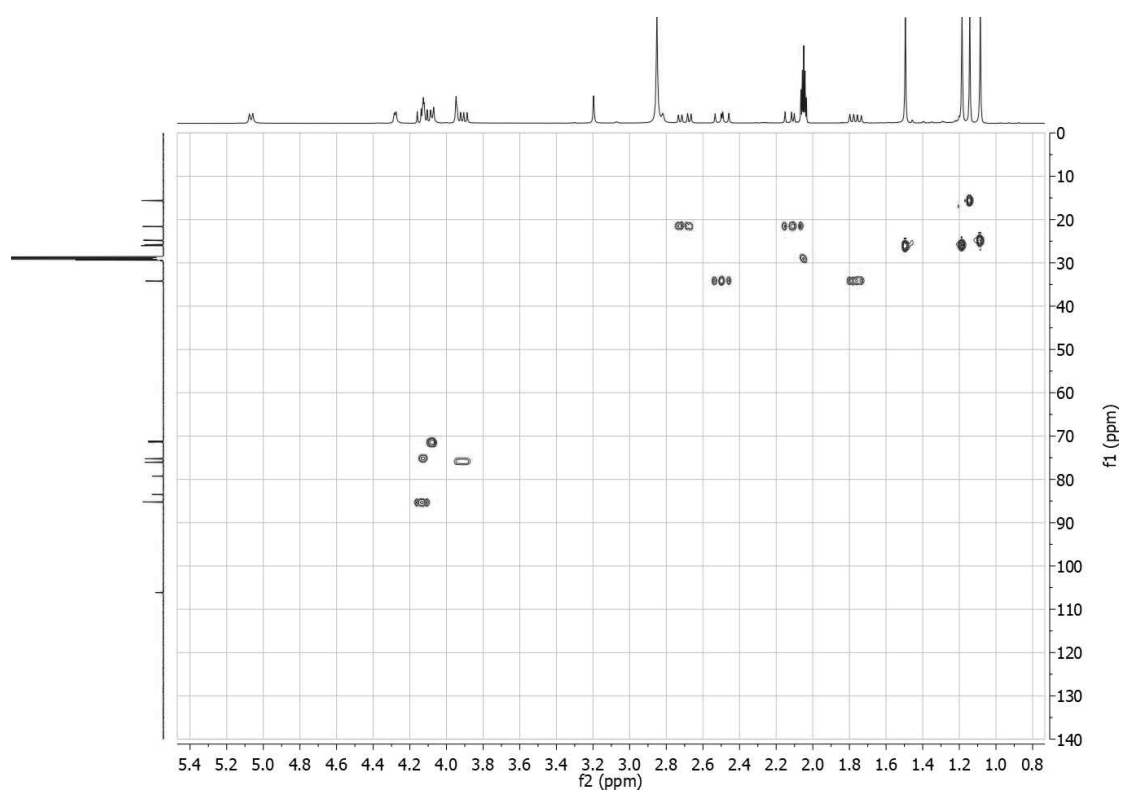


Figure S60. HSQC (600 MHz, Acetone- d_6) spectrum of **8**.

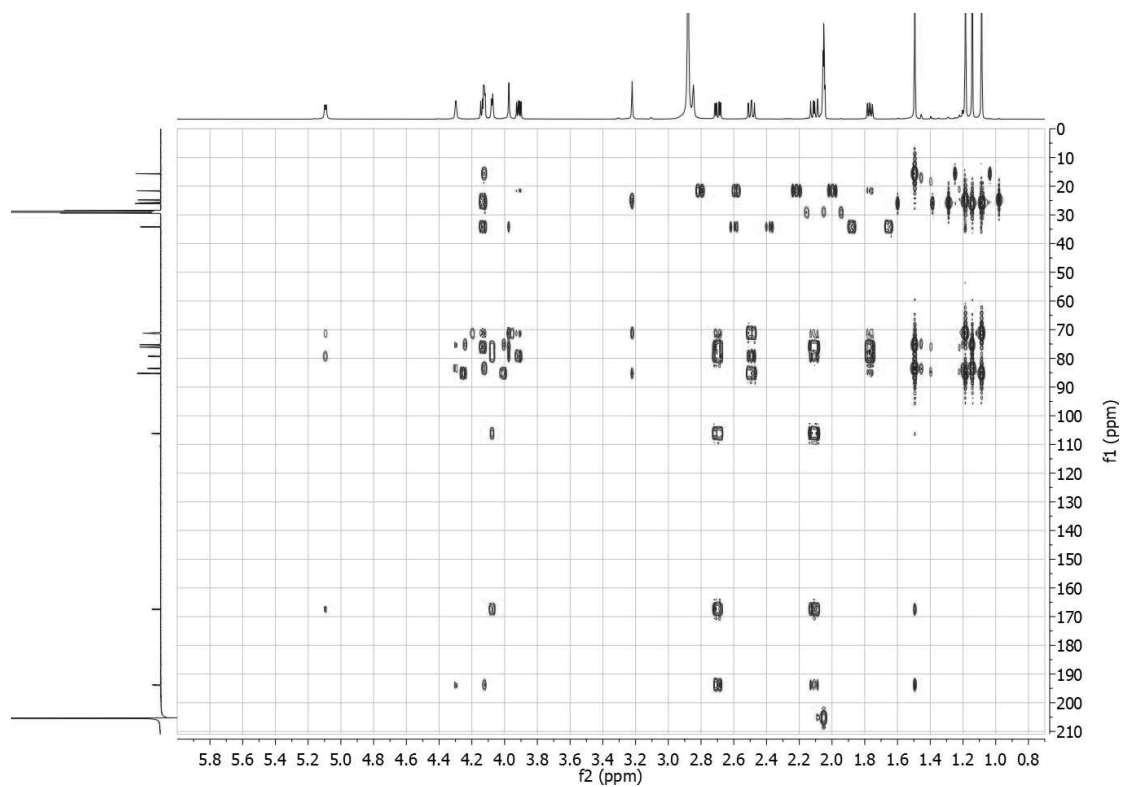


Figure S61. HMBC (600 MHz, Acetone-*d*₆) spectrum of **8**.

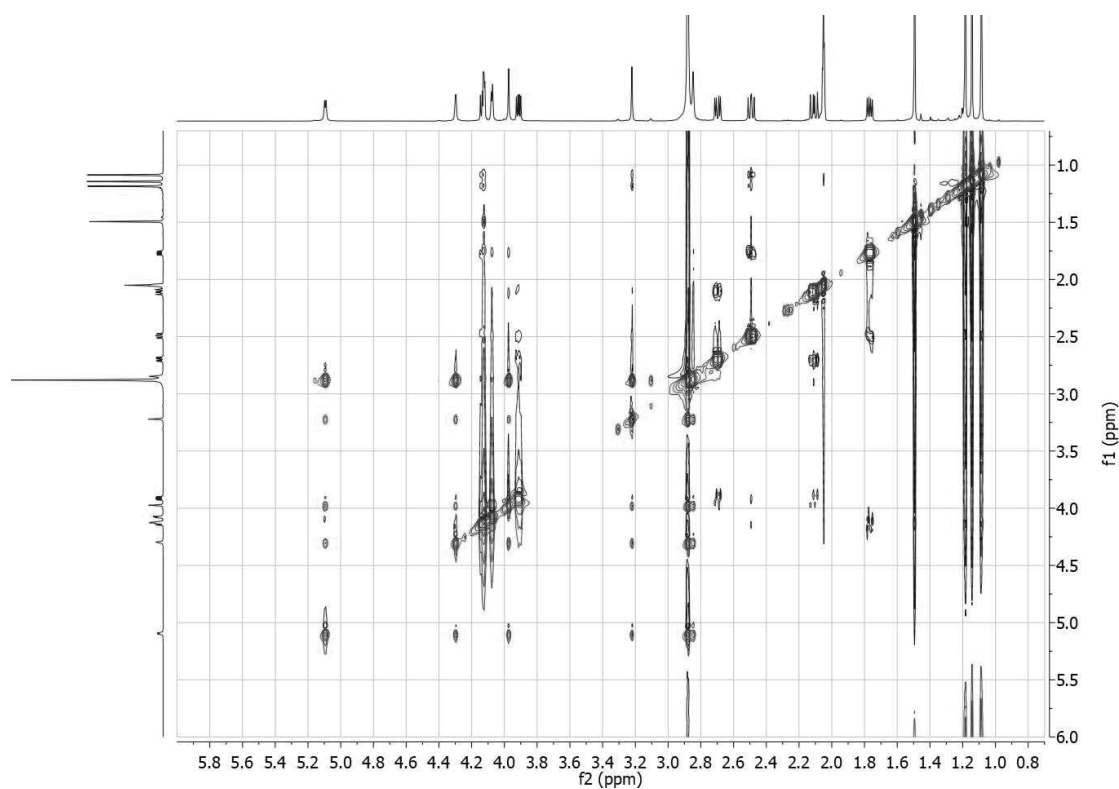
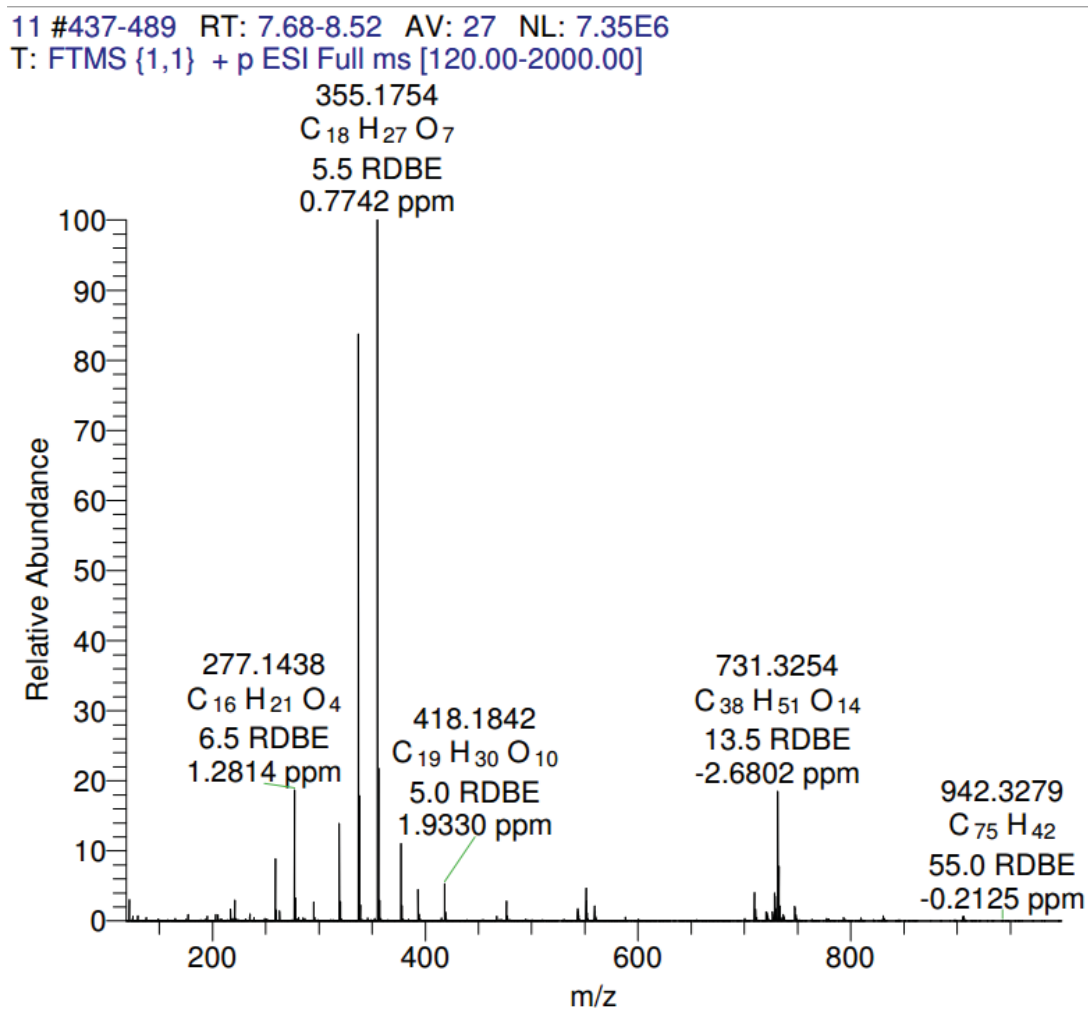
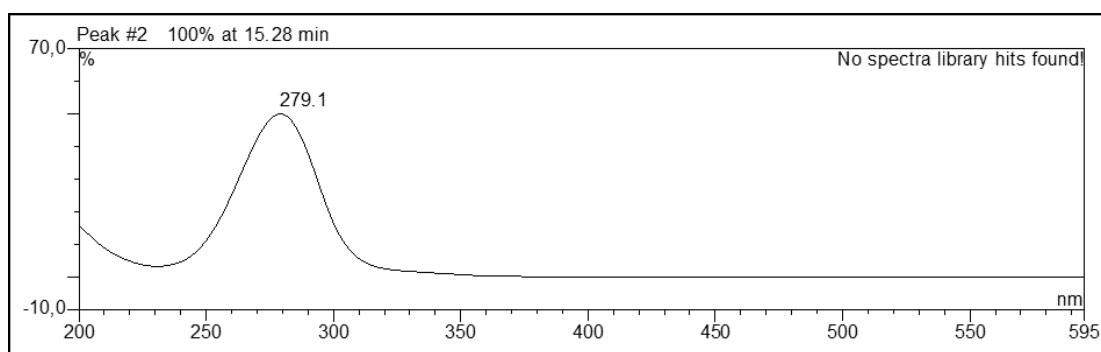


Figure S62. ROESY (600 MHz, Acetone-*d*₆) spectrum of **8**.

Figure S63. HREISMS of **9**.Figure S64. UV spectrum of **9**.

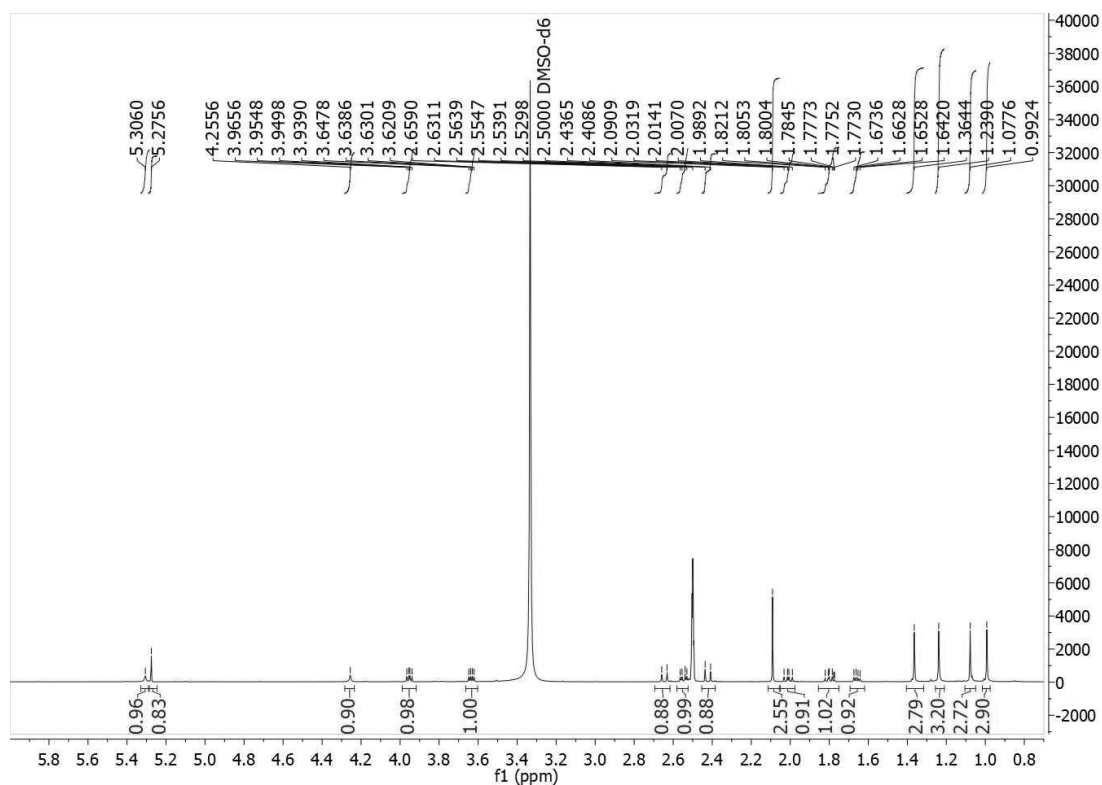


Figure S65. ¹H-NMR (600 MHz, DMSO-*d*₆) spectrum of **9**.

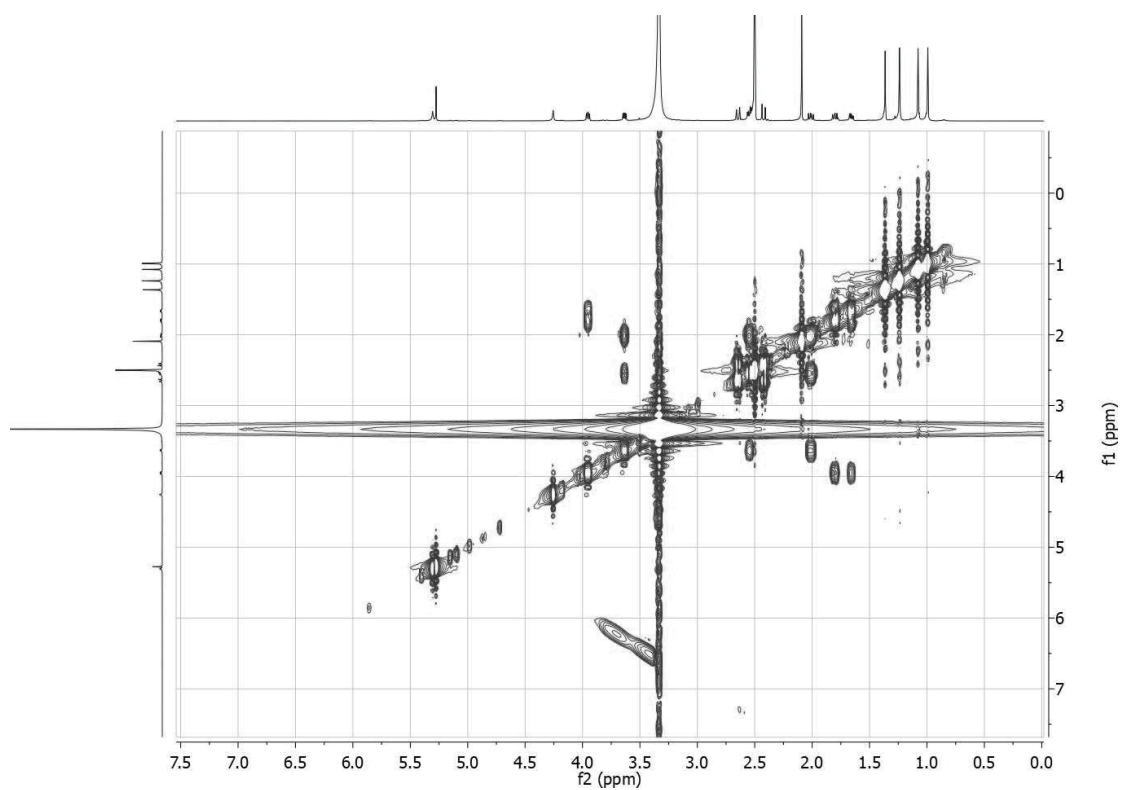


Figure S66. ¹H-¹H COSY (600 MHz, DMSO-*d*₆) spectrum of **9**.

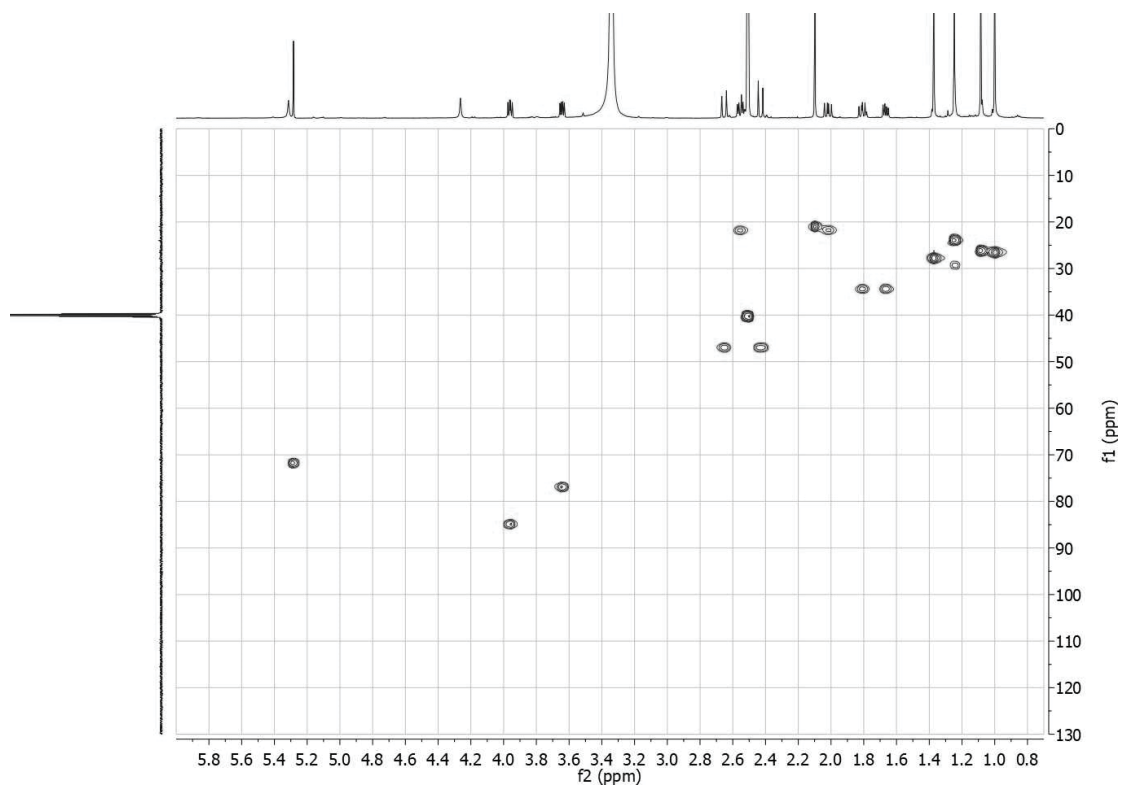


Figure S67. HSQC (600 MHz, DMSO-*d*₆) spectrum of **9**.

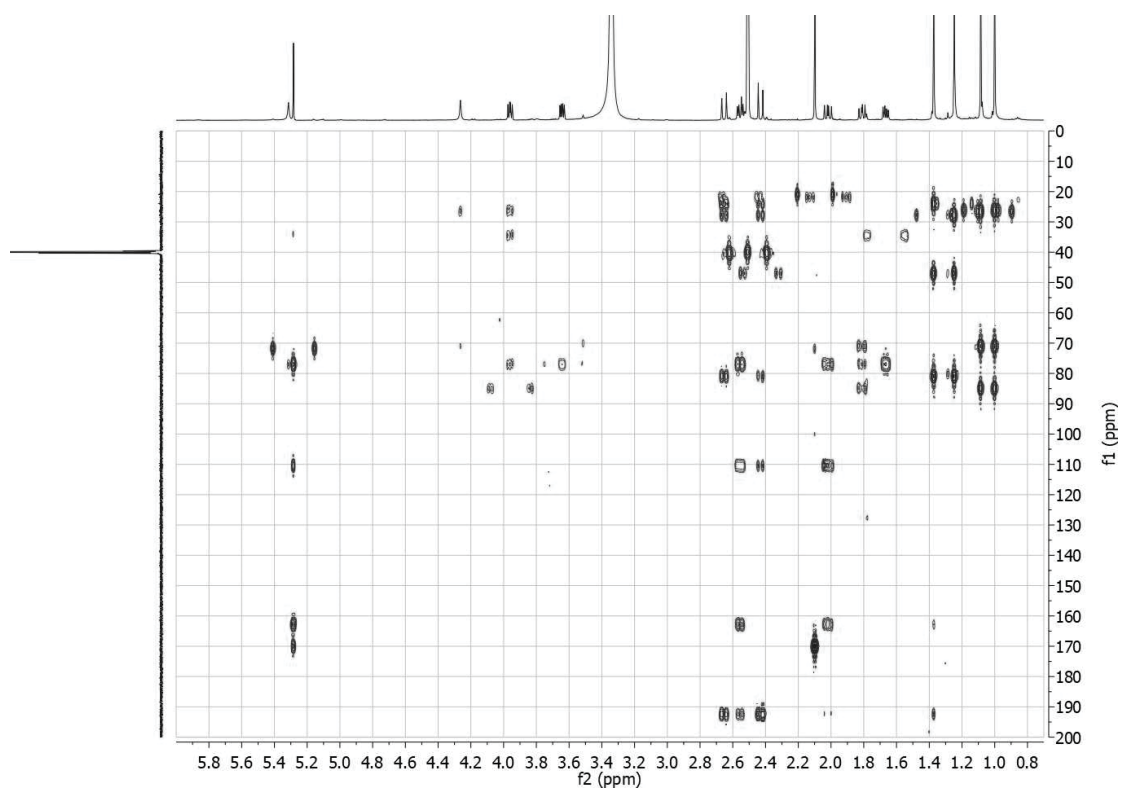


Figure S68. HMBC (600 MHz, DMSO-*d*₆) spectrum of **9**.

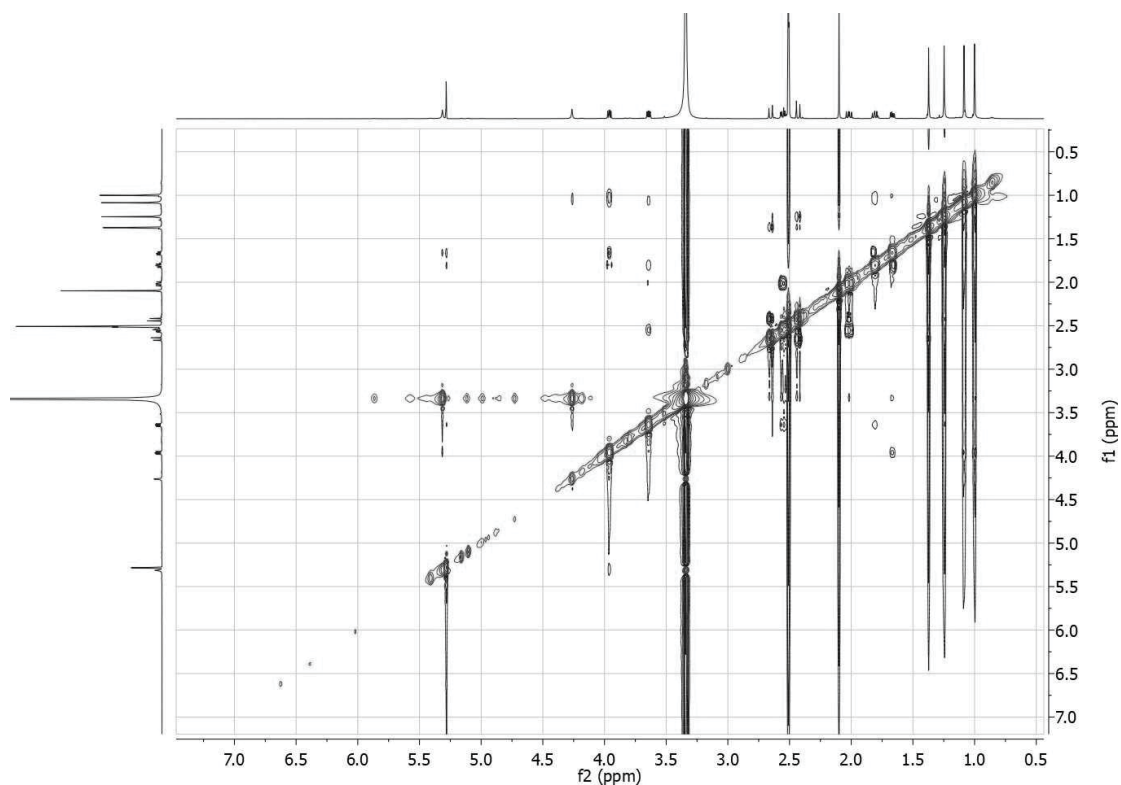
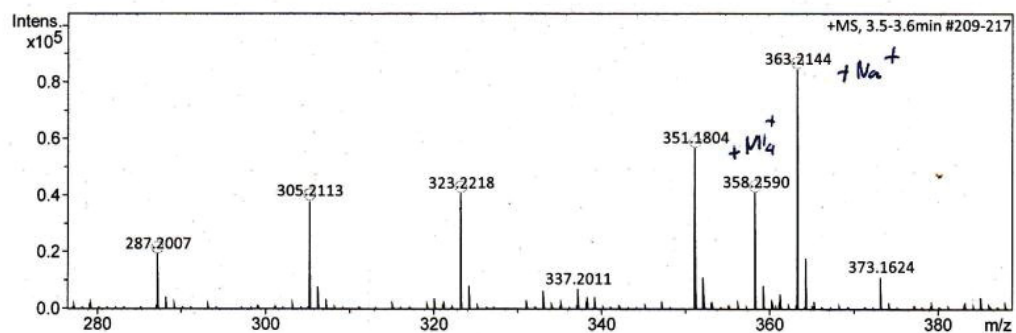


Figure S69. ROESY (600 MHz, DMSO- d_6) spectrum of **9**.

Acquisition Parameter

Source Type	ESI	Ion Polarity	Positive	Set Nebulizer	0.3 Bar
Focus	Not active	Set Capillary	4000 V	Set Dry Heater	180 °C
Scan Begin	50 m/z	Set End Plate Offset	-500 V	Set Dry Gas	4.0 l/min
Scan End	1500 m/z	Set Collision Cell RF	600.0 Vpp	Set Divert Valve	Source



Meas. m/z	#	Ion Formula	m/z	err [ppm]	mSigma	# mSigma	Score	rdb	e ⁻ Conf	N-Rule
287.2007	1	C ₁₉ H ₂₇ O ₂	287.2006	-0.5	42.2	1	100.00	6.5	even	ok
305.2113	1	C ₁₉ H ₂₉ O ₃	305.2111	-0.5	34.9	1	100.00	5.5	even	ok
323.2218	1	C ₁₉ H ₃₁ O ₄	323.2217	-0.4	3.4	1	100.00	4.5	even	ok
351.1804	1	C ₁₉ H ₂₇ O ₆	351.1802	-0.5	6.9	1	100.00	6.5	even	ok
358.2590	1	C ₁₉ H ₃₆ NO ₅	358.2588	-0.6	10.3	1	100.00	2.5	even	ok
363.2144	1	C ₁₉ H ₃₂ NaO ₅	363.2142	-0.7	1.0	1	100.00	3.5	even	ok

Figure S70. HREISMS of **15**.

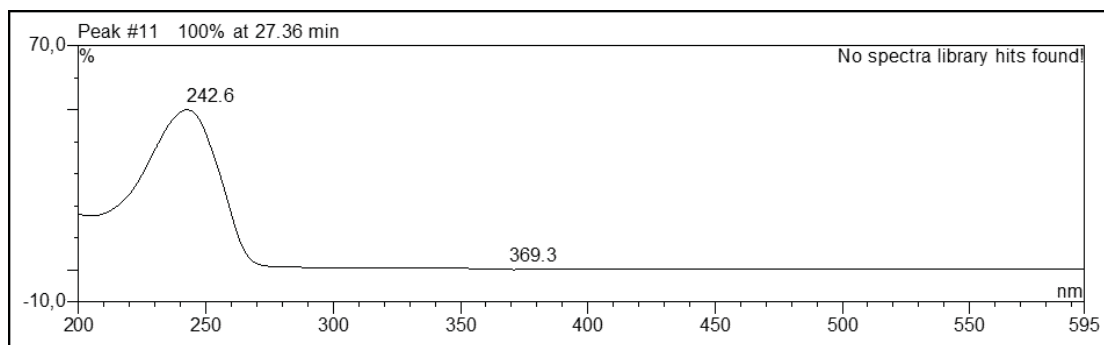


Figure S71. UV spectrum of **15**.

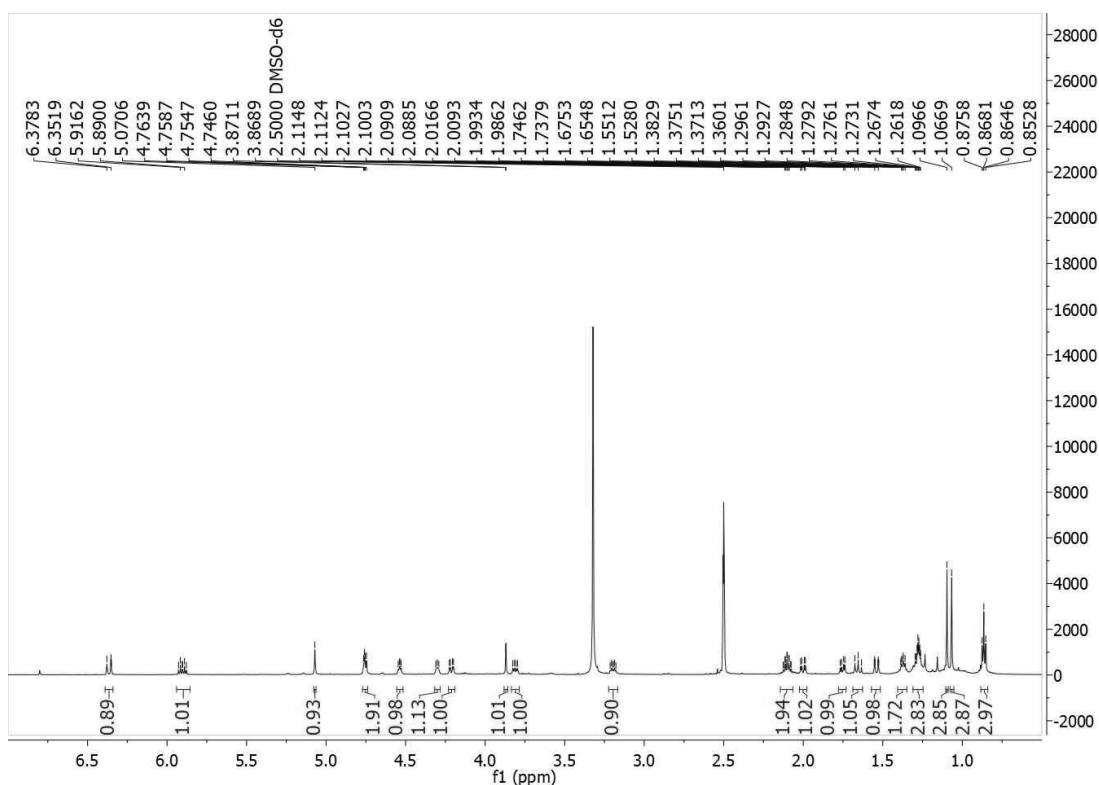


Figure S72. ¹H-NMR (600 MHz, DMSO-*d*₆) spectrum of **15**.

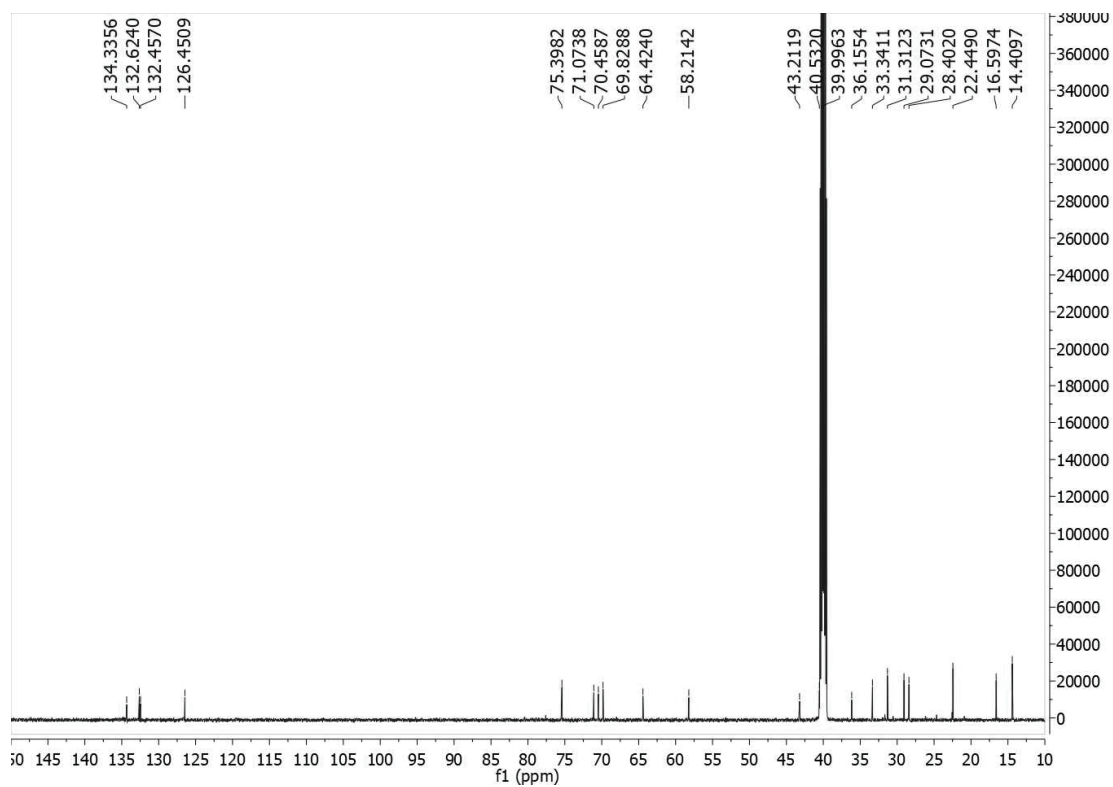


Figure S73. ^{13}C -NMR (150 MHz, $\text{DMSO}-d_6$) spectrum of **15**.

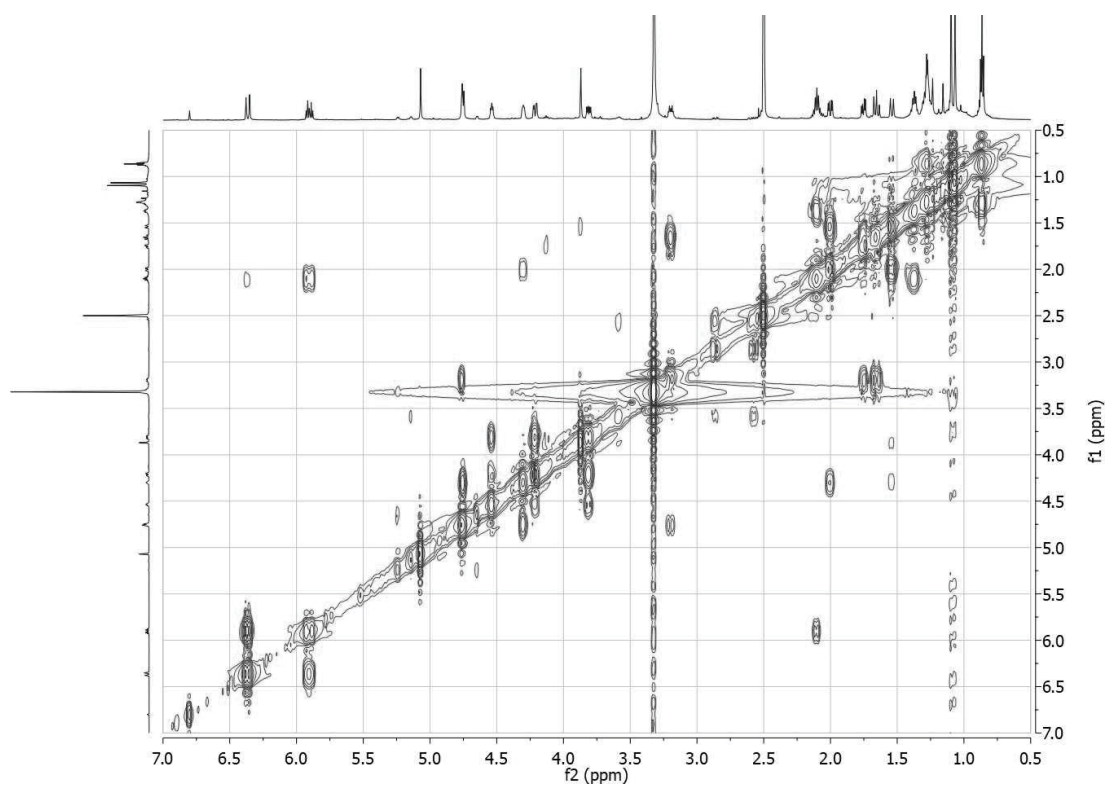


Figure S74. ^1H - ^1H COSY (600 MHz, $\text{DMSO}-d_6$) spectrum of **15**.

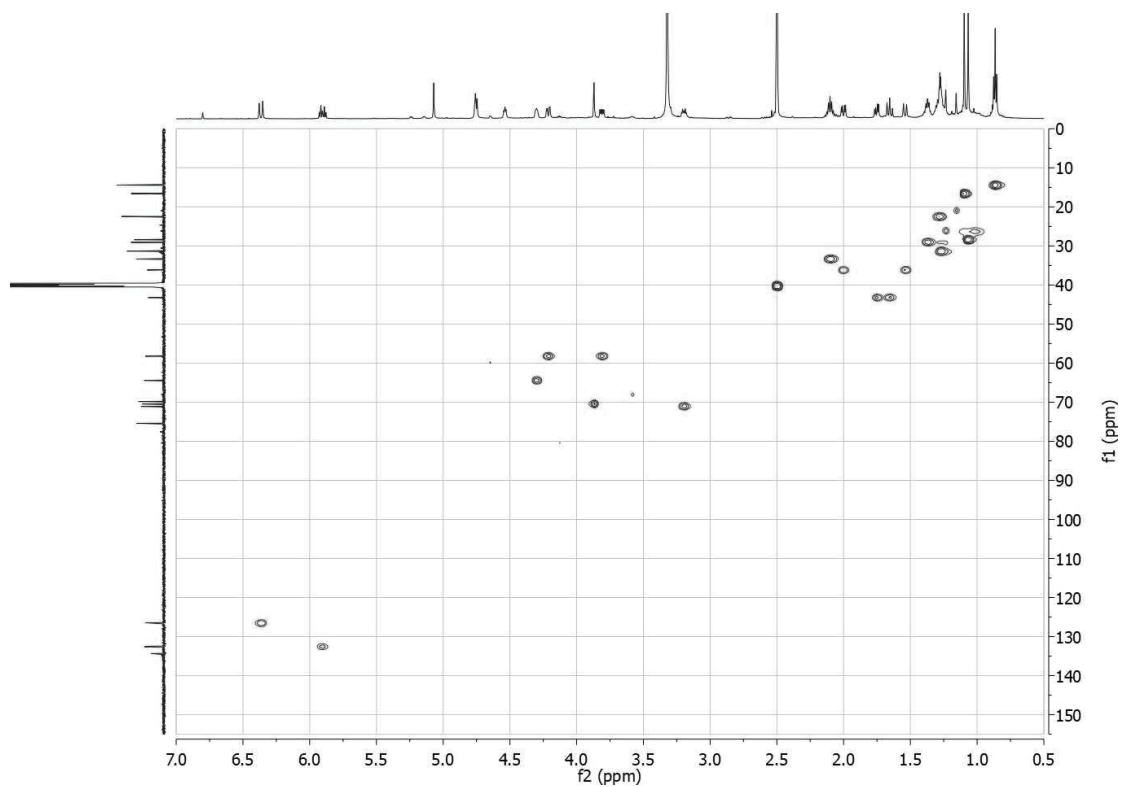


Figure S75. HSQC (600 MHz, DMSO- d_6) spectrum of **15**.

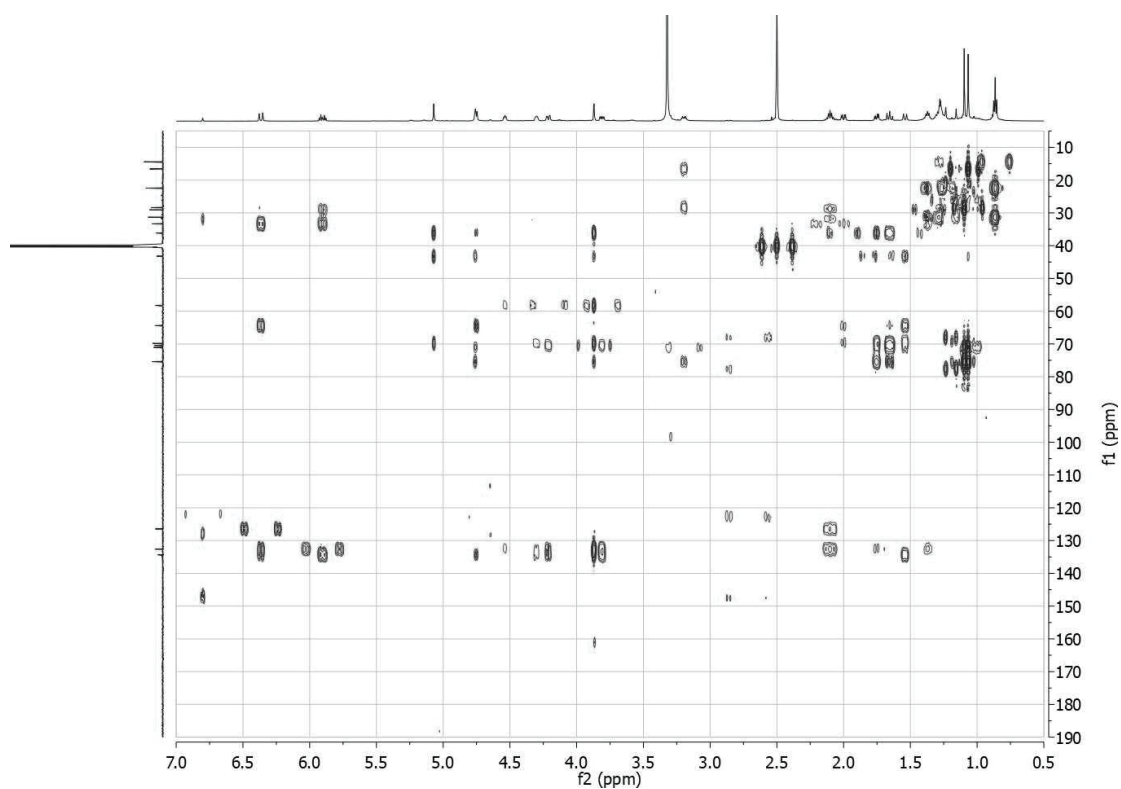


Figure S76. HMBC (600 MHz, DMSO- d_6) spectrum of **15**.

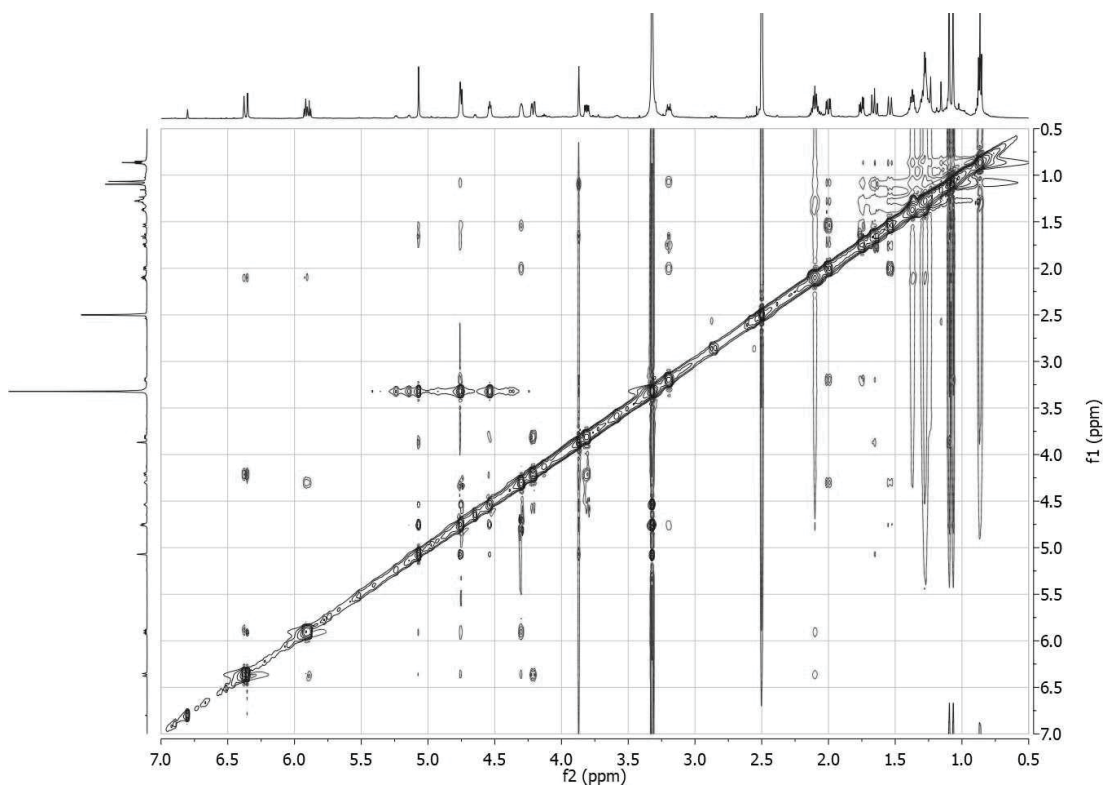


Figure S77. ROESY (600 MHz, DMSO- d_6) spectrum of **15**.

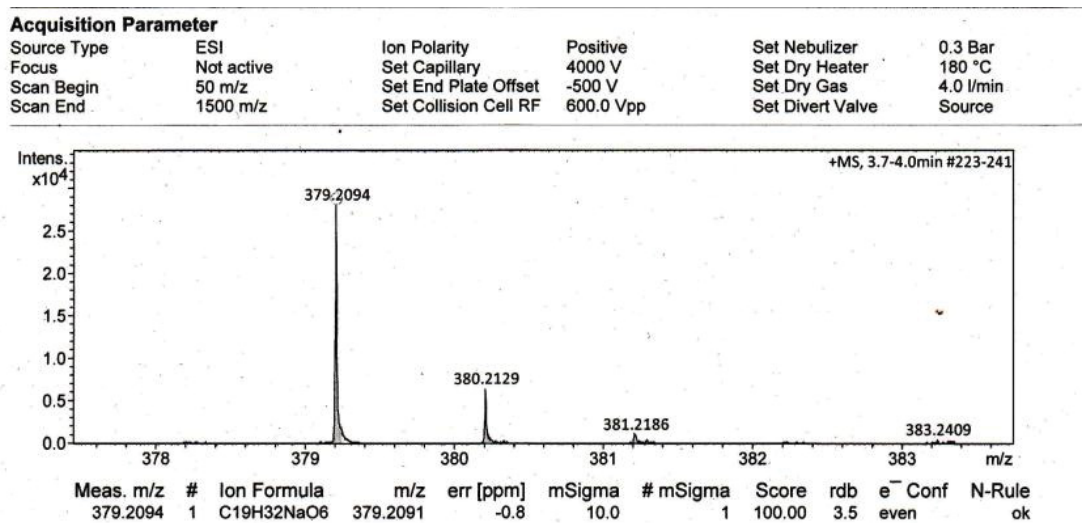


Figure S78. HREISMS of **16**.

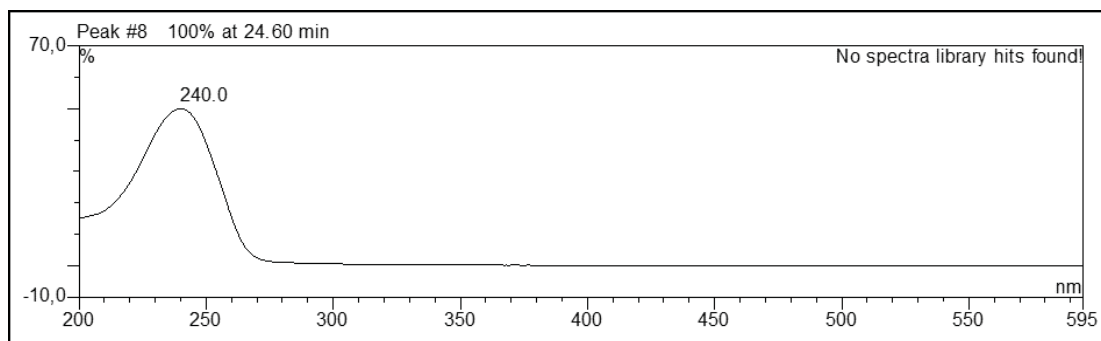


Figure S79. UV spectrum of **16**.

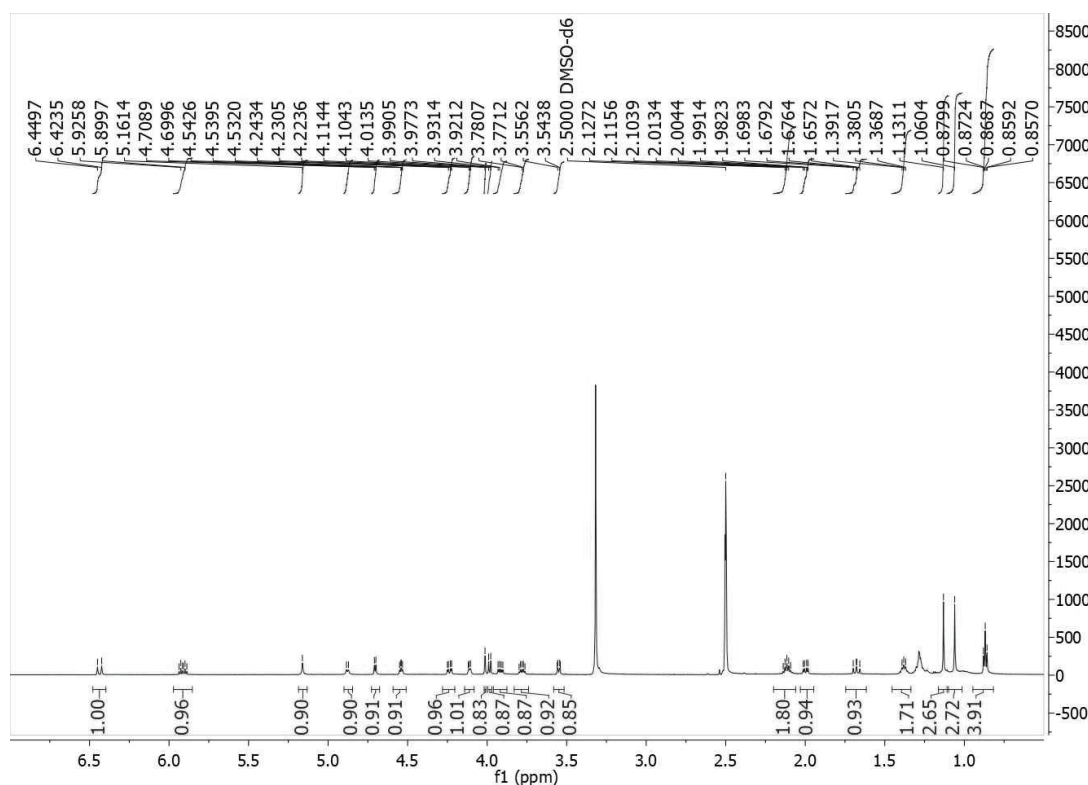


Figure S80. ^1H -NMR (600 MHz, $\text{DMSO}-d_6$) spectrum of **16**.

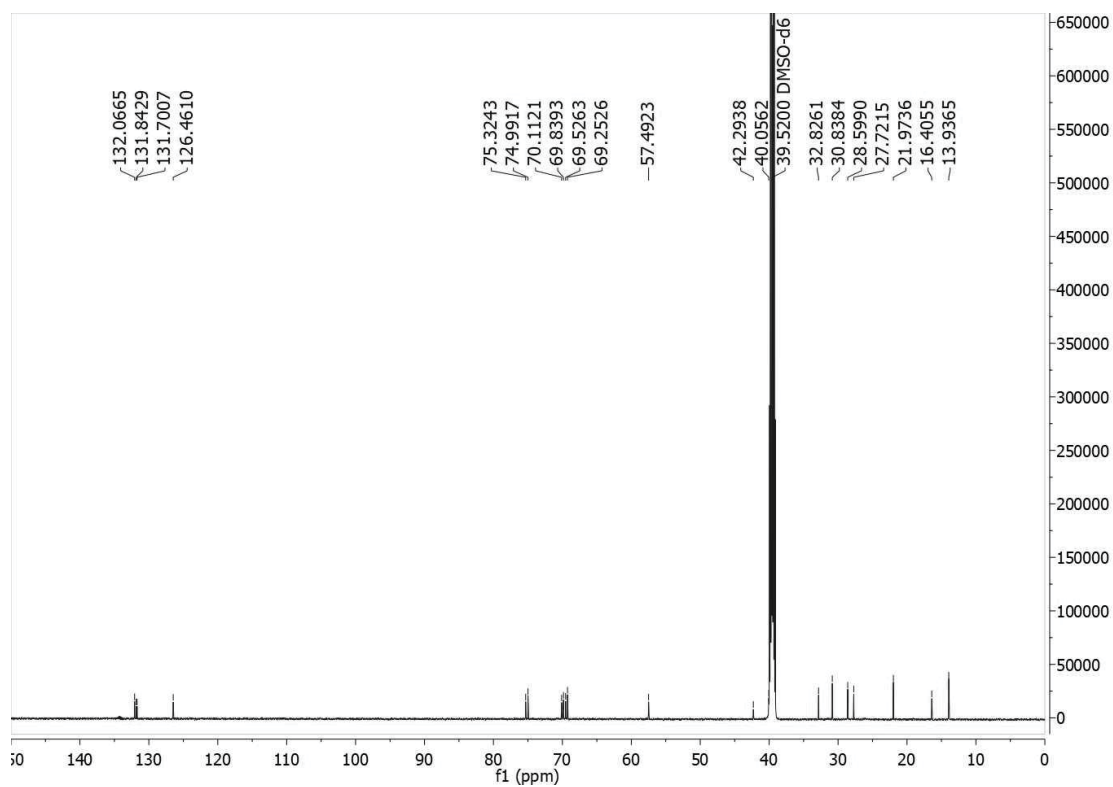


Figure S81. ^{13}C -NMR (150 MHz, $\text{DMSO}-d_6$) spectrum of **16**.

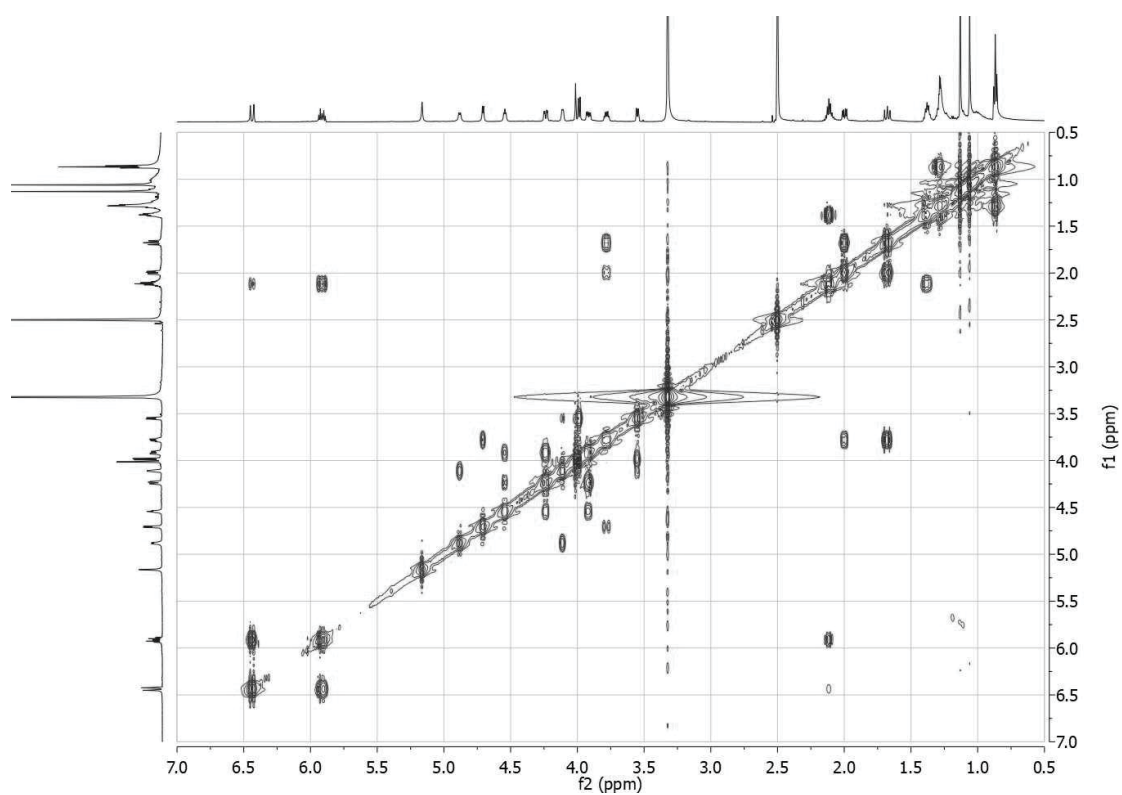


Figure S82. ^1H - ^1H COSY (600 MHz, $\text{DMSO}-d_6$) spectrum of **16**.

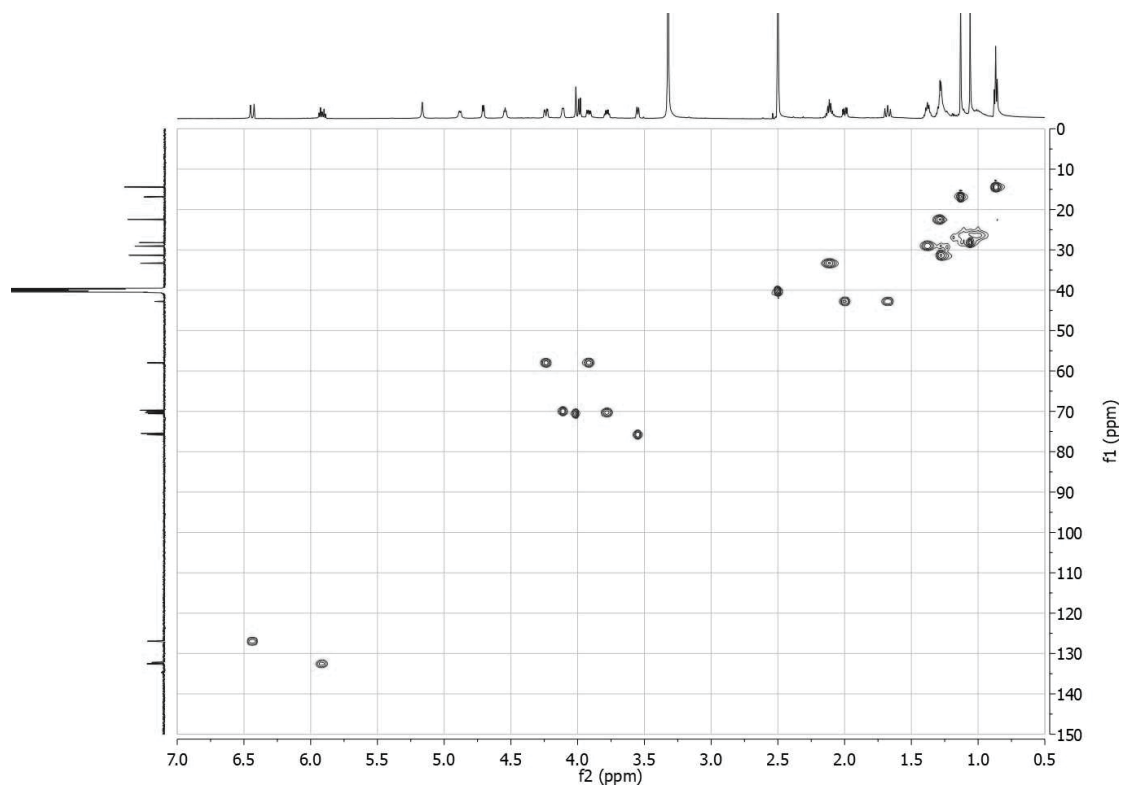


Figure S83. HSQC (600 MHz, DMSO-*d*₆) spectrum of **16**.

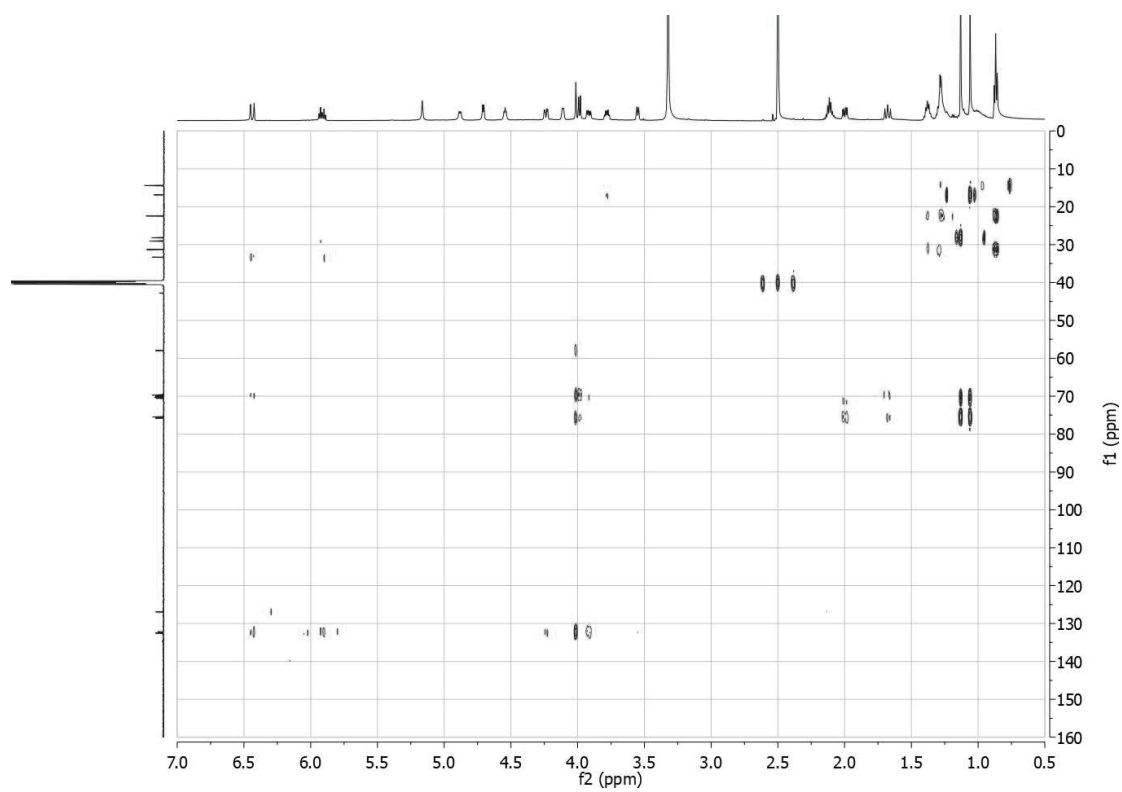
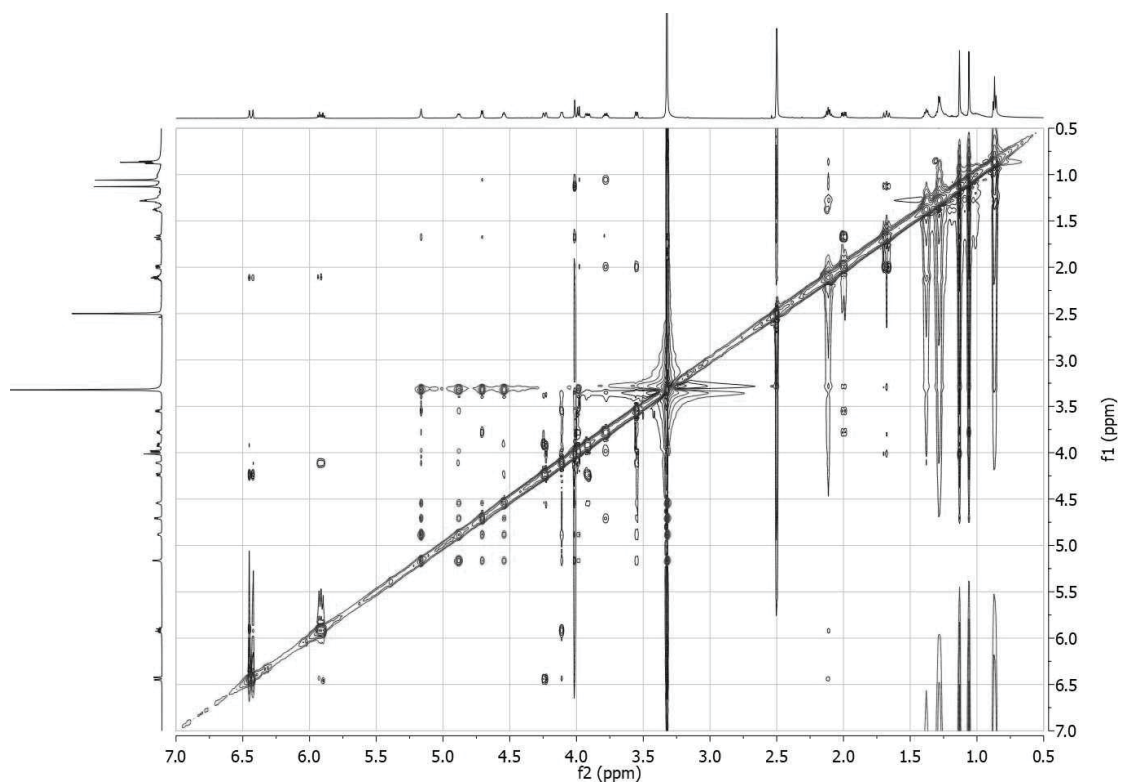
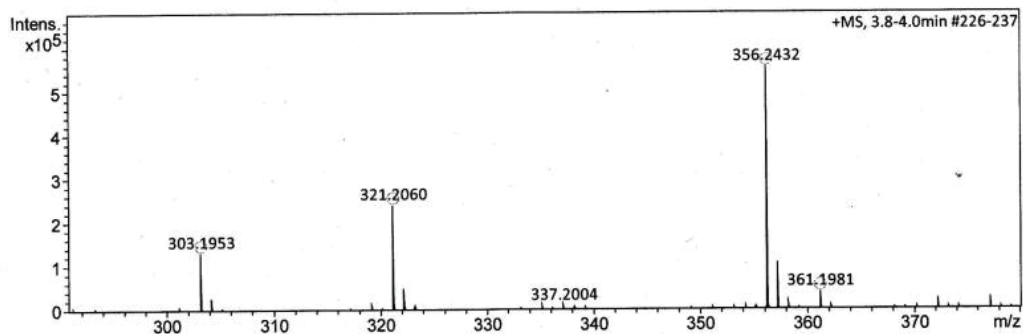


Figure S84. HMBC (600 MHz, DMSO-*d*₆) spectrum of **16**.

Figure S85. ROESY (600 MHz, DMSO-*d*₆) spectrum of **16**.**Acquisition Parameter**

Source Type	ESI	Ion Polarity	Positive	Set Nebulizer	0.3 Bar
Focus	Not active	Set Capillary	4000 V	Set Dry Heater	180 °C
Scan Begin	50 m/z	Set End Plate Offset	-500 V	Set Dry Gas	4.0 l/min
Scan End	1500 m/z	Set Collision Cell RF	600.0 Vpp	Set Divert Valve	Source



Meas. m/z	#	Ion Formula	m/z	err [ppm]	mSigma	# mSigma	Score	rdb	e ⁻ Conf	N-Rule
303.1953	1	C ₁₉ H ₂₇ O ₃	303.1955	0.5	6.3	1	100.00	6.5	even	ok
321.2060	1	C ₁₉ H ₂₉ O ₄	321.2060	0.1	4.9	1	100.00	5.5	even	ok
	2	C ₁₈ H ₂₆ N ₄ Na	321.2050	-3.3	7.5	2	57.53	7.5	even	ok
	3	C ₂₀ H ₂₅ N ₄	321.2074	4.2	18.5	3	38.70	10.5	even	ok
356.2432	1	C ₁₉ H ₃₄ NO ₅	356.2431	-0.2	13.3	1	100.00	3.5	even	ok
	2	C ₁₈ H ₃₁ N ₅ NaO	356.2421	-3.2	14.5	2	57.33	5.5	even	ok

Figure S86. HREISMS of **17**.

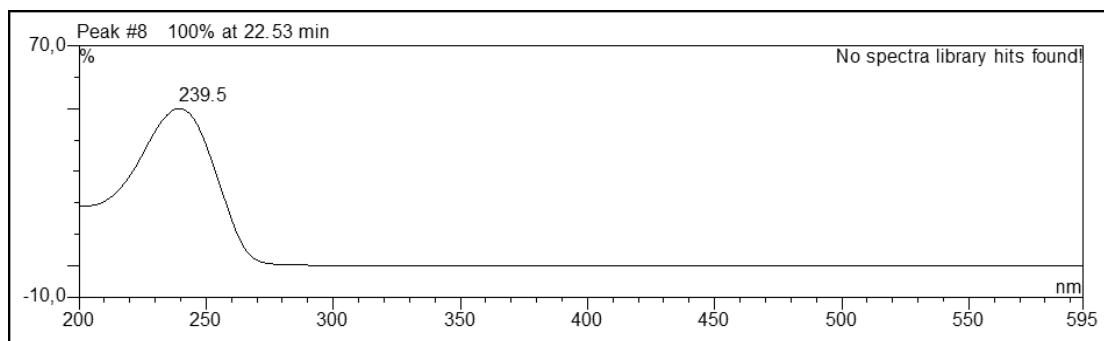


Figure S87. UV spectrum of 17.

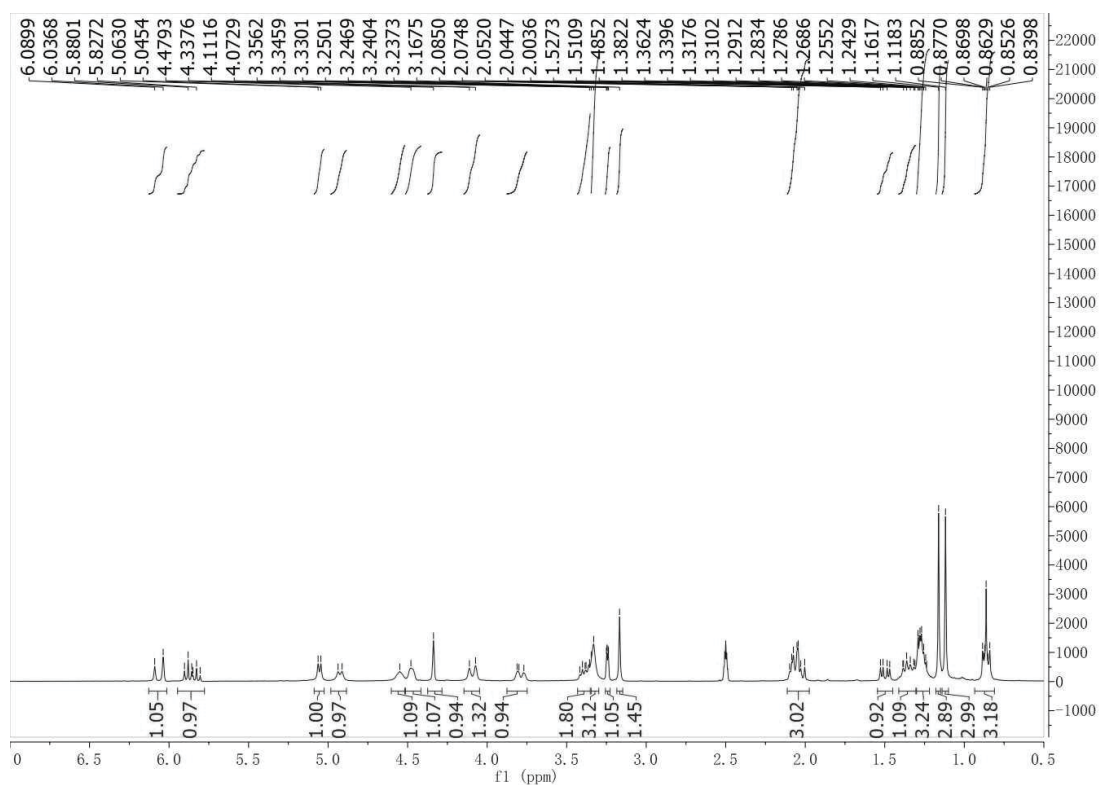


Figure S88. ^1H -NMR (300 MHz, $\text{DMSO}-d_6$) spectrum of 17.

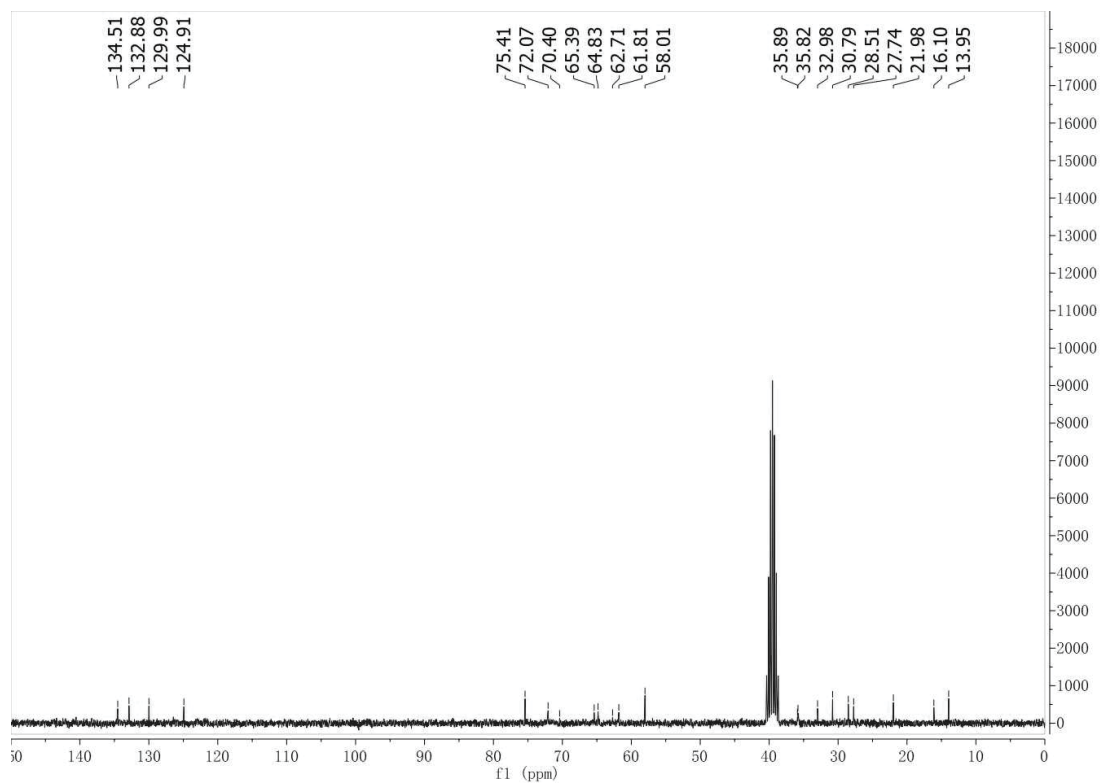


Figure S89. ^{13}C -NMR (75 MHz, $\text{DMSO}-d_6$) spectrum of **17**.

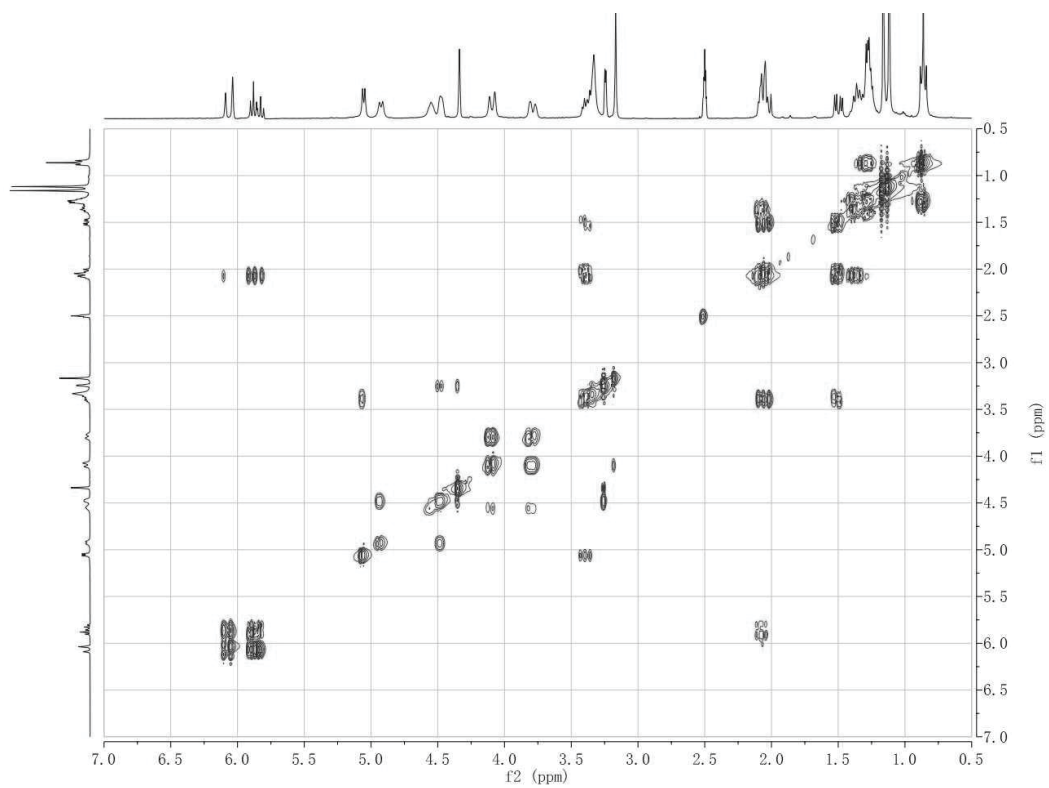


Figure S90. ^1H - ^1H COSY (300 MHz, $\text{DMSO}-d_6$) spectrum of **17**.

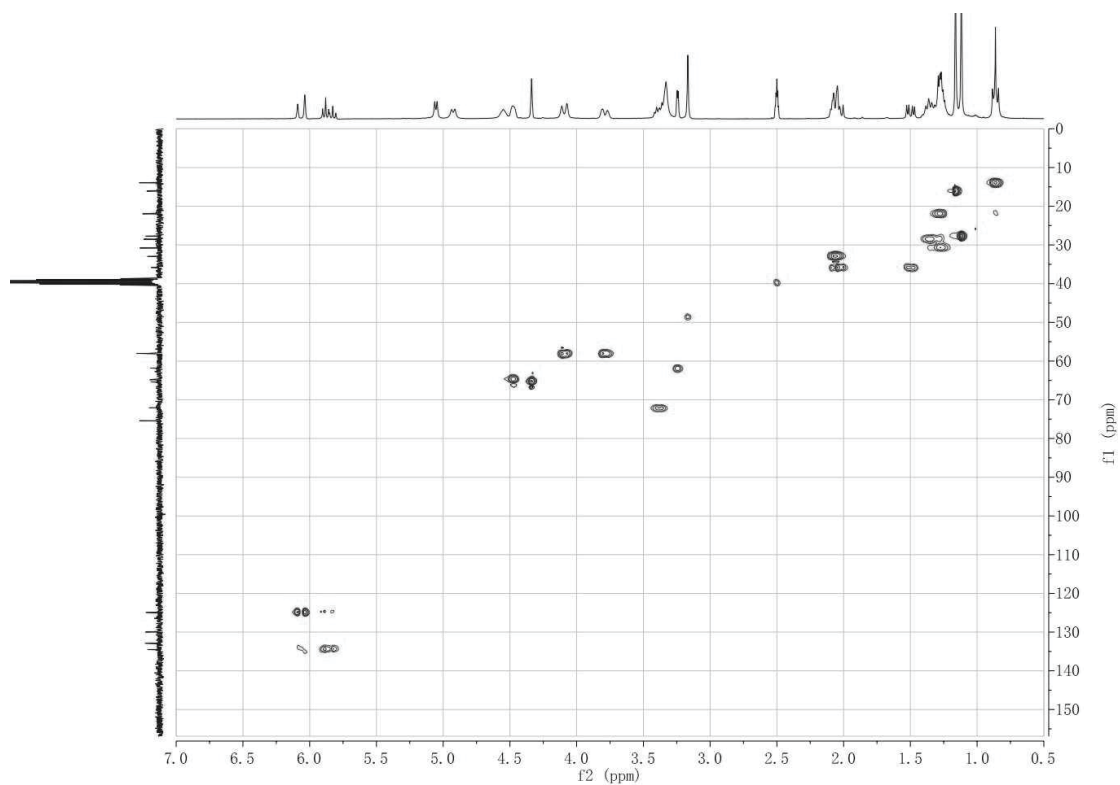


Figure S91. HSQC (300 MHz, DMSO- d_6) spectrum of **17**.

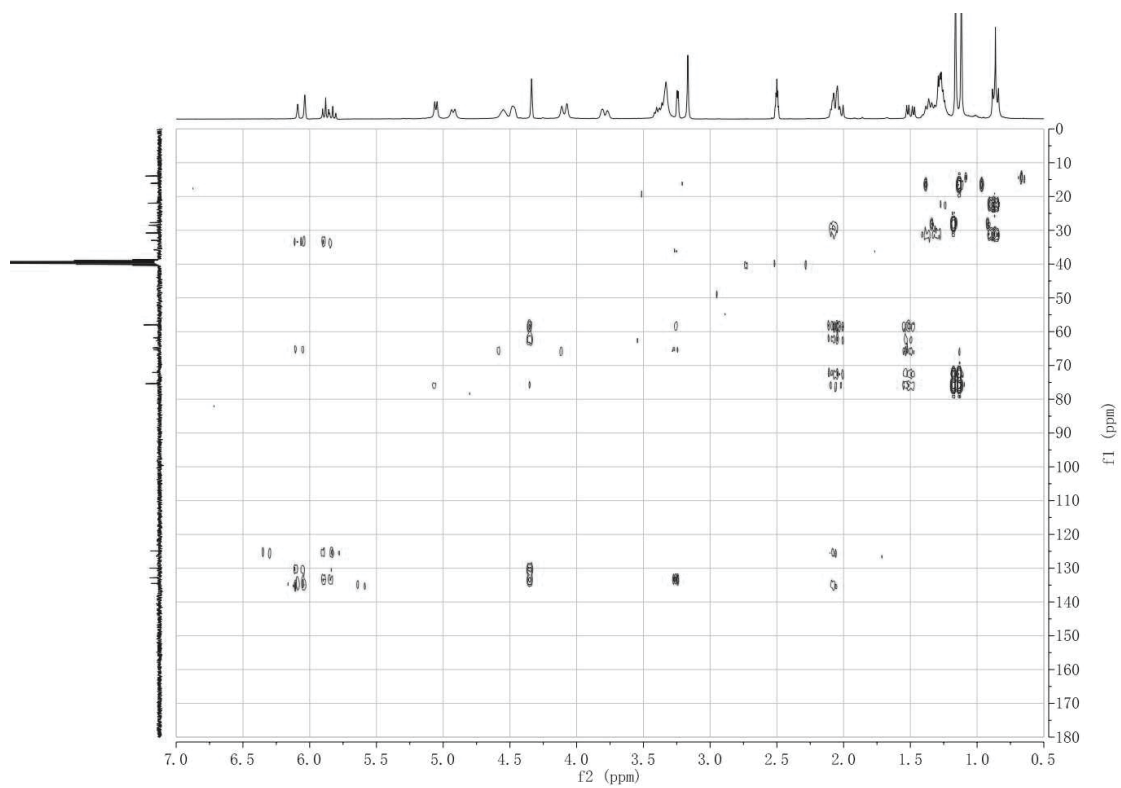


Figure S92. HMBC (300 MHz, DMSO- d_6) spectrum of **17**.

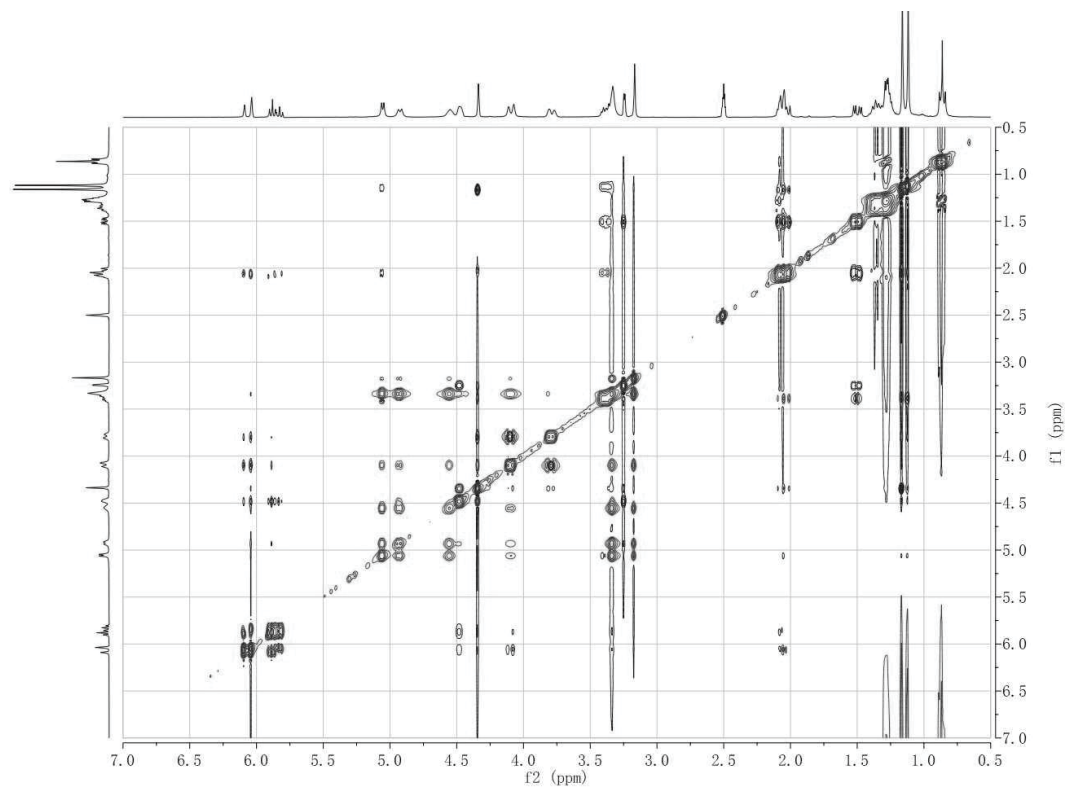


Figure S93. ROESY (300 MHz, DMSO-*d*₆) spectrum of **17**.

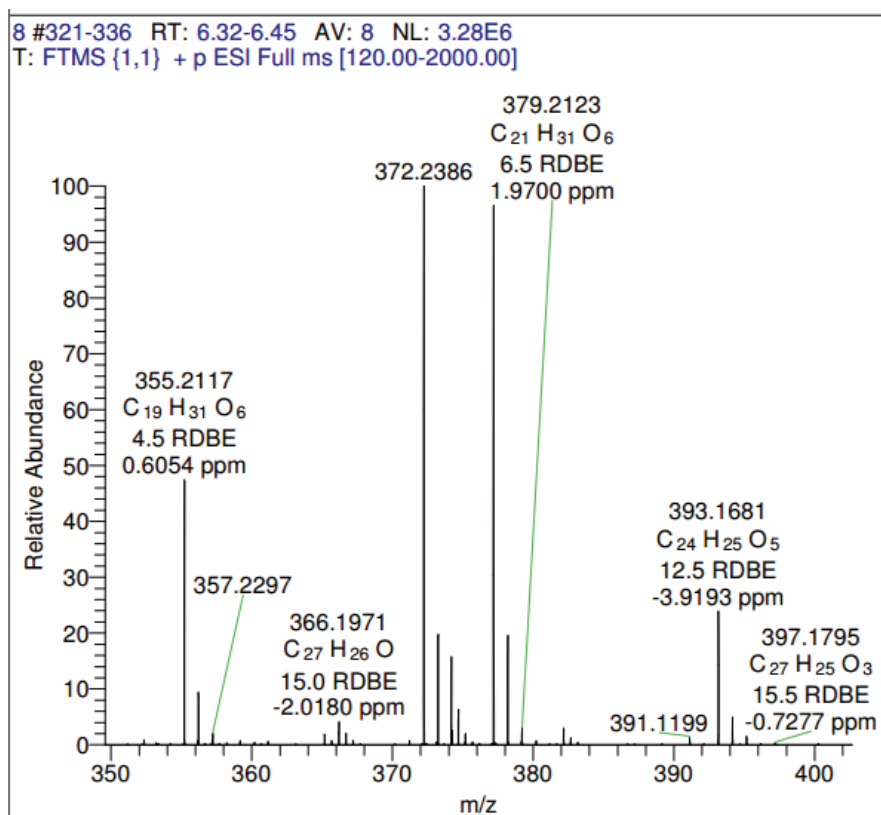


Figure S94. HREISMS of **18**.

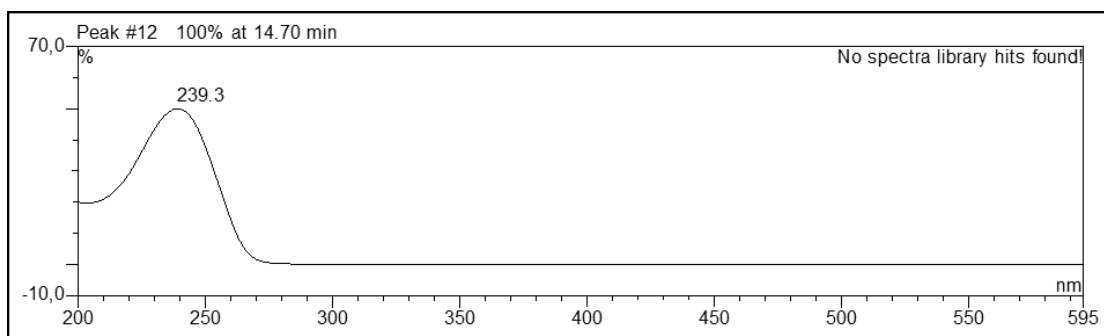


Figure S95. UV spectrum of 18.

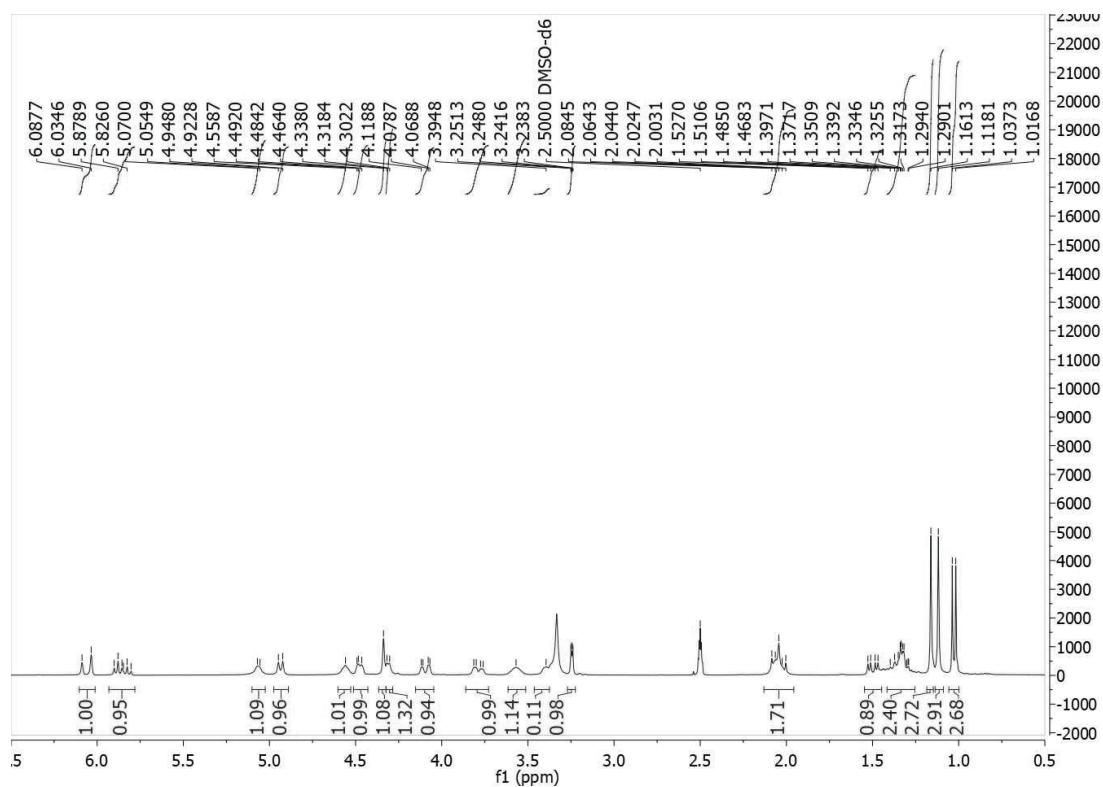


Figure S96. ^1H -NMR (300 MHz, DMSO-d_6) spectrum of 18.

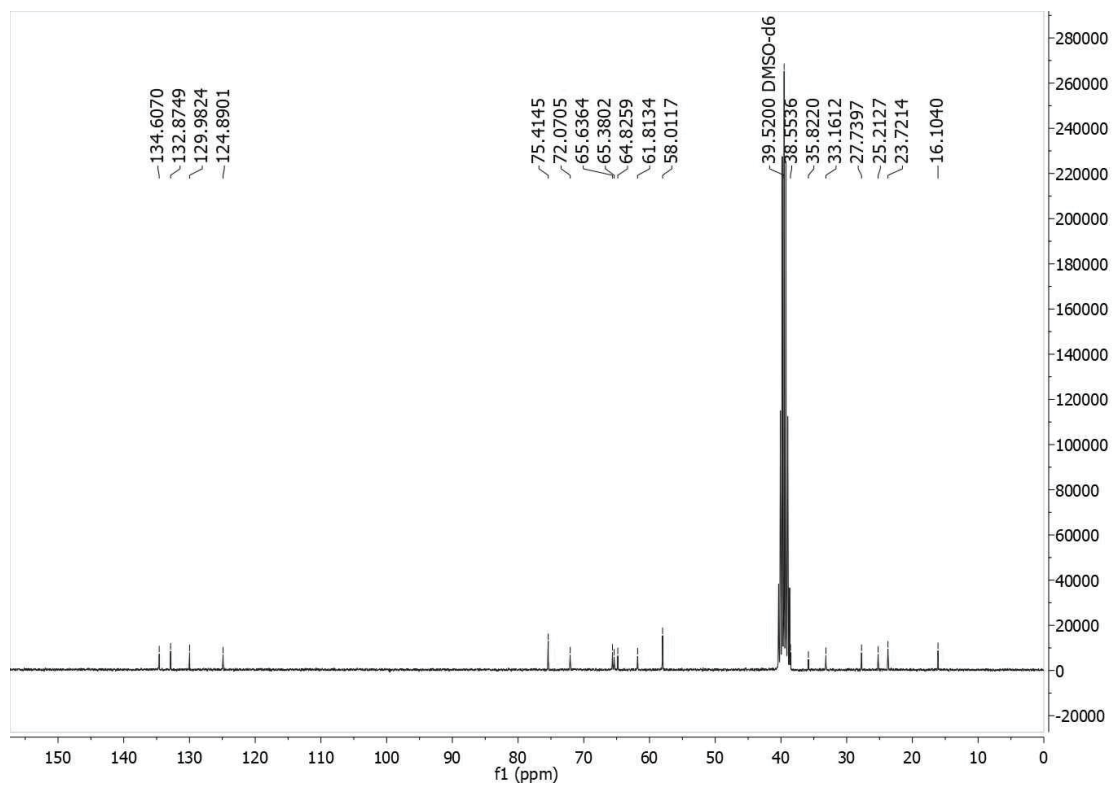


Figure S97. ^{13}C -NMR (75 MHz, $\text{DMSO}-d_6$) spectrum of **18**.

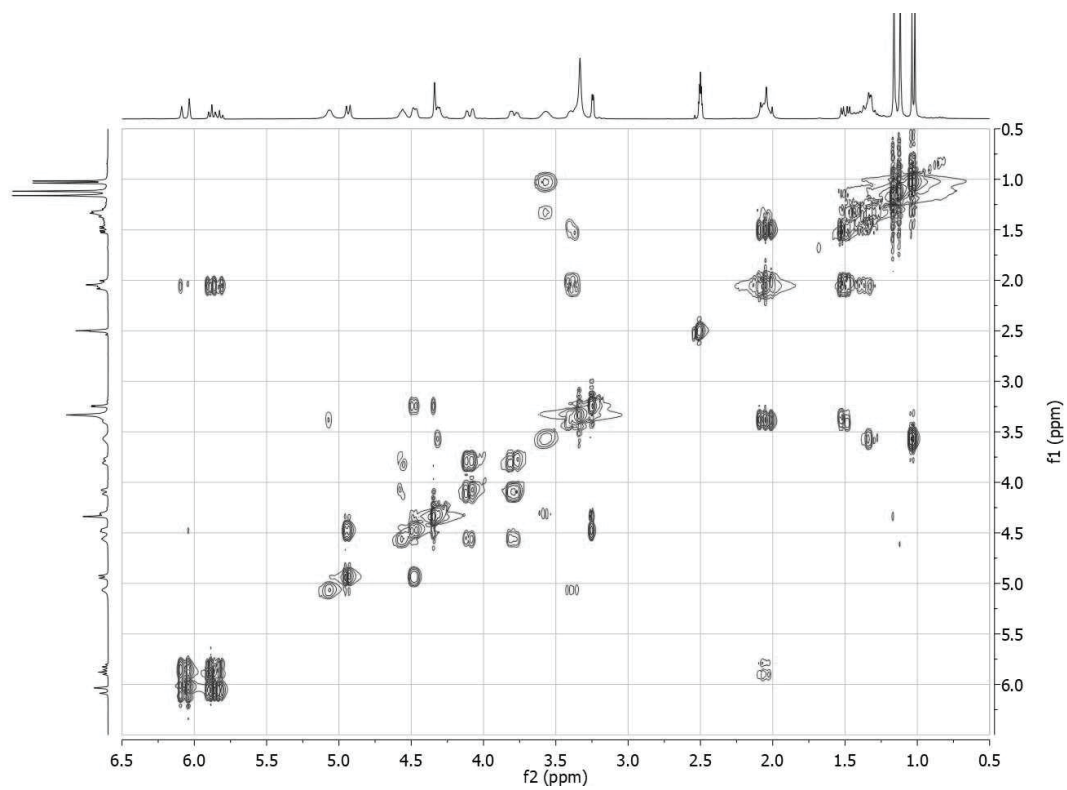


Figure S98. ^1H - ^1H COSY (300 MHz, $\text{DMSO}-d_6$) spectrum of **18**.

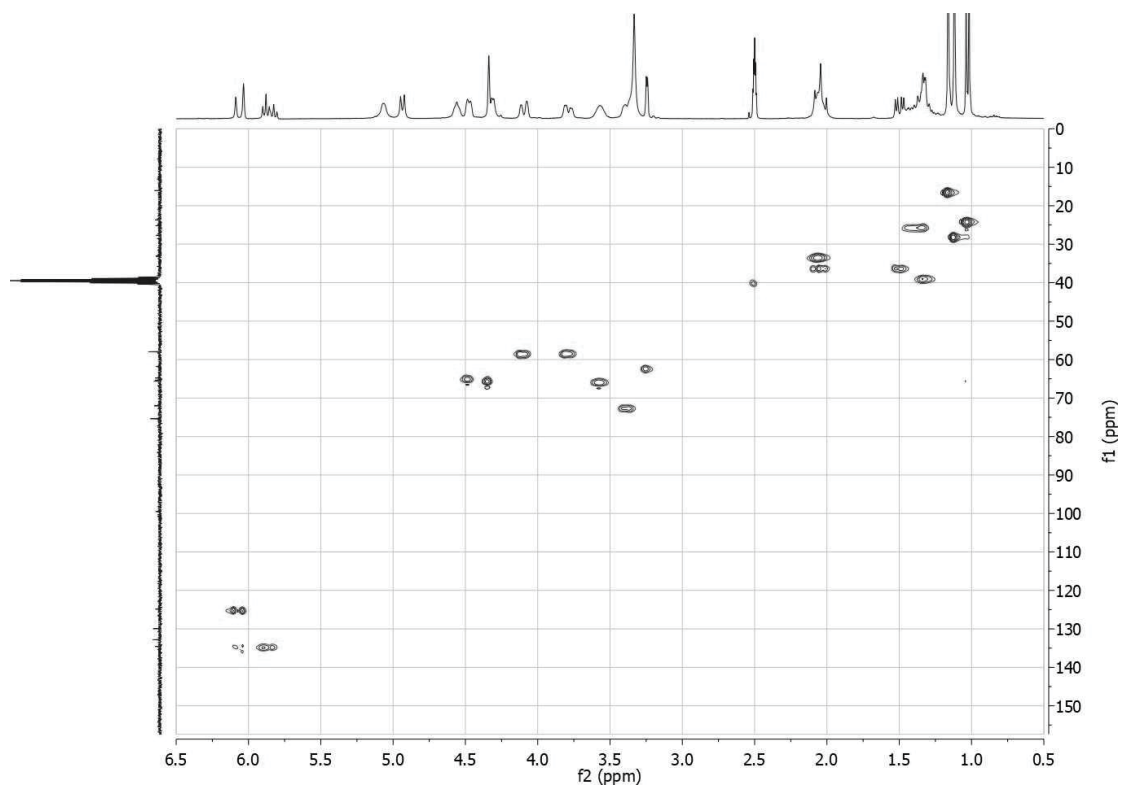


Figure S99. HSQC (300 MHz, DMSO- d_6) spectrum of **18**.

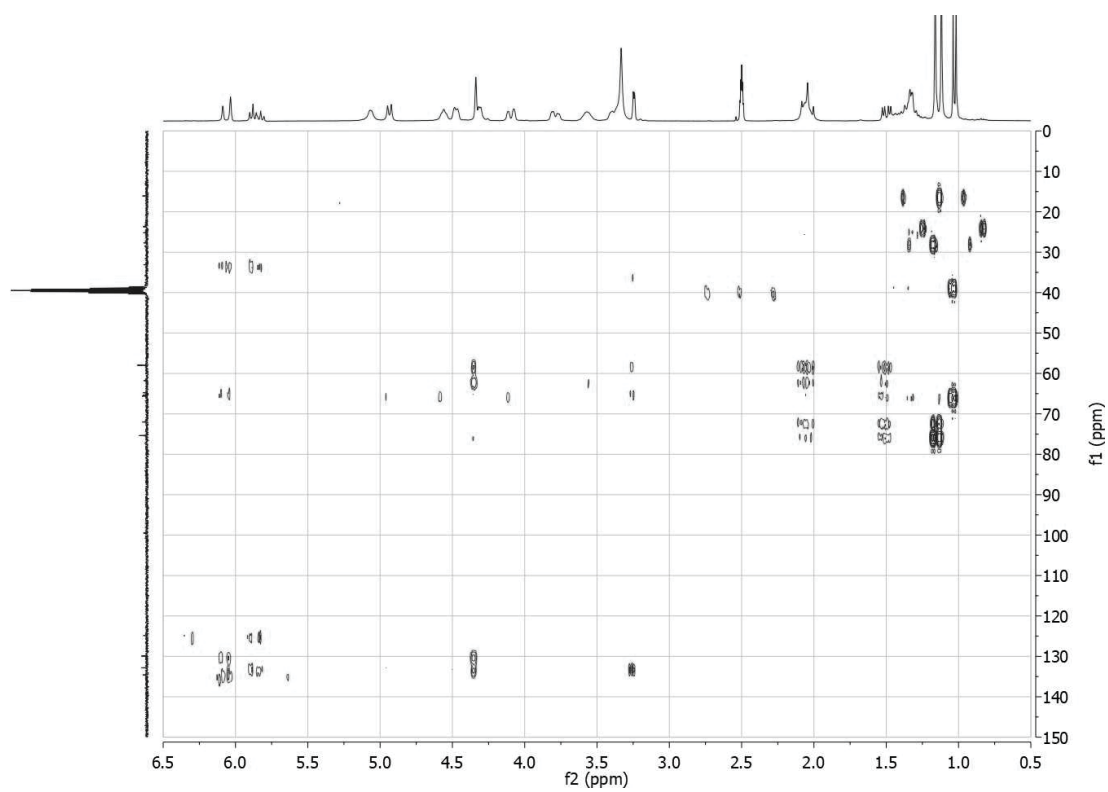


Figure S100. HMBC (300 MHz, DMSO- d_6) spectrum of **18**.

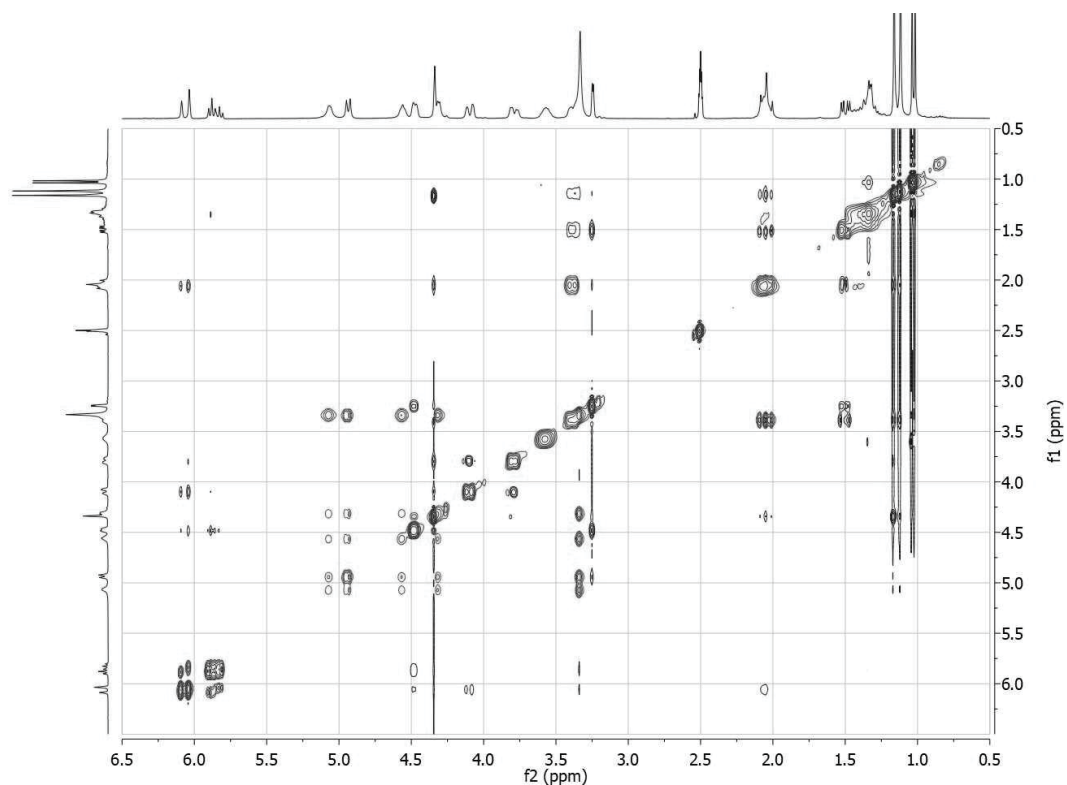


Figure S101. ROESY (300 MHz, DMSO- d_6) spectrum of **18**.

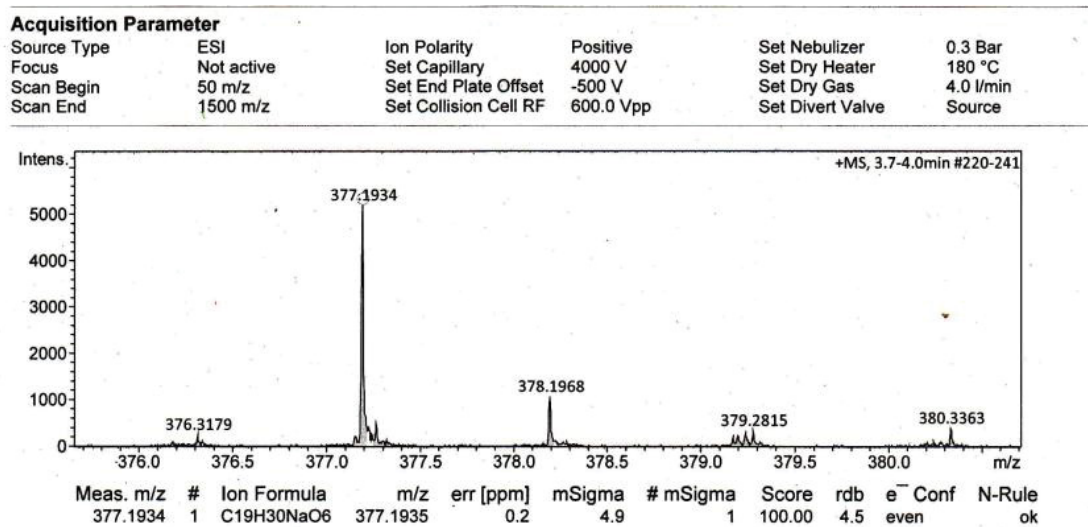


Figure S102. HREISMS of **19**.

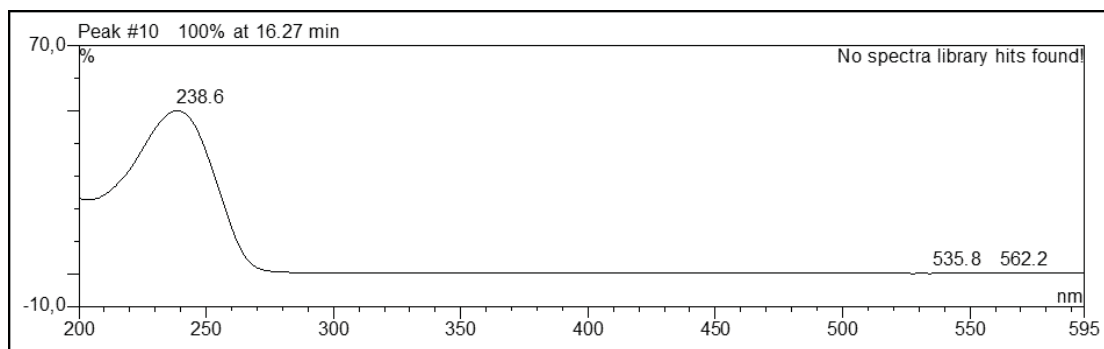


Figure S103. UV spectrum of 19.

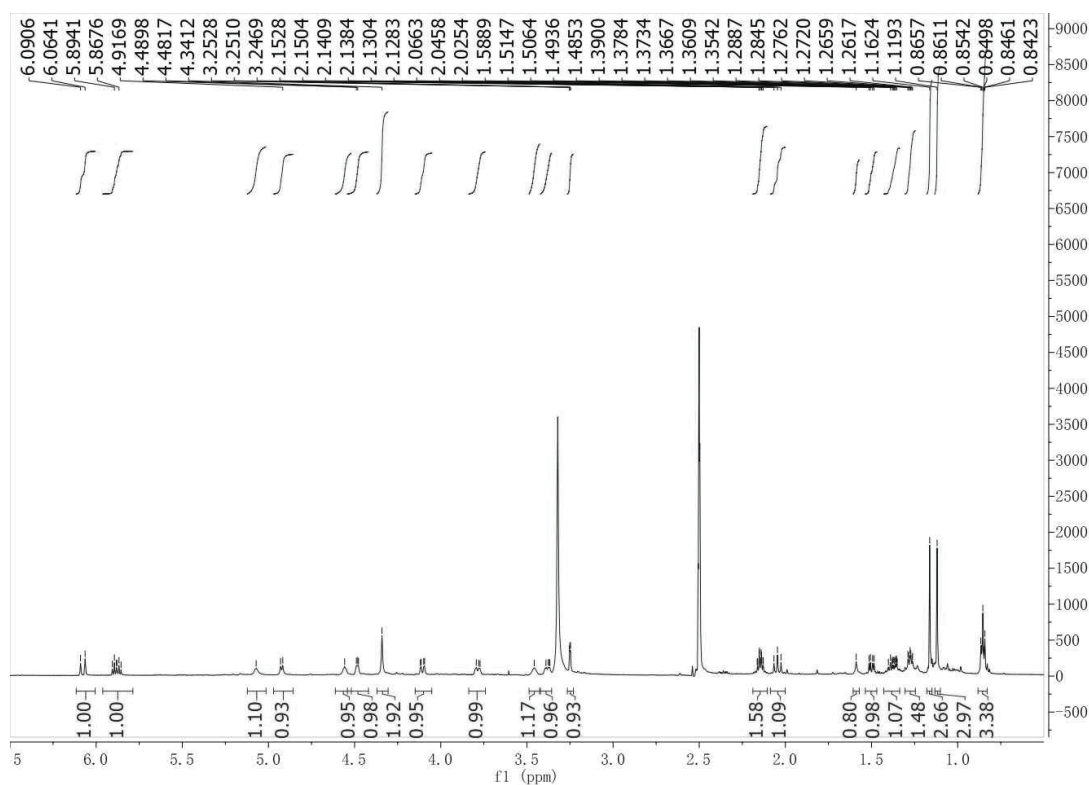


Figure S104. ^1H -NMR (600 MHz, $\text{DMSO}-d_6$) spectrum of 19.



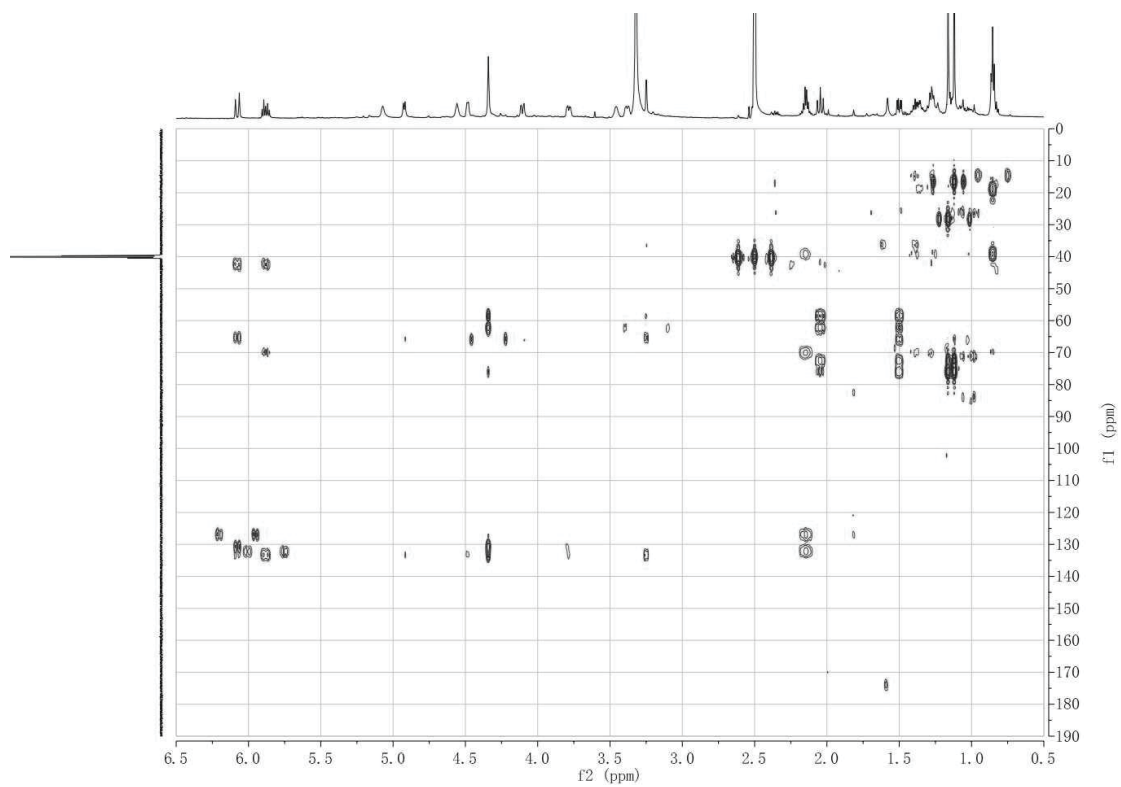


Figure S107. HMBC (600MHz, DMSO-*d*₆) spectrum of **19**.

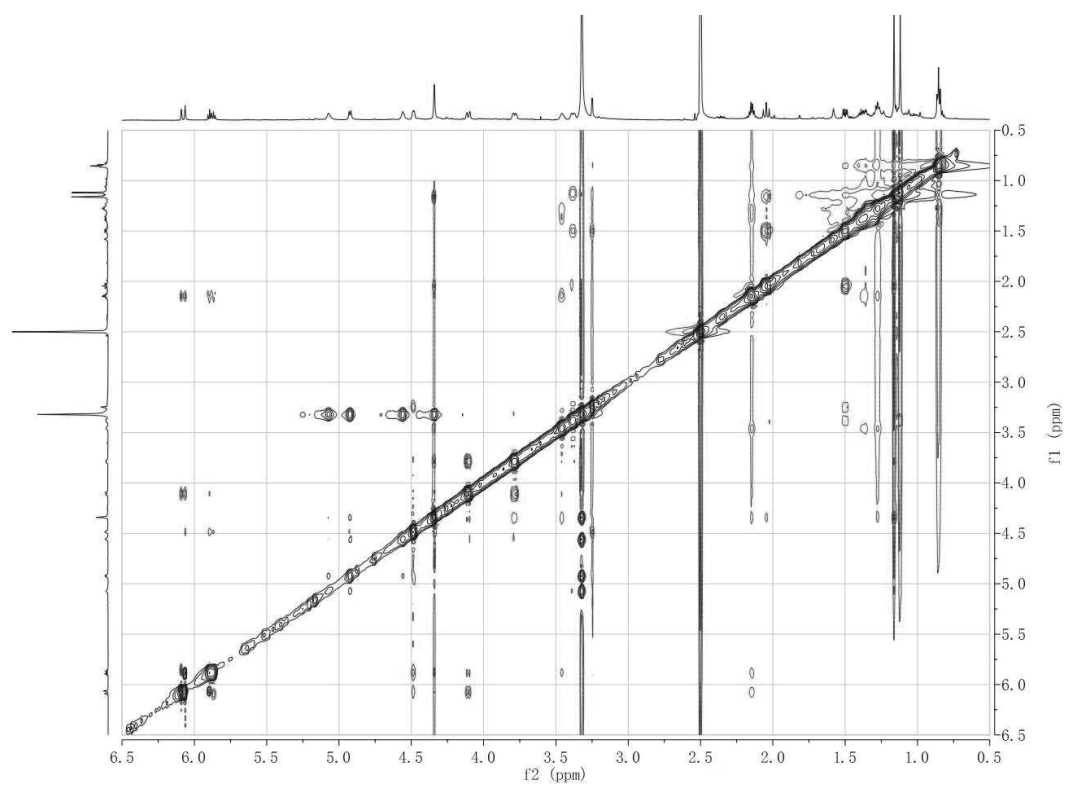
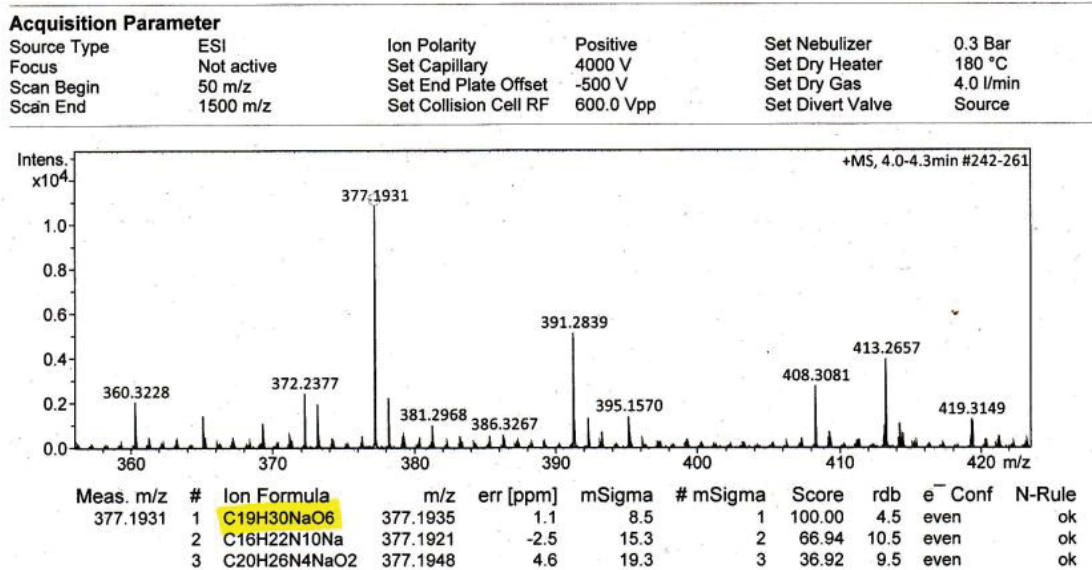
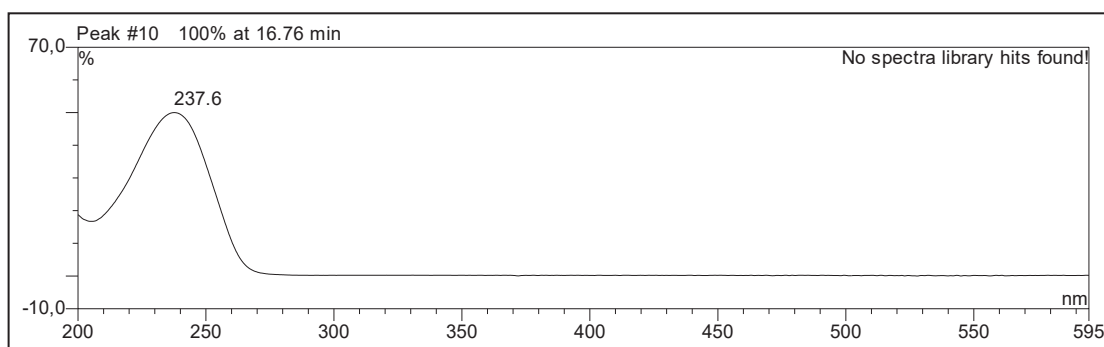


Figure S108. ROESY (600 MHz, DMSO-*d*₆) spectrum of **19**.

Figure S109. HREISMS of **20**.Figure S110. The UV spectrum of **20**.

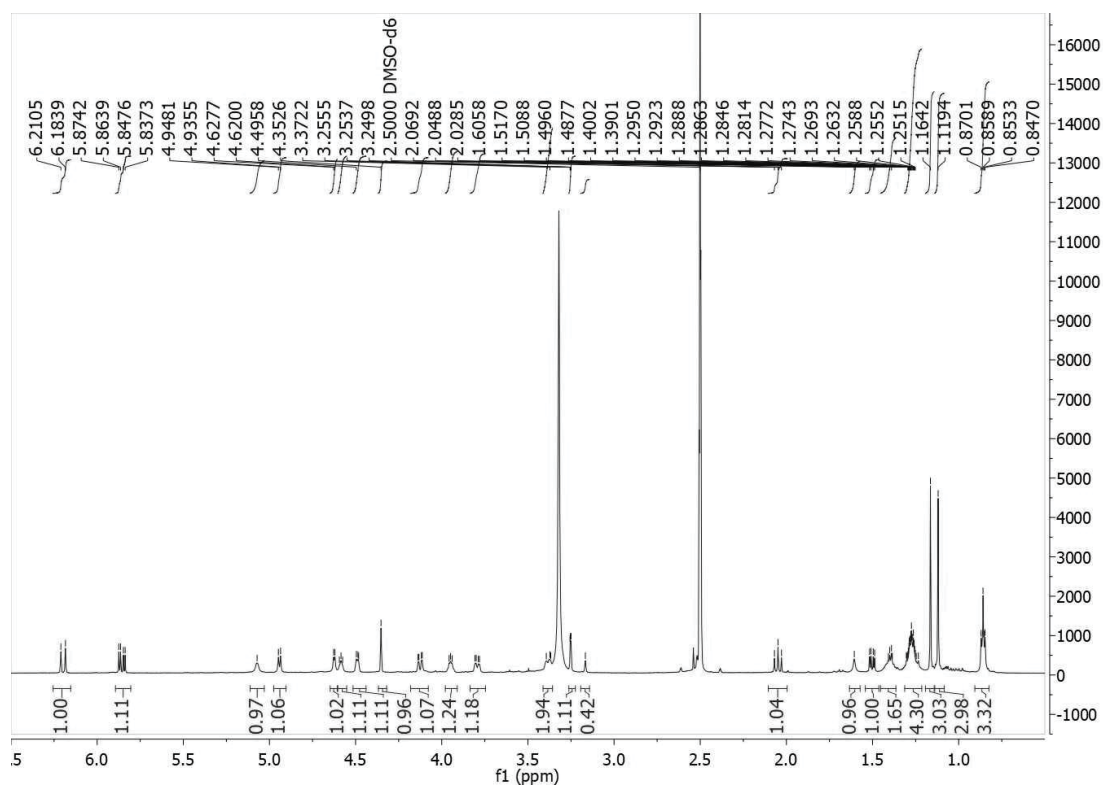


Figure S11. The ¹H-NMR (600 MHz, DMSO-*d*₆) spectrum of **20**.

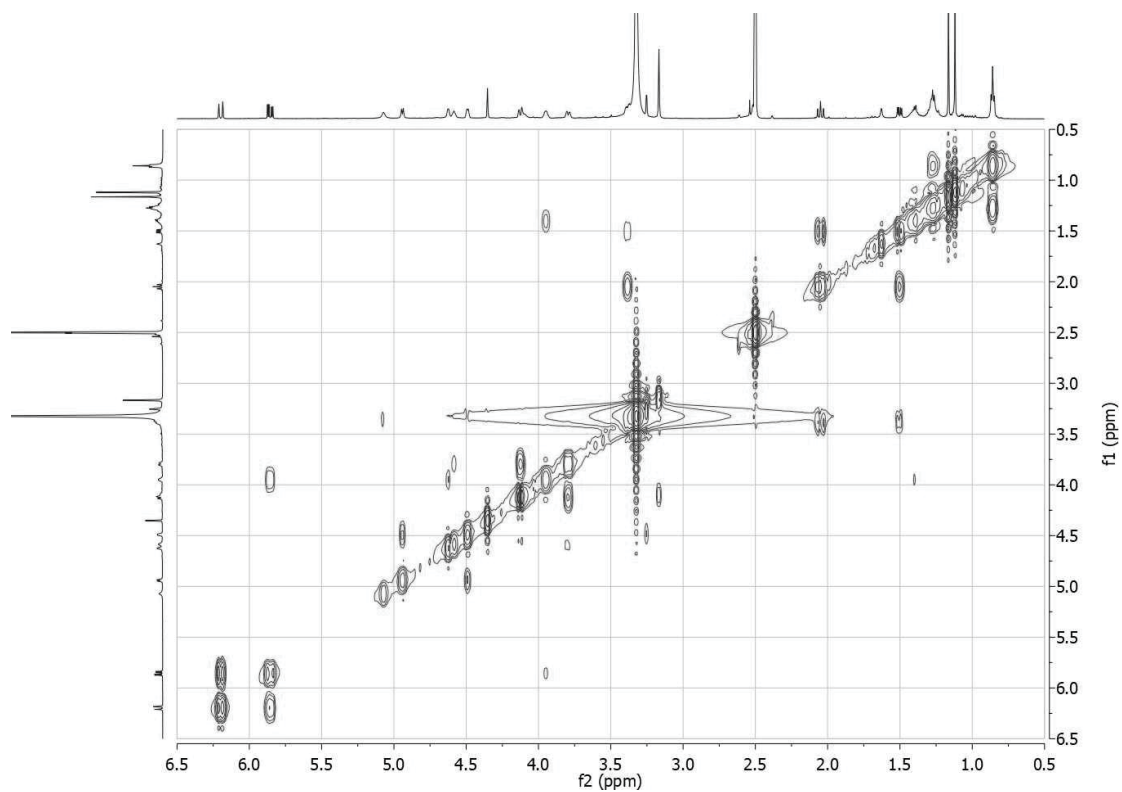


Figure S12. ¹H-¹H COSY (600 MHz, DMSO-*d*₆) spectrum of **20**.

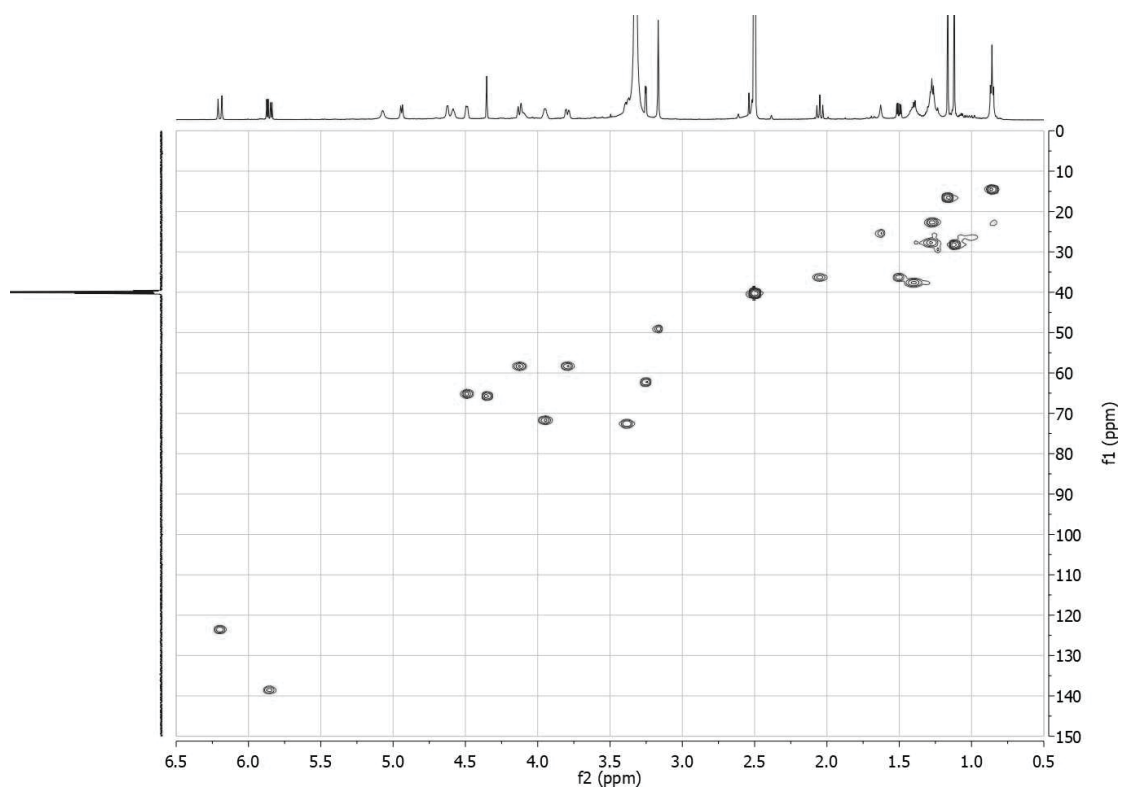


Figure S113. HSQC (600 MHz, DMSO-*d*₆) spectrum of **20**.

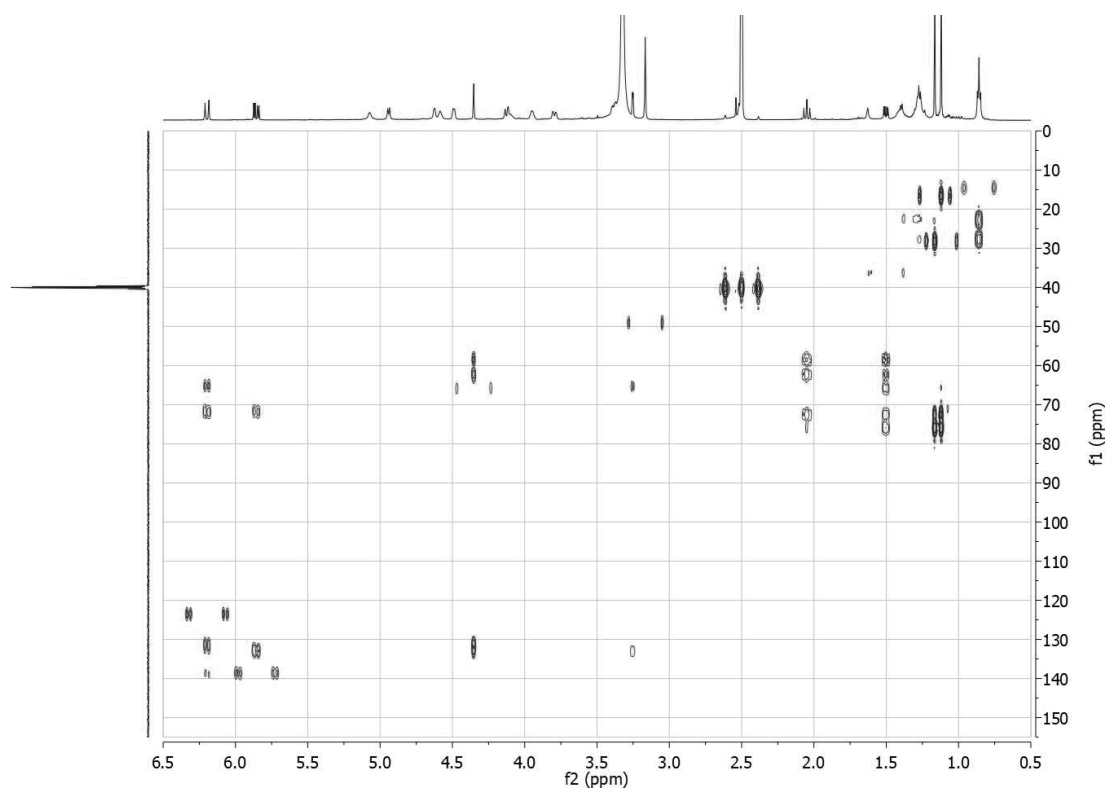


Figure S114. HMBC (600 MHz, DMSO-*d*₆) spectrum of **20**.

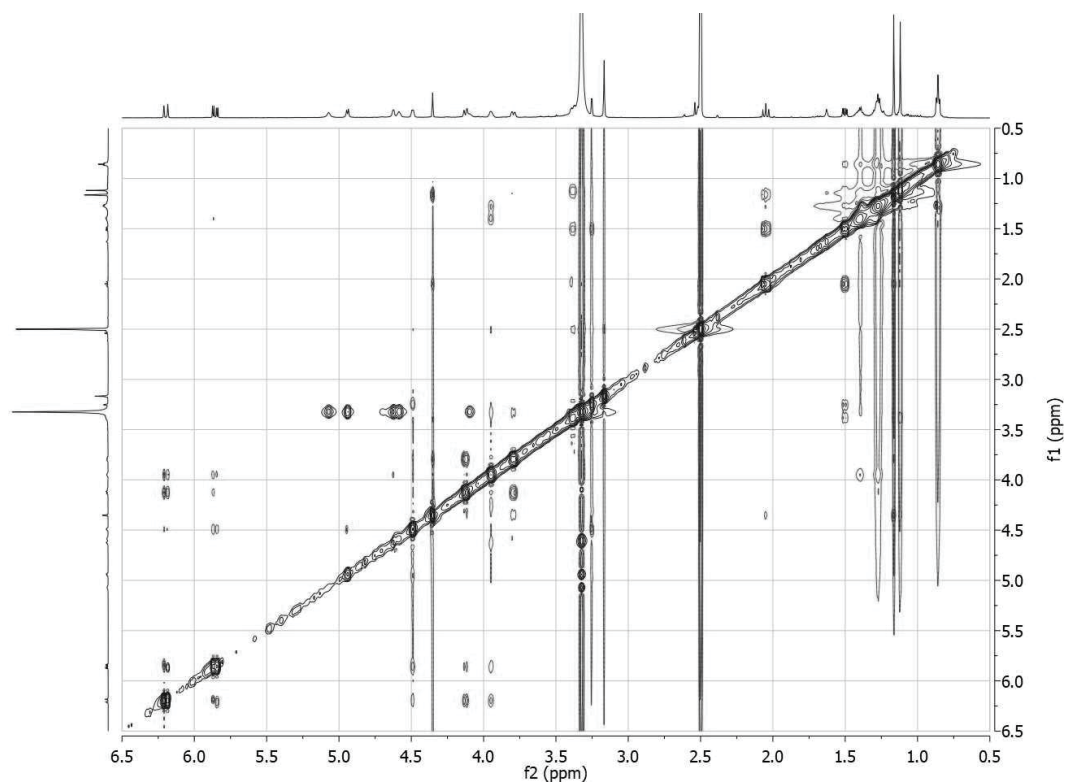


Figure S115. ROESY ((600 MHz, DMSO-*d*₆) spectrum of **20**.

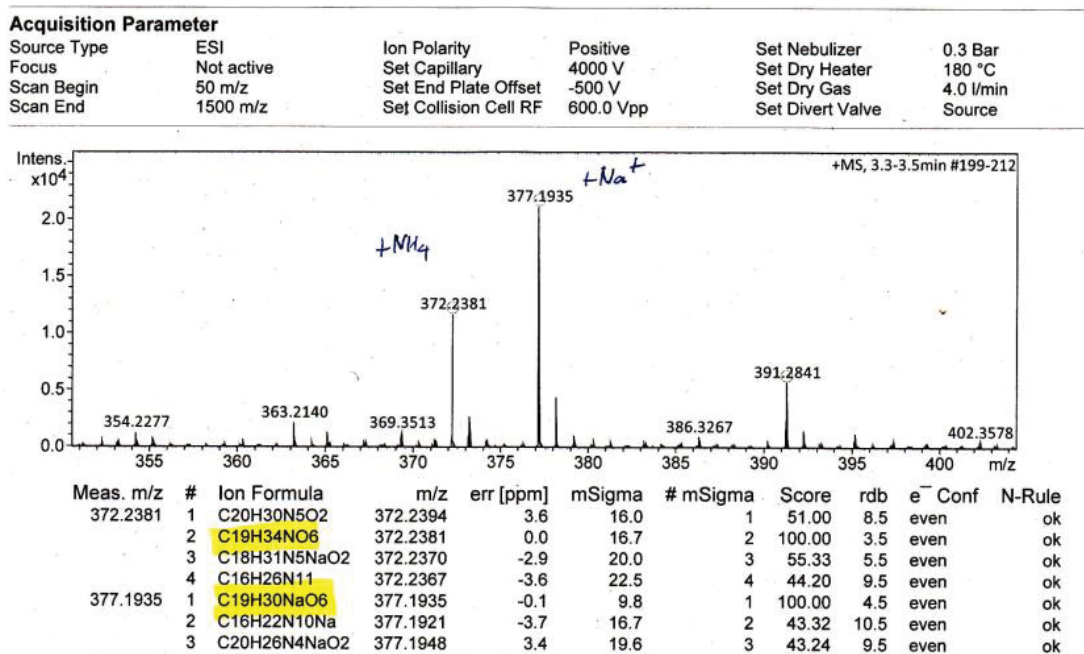


Figure S116. HREISMS of **21**.

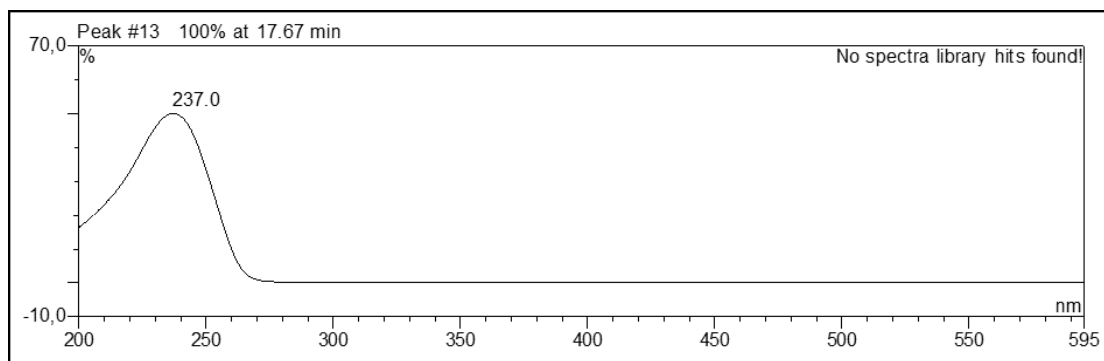


Figure S117. UV spectrum of 21.

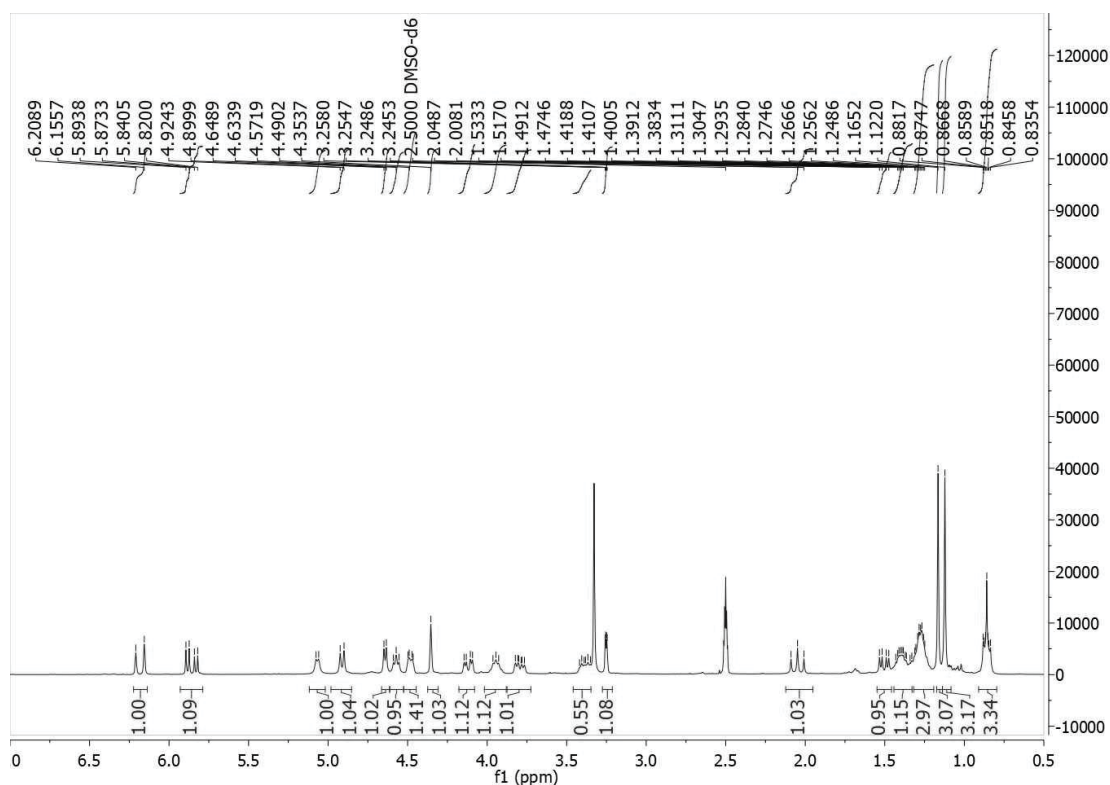


Figure S118. ^1H -NMR (300 MHz, $\text{DMSO}-d_6$) spectrum of 21.

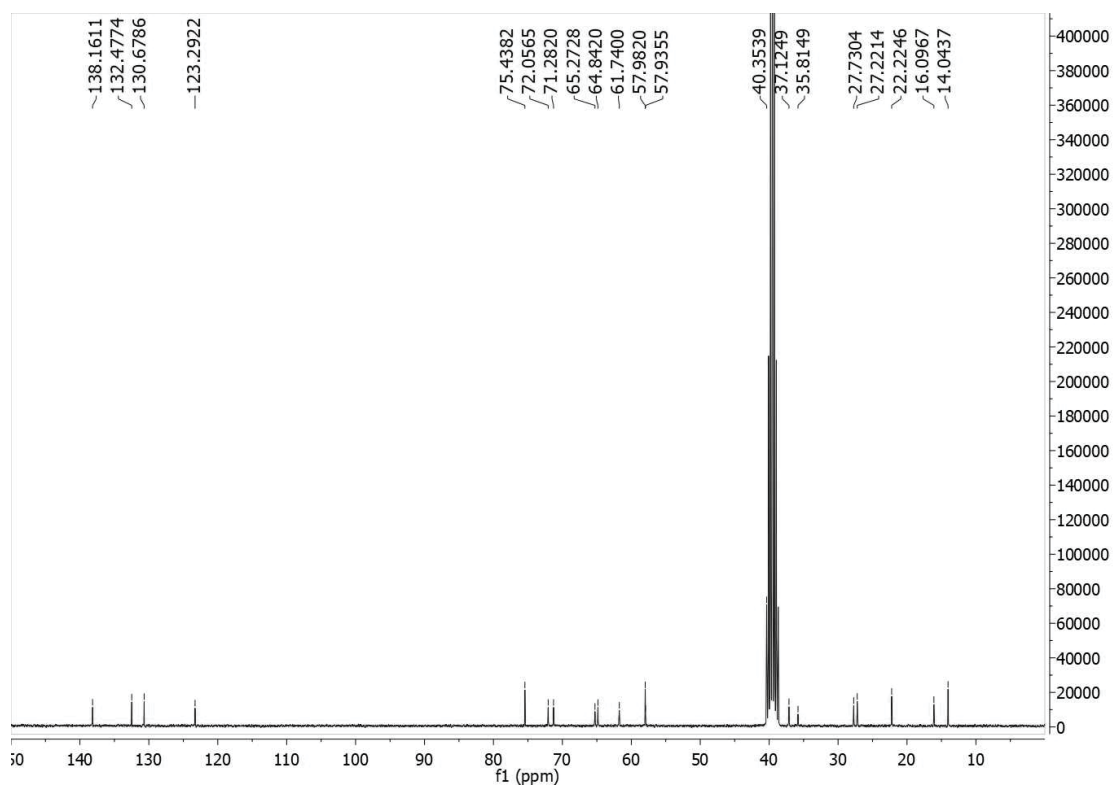


Figure S119. ^{13}C -NMR (75 MHz, $\text{DMSO}-d_6$) spectrum of **21**.

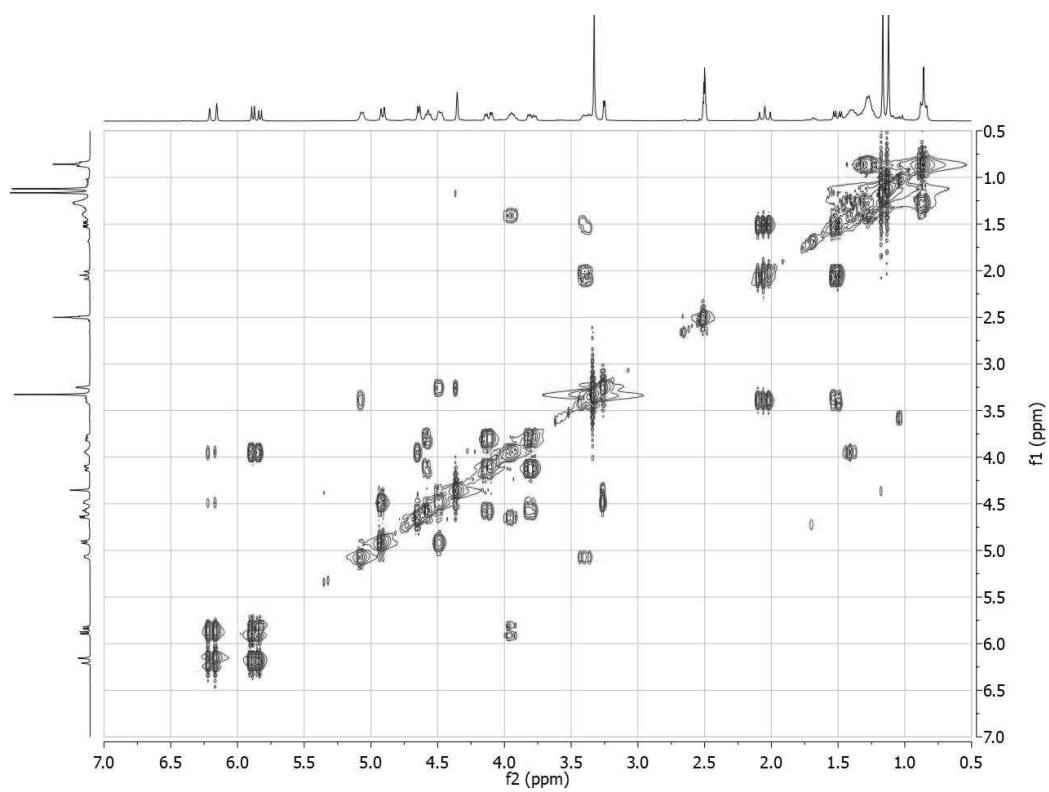


Figure S120. ^1H - ^1H COSY (300 MHz, $\text{DMSO}-d_6$) spectrum of **21**.

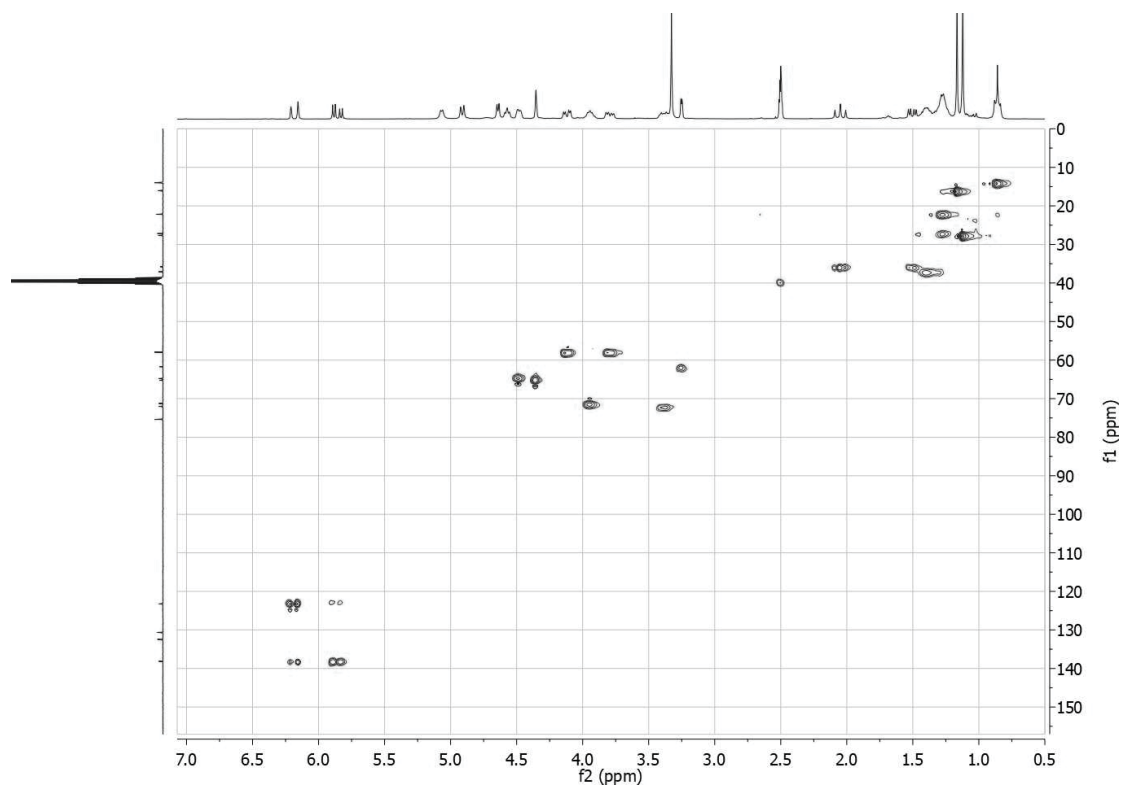


Figure S121. HSQC (300 MHz, DMSO-*d*₆) spectrum of **21**.

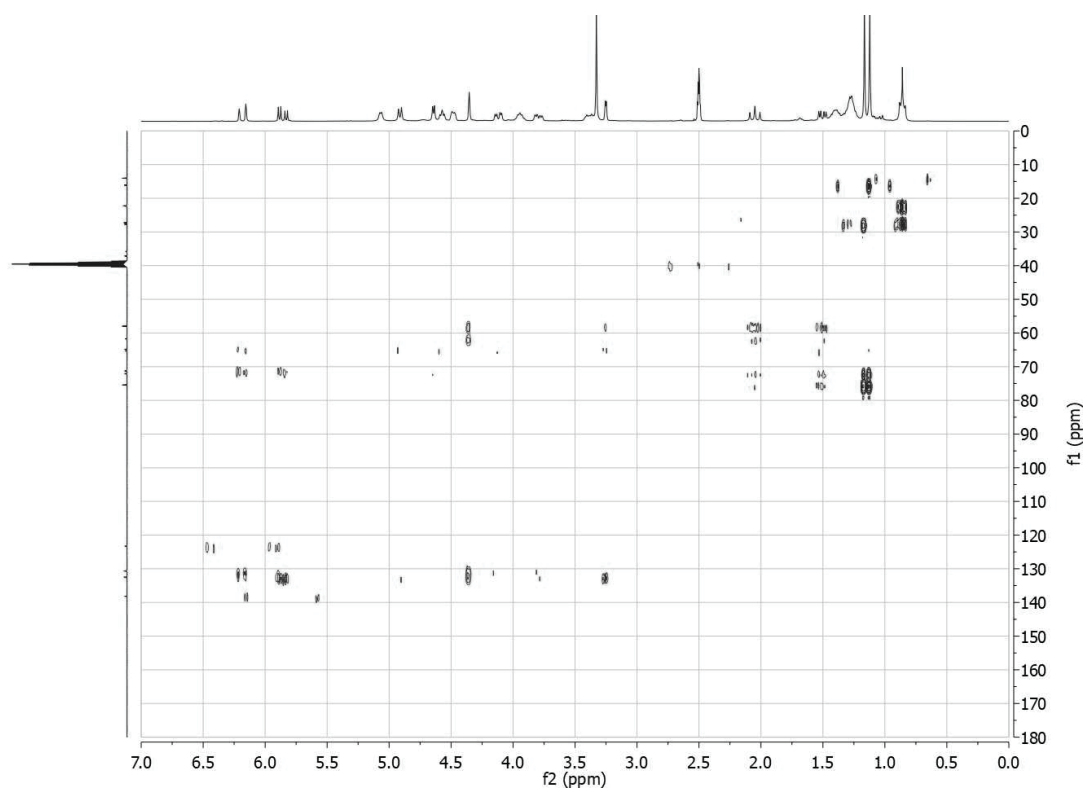


Figure S122. HMBC (300 MHz, DMSO-*d*₆) spectrum of **21**.

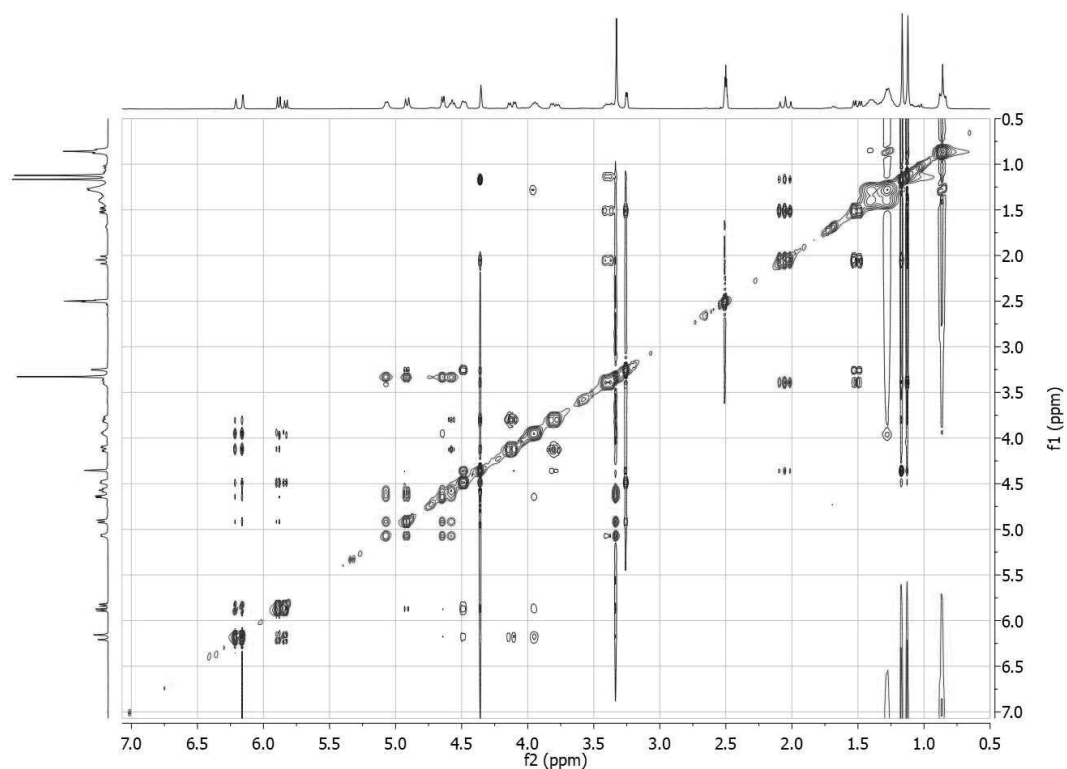


Figure S123. ROESY (300 MHz, DMSO-*d*₆) spectrum of **21**.

Acquisition Parameter

Source Type	ESI	Ion Polarity	Positive	Set Nebulizer	0.3 Bar
Focus	Not active	Set Capillary	4000 V	Set Dry Heater	180 °C
Scan Begin	50 m/z	Set End Plate Offset	-500 V	Set Dry Gas	4.0 l/min
Scan End	1500 m/z	Set Collision Cell RF	600.0 Vpp	Set Divert Valve	Source

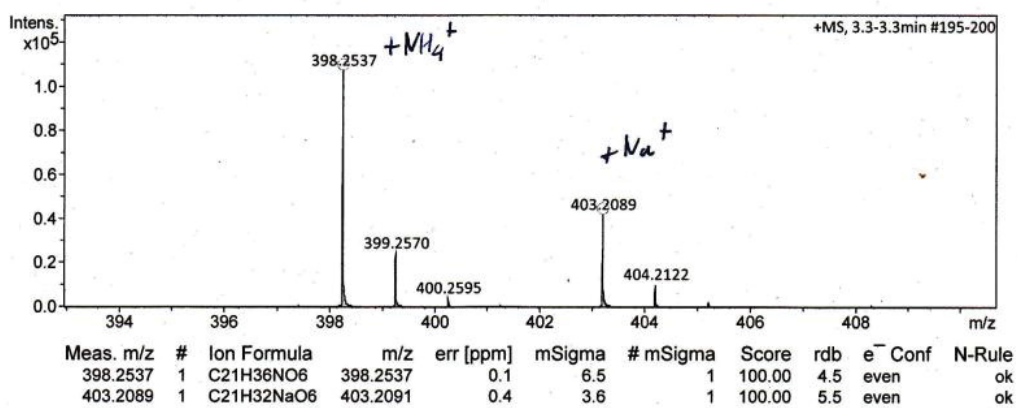


Figure S124. HREISMS of **22**.

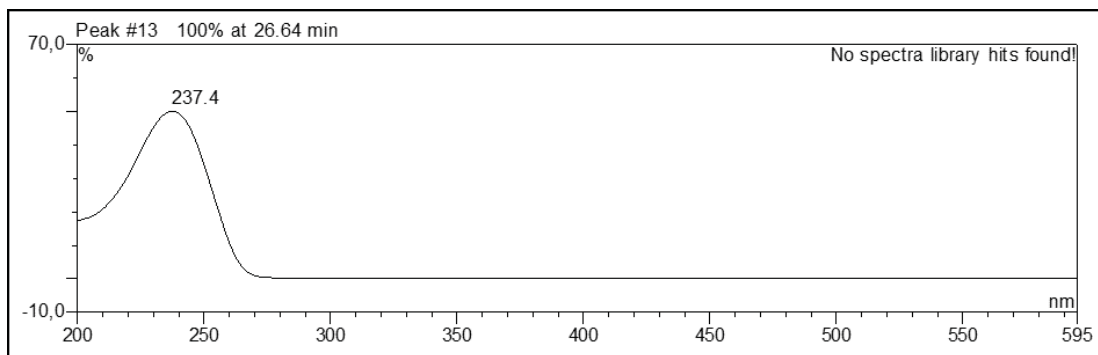


Figure S125. UV spectrum of **22**.

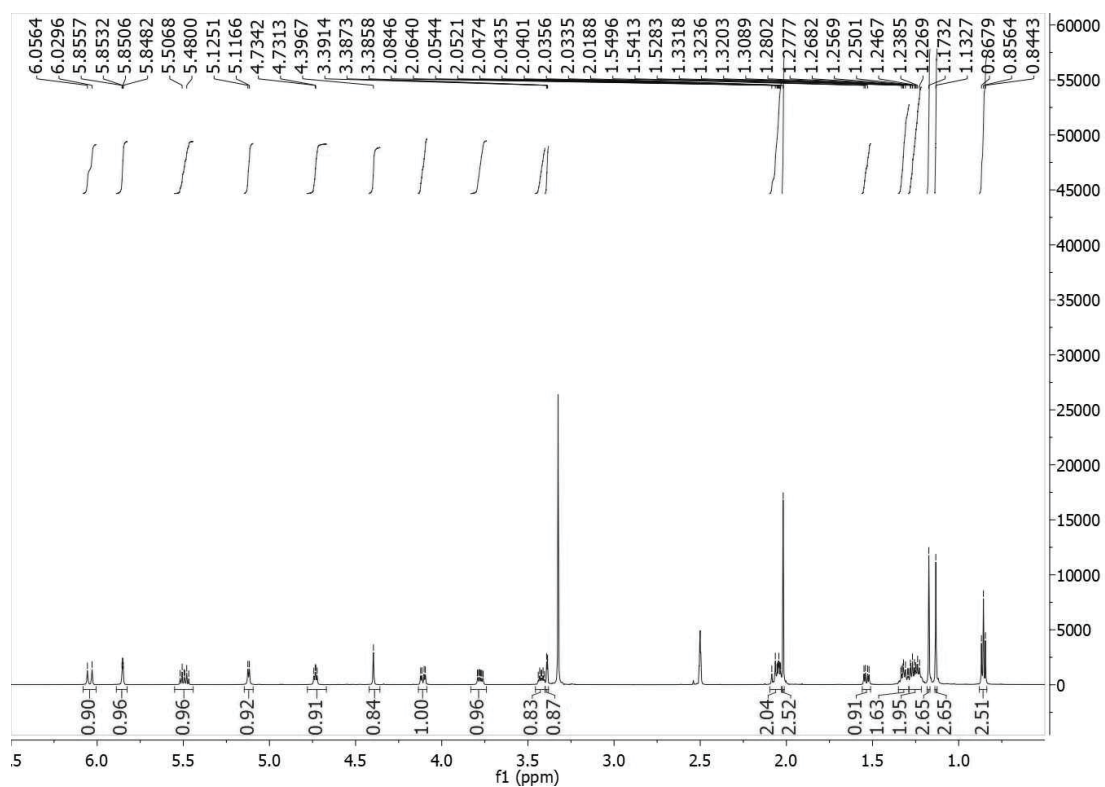


Figure S126. ^1H -NMR (600 MHz, $\text{DMSO}-d_6$) spectrum of **22**.

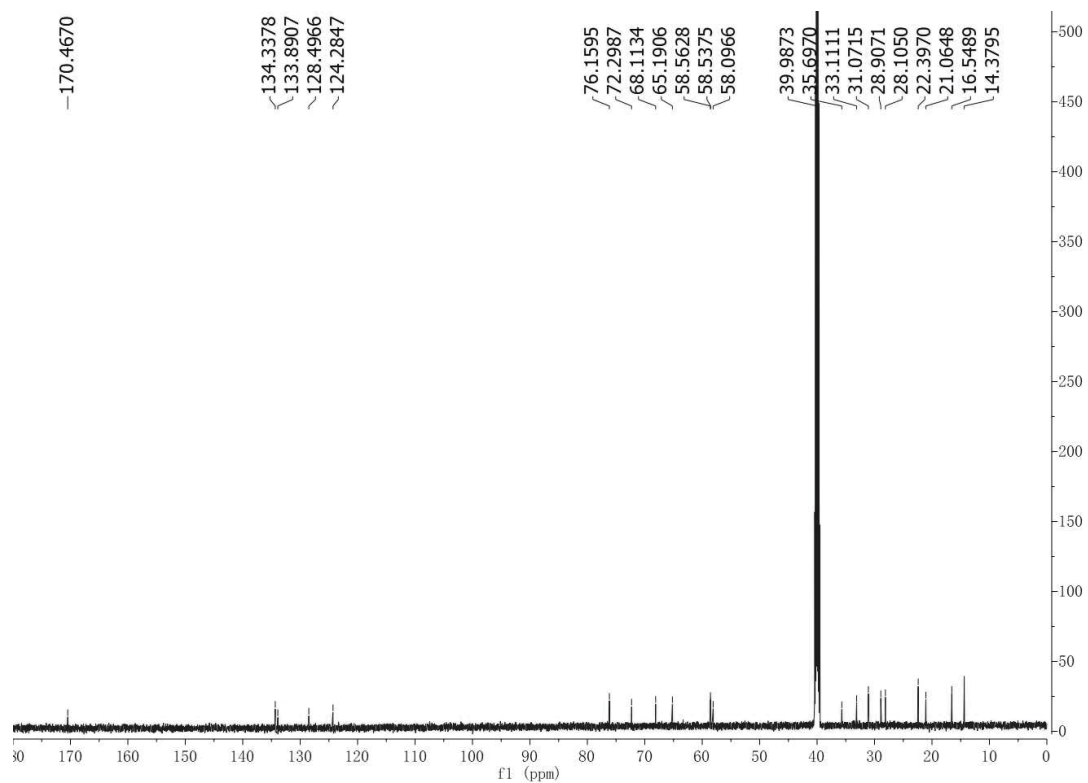


Figure S127. ^{13}C -NMR (150 MHz, $\text{DMSO}-d_6$) spectrum of **22**.

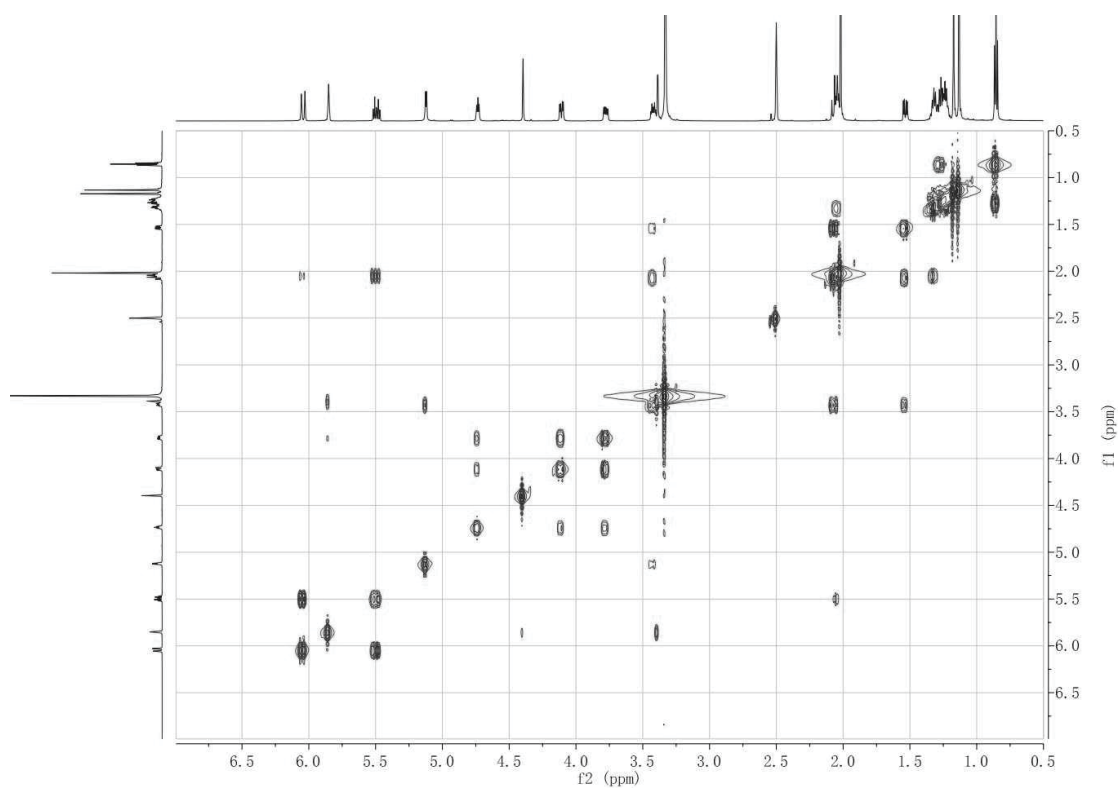


Figure S128. ^1H - ^1H COSY (600 MHz, $\text{DMSO}-d_6$) spectrum of **22**.

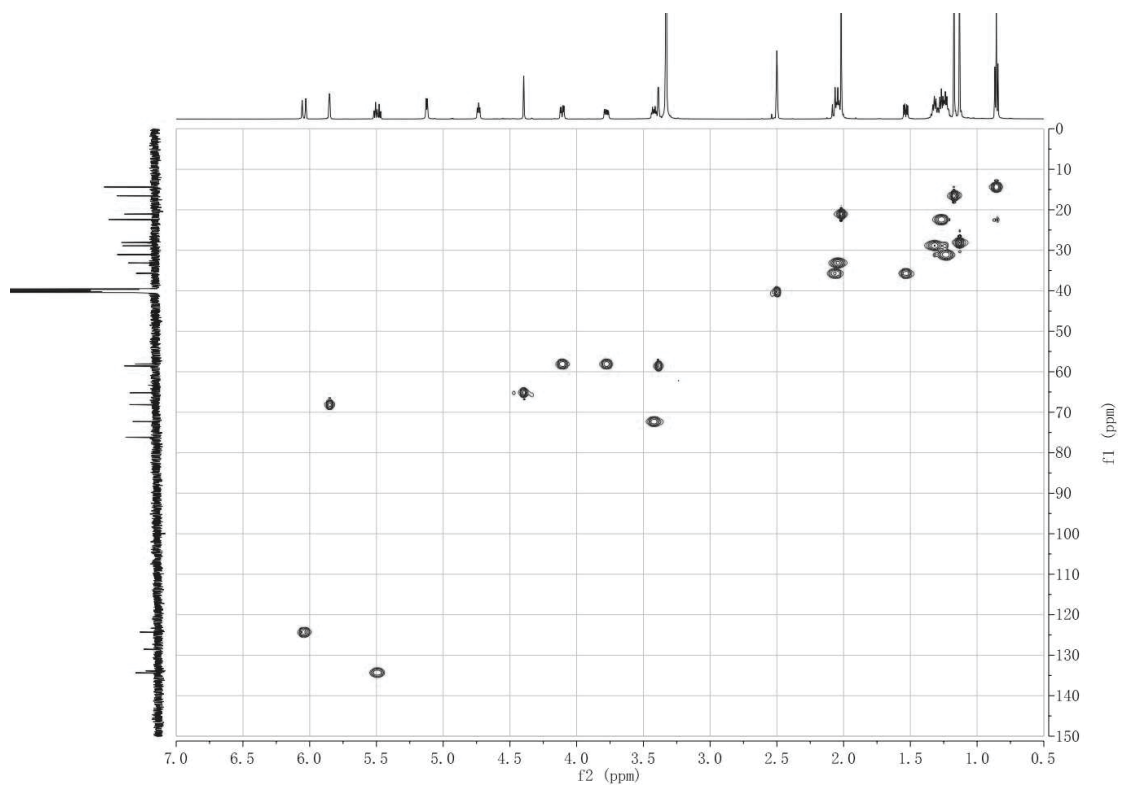


Figure S129. HSQC (600 MHz, DMSO-*d*₆) spectrum of **22**.

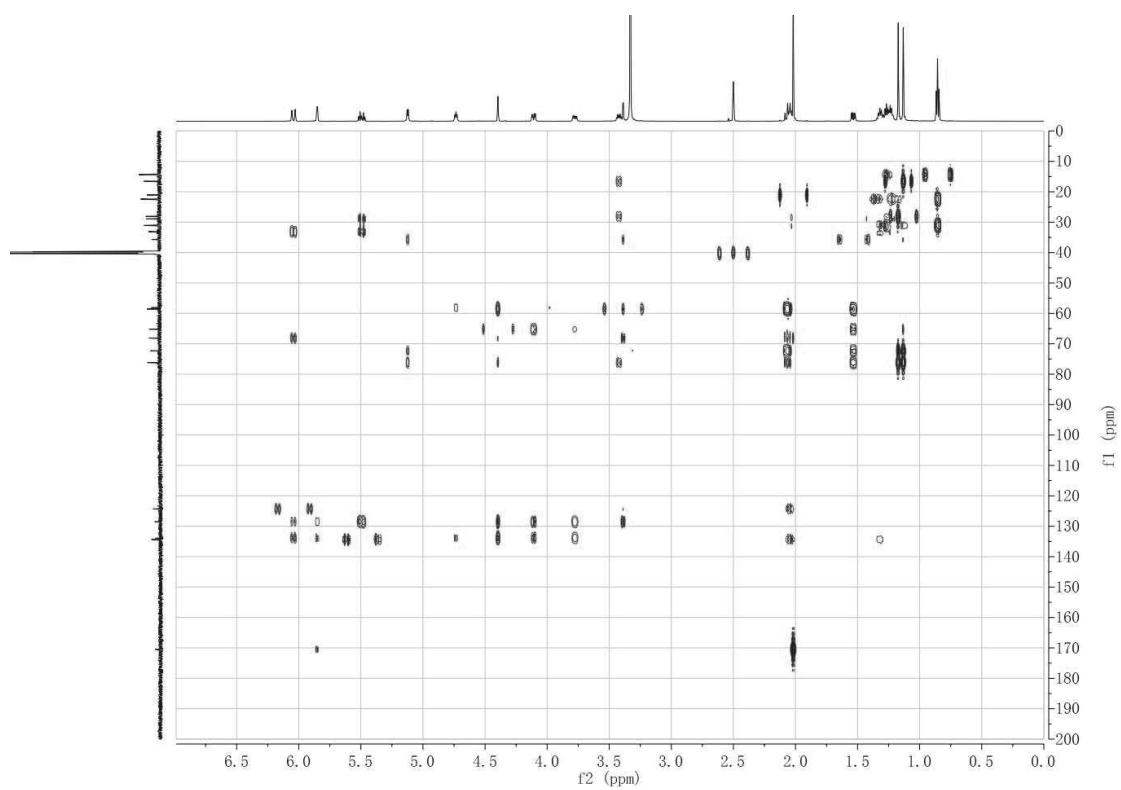


Figure S130. HMBC (600 MHz, DMSO-*d*₆) spectrum of **22**.

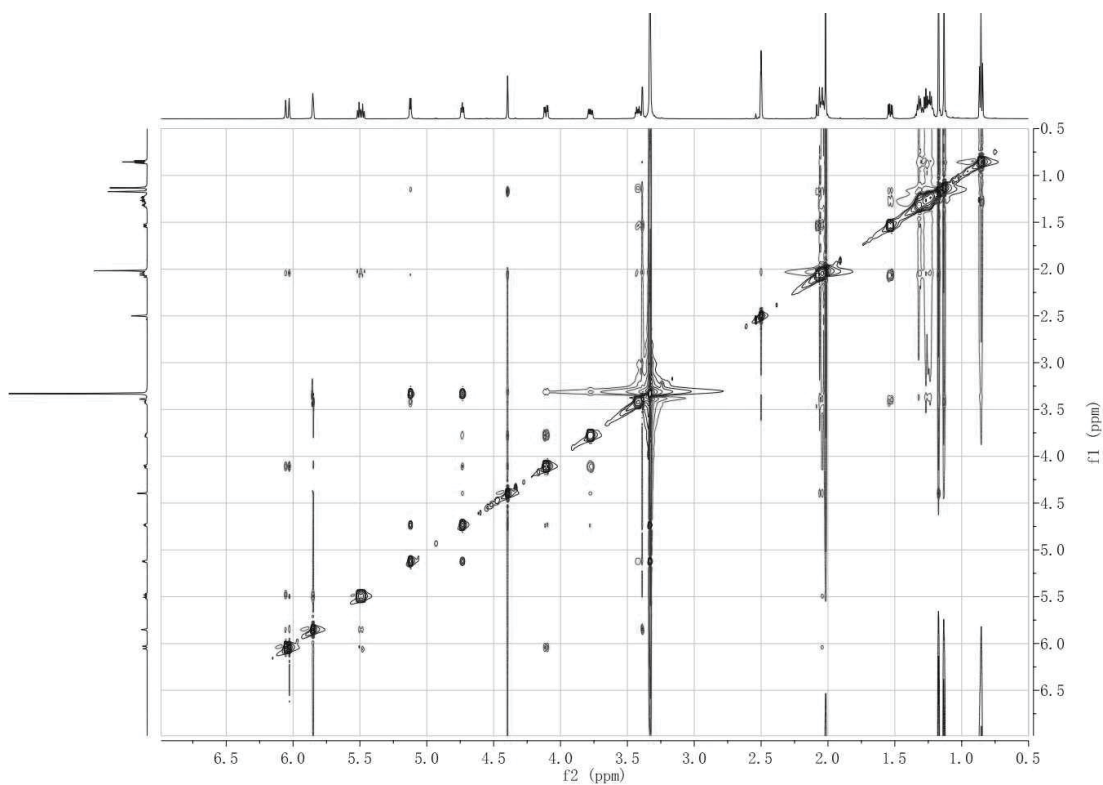


Figure S131. ROESY (600 MHz, DMSO- d_6) spectrum of **22**.

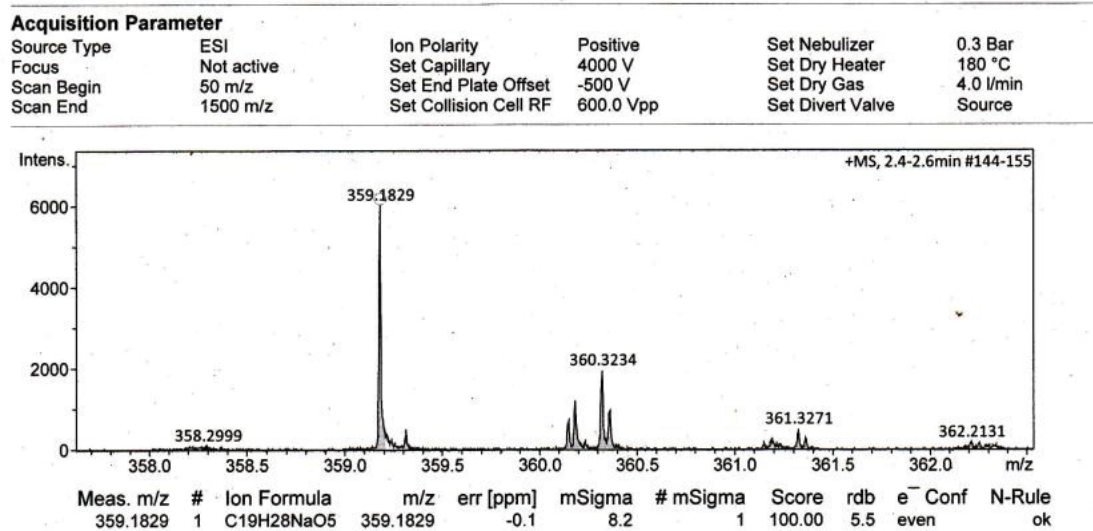


Figure S132. HREISMS of **23**.

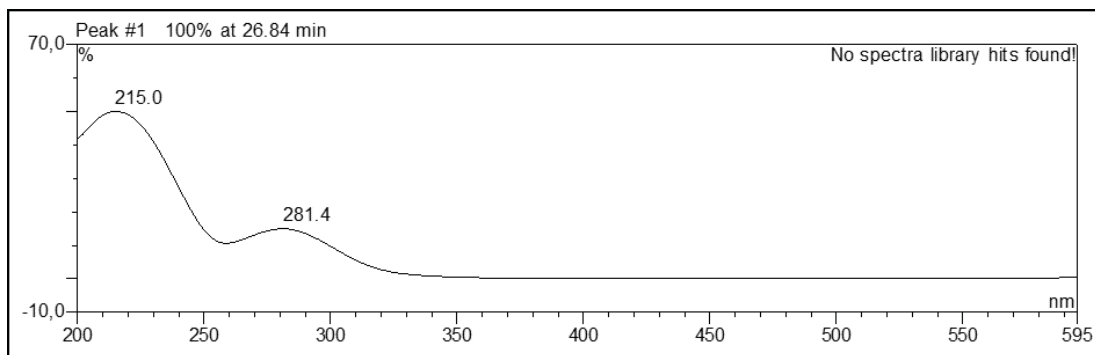


Figure S133. UV spectrum of **23**.

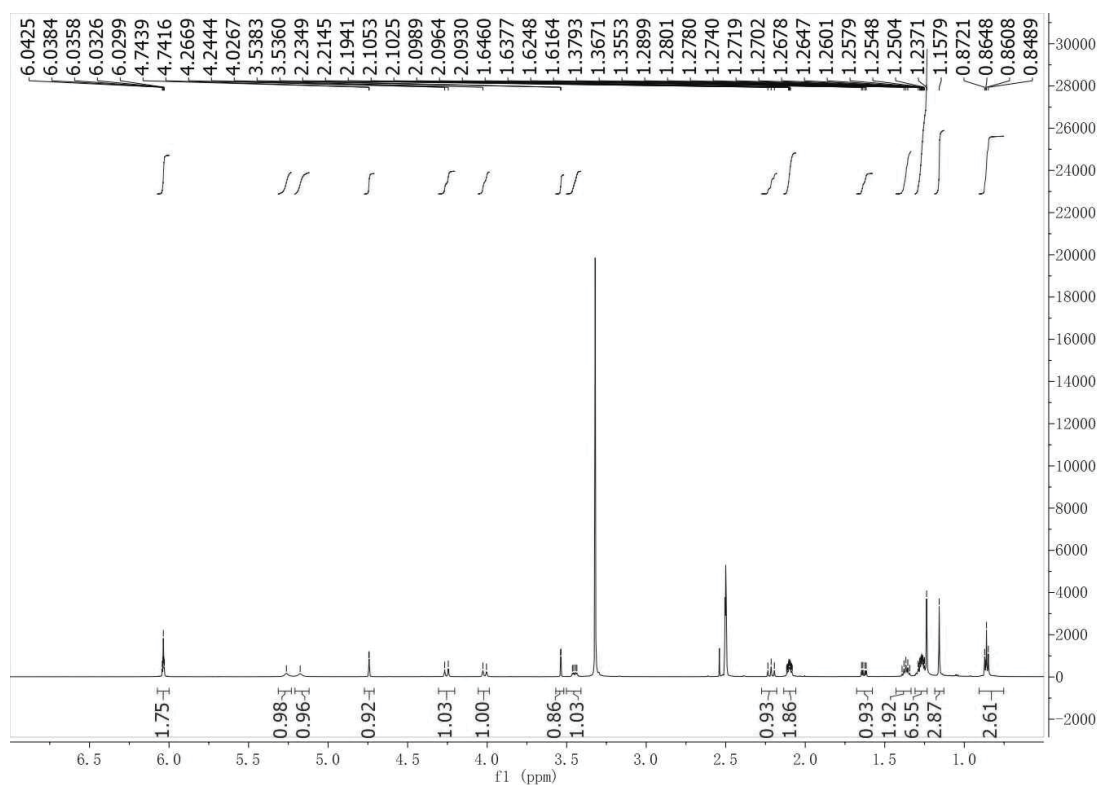


Figure S134. ^1H -NMR (600 MHz, $\text{DMSO}-d_6$) spectrum of **23**.

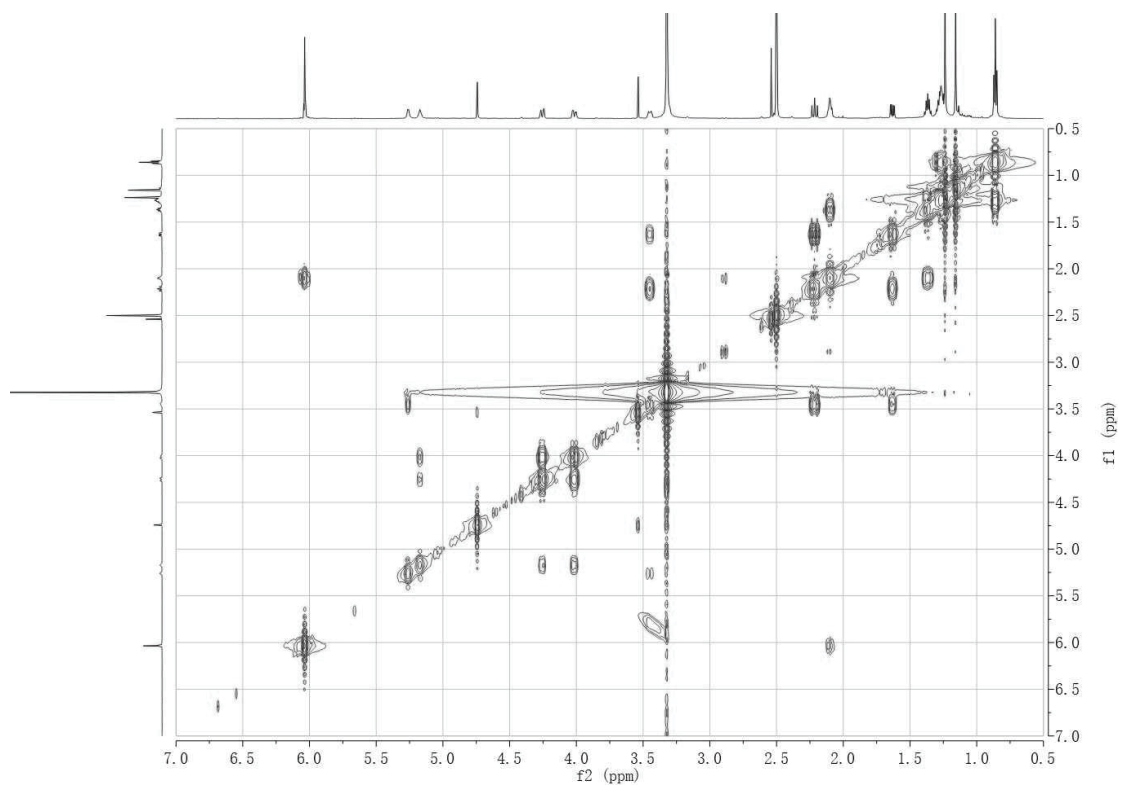


Figure S135. ^1H - ^1H COSY (600 MHz, $\text{DMSO}-d_6$) spectrum of **23**.

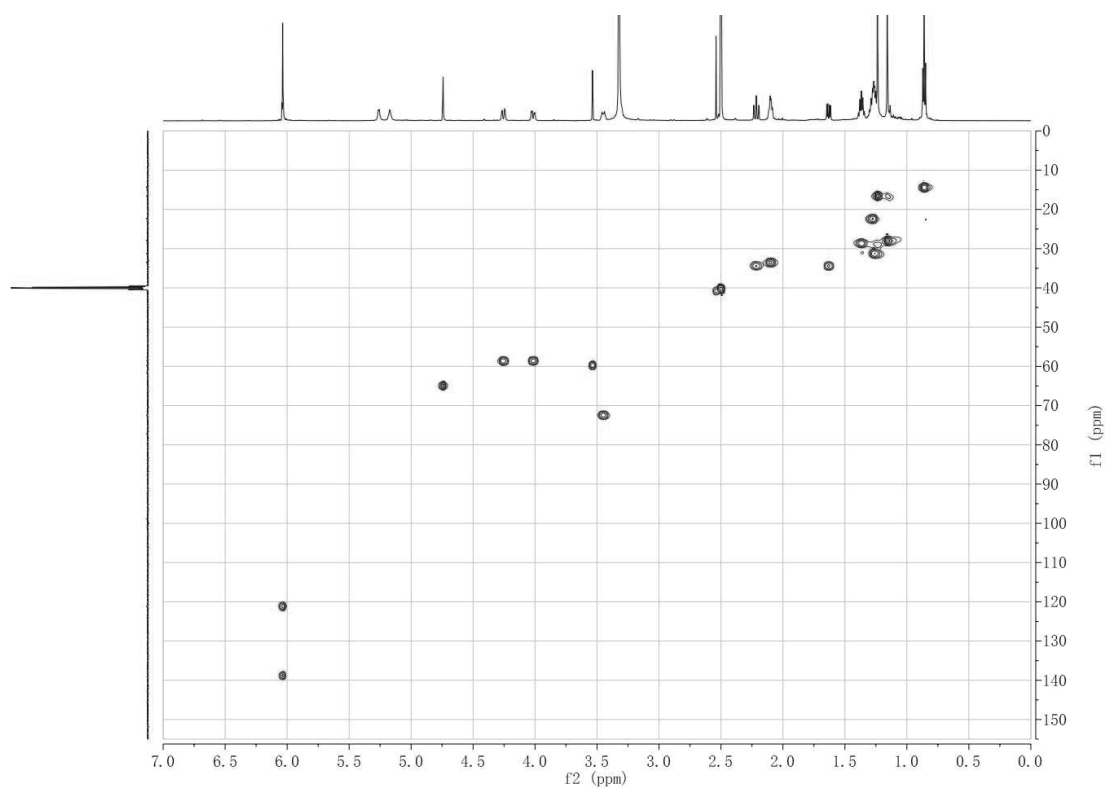


Figure S136. HSQC (600 MHz, $\text{DMSO}-d_6$) spectrum of **23**.

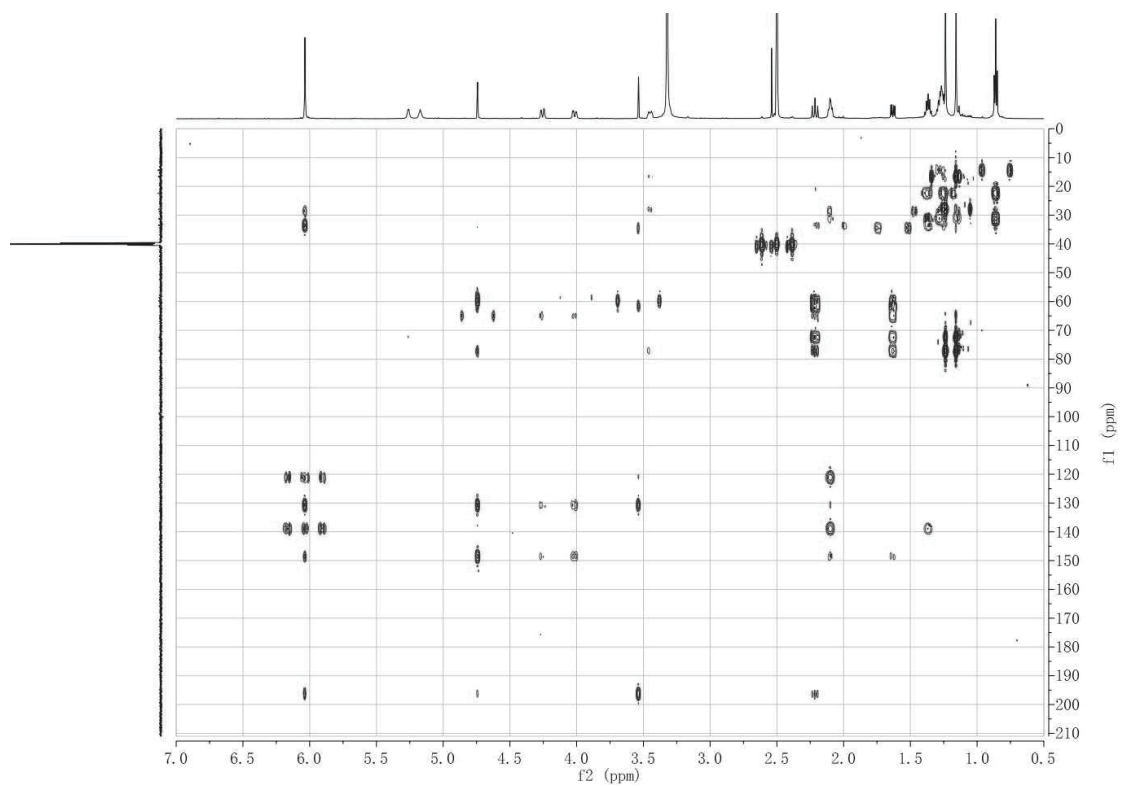


Figure S137. HMBC (600 MHz, DMSO- d_6) spectrum of **23**.

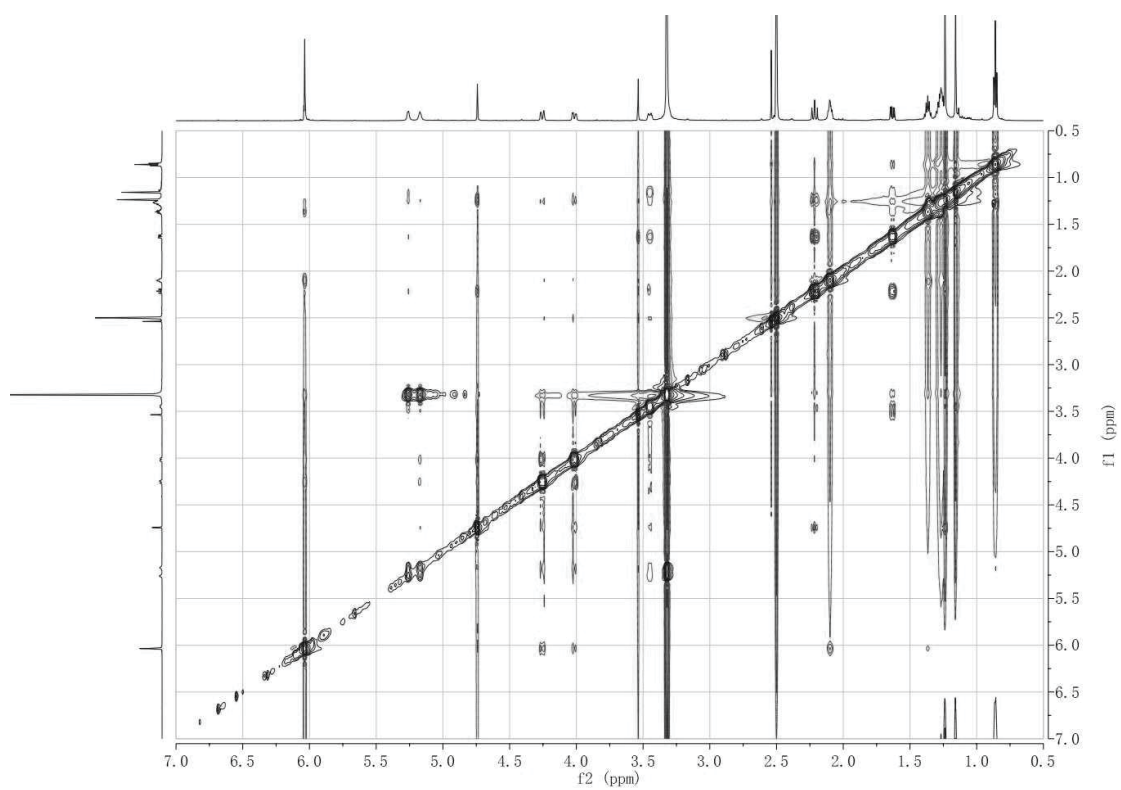


Figure S138. ROESY (600 MHz, DMSO- d_6) spectrum of **23**.

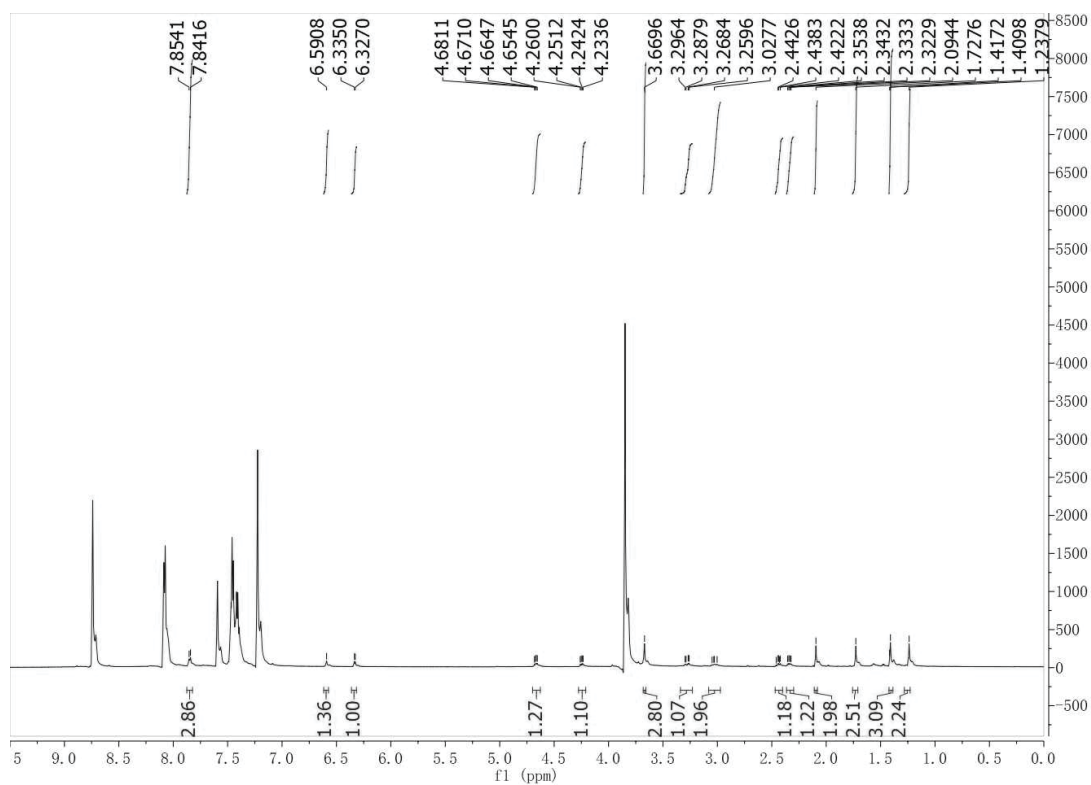


Figure S139. ¹H-NMR (600 MHz, Pyridine-*d*₅) spectrum of **1a**.

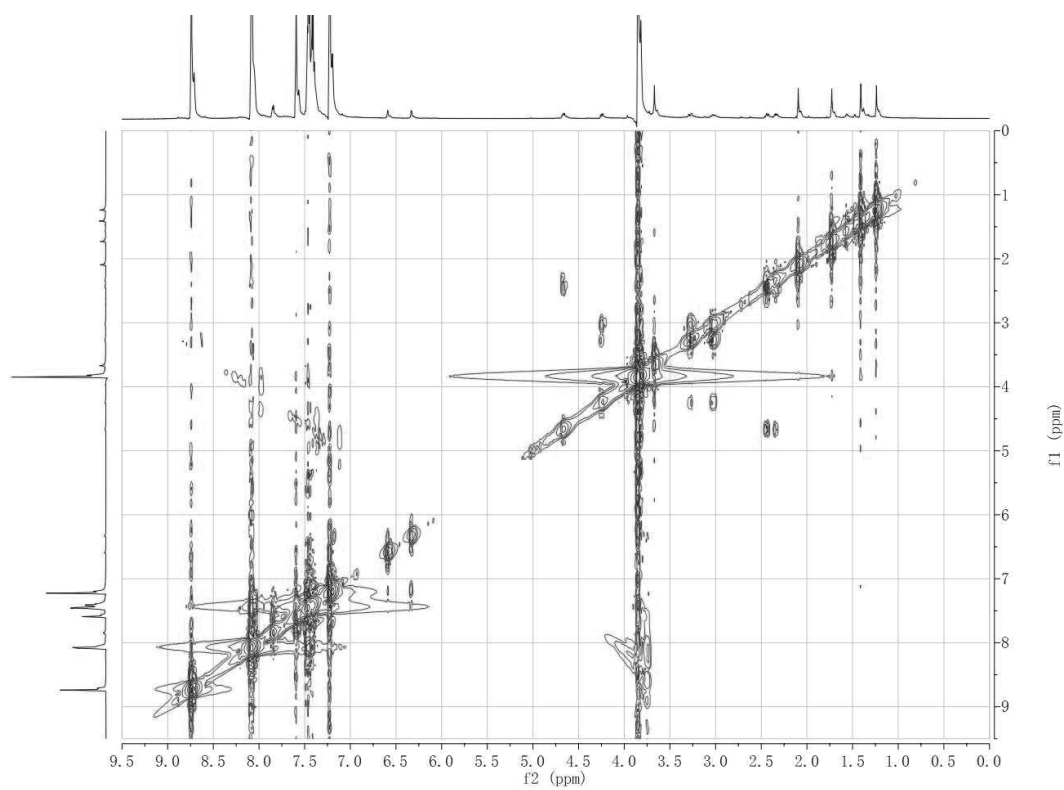


Figure S140. ¹H-¹H COSY (600 MHz, Pyridine-*d*₅) spectrum of **1a**.

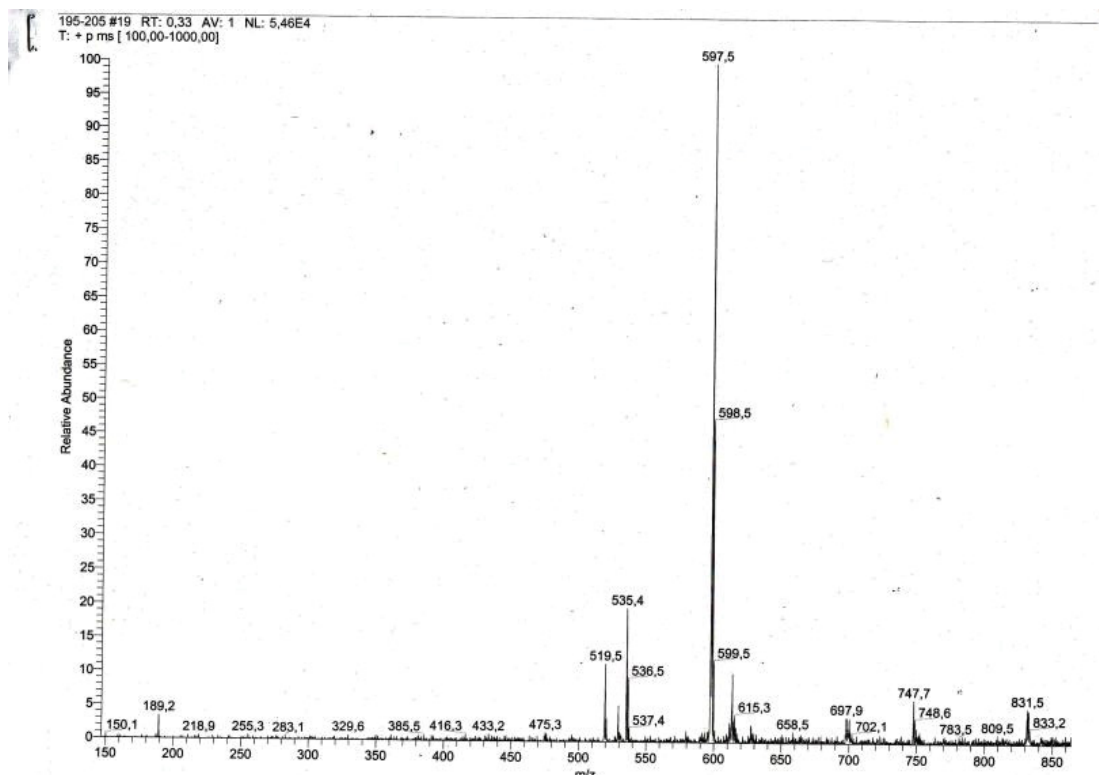


Figure S141. ESIMS of 1a.

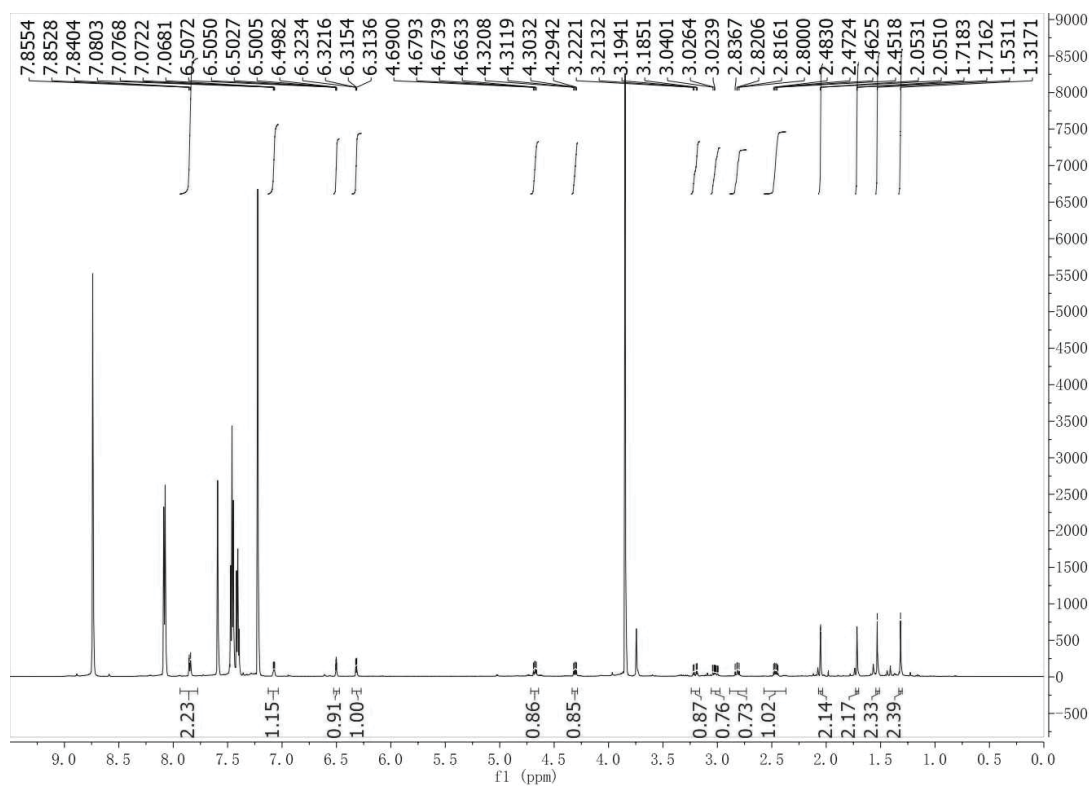


Figure S142. ¹H-NMR (600 MHz, Pyridine-*d*₅) spectrum of 1b.

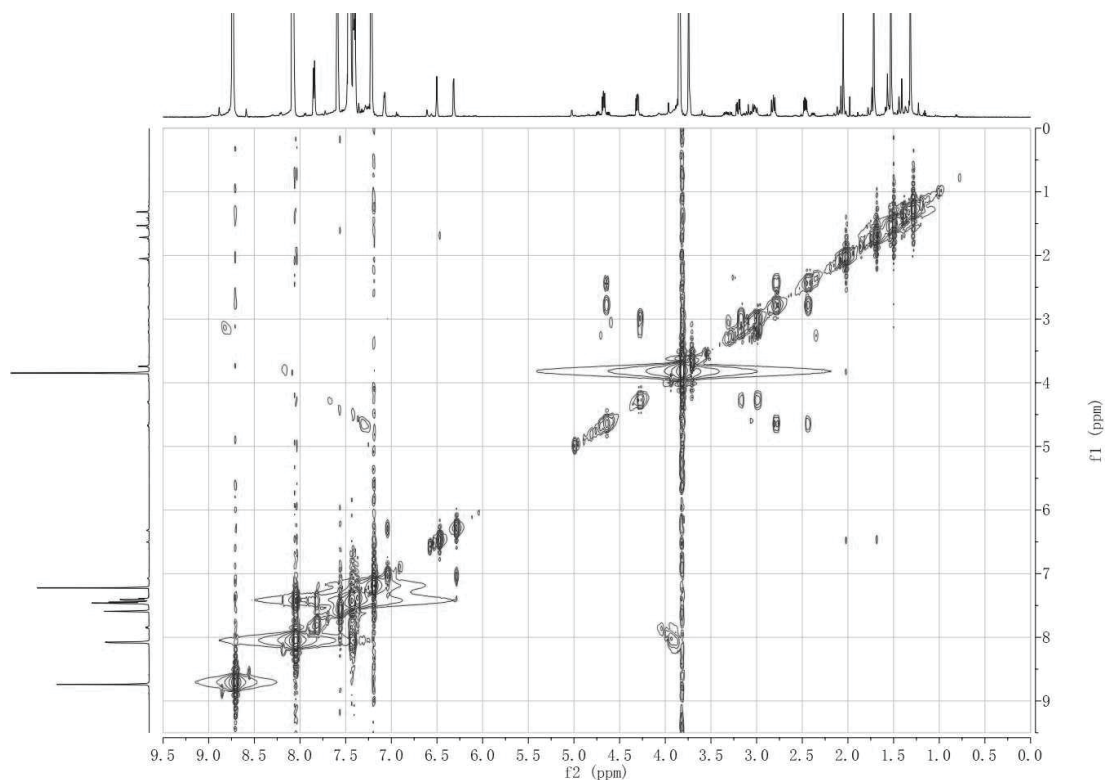


Figure S143. ^1H - ^1H COSY (600 MHz, Pyridine- d_5) spectrum of **1b**.

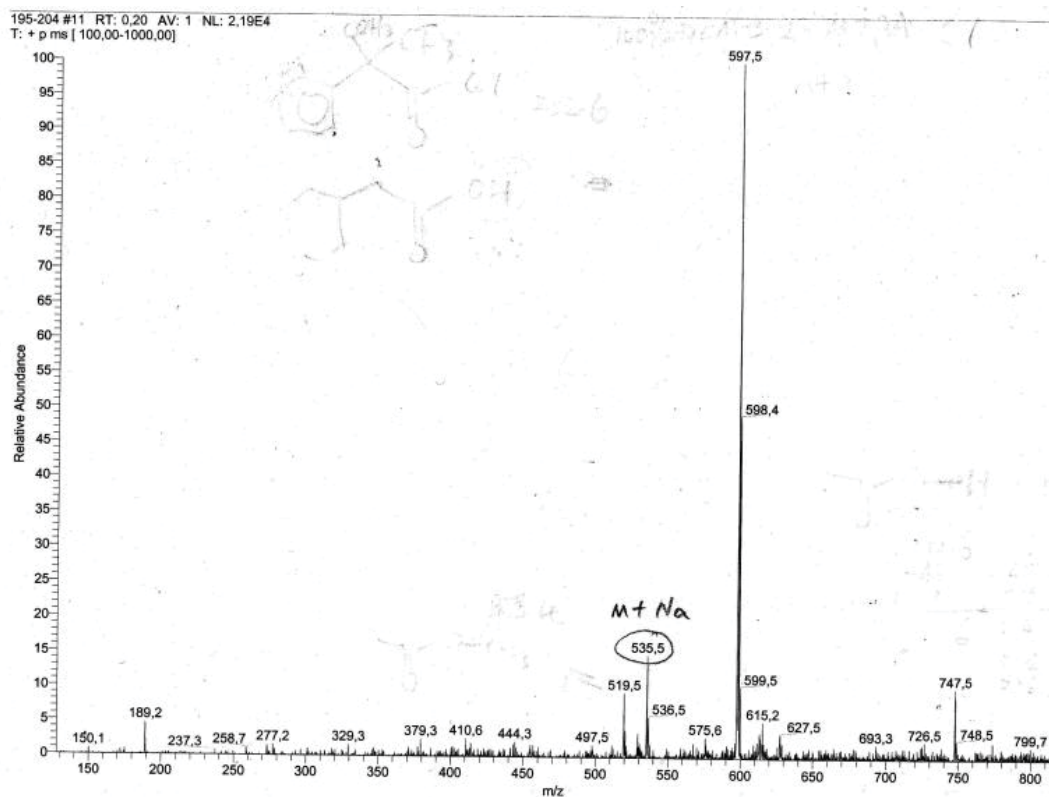


Figure S144. ESIMS of **1b**.

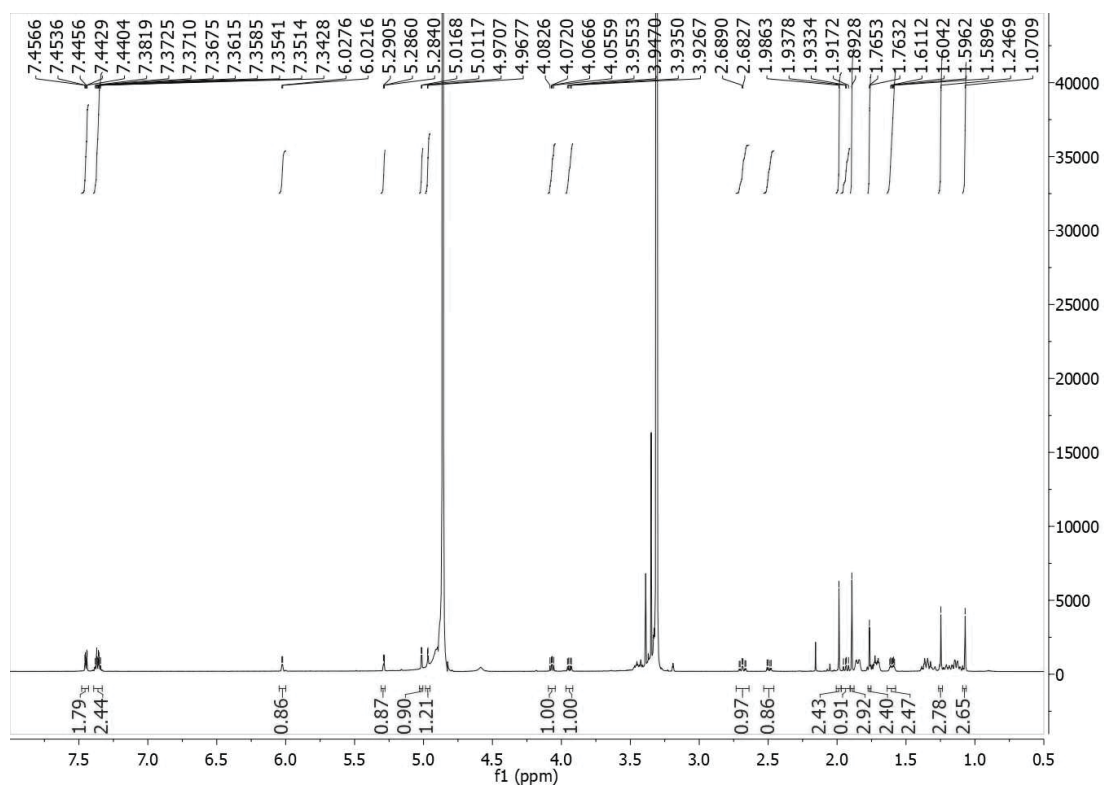


Figure S145. ^1H -NMR (600 MHz, CD_3OD) spectrum of **7a**.

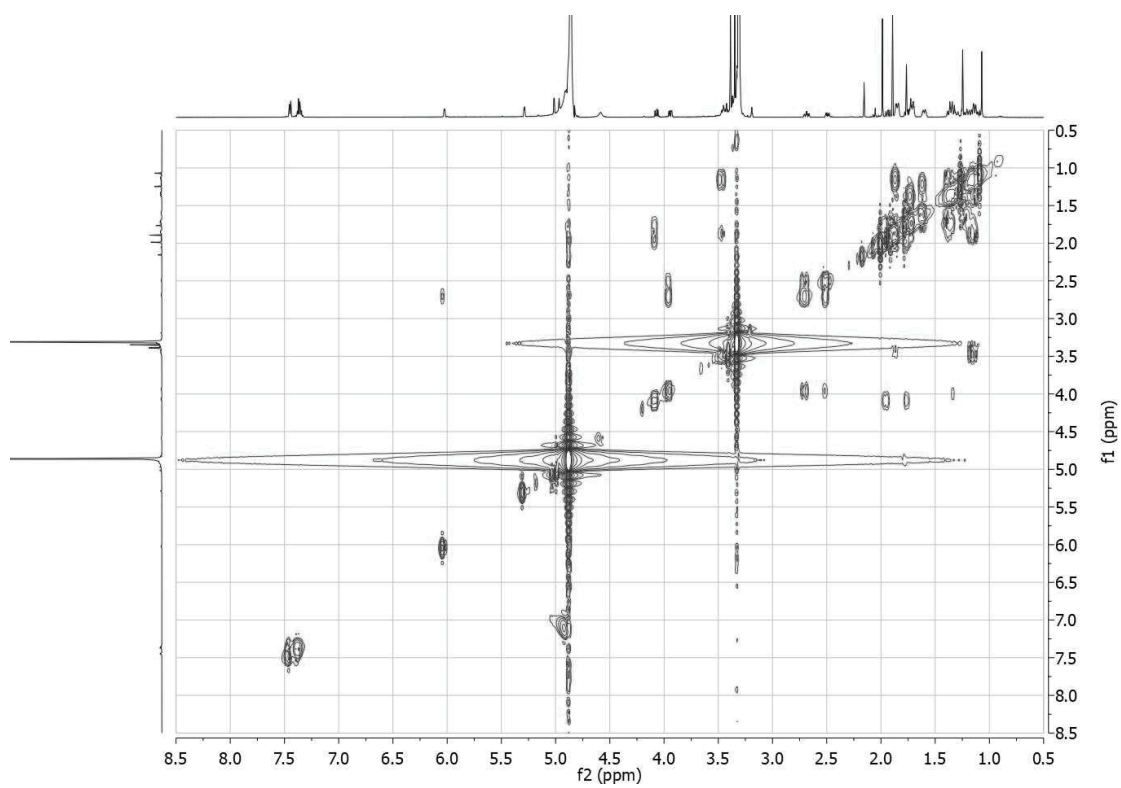


Figure S146. ^1H - ^1H COSY (600 MHz, CD_3OD) spectrum of **7a**.

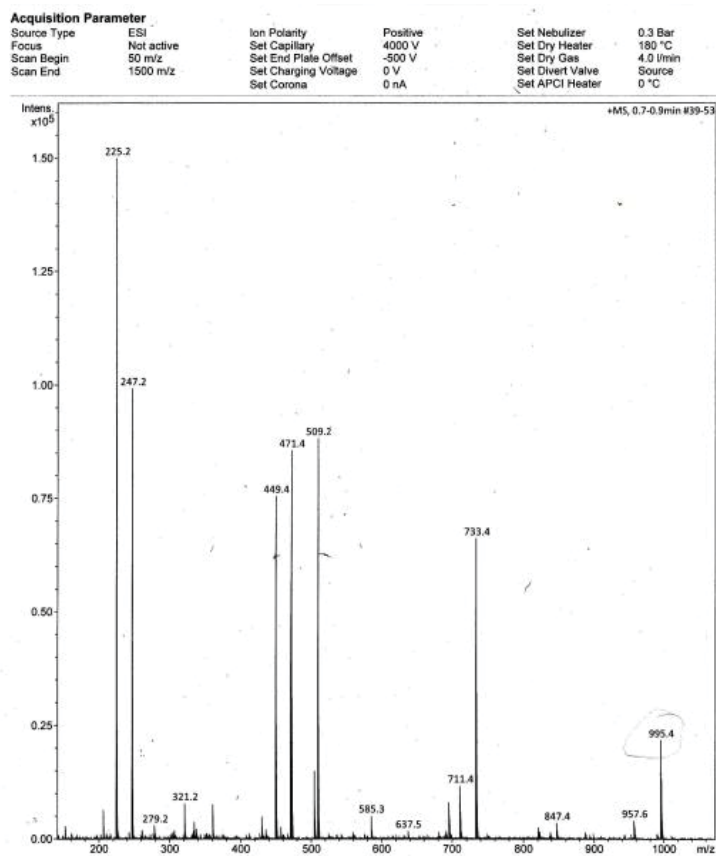


Figure S147. ESIMS of **7a**.

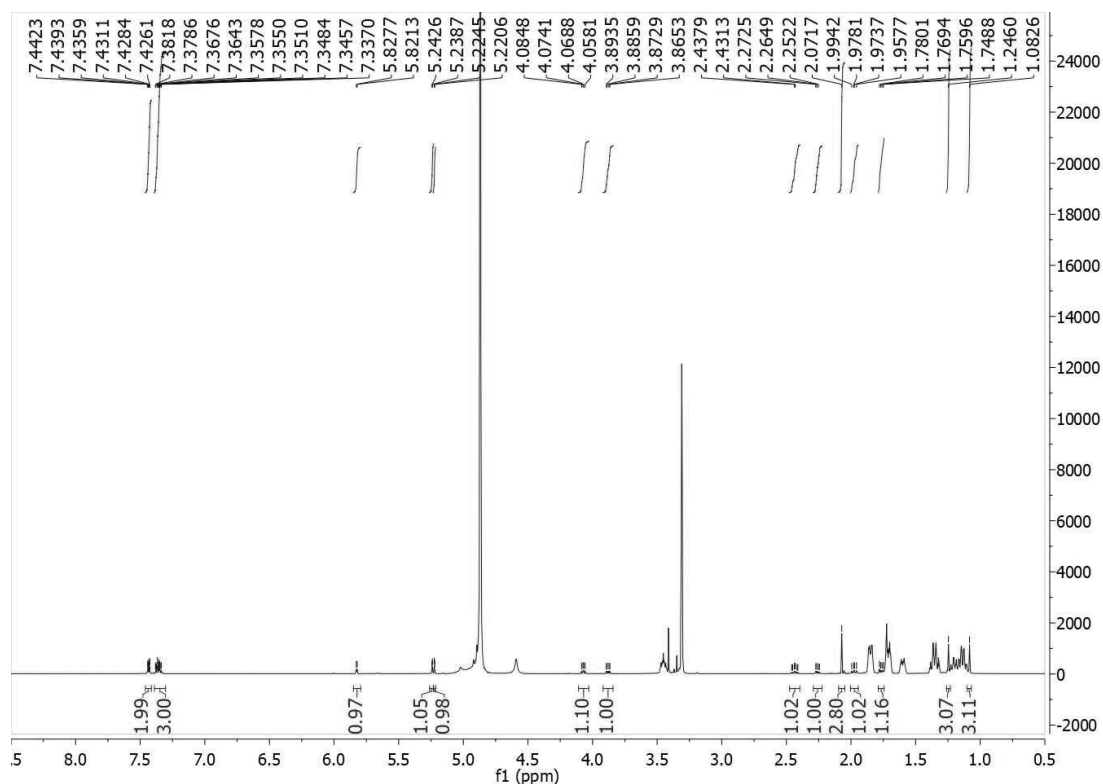


Figure S148. ^1H -NMR (600 MHz, CD_3OD) spectrum of **7b**.

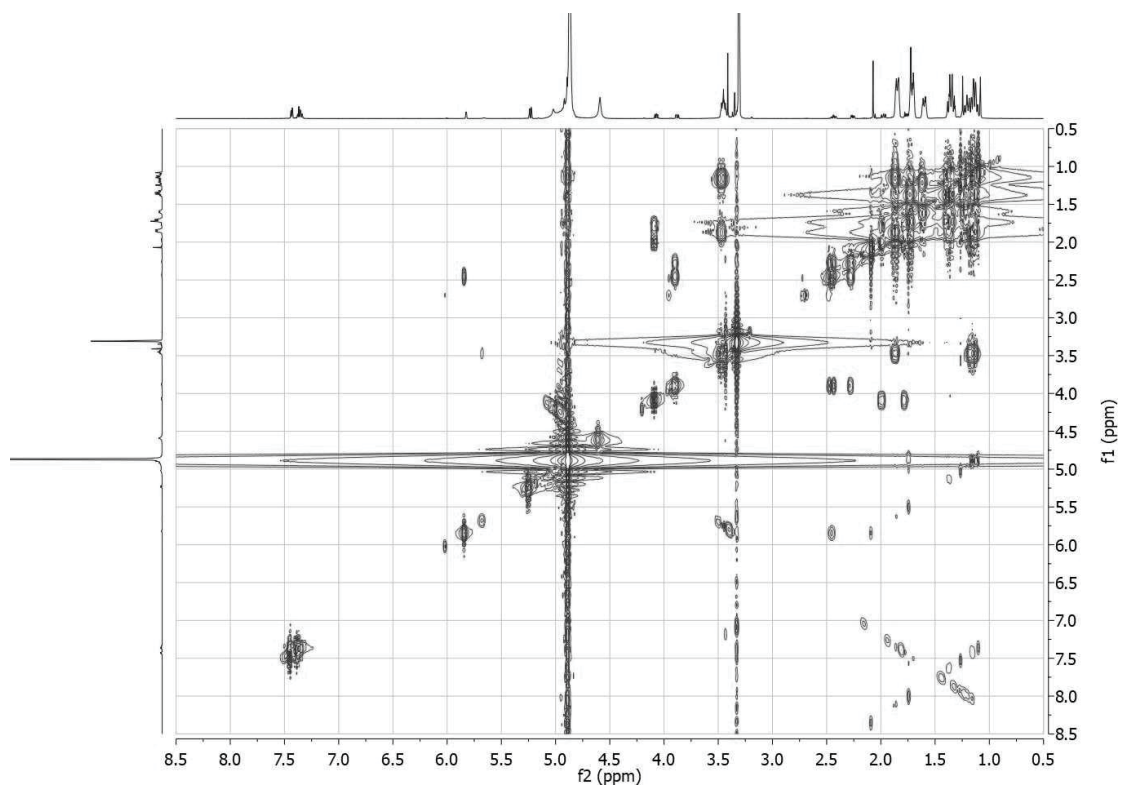


Figure S149. ^1H - ^1H COSY (600 MHz, CD_3OD) spectrum of **7b**.

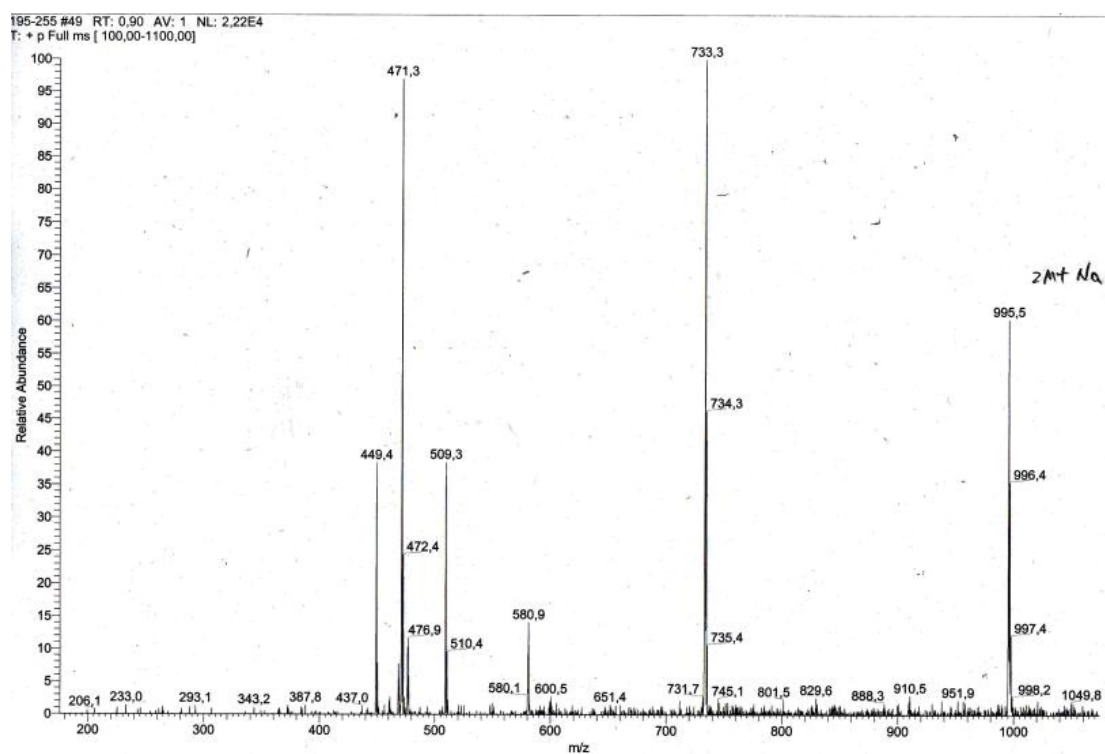


Figure S150. ESIMS of **7b**.

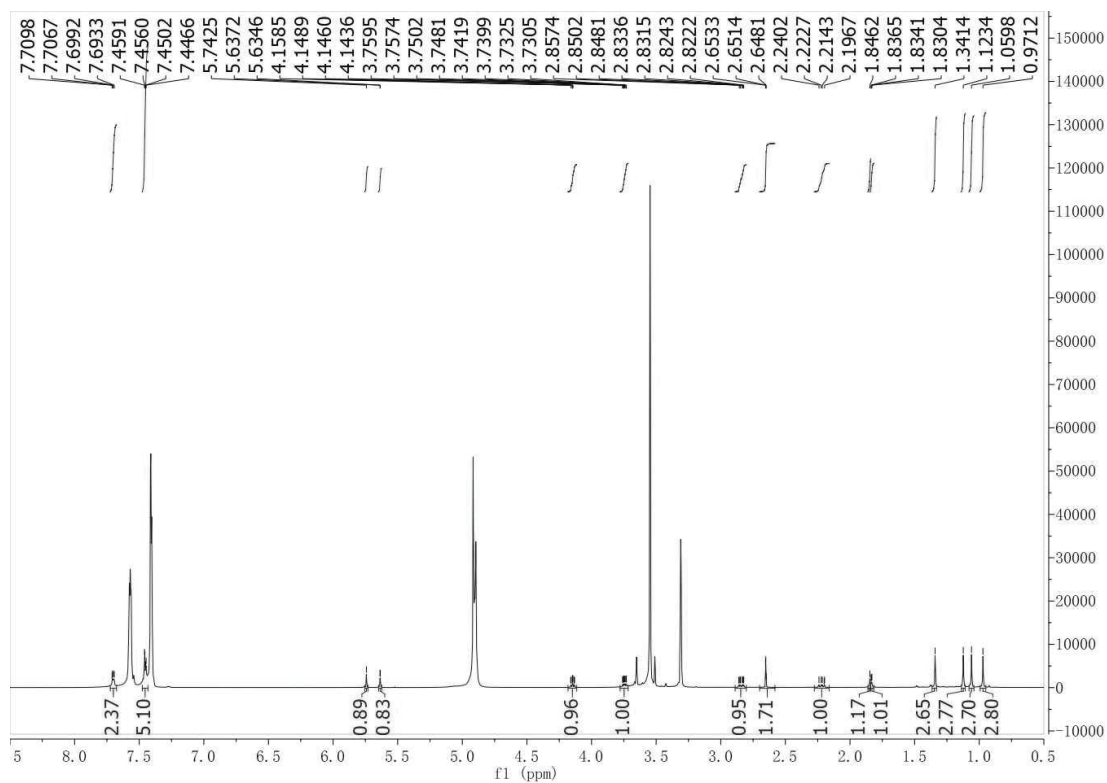


Figure S151. ^1H -NMR (600 MHz, CD_3OD) spectrum of **8a**.

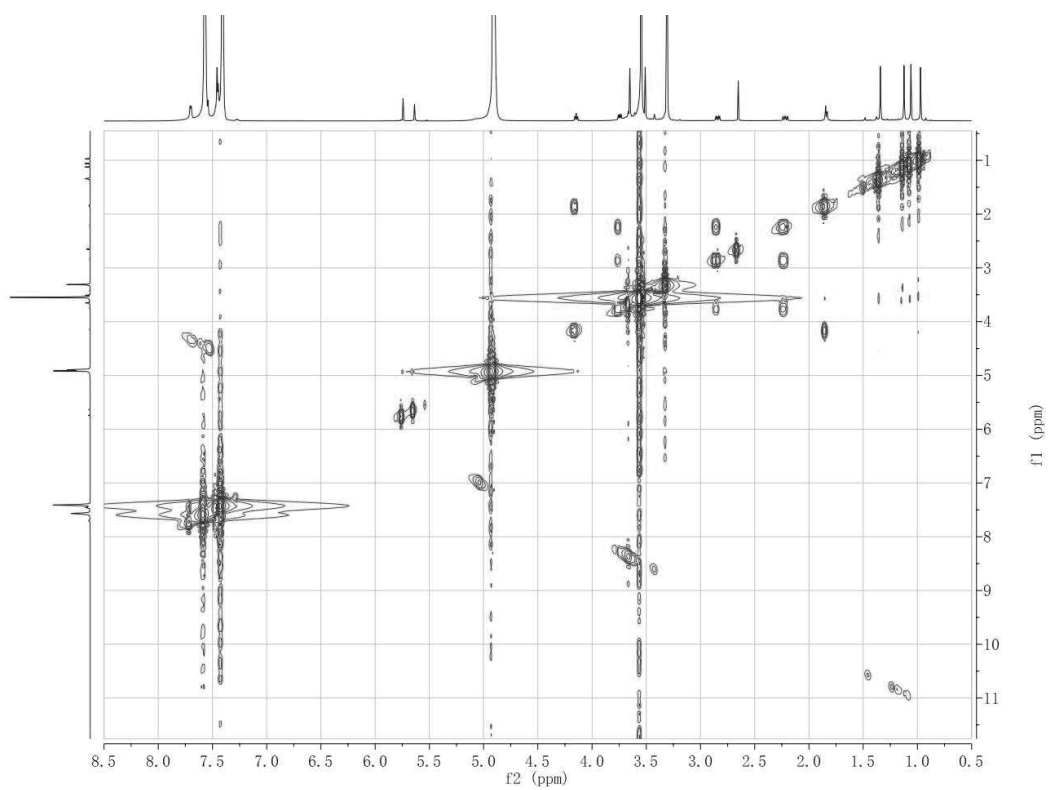


Figure S152. ^1H - ^1H COSY (600 MHz, CD_3OD) spectrum of **8a**.

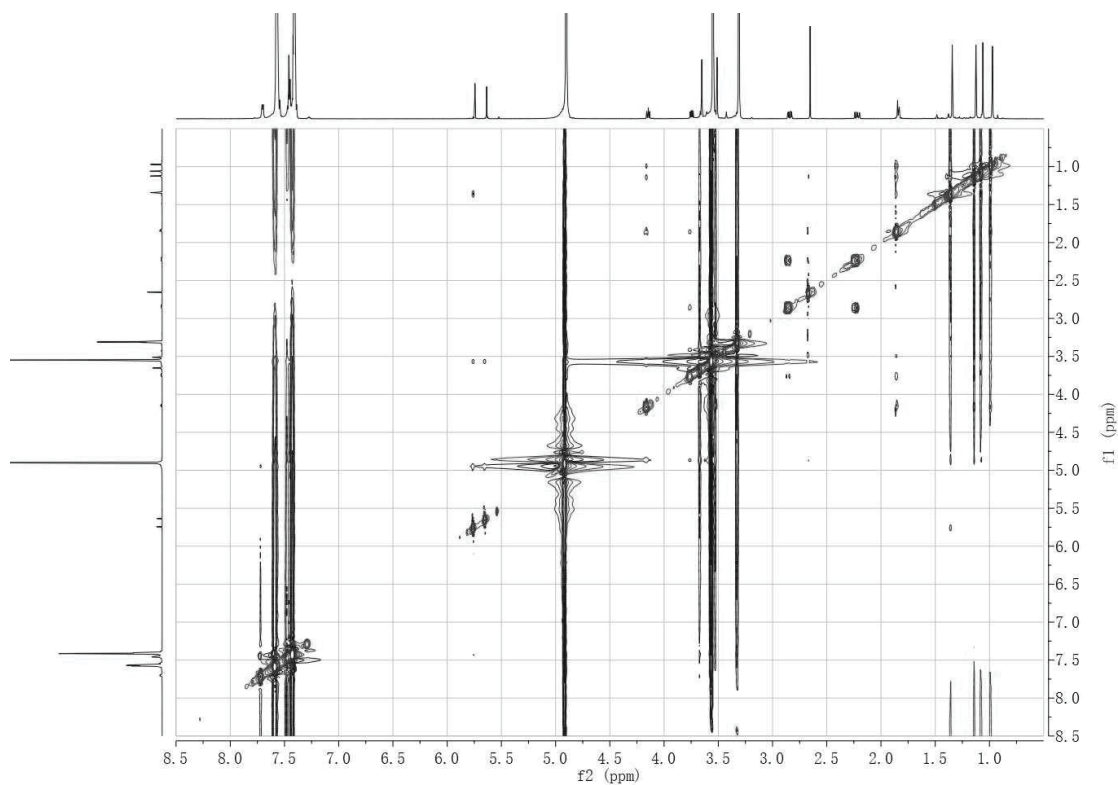


Figure S153. ROESY (600 MHz, CD₃OD) spectrum of **8a**.

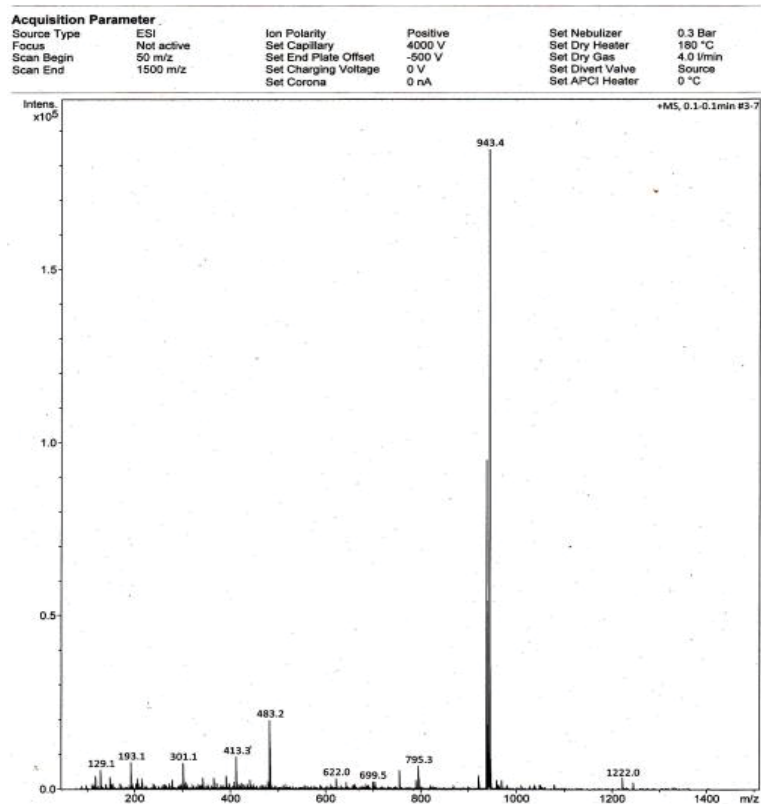


Figure S154. ESIMS of **8a**.

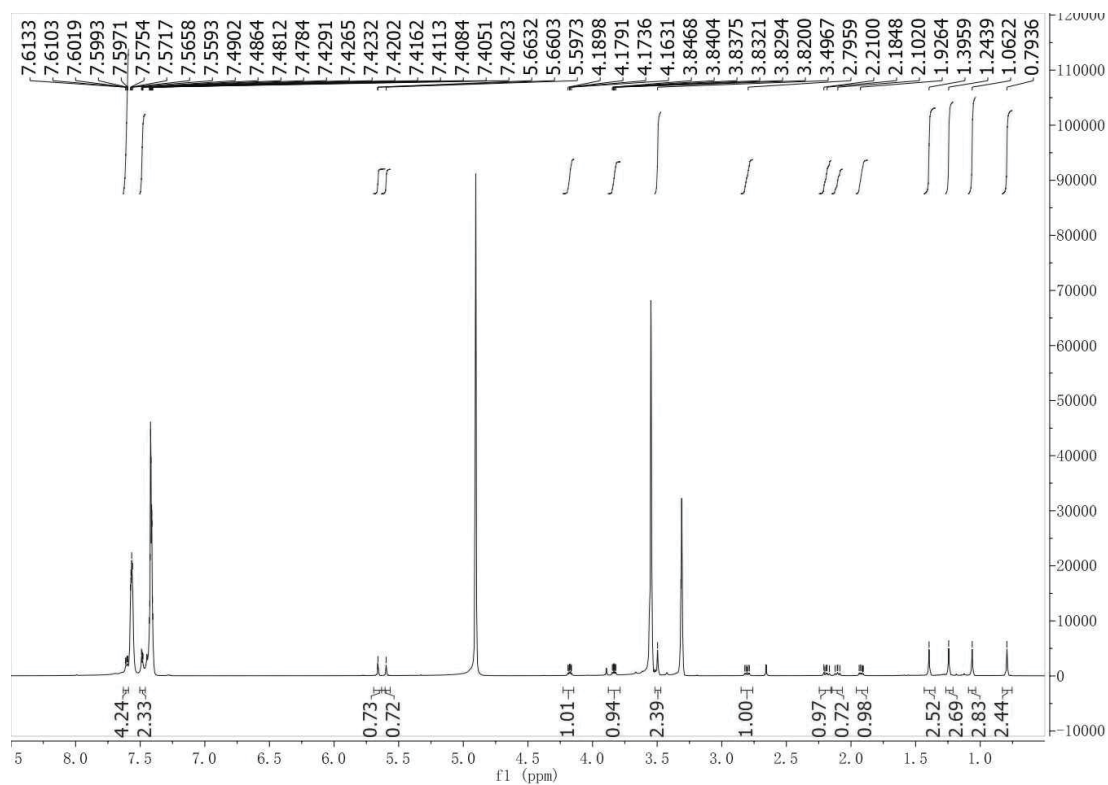


Figure S155. ¹H-NMR (600 MHz, CD₃OD) spectrum of **8b**.

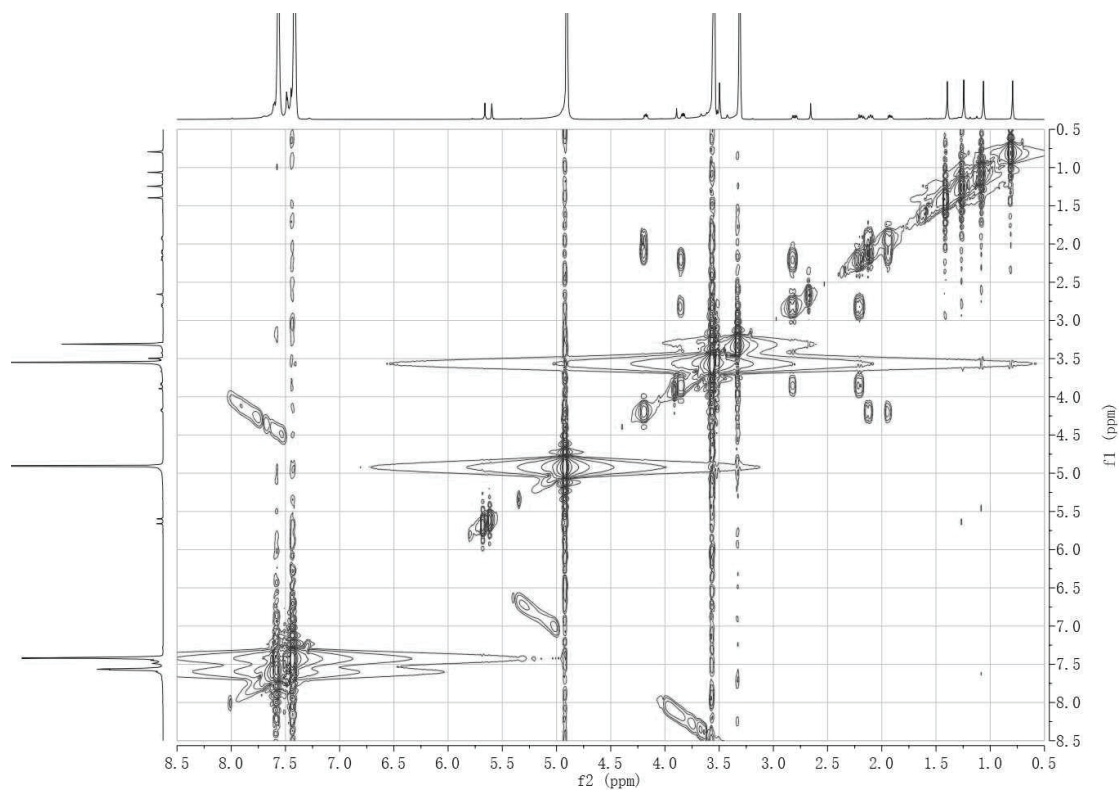


Figure S156. ¹H-¹H COSY (600 MHz, CD₃OD) spectrum of **8b**.

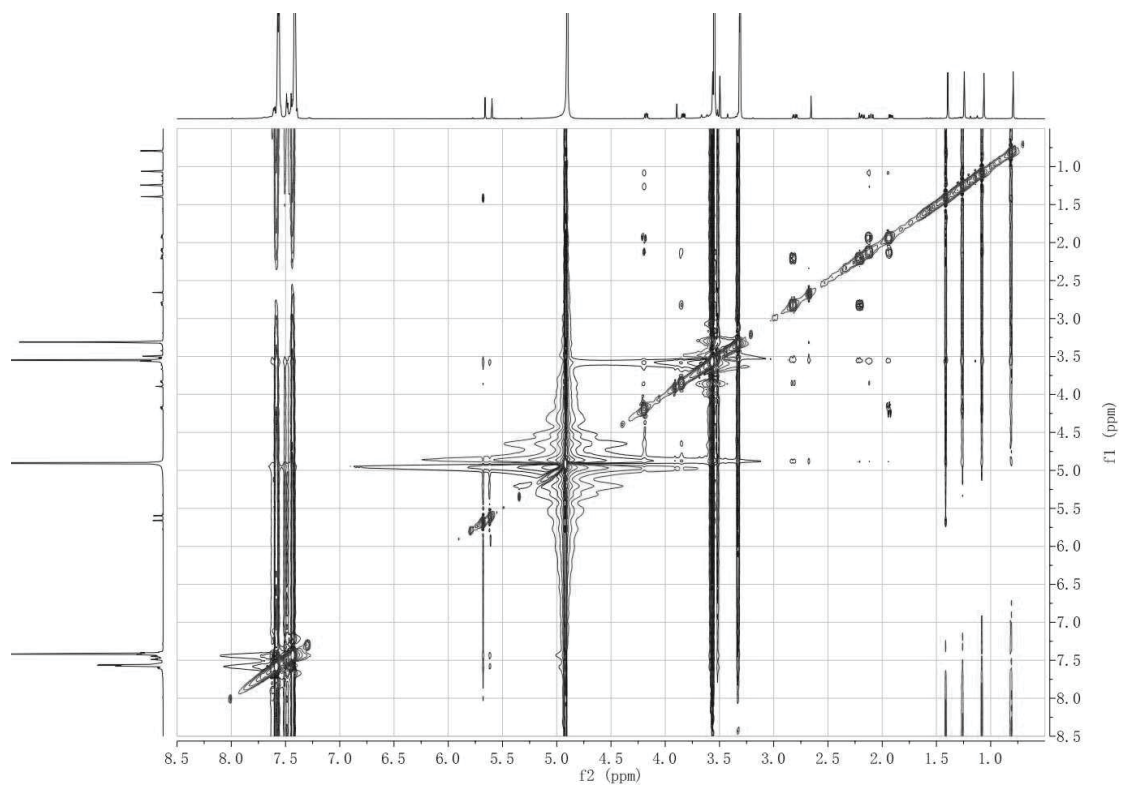


Figure S157. ROESY (600 MHz, CD₃OD) spectrum of **8b**.

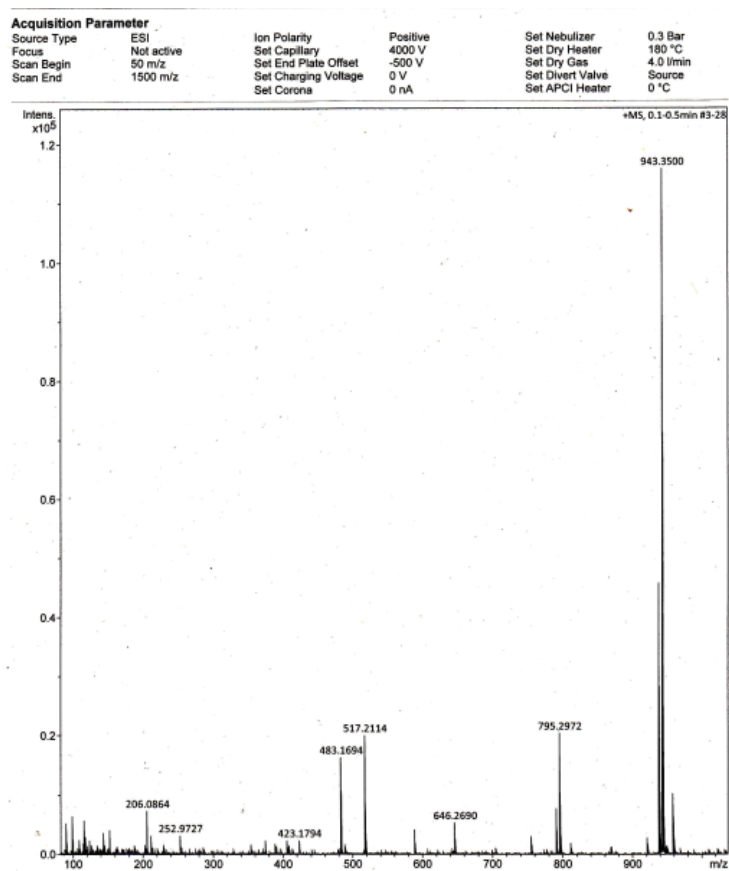


Figure S158. ESIMS of **8b**.

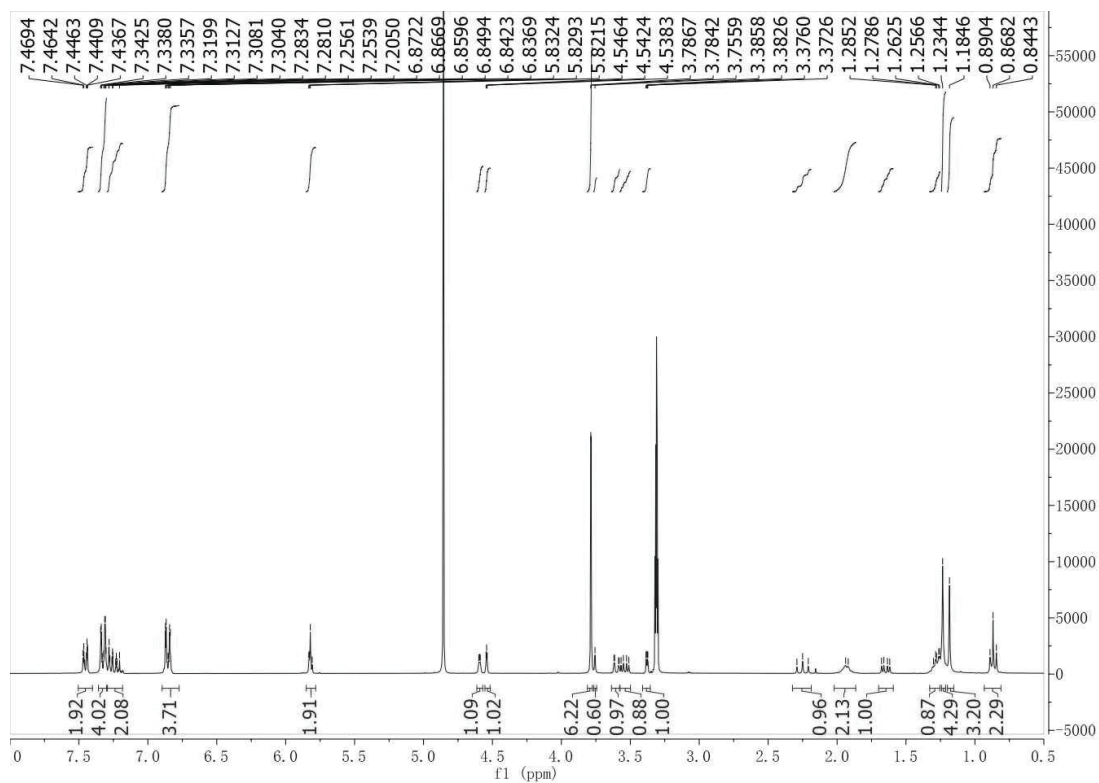


Figure S159. ¹H-NMR (600 MHz, CD₃OD) spectrum of 17a.

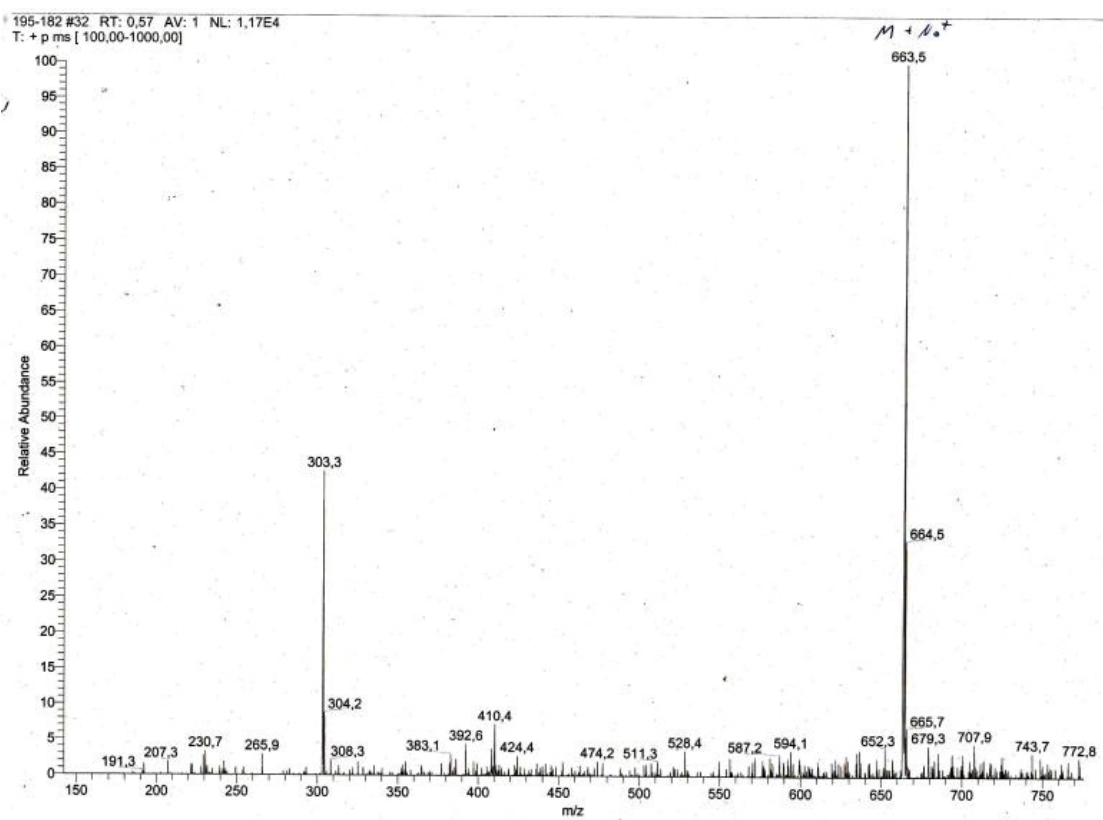


Figure S160. ESIMS of 17a.

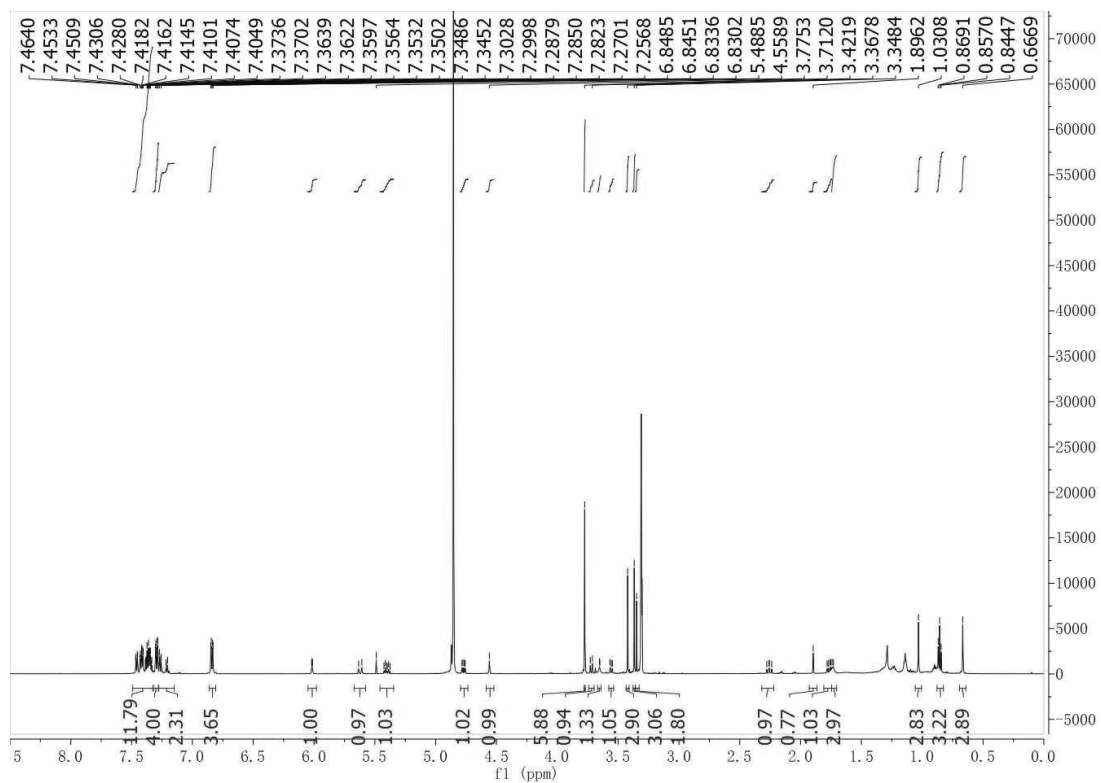


Figure S161. ^1H -NMR (600 MHz, CD_3OD) spectrum of **17b**.

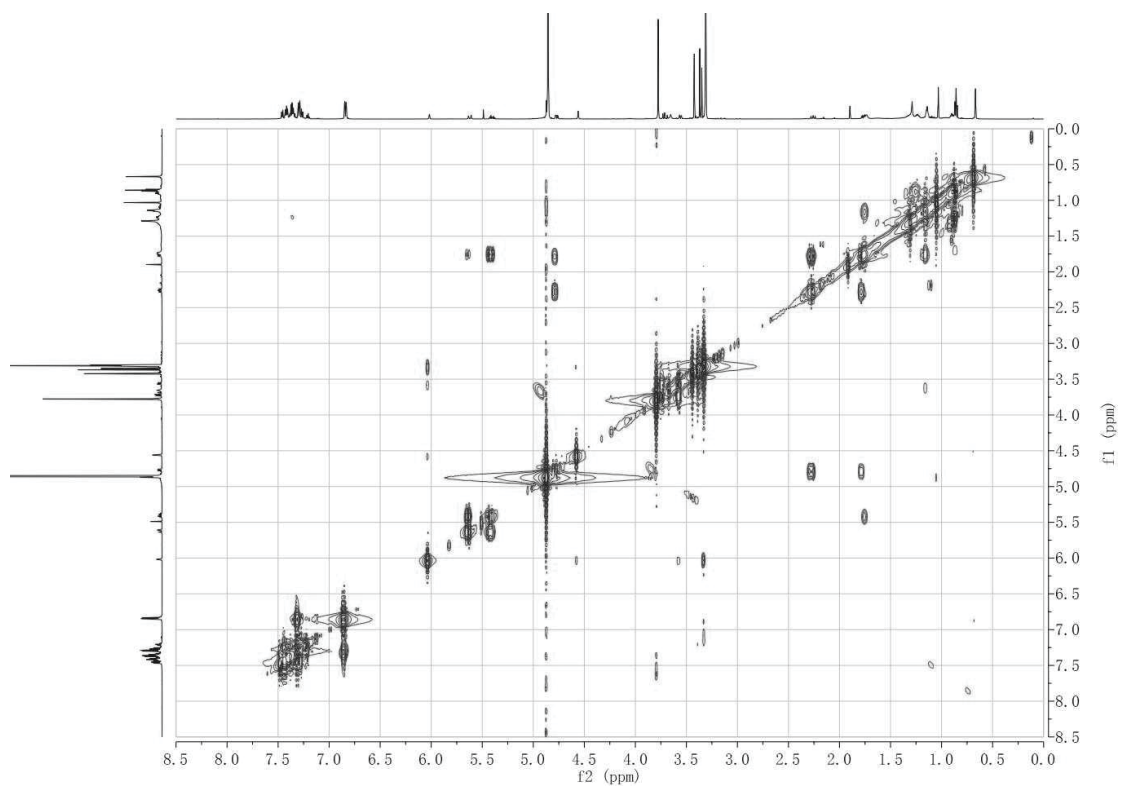


Figure S162. ^1H - ^1H COSY (600 MHz, CD_3OD) spectrum of **17b**.

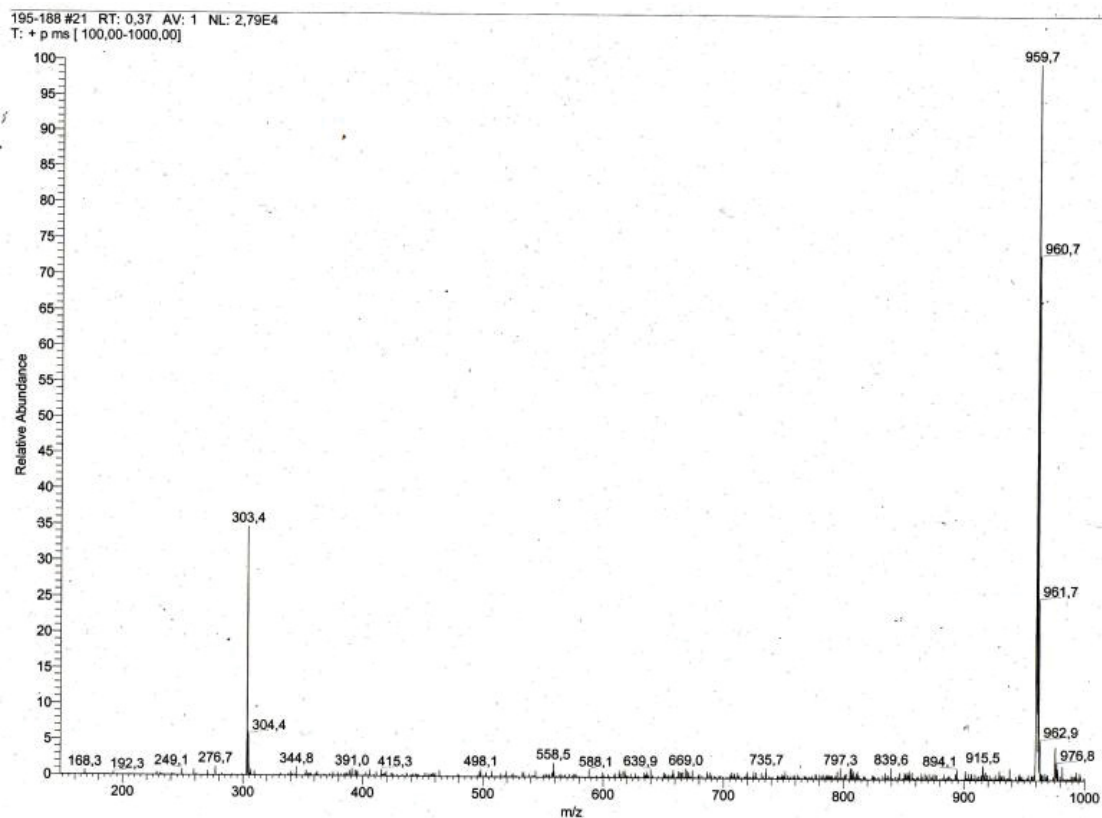


Figure S163. ESIMS of 17b.

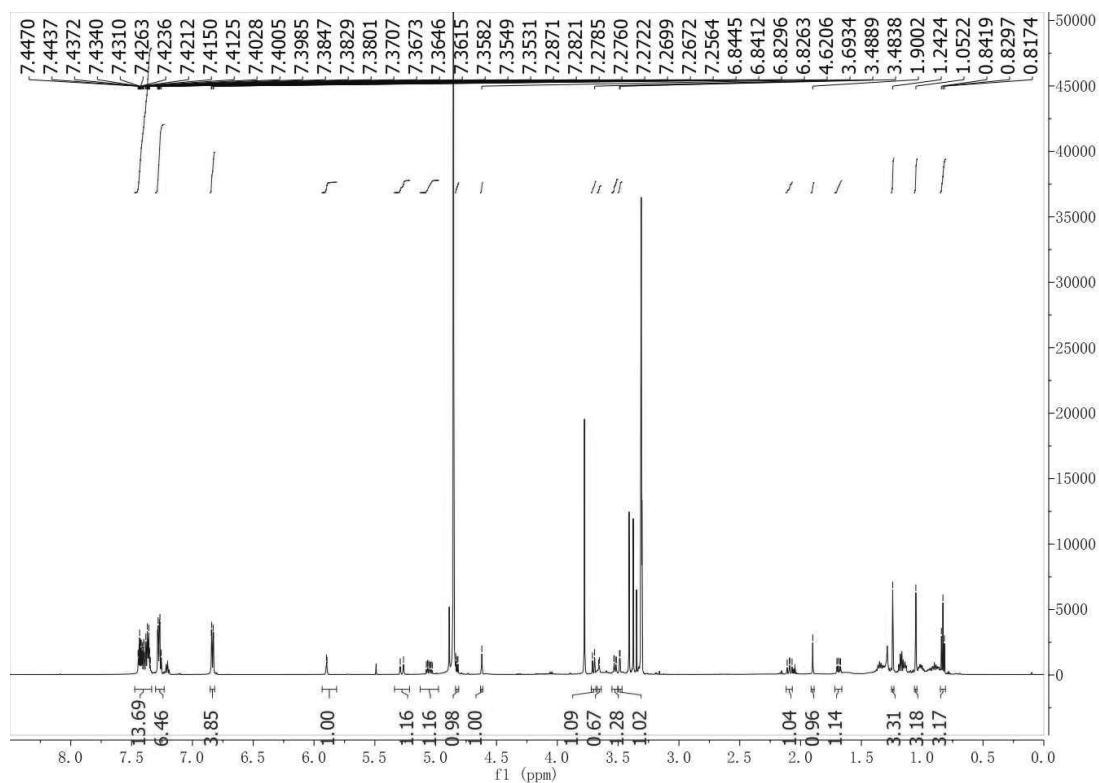


Figure S164. ^1H -NMR (600 MHz, CD_3OD) spectrum of 17c.

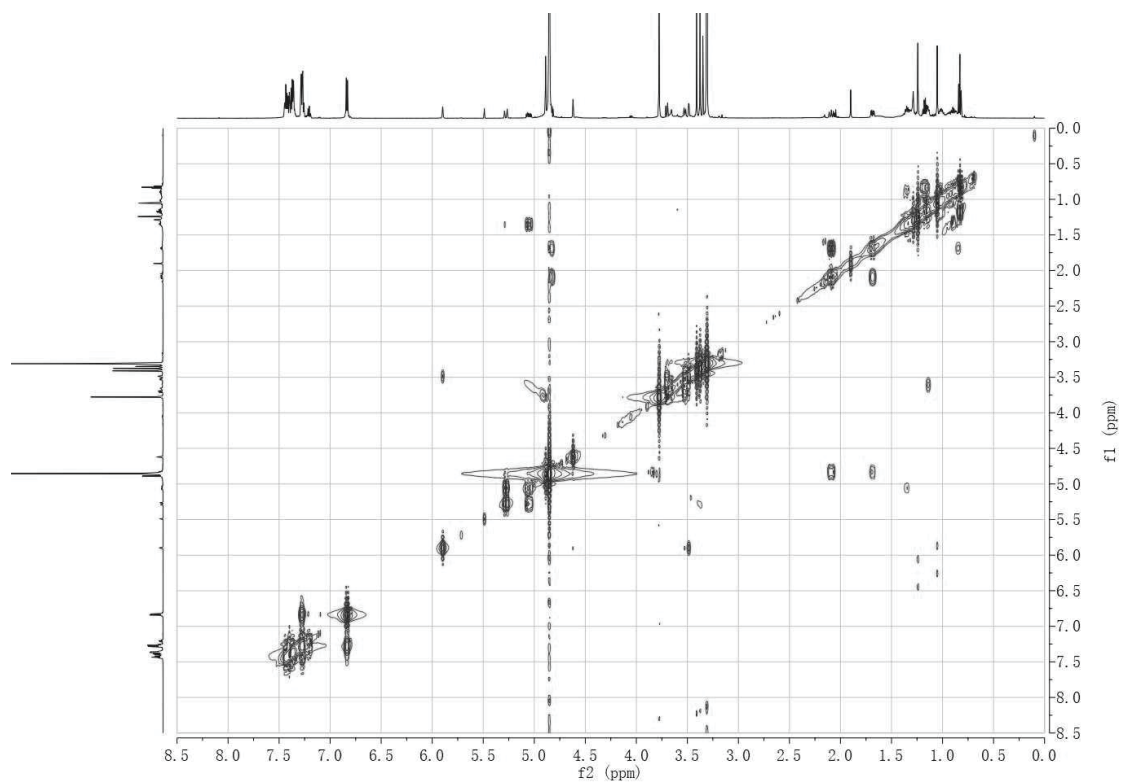


Figure S165. ^1H - ^1H COSY (600 MHz, CD_3OD) spectrum of **17c**.

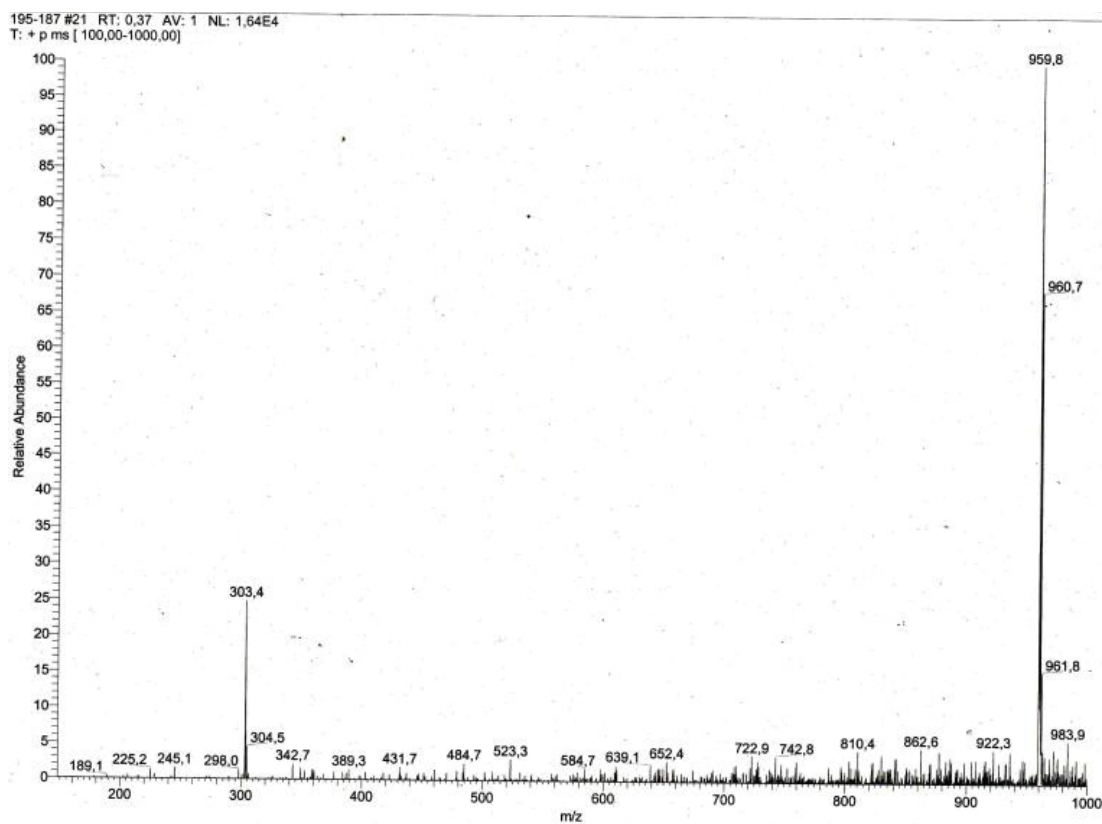


Figure S166. ESIMS of **17c**.

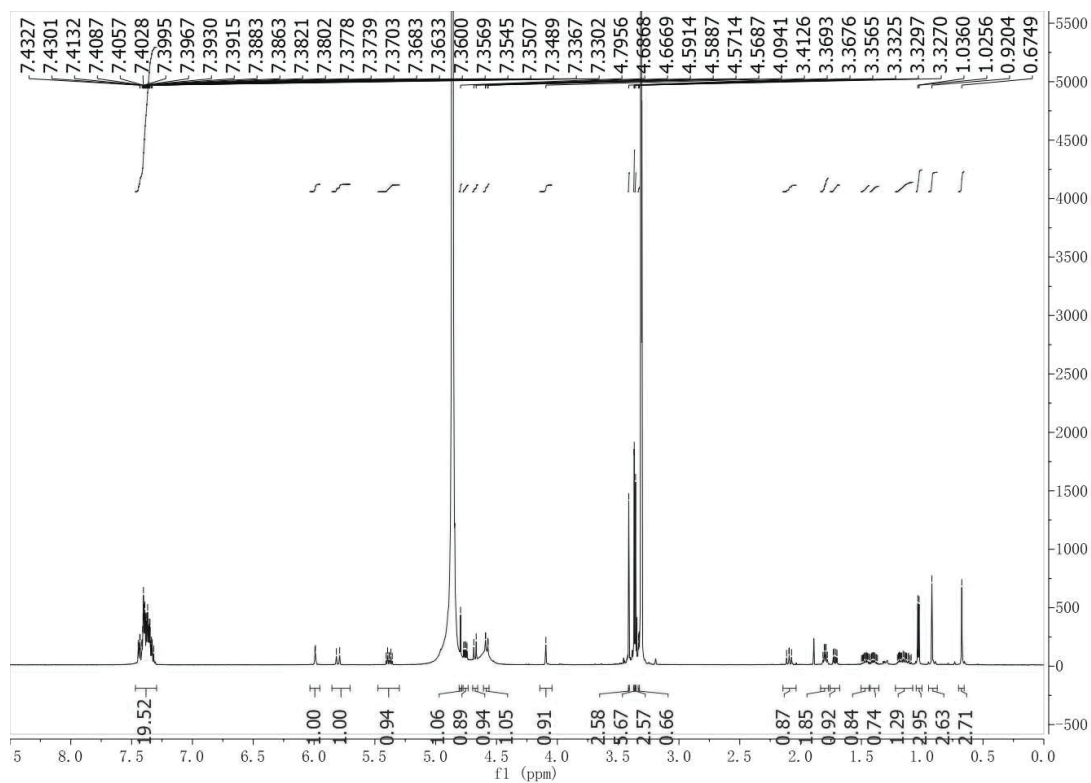


Figure S167. ^1H -NMR (600 MHz, CD_3OD) spectrum of **18a**.

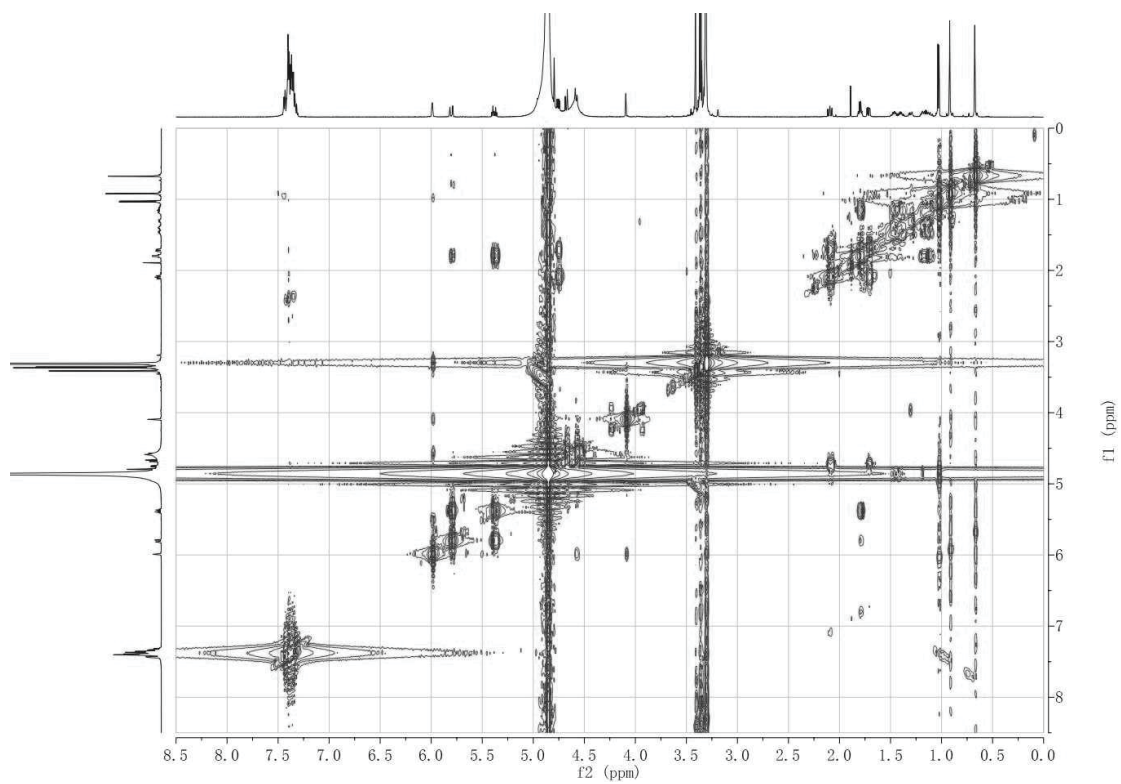


Figure S168. ^1H - ^1H COSY (600 MHz, CD_3OD) spectrum of **18a**.

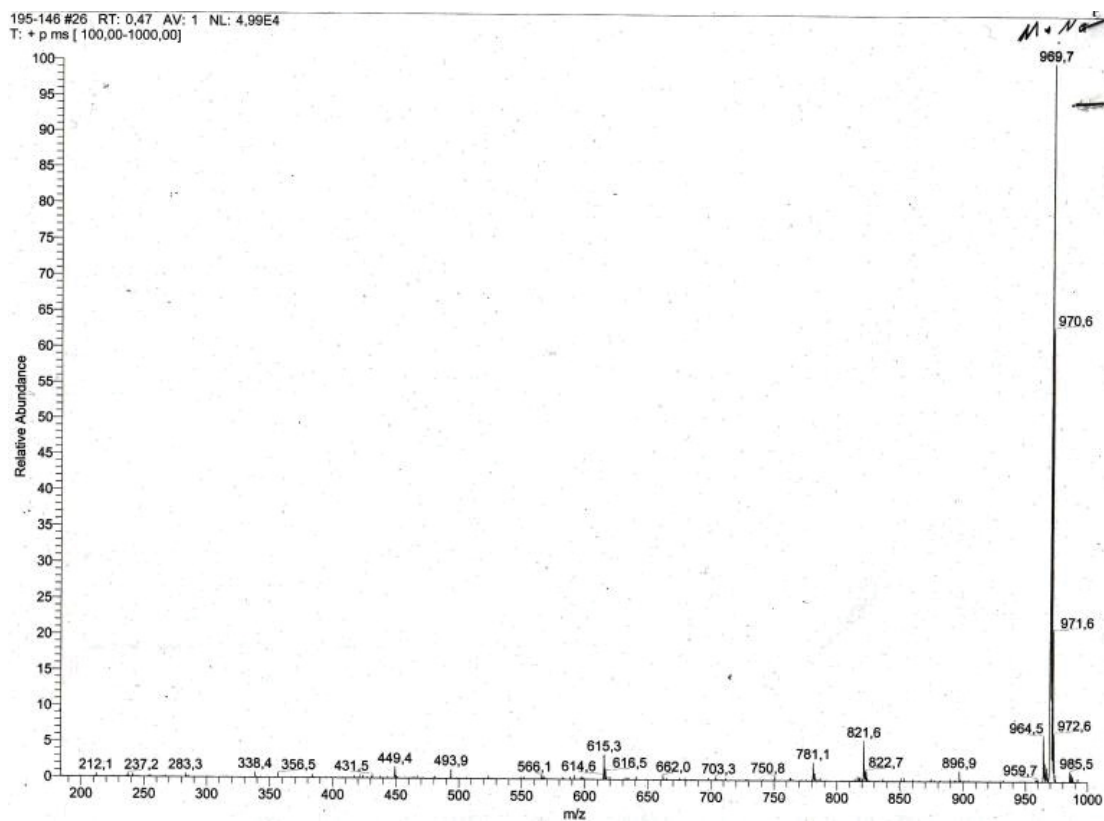


Figure S169. ESIMS of 18a.

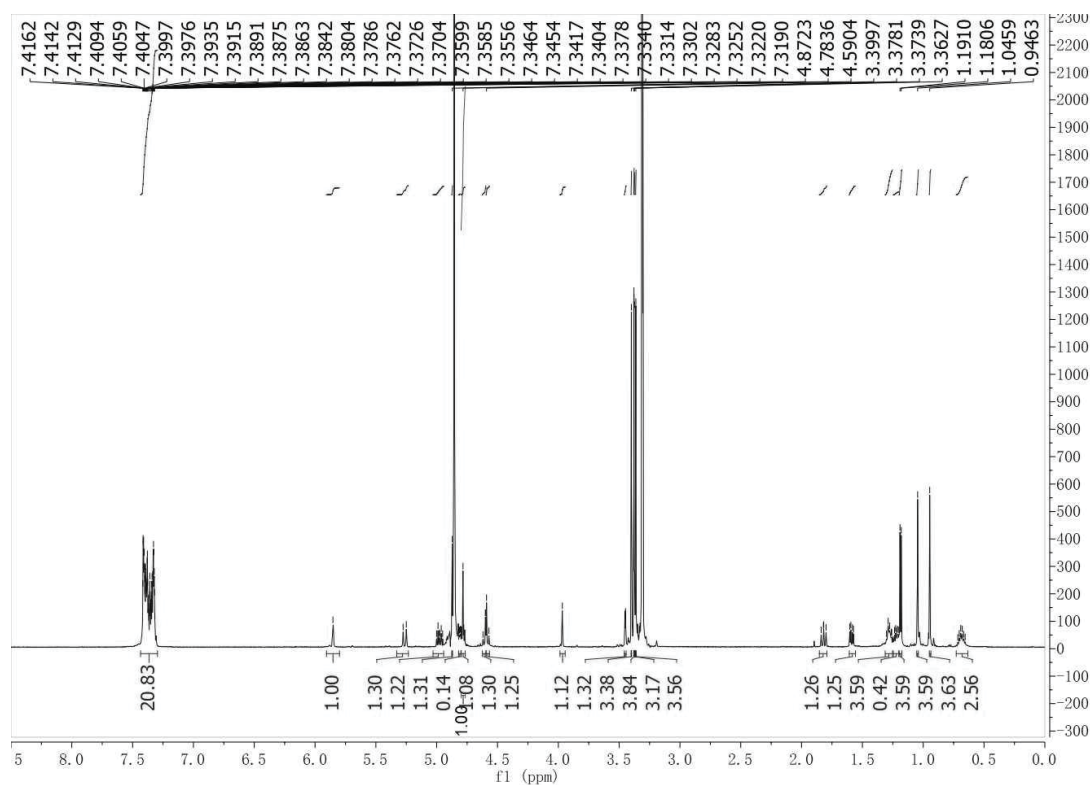


Figure S170. ^1H -NMR (600 MHz, CD_3OD) spectrum of 18b.

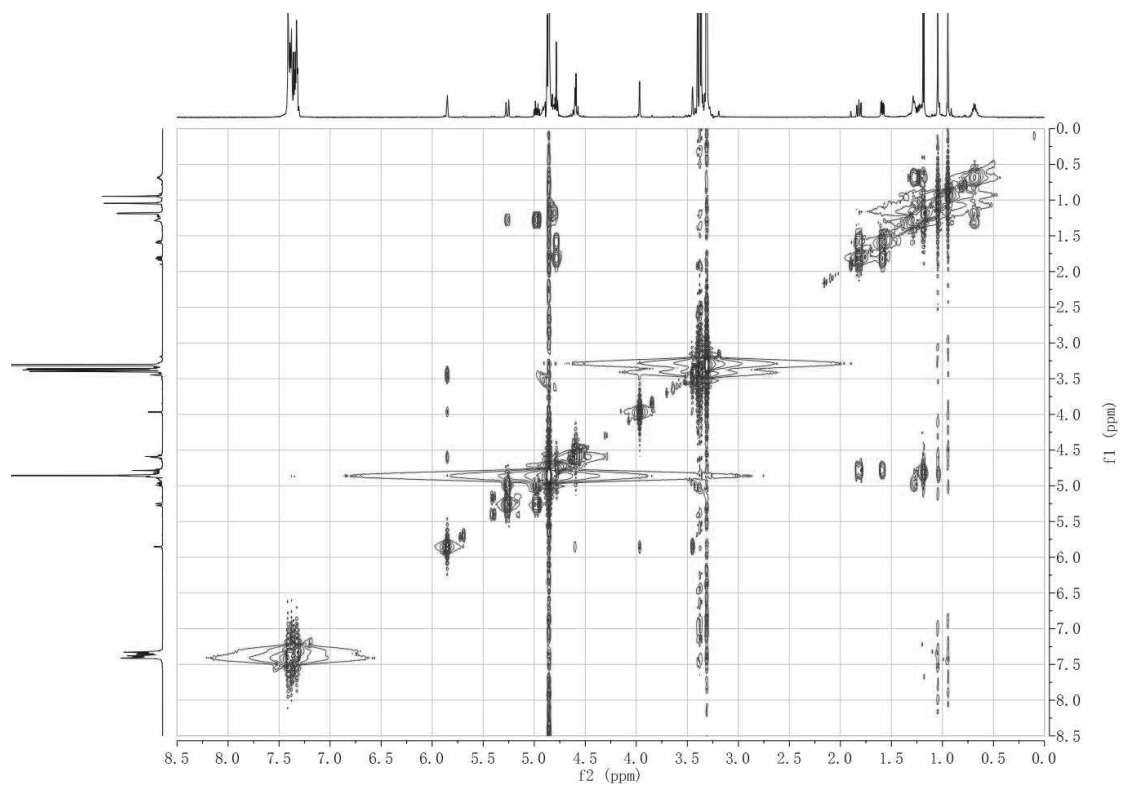


Figure S171. ^1H - ^1H COSY (600 MHz, CD_3OD) spectrum of **18b**.

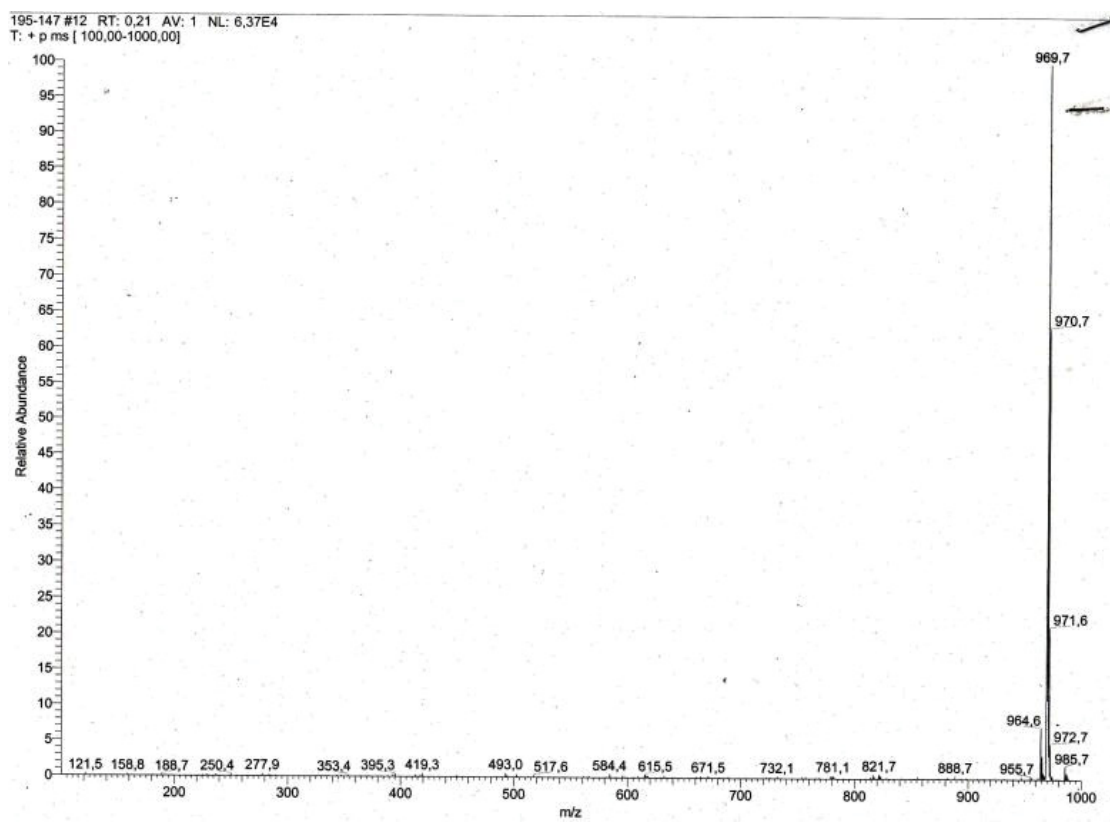


Figure S172. ESIMS of **18b**.

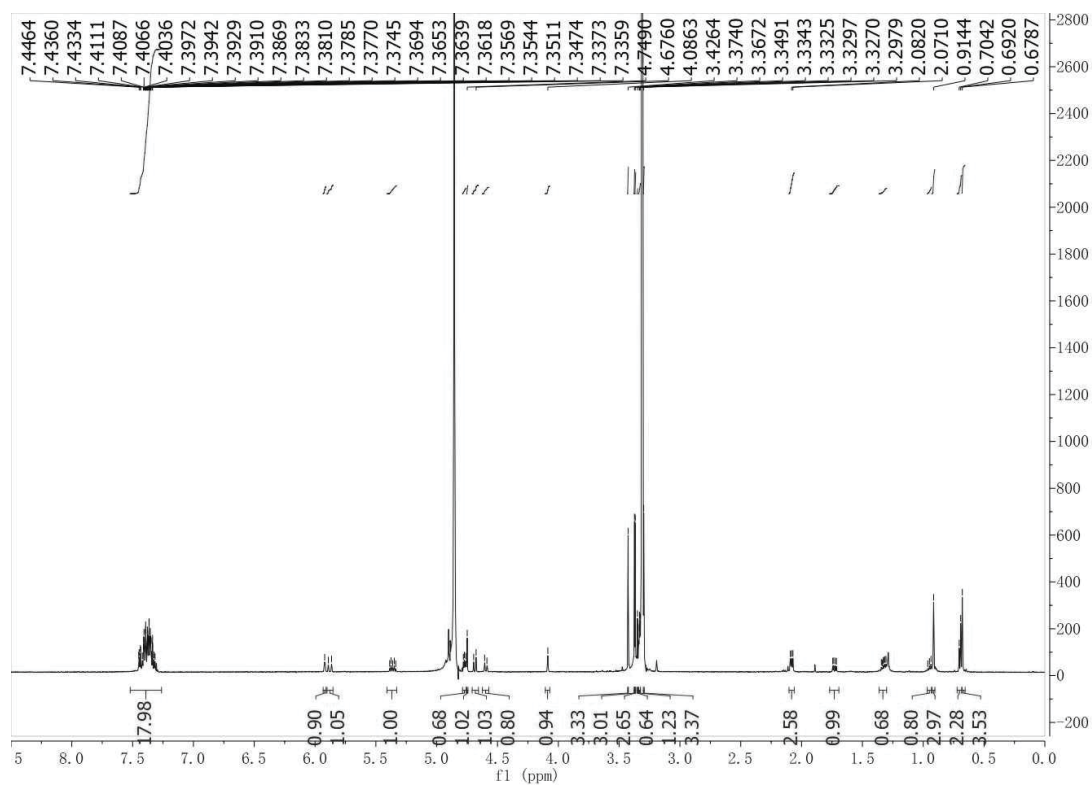


Figure S173. ¹H-NMR (600 MHz, CD₃OD) spectrum of **25a**.

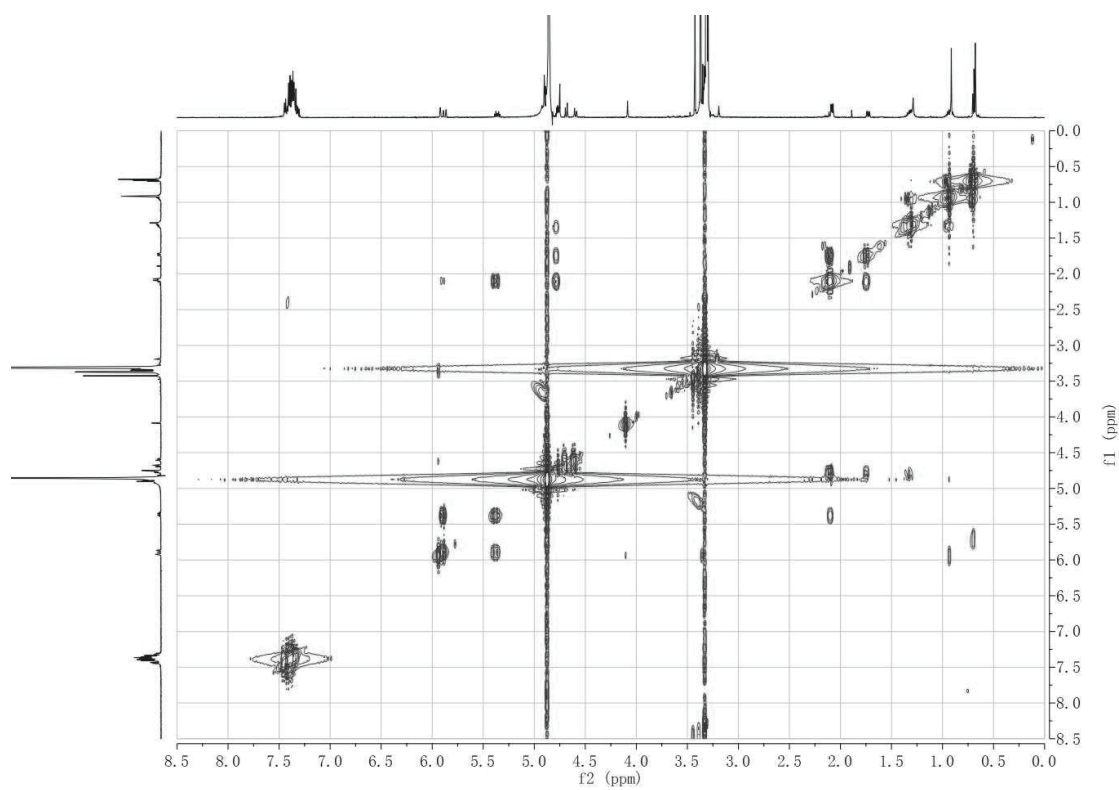


Figure S174. ¹H-¹H COSY (600 MHz, CD₃OD) spectrum of **25a**.

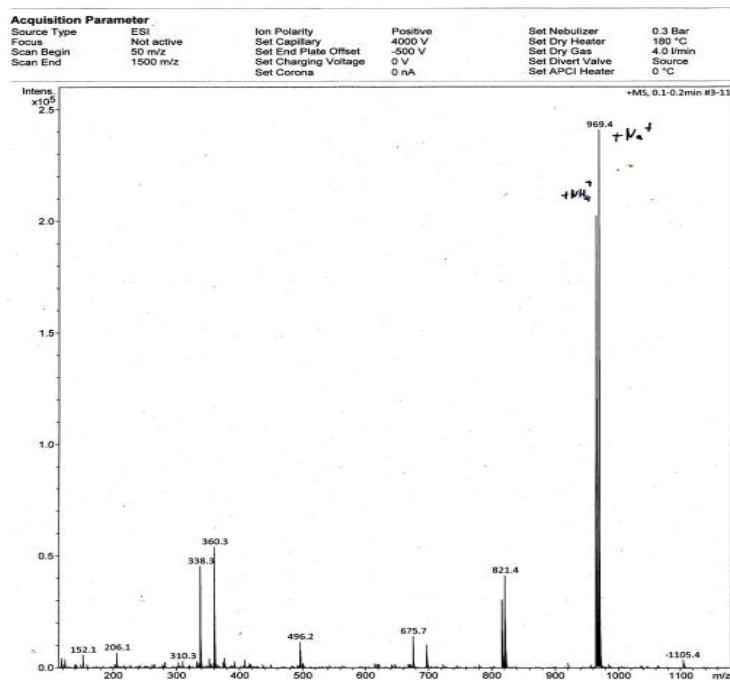


Figure S175. ESIMS of **25a**.

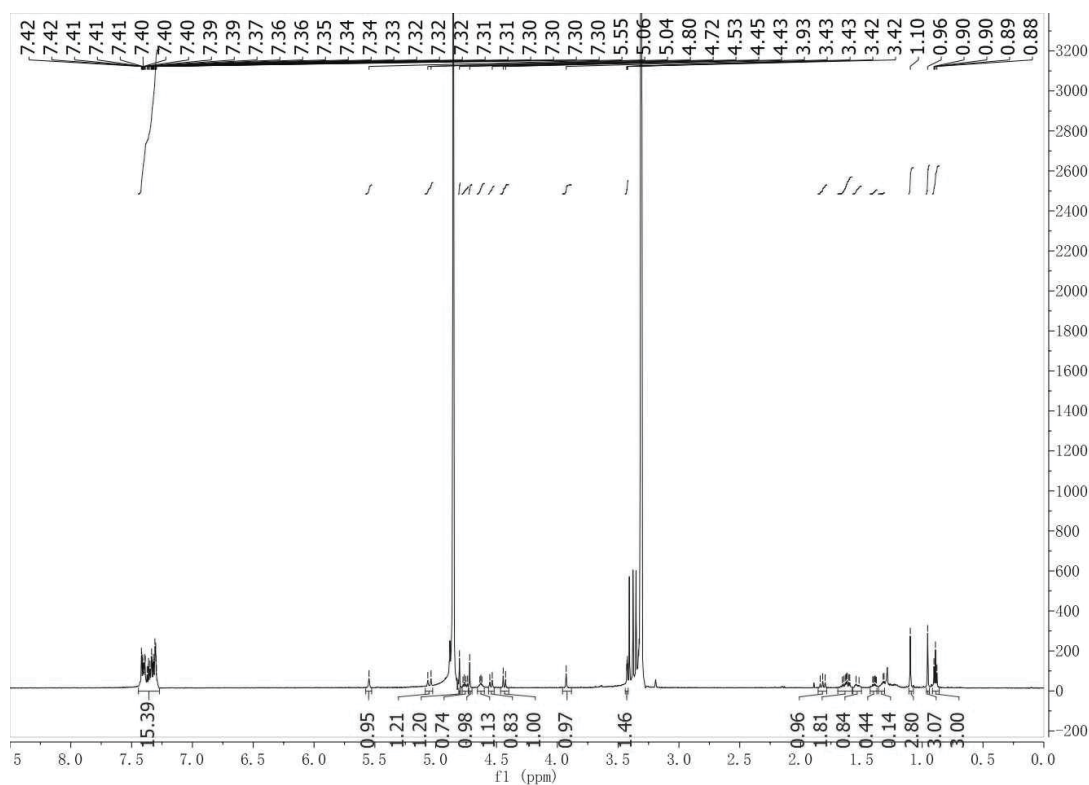


Figure S176. ^1H -NMR (600 MHz, CD_3OD) spectrum of **25b**.

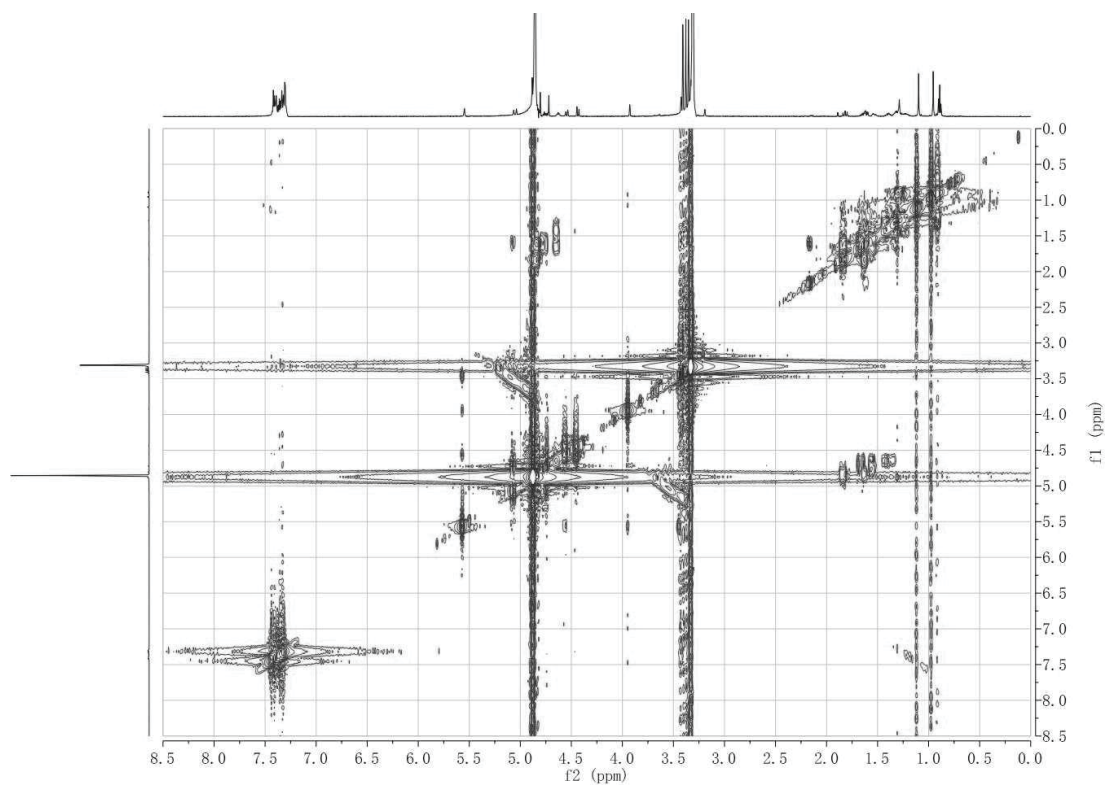


Figure S177. ^1H - ^1H COSY (600 MHz, CD_3OD) spectrum of 25b.

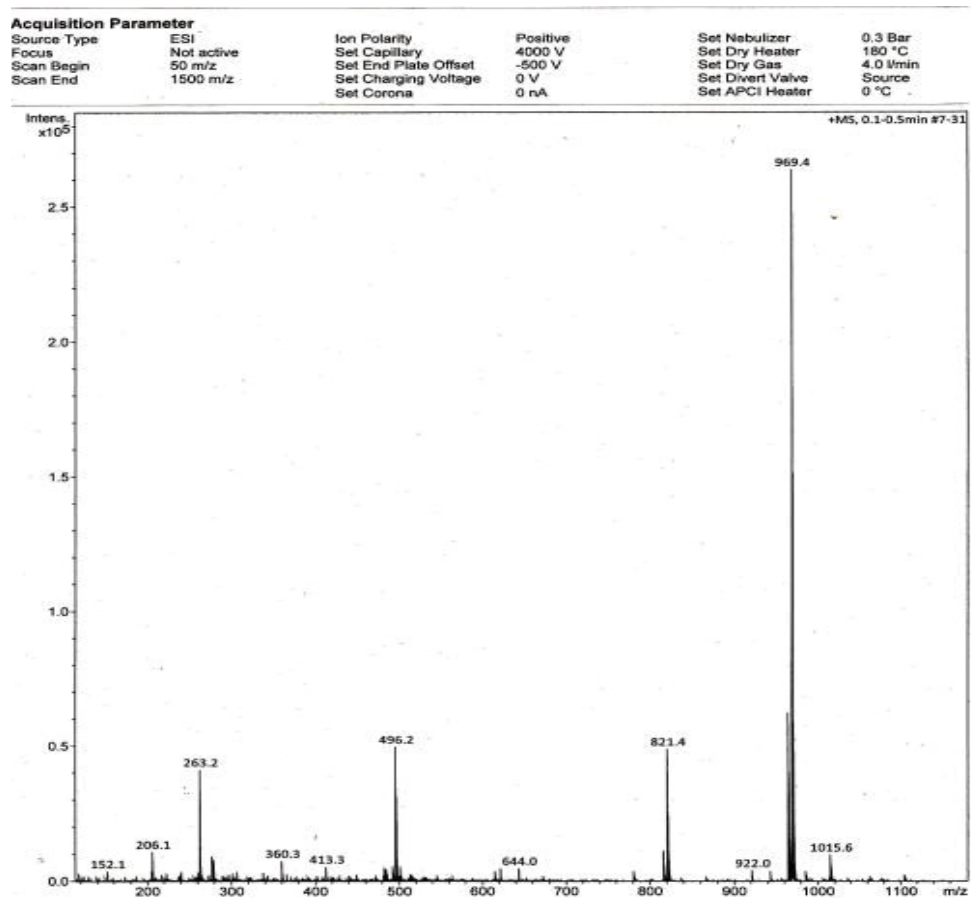


Figure S178. ESIMS of 25b.

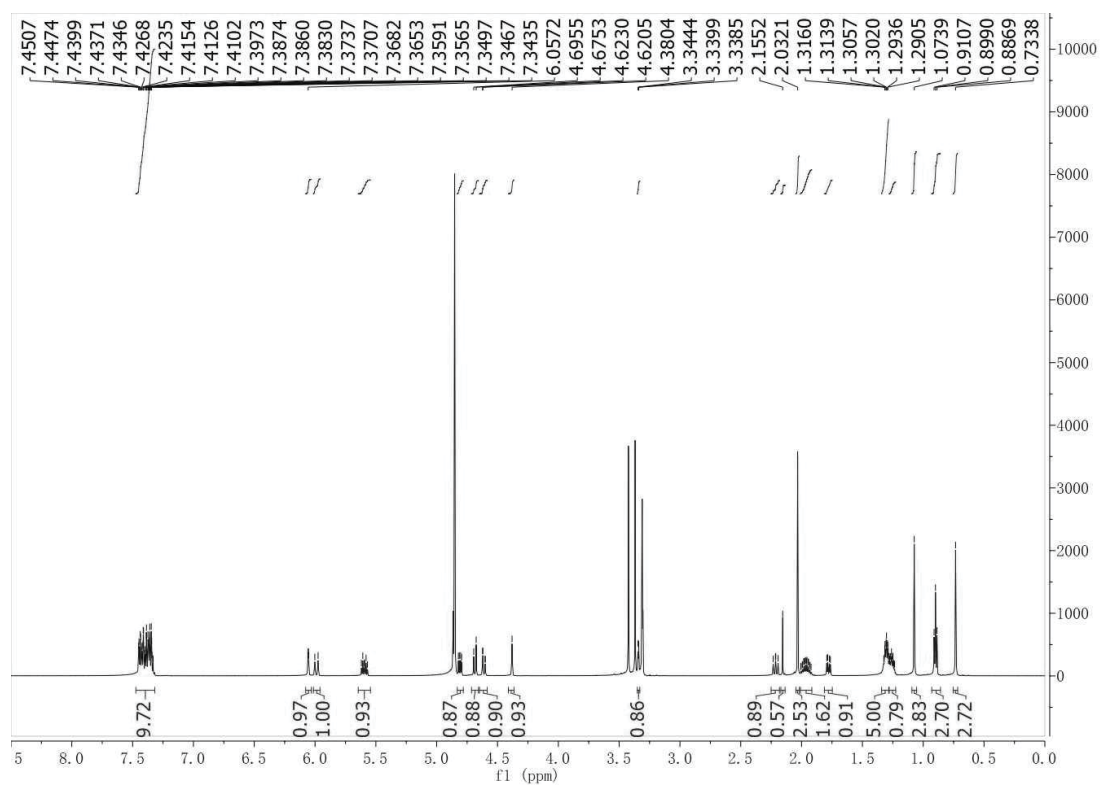


Figure S179. ^1H -NMR (600 MHz, CD_3OD) spectrum of **26a**.

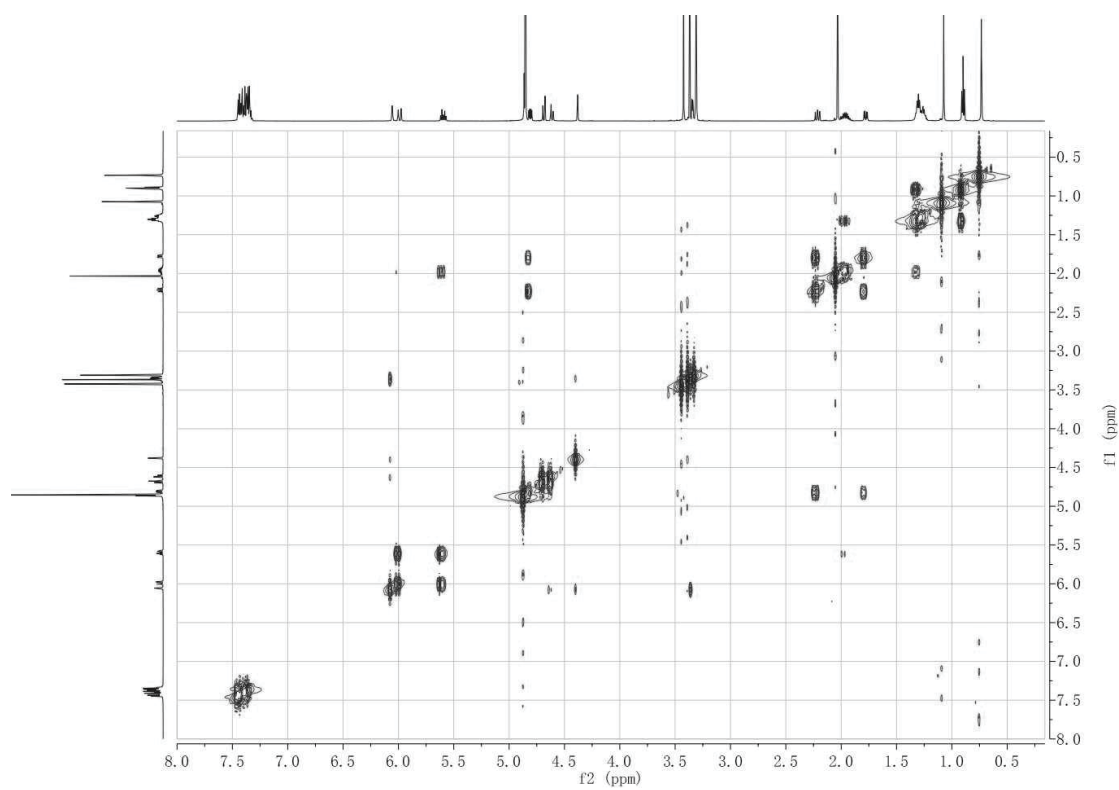


Figure S180. ^1H - ^1H COSY (600 MHz, CD_3OD) spectrum of **26a**.

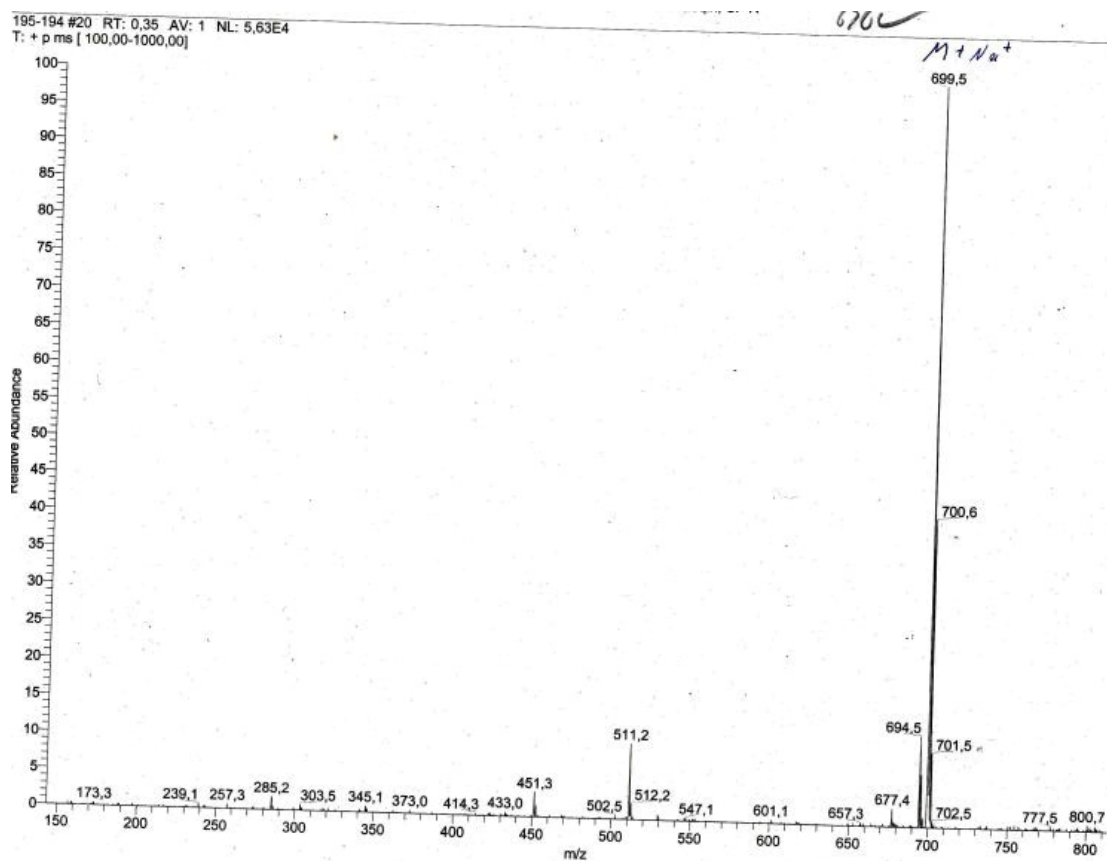
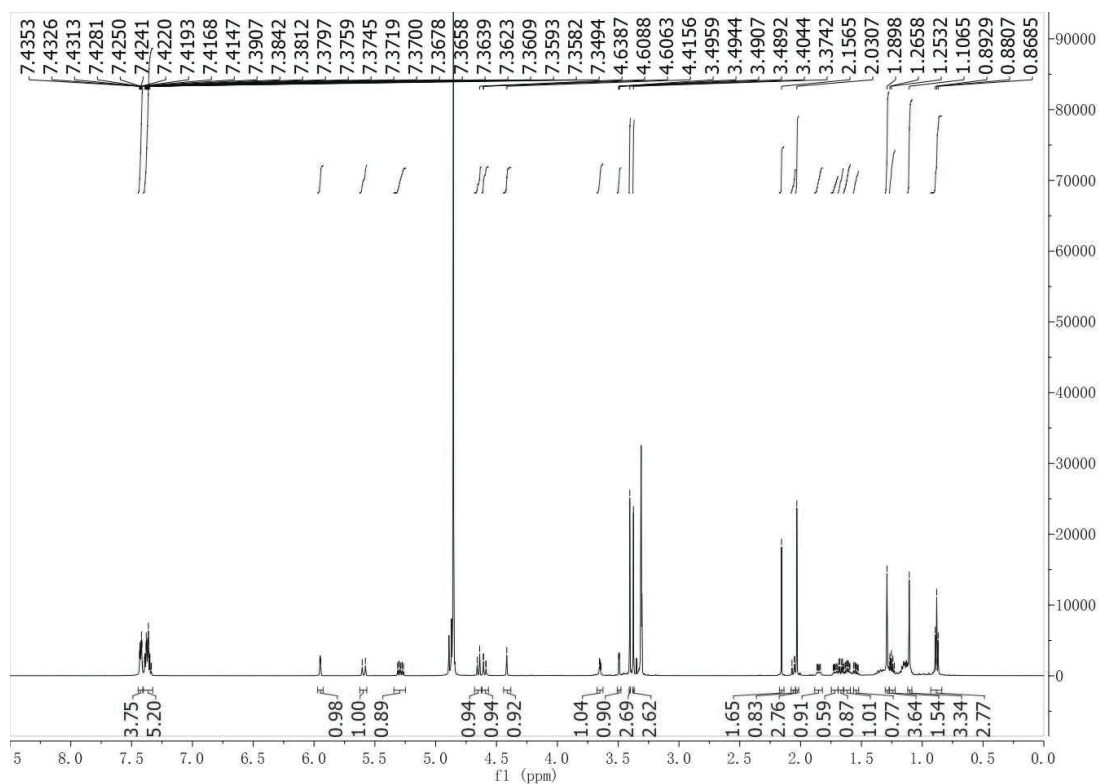


Figure S181. ESIMS of 26a.

Figure S182. ¹H-NMR (600 MHz, CD₃OD) spectrum of 26b.

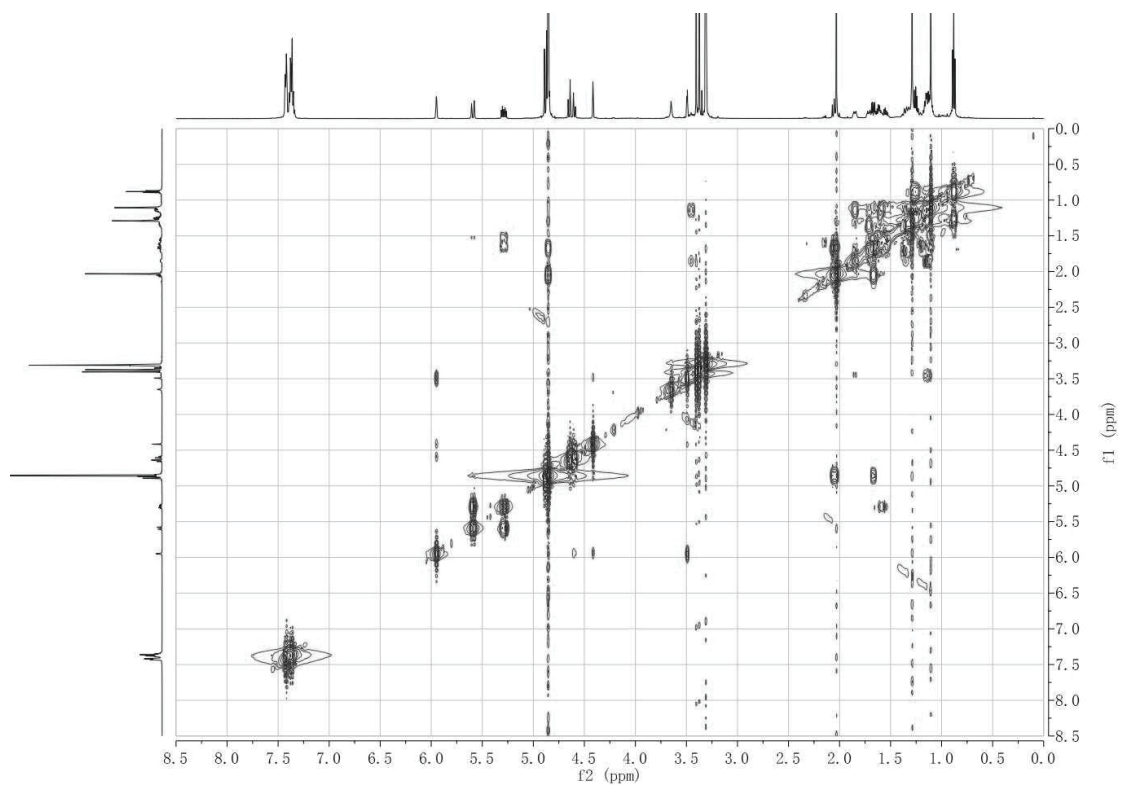


Figure S183. ^1H - ^1H COSY (600 MHz, CD_3OD) spectrum of **26b**.

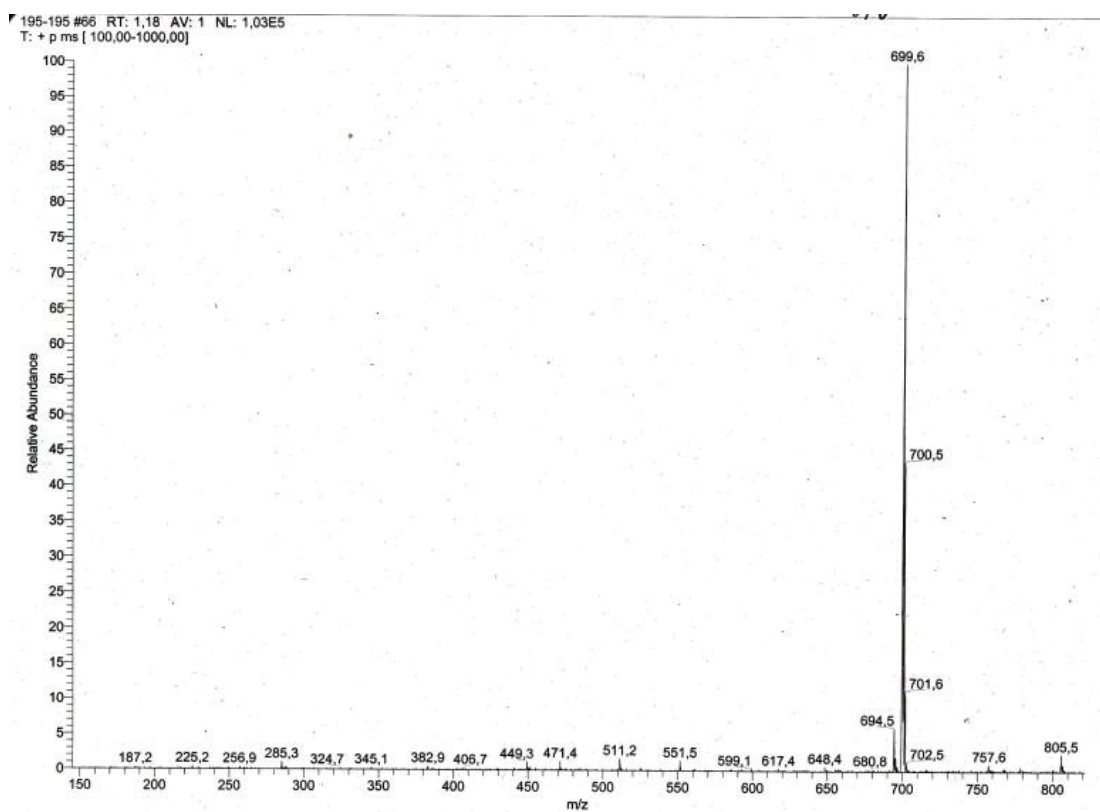


Figure S184. ESIMS of **26b**.

Table S1. SMILES table of compounds **1–26**.

No.	SMILES
1	<chem>CC(C)(O)[C@H](O1)C[C@]2([R1])[C@]1([H])CC(C/C=C(C)/C)=O=C[C@@H]2[R2]</chem>
2	<chem>CC(C)(O)[C@H](O1)C[C@]2([R1])[C@]1([H])CC(C/C=C(C)/C)=O=C[C@H]2[R2]</chem>
3	<chem>CC(C)(O)[C@H](O1)C[C@]23[C@]1([H])C/C([C@@H](O)[C@H]2O3)=C/C=C(CO)/C</chem>
4	<chem>CC(C)(O)[C@H](O1)C[C@]2(O)[C@]1([H])C=C(C#CC(C)=C)[C@@H](O)[C@H]2O</chem>
5	<chem>CC(C)(O)C(O1)C[C@]2(O)[C@]1([H])C=C(C#CC(C)=C)[C@@H](O)[C@H]2O</chem>
6	<chem>CC(C)(O)[C@H](O1)C[C@]2(O)[C@]1([H])CC([C@@H](O)[C@H]2O)=[C@]=CC(C)=C</chem>
7	<chem>CC(C)(O)[C@H](O1)C[C@]2(O)[C@]1([H])CC([C@@H](O)[C@H]2OC(C)=O)=[C@]=CC(C)=C</chem>
8	<chem>CC(C)(O)[C@H](O1)C[C@]2(O)[C@]1([H])CC(C([C@H](O)C(C)(C)O3)=O)=C3[C@@H]2O</chem>
9	<chem>CC(C)(O)[C@H](O1)C[C@]2(O)[C@]1([H])CC(C(C([H])C(C)(C)O3)=O)=C3[C@@H]2OC(C)=O</chem>
10	<chem>C=C(C)C#C[C@H]1C[C@@](OC(C)(C)[C@@H](O)C2)([H])[C@]2(O3)[C@H]3[C@@H]1O</chem>
11	<chem>CC(C)(O)[C@H](O1)C[C@]23[C@]1([H])CC([C@@H](O)[C@H]2O3)=[C@]=CC(C)=C</chem>
12	<chem>CC(C)(O)[C@H](O1)C[C@]2(O)[C@]1([H])CC([C@@H](O)[C@H]2Cl)=[C@]=CC(C)=C</chem>
13	<chem>CC(C)(O)[C@H](O1)C[C@]2(O)[C@]1([H])CC(C(C([H])C(C)(C)O3)=O)=C3[C@@H]2O</chem>
14	<chem>CC1(C)CC(C2=C(O1)C=C(C[C@H](C(C)(O)C)O3)C3=C2)=O</chem>
15	<chem>O[C@@H]1C/C=C/CCCC=C(CO)[C@@]2([H])OC(C)(C)[C@H](O)C[C@@]2(O)C1[H]</chem>
16	<chem>O[C@@H]1C/C=C/CCCC=C(CO)[C@@]2([H])OC(C)(C)[C@H](O)C[C@@]2(O)[C@H]1O</chem>
17	<chem>O[C@@H]1C/C=C/CCCC=C(CO)[C@@]2([H])OC(C)(C)[C@H](O)C[C@@]23[C@@H]1O3</chem>
18	<chem>O[C@@H]1C/C=C/CCC([H])[C@@H](O)C=C(CO)[C@@]2([H])OC(C)(C)[C@H](O)C[C@@]23[C@@H]1O3</chem>
19	<chem>O[C@@H]1C/C=C/C[C@H](O)CCC=C(CO)[C@@]2([H])OC(C)(C)[C@H](O)C[C@@]23[C@@H]1O3</chem>
20	<chem>O[C@@H]1C/C=C/[C@@H](O)CCCC=C(CO)[C@@]2([H])OC(C)(C)[C@H](O)C[C@@]23[C@@H]1O3</chem> or <chem>O[C@@H]1C/C=C/[C@H](O)CCCC=C(CO)[C@@]2([H])OC(C)(C)[C@H](O)C[C@@]23[C@@H]1O3</chem>
21	<chem>O[C@@H]1C/C=C/[C@@H](O)CCCC=C(CO)[C@@]2([H])OC(C)(C)[C@H](O)C[C@@]23[C@@H]1O3</chem> or <chem>O[C@@H]1C/C=C/[C@H](O)CCCC=C(CO)[C@@]2([H])OC(C)(C)[C@H](O)C[C@@]23[C@@H]1O3</chem>
22	<chem>CCCCC/C=C/C1=C(CO)[C@@]2([H])OC(C)(C)[C@H](O)C[C@@]23[C@H](O3)[C@]1([H])OC(C)=O</chem>
23	<chem>CCCCC/C=C/C1=C(CO)[C@@]2([H])OC(C)(C)[C@H](O)C[C@@]23[C@H](O3)C1=O</chem>
24	<chem>O[C@@H]1C/C=C/CCC(O)C([H])C=C(CO)[C@@]2([H])OC(C)(C)[C@H](O)C[C@@]23[C@@H]1O3</chem>
25	<chem>O[C@@H]1C/C=C/C[C@H](O)CCC=C(CO)[C@@]2([H])OC(C)(C)[C@H](O)C[C@@]23[C@@H]1O3</chem>
26	<chem>O[C@@H]1C/C=C/CCCC=C(COC(C)=O)[C@@]2([H])OC(C)(C)[C@H](O)C[C@@]23[C@@H]1O3</chem>

Table S2. Results of cytotoxicity and antibacterial activity assay of compounds **1–26**.

No.	Antibacterial activity (MIC, μ M)					Cell growth (%) at 10 μ g/mL	Cytotoxicity (IC ₅₀ , μ M)
	<i>A. baumannii</i> (BAA1605)	<i>A. baumannii</i> (BAA1605) + colistin (0.1 μ M)	<i>P. aeruginosa</i> (27853)	<i>S. aureus</i> (29213)	<i>M. tuberculosis</i> (H37Rv)	Mouse lymphoma cell line L5178Y	
1	>100	>100	>100	>100	>100	58.5	>20
2	>100	>100	>100	>100	>100	65.4	>20
3	>100	>100	>100	>100	>100	64.8	>20
4	>100	>100	>100	>100	>100	77.4	>20
5	>100	>100	>100	>100	>100	64.3	>20
6	>100	>100	>100	>100	>100	68.3	>20
7	>100	>100	>100	>100	>100	67.1	>20
8	>100	>100	>100	>100	>100	77.8	>20
9	>100	>100	>100	>100	>100	53.0	>20
10	>100	>100	>100	>100	>100	56.1	>20
11	>100	>100	>100	>100	>100	76.5	>20
12	>100	>100	>100	>100	>100	66.7	>20
13	>100	>100	>100	>100	>100	77.5	>20
14	>100	>100	>100	>100	>100	67.2	>20
15	>100	>100	>100	>100	>100	54.4	>20
16	>100	>100	>100	>100	>100	53.2	>20
17	>100	>100	>100	>100	>100	70.5	>20
18	>100	>100	>100	>100	>100	64.8	>20
19	>100	>100	>100	>100	>100	78.1	>20
20	>100	>100	>100	>100	>100	70.1	>20
21	>100	>100	>100	>100	>100	63.6	>20
22	>100	50	>100	>100	>100	44.2	>20
23	>100	100	>100	>100	>100	1.90	3.0
24	>100	>100	>100	>100	>100	80.0	>20
25	>100	>100	>100	>100	>100	77.4	>20
26	>100	>100	>100	>100	>100	65.7	>20

4 Publication 3

Induction of ambuic acid derivatives by the endophytic fungus *Pestalotiopsis lespedezae* through an OSMAC approach

Xiaoqin Yu, Ying Gao, Marian Frank, Attila Mándi, Tibor Kurtán, Werner E. G. Müller, Rainer Kalscheuer, Zhiyong Guo, Kun Zou, Zhen Liu, Peter Proksch

Submitted to “*Tetrahedron*”

Research contribution: the first author contributed 60% to this publication. The first author's work involved all laboratory work including the OSMAC experiments, isolation, structure elucidation, and manuscript preparation for all compounds.

Induction of ambuic acid derivatives by the endophytic fungus *pestalotiopsis lespedezae* through an OSMAC approach

Xiaoqin Yu,^{a,b} Ying Gao,^a Marian Frank,^a Attila Mándi,^c Tibor Kurtán,^c Werner E. G. Müller,^d Rainer Kalscheuer,^a Zhiyong Guo,^b Kun Zou,^b Zhen Liu,^{a,*} Peter Proksch,^{a,b,*}

^aInstitute of Pharmaceutical Biology and Biotechnology, Heinrich-Heine-University Duesseldorf, 40225 Duesseldorf, Germany. Correspondence: zhenfeizi0@sina.com (Z.L.), proksch@uni-duesseldorf.de (P.P.)

^bHubei Key Laboratory of Natural Products Research and Development, College of Biological and Pharmaceutical Sciences, China Three Gorges University, Yichang 443002, People's Republic of China

^cDepartment of Organic Chemistry, University of Debrecen, P.O.B. 400, 4002 Debrecen, Hungary

^dInstitute for Physiological Chemistry, University Medical Center of the Johannes Gutenberg University Mainz Duesbergweg 6, 55128 Mainz, Germany

[†]Electronic supplementary information (ESI) available: MS, 1D and 2D NMR spectra of compounds **1–10**.

ABSTRACT:

Ten new ambuic acid derivatives, pestallic acids **H–Q** (**1–10**) including one new iodinated natural product (**10**) along with two known compounds (**11** and **12**) were obtained through fermentation of the endophytic fungus *Pestalotiopsis lespedezae* on solid rice medium with 3.5% NaI. Compounds **1–10** were undetectable in cultures of the fungus grown on solid rice medium lacking NaI or in those where NaI had been replaced by NaCl or NaBr. The structures of the new metabolites were established on basis of 1D/2D NMR and HRESIMS data. Their absolute configurations were determined by Mosher's method and TDDFT-ECD calculations. The compounds failed to show antibacterial activity against *S. aureus* (ATCC29213), drug-resistant *Acinetobacter baumannii* (BAA1605) or *Mycobacterium*

tuberculosis, as well as cytotoxicity against the mouse lymphoma cell line L5178Y.

Keywords: endophytic fungus, *Pestalotiopsis lespedezae*, pestallic acids, iodinated natural product, TDDFT-ECD.

INTRODUCTION

Fungal metabolites play an important role in drug development.^{1,2} Lovastatin, famous as an inhibitor of 3-hydroxy-3-methylglutaryl-coenzyme A (HMG-CoA) reductase produced by *Aspergillus terreus* was the lead compound for a series of statins which are mainly used for the treatment of dyslipidemia and the prevention of cardiovascular disease.³ Multiple generations of cephalosporins, which are analogues of the fungal antibiotic agent cephalosporin produced by *Cephalosporium acremonium*, have been introduced to the clinics as powerful antibiotics.⁴ Fingolimod, the most recent drug of fungal origin was modelled after the natural product myriocin isolated from various fungi such as *Myricelia sterilia* and is used for the treatment of multiple sclerosis.^{5,6}

The potential of bioactive fungal secondary metabolites has generated considerable interest for bioprospecting. The increasing rate of re-isolation of known compounds, however, is a bottleneck for drug discovery. The latter is partly due to the fact that many secondary metabolite gene clusters are silent under standard laboratory culture conditions thereby seriously limiting the chemical diversity of compounds. This has forced researchers to turn their attention to unlock the trove of metabolic treasures. Several strategies, such as co-cultivation of different microbes, epigenetic modification or the OSMAC (One Strain Many Compounds) approach can be applied to expand the metabolic diversity of fungi.⁷ The OSMAC approach is a powerful method which relies on modification of cultivation parameters such as temperature, media composition, shape of culturing flask or aeration.^{8,9} For instance, a new amidepsine derivative 5-*epi*-pestafolide A was obtained from the endophytic fungus *Trichocladium* sp. when grown on rice medium while new sesquiterpene and bismacrolactone derivatives were isolated following fermentation of the fungus on peas.¹⁰ Adding a mixture of salts (MgSO₄, NaNO₃ and NaCl) to solid Czapek's medium induced the endophytic fungus *Bulgaria inquinans* to accumulate a new butyrolactone derivative, two unusual 1,3-oxazine containing

natural products as well as five new α -pyrones.¹¹ Interestingly, several bioactive brominated or chlorinated natural products were reported as fungal metabolites following cultivation of fungi in media containing halogen salts. For example, new cytotoxic brominated tyrosine-derived alkaloids were isolated from the fungus *Gymnascella dankaliensis* when cultivated on solid rice medium following addition of NaBr.¹² When the same fungus was cultured on rice medium spiked with 3.5% NaCl the chlorinated metabolites gymnastatin A and gymnastatin B were obtained.¹³

These successful examples inspired our current study on expanding the chemical diversity of the endophytic fungus *Pestalotiopsis lespedezae* isolated from roots of the plant *Youngia japonica* (Asteraceae) from China by adding halogen salts such as NaCl, NaBr and NaI to solid rice media. Addition of NaI yielded ten new ambuic acid derivatives pestallic acids H–Q (**1**–**10**), including one iodinated new natural product (**10**) (Fig. 1). Iodinated natural products are extremely rare, the few examples reported so far include iodinated meroditerpenes and polyhalogenated indoles from the red algae *Callophycus* sp. and *Rhodophyllis membranacea*, respectively.^{14,15} When *P. lespedezae* was grown on solid rice medium lacking NaI, two known compounds including ambuic acid (**11**) and its derivative **12** were as major metabolites thus highlighting the power of this OSMAC approach.^{16,17} No significant difference, however, was observed in the chromatographic profiles following the addition of NaCl to solid rice medium when compared to chromatograms of the fungus grown on rice medium without salts.

Here we report the isolation and structure elucidation of the new natural products obtained as well as results following screening of the compounds for antibiotic activity and cytotoxicity. A plausible biosynthetic pathway of ambuic acid (**11**) and its derivatives (**1**–**10** and **12**) is also suggested.

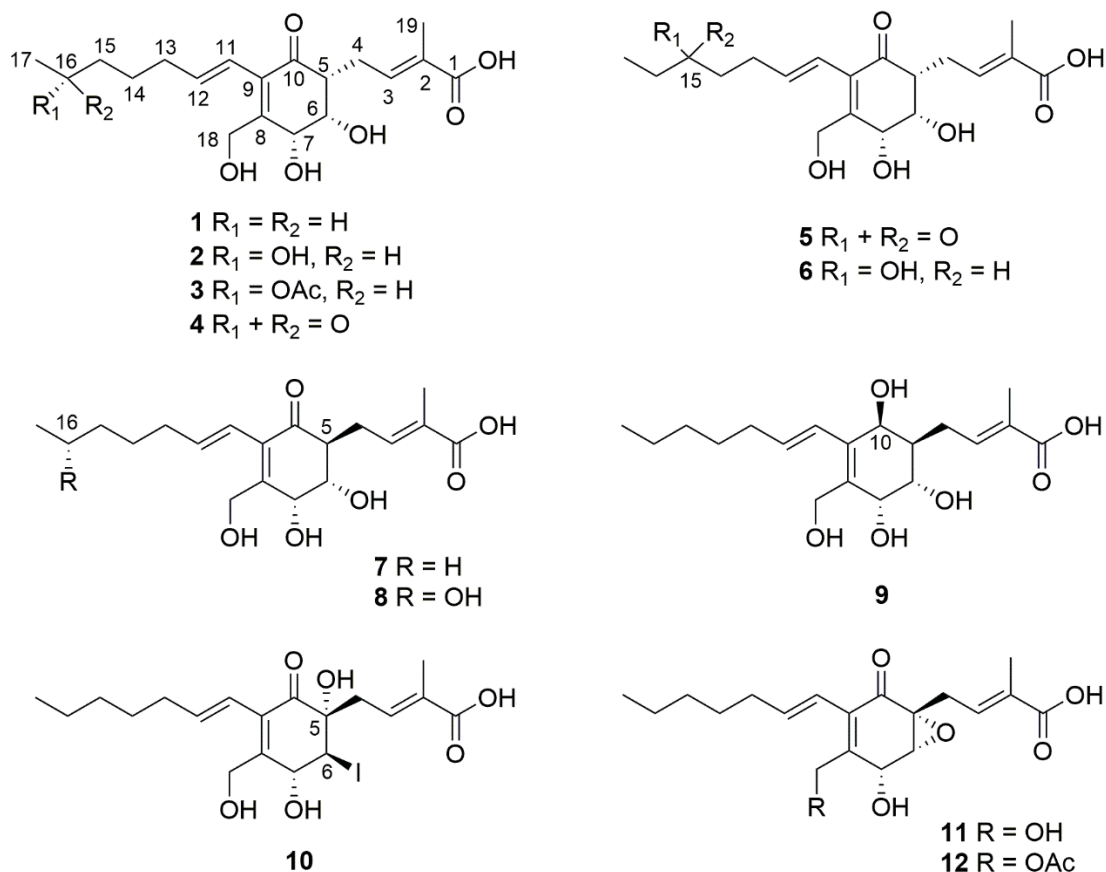


Figure. 1 Structures of compounds **1**–**12** from *P. lespedezae*.

RESULTS AND DISCUSSION

The molecular formula of pestallic acid H (**1**) was determined as $C_{19}H_{28}O_6$ by HRESIMS, with six degrees of unsaturation, thus differing from the co-isolated known ambuic acid (**11**) by two additional mass units. The ^{13}C NMR data (Table 1) for **1** revealed the presence of two carbonyl carbons at δ_C 200.3 (C-10) and 171.8 (C-1), and six olefinic carbons at δ_C 152.5 (C-8), 141.4 (C-3), 139.9 (C-12), 135.3 (C-9), 130.8 (C-2), and 123.1 (C-11), accounting for five degrees of unsaturation. Thus, **1** was suggested to be monocyclic. Further analysis of the 1D and 2D NMR spectroscopic data (Fig. 2) confirmed **1** to be similar to the co-isolated known compound ambuic acid (**11**), which was first obtained from the endophytic fungi *Pestalotiopsis* spp. and *Monochaetia* sp.¹⁷ The major difference between **1** and **11** resided in the substitution of the six-membered ring. Whereas ambuic acid (**11**) exhibited an epoxy substituent at C-5/C-6 with an oxygenated carbon signal at δ_C 61.3 (C-5) and signals for H-6 and C-6 at δ_H 3.74 and δ_C 61.0, **1** featured signals for H-5 and C-5 at δ_H 2.67 and δ_C 52.4 and for H-6 and C-6 at δ_H

4.17 and δ_C 73.5, respectively, as revealed by the HSQC spectrum of **1**. The absence of the epoxy substituent at C-5/C-6 of ambuic acid (**11**) in **1** was further supported by COSY relationships between H_{ab} -4/H-5/H-6/H-7. Therefore, the planar structure of **1** was determined as shown. The relative configuration of **1** was determined by analysis of the coupling constants and NOE data. The olefinic double bond at C-11/C-12 was suggested to be *E*-configured as indicated by the large coupling constant of 15.9 Hz. The double bond at C-2/C-3 was likewise *E*-configured as shown by the NOE correlation between H_b -4 (δ_H 2.46) and Me-19 (δ_H 1.87). The small coupling constant of $^2J_{H-5,H-6}$ (2.0 Hz) and $^2J_{H-6,H-7}$ (3.3 Hz) aided by the ROESY correlations between H-5/H-6, H-6/H-7, H-7/H-5 indicated that those protons were on the same side of the cyclohexene ring.

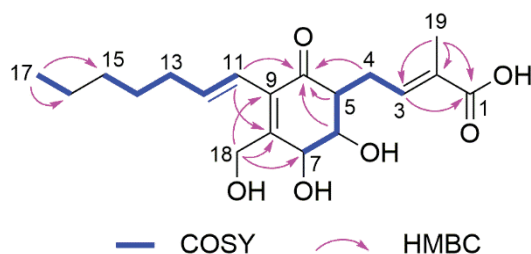


Figure. 2 Key COSY and HMBC correlations for **1**.

To elucidate the absolute configuration of **1**, the solution TDDFT-ECD method was applied on the arbitrarily chosen (*5R,6S,7R*) epimer.^{18,19} The truncated model compound **1a** (Fig. 3), in which the C-9 hept-1-en-1-yl side-chain was replaced by a prop-1-en-1-yl one, was used for the calculation to decrease the number of computed conformers.^{20,21} The initial Merck Molecular Force Field (MMFF) conformational search of (*5R,6S,7R*)-**1a** resulted in 205 conformers in a 21 kJ/mol energy window. ω B97X/TZVP²² PCM/MeOH re-optimization of these structures yielded 24 low-energy conformers above 1% Boltzmann-distribution. ECD calculations performed at various levels gave acceptable overall agreement with the experimental spectrum of **1** (Fig. 4). A positive Cotton effect (CE) below 300 nm appears in the Boltzmann-weighted ECD spectrum,²³ which was missing from the experimental ECD curve. A different Boltzmann distribution of the conformers would have produced a much better agreement, since some minor conformers (around 1% population) reproduced this part of the spectrum better,²⁴ but due to their low populations, they have negligible contribution and the

truncation may have adversely affected the computed conformational ensemble.²⁵ All low-energy conformers over 1% Boltzmann population had the same *P* helicity in the cyclohexenone ring and differed only in the orientation of the C-5 side chain and the OH groups (Fig. 5). Regarding the orientation of the truncated C-9 side-chain, only the 24th conformer had different arrangement. Consequently, conformers A-W had similar spectra and rather different from those of conformer X and many other minor conformers with lower population than 1%. We checked whether we can produce a better agreement by increasing the underestimated populations of the minor conformers. Thus, we re-clustered the 205 DFT-optimized conformers considering only the cyclohexenone ring, the connecting first atoms and the truncated C-9 side-chain and neglecting the orientation of the oxygens and the C-5 side-chain, since their different orientations did not change the computed ECD transitions. Six groups of conformers were identified and ECDs were computed for the lowest-energy conformers of each group and the results were weighted by the new Boltzmann populations of the six conformers. This approach increased the population of the X-type conformer from 1.0% to 9.3% with 79.6% population of the A-type conformers. However, even this change could not significantly improve the overall agreement and it gave a similar result to the conventional approach. We suppose that a better reproduction of the disputed region below 300 nm may be achieved if conformers A and X have comparable populations with higher percentage for conformer A. The acceptable overall agreement and the good reproduction of the high-energy CEs and the transitions above 300 nm allowed elucidation of the absolute configuration as (5*R*,6*S*,7*R*).

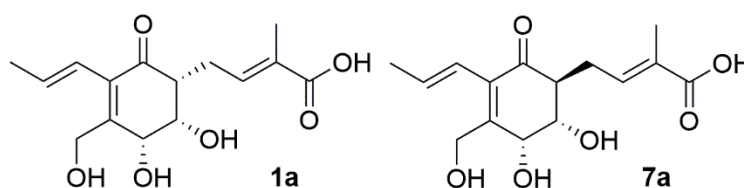


Figure. 3 Structures of the truncated model compounds of **1** (**1a**) and **7** (**7a**) applied for the TDDFT-ECD calculations.

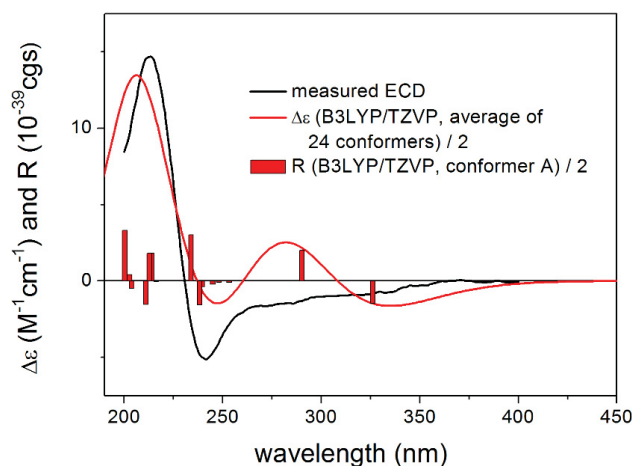


Figure. 4 Experimental ECD spectrum of **1** in MeOH compared with the Boltzmann-weighted B3LYP/TZVP PCM/MeOH ECD spectrum of (5*R*,6*S*,7*R*)-**1a**. Level of optimization: ω B97X/TZVP PCM/MeOH. Bars represent the rotatory strength values of the lowest-energy conformer.

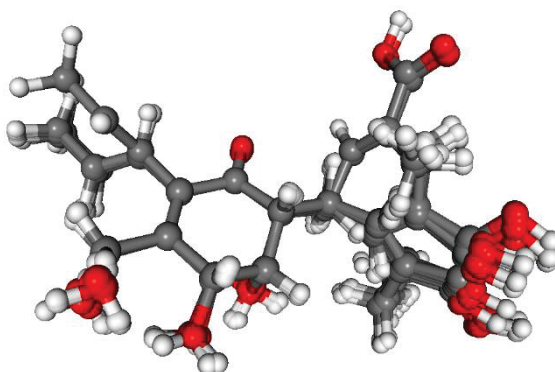


Figure. 5 Overlapped geometries of the 24 low-energy ω B97X/TZVP PCM/MeOH conformers of (5*R*,6*S*,7*R*)-**1a**.

The molecular formula of **2** was established as $C_{19}H_{28}O_7$ by HRESIMS, containing an additional oxygen atom when compared to **1**. The 1H and ^{13}C NMR data (Table 1) were similar to those of **1** except for signals in the long alkyl side chain. An extra oxygenated methine at δ_C 68.4 and δ_H 3.74 (CH-16) and a doublet peak at δ_H 1.16 (Me-17) for the terminal methyl group indicated C-16 to carry a hydroxy substituent when compared to **1**, which was further supported by COSY correlations of Me-17/H-16/H₂-15 and the HMBC correlations from Me-17 to C-16 and C-15. The remaining structure of **2** including relative configuration in the cyclohexene ring was identical to that of **1** as shown (Fig. 1). A sample of **2** was submitted for methylation giving

the derivative **2a**. Modified Mosher's method was applied for the determination of the absolute configuration at C-16 of **2a**. Due to the interference of multiple Mosher esters, only the key values of $\Delta\delta^{SR}$ for the MTPA esters are displayed. Based on the summarized data (Fig. 6), the absolute configuration of C-16 was suggested to be (*R*).

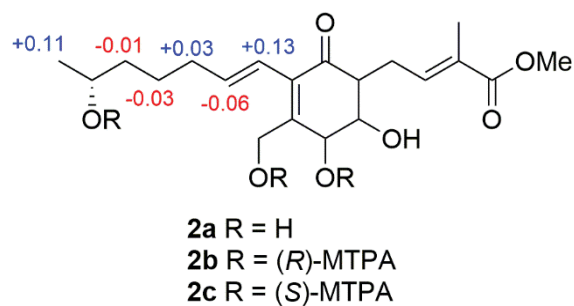


Figure. 6 Key values of $\Delta\delta^{SR}$ (in ppm) for the MTPA esters of **2a**.

Table 1 NMR data for compounds **1–3** in CD₃OD.

NO.	1^a		2^b		3^a	
	δ_{C} , type	δ_{H} (J in Hz)	δ_{C} , type	δ_{H} (J in Hz)	δ_{C} , type ^c	δ_{H} (J in Hz)
1	171.8, C		171.9, C		172.2, C	
2	130.8, C		131.0, C		131.1, C	
3	141.4, CH	6.83, t (7.5)	141.2, CH	6.80, t (7.6)	140.9, CH	6.78, t (7.5)
4	26.3, CH ₂	2.79, ddd (15.2, 7.5, 5.1) 2.46, ddd (15.2, 8.7, 7.5)	26.3, CH ₂	2.78, ddd (15.3, 7.6, 5.1) 2.45, ddd (15.3, 8.6, 7.6)	26.6, CH ₂	2.78, ddd (15.1, 7.5, 5.0) 2.45, ddd (15.1, 8.5, 7.5)
5	52.4, CH	2.67, ddd (8.7, 5.1, 2.0)	52.5, CH	2.67, ddd (8.6, 5.1, 2.1)	52.9, CH	2.66, ddd (8.5, 5.0, 2.0)
6	73.5, CH	4.17, dd (3.3, 2.0)	73.5, CH	4.17, dd (3.4, 2.1)	73.9, CH	4.17, dd (3.2, 2.0)
7	71.4, CH	4.70, d (3.3)	71.5, CH	4.70, d (3.4)	71.8, CH	4.70, d (3.2)
8	152.5, C		152.4, C		152.4, C	
9	135.3, C		135.3, C		135.1, C	
10	200.3, C		200.2, C		200.0, C	
11	123.1, CH	6.05, d (15.9)	123.3, CH	6.07, d (16.0)	124.0, CH	6.07, d (15.8)
12	139.9, CH	5.87, dt (15.9, 6.9)	139.6, CH	5.89, dt (16.0, 6.9)	139.6, CH	5.87, dt (15.8, 7.0)
13	34.5, CH ₂	2.17, m	34.5, CH ₂	2.19, m	34.6, CH ₂	2.19, m
14	30.0, CH ₂	1.46, m	26.4, CH ₂	1.56, m; 1.48, m	26.4, CH ₂	1.48, m
15	32.5, CH ₂	1.34, m	39.6, CH ₂	1.46, m	36.7, CH ₂	1.62, m; 1.57, m
16	23.6, CH ₂	1.35, m	68.4, CH	3.74, m	72.6, CH ₂	4.90, m
17	14.4, CH ₃	0.92, t (7.0)	23.5, CH ₃	1.16, d (6.2)	20.5, CH ₃	1.21, d (6.2)
18	60.8, CH ₂	4.53, d (12.5); 4.49, d (12.5)	60.9, CH ₂	4.53, d (12.5); 4.49, d (12.5)	61.2, CH ₂	4.52, d (12.5); 4.49, d (12.5)
19	12.7, CH ₃	1.87, s	12.7, CH ₃	1.87, s	13.2, CH ₃	1.87, s
16-OAc					21.6, CH ₃	2.01, s
					172.4, C	

^a recorded at 600 MHz (¹H) and 150 MHz (¹³C); ^b recorded at 300 MHz (¹H) and 75 MHz (¹³C); ^c Data were extracted from HSQC and HMBC.

The HRESIMS of pestallic acid J (**3**) indicated a molecular formula of $C_{21}H_{31}O_8$, thus differing from **2** by 42 additional mass units. This difference of molecular weight was accounted for by an acetyl group, which was evident from the presence of an additional carbonyl carbon at δ_C 172.4 and an additional methyl group at δ_C 21.6 and δ_H 2.01 in the NMR spectra of **3** (Table 1). The attachment of the acetyl group at C-16 was confirmed by the HMBC correlations from the methyl group (δ_H 2.01) and deshielded H-16 (δ_H 4.90) to the carbonyl carbon (δ_C 172.4). The remaining structure of **3** was identical to that of **2**.

Pestallic acid K (**4**) had the molecular formula $C_{19}H_{26}O_7$ as established by HRESIMS. Its 1H and ^{13}C NMR data (Table 2) revealed a close structural similarity to **2** except for the replacement of the oxygenated methine at C-16 (δ_H 3.74 and δ_C 68.4) of **2** by a carbonyl group (δ_C 211.9) in **4**. This was supported by the HMBC correlations from Me-17 (δ_H 2.14), H₂-15 (δ_H 2.54) and H₂-14 (δ_H 1.70) to C-16 (δ_C 211.9). Thus, the structure of **4** was elucidated as shown.

The HRESIMS of **5** indicated the same molecular formula $C_{19}H_{26}O_7$ as that of **4**. Comparison of the NMR data of **5** and **4** (Table 2) indicated that both compounds differ in the position of the carbonyl function in the alkyl side chain. In compound **5** the carbonyl group resided at C-15 instead of C-16 as in **4** based on the COSY correlations between Me-17 (δ_H 1.02) and H₂-16 (δ_H 2.50), together with the HMBC correlations from Me-17, H₂-16, H₂-14 (δ_H 2.61) and H₂-13 (δ_H 2.41) to C-15 (δ_C 212.5).

Pestallic acid M (**6**) gave the molecular formula $C_{19}H_{28}O_7$ as determined by HRESIMS, indicating the loss of one degree of unsaturation compared to **5**. The NMR data of **6** (Table 2) displayed signals for an oxygenated methine at δ_H 3.49 and δ_C 72.9 (CH-15) that were absent in **5**. The above data indicated reduction of a carbonyl group of **5** and presence of an additional hydroxy substituent in **6**. The COSY correlations of Me-17/H_{ab}-16/H-15/H_{ab}-14 revealed the presence of the extra hydroxy group of **6** at C-15. Detailed analysis of the 2D NMR spectra of **6** revealed that the remaining substructure and the relative configuration in the cyclohexene ring of **6** were identical to those of **5**. However, the absolute configuration at C-15 of **6** remained undetermined due to the low amount of isolated compound.

Table 2 NMR data for compounds **4–6** in CD₃OD.

NO.	4^a		5^a		6^a	
	δ_{C} , type	δ_{H} (J in Hz)	δ_{C} , type ^b	δ_{H} (J in Hz)	δ_{C} , type ^b	δ_{H} (J in Hz)
1	171.5, C		172.7, C		172.5, C	
2	130.7, C		132.0, C		131.8, C	
3	141.4, CH	6.82, t (7.6)	139.9, CH	6.73, t (7.3)	139.7, CH	6.75, t (7.4)
4	26.3, CH ₂	2.79, ddd (15.2, 7.6, 5.2) 2.46, ddd (15.2, 8.6, 7.6)	26.2, CH ₂	2.77, ddd (15.2, 7.3, 5.2) 2.44, ddd (15.2, 8.9, 7.3)	25.9, CH ₂	2.77, ddd (15.1, 7.4, 5.0) 2.44, ddd (15.1, 8.7, 7.4)
5	52.5, CH	2.68, ddd (8.6, 5.2, 2.2)	52.6, CH	2.65, ddd (8.9, 5.2, 2.1)	52.2, CH	2.66, ddd (8.7, 5.0, 2.2)
6	73.5, CH	4.17, dd (3.3, 2.2)	73.5, CH	4.17, dd (3.1, 2.1)	73.2, CH	4.18, dd (3.1, 2.2)
7	71.4, CH	4.71, d (3.3)	71.5, CH	4.68, d (3.1)	71.2, CH	4.70, d (3.1)
8	152.7, C		152.7, C		151.9, C	
9	135.1, C		134.9, C		135.1, C	
10	200.2, C		200.0, C		200.1, C	
11	123.9, CH	6.06, d (15.9)	123.8, CH	6.08, d (15.9)	123.0, CH	6.09, d (15.9)
12	138.7, CH	5.85, dt (15.9, 7.0)	138.0, CH	5.88, dt (15.9, 6.8)	139.2, CH	5.90, dt (15.9, 6.9)
13	33.8, CH ₂	2.18, m	28.7, CH ₂	2.41, m	30.5, CH ₂	2.32, m; 2.23, m
14	24.2, CH ₂	1.70, m	42.3, CH ₂	2.61, t (7.3)	37.1, CH ₂	1.59, m; 1.53, m
15	43.4, CH ₂	2.54, m	212.5, C		72.9, CH	3.49, m
16	211.9, C		36.7, CH ₂	2.50, q (7.3)	30.8, CH ₂	1.50, m 1.43, m
17	29.9, CH ₃	2.14, s	8.0, CH ₃	1.02, t (7.3)	10.1, CH ₃	0.95, t (7.4)
18	60.7, CH ₂	4.51, d (12.6); 4.48, d (12.6)	60.7, CH ₂	4.49, d (12.6); 4.46, d (12.6)	60.5, CH ₂	4.52, d (12.5); 4.49, d (12.5)
19	12.7, CH ₃	1.87, s	12.9, CH ₃	1.87, s	12.6, CH ₃	1.87, s

^a recorded at 600 MHz (¹H) and 150 MHz (¹³C); ^b Data were extracted from HSQC and HMBC.

Pestallic acid **7** shared the same molecular formula as **1** as determined by HRESIMS. The ^1H and ^{13}C NMR data of **7** (Table 3) closely matched those of **1** indicating that the planar structures of the two compounds were identical whereas they differed in the configuration of C-5 as evident from analysis of the coupling constants and of the ROESY spectra. The double bonds at C-2/C-3 and C-11/C-12 of **7** were *E*-configured based on the NOE correlation between H_b -4 (δ_H 2.62) and Me-19 (δ_H 1.88) and the large coupling constants (16.0 Hz) observed for H-11 and H-12. The small *J* value (3.5 Hz) of H-6 and H-7 suggested their *cis* orientation. However, the coupling constant between H-5 and H-6 was 10.8 Hz for **7**, whereas only a small coupling constant of 2.0 Hz was observed for the corresponding protons of **1**. These data, together with the NOE correlation between H_ab -4 and H-6 and the lack of a NOE correlation between H-5 and H-7 observed in **1** indicated that **7** differed from **1** in the relative configuration of C-5.

The above ECD computational protocol was also carried out on the truncated model compound of **7** [(5*S*,6*S*,7*R*)-**7a**]. DFT re-optimization of the 361 MMFF conformers resulted in 28 low-energy structures over 1% Boltzmann distribution. In contrast to **1a**, the cyclohexenone ring of the DFT conformers of **7a** adopted both *M* and *P* helicity in comparable ratio. The ECD spectra computed at four levels gave moderate to good agreement with the experimental ECD spectrum allowing elucidation of the absolute configuration as (5*S*,6*S*,7*R*). The BH&HLYP/TZVP PCM/MeOH ECD calculation provided the best agreement (Fig.7).

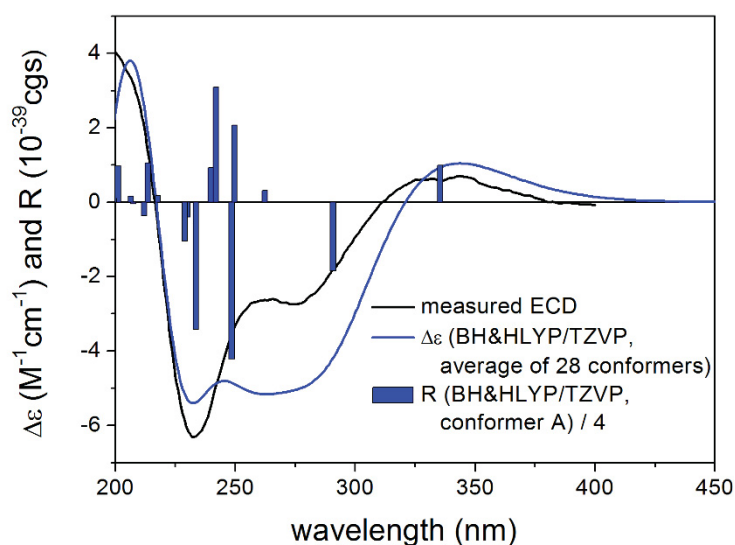


Figure. 7 Experimental ECD spectrum of **7** in MeOH compared with the Boltzmann-weighted B3LYP/TZVP PCM/MeOH ECD spectrum of (5*S*,6*S*,7*R*)-**7a**. Level of optimization: ω B97X/TZVP PCM/MeOH. Bars represent the rotatory strength values of the lowest-energy conformer.

The molecular formula of pestallic acid O (**8**) was identical to that of **2** according to the HRESIMS data. Analysis of the ^1H and ^{13}C NMR data (Table 3) revealed that **8** and **2** share the same planar structure. Analysis of the coupling constant between H-5 and H-6 (10.8 Hz) and of the NOE correlations, however, indicated **8** to be a derivative of **7** rather than of **2** with regard to the configuration of C-5. The absolute configuration at C-16 of **8** remained undetermined due to the limited amount of compound isolated. However, based on the identical NMR data for the alkyl side chain of **2** and **8**, the absolute configuration at C-16 of **8** was suggested to be (*R*) as shown for **2**.

Table 3 NMR data for compounds **7–10** in CD₃OD.

NO.	7^a		8^b		9^b		10^b	
	δ_C , type	δ_H (<i>J</i> in Hz)	δ_C , type	δ_H (<i>J</i> in Hz)	δ_C , type ^c	δ_H (<i>J</i> in Hz)	δ_C , type	δ_H (<i>J</i> in Hz)
1	171.8, C		172.1, C		173.8, C		170.9, C	
2	130.2, C		130.5, C		131.4, C		132.3, C	
3	141.1, CH	6.75, t (7.4)	140.7, CH	6.73, t (7.5)	141.4, CH	6.88, t (7.2)	135.6, CH	6.66, dd (8.9, 6.3)
4	26.0, CH ₂	2.75, ddd (15.1, 7.4, 4.1) 2.62, ddd (15.1, 7.4, 6.1)	25.9, CH ₂	2.74, ddd (15.0, 7.5, 4.2) 2.62, ddd (15.0, 7.5, 6.0)	26.8, CH ₂	2.66, m 2.44, m	37.9, CH ₂	2.79, dd (14.9, 6.3) 2.57, dd (14.9, 8.9)
5	49.8, CH	2.93, ddd (10.8, 6.1, 4.1)	49.6, CH	2.93, ddd (10.8, 6.0, 4.2)	41.6, CH	1.96, m	80.0, C	
6	71.3, CH	3.73, dd (10.8, 3.5)	71.1, CH	3.74, dd (10.8, 3.4)	69.6, CH	3.77, dd (11.8, 4.0)	47.5, CH	4.30, d (8.9)
7	67.8, CH	4.65, d (3.5)	67.7, CH	4.65, d (3.4)	69.4, CH	4.26, d (4.0)	74.4, CH	4.76, d (8.9)
8	152.9, C		153.1, C		135.2, C		154.1, C	
9	135.7, C		135.7, C		137.8, C		132.8, C	
10	201.1, C		201.1, C		67.5, CH	4.38, d (3.2)	197.4, C	
11	122.7, CH	6.06, d (16.0)	122.9, CH	6.08, d (16.0)	126.7, CH	6.39, d (15.8)	121.9, CH	6.08, d (16.0)
12	140.3, CH	5.85, dt (16.0, 6.9)	140.0, CH	5.87, dt (16.0, 7.0)	135.4, CH	6.03, dt (15.8, 7.0)	141.3, CH	6.03, dt (16.0, 6.7)
13	34.5, CH ₂	2.17, m	34.5, CH ₂	2.19, m	34.5, CH ₂	2.18, m	34.6, CH ₂	2.16, m
14	29.9, CH ₂	1.46, m	26.4, CH ₂	1.57, m; 1.48, m	30.1, CH ₂	1.45, m	29.8, CH ₂	1.42, m
15	32.5, CH ₂	1.34, m	39.6, CH ₂	1.47, m	32.6, CH ₂	1.33, m	32.5, CH ₂	1.31, m
16	23.5, CH ₂	1.35, m	68.4, CH	3.73, m	23.6, C	1.34, m	23.5, CH ₂	1.34, m
17	14.3, CH ₃	0.91, t (7.0)	23.5, CH ₃	1.15, d (6.2)	14.4, CH ₃	0.91, t (7.0)	14.4, CH ₃	0.91, t (7.0)
18	61.1, CH ₂	4.55, d (13.2) 4.37, d (13.2)	61.0, CH ₂	4.55, d (13.2) 4.37, d (13.2)	60.0, CH ₂	4.41, d (12.1) 4.19, d (12.1)	60.0, CH ₂	4.51, d (13.0) 4.48, d (13.0)
19	12.7, CH ₃	1.88, s	12.8, CH ₃	1.88, s	13.1, CH ₃	1.89, s	12.9, CH ₃	1.73, s

^a recorded at 300 MHz (¹H) and 75 MHz (¹³C); ^b recorded at 600 MHz (¹H) and 150 MHz (¹³C); ^c Data were extracted from HSQC and HMBC.

Pestallic acid P (**9**) had the molecular formula $C_{19}H_{30}O_6$ as determined by HRESIMS data, indicating the loss of one degree of unsaturation compared to **7**. Extra signals for an oxygenated methine at δ_H 4.38 and δ_C 67.5 in the 1H and ^{13}C NMR spectra of **9**, together with the loss of the carbonyl carbon signal of C-10 of **1–8**, indicated reduction of the carbonyl functionality at C-10 in compound **9**. This was further supported by the COSY correlations of H-10/H-5/H-6/H-7 and the HMBC correlations from H-10 to C-8 (δ_C 135.2) and C-11 (δ_C 126.7). Therefore, the gross structure of **9** was established as shown. The olefinic double bonds at C-2/C-3 and C-11/C-12 in **9** were both assigned to have *E*-geometry as described for **1** and **7**. The small *J* values between H-6 and H-7 (4.0 Hz) indicated the *cis* orientation of these two protons. Similarly, *cis* orientation of H-5 and H-10 was suggested based on the small coupling constants of 3.2 Hz. Neither H-5 nor H-10 showed correlations to H-7 in the ROESY spectrum. However, the large coupling constant between H-5 and H-6 (11.8 Hz) and the NOE correlations from H_{ab}-4 to H-6 indicated that the latter protons resided on the same face of the plain whereas H-5 and H-10 had an opposite orientation.

The molecular formula of pestallic acid Q (**10**) was $C_{19}H_{27}IO_6$ as determined by HRESIMS, indicating six degrees of unsaturation. The ^{13}C NMR data (Table 3) for **10** exhibited eight unsaturated carbons including two carbonyl carbons at δ_C 170.9 (C-1) and 197.4 (C-10) and six olefinic carbons at δ_C 154.1 (C-8), 141.3 (C-12), 135.6 (C-3), 132.8 (C-9), 132.3 (C-2), and 121.9 (C-11), accounting for five degrees of unsaturation. Thus, **10** was suggested to be monocyclic. The 1H and ^{13}C NMR data (Table 3) of **10** were similar to those of **1** except for differences in the substitution of the six-membered ring. The signals at δ_H 2.67 and δ_C 52.4 of the methine functionality at C-5 in **1** were absent in **10** as revealed by the HSQC spectrum of the latter. Instead, an extra signal for an oxygenated carbon and the HMBC correlations from H-3 and H_{ab}-4 to this oxygenated carbon were observed for **10**, indicating hydroxylation at C-5. The chemical shifts for the oxygenated methine at C-7 in **10** were similar to those of **1** whereas the chemical shift of C-6 was shifted upfield from 73.5 ppm in **1** to 47.5 ppm in **10** as evident from the ^{13}C NMR data of the latter. Therefore, the attachment of the iodine

atom was at C-6 when the inductive effect of the iodine atom was taken into consideration. Thus, the planar structure of **10** was elucidated as shown (Fig. 1). The relative configuration of **10** was assigned by analysis of the coupling constants and ROESY relationships. The large coupling constant of 16.0 Hz and the NOE correlation between H_b-4 (δ_{H} 2.57) and Me-19 (δ_{H} 1.73) indicated that the double bonds at C-11/C-12 and C-2/C-3 were both *E* configured. The regioselective conversion of epoxides to halohydrins resulted in different orientations of the hydroxy group at C-5 and of the iodine atom at C-6.^{26,27} The coupling constant of 8.9 Hz between H-6 and H-7 indicated their *trans* orientation whereas the NOE correlation between H-7 and H_b-4 confirmed that the latter protons had a co-facial orientation.

The isolated ambuic acid (**11**) derivatives including the new compounds **1–10** originate from the polyketide pathway (Fig. 8).^{28,29} Elimination of water from the hypothetical precursor **a** is suggested to yield product **b** which features a double bond at C-5/C-6. A Michael addition reaction of **b** with H₂O will generate **1** and **7** which will undergo oxidation, reduction or acetylation to form **2–6**, **8** and **9**. On the other hand, ambuic acid (**11**) likely originates from intermediate **b** via oxidation.³⁰ Compound **12** is derived from **11** via acetylation while the iodized compound **10** may be assumed to be derived via a ring-opening reaction of the epoxide group of **11** with iodine.²⁶ In order to exclude that compound **10** might be an artifact formed during fermentation of the fungus in presence of NaI, ambuic acid (**11**) was incubated in a mixture of MeOH and water adjusted to pH of 3 in presence of 3.5% NaI for 48 h at room temperature. No generation of **10** was observed.

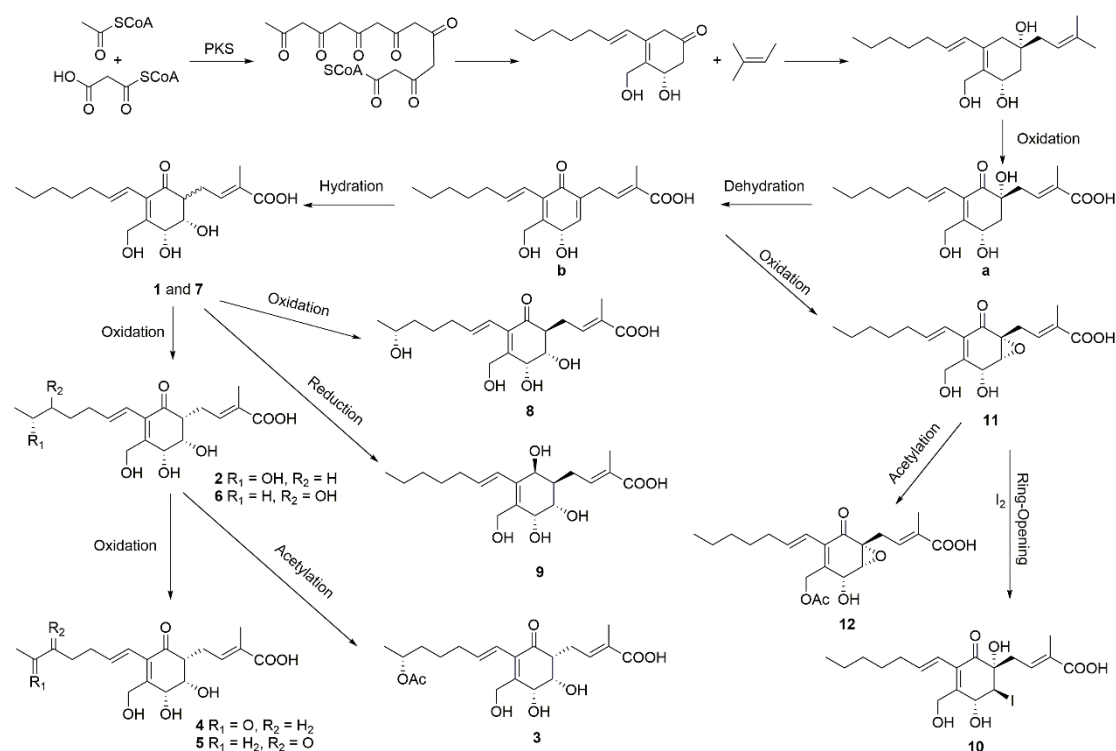


Figure. 8 Plausible biogenetic pathways of ambuic acid (11) and derivatives.

In a previous report, the known compounds ambuic acid (11) and 12 displayed antimicrobial activity against the Gram-positive bacterium *Staphylococcus aureus* (ATCC6538) with IC_{50} values of 43.9 and 27.8 μ M, respectively.¹⁶ Consequently, compounds 1–10 were tested for antibacterial activity against *S. aureus* (ATCC29213), drug-resistant *Acinetobacter baumannii* (BAA1605) and *Mycobacterium tuberculosis*. Cytotoxicity was also tested against the mouse lymphoma cell line L5178Y. However, none of the analyzed compounds were active.

EXPERIMENTAL SECTION

General Experimental Procedures. Optical rotations were measured with a Jasco P-2000 polarimeter. ECD spectra were recorded on a JASCO J-810 spectropolarimeter. NMR spectra were recorded on Bruker ARX 400 or 600 NMR spectrometers. Chemical shifts were referenced to the solvent residual peaks. Mass spectra (ESI) were recorded with a LC-MS HP1100 Agilent Finnigan LCQ Deca XP Thermoquestman spectrometer and HRESIMS were recorded on a UHR-QTOF maXis 4G (Bruker Daltonics) mass spectrometer. HPLC analysis was performed with a

Dionex UltiMate-3400SD system coupled to a LPG-3400SD pump and a photodiode array detector (DAD 300RS). The analytical column (125 × 4 mm) was prefilled with Eurosphere-10 C18 (Knauer, Germany), and the following gradient was used (MeOH, 0.1% formic acid in H₂O): 0 min (10% MeOH); 5 min (10% MeOH); 35 min (100% MeOH); 45 min (100% MeOH). Semi-preparative HPLC was performed using a Merck Hitachi HPLC System (UV detector L-7400; pump L-7100; Eurosphere-100 C18, 300 × 8 mm), with a mixture of MeOH-H₂O as mobile phase. Column chromatography was done using Merck MN silica gel 60M (0.04–0.063 mm), silica gel 90 C₁₈-reversed phase and Sephadex LH-20. TLC plates precoated with silica gel F₂₅₄ (Merck) were used to monitor and collect fractions; detection was under 254 and 366 nm or by spraying the plates with anisaldehyde reagent. Distilled and spectral grade solvents were used for column chromatography and spectroscopic measurements, respectively.

Fungal Material and Identification. The fungus was isolated from roots of the plant *Youngia japonica* (L.) DC (Asteraceae) collected in April 2018 at Guiyang, Guizhou Province, P.R. China by Prof. Han Xiao from Guizhou Nationalities University. It was identified as *Pestalotiopsis lespedezae* (GenBank accession number MT521347) by DNA amplification and sequencing of its ITS region. Details of protocol have been described before.²⁷

Fermentation, Extraction and Isolation. The fungus was cultivated on solid rice medium in 10 Erlenmeyer flasks, which contained 100 g rice and 110 mL demineralized water per flask and had been autoclaved at 121 °C for 20 min before inoculation. For extraction EtOAc (500 mL) was added to each flask, followed by shaking at 140 rpm for 8 h after fermentation of the fungus for 14 days at 20 °C. For the OSMAC experiments 3.5 g NaCl, 3.5 g NaBr or 3.5 g NaI were added to each Erlenmeyer flask containing 100 g rice and 110 mL demineralized water prior to autoclaving.

The crude EtOAc extract (8.5 g) from *P. lespedezae* after fermentation on solid rice medium without salts was subjected to liquid-liquid partitioning between *n*-hexane and 90% aq. MeOH. The MeOH fraction (4.6 g) was subjected to vacuum liquid silica

gel column chromatography using a gradient solvent system of *n*-hexane and EtOAc (100:1 to 0:100; v/v) to obtain 5 fractions (Fr.1–5). Fr.3 (1.0 g) was separated into 4 subfractions (Fr.3.1–3.4) by column chromatography on Sephadex LH-20 (3 × 60 cm) with MeOH as mobile phase, yielding **11** (14.0 mg) and **12** (8.9 mg) following purification by semi-preparative HPLC (MeOH-H₂O: 0–2 min, 55%; 2–27 min, from 55% to 70%; 27–32 min, 100%).

The crude extract (10.1 g) from a large scale fermentation of *P. lespedezae* on rice medium in presence of NaI was subjected to vacuum liquid silica gel column chromatography using a gradient solvent system of *n*-hexane and EtOAc (100:1 to 0:100; v/v) to give 4 subfractions (Fr.1–4). Fr.2 (2.3 g) was separated into subfractions Fr.2.1–2.3 by vacuum liquid RP-18 column (6 × 20 cm) chromatography. Fr.2.1 was subjected to a Sephadex LH-20 column (3 × 60 cm) with MeOH as mobile phase, followed by purification using semi-preparative HPLC to yield **2** (6.0 mg) and **6** (2.2 mg). Compounds **8** (2.5 mg), **5** (2.4 mg), **4** (2.5 mg) and **9** (2.1 mg) were obtained from Fr.2.2 (68 mg) by semi-preparative HPLC (MeOH-H₂O: 0–2 min, 40%; 2–22 min, from 40% to 58%; 22–30 min, 100%). Fr.3 (2.0 g) was separated into 5 subfractions (Fr.3.1–3.5) by vacuum liquid RP-18 column chromatography (6 × 20 cm). From Fr.3.2, **10** (5.5 mg), **7** (3.4 mg), **1** (3.0 mg) and **3** (1.1 mg) were obtained by semi-preparative HPLC (MeOH-H₂O: 0–2 min, 35%; 2–27 min, from 35% to 65%; 27–30 min, 100%).

Preparation of methyl ester 2a. To a stirred solution of **2** (5.4 mg, 0.014 mmol) in approximately 10 mL of toluene-MeOH (3:2), an etheric solution of TMSCHN₂ was added dropwise until the yellow color persisted (1.1–1.5 mmol).³¹ The mixture was stirred for 30 min at room temperature and concentrated to give the corresponding methyl ester **2a**, which was further purified by CC using CH₂Cl₂-MeOH (5:1) as eluent.

Preparation of (R)- and (S)-MTPA esters. Compound **2a** (1.8 mg) was dissolved in pyridine (500 µL) and then transferred to an NMR tube. (S)-MTPACl (15.0 µL, 0.075 mmol) was added quickly. By shaking the NMR tube, the reagent and the dissolved compound were mixed. After 10 h at room temperature and removal of pyridine, ¹H NMR data were obtained in CD₃OD for the (R)-MTPA ester (**2b**).

Following the same protocol, the (*S*)-MTPA ester (**2c**) was produced.

Pestallic acid H (**1**): colorless needles; $[\alpha]_{\text{D}}^{20}$ -25 (*c* 0.125, MeOH); UV (MeOH) λ_{max} 205 nm; ECD (0.213 mM, MeOH), λ_{max} ($\Delta\epsilon$) 333sh (-0.77), 272sh (-1.64), 242 (-5.13), 213 ($+14.68$) nm; ^1H and ^{13}C NMR data, Table 1; HRESIMS m/z 370.2224 $[\text{M}+\text{Na}]^+$ ($\text{C}_{22}\text{H}_{28}\text{O}_7\text{Na}$, calcd. 370.2224).

Pestallic acid I (**2**): colorless needles; $[\alpha]_{\text{D}}^{20}$ -14 (*c* 0.125, MeOH); UV (MeCN) λ_{max} 207 nm; ^1H and ^{13}C NMR data, Table 1; HRESIMS m/z 369.1909 $[\text{M}+\text{H}]^+$ ($\text{C}_{12}\text{H}_{29}\text{O}_7$, calcd. 369.1908).

Pestallic acid J (**3**): yellowish oil; $[\alpha]_{\text{D}}^{20}$ $+4.5$ (*c* 0.15, MeOH); UV (MeOH) λ_{max} 203 nm; ^1H and ^{13}C NMR data, Table 1; HRESIMS m/z 411.2016 $[\text{M}+\text{H}]^+$ ($\text{C}_{21}\text{H}_{31}\text{O}_8$, calcd. 411.2013).

Pestallic acid K (**4**): colorless needles; $[\alpha]_{\text{D}}^{20}$ -24 (*c* 0.10, MeOH); UV (MeOH) λ_{max} 209 nm; ^1H and ^{13}C NMR data, Table 2; HRESIMS m/z 384.2014 $[\text{M}+\text{NH}_4]^+$ ($\text{C}_{19}\text{H}_{30}\text{NO}_7$, calcd. 384.2017).

Pestallic acid L (**5**): colorless needles; $[\alpha]_{\text{D}}^{20}$ -20 (*c* 0.10, MeOH); UV (MeOH) λ_{max} 202 nm; ^1H and ^{13}C NMR data, Table 2; HRESIMS m/z 384.2023 $[\text{M}+\text{NH}_4]^+$ ($\text{C}_{19}\text{H}_{30}\text{NO}_7$, calcd. 384.2017).

Pestallic acid M (**6**): colorless needles; $[\alpha]_{\text{D}}^{20}$ -26 (*c* 0.10, MeOH); UV (MeOH) λ_{max} 210 nm; ^1H and ^{13}C NMR data, Table 2; HRESIMS m/z 391.1728 $[\text{M}+\text{H}]^+$ ($\text{C}_{19}\text{H}_{28}\text{O}_7\text{Na}$, calcd. 391.1727).

Pestallic acid N (**7**): yellowish oil; $[\alpha]_{\text{D}}^{20}$ -47 (*c* 0.1, MeOH); UV (MeOH) λ_{max} 203 nm; ECD (0.213 mM, MeOH), λ_{max} ($\Delta\epsilon$) 343 ($+0.70$), 274sh (-2.75), 233 (-6.31), 206sh ($+3.39$) nm; ^1H and ^{13}C NMR data, Table 3; HRESIMS m/z 370.2228 $[\text{M}+\text{NH}_4]^+$ ($\text{C}_{19}\text{H}_{32}\text{NO}_6$, calcd. 370.2224).

Pestallic acid O (**8**): colorless oil; $[\alpha]_{\text{D}}^{20}$ -43 (*c* 0.10, MeOH); UV (MeCN) λ_{max} 209 nm; ^1H and ^{13}C NMR data, Table 3; HRESIMS m/z 391.1729 $[\text{M}+\text{Na}]^+$ ($\text{C}_{19}\text{H}_{28}\text{O}_7\text{Na}$, calcd. 391.1727).

Pestallic acid P (**9**): yellowish oil; $[\alpha]_{\text{D}}^{20}$ -97 (*c* 0.10, MeOH); UV (MeOH) λ_{max} 207 nm; ^1H and ^{13}C NMR data, Tables 3; HRESIMS m/z 377.1930 $[\text{M}+\text{Na}]^+$

(C₁₉H₃₀O₆Na, calcd. 377.1935).

Pestallic acid Q (**10**): yellowish oil; $[\alpha]_D^{20}$ -46 (c 0.15, MeOH); UV (MeOH) λ_{\max} 211 nm; ¹H and ¹³C NMR data, Table 3; HRESIMS m/z 501.0742 [M+Na]⁺ (C₁₉H₂₇IO₆Na, calcd. 501.0745).

Cytotoxicity and Antibacterial Assay. Kahalalide F (IC₅₀ 4.3 μ M) and medium with 0.1% ethylene glycol monomethyl ether (EGME) in DMSO were used as positive and negative controls, respectively, while the MTT method was applied for measuring cytotoxicity against the mouse lymphoma cell line L5178Y as described before.³² Antibacterial activity against Gram-positive bacteria *Staphylococcus aureus* (ATCC29213), drug-resistant *Acinetobacter baumannii* (BAA1605) and *Mycobacterium tuberculosis* was evaluated using the microdilution method in alignment with the CLSI guidelines using Muller Hinton broth for bacteria and 7H9 broth for Mycobacteria.³³

Computational Section. Mixed torsional/low-frequency mode conformational searches were carried out by means of the MacroModel 10.8.011 software by using the MMFF with an implicit solvent model for CHCl₃.³⁴ Geometry re-optimizations were carried out at the ω B97X/TZVP level with the PCM solvent model for MeOH. TDDFT-ECD calculations were run with various functionals (B3LYP, BH&HLYP, CAM-B3LYP, and PBE0), the TZVP basis set and the same PCM/MeOH solvent model as implemented in the Gaussian 09 package.³⁵ Electronic circular dichroism spectra were generated as sums of Gaussians with 3600 and 4800 cm⁻¹ width at half-height, using dipole-velocity-computed rotational strength values.³⁶ Boltzmann distributions were estimated from the ω B97X energies. The MOLEKEL software package was used for visualization of the results.³⁷

ACKNOWLEDGMENTS

X.Y. wants to thank China Scholarship Council, the Ministry of Education of China for a doctoral scholarship, and Prof. Han Xiao for plant sample collection. P.P. wants to thank the Manchot Foundation for support. The Hungarian authors were supported by the EU and co-financed by the European Regional Development Fund

under the project GINOP-2.3.2-15-2016-00008. T.K. thanks the National Research Development and Innovation Office (K120181) and A.M. by the János Bolyai Research Scholarship of the Hungarian Academy of Sciences. The Governmental Information-Technology Development Agency (KIFÜ) is acknowledged for CPU time.

REFERENCES

1. F. Surup and M. Stadler, *Angew. Chem.* 2015, **127**, 8999-9000.
2. A. H. Aly, A. Debbab and P. Proksch, *Fungal Divers.* 2011, **50**, 3-19.
3. J. A. Tobert, *Nat. Rev. Drug. Discov.* 2003, **2**, 517-526.
4. G. Bo, *Clin. Microbiol. Infect.* 2000, **6**, 6-9.
5. C. R. Strader, C. J. Pearce and N. H. Oberlies, *J. Nat. Prod.* 2011, **74**, 900-907.
6. T. Fujita, K. Inoue, S. Yamamoto, T. Ikumoto, S. Sasaki, R. Toyama, K. Chiba, Y. Hoshino and T. Okumoto, *J. Antibiot.* 1994, **47**, 208-215.
7. F. L. Cherblanc, R. W. Davidson, P. Di Fruscia, N. Srimongkolpithak and M. Fuchter, *J. Nat. Prod. Rep.* 2013, **30**, 605-624.
8. P. J. Rutledge and G. L. Challis, *Nat. Rev. Microbiol.* 2015, **13**, 509-523.
9. G. Daletos, W. Ebrahim, E. Ancheeva, M. El-Neketi, W. H. Lin and P. Proksch, *Chemical Biology of Natural Products; Grothaus, P., Cragg, GM, Newman, DJ, Eds* 2017, 233-284.
10. N. M. Tran-Cong, A. Mándi, T. Kurtán, W. E. G. Müller, R. Kalscheuer, W. H. Lin, Z. Liu and P. Proksch, *RSC Advances* 2019, **9**, 27279-27288.
11. N. P. Ariantari, G. Daletos, A. Mándi, T. Kurtán, W. E. G. Müller, W. H. Lin, E. Ancheeva and P. Proksch, *RSC Advances* 2019, **9**, 25119-25132.
12. H. Wang, H. F. Dai, C. Heering, C. Janiak, W. H. Lin, R. S. Orfali, W. E. G. Müller, Z. Liu and P. Proksch, *RSC Advances* 2016, **6**, 81685-81693.
13. L. Hammerschmidt, A. H. Aly, M. Abdel-Aziz, W. E. G. Müller, W. H. Lin, G. Daletos and P. Proksch, *Bioorg. Med. Chem.* 2015, **23**, 712-719.
14. S. Lavoie, D. Brumley, T. S. Alexander, C. Jasmin, F. A. Carranza, K. Nelson, C. L. Quave and J. Kubanek, *J. Org. Chem.* 2017, **82**, 4160-4169.
15. V. H. Woolner, C. M. Jones, J. J. Field, N. H. Fadzilah, A. B. Munkacsi, J. H. Miller, R. A. Keyzers and P. T. Northcote, *J. Nat. Prod.* 2016, **79**, 463-469.
16. G. Ding, Y. Li, S. Fu, S. Liu, J. Wei and Y. Che, *J. Nat. Prod.* 2009, **72**, 182-186.
17. J. Y. Li, J. K. Harper, D. M. Grant, B. O. Tombe, B. Bashyal, W. M. Hess and G. A. Strobel, *Phytochemistry* 2001, **56**, 463-468.
18. S. Superchi, P. Scafato, M. Gorecki and G. Pescitelli, *Curr. Med. Chem.* 2018, **25**, 287-320.
19. A. Mándi and T. Kurtán, *Nat. Prod. Rep.* 2019, **36**, 889-918.
20. A. Mándi, I. W. Mudianta, T. Kurtán and M. J. Garson, *J. Nat. Prod.* 2015, **78**, 2051-2056.
21. X. F. Hou, S. Yao, A. Mándi, T. Kurtán, C. P. Tang, C. Q. Ke, X. Q. Li and Y. Ye, *Org. Lett.* 2012, **14**, 460-463.

22. J. D. Chai and M. Head-Gordon, *J. Chem. Phys.* 2008, **128**, 084106.
23. P. Sun, D. X. Xu, A. Mándi, T. Kurtán, T. J. Li, B. Schulz and W. Zhang, *J. Org. Chem.* 2013, **78**, 7030–7047.
24. Y. Zhou, A. Mándi, A. Debbab, V. Wray, B. Schulz, W. E. G. Müller, W. H. Lin, P. Proksch, T. Kurtán and A. H. Aly, *Eur. J. Org. Chem.* 2011, **2011**, 6009-6019.
25. A. Mándi, M. M. M. Swamy, T. Taniguchi, M. Anetai and K. Monde, *Chirality* 2016, **28**, 453-459.
26. J. Wu, X. Sun, W. Sun and S. Ye, *Synlett.* 2006, **2006**, 2489-2491.
27. J. Kjer, A. Debbab, A. H. Aly and P. Proksch, *Nat. Protoc.* 2010, **5**, 479-490.
28. C. Li, R. P. Johnson and J. A. Porco, *J. Am. Chem. Soc.* 2003, **125**, 5095-5106.
29. C. Yuan, G. Ding, H. Y. Wang, Y. H. Guo, H. Shang, X. J. Ma and Z. M. Zou, *Biomed. Res. Int.* 2017, **2017**, 6961928.
30. L. A. M. Murray, S. M. K. McKinnie, H. P. Pepper, R. Erni, Z. D. Miles, M. C. Cruickshank, B. López-Pérez, B. S. Moore and J. H. George, *Angew. Chem. Int. Ed. Engl.* 2018, **57**, 11009-11014.
31. A. Presser and A. Hofner, *Monatshefte für Chemie* 2004, **135**, 1015-1022.
32. M. Ashour, R. Edrada, R. Ebel, V. Wray, W. Watjen, K. Padmakumar, W. E. G. Müller, W. H. Lin and P. Proksch, *J. Nat. Prod.* 2006, **69**, 1547-53.
33. F. R. Cockerill, M. A. Wikler, J. Alder, M. N. Dudley, G. M. Eliopoulos, M. J. Ferraro, D. J. Hardy, D. W. Hecht, J. A. Hindler and J. B. Patel, *Clin. Lab. Stand. Inst.* 2012, **32**, M07-A9.
34. MacroModel, Schrödinger LLC, 2015, <http://www.schrodinger.com/MacroModel>.
35. M. J. Frisch, G. W. Trucks, H. B. Schlegel, G. E. Scuseria, M. A. Robb, J. R. Cheeseman, V. Scalmani, G. Barone, B. Mennucci, G. A. Petersson, H. Nakatsuji, M. Caricato, X. Li, H. P. Hratchian, A. F. Izmaylov, J. Bloino, G. Zheng, J. L. Sonnenberg, M. Hada, M. Ehara, K. Toyota, R. Fukuda, J. Hasegawa, M. Ishida, T. Nakajima, Y. Honda, O. Kitao, H. Nakai, T. Vreven, J. A., Jr. Montgomery, J. E. Peralta, F. Ogliaro, M. Bearpark, J. J. Heyd, E. Brothers, K. N. Kudin, V. N. Staroverov, R. Kobayashi, J. Normand, K. Raghavachari, A. Rendell, J. C. Burant, S. S. Iyengar, J. Tomasi, M. Cossi, N. Rega, J. M. Millam, M. Klene, J. E. Knox, J. B. Cross, V. Bakken, C. Adamo, J. Jaramillo, R. Gomperts, R. E. Stratmann, O. Yazyev, A. J. Austin, R. Cammi, C. Pomelli, J. W. Ochterski, R. L. Martin, K. Morokuma, V. G. Zakrzewski, G. A. Voth, P. Salvador, J. J. Dannenberg, S. Dapprich, A. D. Daniels, . Farkas, J. B. Foresman, J. V. Ortiz, J. Cioslowski, D. J. Fox, *Gaussian 09 (Revision E.01)*, Gaussian, Inc., Wallingford, CT, 2013.
36. P. J. Stephens, N. Harada, *Chirality* 2009, **22**, 229–233.
37. U. Varetto, *MOLEKEL 5.4*, Swiss National Supercomputing Centre, Manno, Switzerland, 2009.

Support Information

Inducing new secondary metabolites from the endophytic fungus *Pestalotiopsis lespedezae* through an OSMAC approach

Xiaoqin Yu ^{a,b}, Ying Gao ^a, Marian Frank ^a, Attila Mándi,^c Tibor Kurtán,^c Werner E. G. Müller ^a, Rainer Kalscheuer ^a, Zhiyong Guo ^b, Kun Zou ^b, Zhen Liu ^a, Peter Proksch^{a,b}

^a Institute of Pharmaceutical Biology and Biotechnology, Heinrich-Heine-University Duesseldorf, 40225 Duesseldorf, Germany

^b Hubei Key Laboratory of Natural Products Research and Development, College of Biological and Pharmaceutical Sciences, China Three Gorges University, Yichang 443002, People's Republic of China

^c Department of Organic Chemistry, University of Debrecen, P.O.B. 400, 4002 Debrecen, Hungary

Table of contents

Figure S1. HRESIMS of 1 .	183
Figure S2. UV spectrum of 1 .	183
Figure S3. ¹ H-NMR (600 MHz, CD ₃ OD) spectrum of 1 .	184
Figure S4. ¹³ C-NMR (150 MHz, CD ₃ OD) spectrum of 1 .	184
Figure S5. ¹ H- ¹ H COSY (600 MHz, CD ₃ OD) spectrum of 1 .	185
Figure S6. HSQC (600 MHz, CD ₃ OD) spectrum of 1 .	185
Figure S7. HMBC (600 MHz, CD ₃ OD) spectrum of 1 .	186
Figure S8. ROESY (600 MHz, CD ₃ OD) spectrum of 1 .	186
Figure S9. Structure and population of the low-energy ($\geq 1\%$) ω B97X/TZVP PCM/MeOH conformers of (5 <i>R</i> ,6 <i>S</i> ,7 <i>R</i>)- 1a .	187
Figure S10. HRESIMS of 2 .	187
Figure S11. UV spectrum of 2 .	188
Figure S12. ¹ H-NMR (300 MHz, CD ₃ OD) spectrum of 2 .	188
Figure S13. ¹³ C NMR (75 MHz, CD ₃ OD) spectrum of 2 .	189
Figure S14. ¹ H- ¹ H COSY (300 MHz, CD ₃ OD) spectrum of 2 .	189
Figure S15. HSQC (300 MHz, CD ₃ OD) spectrum of 2 .	190
Figure S16. HMBC (300 MHz, CD ₃ OD) spectrum of 2 .	190
Figure S17. ROESY (600 MHz, CD ₃ OD) spectrum of 2 .	191
Figure S18. HRESIMS of 3 .	191
Figure S19. UV spectrum of 3 .	192
Figure S20. ¹ H-NMR (600 MHz, CD ₃ OD) spectrum of 3 .	192
Figure S21. ¹ H- ¹ H COSY (600 MHz, CD ₃ OD) spectrum of 3 .	193
Figure S22. HSQC (600 MHz, CD ₃ OD) spectrum of 3 .	193
Figure S23. HMBC (600 MHz, CD ₃ OD) spectrum of 3 .	194
Figure S24. ROESY (600 MHz, CD ₃ OD) spectrum of 3 .	194
Figure S25. HRESIMS of 4 .	195
Figure S26. UV spectrum of 4 .	195
Figure S27. ¹ H-NMR (600 MHz, CD ₃ OD) spectrum of 4 .	196
Figure S28. ¹ H- ¹ H COSY (600 MHz, CD ₃ OD) spectrum of 4 .	196
Figure S29. HSQC (600 MHz, CD ₃ OD) spectrum of 4 .	197
Figure S30. HMBC (600 MHz, CD ₃ OD) spectrum of 4 .	197
Figure S31. ROESY (600 MHz, CD ₃ OD) spectrum of 4 .	198
Figure S32. HRESIMS of 5 .	198
Figure S33. UV spectrum of 5 .	199
Figure S34. ¹ H-NMR (600 MHz, CD ₃ OD) spectrum of 5 .	199
Figure S35. ¹ H- ¹ H COSY (600 MHz, CD ₃ OD) spectrum of 5 .	200
Figure S36. HSQC (600 MHz, CD ₃ OD) spectrum of 5 .	200
Figure S37. HMBC (600 MHz, CD ₃ OD) spectrum of 5 .	201
Figure S38. ROESY (600 MHz, CD ₃ OD) spectrum of 5 .	201
Figure S39. HRESIMS of 6 .	202
Figure S40. UV spectrum of 6 .	202
Figure S41. ¹ H-NMR (600 MHz, CD ₃ OD) spectrum of 6 .	203
Figure S42. ¹ H- ¹ H COSY (600 MHz, CD ₃ OD) spectrum of 6 .	203

Figure S43. HSQC (600 MHz, CD ₃ OD) spectrum of 6	204
Figure S44. HMBC (600 MHz, CD ₃ OD) spectrum of 6	204
Figure S45. ROESY (600 MHz, CD ₃ OD) spectrum of 6	205
Figure S46. HRESIMS of 7	205
Figure S47. UV spectrum of 7	206
Figure S48. ¹ H-NMR (300 MHz, CD ₃ OD) spectrum of 7	206
Figure S49. ¹³ C-NMR (75 MHz, CD ₃ OD) spectrum of 7	207
Figure S50. ¹ H- ¹ H COSY (300 MHz, CD ₃ OD) spectrum of 7	207
Figure S51. HSQC (300 MHz, CD ₃ OD) spectrum of 7	208
Figure S52. HMBC (300 MHz, CD ₃ OD) spectrum of 7	208
Figure S53. ROESY (600 MHz, DMSO- <i>d</i> ₆) spectrum of 7	209
Figure S54. Structure and population of the low-energy ($\geq 1\%$) ω B97X/TZVP PCM/MeOH conformers of (5 <i>S</i> ,6 <i>S</i> ,7 <i>R</i>)- 7a	209
Figure S55. HREISMS of 8	210
Figure S56. UV spectrum of 8	210
Figure S57. ¹ H-NMR (600 MHz, CD ₃ OD) spectrum of 8	211
Figure S58. ¹³ C-NMR (150 MHz, CD ₃ OD) spectrum of 8	211
Figure S59. ¹ H- ¹ H COSY (600 MHz, CD ₃ OD) spectrum of 8	212
Figure S60. HSQC (600 MHz, CD ₃ OD) spectrum of 8	212
Figure S61. HMBC (600 MHz, CD ₃ OD) spectrum of 8	213
Figure S62. ROESY (600 MHz, CD ₃ OD) spectrum of 8	213
Figure S63. HREISMS of 9	214
Figure S64. UV spectrum of 9	214
Figure S65. ¹ H-NMR (600 MHz, CD ₃ OD) spectrum of 9	215
Figure S66. ¹ H- ¹ H COSY (600 MHz, CD ₃ OD) spectrum of 9	215
Figure S67. HSQC (600 MHz, CD ₃ OD) spectrum of 9	216
Figure S68. HMBC (600 MHz, CD ₃ OD) spectrum of 9	216
Figure S69. ROESY (600 MHz, CD ₃ OD) spectrum of 9	217
Figure S70. HREISMS of 10	217
Figure S71. UV spectrum of 10	218
Figure S72. ¹ H-NMR (600 MHz, CD ₃ OD) spectrum of 10	218
Figure S73. ¹³ C-NMR (150 MHz, CD ₃ OD) spectrum of 10	219
Figure S74. ¹ H- ¹ H COSY (600 MHz, CD ₃ OD) spectrum of 10	219
Figure S75. HSQC (600 MHz, CD ₃ OD) spectrum of 10	220
Figure S76. HMBC (600 MHz, CD ₃ OD) spectrum of 10	220
Figure S77. ROESY (600 MHz, CD ₃ OD) spectrum of 10	221
Figure S78. ¹ H-NMR (600 MHz, CD ₃ OD) spectrum of 2a	221
Figure S79. EISMS of 2a	222
Figure S80. ¹ H-NMR (600 MHz, CD ₃ OD) spectrum of 2b	222
Figure S81. ¹ H- ¹ H COSY (600 MHz, CD ₃ OD) spectrum of 2b	223
Figure S82. HRESIMS of 2b	223
Figure S83. ¹ H-NMR (600 MHz, CD ₃ OD) spectrum of 2c	224
Figure S84. ¹ H- ¹ H COSY (600 MHz, CD ₃ OD) spectrum of 2c	224
Figure S85. HRESIMS of 2c	225

Acquisition Parameter

Source Type	ESI	Ion Polarity	Positive	Set Nebulizer	0.3 Bar
Focus	Not active	Set Capillary	4000 V	Set Dry Heater	180 °C
Scan Begin	50 m/z	Set End Plate Offset	-500 V	Set Dry Gas	4.0 l/min
Scan End	1500 m/z	Set Collision Cell RF	600.0 Vpp	Set Divert Valve	Source

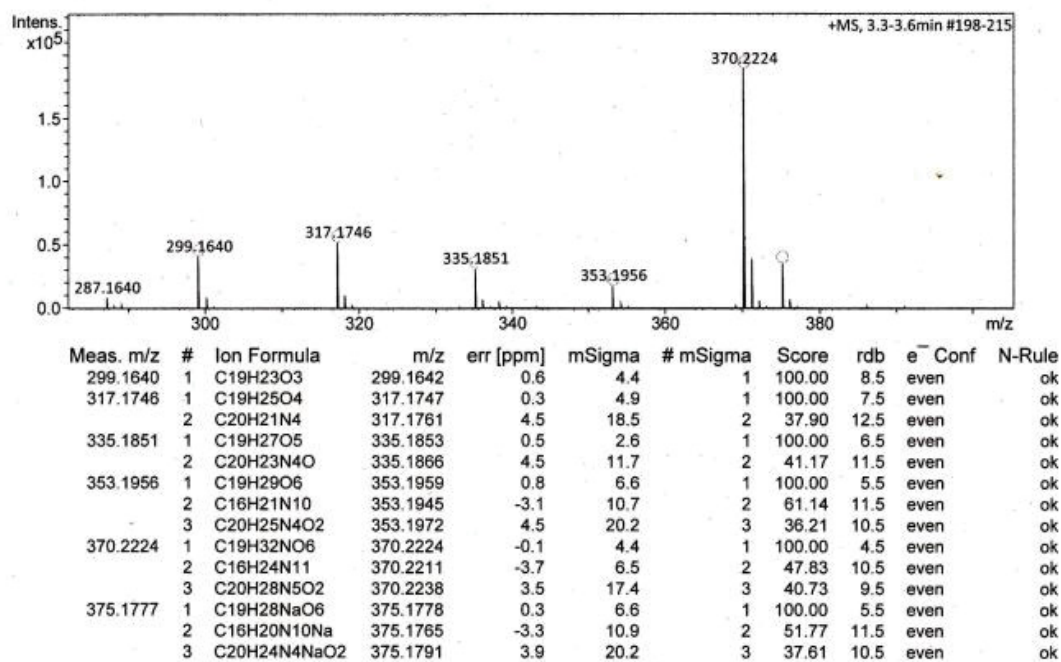


Figure S1. HRESIMS of 1.

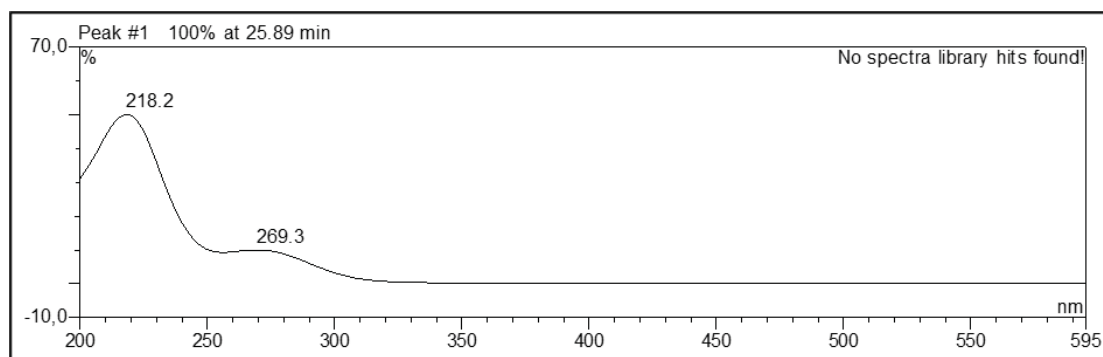


Figure S2. UV spectrum of 1.

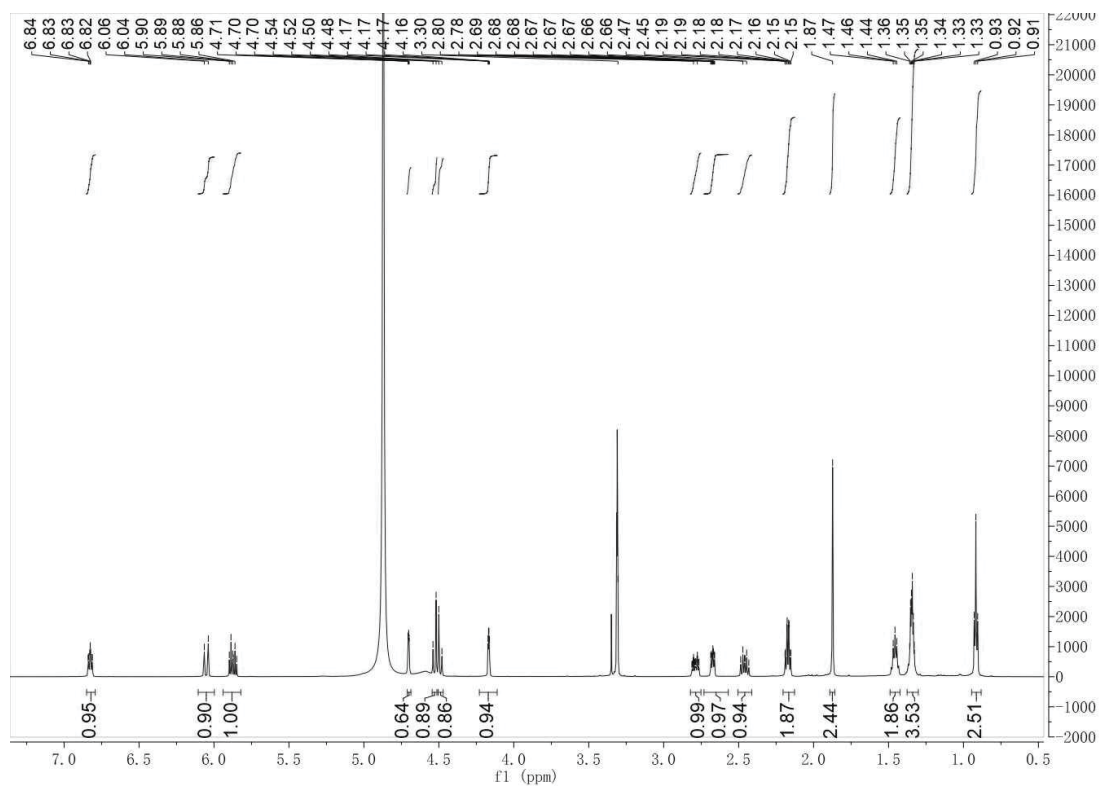


Figure S3. ¹H-NMR (600 MHz, CD₃OD) spectrum of 1.

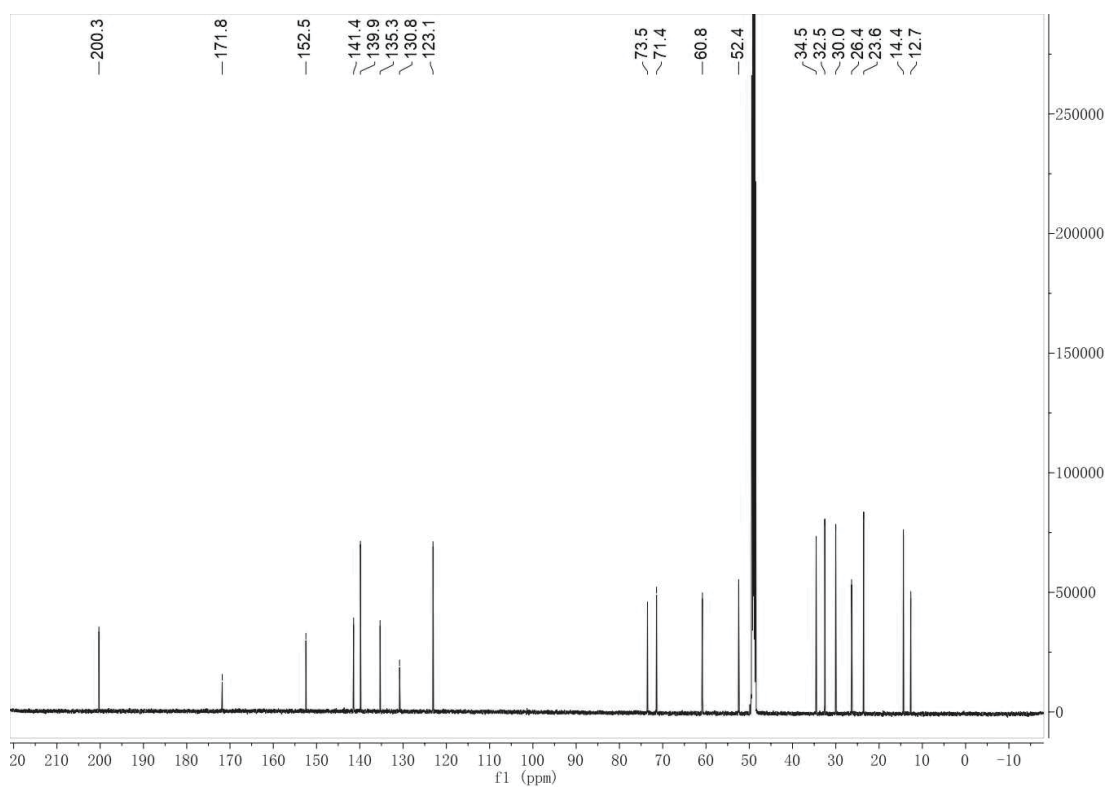


Figure S4. ¹³C-NMR (150 MHz, CD₃OD) spectrum of 1.



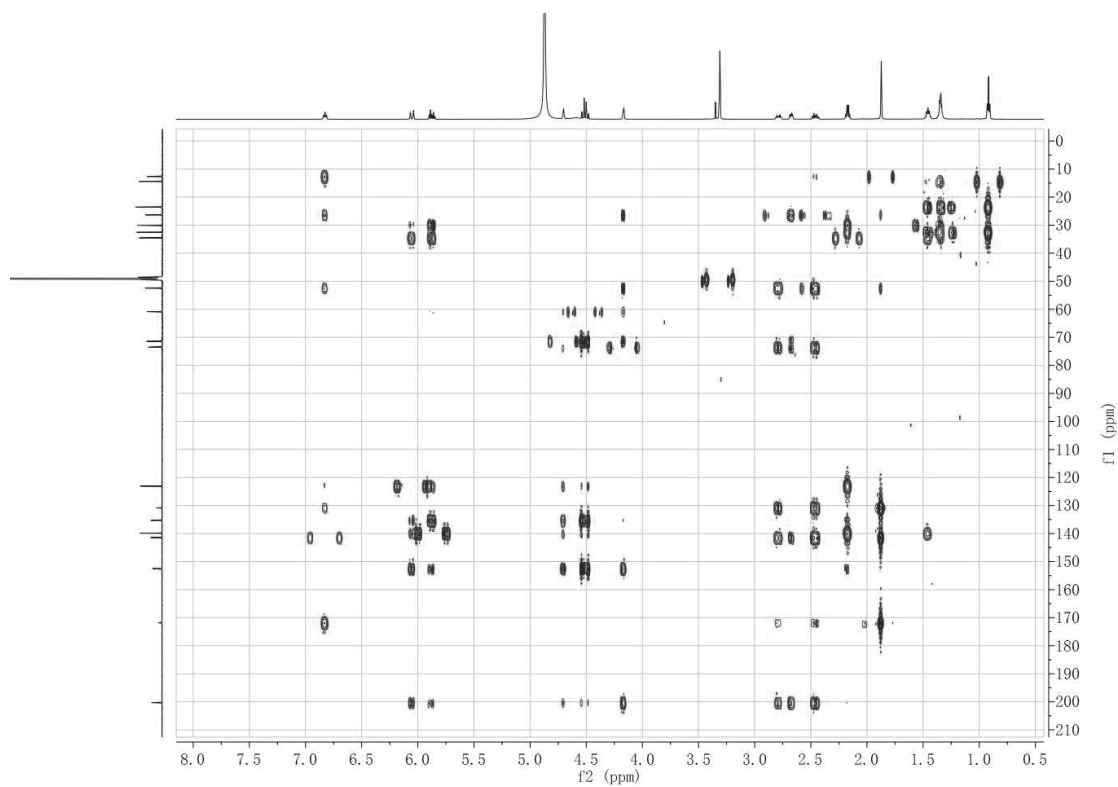


Figure S7. HMBC (600 MHz, CD₃OD) spectrum of **1**.

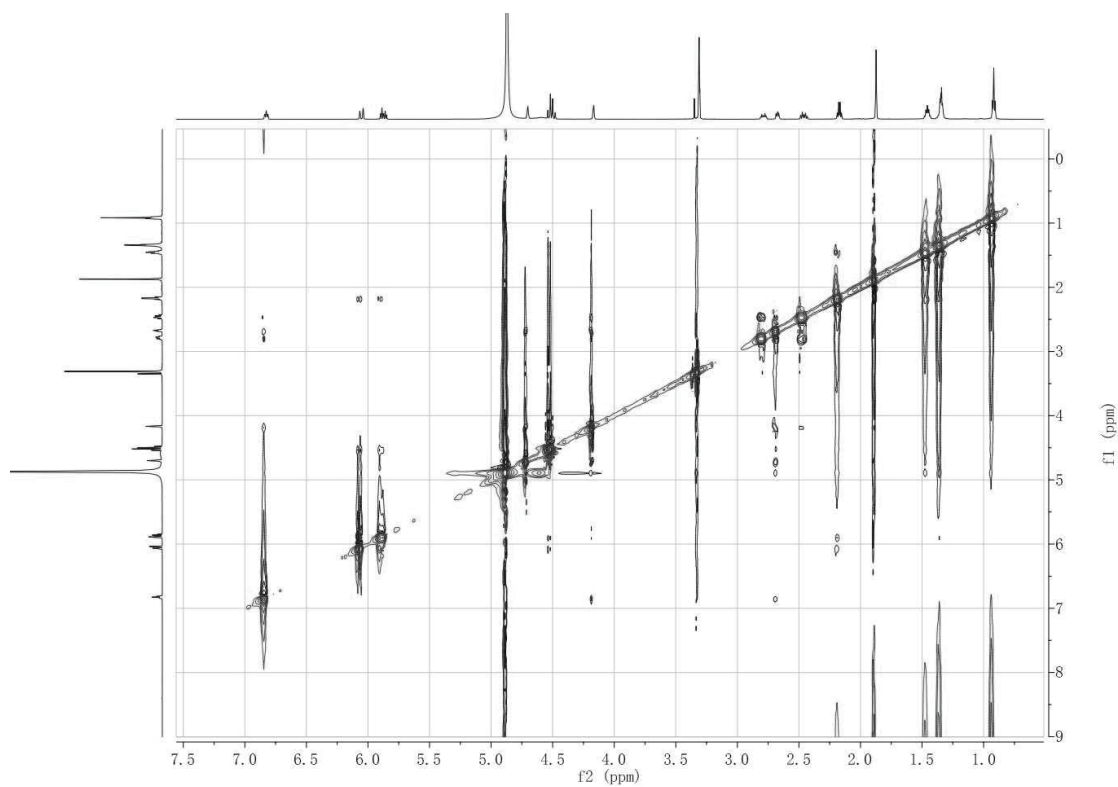


Figure S8. ROESY (600 MHz, CD₃OD) spectrum of **1**.

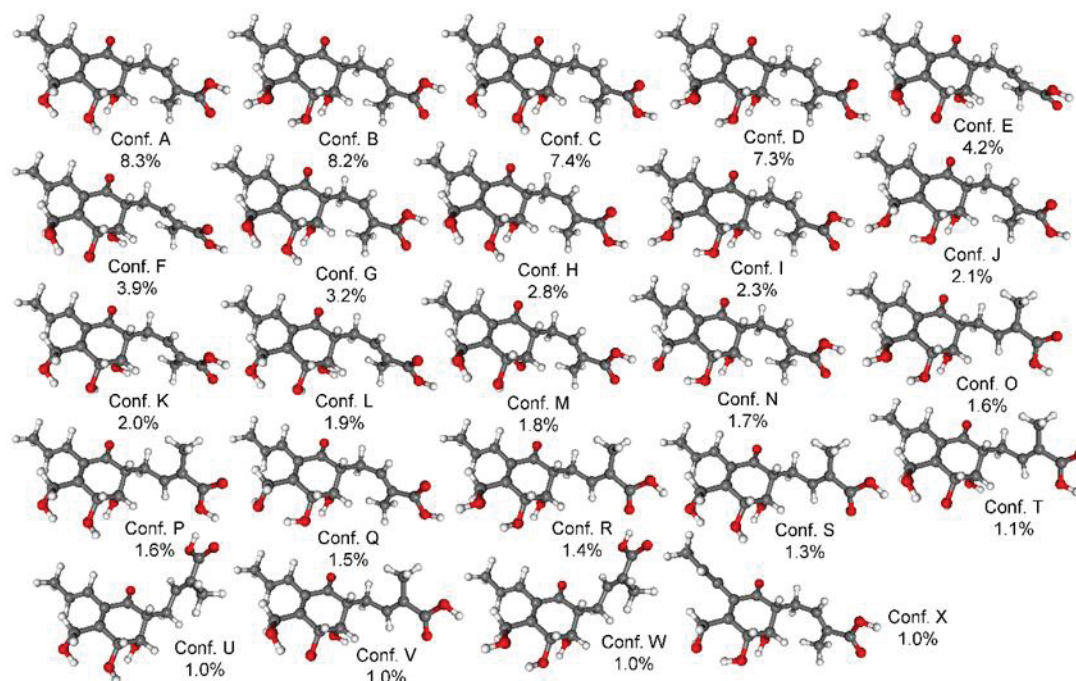


Figure S9. Structure and population of the low-energy ($\geq 1\%$) ω B97X/TZVP PCM/MeOH conformers of (5*R*,6*S*,7*R*)-**1a**.

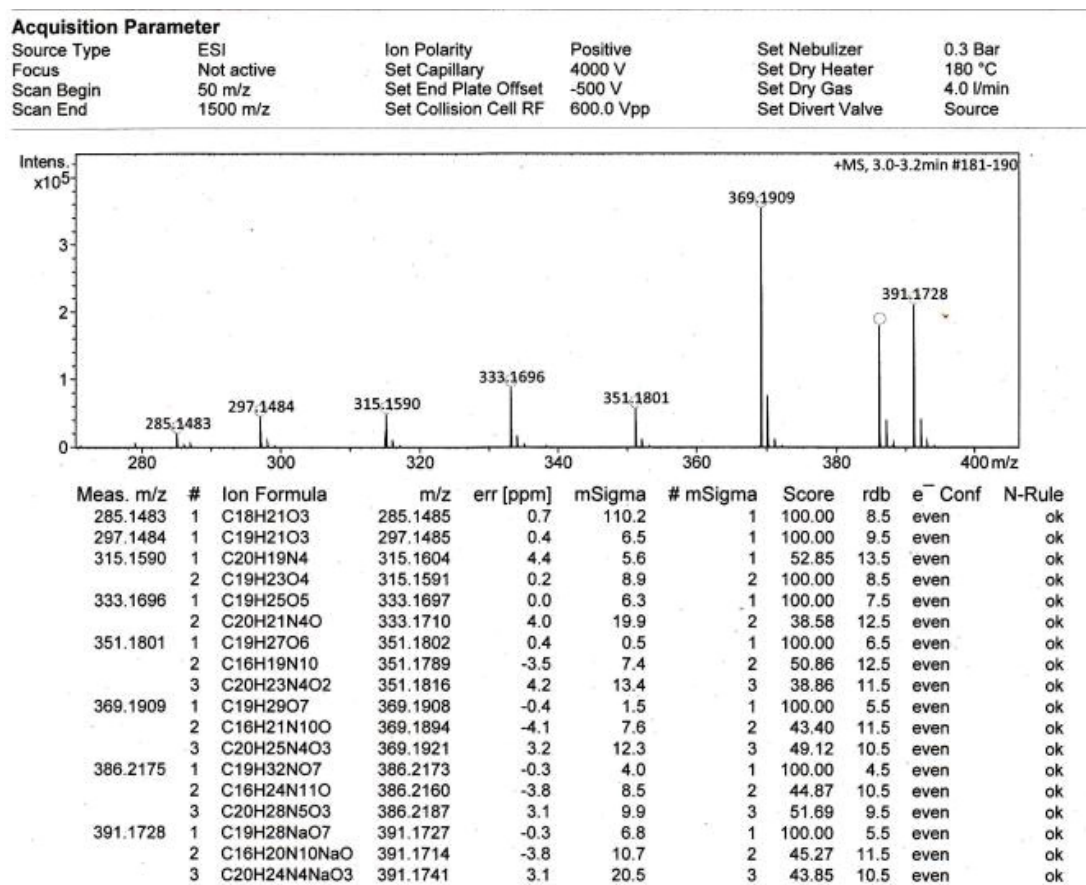


Figure S10. HRESIMS of **2**.

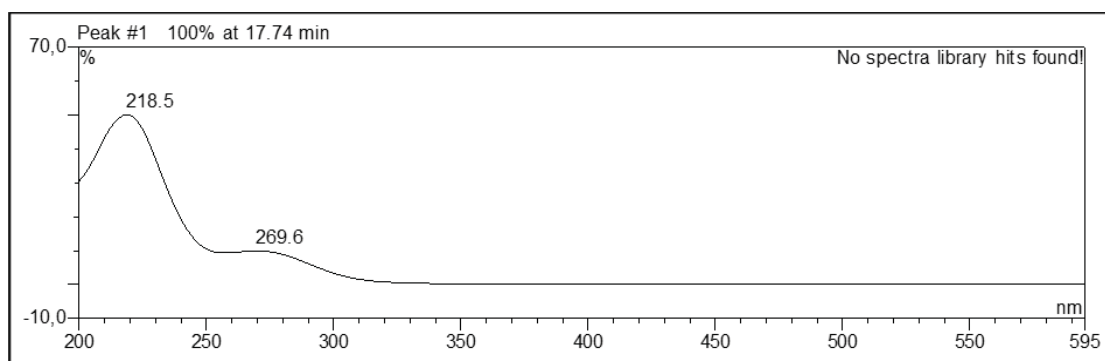


Figure S11. UV spectrum of **2**.

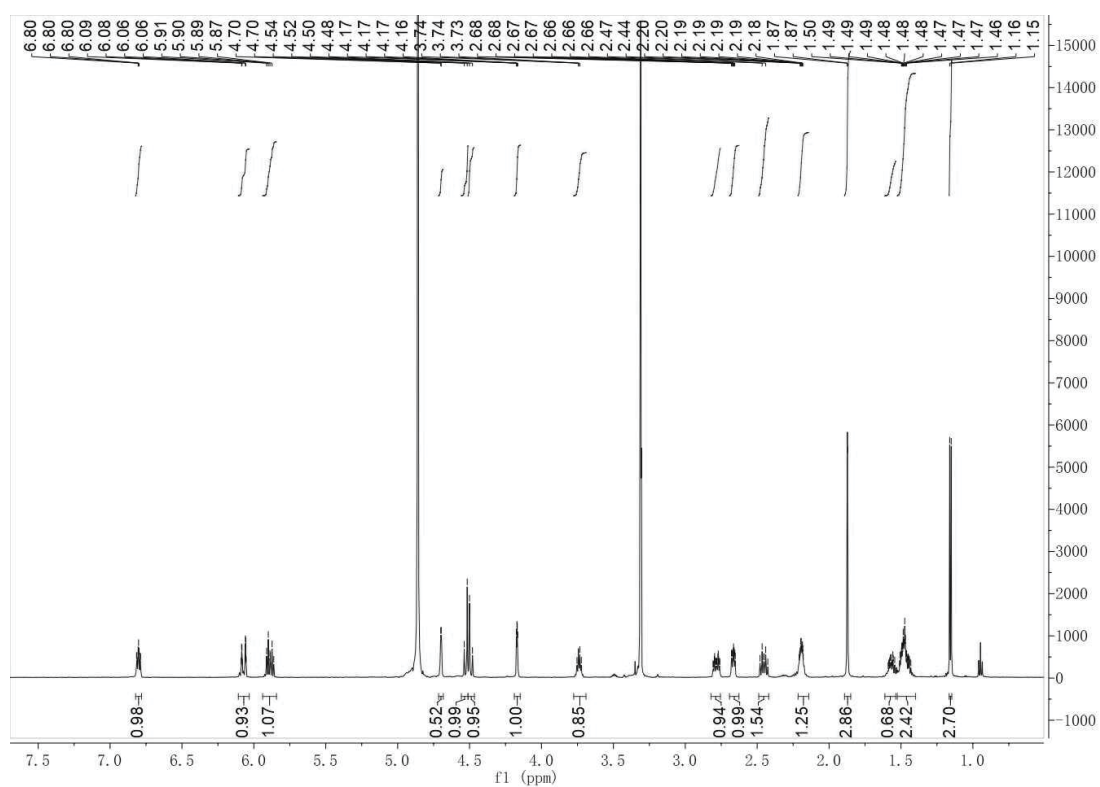


Figure S12. ^1H -NMR (300 MHz, CD_3OD) spectrum of **2**.

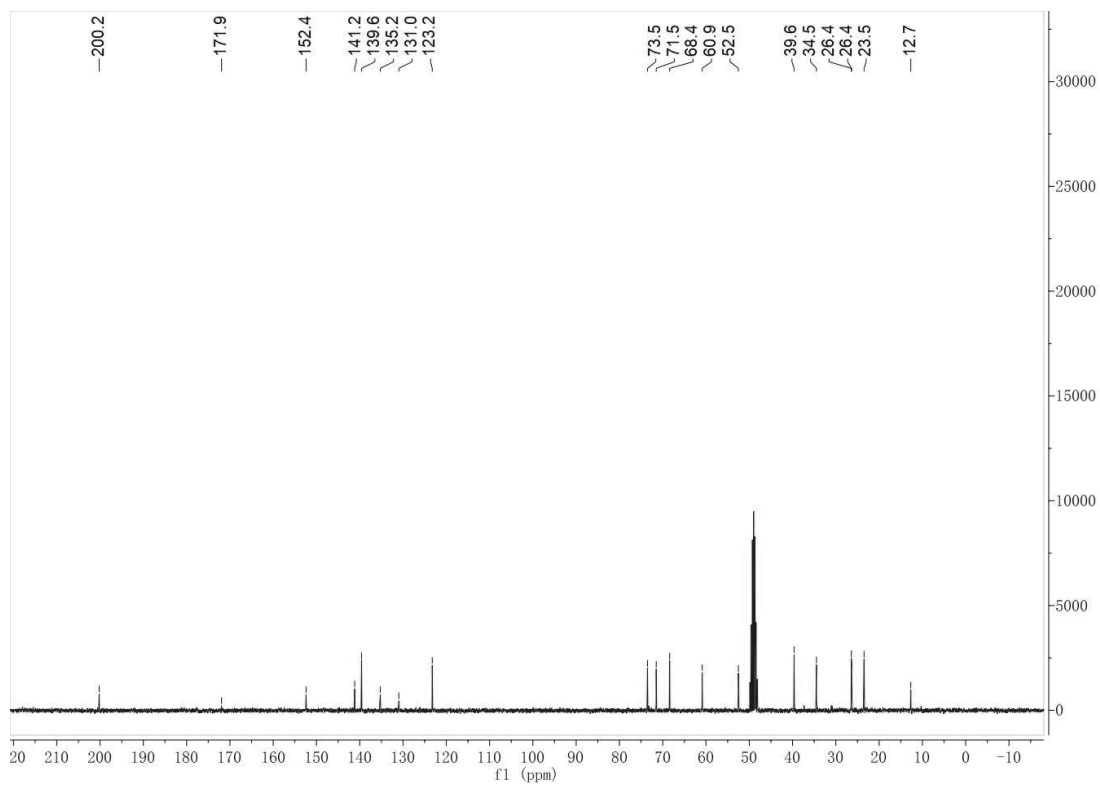


Figure S13. ^{13}C NMR (75 MHz, CD_3OD) spectrum of 2.

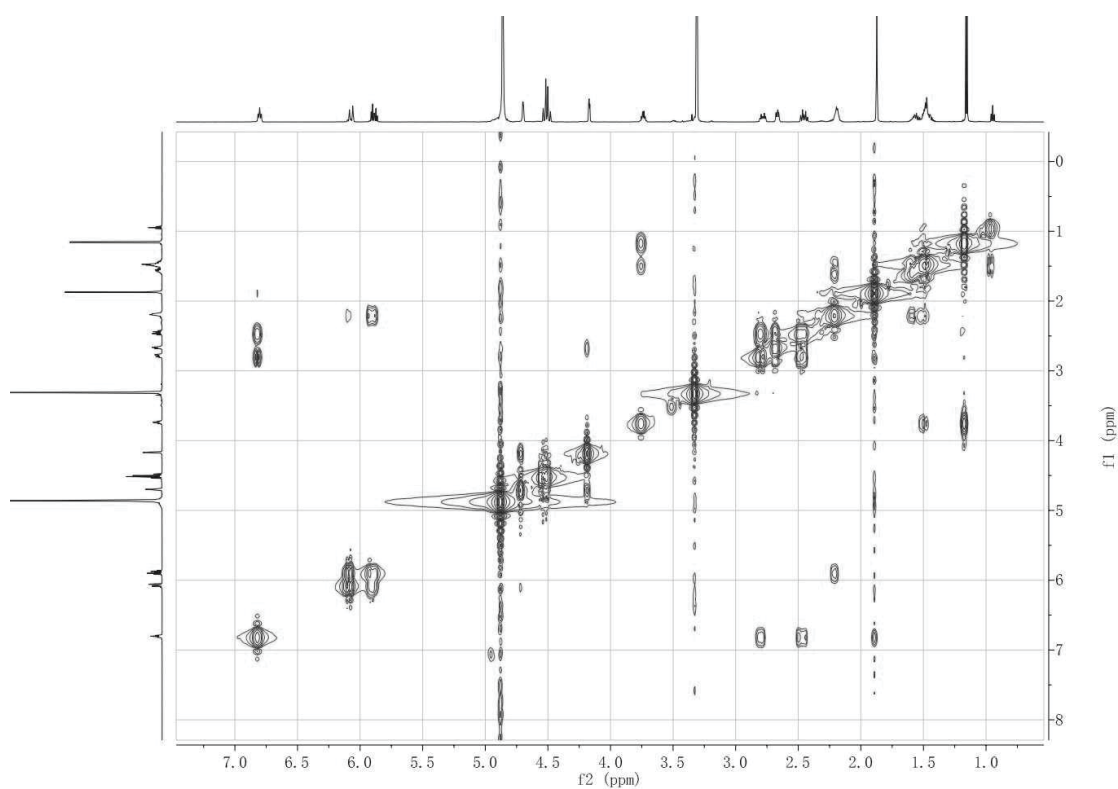


Figure S14. ^1H - ^1H COSY (300 MHz, CD_3OD) spectrum of 2.

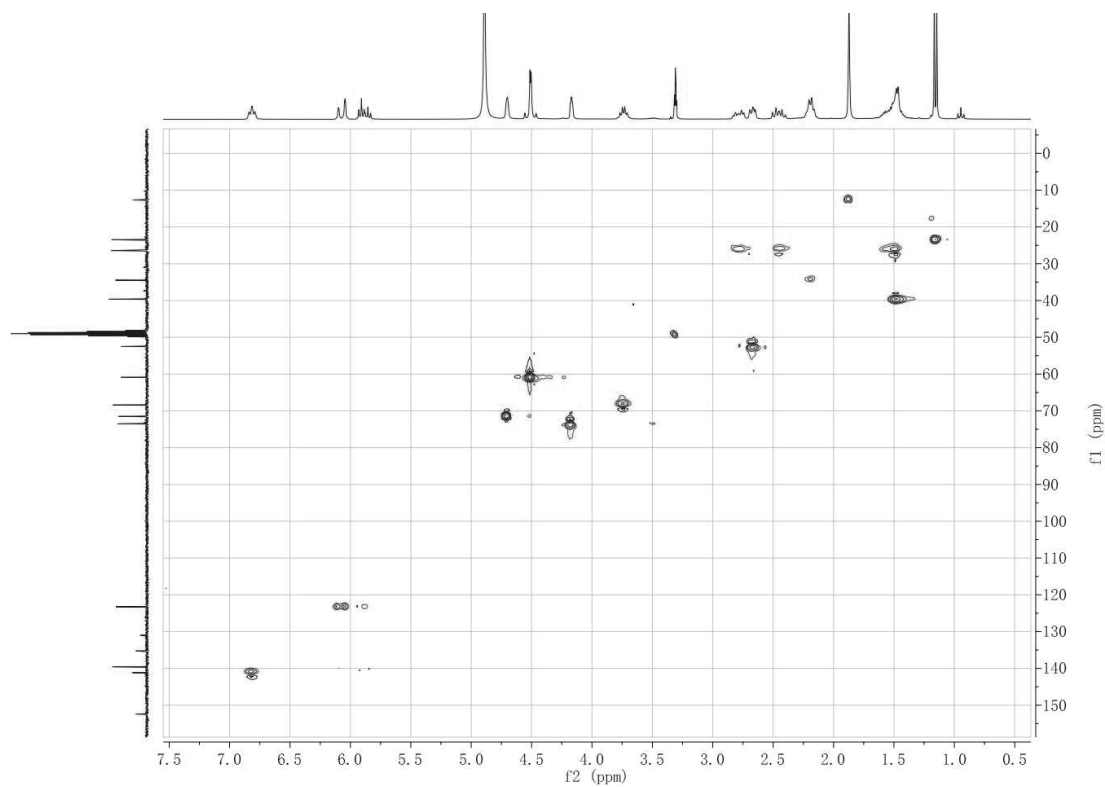


Figure S15. HSQC (300 MHz, CD₃OD) spectrum of **2**.

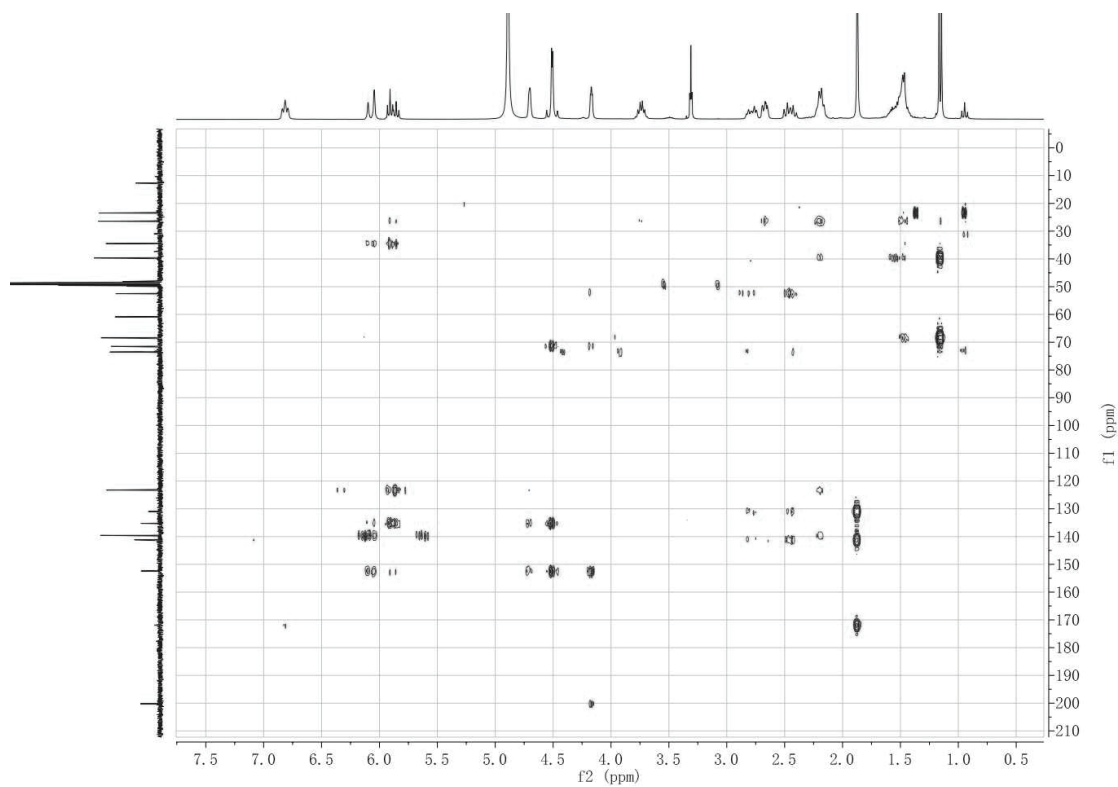


Figure S16. HMBC (300 MHz, CD₃OD) spectrum of **2**.

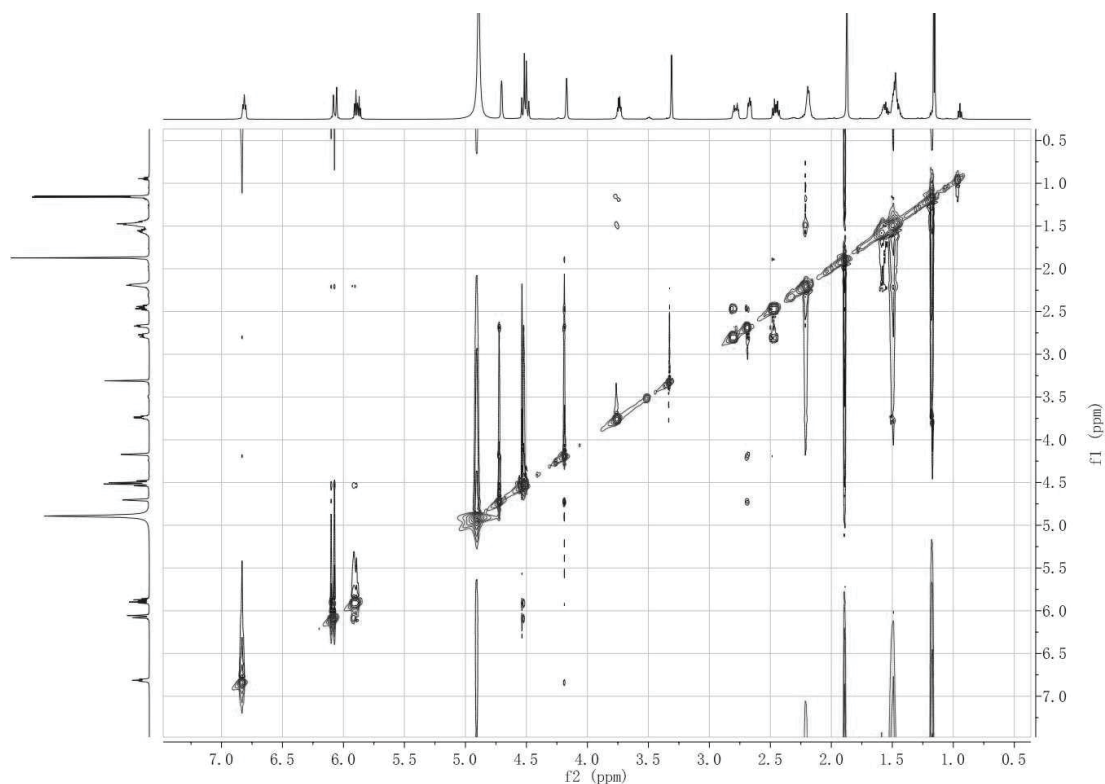


Figure S17. ROESY (600 MHz, CD₃OD) spectrum of **2**.

Acquisition Parameter

Source Type	ESI	Ion Polarity	Positive	Set Nebulizer	0.3 Bar
Focus	Not active	Set Capillary	4000 V	Set Dry Heater	180 °C
Scan Begin	50 m/z	Set End Plate Offset	-500 V	Set Dry Gas	4.0 l/min
Scan End	1500 m/z	Set Collision Cell RF	600.0 Vpp	Set Divert Valve	Source

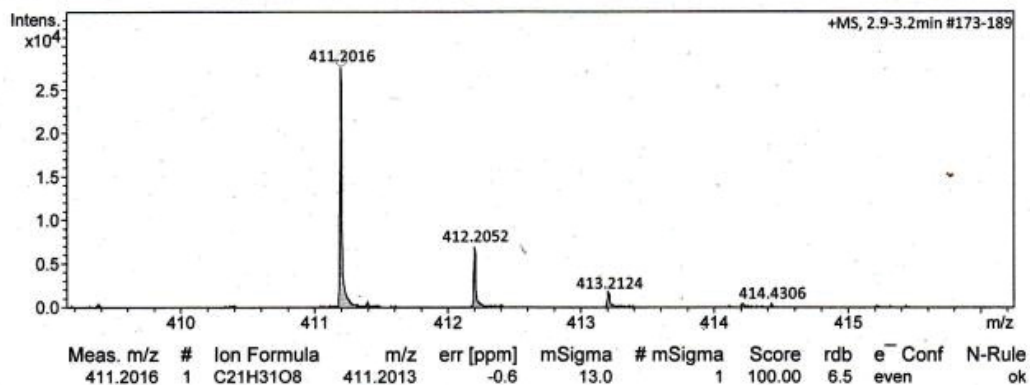


Figure S18. HRESIMS of **3**.

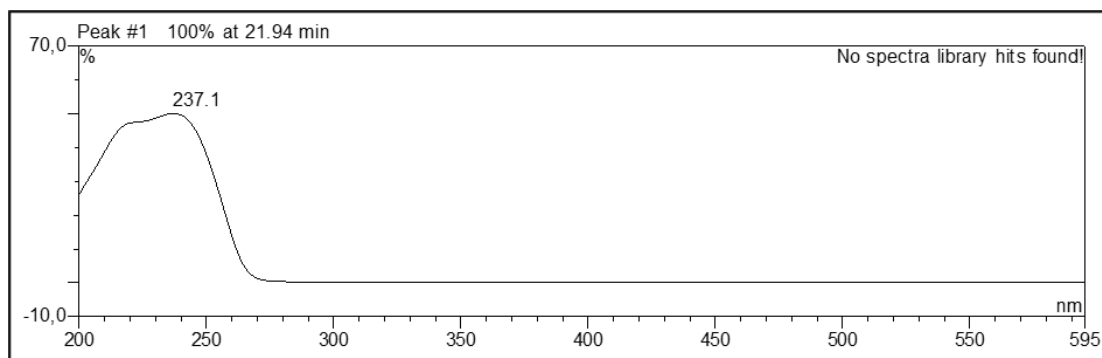


Figure S19. UV spectrum of **3**.

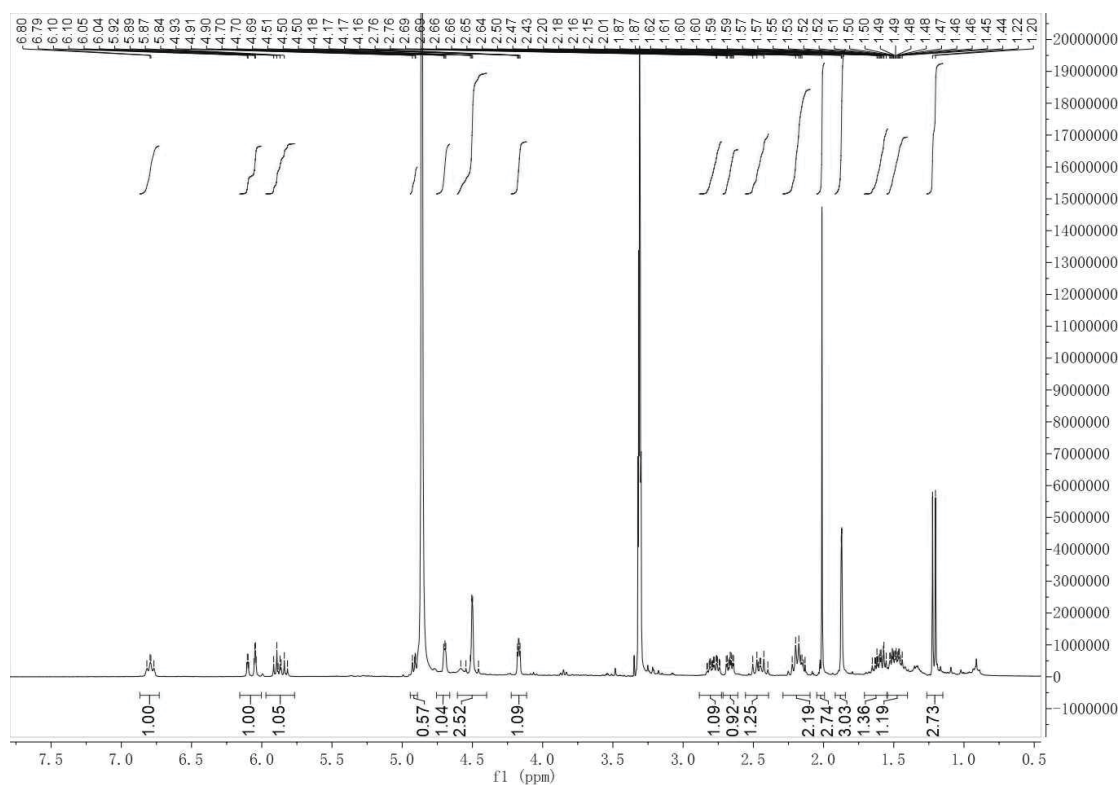


Figure S20. ^1H -NMR (600 MHz, CD_3OD) spectrum of **3**.

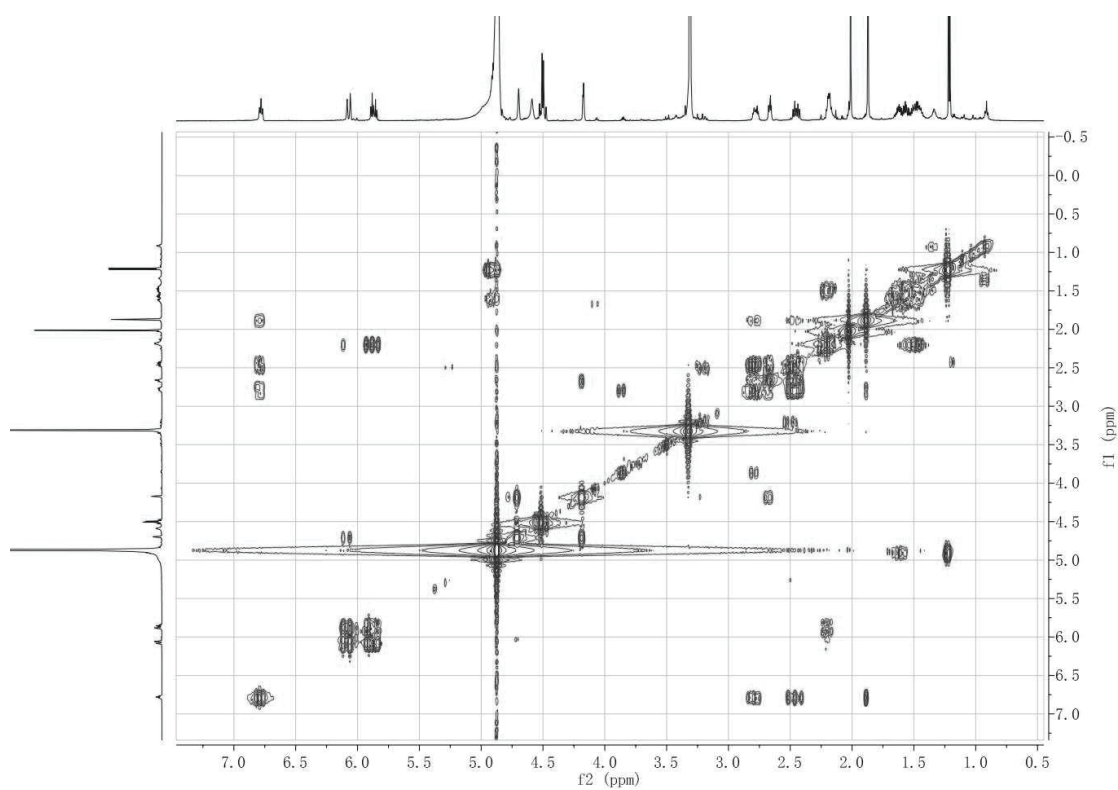


Figure S21. ^1H - ^1H COSY (600 MHz, CD_3OD) spectrum of **3**.

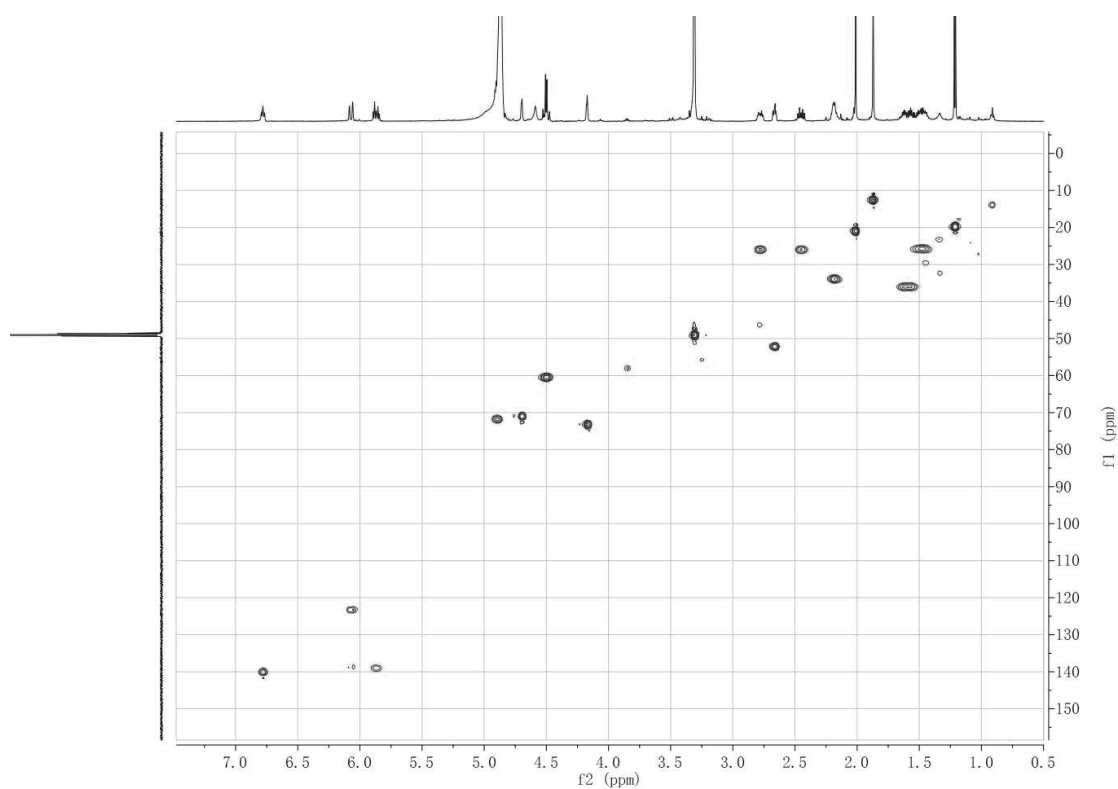


Figure S22. HSQC (600 MHz, CD_3OD) spectrum of **3**.

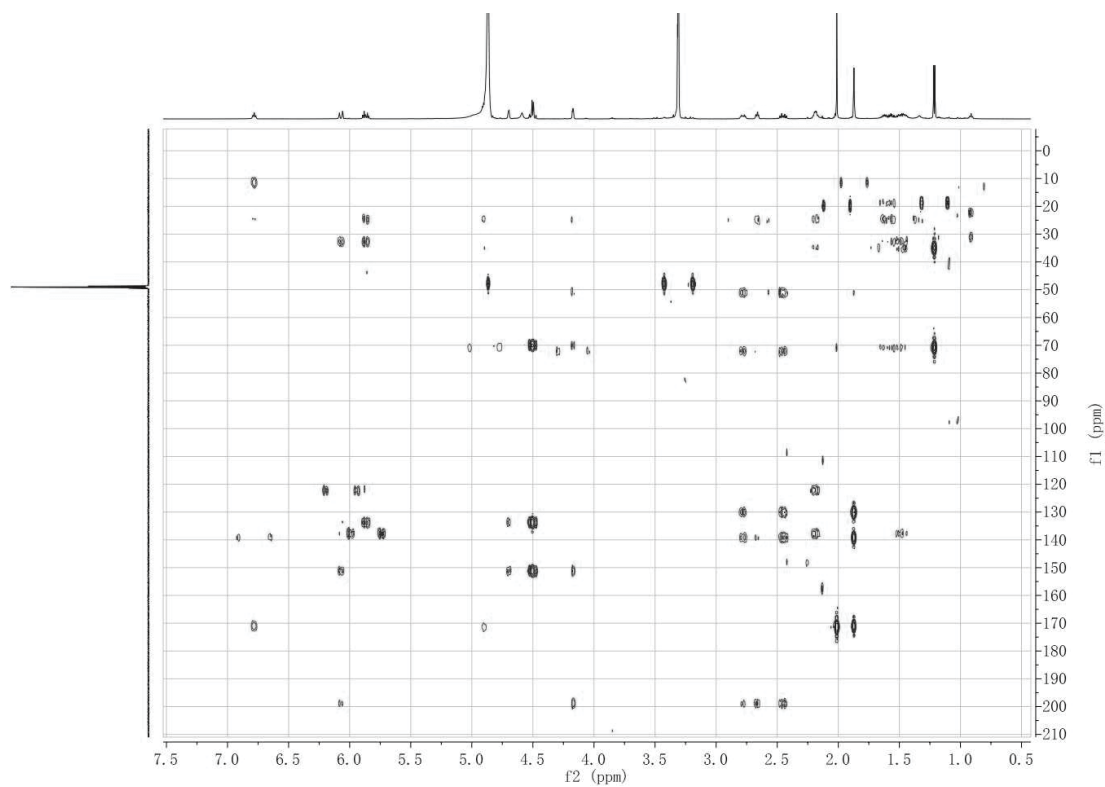


Figure S23. HMBC (600 MHz, CD₃OD) spectrum of **3**.

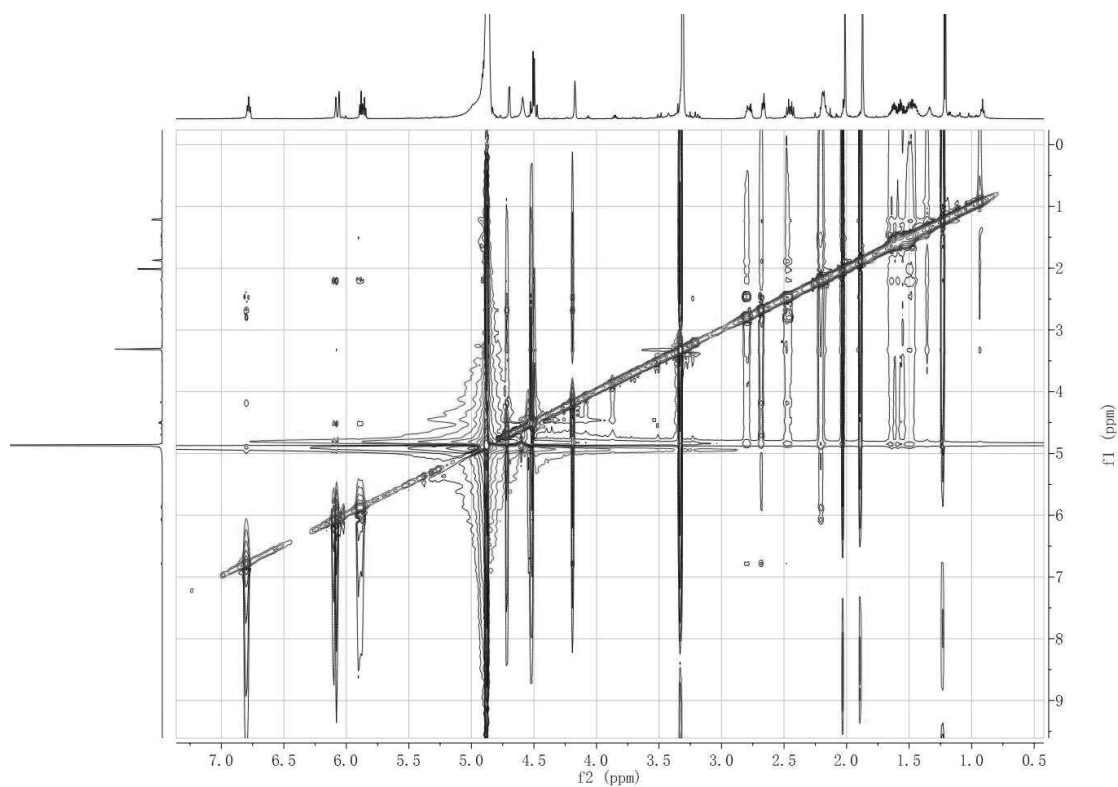
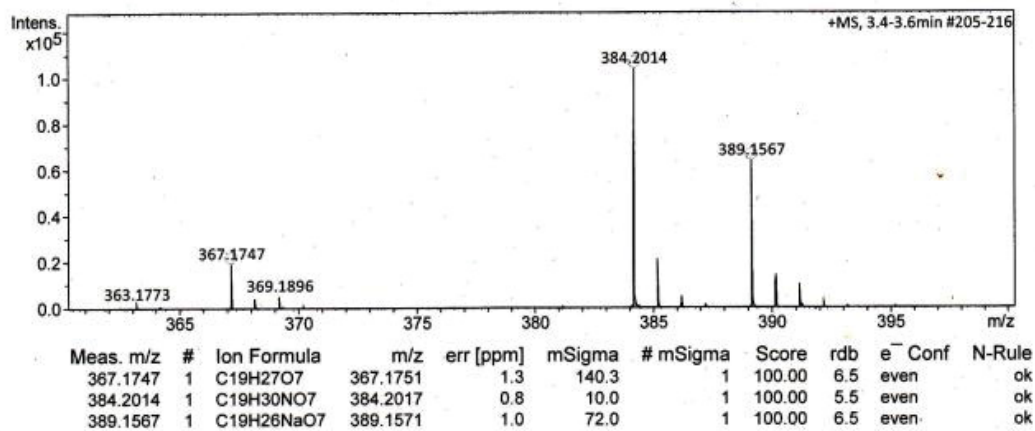
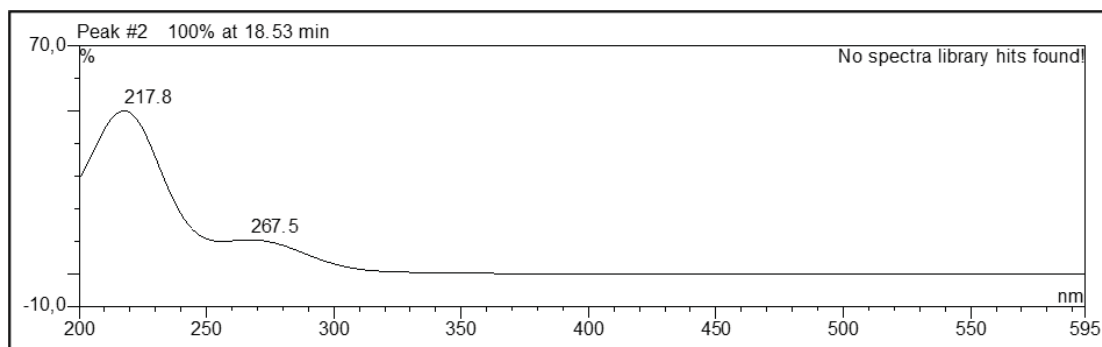


Figure S24. ROESY (600 MHz, CD₃OD) spectrum of **3**.

Acquisition Parameter

Source Type	ESI	Ion Polarity	Positive	Set Nebulizer	0.3 Bar
Focus	Not active	Set Capillary	4000 V	Set Dry Heater	180 °C
Scan Begin	50 m/z	Set End Plate Offset	-500 V	Set Dry Gas	4.0 l/min
Scan End	1500 m/z	Set Collision Cell RF	600.0 Vpp	Set Divert Valve	Source

**Figure S25.** HRESIMS of **4**.**Figure S26.** UV spectrum of **4**.

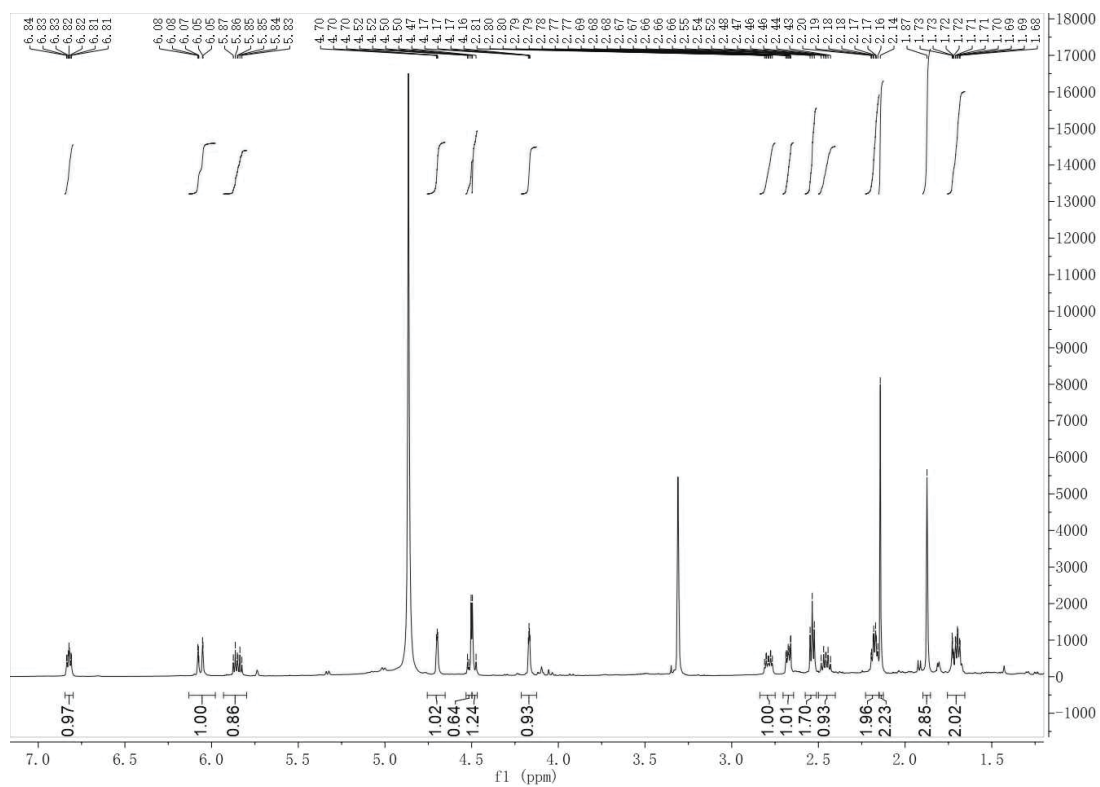


Figure S27. ¹H-NMR (600 MHz, CD₃OD) spectrum of 4.

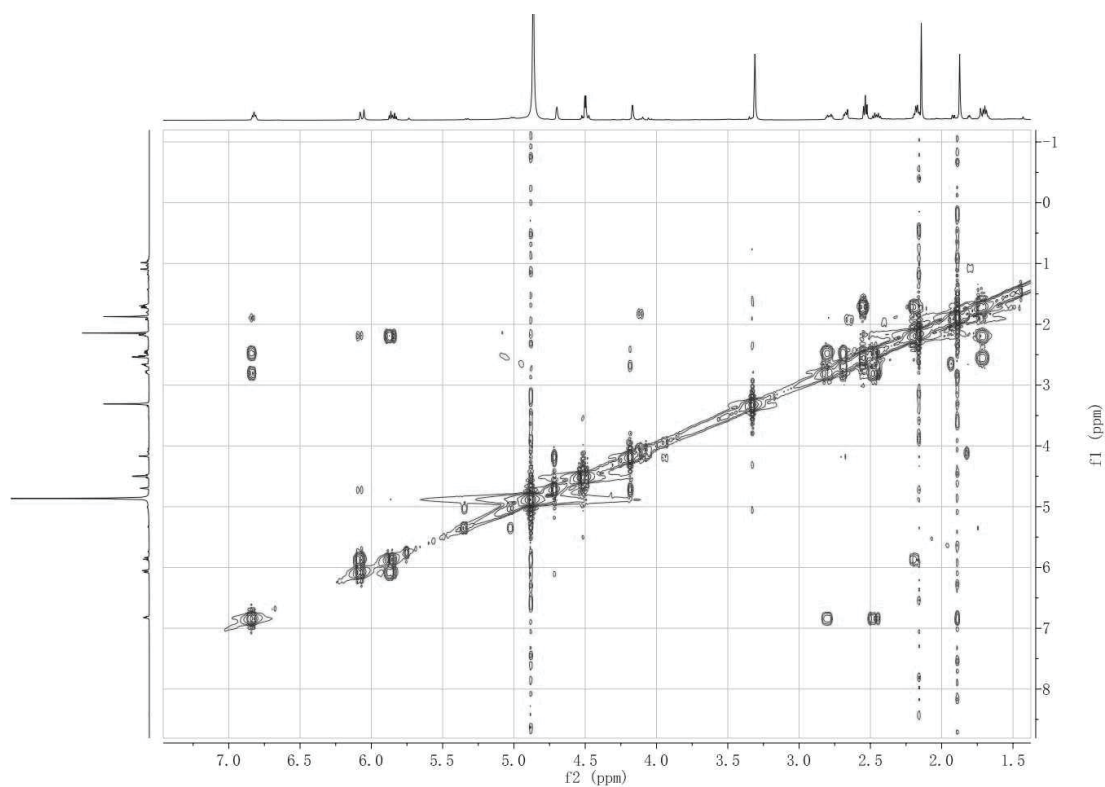


Figure S28. ¹H-¹H COSY (600 MHz, CD₃OD) spectrum of 4.

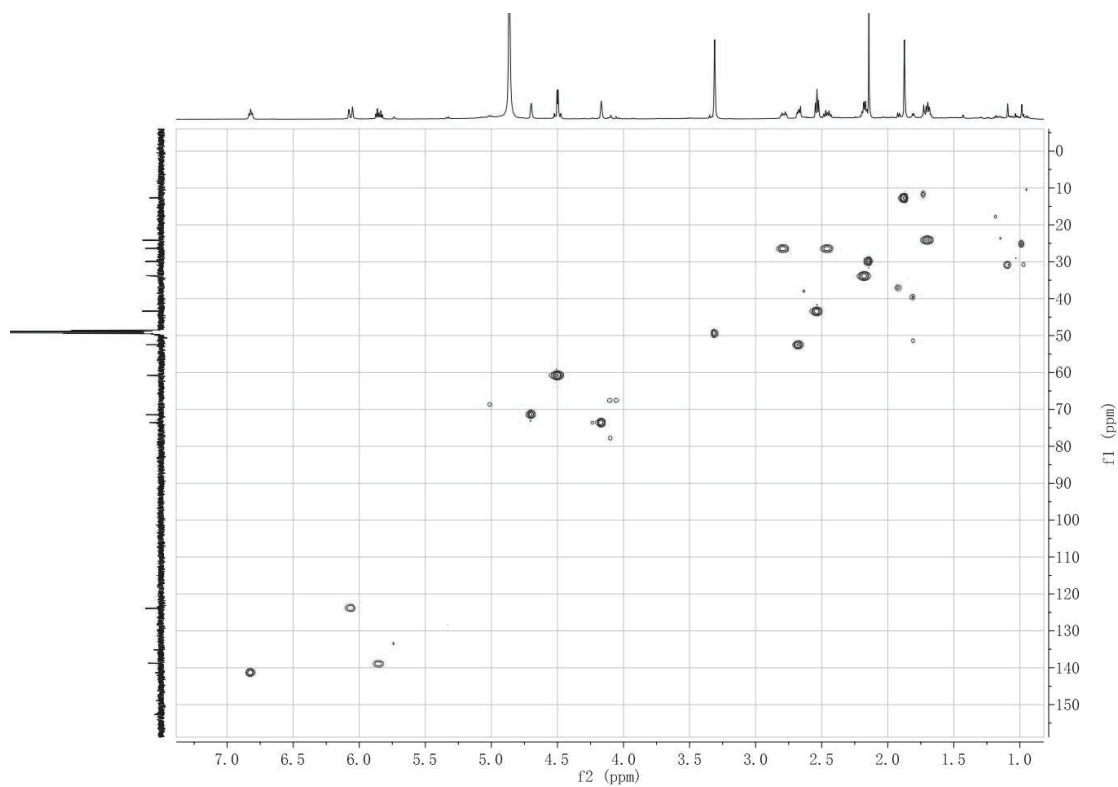


Figure S29. HSQC (600 MHz, CD₃OD) spectrum of **4**.

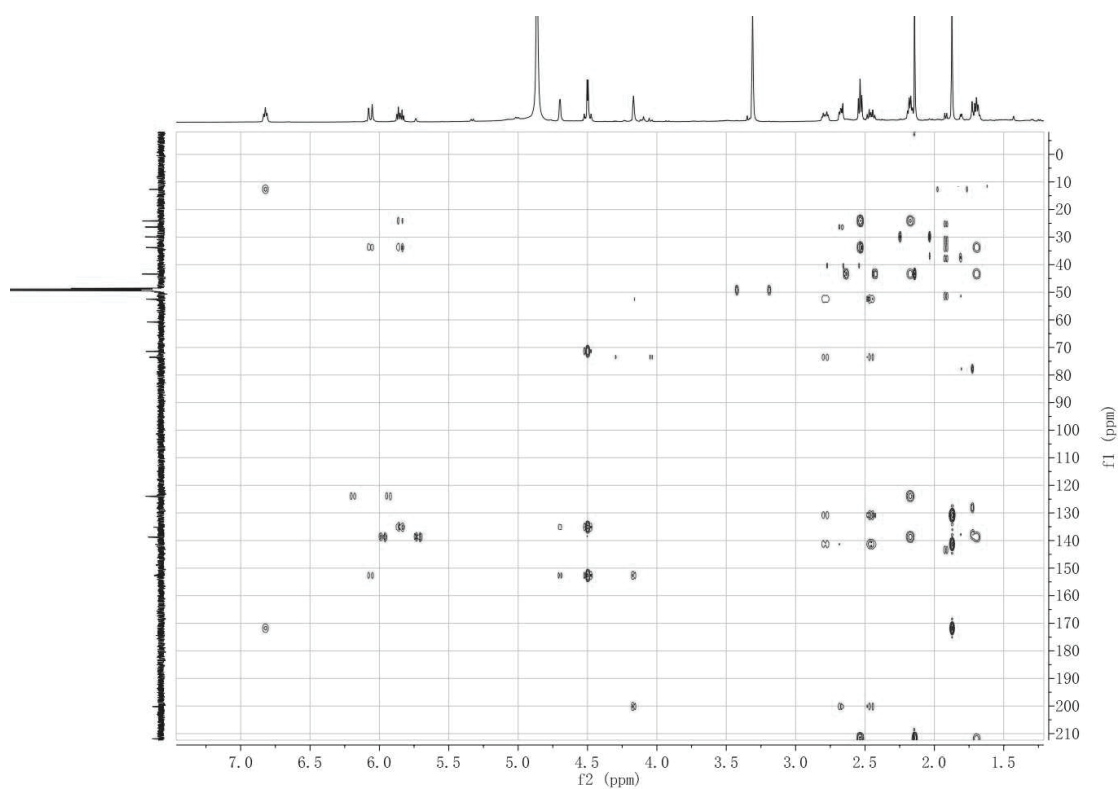


Figure S30. HMBC (600 MHz, CD₃OD) spectrum of **4**.

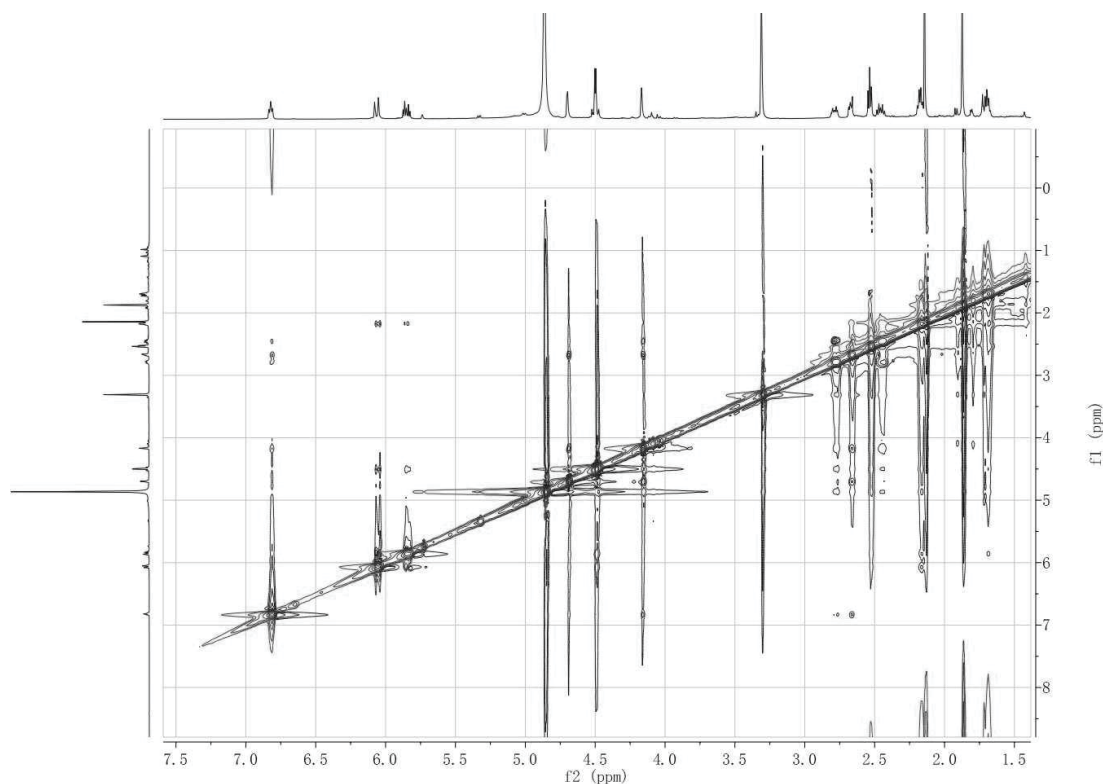
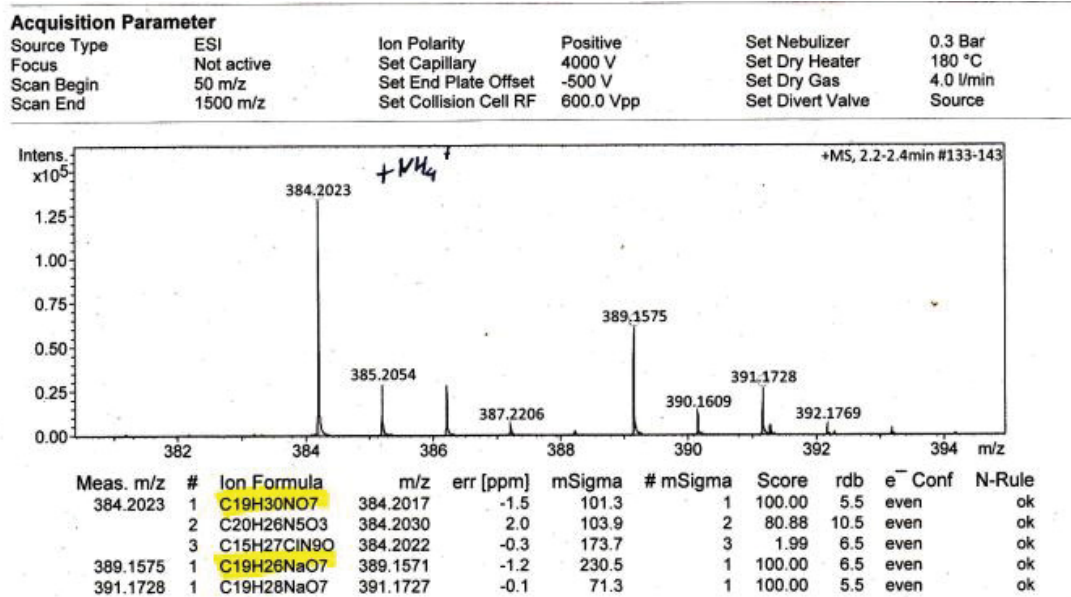
Figure S31. ROESY (600 MHz, CD₃OD) spectrum of 4.

Figure S32. HRESIMS of 5.

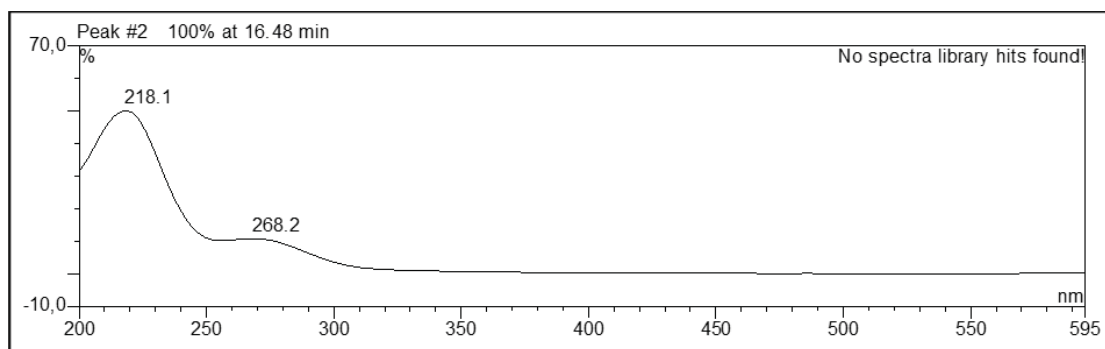


Figure S33. UV spectrum of **5**.

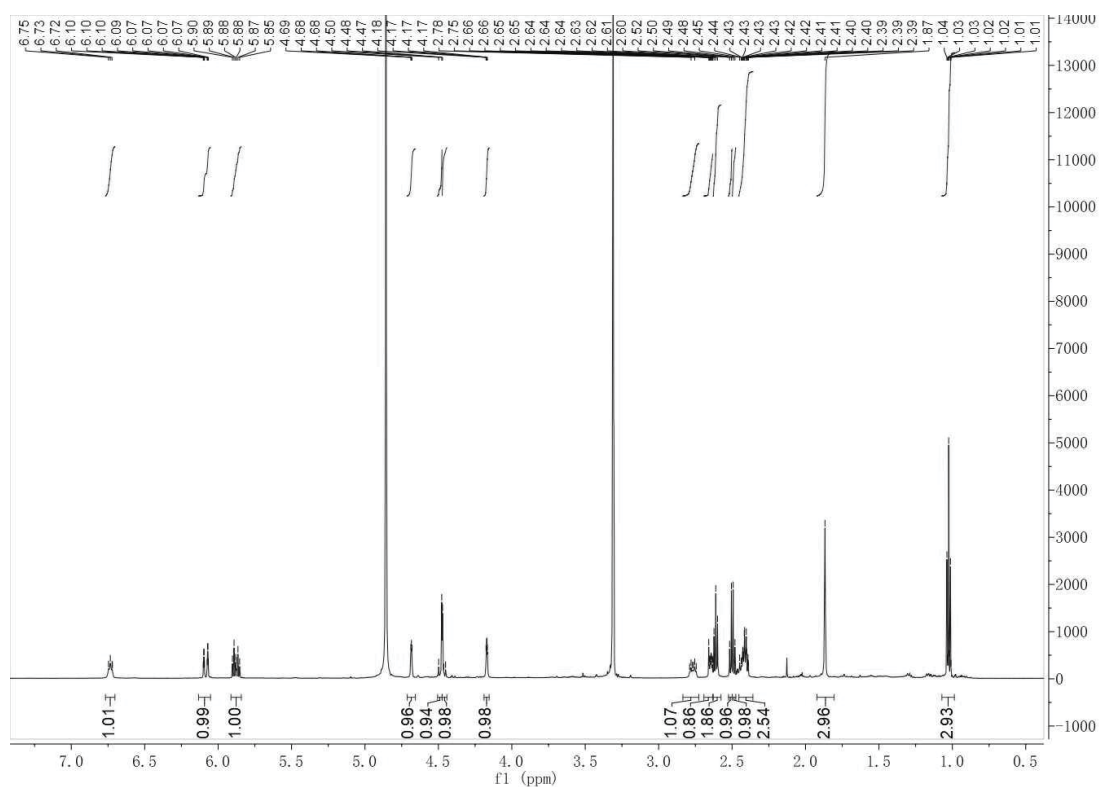


Figure S34. ^1H -NMR (600 MHz, CD_3OD) spectrum of **5**.

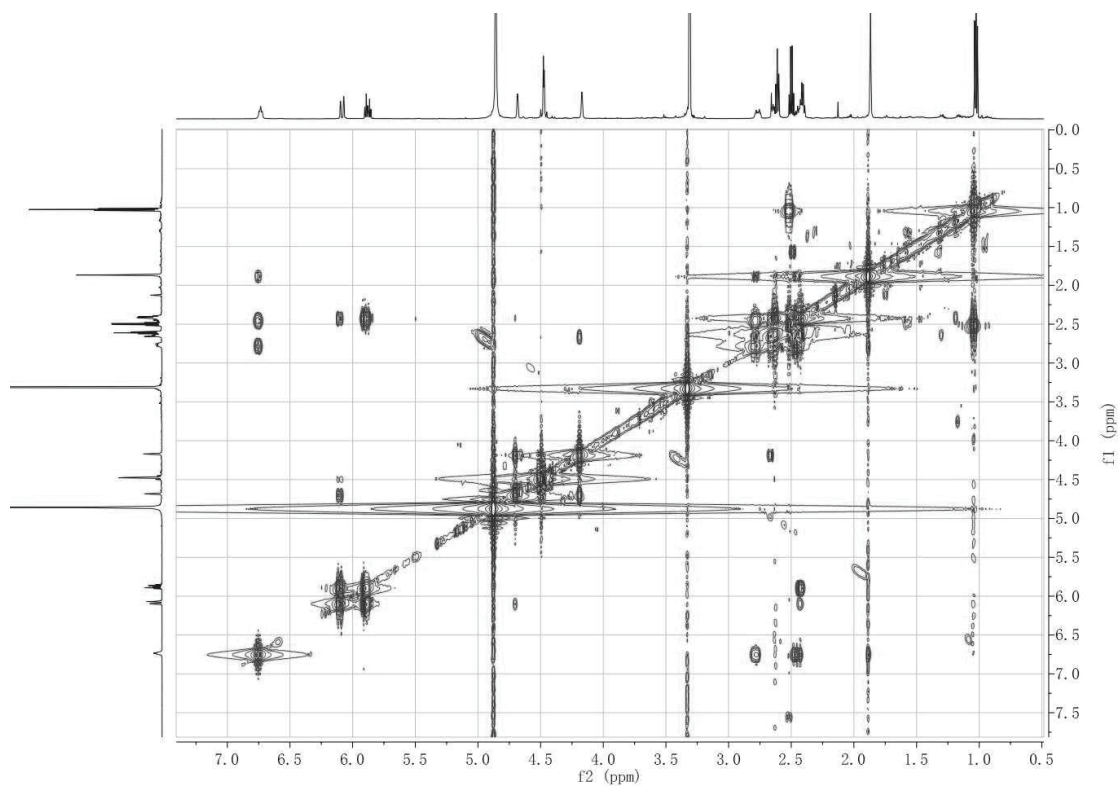


Figure S35. ^1H - ^1H COSY (600 MHz, CD_3OD) spectrum of **5**.

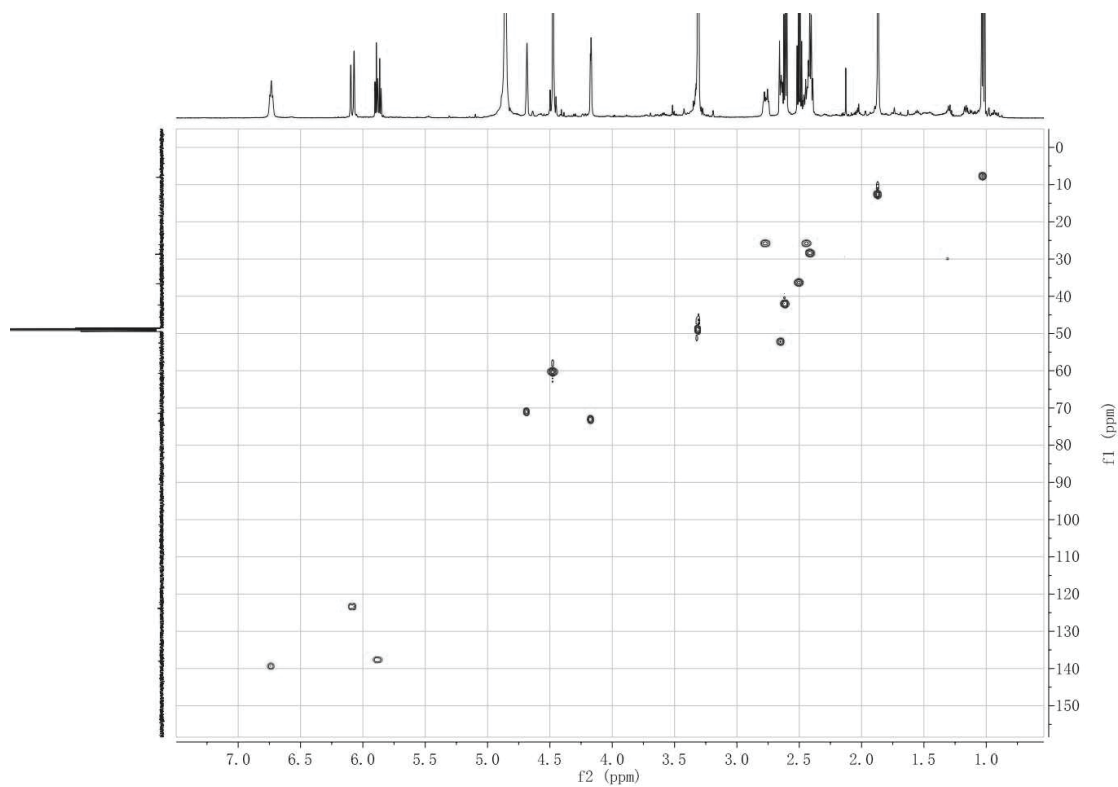


Figure S36. HSQC (600 MHz, CD_3OD) spectrum of **5**.

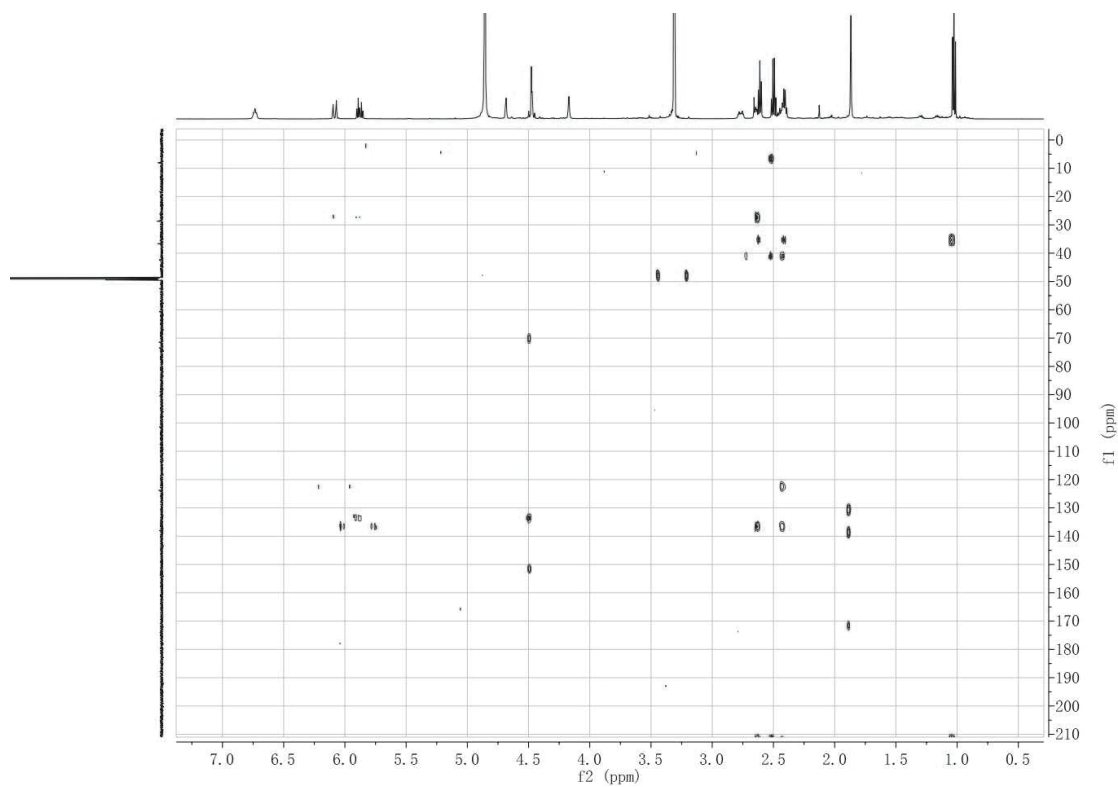


Figure S37. HMBC (600 MHz, CD₃OD) spectrum of **5**.

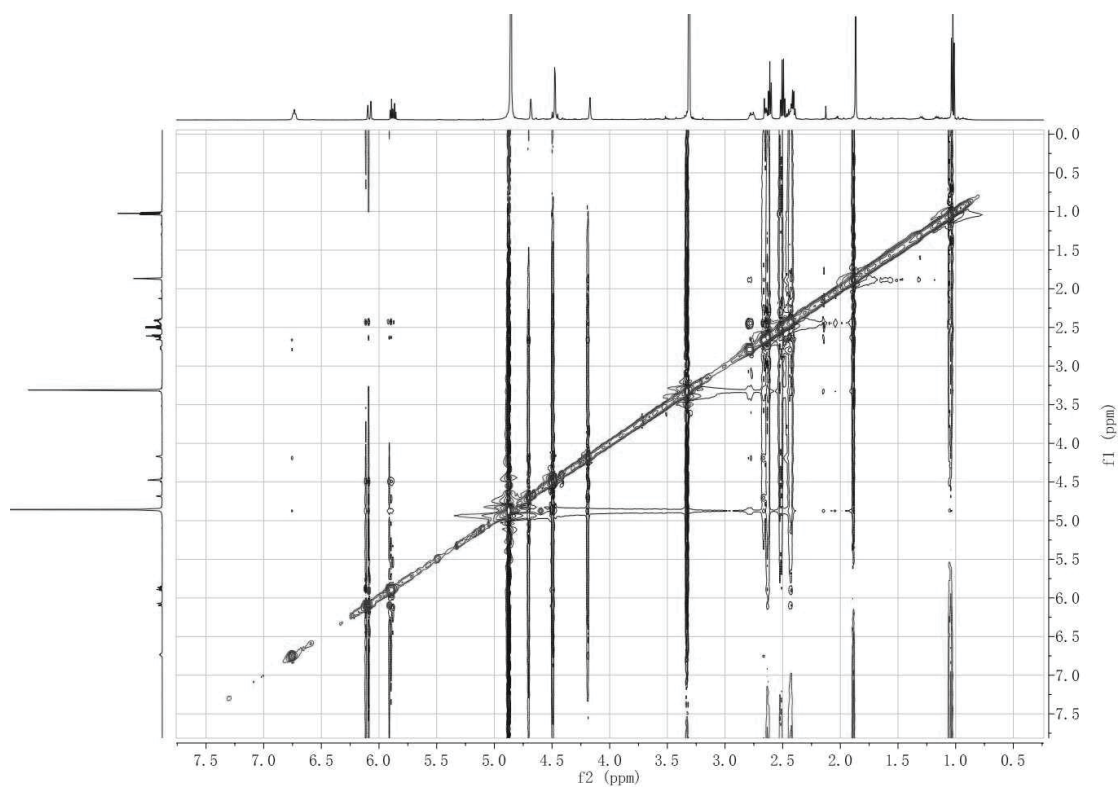
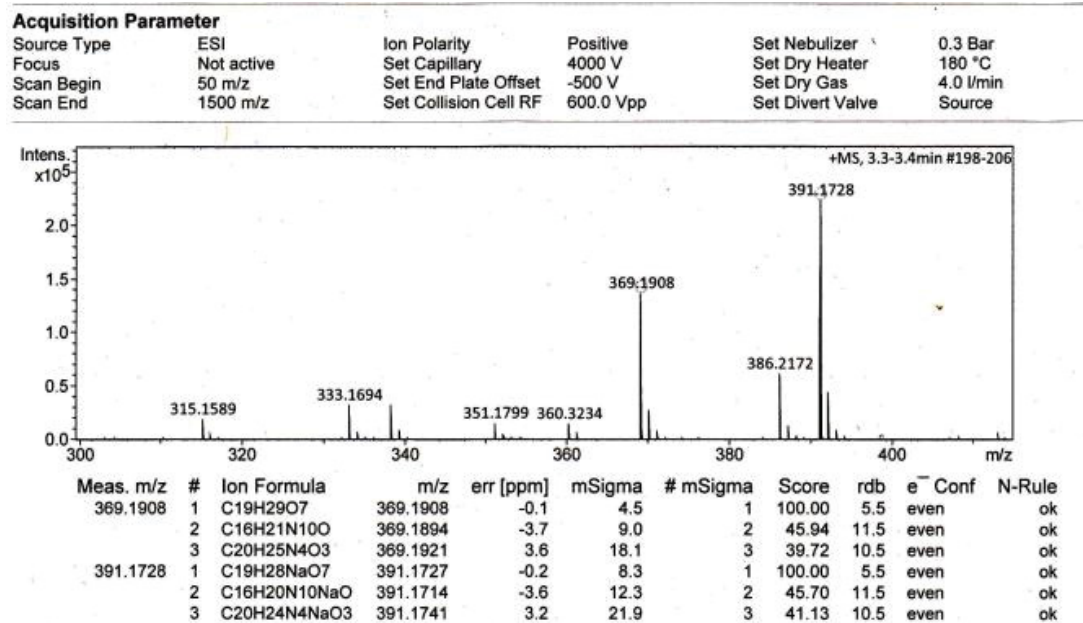
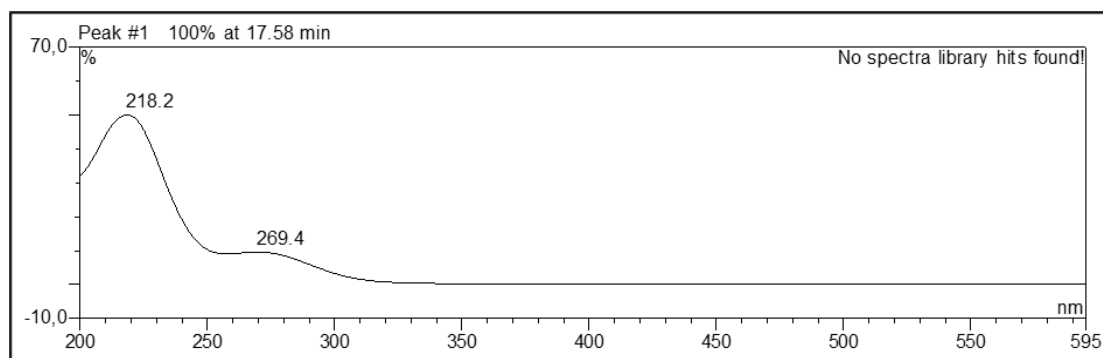
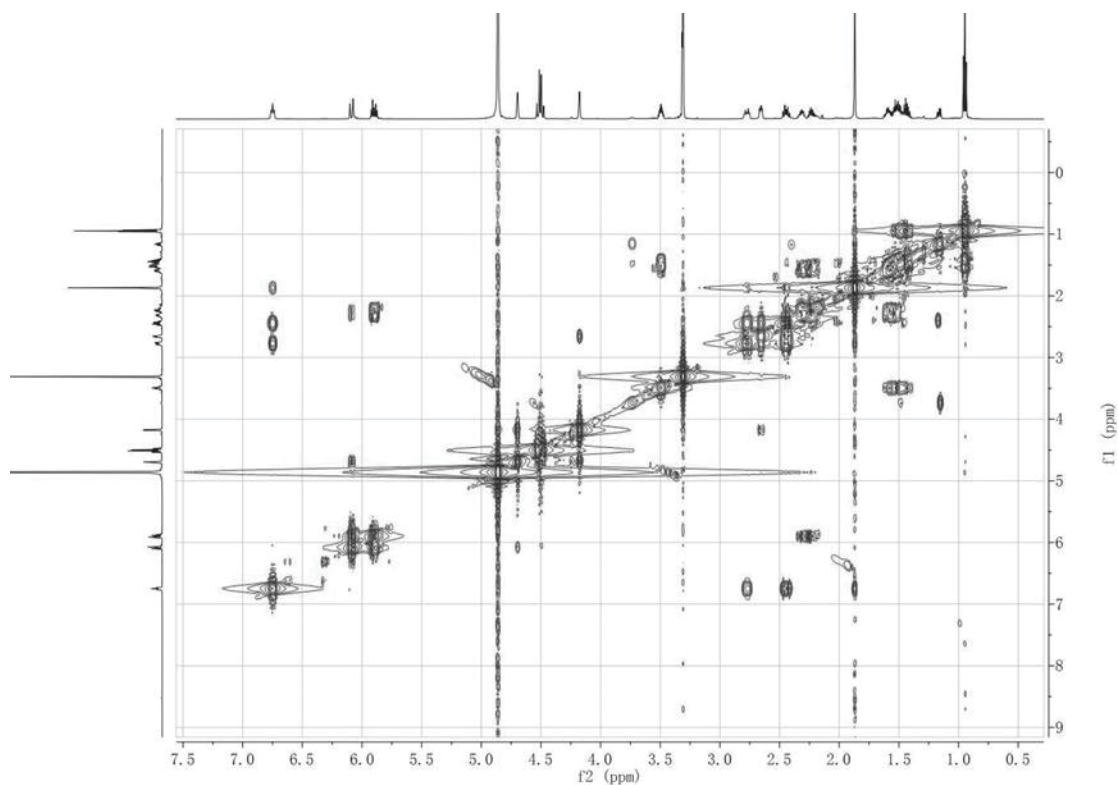
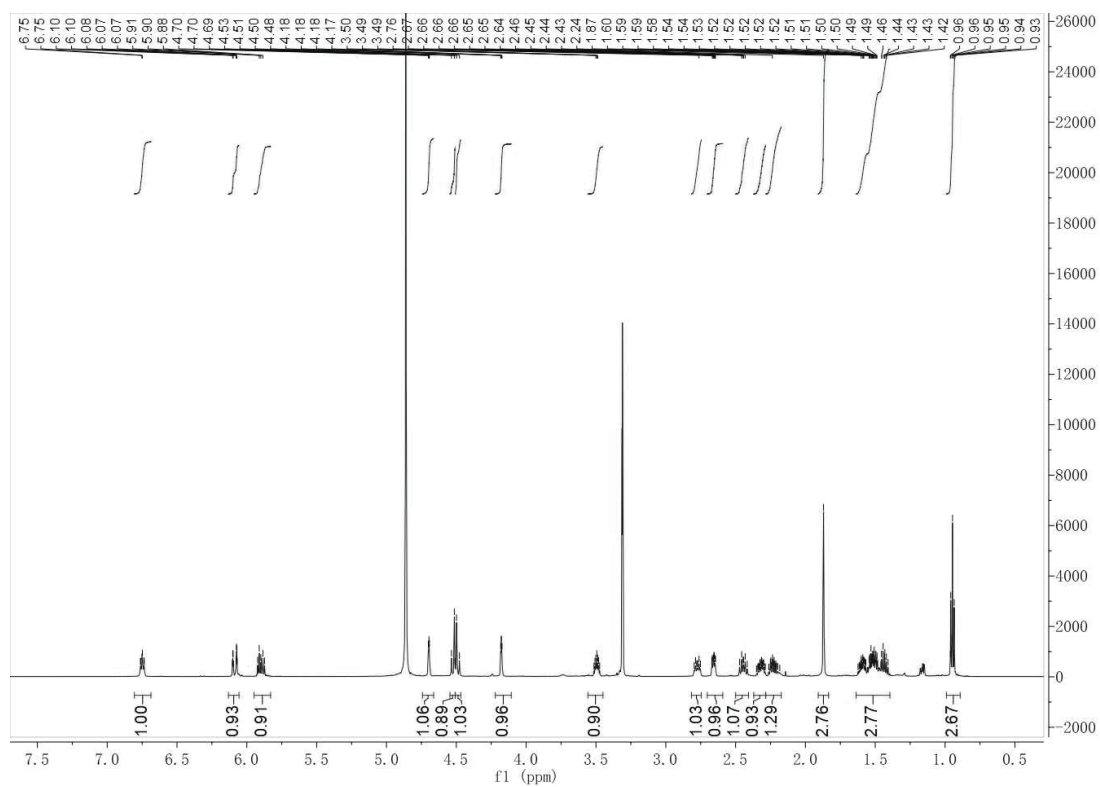


Figure S38. ROESY (600 MHz, CD₃OD) spectrum of **5**.

Figure S39. HRESIMS of **6**.Figure S40. UV spectrum of **6**.



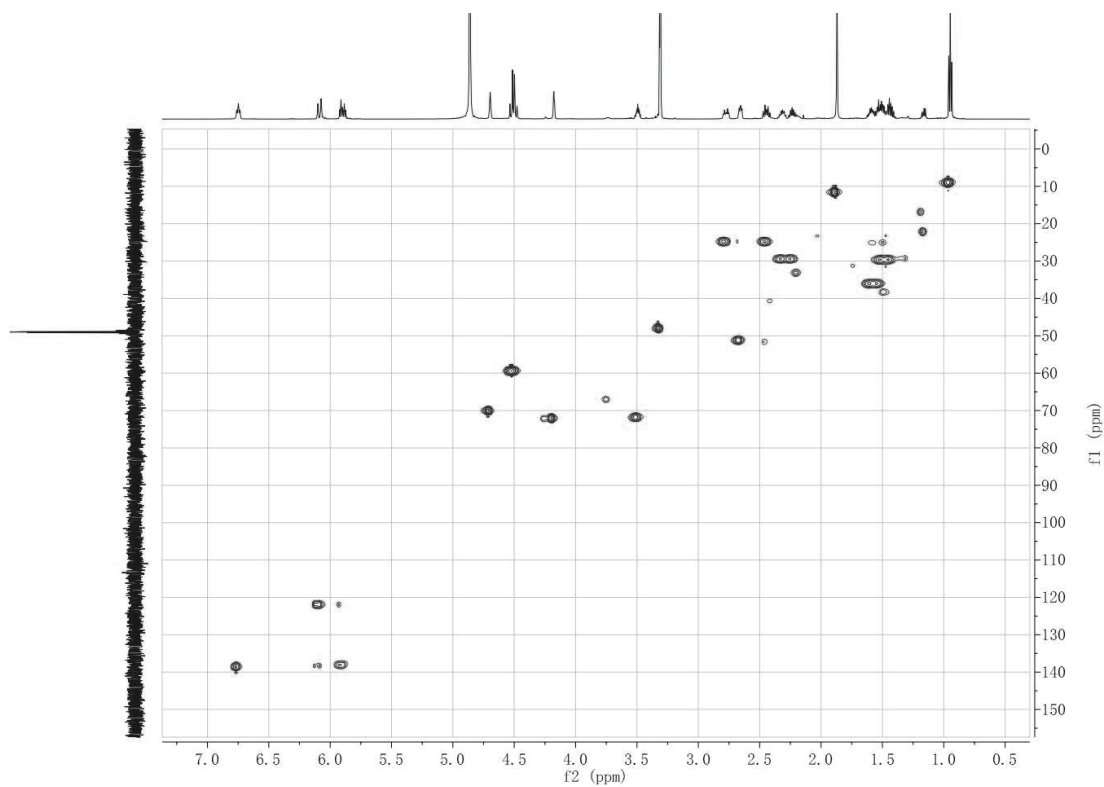


Figure S43. HSQC (600 MHz, CD₃OD) spectrum of **6**.

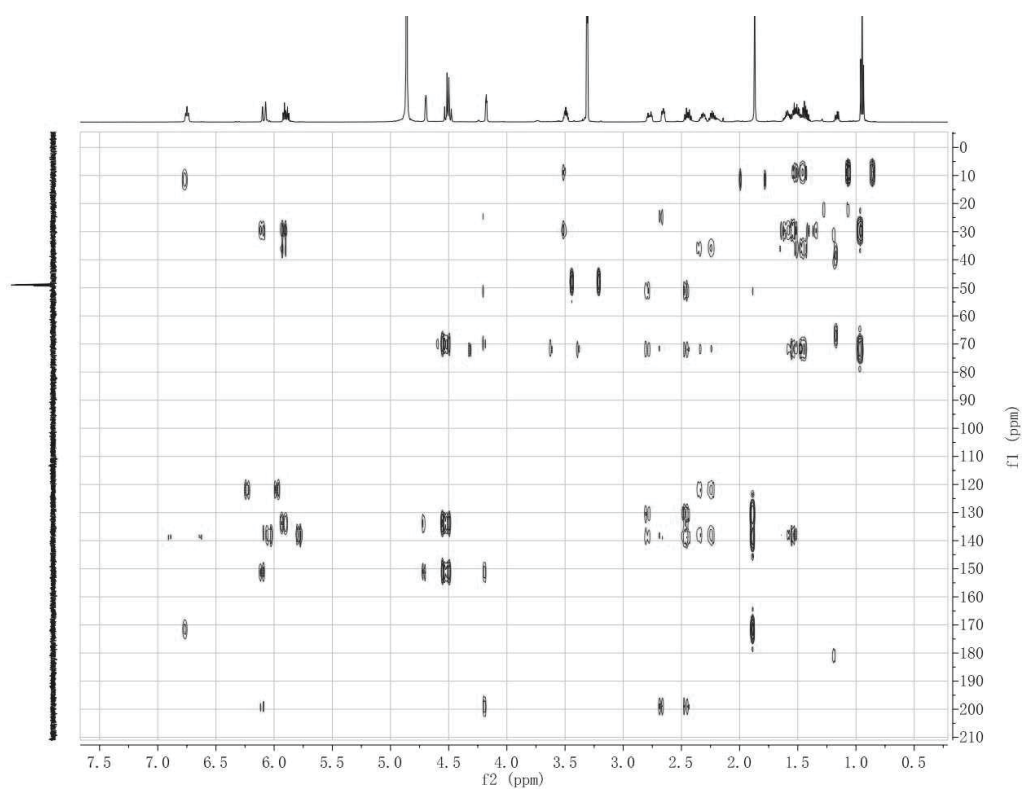
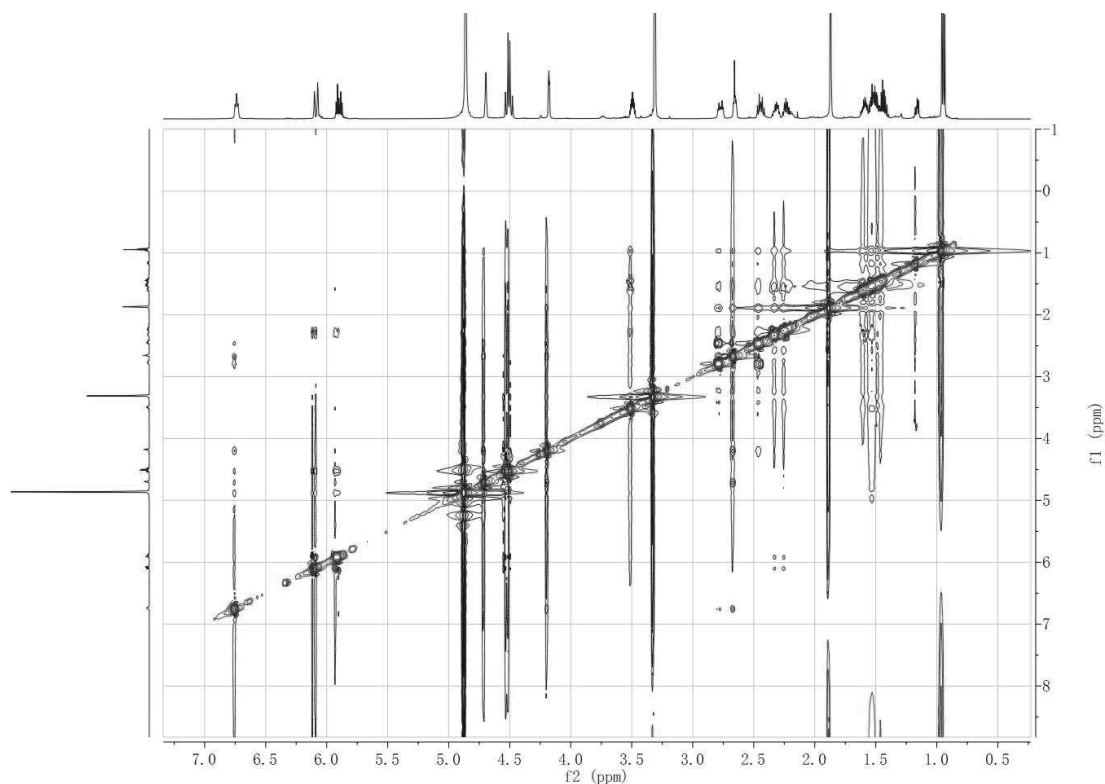
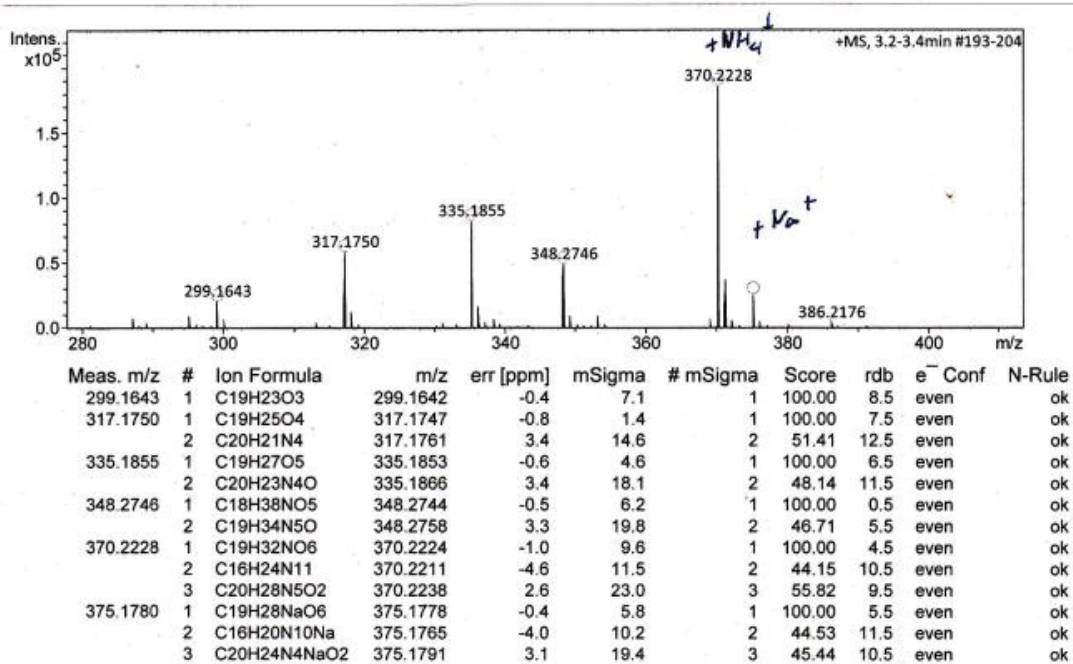


Figure S44. HMBC (600 MHz, CD₃OD) spectrum of **6**.

Figure S45. ROESY (600 MHz, CD₃OD) spectrum of **6**.**Acquisition Parameter**

Source Type	ESI	Ion Polarity	Positive	Set Nebulizer	0.3 Bar
Focus	Not active	Set Capillary	4000 V	Set Dry Heater	180 °C
Scan Begin	50 m/z	Set End Plate Offset	-500 V	Set Dry Gas	4.0 l/min
Scan End	1500 m/z	Set Collision Cell RF	600.0 Vpp	Set Divert Valve	Source

Figure S46. HRESIMS of **7**.

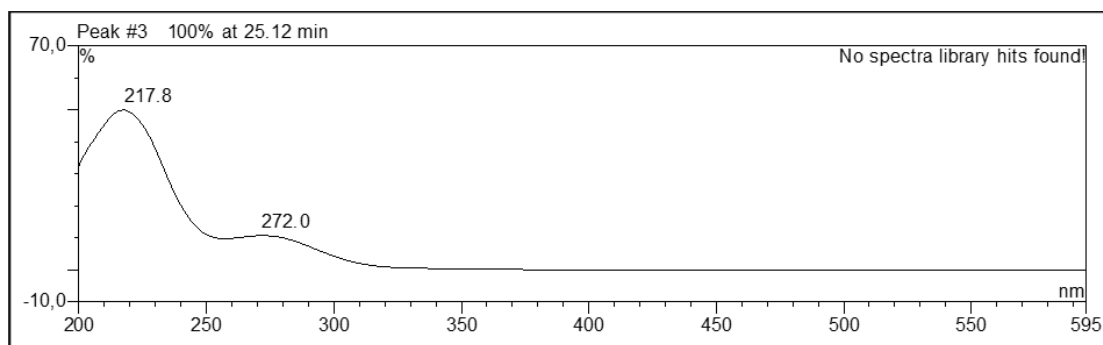


Figure S47. UV spectrum of **7**.

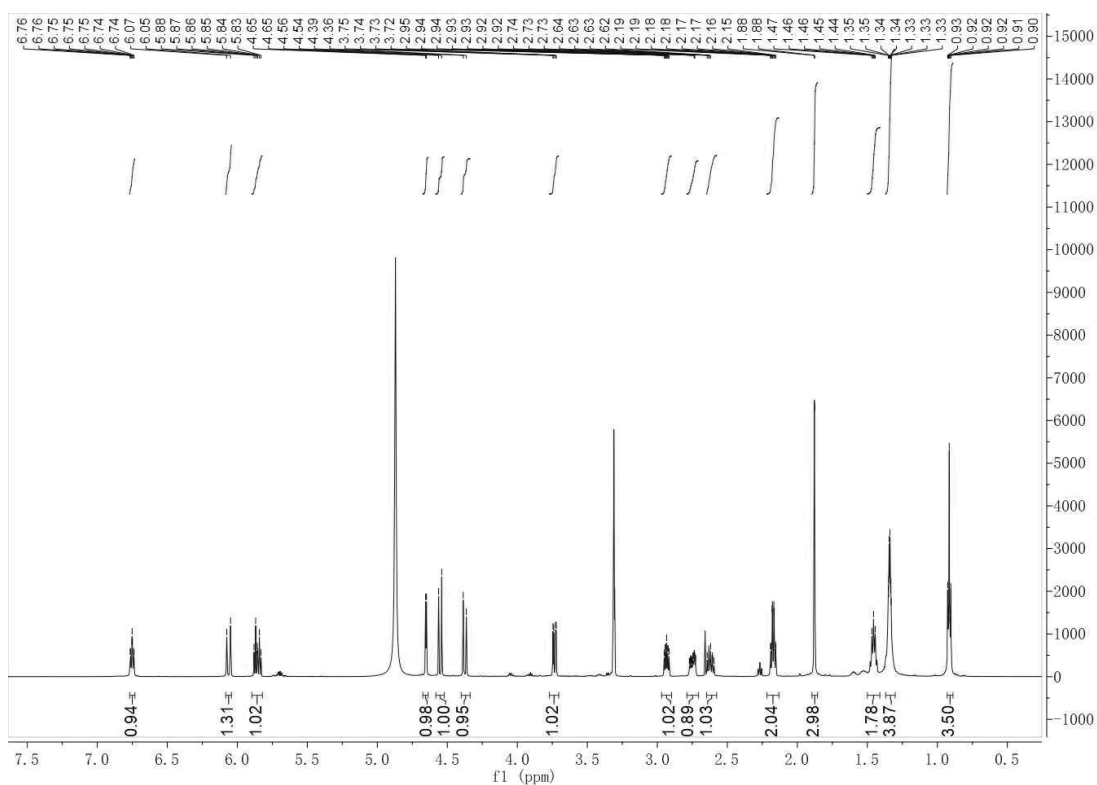


Figure S48. ^1H -NMR (300 MHz, CD_3OD) spectrum of **7**.

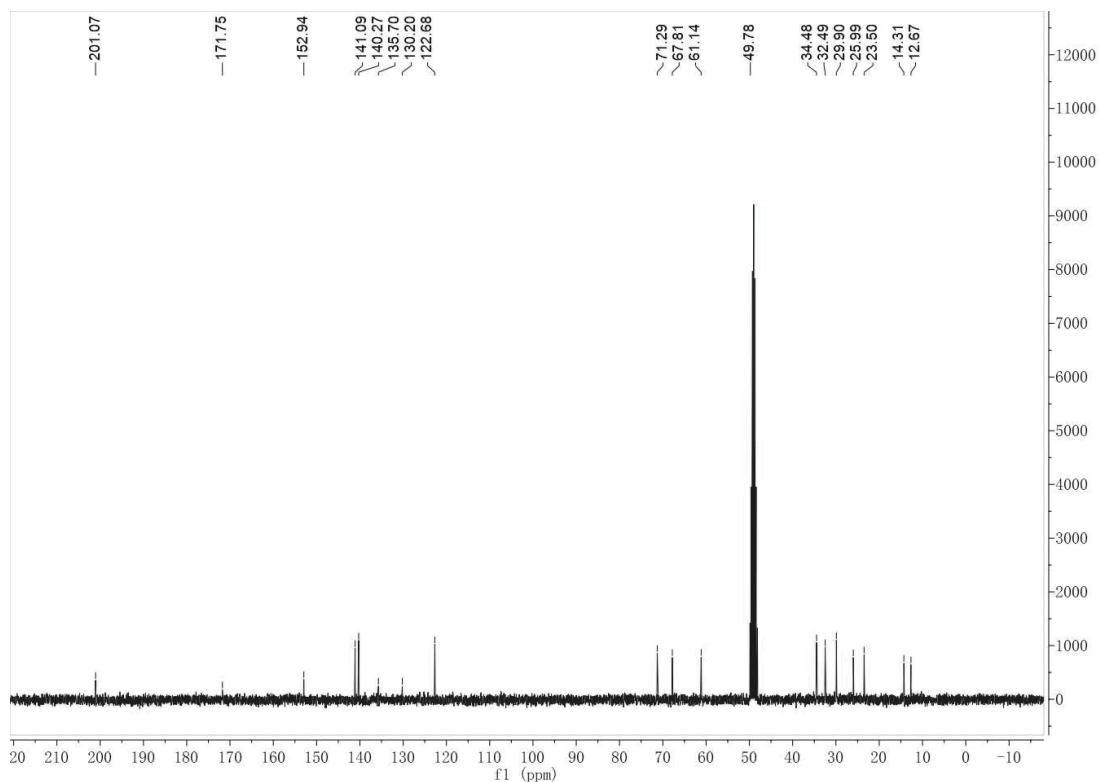


Figure S49. ^{13}C -NMR (75 MHz, CD_3OD) spectrum of 7.

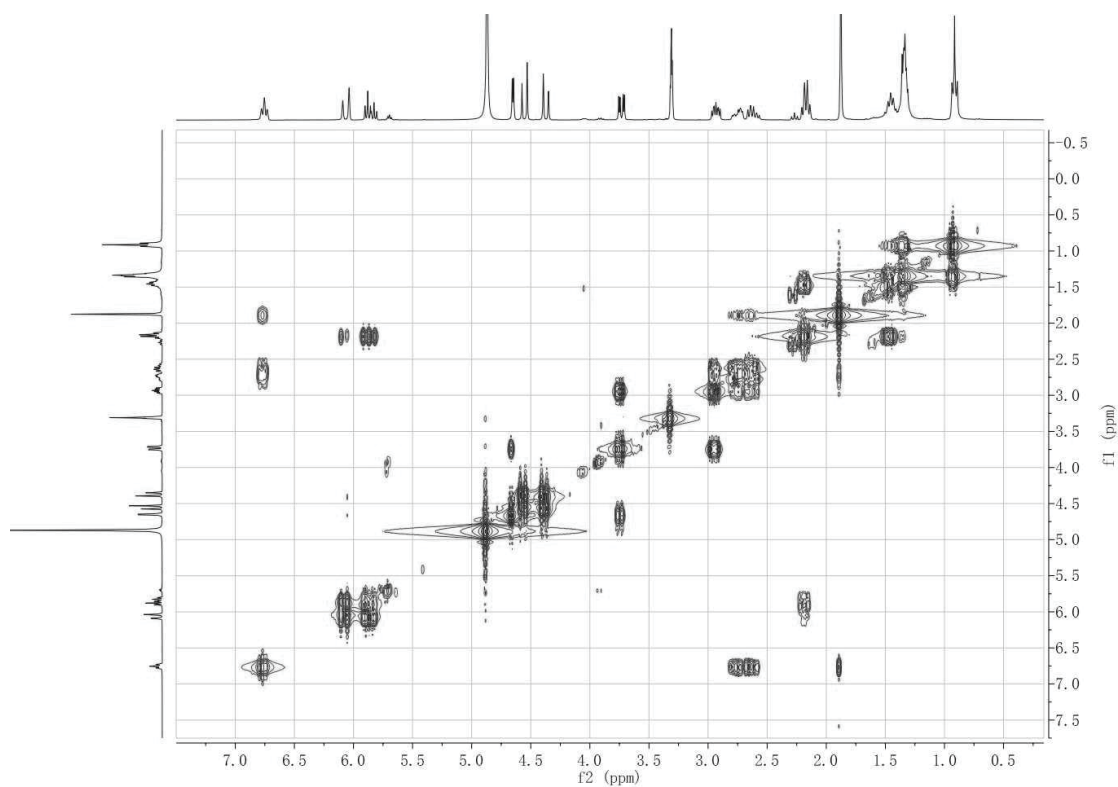


Figure S50. ^1H - ^1H COSY (300 MHz, CD_3OD) spectrum of 7.

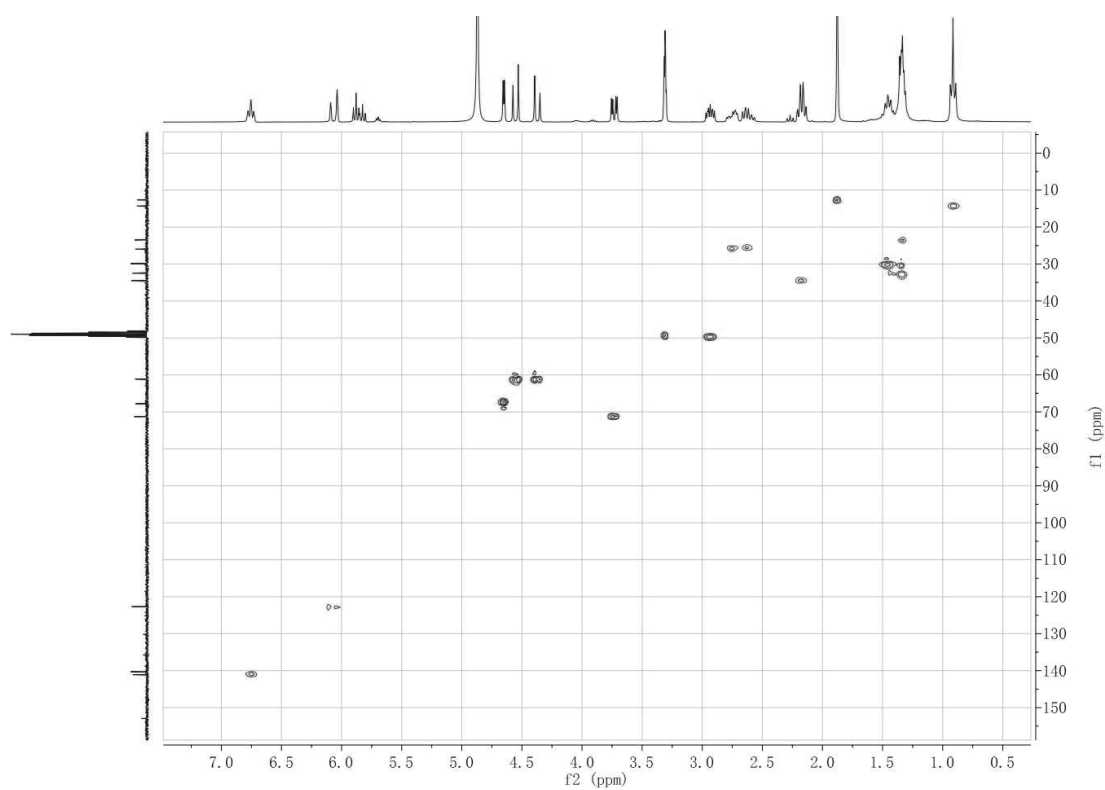


Figure S51. HSQC (300 MHz, CD₃OD) spectrum of **7**.

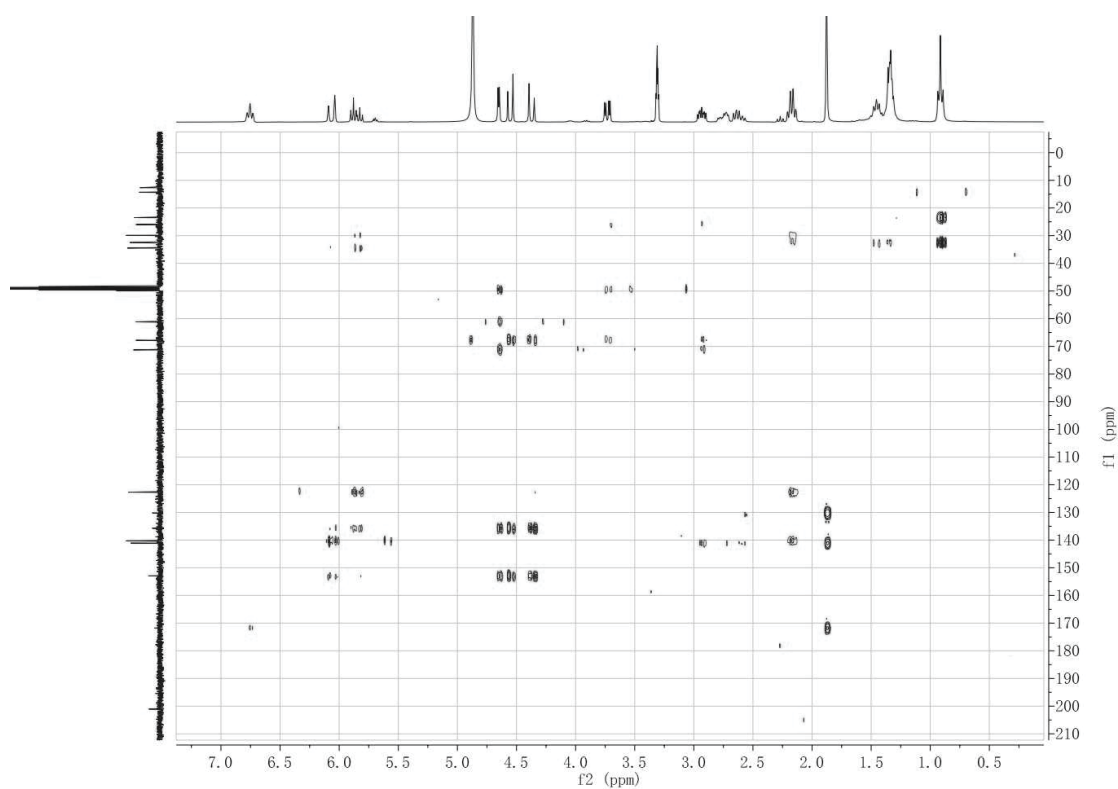


Figure S52. HMBC (300 MHz, CD₃OD) spectrum of **7**.

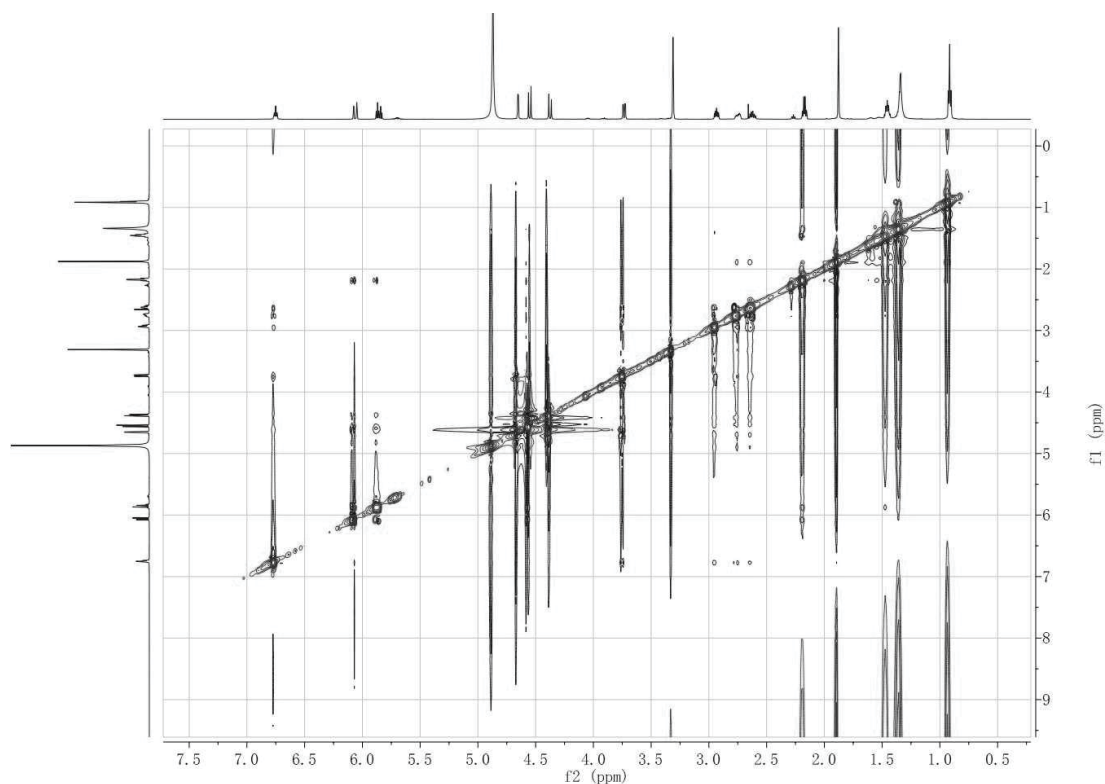


Figure S53. ROESY (600 MHz, DMSO- d_6) spectrum of **7**.

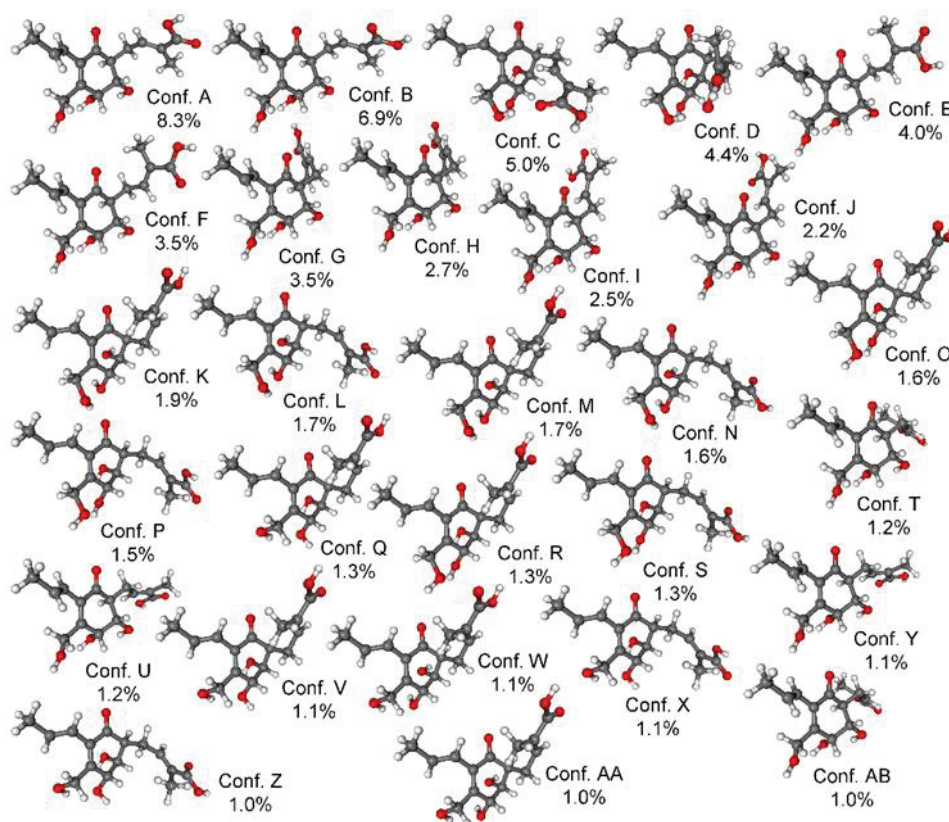
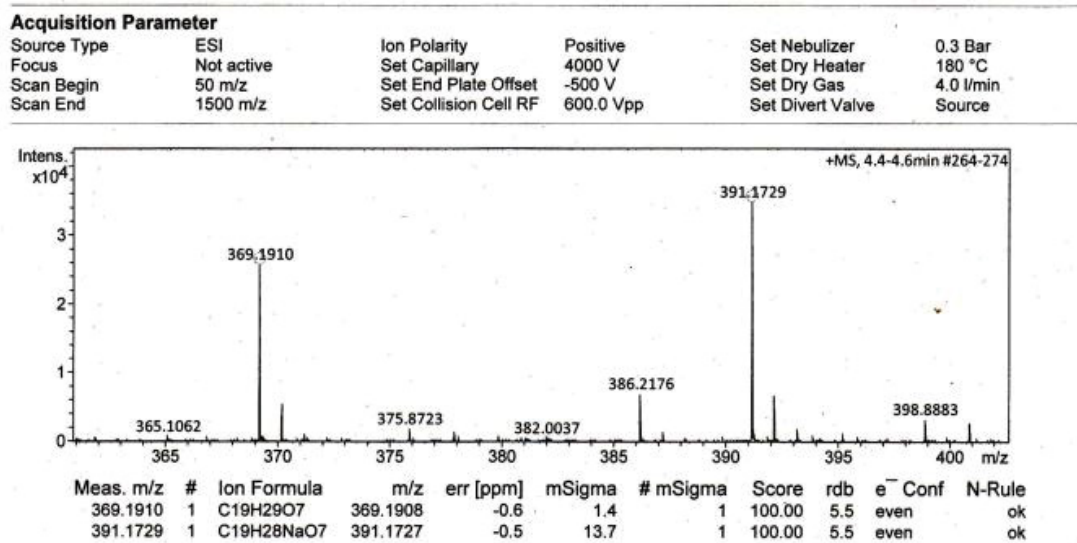
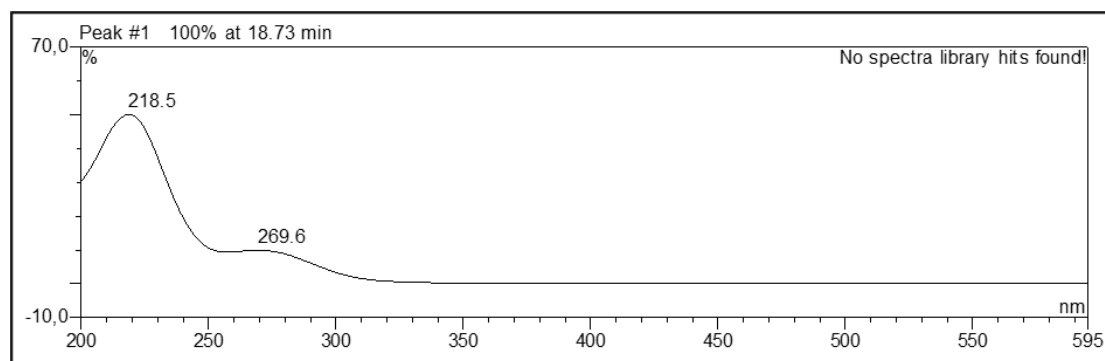


Figure S54. Structure and population of the low-energy ($\geq 1\%$) ω B97X/TZVP PCM/MeOH conformers of (5*S*,6*S*,7*R*)-**7a**.

Figure S55. HREISMS of **8**.Figure S56. UV spectrum of **8**.

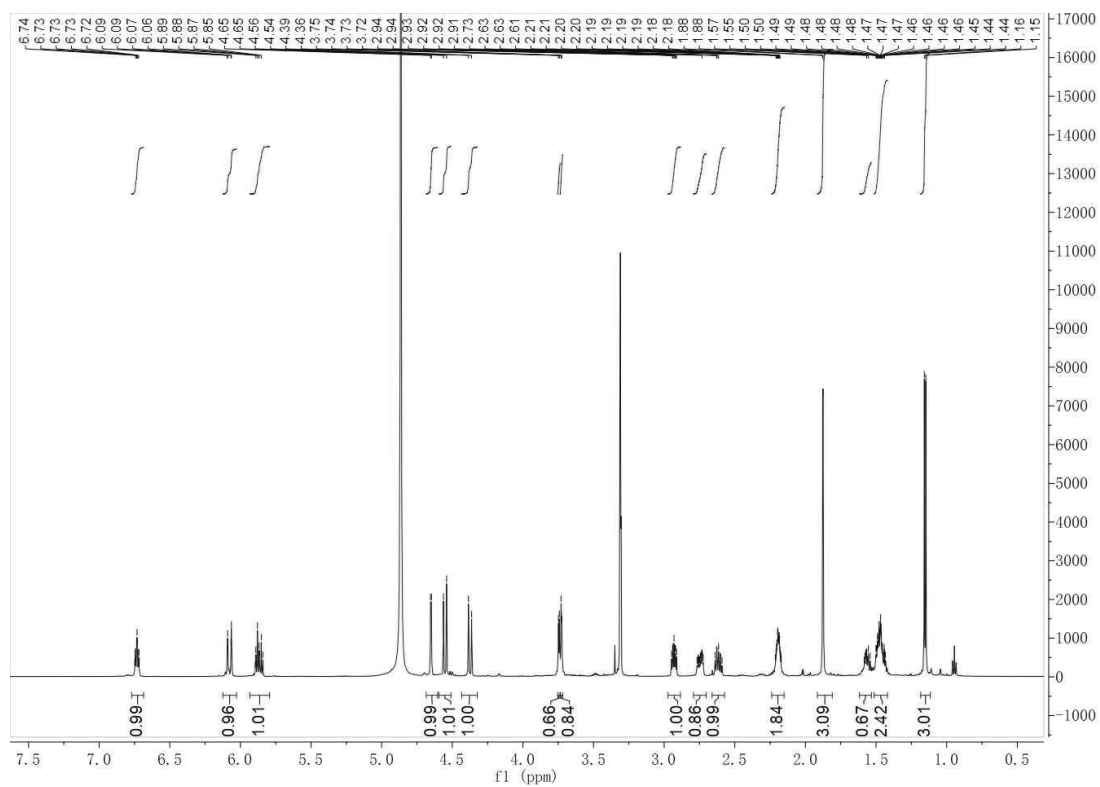


Figure S57. ^1H -NMR (600 MHz, CD_3OD) spectrum of **8**.

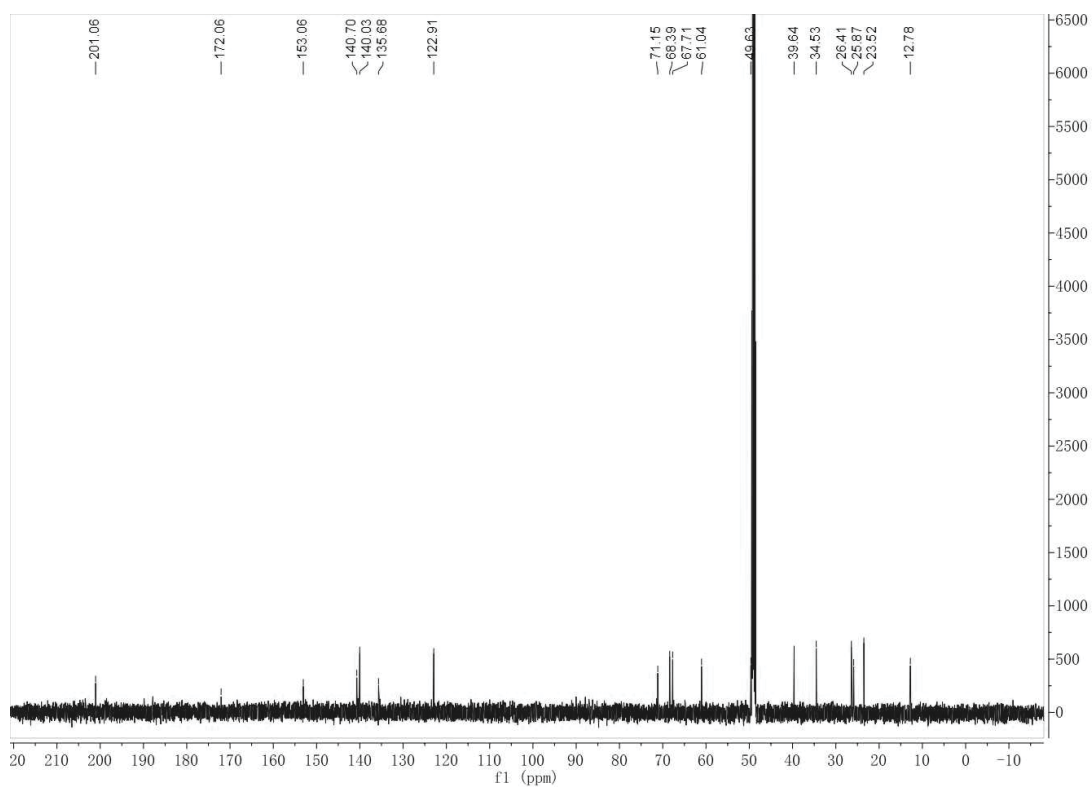


Figure S58. ^{13}C -NMR (150 MHz, CD_3OD) spectrum of **8**.

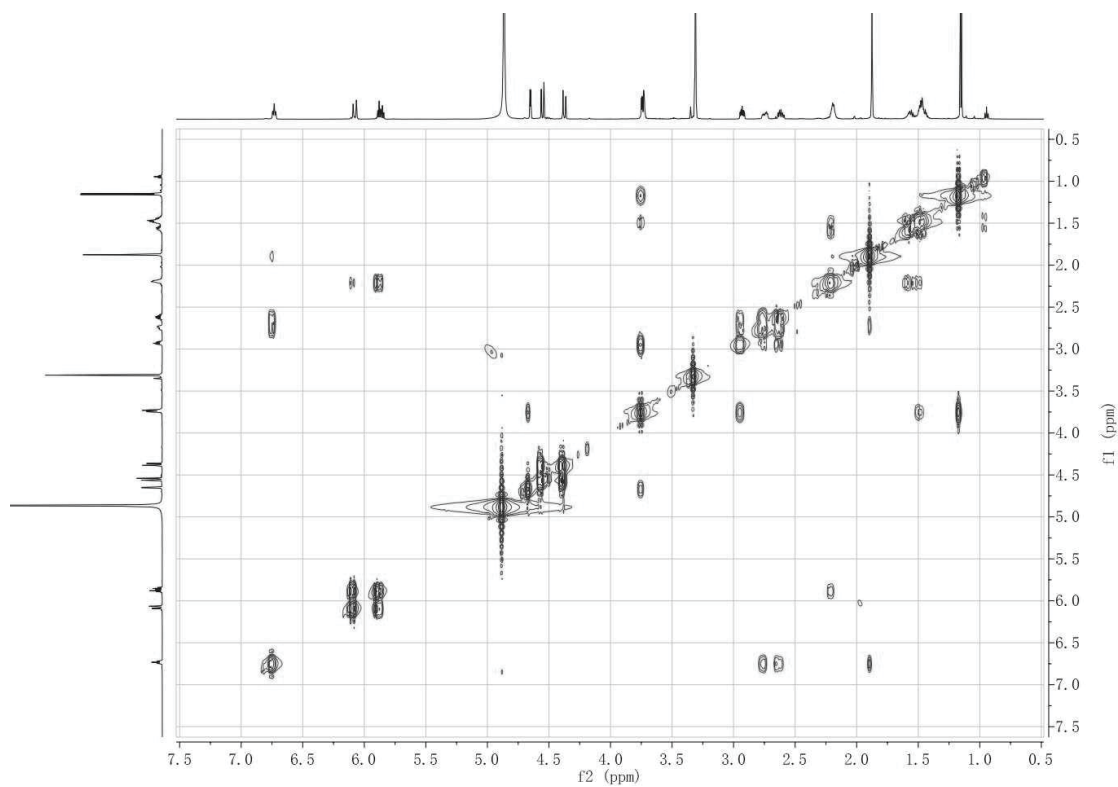


Figure S59. ^1H -H COSY (600 MHz, CD_3OD) spectrum of **8**.

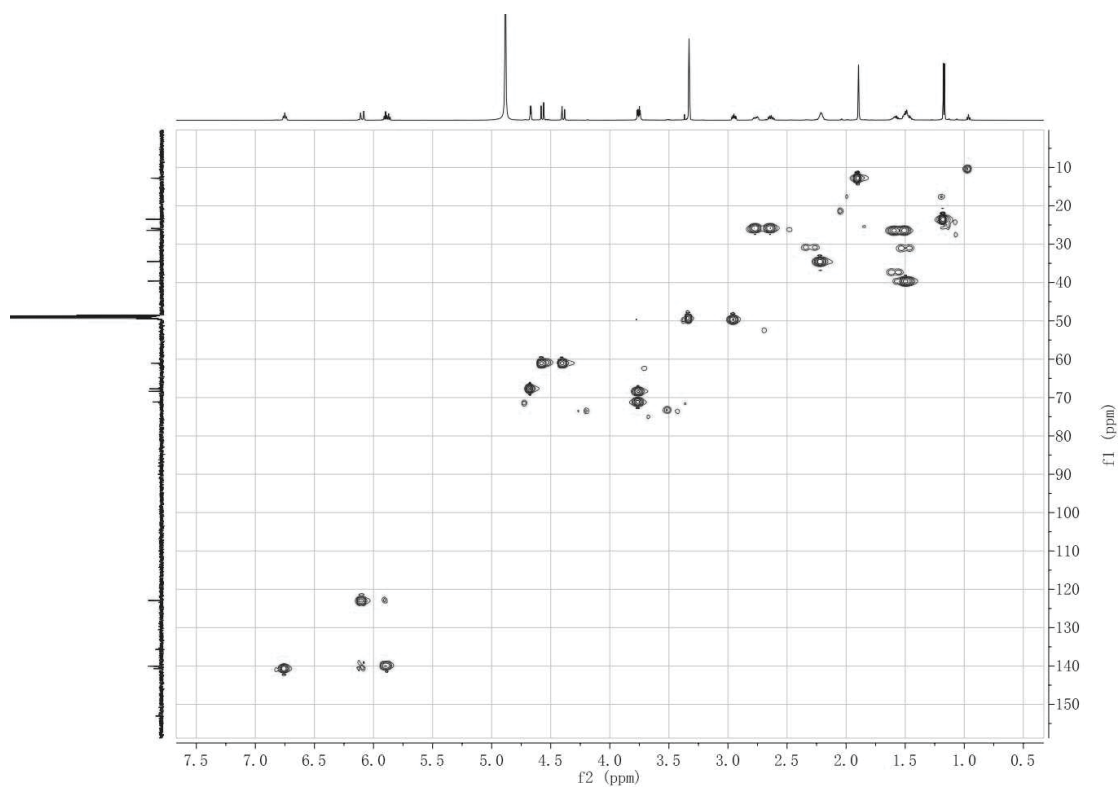


Figure S60. HSQC (600 MHz, CD_3OD) spectrum of **8**.

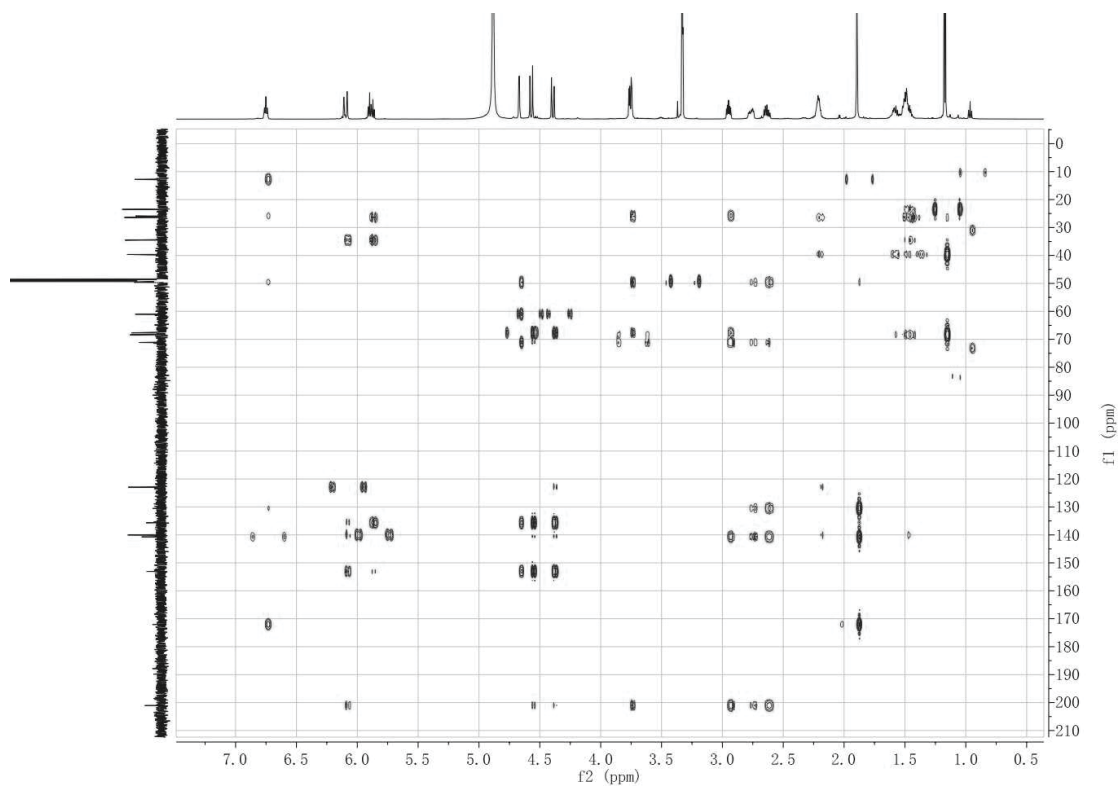


Figure S61. HMBC (600 MHz, CD₃OD) spectrum of **8**.

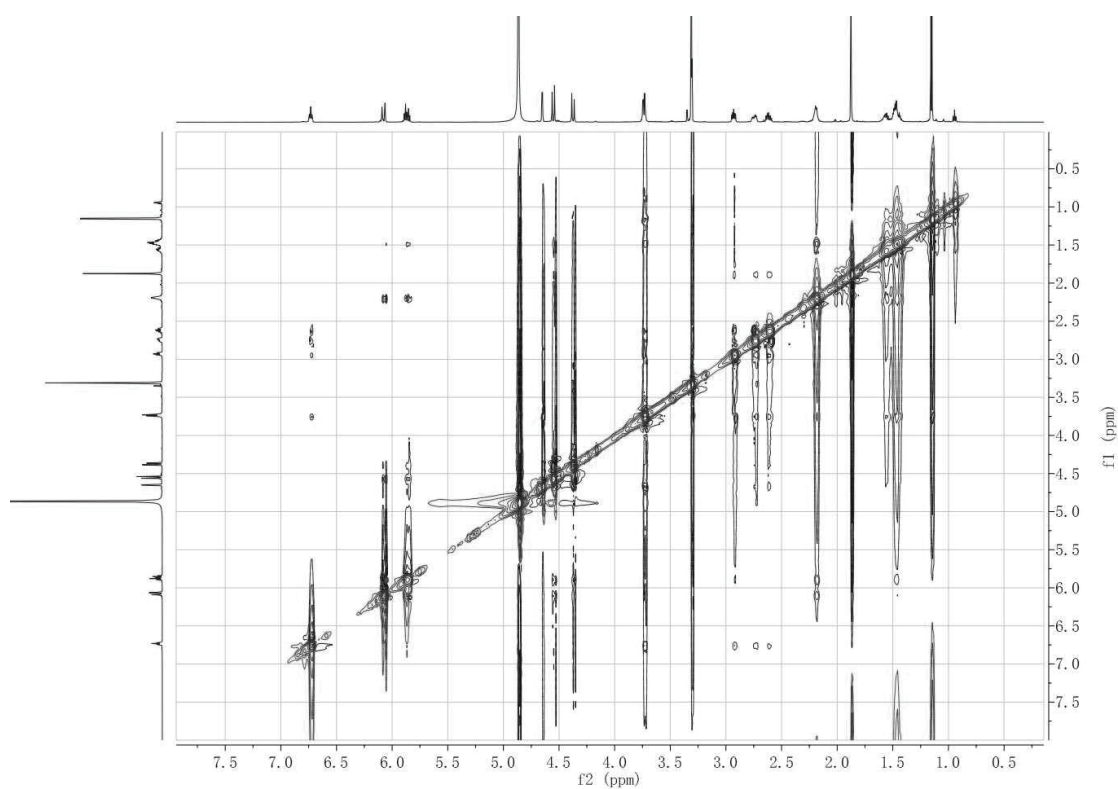
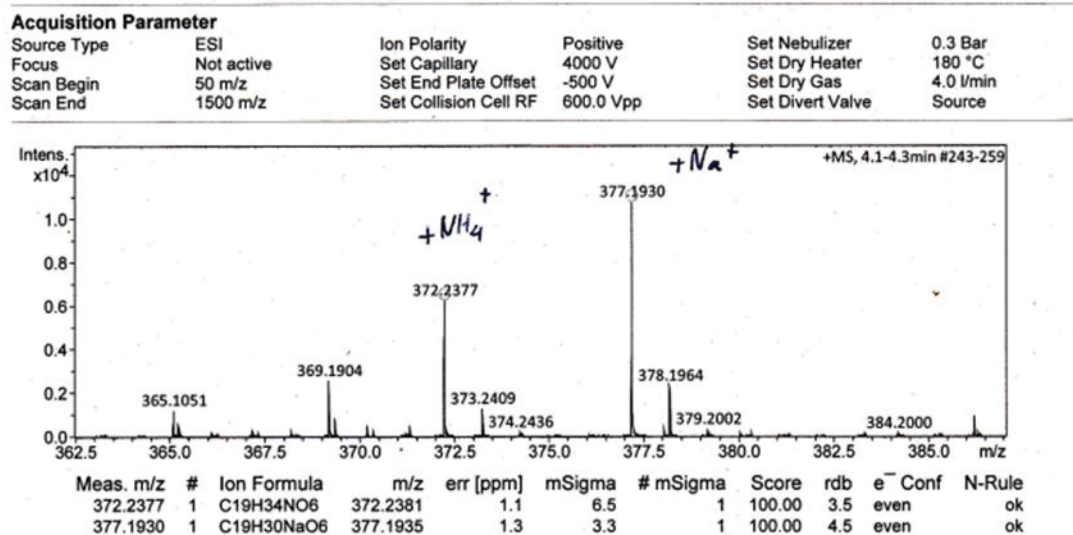
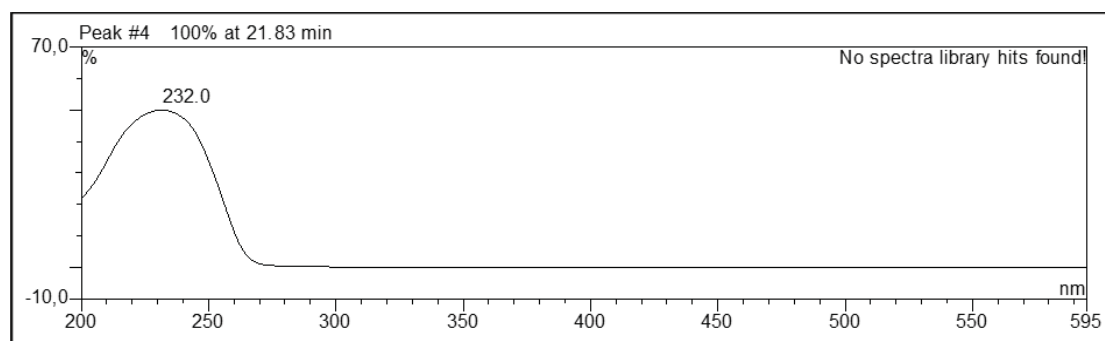


Figure S62. ROESY (600 MHz, CD₃OD) spectrum of **8**.

Figure S63. HREISMS of **9**.Figure S64. UV spectrum of **9**.

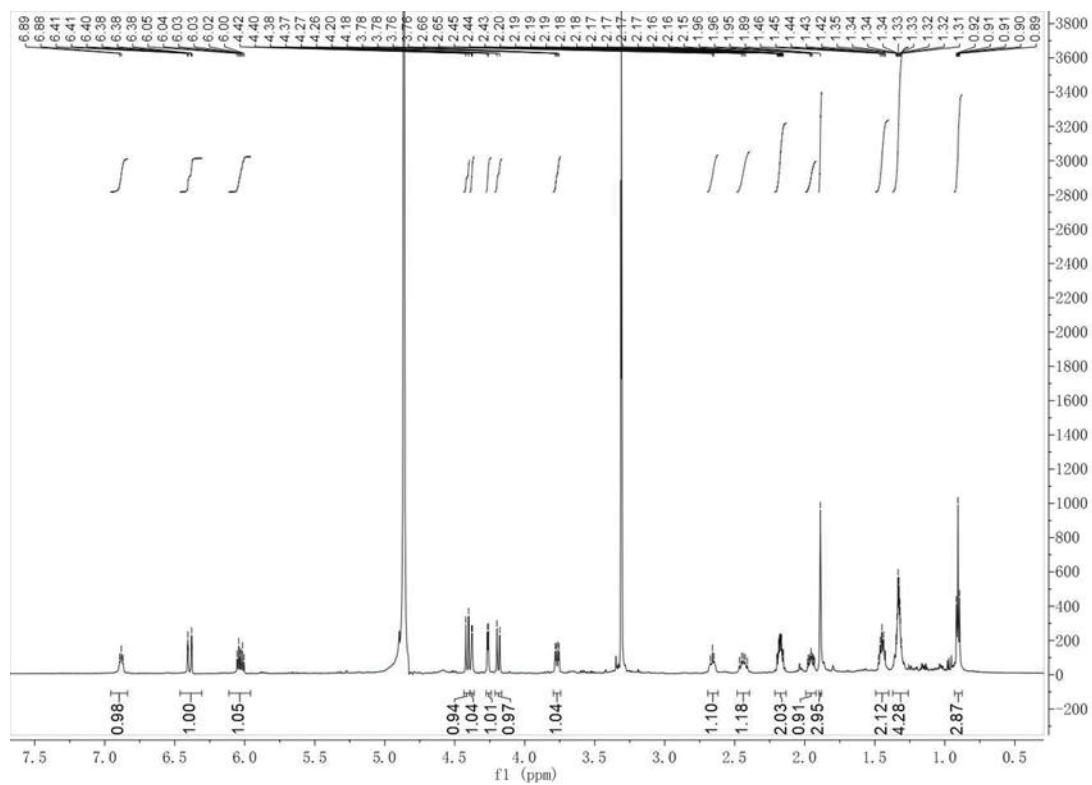


Figure S65. ^1H -NMR (600 MHz, CD_3OD) spectrum of **9**.

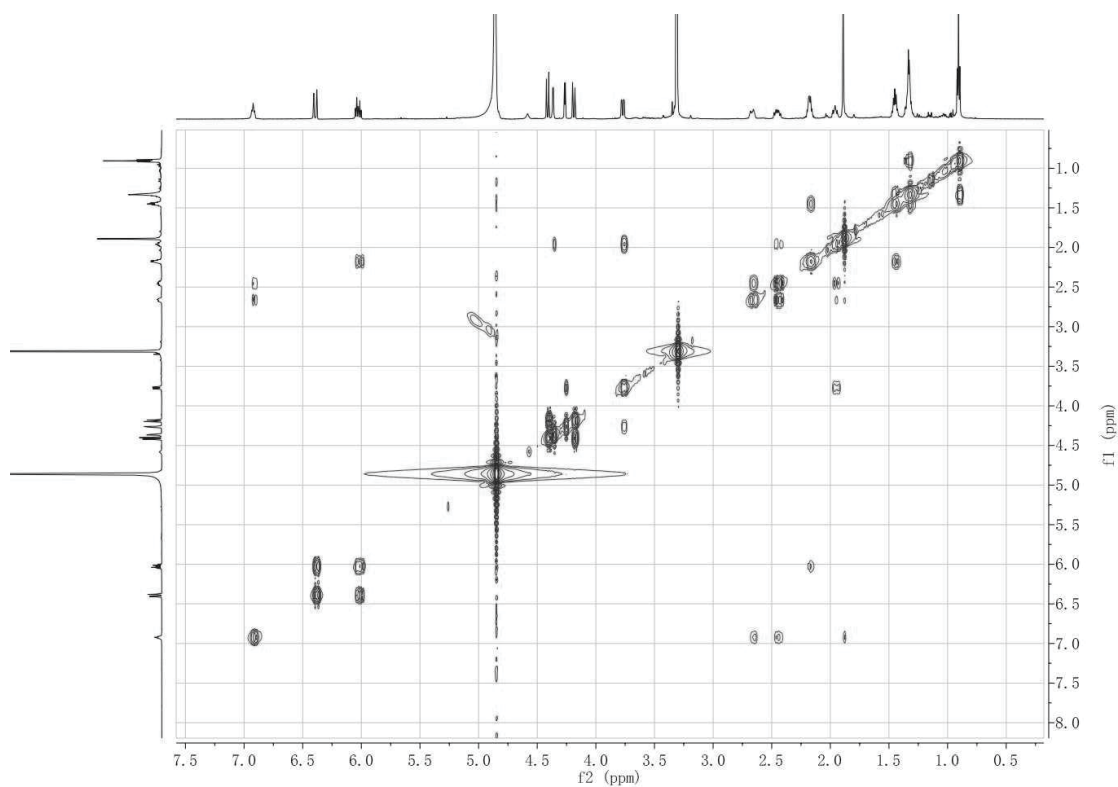


Figure S66. ^1H - ^1H COSY (600 MHz, CD_3OD) spectrum of **9**.

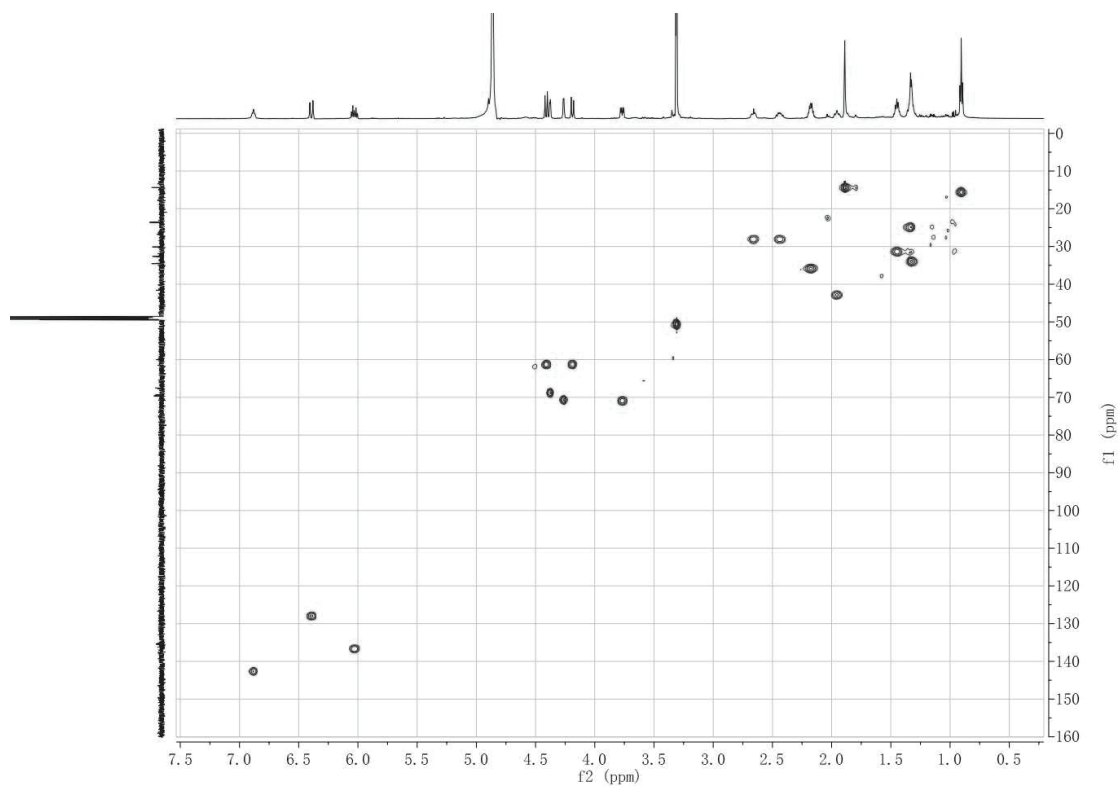


Figure S67. HSQC (600 MHz, CD₃OD) spectrum of **9**.

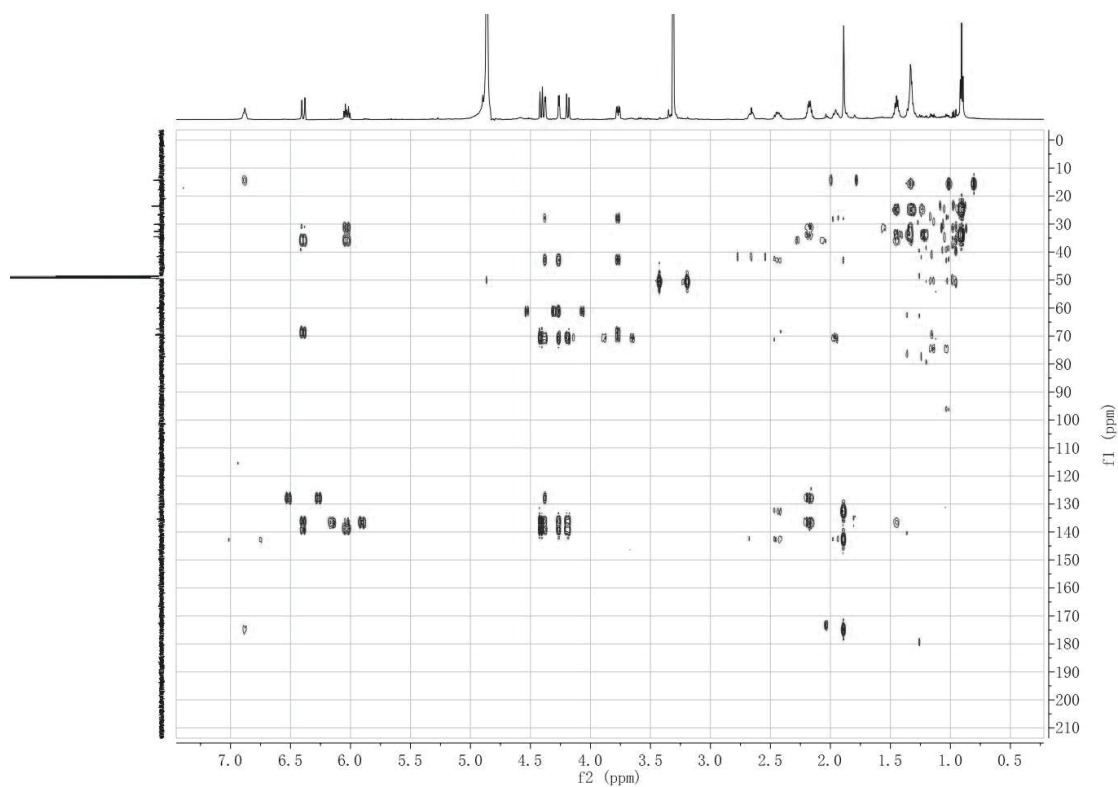
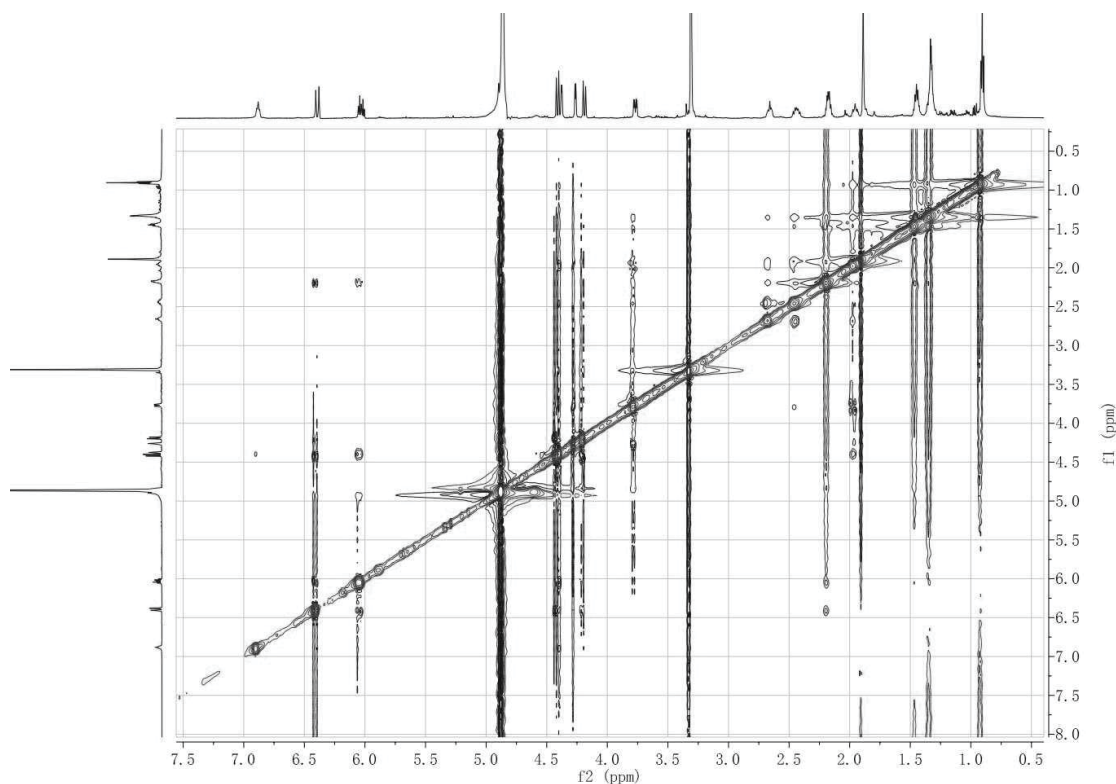


Figure S68. HMBC (600 MHz, CD₃OD) spectrum of **9**.

Figure S69. ROESY (600 MHz, CD₃OD) spectrum of 9.

Acquisition Parameter

Source Type	ESI	Ion Polarity	Positive	Set Nebulizer	0.3 Bar
Focus	Not active	Set Capillary	4000 V	Set Dry Heater	180 °C
Scan Begin	50 m/z	Set End Plate Offset	-500 V	Set Dry Gas	4.0 l/min
Scan End	1500 m/z	Set Collision Cell RF	600.0 Vpp	Set Divert Valve	Source

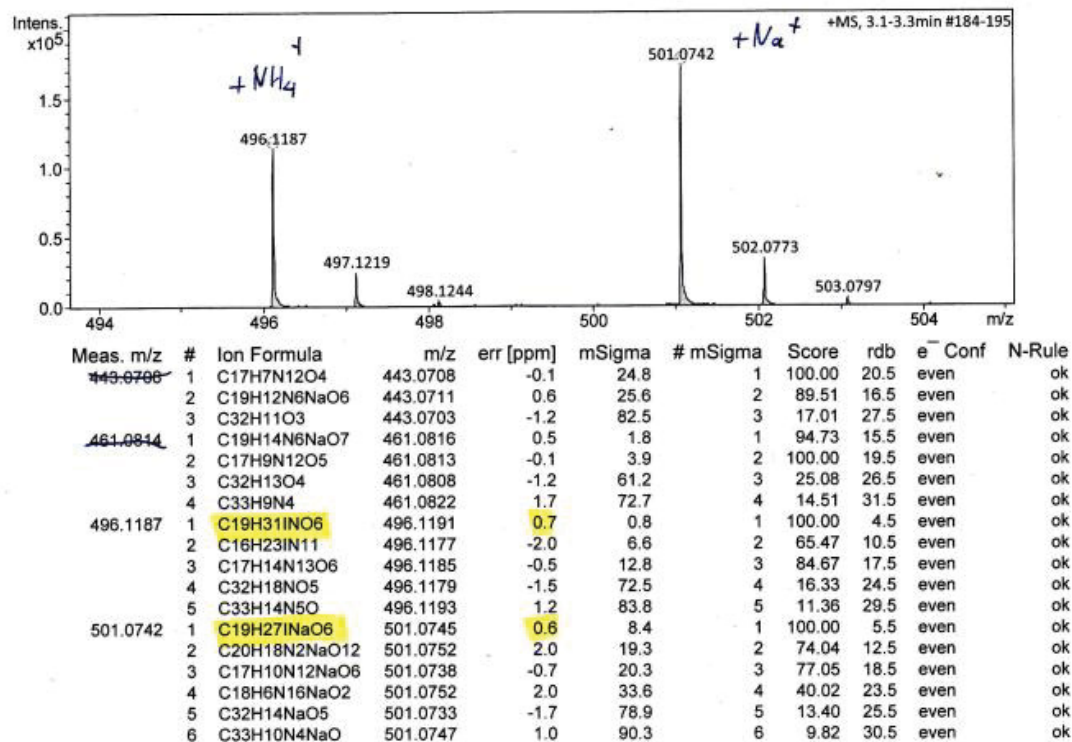


Figure S70. HREISMS of 10.

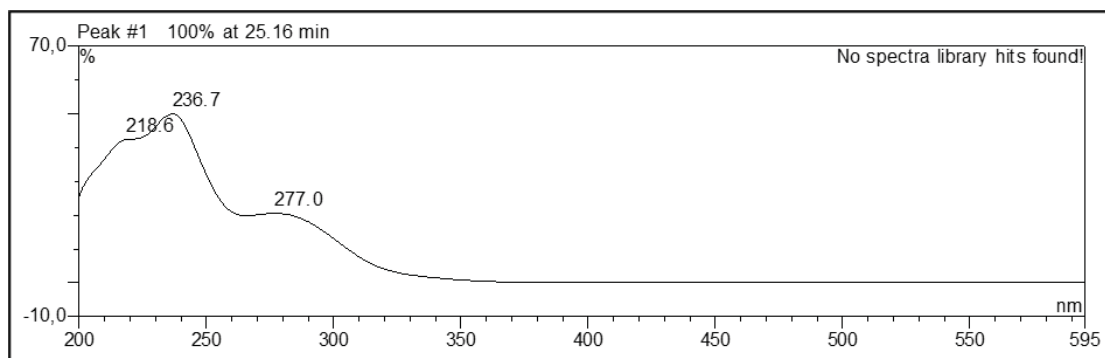


Figure S71. UV spectrum of **10**.

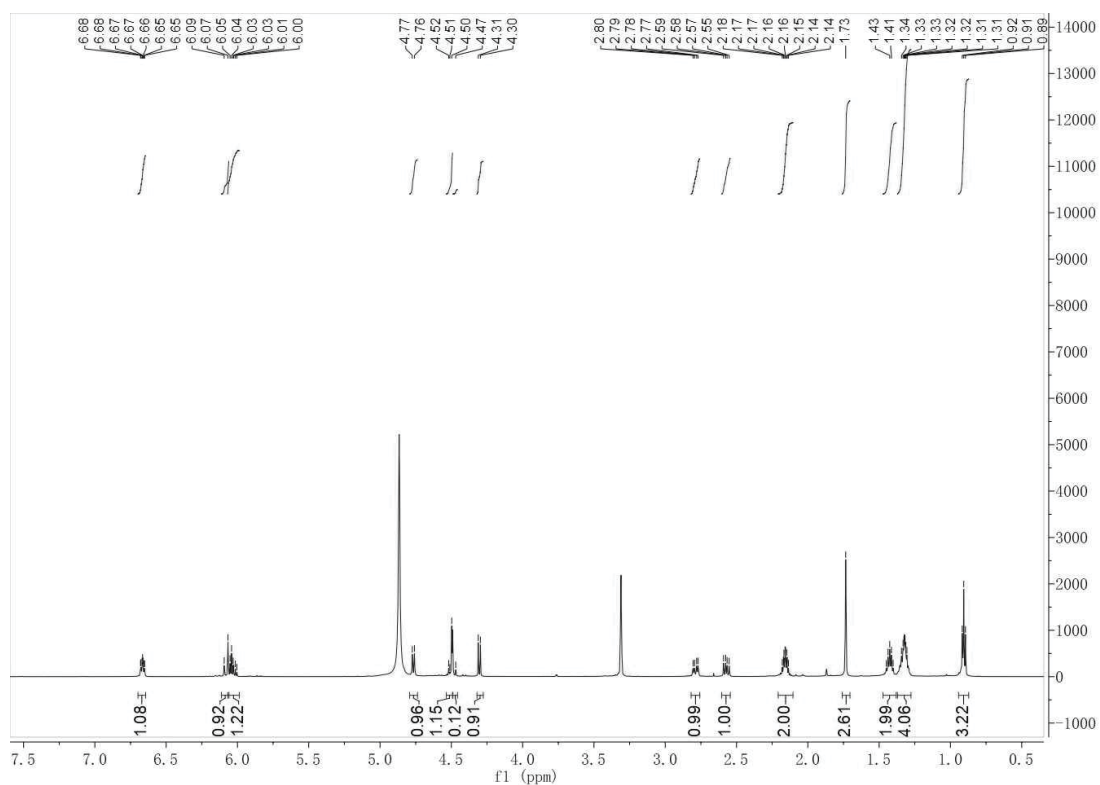


Figure S72. ^1H -NMR (600 MHz, CD_3OD) spectrum of **10**.

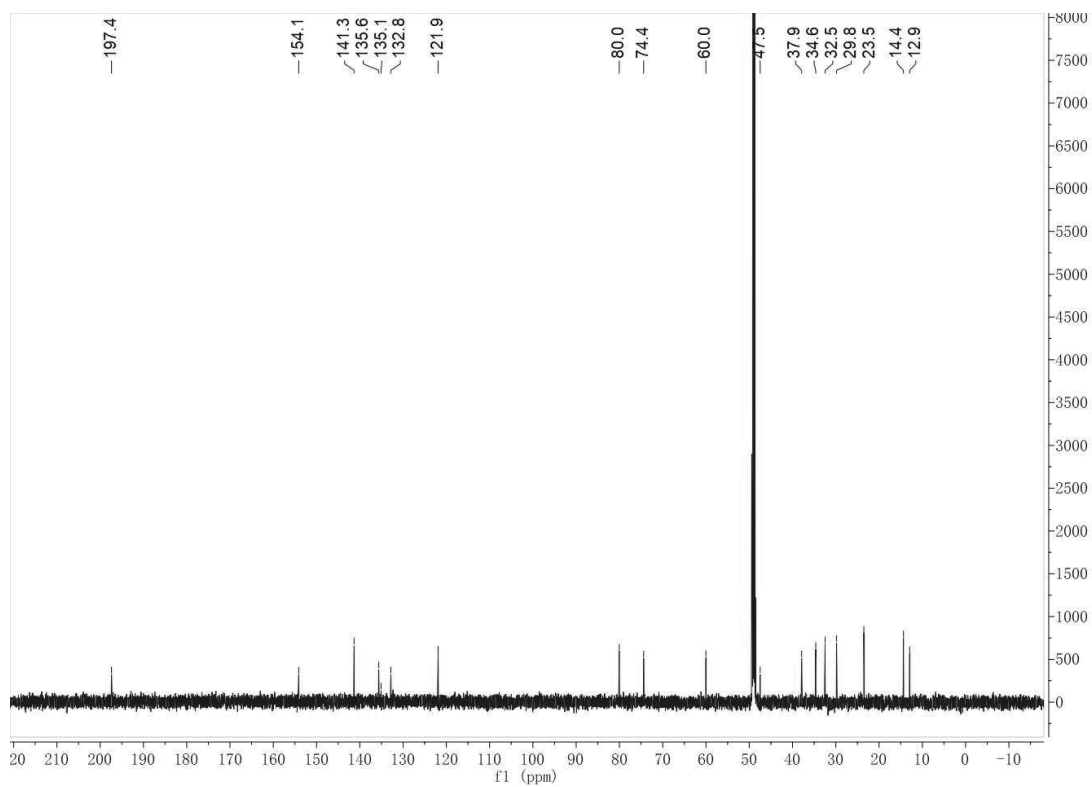


Figure S73. ^{13}C -NMR (150 MHz, CD_3OD) spectrum of **10**.

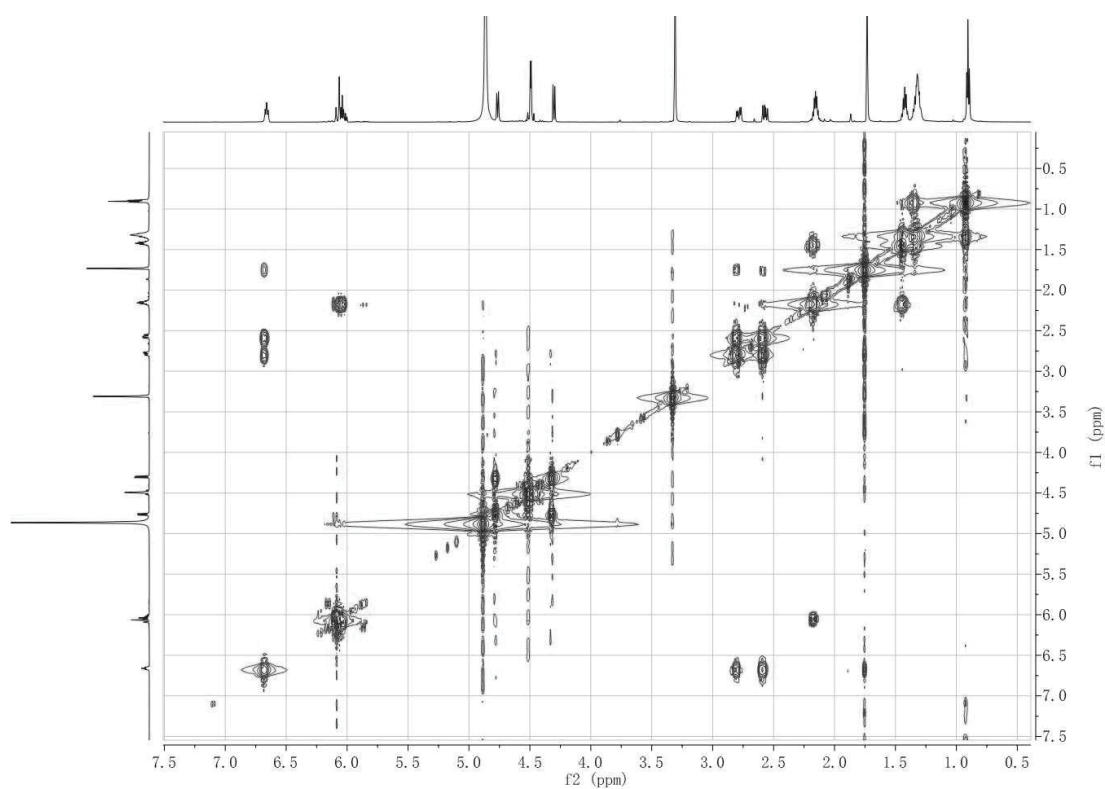


Figure S74. ^1H - ^1H COSY (600 MHz, CD_3OD) spectrum of **10**.

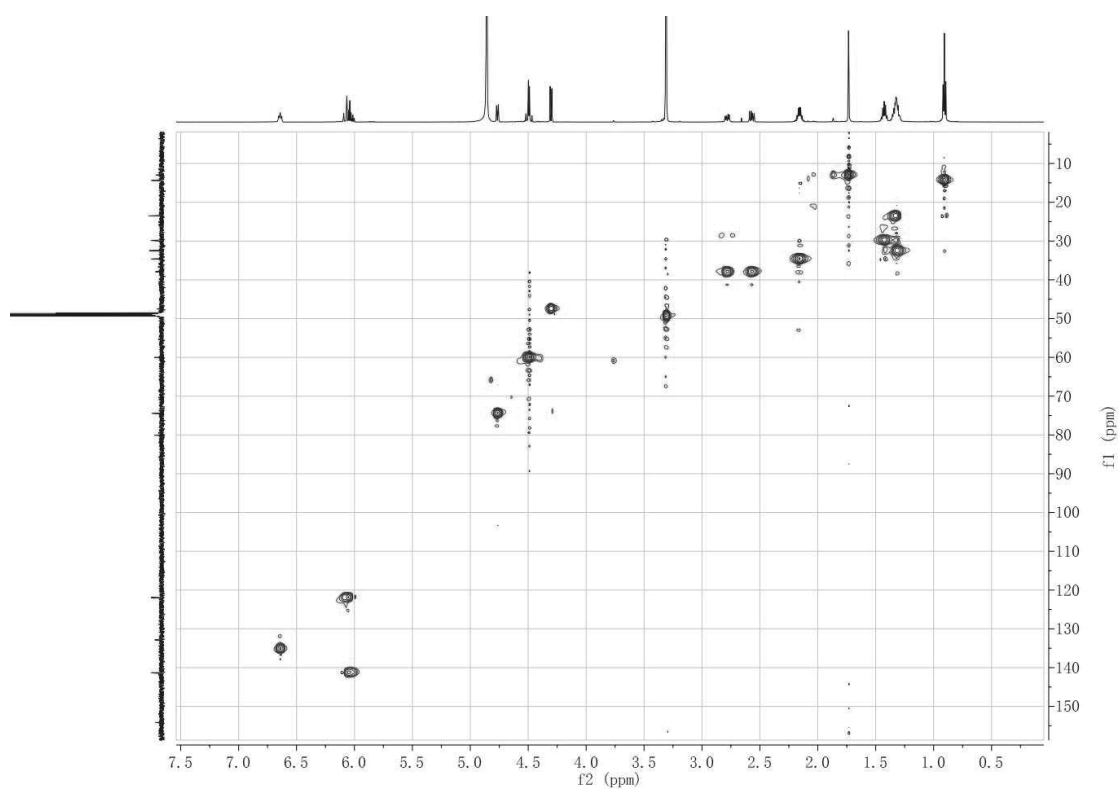


Figure S75. HSQC (600 MHz, CD₃OD) spectrum of **10**.

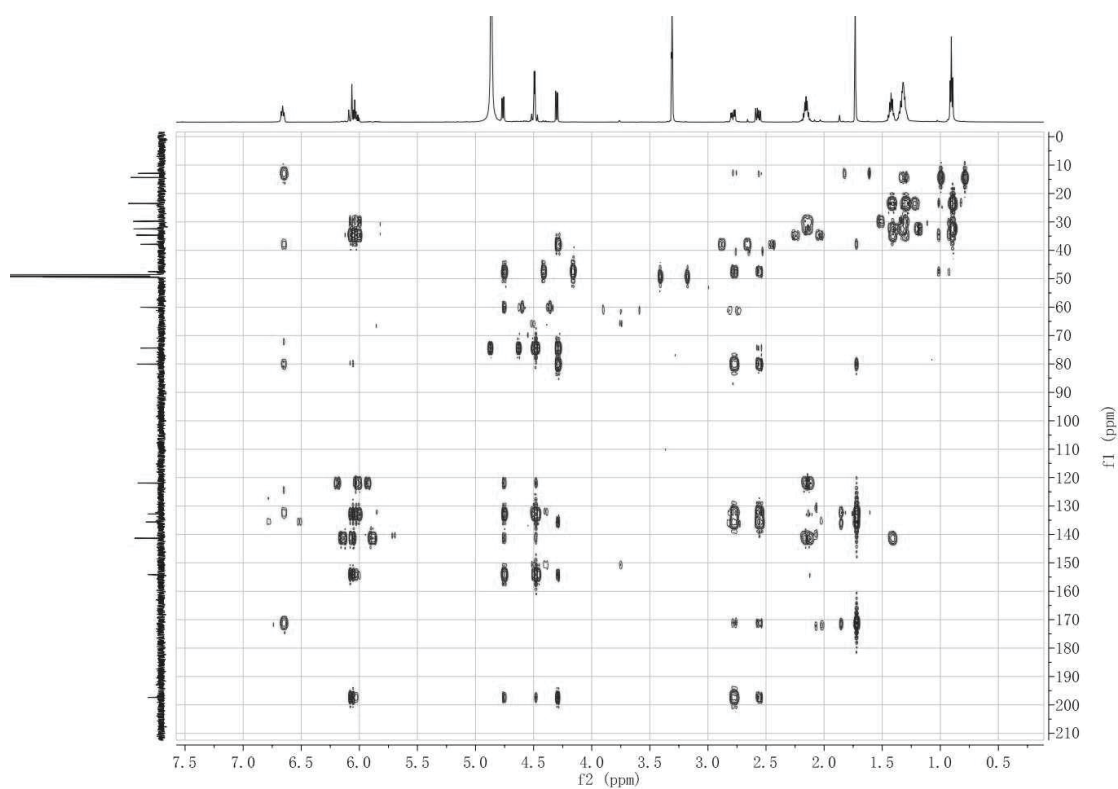


Figure S76. HMBC (600 MHz, CD₃OD) spectrum of **10**.

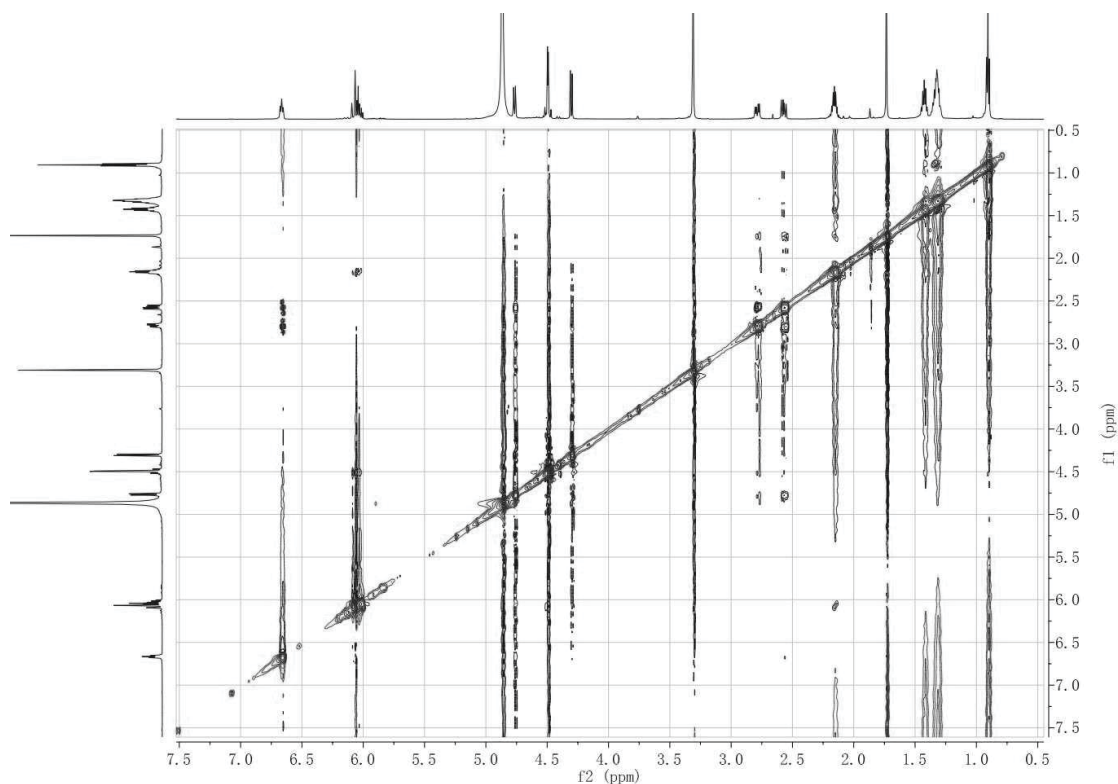


Figure S77. ROESY (600 MHz, CD₃OD) spectrum of **10**.

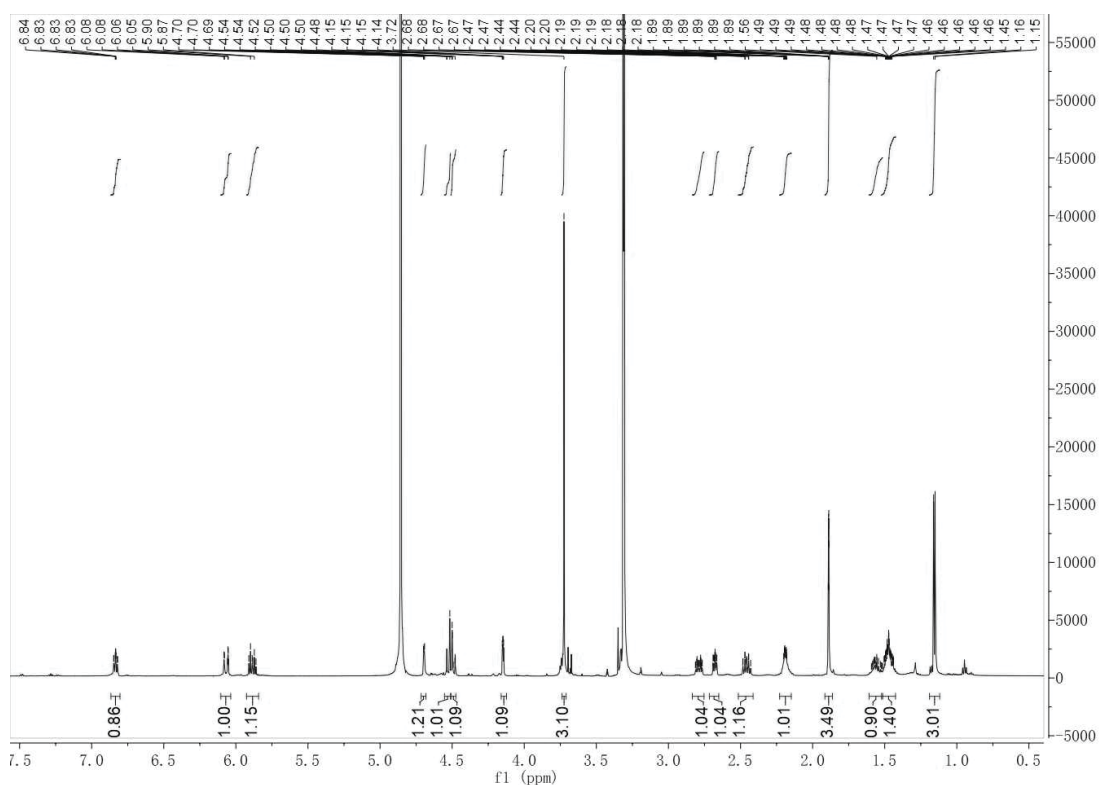
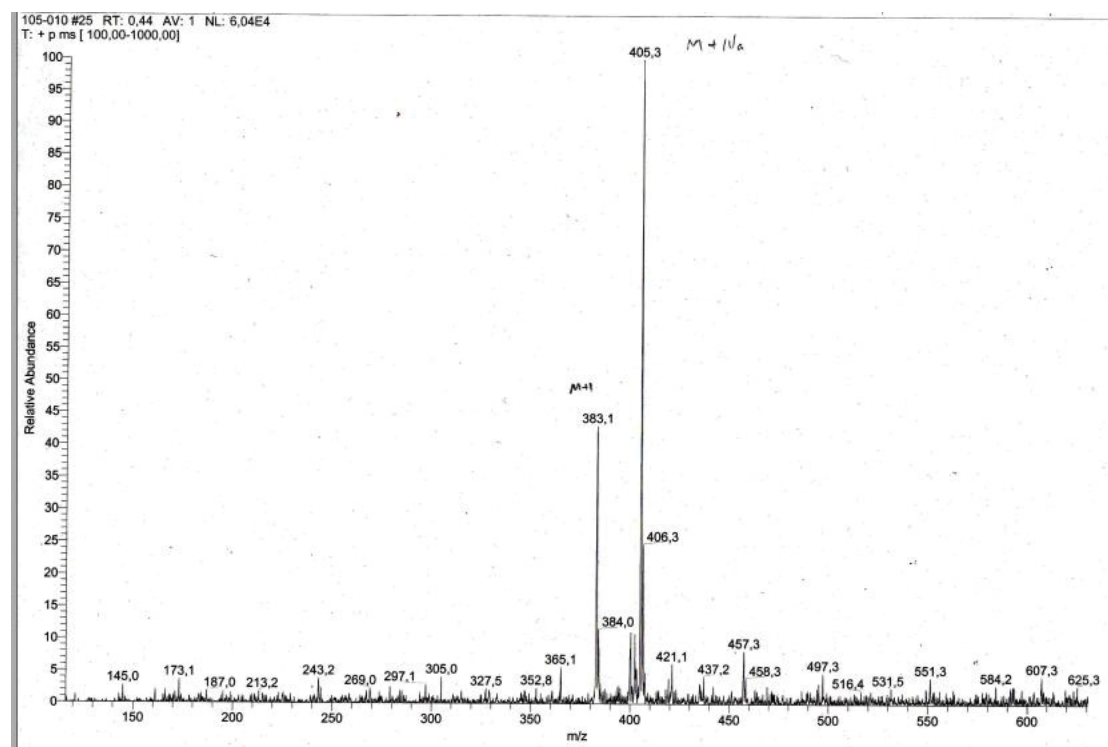
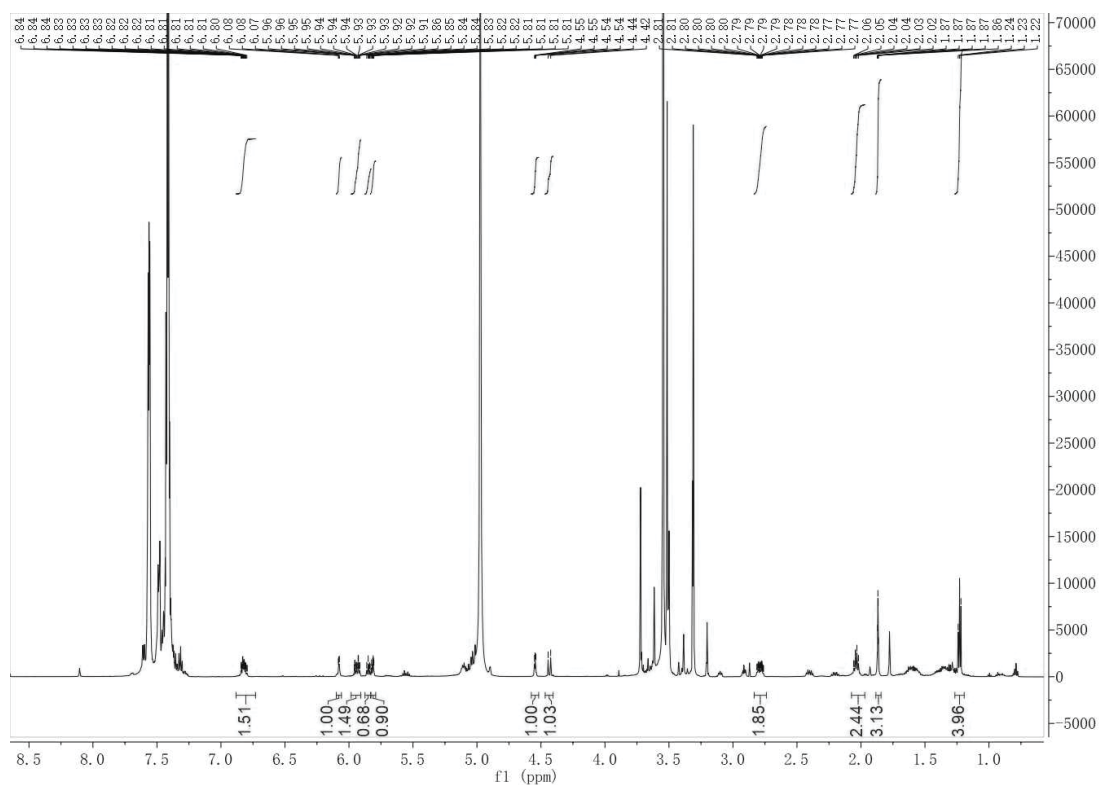


Figure S78. ¹H-NMR (600 MHz, CD₃OD) spectrum of **2a**.

**Figure S79.** EISMS of **2a**.**Figure S80.** ^1H -NMR (600 MHz, CD_3OD) spectrum of **2b**.

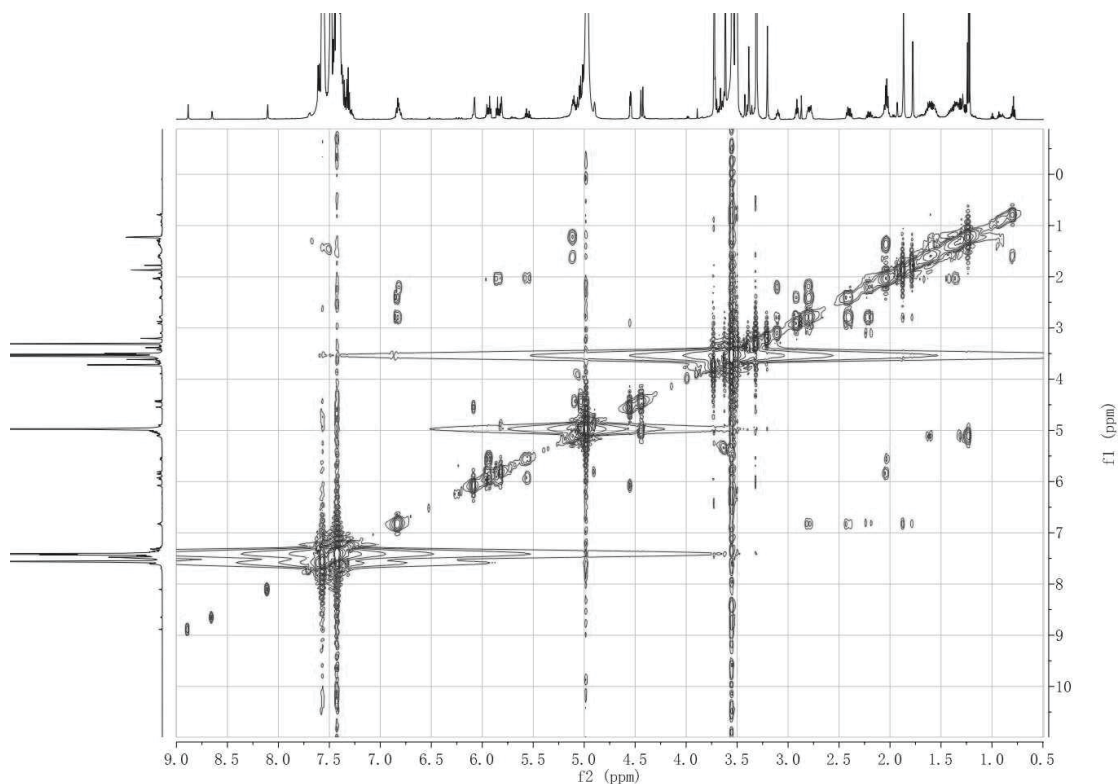


Figure S81. ^1H -H COSY (600 MHz, CD_3OD) spectrum of **2b**.

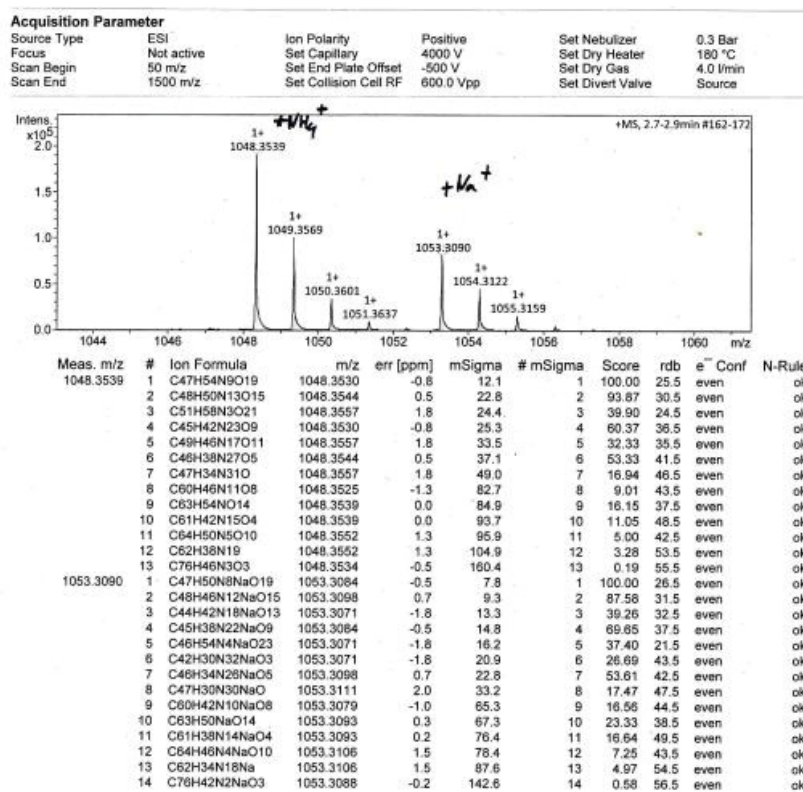


Figure S82. HRESIMS of **2b**.

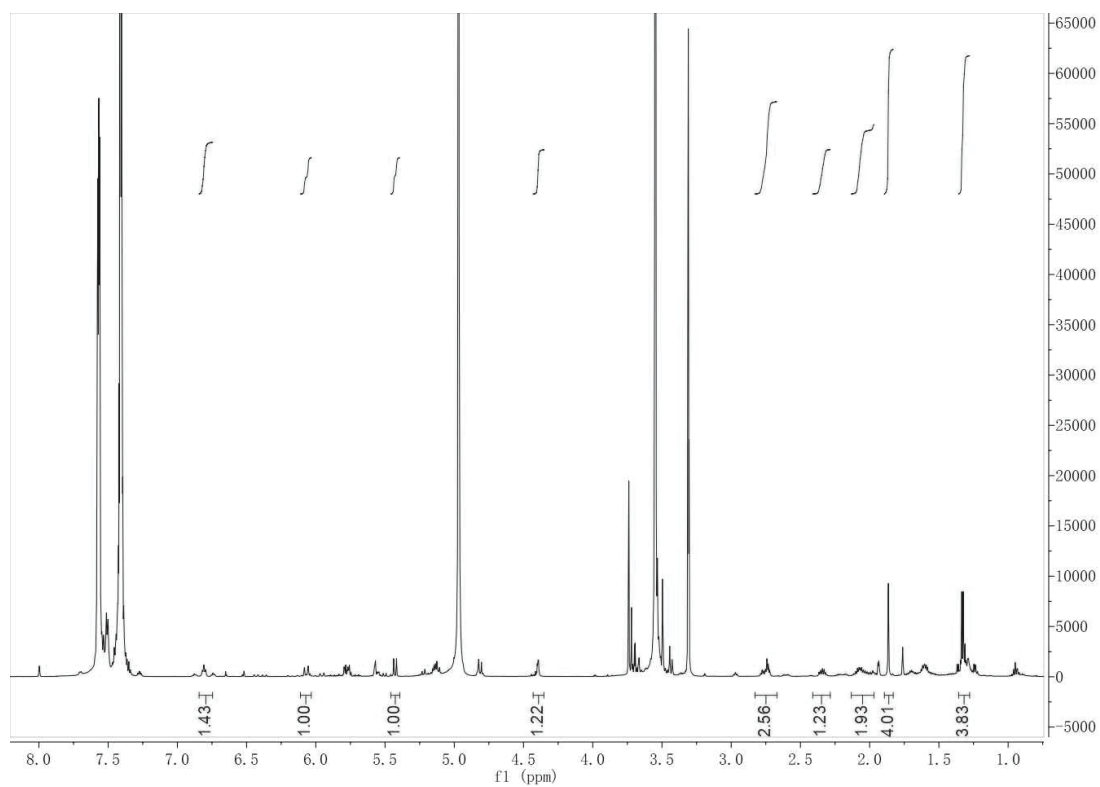


Figure S83. ^1H -NMR (600 MHz, CD_3OD) spectrum of **2c**.

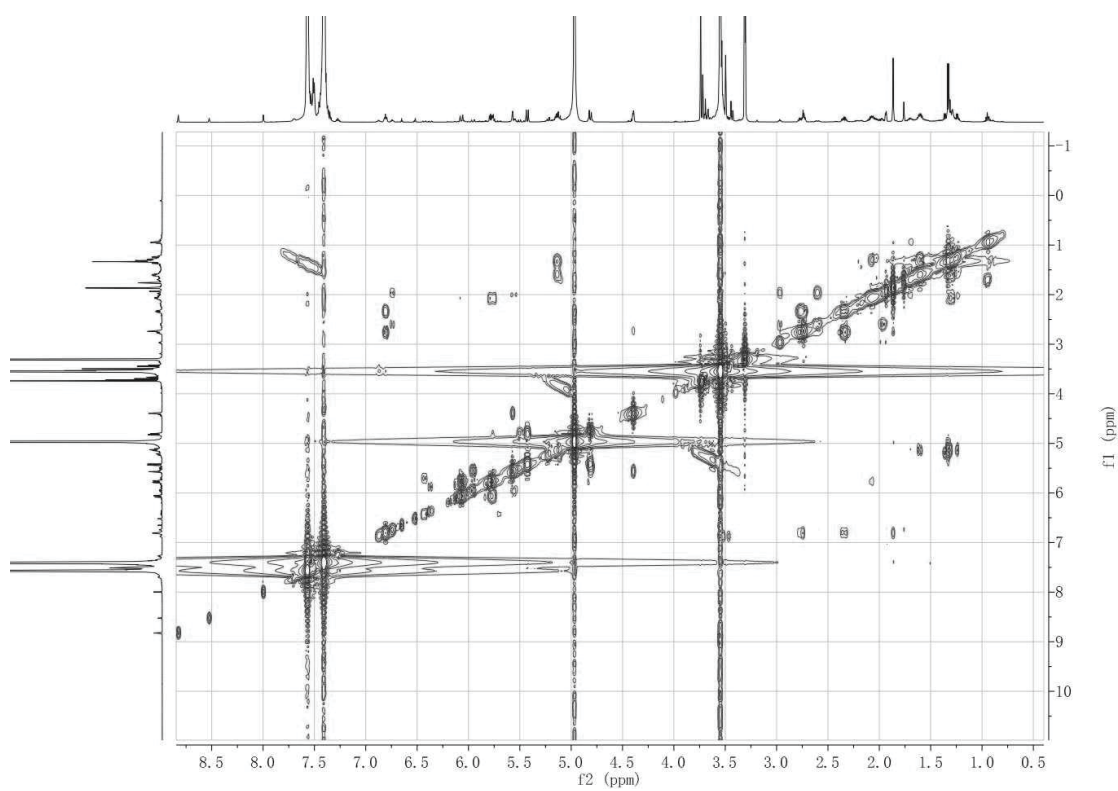


Figure S84. ^1H - ^1H COSY (600 MHz, CD_3OD) spectrum of **2c**.

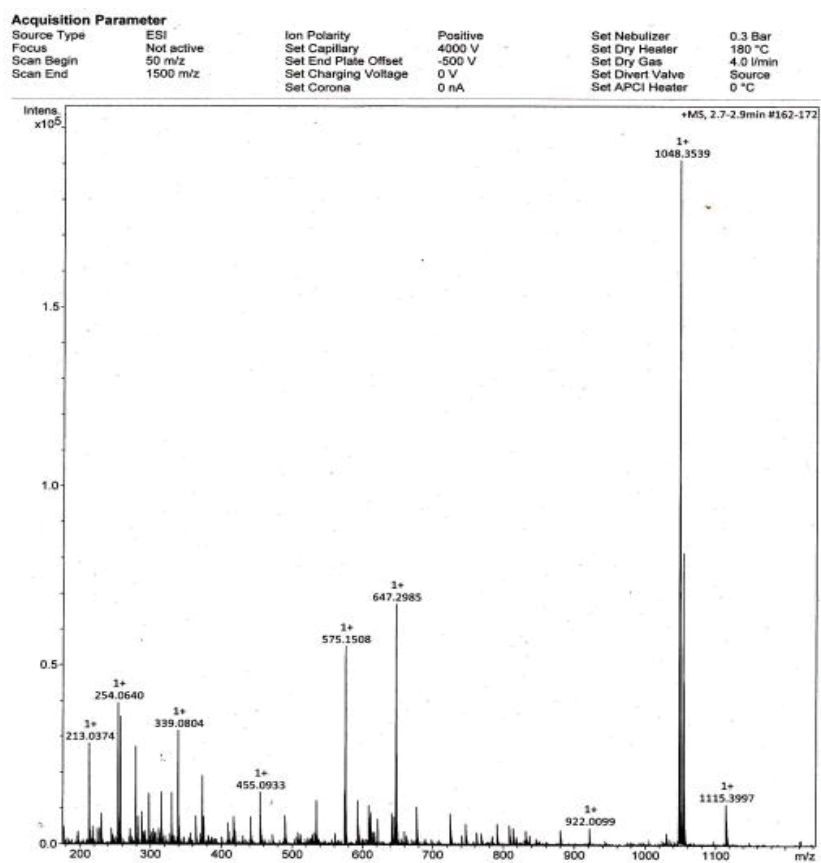


Figure S85. HRESIMS of 2c.

5. Discussion

5.1. Prenylated indole alkaloids from *Aphanoascus fulvescens*

Aphanoascus fulvescens is a keratinophilic saprotrophous fungus. The previous studies related to *A. fulvescens* were mainly focused on its ability for biodegradation of feather waste keratin rather than secondary metabolites except for the discovery of two amines WF14865 A and B (Bohacz, 2017; Otsuk *et al.*, 2000). As mentioned in chapter 2 (publication 1), five new prenylated indole alkaloids okaramines V–Z, together with eleven known derivatives were obtained from solid rice medium fermentation of coprophilous fungus *A. fulvescens*.

Okaramines are representative prenylated cyclic dipeptide derivatives consisting of two L-tryptophan molecules. Most of them were isolated from *Aspergillus* spp. and *Penicillium* spp. (Matsuda, 2018). In addition to the remarkable polycyclic structures, okaramine analogues are different in the numbers and positions of regular or reverse prenyl moiety in the indole ring (Figure 5.1.1). For example, okaramine V (Figure 5.1.2) possesses two reverse prenyl moieties at C-2 and N-1, S possesses two regular prenys at C-7 while Z features two reverse prenyl moieties at N1. Interestingly, in the structures of okaramines reported so far, prenylation at C-1, C-2, C-7 and N-1 was observed, however, no prenylation at C-6 was found until the isolation of okaramine W from *A. fulvescens*.

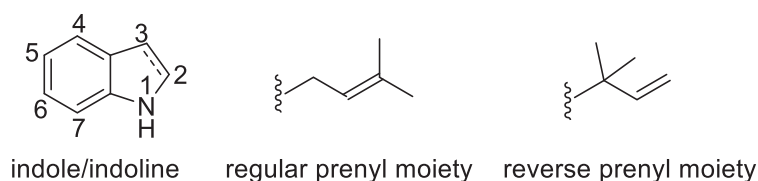


Figure 5.1.1. Numbering of prenyl and indole/indoline moieties.

The biosynthetic pathway of okaramines, as well as other prenylated indole alkaloids such as aszonalenin, roquefortine C was suggested to start from tryptophan and dimethylallyl diphosphate (DMAPP) based on feeding experiments with isotope-labelled precursors (Jakubczyk *et al.*, 2014). Cyclo-L-Trp-L-Trp was assumed to be the common precursor for okaramine W and its analogues due to the high similarity of core structures. The distinct prenylation at C-6 in okaramine W from *A. fulvescens* might result from yet unknown prenyltransferases which can accept the tryptophan-containing cyclic dipeptide (**a**) and convert

it to derivative with a prenyl moiety at position C-6.

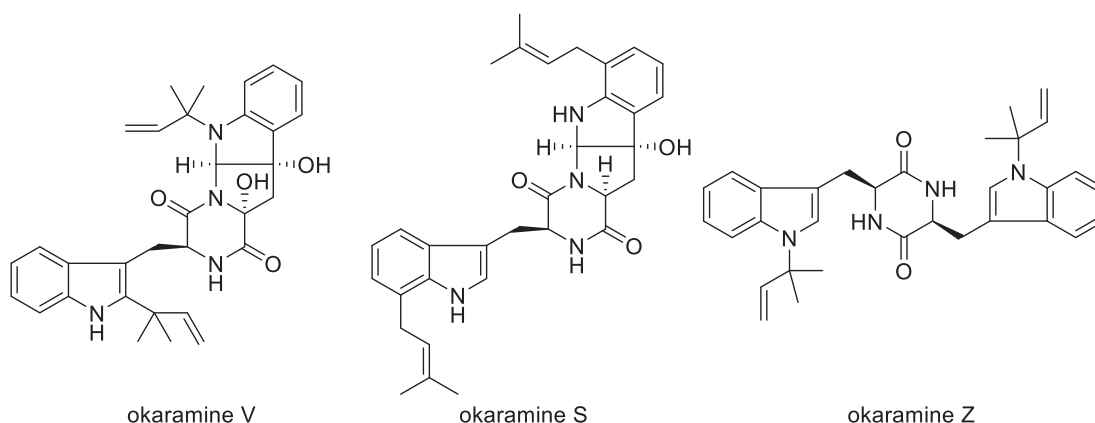


Figure 5.1.2. Structures of okaramines.

As far as we know, several prenyltransferases such as 7-DMATS, FgaPT2 and FtmPT1 were shown to participate in prenyl transfer reactions (Grundmann and Li, 2005). These enzymes were suggested to accept dimethylallyl diphosphate as specific prenyl donor (Steffan *et al.*, 2009). Moreover, tryptophan derivatives, such as tryptophan-containing cyclic dipeptides (**a**) could be converted to different prenylated metabolites by them. For example, purified prenyltransferase gene FtmPT1 was identified in the genome sequence of *Aspergillus fumigatus*. It encoded for an enzyme which catalyzes the prenylation of cyclo-L-trp-L-Pro (brevianamide F) at the C-2 position of the indole nucleus (Grundmann and Li, 2005). With the same strategy as shown in figure 5.1.3 (Li, 2010), corresponding derivatives with prenyl moieties at N-1, C-2, C-3, C-4 and C-7 could be obtained. In addition to okaramine W, prenylated peptide arestrictin B from *Aspergillus penicilloides* (Itabashi *et al.*, 2006), isocochliodinol from *Chaetomium* spp. (Sekita, 1983) were also obtained with regular prenylation at positions C-6. These cases make it interesting to assume that one or a group of indoles prenyltransferase genes could be identified in the genome sequences of fungi strains including *A. fulvescens* as well as *Aspergillus penicilloides* and *Chaetomium* spp. to catalyze the prenylation at the C-6 in cyclic dipeptides. Further molecular biological and biochemical work following the procedures for discovery of FtmPT1 needs to be conducted to prove our assumption above.

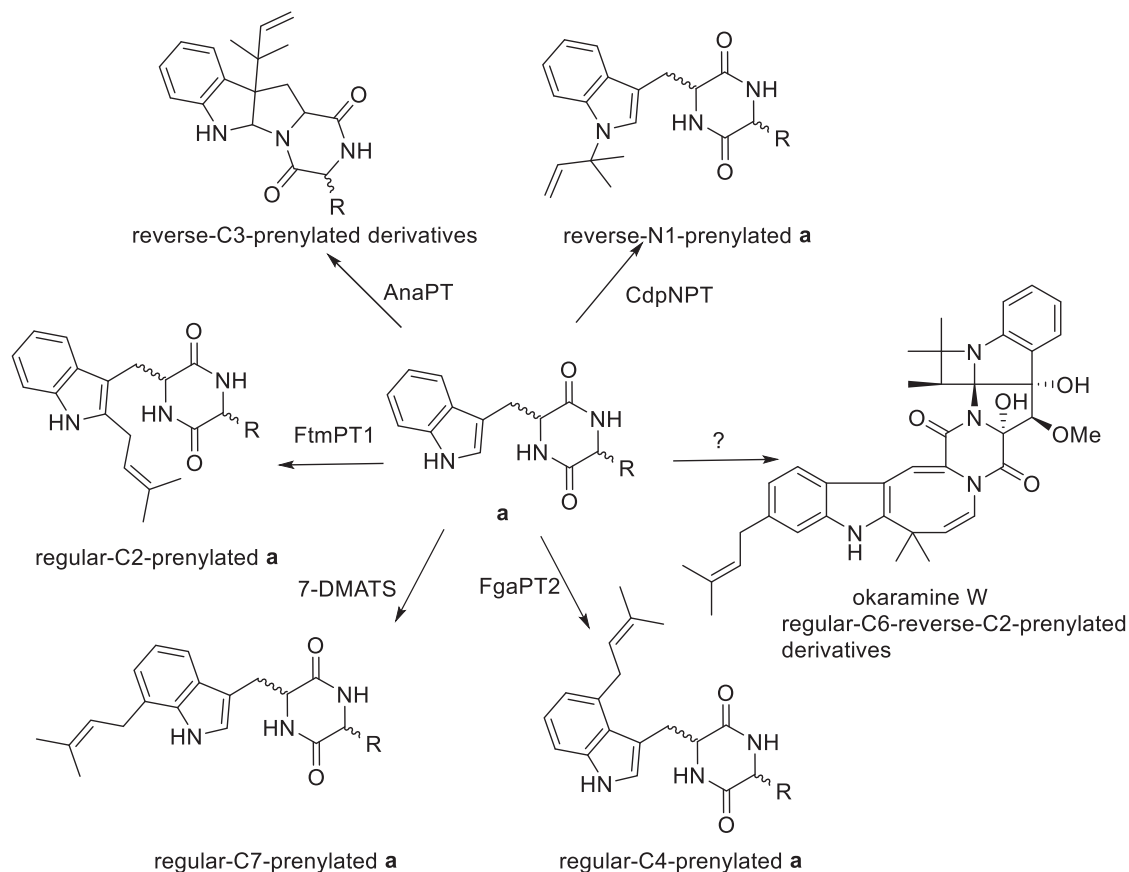


Figure 5.1.3. Prenyltransfer reactions catalyzed by different prenyltransferases.

5.2. Acetylenic natural products from *Pseudopestalotiopsis theae*

As described in publication 2, eighteen new polyketide derivatives named pestalothols I–Q and cytosporins O–W were identified during the chemical investigation of secondary metabolites from the endophytic fungus *Pseudopestalotiopsis theae*. These compounds can be divided into two groups based on their structural features. Pestalothols I–Q feature an alkenyl or alkynyl group, while cytosporins O–W possess alkyl side chains. New metabolites pestalothols L, M and the co-isolated known compound truncateol B bear internal alkynyl functions between C-10 and C-11, making them distinct from other analogues.

Acetylenic natural products include compounds which possess a carbon-carbon triple bond or alkynyl functional group. They occur in fungi, marine algae, plants and other sources. There are a number of drugs on the market containing alkyne groups. Efavirenz (EFV) which was sold under the brand names Sustiva, is a drug widely used for prevention and treatment of HIV-AIDS (Bastos *et al.*, 2016). Bacterium (*Micromonospora echinospora*) derived

theae.

o-Prenylated phenol (**a**) which might undergo prenylation and alkynylation reactions is suggested to be the precursor of **b**. Pestalothel D which undertakes reduction, epoxidation to form pestalothel A and P, is assumed to be one of the products during the formation of **b** by oxidation and heterocyclization. Pestalothel Q is thus formed from P via acetylation. An epoxide group at the isoprenyl side chain is derived in key intermediates **c** and **d** via oxygenation and reduction. Pestalothel K, truncateol B and D are supposed to be derived from **c** by reduction, olefinic rearrangement. Meanwhile, **d** undertakes cyclization, reduction and hydrolysis in the hydroquinone ring to generate pestalothel M and L, respectively. On the one hand, pestalothel M undergoes a double hydride reduction (Gubbels *et al.*, 2016) to generate pestalothel N, which produces pestalothel I by olefinic rearrangement, hydration and oxidation. At the same time, the compound may undertake C-5 chlorination and acetylation to form truncateol H and pestalothel O, respectively. On the other hand, pestalothel J is derived from M via the same way as for pestalothel I.

As we can see, all compounds in figure 5.2 displayed *R* configuration at C-6 and *S* at C-9. This may imply that the reduction of intermediate **b** to form hydroxy group in **c** is stereospecific, which is different from the case for truncateols (Zhao *et al.*, 2018). Moreover, the hydrolysis in the hydroquinone ring of **d** made it possible for the co-existence of pestalothel I, N and J, L. Except for the examples of acetylenases in biosynthesis of the alkyne moiety, the genetic basis for alkyne formation is still poorly understood. Therefore, there is a long way to go for the exact gene cluster and biosynthetic pathway of acetylenic compounds from *Pseudopestalotiopsis theae*.

5.3. Inducing iodinated secondary metabolites through halogen incorporation experiment

Fermentation of the endophytic fungus *Pestalotiopsis lespedezae* on solid rice medium led to the isolation of ambuic acid and one of its derivatives as major metabolites. These two compounds displayed antimicrobial activity against the Gram-positive bacterium *Staphylococcus aureus* as reported (Ding *et al.*, 2009). In order to expand the chemical diversity of the fungus *P. lespedezae*, halogen incorporation experiments were conducted by adding

halide salts such as 3.5 % sodium chloride, 3.5 % sodium bromide and 3.5 % sodium iodine to solid rice medium. Based on previous research, the experiment of sodium fluoride was excluded (Li *et al.*, 2013). Chromatographic profiles from crude extracts with or without addition of different salts to solid rice medium suggested that halogen incorporation experiments with sodium bromide were s most interesting due to the appearance of new peaks. Further separation of its crude extract yielded ten new ambuic acid derivatives, pestallic acids H–Q, including one iodinated new natural product, pestallic acid Q. These new metabolites were not detected in cultures of the fungus grown on solid rice medium lacking sodium iodide or in those where sodium iodide had been replaced by sodium chloride or sodium bromide, thus highlighting the power of halogen incorporation experiment. As described, the structures were determined by 1D and 2D NMR data in combination with HRESI results. Mosher’s method and TDDFT-ECD calculations were applied for absolute configuration assignment.

Pestallic acids H–P are new analogues of the known compound ambuic acid, but mainly differ from it by the absence of epoxides between C-5 and C-6. The new compounds can be divided into three groups, H–M, N–P and Q according to the difference at C-5. Pestallic acids H–M were assigned as 5*R* while N–P were determined as 5*S*. Moreover, the hydroxy group that is attached to C-6 in co-isolated pestallic acids H–P, was converted to C-5 in pestallic acid Q. Meanwhile, regioselective conversion of epoxides to halohydrins resulted in different orientations of the hydroxy group at C-5 and of the iodine atom at C-6 (Wu *et al.*, 2006). Therefore, ambuic acid was suggested to be the precursor of pestallic acid Q. The intermediate **b** which features a double bond at C-5/C-6 may be the key precursor in the biosynthetic pathway. A Michael addition reaction of **b** with H₂O will generate C-5 epimers, which is reasonable for the formation of H–N and O–P, respectively. Ambuic acid was suggested to be the precursor of pestallic acid Q.

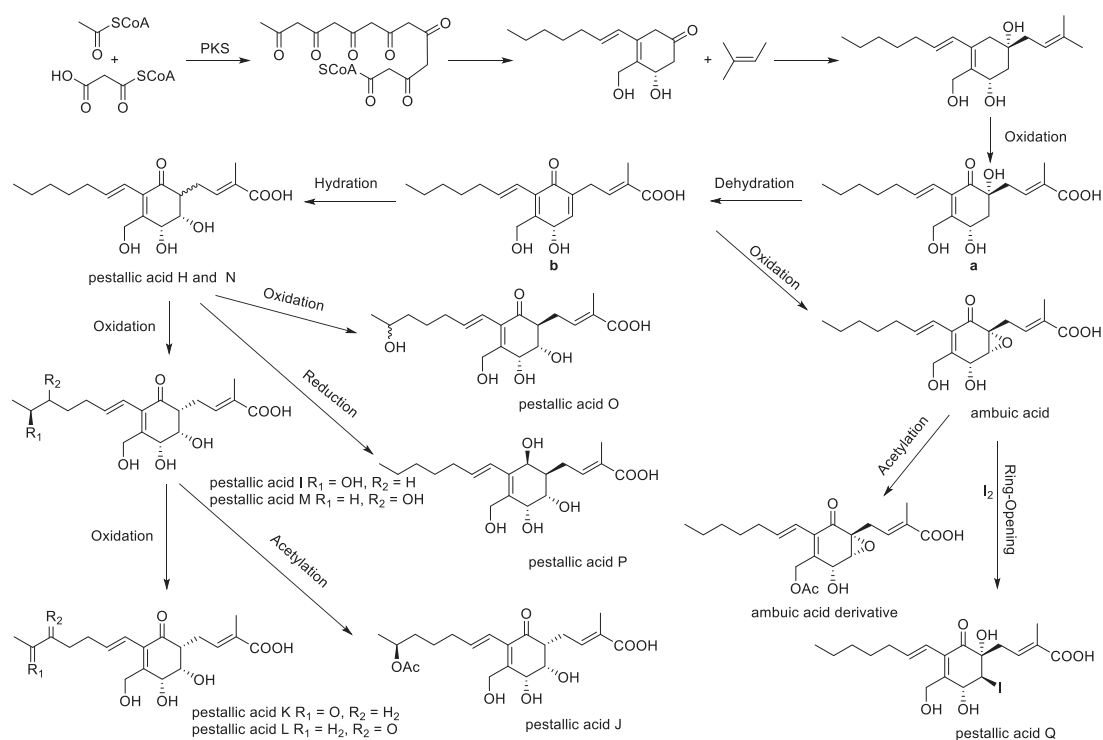


Figure 5.3.1. Plausible biogenetic pathway of ambuic acid derivatives.

Above all, a plausible biogenetic pathway was given. The isolated ambuic acid derivatives including the new compounds pestallic acid H–Q originate from the polyketide pathway (Yuan *et al.*, 2017). Elimination of water from the hypothetical precursor **a** is suggested to yield product **b** which features a double bond at C5/C6. A Michael addition reaction of **b** with H₂O in two manners will generate pestallic acids H and N which will undergo oxidation, reduction or acetylation to form pestallic acids I–M, O and P. On the other hand, ambuic acid likely originates from intermediate **b** via oxidation (Murray *et al.*, 2018). Ambuic acid derivatives are derived from ambuic acid via acetylation while the iodinated compound pestallic acid Q may be assumed to be derived via a ring-opening reaction of the epoxide group of ambuic acid with iodine (Wu *et al.*, 2006). Exposed to air, iodine anions (I[−]) from NaI solutions are slowly oxidized by atmospheric oxygen to molecule iodine (Figure 5.3.2) (Galvez, *et al.*, 2016). The appearance of intermediate **b** is reasonable as both 5*R* and 5*S* isomers (H and N, I and O) coexist. In order to exclude that pestallic acid Q might be an artifact formed during fermentation of the fungus in presence of NaI, ambuic acid was incubated in a mixture of MeOH and water adjusted to pH value of 3 in presence of 3.5% NaI for more than 48 h at room temperature. No generation of pestallic acid Q was observed.

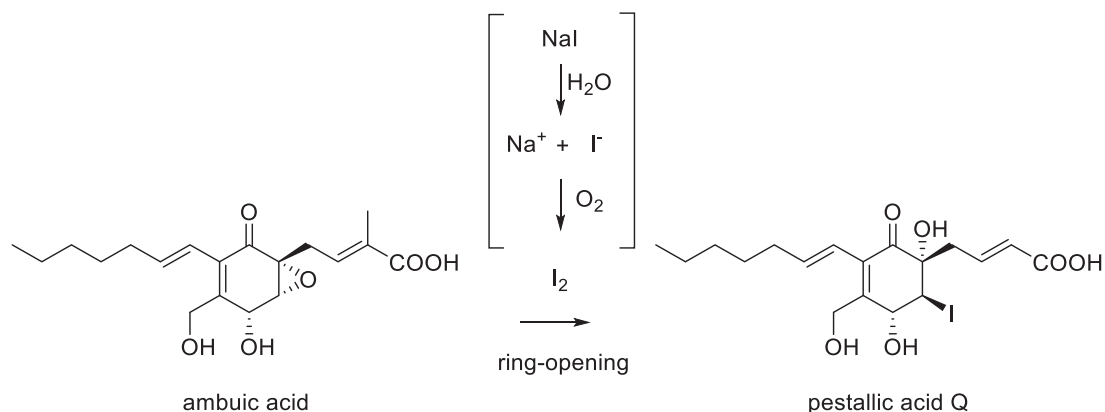


Figure 5.3.2. Plausible strategy for generation of pestallic acid Q.

Several chlorinated and brominated natural products were obtained from fungal endophytes (Li *et al.*, 2008; Wang *et al.*, 2016). However, iodinated natural products are extremely rare, the few examples reported so far include iodinated meroterpenes and polyhalogenated indoles from the red algae *Callophycus* sp. and *Rhodophyllis membranacea*, respectively (Lavoie *et al.*, 2017; Woolner *et al.*, 2016). As far as we know, fungi will not accept iodine, further interesting research on specific enzymatic halogenation *in vitro* and *in vivo* may be possible to support the biosynthetic pathway supposed above and the enzymatic catalysis of iodinated metabolite in the future (Weichold *et al.*, 2016).

In recent years, there were several top-selling halogens containing drugs on the market, examples include the brominated anti-anxiety agent bromazepam, fluorinated statins rosuvastatin and ledipasvir (Zhou *et al.*, 2016). Halogen substituents in natural molecules play an important role for their bioactivities. The chlorine substituent in salinosporamide A, a promising drug candidate entering the phase I human clinical trials for multiple myeloma treatment as 20S proteasome inhibitor (Niewerth *et al.*, 2014), may enhance proteasome inhibition through more favorable binding energy while providing the parallel benefit of increased potential for membrane permeability (Groll *et al.*, 2006). Compared to chemical halogenation, which most of the time requires harsh conditions, biosynthesis of halogenated natural products has a great advantage and should be a valuable approach for structural modification of the natural products for drugs research.

References

- Agrawal, S., Deshmukh, S. K., Reddy, M. S., Prasad R. and Goel, M. (2020). Endolichenic fungi: A hidden source of bioactive metabolites. *South African Journal of Botany*: Ahead of Print.
- Ariantari, N. P., Daletos, G., Mandi, A., Kurtan, T., Muller, W. E. G., Lin, W. H., Ancheeva, E. and Proksch, P. (2019). Expanding the chemical diversity of an endophytic fungus *Bulgaria inquinans*, an ascomycete associated with mistletoe, through an OSMAC approach. *RSC Advances*, **9**(43), 25119–25132.
- Baltz, R. H. (2016). Genetic manipulation of secondary metabolite biosynthesis for improved production in *Streptomyces* and other actinomycetes. *Journal of Industrial Microbiology and Biotechnology*, **43**(2–3), 343–370.
- Bastos, M. M., Costa, C. C., Bezerra, T. C., da Silva, F. D. C. and Boechat, N. (2016). Efavirenz a nonnucleoside reverse transcriptase inhibitor of first-generation: Approaches based on its medicinal chemistry. *European Journal of Medicinal Chemistry*, **108**, 455–465.
- Bohacz, J. (2017). Biodegradation of feather waste keratin by a keratinolytic soil fungus of the genus *Chrysosporium* and statistical optimization of feather mass loss. *World Journal of Microbiology and Biotechnology*, **33**(1), 13.
- Bryskier, A. (2000). Cepheids: fifty years of continuous research. *The Journal of Antibiotics*, **53**(10), 1028–1037.
- Butler, M. S. and Paterson, D. L. (2020). Antibiotics in the clinical pipeline in October 2019. *The Journal of Antibiotics*, 1–36.
- Carroll, A. R., Copp, B. R., Davis, R. A., Keyzers, R. A. and Prinsep, M. R. (2020). Marine natural products. *Natural Product Reports*, **37**(2), 175–223.
- Chalearmsrimuang, T., Ismail, S. I., Mazlan, N., Suasaard, S. and Dethoup, T. (2019). Marine-derived fungi: a promising source of halo tolerant biological control agents against plant pathogenic fungi. *Journal of Pure & Applied Microbiology*, **13**(1), 209–223.
- Chang, S. T. (1977). The origin and early development of straw mushroom cultivation. *Economic Botany*, **31**(3), 374–376.
- Che, Y., Gloer, J. B., Koster, B. and Malloch, D. (2002). Decipinin A and decipienolides A and B: New bioactive metabolites from the coprophilous fungus *Podospora decipiens*. *Journal of Natural Products*, **65**(6), 916–919.
- Chen, H., Ma, A., Daloze, P. and CQ, M. (2015). Historical remarks of immunosuppressive therapy in organ transplantation. *Current Immunosuppressive Therapy in Organ Transplantation*, **51**.
- Choi, S. S., Katsuyama, Y., Bai, L., Deng, Z., Ohnishi, Y. and Kim, E. S. (2018). Genome engineering for microbial natural product discovery. *Current Opinion in Microbiology*, **45**, 53–60.
- Chu, C. H., Li, K. M., Lin, S. W., Chang, M. D. T., Jiang, T. Y. and Sun, Y. J. (2014). Crystal structures of starch binding domain from *Rhizopus oryzae* glucoamylase in complex with isomaltooligosaccharide: insights into polysaccharide binding mechanism of CBM21 family. *Proteins: Structure, Function, and Bioinformatics*, **82**(6), 1079–1085.
- Chun, J. and Hartung, H. P. (2010). Mechanism of action of oral fingolimod (FTY720) in multiple sclerosis. *Clinical Neuropharmacology*, **33**(2), 91.

- Cochrane, S. A. and Vederas, J. C. (2016). Lipopeptides from *Bacillus* and *Paenibacillus* spp.: a gold mine of antibiotic candidates. *Medicinal Research Reviews*, **36**(1), 4–31.
- Cosme, M., Lu, J., Erb, M., Stout, M. J., Franken, P. and Wurst, S. (2016). A fungal endophyte helps plants to tolerate root herbivory through changes in gibberellin and jasmonate signaling. *New Phytologist*, **211**(3), 1065–1076.
- Ding, G., Li, Y., Fu, S., Liu, S., Wei, J. and Che, Y. (2009). Ambuic acid and torreyanic acid derivatives from the endolichenic fungus *Pestalotiopsis* sp.. *Journal of Natural Products*, **72**(1), 182–186.
- El-hawary, S. S., Moawad, A. S., Bahr, H. S., Abdelmohsen, U. R. and Mohammed, R. (2020). Natural product diversity from the endophytic fungi of the genus *Aspergillus*. *RSC Advances*, **10**(37), 22058–22079.
- Endo, A. (2004). The origin of the statins. *International Congress Series*, **1262**, 3–8.
- Endo, A. (2017). Discovery and development of statins. *Natural Product Communications*, **12**(8), 1934578X1701200801.
- Endo, A., Kuroda, M. and Tsujita, Y. (1976). ML-236A, ML-236B, and ML-236C, new inhibitors of cholesterologenesis produced by *Penicillium citrinum*. *The Journal of Antibiotics*, **29**(12), 1346–1348.
- Eugui, E. M., Almquist, S. J., Muller, C. D. and Allison, A. C. (1991). Lymphocyte-selective cytostatic and immunosuppressive effects of mycophenolic acid in vitro: role of deoxyguanosine nucleotide depletion. *Scandinavian Journal of Immunology*, **33**(2), 161–173.
- Fleming, A. (1979). On the antibacterial action of cultures of a *penicillium*, with special reference to their use in the isolation of *B. influenzae*. *British Journal of Experimental Pathology*, **60**(1), 3–13.
- Fujita, T., Inoue, K., Yamamoto, S., Ikumoto, T., Sasaki, S., Toyama, R., Chiba K, Hoshino Y and Okumoto, T. (1994). Fungal metabolites. Part 11. A potent immunosuppressive activity found in *Isaria sinclairii* metabolite. *The Journal of Antibiotics*, **47**(2), 208–215.
- Fyrst, H. and Saba, J. D. (2010). An update on sphingosine-1-phosphate and other sphingolipid mediators. *Nature Chemical Biology*, **6**(7), 489–497.
- Gálvez, Ó., Baeza-Romero, M. T., Sanz, M. and Pacios, L. F. (2016). A theoretical study on the reaction of ozone with aqueous iodide. *Physical Chemistry Chemical Physics*, **18**(11), 7651–7660.
- García-Estrada, C. and Martín, J. F. (2016). Biosynthetic gene clusters for relevant secondary metabolites produced by *Penicillium roqueforti* in blue cheeses. *Applied Microbiology and Biotechnology*, **100**(19), 8303–8313.
- Groll, M., Huber, R. and Potts, B. C. (2006). Crystal structures of salinosporamide A (NPI-0052) and B (NPI-0047) in complex with the 20S proteasome reveal important consequences of β -lactone ring opening and a mechanism for irreversible binding. *Journal of the American Chemical Society*, **128**(15), 5136–5141.
- Grundmann, A. and Li, S. M. (2005). Overproduction, purification and characterization of FtmPT1, a brevianamide F prenyltransferase from *Aspergillus fumigatus*. *Microbiology*, **151**(7), 2199–2207.
- Gubbels, M. A., Hulce, M., Kum, J. M., Urick, A. K. and Villa, E. M. (2016). Stereoselective synthesis of exocyclic allenes by double hydride reduction of 3-alkynyl-2-

- cycloalkenones. *Tetrahedron*, **72**(40), 6052–6063.
- Guzera, M., Szulc-Dąbrowska, L., Cywińska, A., Archer, J. and Winnicka, A. (2016). In vitro influence of mycophenolic acid on selected parameters of stimulated peripheral canine lymphocytes. *PloS one*, **11**(5), e0154429.
- Hemphill, C. F. P., Sureechatchaiyan, P., Kassack, M. U., Orfali, R. S., Lin, W., Daletos, G. and Proksch, P. (2017). OSMAC approach leads to new fusarielin metabolites from *Fusarium tricinctum*. *The Journal of Antibiotics*, **70**(6), 726–732.
- Hwu, J. R., Ethiraj, K. S. and Hakimelahi, G. H. (2003). Biological activity of some monocyclic-and bicyclic beta-lactams with specified functional groups. *Mini Reviews in Medicinal Chemistry*, **3**(4), 305–313.
- Itabashi, T., Matsuishi, N., Hosoe, T., Toyazaki, N., Udagawa, S. I., Imai, T. and Kawai, K. I. (2006). Two new dioxopiperazine derivatives, arestrictins A and B, isolated from *Aspergillus restrictus* and *Aspergillus penicilloides*. *Chemical and Pharmaceutical Bulletin*, **54**(12), 1639–1641.
- Jakubczyk, D., Cheng, J. Z. and O'Connor, S. E. (2014). Biosynthesis of the ergot alkaloids. *Natural Product Reports*, **31**(10), 1328–1338.
- Jakubczyk, D. and Dussart, F. (2020). Selected fungal natural products with antimicrobial properties. *Molecules*, **25**(4), 911.
- Jayanetti, D. R., Yue, Q., Bills, G. F. and Gloer, J. B. (2015). Hypocoprins A–C: new sesquiterpenoids from the coprophilous fungus *Hypocopa rostrata*. *Journal of Natural Products*, **78**(3), 396–401.
- Jeon, J. E., Kim, J. G., Fischer, C. R., Mehta, N., Dufour-Schroif, C., Wemmer, K. and Sattely, E. (2020). A pathogen-responsive gene cluster for highly modified fatty acids in tomato. *Cell*, **180**(1), 176–187.
- Jia, M., Chen, L., Xin, H. L., Zheng, C. J., Rahman, K., Han, T. and Qin, L. P. (2016). A friendly relationship between endophytic fungi and medicinal plants: a systematic review. *Frontiers in Microbiology*, **7**, 906.
- Kim, G. S., Ko, W., Kim, J. W., Jeong, M. H., Ko, S. K., Hur, J. S. and Ahn, J. S. (2018). Bioactive α -pyrone derivatives from the endolichenic fungus *Dothideomycetes* sp. EL003334. *Journal of Natural Products*, **81**(4), 1084–1088.
- Klaiklay, S., Rukachaisirikul, V., Tadpetch, K., Sukpondma, Y., Phongpaichit, S., Buatong, J. and Sakayaroj, J. (2012). Chlorinated chromone and diphenyl ether derivatives from the mangrove-derived fungus *Pestalotiopsis* sp. PSU-MA69. *Tetrahedron*, **68**(10), 2299–2305.
- Knoll, G. A., MacDonald, I., Khan, A. and van Walraven, C. (2003). Mycophenolate mofetil dose reduction and the risk of acute rejection after renal transplantation. *Journal of the American Society of Nephrology*, **14**(9), 2381–2386.
- Kobashigawa, J. A. and Meiser, B. M. (2005). Review of major clinical trials with mycophenolate mofetil in cardiac transplantation. *Transplantation*, **80**(2S), S235–S243.
- Lafont, P., J. P. Debeauvais, Gaillardin, M. and Payen, J. (1979). Production of mycophenolic acid by *Penicillium roqueforti* strains. *Applied and Environmental Microbiology*, **37**(3), 365–368.
- Lavoie, S., Brumley, D., Alexander, T. S., Jasmin, C., Carranza, F. A., Nelson, K. and Kubanek, J. (2017). Iodinated meroditerpenes from a red alga *Callophycus* sp. *The Journal of*

- Organic Chemistry*, **82**(8), 4160–4169.
- Li, E., Jiang, L., Guo, L., Zhang, H. and Che, Y. (2008). Pestalachlorides A–C, antifungal metabolites from the plant endophytic fungus *Pestalotiopsis adusta*. *Bioorganic & Medicinal Chemistry*, **16**(17), 7894–7899.
- Li, H. T., Liu, T., Yang, R., Xie, F., Yang, Z., Yang, Y. and Ding, Z. T. (2020). Phomretones A–F, C-12 polyketides from the co-cultivation of *Phoma* sp. YUD17001 and *Armillaria* sp. *RSC Advances*, **10**(31), 18384–18389.
- Li, L., Jiang, W. and Lu, Y. (2017). New strategies and approaches for engineering biosynthetic gene clusters of microbial natural products. *Biotechnology Advances*, **35**(8), 936–949.
- Li, S., Smith, K. D., Davis, J. H., Gordon, P. B., Breaker, R. R. and Strobel, S. A. (2013). Eukaryotic resistance to fluoride toxicity mediated by a widespread family of fluoride export proteins. *Proceedings of the National Academy of Sciences*, **110**(47), 19018–19023.
- Li, S. M. (2010). Prenylated indole derivatives from fungi: structure diversity, biological activities, biosynthesis and chemoenzymatic synthesis. *Natural Product Reports*, **27**(1), 57–78.
- Liu, S., Dai, H., Makhoulfi, G., Heering, C., Janiak, C., Hartmann, R. and Lin, W. (2016). Cytotoxic 14-membered macrolides from a mangrove-derived endophytic fungus *Pestalotiopsis microspora*. *Journal of Natural Products*, **79**(9), 2332–2340.
- Loron, C. C., François, C., Rainbird, R. H., Turner, E. C., Borensztajn, S. and Javaux, E. J. (2019). Early fungi from the Proterozoic era in Arctic Canada. *Nature*, **570**(7760), 232–235.
- Abe, I., Lv, J. M., Gao, Y. H., Zhao, H., Awakawa, T., Liu, L. and Gao, H. (2020). Biosynthesis of biscognienyne B involving a cytochrome P450-dependent alkynylation. *Angewandte Chemie International Edition*, **59**(32), 13531–13536.
- Marchand, J. A., Neugebauer, M. E., Ing, M. C., Lin, C. I., Pelton, J. G. and Chang, M. C. Y. (2019). Discovery of a pathway for terminal-alkyne amino acid biosynthesis. *Nature*, **567**(7748), 420–424.
- Martins, A., Vieira, H., Gaspar, H. and Santos, S. (2014). Marketed marine natural products in the pharmaceutical and cosmeceutical industries: Tips for success. *Marine Drugs*, **12**(2), 1066–1101.
- Matsuda, K. (2018). Okaramines and other plant fungal products as new insecticide leads. *Current Opinion in Insect Science*, **30**, 67–72.
- Meng, L. H., Li, X. M., Liu, Y., Xu, G. M. and Wang, B. G. (2017). Antimicrobial alkaloids produced by the mangrove endophyte *Penicillium brocae* MA-231 using the OSMAC approach. *RSC Advances*, **7**(87), 55026–55033.
- Murray, L. A., McKinnie, S. M., Pepper, H. P., Erni, R., Miles, Z. D., Cruickshank, M. C. and George, J. H. (2018). Total synthesis establishes the biosynthetic pathway to the naphterpin and marinone natural products. *Angewandte Chemie International Edition*, **57**(34), 11009–11014.
- Newman, D. J. and Cragg, G. M. (2015). Endophytic and epiphytic microbes as “sources” of bioactive agents. *Frontiers in Chemistry*, **3**, 34.
- Newman, D. J. and Cragg, G. M. (2020). Natural products as sources of new drugs over the nearly four decades from 01/1981 to 09/2019. *Journal of Natural Products*, **83**(3), 770–

- 803.
- Newman, D. J. and Cragg, G. M. (2020). Plant endophytes and epiphytes: Burgeoning sources of known and "unknown" cytotoxic and antibiotic agents? *Planta Medica*, **86**(13–14), 891–905.
- Niewerth, D., Jansen, G., Riethoff, L. F., van Meerloo, J., Kale, A. J., Moore, B. S. and Cloos, J. (2014). Antileukemic activity and mechanism of drug resistance to the marine *Salinispora tropica* proteasome inhibitor salinosporamide A (Marizomib). *Molecular Pharmacology*, **86**(1), 12–19.
- Ola, A. R., Thomy, D., Lai, D., Brötz-Oesterhelt, H. and Proksch, P. (2013). Inducing secondary metabolite production by the endophytic fungus *Fusarium tricinctum* through co-culture with *Bacillus subtilis*. *Journal of Natural Products*, **76**(11), 2094–2099.
- Otsuka, T., Muramatsu, Y., Nakanishi, T., Hatanaka, H., Okamoto, M., Hino, M. and Hashimoto, S. (2000). WF14865A and B, new cathepsins B and L inhibitors produced by *Aphanoascus fulvescens*. *The Journal of Antibiotics*, **53**(5), 449–458.
- Pan, R., Bai, X., Chen, J., Zhang, H. and Wang, H. (2019). Exploring structural diversity of microbe secondary metabolites using OSMAC strategy: a literature review. *Frontiers in Microbiology*, **10**, 294.
- Pang, K. L., Overy, D. P., Jones, E. G., da Luz Calado, M., Burgaud, G., Walker, A. K. and Bills, G. F. (2016). ‘Marine fungi’ and ‘marine-derived fungi’ in natural product chemistry research: toward a new consensual definition. *Fungal Biology Reviews*, **30**(4), 163–175.
- Parapouli, M., Vasileiadis, A., Afendra, A. S. and Hatziloukas, E. (2020). *Saccharomyces cerevisiae* and its industrial applications. *AIMS Microbiology*, **6**(1), 1.
- Patel, P. D. (2000). *Encyclopedia of Food Microbiology* (No. 664.03 E6).
- Qiao, Y., Xu, Q., Feng, W., Tao, L., Li, X. N., Liu, J., Zhu, H., Lu, Y., Wang, J., Qi, C., Xue, Y. and Zhang, Y. (2019). Asperpyridone A: An unusual pyridone alkaloid exerts hypoglycemic activity through the insulin signaling pathway. *Journal of Natural Products*, **82**(10), 2925–2930.
- Salque, M., Bogucki, P. I., Pyzel, J., Sobkowiak-Tabaka, I., Grygiel, R., Szmyt, M. and Evershed, R. P. (2013). Earliest evidence for cheese making in the sixth millennium BC in northern Europe. *Nature*, **493**(7433), 522–525.
- Sekita, S. (1983). Isocochliodinol and neocochliodinol, bis(3-indolyl)-benzoquinones from *Chaetomium* spp.. *Chemical and Pharmaceutical Bulletin*, **31**(9), 2998–3001.
- Shao, Z., Luo, Y. and Zhao, H. (2011). Rapid characterization and engineering of natural product biosynthetic pathways via DNA assembler. *Molecular BioSystems*, **7**(4), 1056–1059.
- Shen, B., Yan, X., Huang, T., Ge, H., Yang, D., Teng, Q., Rudolf, J. D. and Lohman, J. R. (2015). Eneidyne: Exploration of microbial genomics to discover new anticancer drug leads. *Bioorganic & Medicinal Chemistry Letters*, **25**(1), 9–15.
- Show, P. L., Oladele, K. O., Siew, Q. Y., Aziz Zakry, F. A., Lan, J. C. W. and Ling, T. C. (2015). Overview of citric acid production from *Aspergillus niger*. *Frontiers in Life Science*, **8**(3), 271–283.
- Singh, G. S. (2004). Beta-lactams in the new millennium. Part-II: cepheems, oxacepheems, penams and sulbactam. *Mini-Reviews in Medicinal Chemistry*, **4**(1), 93–109.
- Steffan, N., Grundmann, A., Yin, W. B., Kremer, A. and Li, S. M. (2009). Indole

- prenyltransferases from fungi: a new enzyme group with high potential for the production of prenylated indole derivatives. *Current Medicinal Chemistry*, **16**(2), 218–231.
- Stierle, A., Strobel, G. and Stierle, D. (1993). Taxol and taxane production by *Taxomyces andreanae*, an endophytic fungus of *Pacific yew*. *Science*, **260**(5105), 214–216.
- Strader, C. R., Pearce, C. J. and Oberlies, N. H. (2011). Fingolimod (FTY720): a recently approved multiple sclerosis drug based on a fungal secondary metabolite. *Journal of Natural Products*, **74**(4), 900–907.
- Stuart, K. A., Welsh, K., Walker, M. C. and Edrada-Ebel, R. (2020). Metabolomic tools used in marine natural product drug discovery. *Expert Opinion on Drug Discovery*, **15**(4), 499–522.
- Tan, R. X. and Zou, W. X. (2001). Endophytes: a rich source of functional metabolites. *Natural Product Reports*, **18**(4), 448–459.
- Thirumurugan, P., Matosiuk, D. and Jozwiak, K. (2013). Click chemistry for drug development and diverse chemical-biology applications. *Chemical Reviews*, **113**(7), 4905–4979.
- Tomm, H. A., Ucciferri, L. and Ross, A. C. (2019). Advances in microbial culturing conditions to activate silent biosynthetic gene clusters for novel metabolite production. *Journal of Industrial Microbiology and Biotechnology*, **46**(9–10), 1381–1400.
- Tran-Cong, N. M., Mándi, A., Kurtán, T., Müller, W. E., Kalscheuer, R., Lin, W. H., Liu, Z. and Proksch, P. (2019). Induction of cryptic metabolites of the endophytic fungus *Trichocladium* sp. through OSMAC and co-cultivation. *RSC Advances*, **9**(47), 27279–27288.
- Vagelos, P. R. (1991). Are prescription drug prices high? *Science*, **252**(5009), 1080–1084.
- Valverde, M. E., Hernandez-Perez, T. and Paredes-Lopez, O. (2015). Edible mushrooms: improving human health and promoting quality life. *International Journal of Medical Microbiology*, **2015**, 376387.
- Verhoff, F. H. and Bauweleers, H. (2000). Citric Acid. *Ullmann's encyclopedia of Industrial Chemistry*, 1–11.
- Wang, H., Dai, H., Heering, C., Janiak, C., Lin, W., Orfali, R. S., W. E. G., Liu, Z. and Proksch, P. (2016). Targeted solid phase fermentation of the soil dwelling fungus *Gymnascella dankaliensis* yields new brominated tyrosine-derived alkaloids. *RSC Advances*, **6**(85), 81685–81693.
- Wang, H., Li, Z., Jia, R., Hou, Y., Yin, J., Bian, X., Li, A., Muller, R., Stewart, A. F., Fu, J. and Zhang, Y. (2016). RecET direct cloning and Redαβ recombineering of biosynthetic gene clusters, large operons or single genes for heterologous expression. *Natural Protocol*, **11**(7), 1175–1190.
- Wang, H. H., Li, G., Qiao, Y. N., Sun, Y., Peng, X. P. and Lou, H. X. (2019). Chamiside A, a cytochalasan with a tricyclic core skeleton from the endophytic fungus *Chaetomium nigricolor* F5. *Organic Letters*, **21**(9), 3319–3322.
- Wang, Y., Gloer, J. B., Scott, J. A. and Malloch, D. (1993). Appenolides A–C: three new antifungal furanones from the coprophilous fungus *Podospora appendiculata*. *Journal of Natural Products*, **56**(3), 341–344.
- Wani, M. C., Taylor, H. L., Wall, M. E., Coggon, P. and McPhail, A. T. (1971). Plant antitumor agents. VI. Isolation and structure of taxol, a novel antileukemic and antitumor agent

- from *Taxus brevifolia*. *Journal of the American Chemical Society*, **93**(9), 2325–2327.
- Weichold, V., Milbredt, D. and van Pée, K. H. (2016). Specific enzymatic halogenation—from the discovery of halogenated enzymes to their applications in *vitro* and in *vivo*. *Angewandte Chemie International Edition*, **55**(22), 6374–6389.
- Wijesekera, K., Mahidol, C., Ruchirawat, S. and Kittakoop, P. (2017). Metabolite diversification by cultivation of the endophytic fungus *Dothideomycete* sp. in halogen containing media: Cultivation of terrestrial fungus in seawater. *Bioorganic & Medicinal Chemistry*, **25**(11), 2868–2877.
- Willems, T., De Mol, M. L., De Bruycker, A., De Maeseneire, S. L. and Soetaert, W. K. (2020). Alkaloids from arine fungi: Promising antimicrobials. *Antibiotics*, **9**(6), 340.
- Woolner, V. H., Jones, C. M., Field, J. J., Fadzilah, N. H., Munkacsi, A. B., Miller, J. H., Keyzers, R. A. and Northcote, P. T. (2016). Polyhalogenated indoles from the red alga *Rhodophyllis membranacea*: The first isolation of bromo-chloro-iodo secondary metabolites. *Journal of Natural Products*, **79**(3), 463–469.
- Wu, B., Hussain, M., Zhang, W., Stadler, M., Liu, X. and Xiang, M. (2019). Current insights into fungal species diversity and perspective on naming the environmental DNA sequences of fungi. *Mycology*, **10**(3), 127–140.
- Wu, J., Sun, X., Sun, W. and Ye, S. (2006). Unexpected highly efficient ring-opening of aziridines or epoxides with iodine promoted by thiophenol. *Synlett*, **2006**(15), 2489–2491.
- Xu, J., Yi, M., Ding, L. and He, S. (2019). A review of anti-inflammatory compounds from marine fungi, 2000–2018. *Marine Drugs*, **17**(11), 636.
- Yu, H., Sperlich, J., Höfert, S. P., Janiak, C., Teusch, N., Stuhldreier, F. and Liu, Z. (2019). Azaphilone pigments and macrodiolides from the coprophilous fungus *Coniella fragariae*. *Fitoterapia*, **137**, 104249.
- Yuan, C., Ding, G., Wang, H. Y., Guo, Y. H., Shang, H., Ma, X. J. and Zou, Z. M. (2017). Polyketide-terpene hybrid metabolites from an endolichenic fungus *Pestalotiopsis* sp. *BioMed Research International*, **2017**.
- Yurchenko, A. N., Smetanina, O. F., Kalinovskiy, A. I., Pushilin, M. A., Glazunov, V. P., Khudyakova, Y. V. and Afiyatulloev, S. S. (2014). Oxirapentyns F–K from the marine-sediment-derived fungus *Isaria felina* KMM 4639. *Journal of Natural Products*, **77**(6), 1321–1328.
- Zaffiri, L., Gardner, J. and Toledo-Pereyra, L. H. (2012). History of antibiotics from salvarsan to cephalosporins. *Journal of Investigative Surgery*, **25**(2), 67–77.
- Zang, Y., Gong, Y., Gong, J., Liu, J., Chen, C., Gu, L. and Zhang, Y. (2020). Fungal polyketides with three distinctive ring skeletons from the fungus *Penicillium canescens* uncovered by OSMAC and molecular networking strategies. *The Journal of Organic Chemistry*, **85**(7), 4973–4980.
- Zhang, F., Li, L., Niu, S., Si, Y., Guo, L., Jiang, X. and Che, Y. (2012). A thiopyranchromenone and other chromone derivatives from an endolichenic fungus *Preussia africana*. *Journal of Natural Products*, **75**(2), 230–237.
- Zhang, J. J. and Moore, B. S. (2020). Site-directed mutagenesis of large biosynthetic gene clusters via oligonucleotide recombineering and CRISPR/Cas9 targeting. *ACS Synthetic Biology*, **9**(7), 1917–1922.

- Zhao, H., Wang, G. Q., Tong, X. P., Chen, G. D., Huang, Y. F., Cui, J. Y. and Gao, H. (2014). Diphenyl ethers from *Aspergillus* sp. and their anti-A β 42 aggregation activities. *Fitoterapia*, **98**, 77–83.
- Zhao, J. Y., Wang, X. J., Liu, Z., Meng, F. X., Sun, S. F., Ye, F. and Liu, Y. B. (2019). Nonadride and spirocyclic anhydride derivatives from the plant endophytic fungus *Talaromyces purpurogenus*. *Journal of Natural Products*, **82**(11), 2953–2962.
- Zhao, Y., Liu, D., Proksch, P., Zhou, D. and Lin, W. (2018). Truncateols O–V, further isoprenylated cyclohexanols from the sponge-associated fungus *Truncatella angustata* with antiviral activities. *Phytochemistry*, **155**, 61–68.
- Zhou, Y., Wang, J., Gu, Z., Wang, S., Zhu, W., Ace , J. L. and Liu, H. (2016). Next generation of fluorine-containing pharmaceuticals, compounds currently in phase II–III clinical trials of major pharmaceutical companies: new structural trends and therapeutic areas. *Chemical Reviews*, **116**(2), 422–518.
- Zhou, Y. M., Ju, G. L., Xiao, L., Zhang, X. F. and Du, F. Y. (2018). Cyclodepsipeptides and sesquiterpenes from marine-derived fungus *Trichothecium roseum* and their biological functions. *Marine Drugs*, **16**(12), 519.
- Zhu, X., Liu, J. and Zhang, W. (2015). De novo biosynthesis of terminal alkyne-labeled natural products. *Nature Chemical Biology*, **11**(2), 115–120.

List of abbreviations

BGCs	Biosynthetic gene clusters
CD ₃ OD	Deuterated methanol
CDCl ₃	Deuterated chloroform
CH ₂ Cl ₂	Dichloromethane
COSY	Correlation spectroscopy
1D	One dimensional
2D	Two dimensional
DMAPP	Dimethylallyl pyrophosphate
DMSO	Dimethyl sulfoxide
DMTCI	4,4'-Dimethoxytrityl chloride
<i>et al.</i>	et altera (and others)
ECD	Electronic circular dichroism
EtOAc	Ethyl acetate
FDA	Food and drug administration (United States)
HMBC	Heteronuclear multiple bond connectivity
HMG-CoA	3-Hydroxy-3-methyl-glutaryl-CoA
HPLC	High performance liquid chromatography
HRESIMS	High resolution electrospray ionisation mass
HSQC	Heteronuclear single quantum coherence spectroscopy
Hz	Hertz
IC ₅₀	Half maximal inhibitory concentration
ITS	Iternal transcriber spacers
IL	Interleukin
KBr	Sodium bromide
LPS	Lipopolysaccharides
MeOH	Methanol
mg	Milligram
mm	Millimeter

mL	Milliliter
MS	Mass spectrometry
MHz	Mega Herz
min	Minute
MIC	Minimum inhibitory concentration
MTT	3-(4,5-dimethylthiazol-2-yl)-2,5-diphenyltetrazolium bromide
(R)-MTPA-Cl	(R)-(-)- α -methoxy- α -(trifluoromethyl)phenylacetyl chloride
(S)-MTPA-Cl	(S)-(+)- α -methoxy- α -(trifluoromethyl)phenylacetyl chloride
MW	Molecular weight
NaCl	Sodium chloride
NaF	Sodium fluoride
NaI	Sodium iodide
NMR	Nuclear magnetic resonance spectrometry
NOE	Nuclear Overhauser effect
OSMAC	One Strain MAny Compounds
PDB	Potato dextrose broth
ROESY	Rotating frame overhauser effect spectroscopy
RP 18	Reversed phase C18
TNF- α	tumor necrosis factor α
TDDFT-ECD	Time-dependent density functional theory-electronic circular dichroism
UV	Ultra-violet
VLC	Vacuum liquid chromatography
μ M	Micromolar

Acknowledgements

First of all, I would like to give my deepest appreciation to my supervisor Prof. Dr. Dr. Peter Proksch for providing me this precious opportunity to pursue my doctoral research in fungal secondary metabolites as well as for the excellent working conditions and facilities at the Institute of Pharmaceutical Biology and Biotechnology, Heinrich Heine University, Duesseldorf. I would like to convey my deep thanks and heartfelt gratitude for his patient guidance, helpful suggestions and fruitful discussions for my study in Duesseldorf.

My deep thanks to Prof. Dr. Kun Zou and Prof. Dr. Zhiyong Guo (Hubei Key Laboratory of Natural Products Research and Development, College of Biological and Pharmaceutical Sciences, China Three Gorges University, Yichang) for introducing me to Prof. Proksch as a visiting student during my master study so that I can have this great chance for further doctoral research, thanks to their help to study in Germany.

I am deeply indebted to Dr. Zhen Liu for his help on valuable suggestions on my experiments, structure elucidations of compounds and preparations of manuscripts for publications. I am heavily indebted to Dr. Marian Frank for his safety introduction, scientific guidance, fruitful discussions and his kind help for preparation of manuscripts.

I would like to express my appreciation to Prof. Dr. Rainer Kalscheuer (Institute of Pharmaceutical Biology and Biotechnology, Heinrich Heine University) for estimating my PhD study as second referee and for the help on antibiotic assays. My sincere thanks to Prof. Dr. Werner E. G. Müller (Institute of Physiological Chemistry and Pathobiochemistry, University of Mainz) for cytotoxicity tests and Ms. Breuer for their NMR measurements, to Dr. Peter Tommes (Institute of Inorganic and Structure Chemistry, Heinrich Heine University, Düsseldorf) for carrying out MS experiments.

I would like to express my sincere gratitude to Prof. Dr. Tibor Kurtán and Dr. Attila Mándi (Department of Organic Chemistry, University of Debrecen, Hungary) for kind help in ECD measurement and calculation.

My deep thanks to Mrs. Claudia Eckelskemper for her generous help of administration, and the technicians Mrs. Simone Miljanovic, Mrs. Waltraud Schlag,

Mrs. Katja Friedrich, Mrs. Simone Mönninghoff-Pützer, Mrs. Eva Müller, Ms. Linda Wiegand, Mrs. Heike Goldbach-Gecke and Mrs. Maryam Masrouri, for their generous help and support.

My sincere thanks to all former postdocs at the Institute, Dr. Daowan Lai, Dr. Elena Ancheeva, Dr. Georgios Daletos, Dr. Ramsay Kadeem, Dr. Sergi Herve Akone and Dr. Yang Liu, for nice discussions. I would like to profound my sincere thanks to my colleagues and friends, Dr. Amin Mokhlesi, Dr. Catalina Perez Hemphill, Ms. Dina Elkashef, Mr. Feng Pan, Mr. Ferhat Oezkaya, Dr. Festus Okoye, Mr. Haiqian Yu, Prof. Han Xiao, Mr. Harwoko, Ms. Kim Thao Lee, Mr. Lei Wang, Mr. Lin Wang, Ms. Mariam Moussa, Ms. Miada Sakr, Ms. Nada Mohamed, Mr. Nam Michael Tran-Cong, Ms. Nihal Aktas, Dr. Peter Eze, Dr. Rini Muharini, Dr. Shuai Liu, Mr. Tino Seidemann and Ms. Ying Gao, for assistances and sharing nice time together in the Institute. I would like to extend my sincere thanks to Mr. Dieter Meier for their help in the antibacterial assay.

My sincere thanks to the China Scholarship Council, Ministry of Education of China for the financial support in Germany. My sincere thanks to the Heine Research Academies (Heinrich Heine University) for providing corona emergency grants as the financial support for the end of my doctoral research.

My deep thanks to my friends in China for their encourage and support.

In the end, I would like to express my deepest gratitude to my parents, my little sister and brother for their great support.

Curriculum vitae

Name: Xiaoqin Yu

Nationality: Chinese

Address: Heinrich Heine University Duesseldorf
Universitätsstraße 1
40225 Duesseldorf

E-Mail: Xiyu101@hhu.de

Educational background:

Sept. 2017 – present: PhD student in Pharmacy, Institute of Pharmaceutical Biology and Biotechnology, Heinrich Heine University, Duesseldorf, Germany

June 2017 – Sept. 2014: Master of Pharmacy, College of Biological and Pharmaceutical Sciences, Three Gorges University, P. R. China

June 2014 – Sept. 2010: Bachelor of Bioengineering, College of Biological and Pharmaceutical Sciences, Three Gorges University, P. R. China

Publications:

1. **Xiaoqin Yu**, Werner E. G. Müller, Dieter Meier, Rainer Kalscheuer, Zhiyong Guo, Kun Zou, Blessing O. Umeokoli, Zhen Liu and Peter Proksch. Polyketide derivatives from mangrove derived endophytic fungus *Pseudopestalotiopsis theae*. *Marine drugs*, **2020**, 18, 129.
2. **Xiaoqin Yu**, Werner E.G. Müller, Zhiyong Guo, Wenhan Lin, Kun Zou, Zhen Liu and Peter Proksch. Indole alkaloids from the coprophilous fungus *Aphanoascus fulvescens*. *Fitoterapia*, **2019**, 136, 104168.
3. **Xiaoqin Yu**, Qingqing Zhang, Li Tian, Zhiyong Guo, Chengxiong Liu, Jianfeng Chen, Weaam Ebrahim, Zhen Liu, Peter Proksch, Kun Zou. Germacrane-type sesquiterpenoids with antiproliferative activities from *Eupatorium chinense*. *J.*

Nat. Prod. **2018**, 81 (1), 85–91

4. **Xiaoqin Yu**, Qingqing Zhang, Weihong Yan, Lei Wang, Zhiyong Guo, Qingqing Yang, Chengxiong Liu, Hai-Bo He, Kun Zou. Three new terpenoids from the *Eupatorium chinense*. *Phytochem Lett.* **2017**, 20, 224–227.
5. Chengxiong Liu, **Xiaoqin Yu**, Zhiyong Guo, Haibo He, Xuan Tu, Zhangshuang Deng, Kun Zou. Structural elucidation and NMR spectral assignments of paraconifuranones I-M from the insect-associated fungus *Paraconiothyrium brasiliense*. *Magn. Reson. Chem.* **2016**, 54 (11), 916–921.